Developing and Testing Novel Glutamate Receptor Antagonist Delivery Systems for the Treatment of Post Traumatic Osteoarthritis

Thesis submitted in the fulfilment of the requirement of the degree of Doctor of Philosophy

Benjamin Joseph Egan

School of Biosciences – Cardiff University
UK
November 2020

Abstract

Joint injury is a major risk factor towards developing osteoarthritis (OA) later in life. Post traumatic OA (PTOA) accounts for at least 12% of all OA cases, developing in 50–70% of patients with ACL ruptures or meniscal damage, 10–15 years after the injury. Current therapies do not prevent or cure OA and are limited to symptom management and end stage joint replacement. Synovial fluid (SF) glutamate concentrations increase in arthritis. NBQX and DNQX are AMPA/kainate glutamate receptor (GluR) antagonists developed as antiepileptic drugs. Previous work revealed intra-articular NBQX reduced knee swelling, cartilage destruction, synovial inflammation, gait abnormalities and bone erosions in rodent antigen induced arthritis and PTOA. This project aims to determine whether GluR antagonists can be incorporated into sustained release poly(lactic-co-glycolic) acid (PLGA) nanoparticles and thermoresponsive hydrogels and investigates GluR antagonists' protective effects on inflammatory or mechanically driven pathways in bone *in vitro.*

PLGA nanoparticles were developed within the nanoscale range and demonstrated sustained delivery of both NBQX and DNQX for up to 5 weeks in phosphate buffered saline (PBS). A freeze-drying methodology was developed that did not alter particle physical properties (size, poly-dispersal index) facilitating long term nanoparticle storage. PLGA nanoparticles did not elicit a cytotoxic response from primary human osteoblasts. Sustained GluR antagonist delivery was not detected in bovine SF and nanoparticle physical properties were altered when suspended in bovine SF with a decrease in particle size (5.1-fold, $p<0.0001$) and zeta potential (5700-fold, $p<0.0001$) detected vs PBS suspended nanoparticles. These findings indicated a potentially detrimental impact to particle stability in suspension media reflecting *in vivo* conditions.

GluR antagonists were incorporated into thermoresponsive hydrogels for sustained subcutaneous delivery. Pluronic F-127 and Carbopol 934 based hydrogels were rheologically tested across a range of Pluronic F-127 concentrations (19-28% w/v). 22% and 25% w/v Pluronic F-127 hydrogels had appropriate gelation temperatures and viscosity characteristics for gelation upon subcutaneous injection. DNQX delivery was sustained over 27hrs through a semi permeable membrane into PBS and over 24hrs through extracted bovine synovial membranes from 25% w/v hydrogels. Hydrogels reduced primary human osteoblast viability by 8-fold vs controls at 1:1 volumetric ratio hydrogel:media but not at 1:8 hydrogel:media (7 days exposure).

The effect of AMPA/KA GluR antagonist delivery was investigated in osteoblasts. Both NBQX and DNQX reduced osteoblast mineralisation 1.8-fold and 1.2-fold ($p=0.004$) at 200μM concentrations in 2D human primary osteoblast and human Y201 MSCs differentiated to osteoblasts. Human Y201s, were embedded in type I collagen and osteogenically differentiated into dendritic, osteocyte-like cells (expressing bone markers OPG, OCN, ALP and COL-1A1) and either stimulated with IL-6 and sIL-6r, or mechanically loaded, to mimic inflammatory and loading effects on osteocytes relevant to joint degeneration. The effects of either unencapsulated NBQX or unencapsulated NBQX combined with sustained release NBQX loaded PLGA nanoparticles was determined. IL-6/sIL-6r treatment increased nitrite levels indicating oxidative stress. Multivariate analysis identified a decrease following IL-6/sIL-6r treatment on bone turnover (*opg* 1.9-fold, *alp* 2.0-fold), inflammatory markers (*il-6* 2.5-fold) and glutamate signalling machinery (*gria-1* 3.1-fold) vs controls. Short term NBQX exposure decreased glutamate release vs controls (1.2-fold, $p=0.030$). *alp* expression was significantly reduced at 24hrs following IL-6 exposure and corrected by short term NBQX treatment. Anti-inflammatory cytokines (IL-4, IL-10, IL-13) release was upregulated by short term NBQX treatment at 24hrs. Nanoparticle treated cells did not differ to IL-6/sIL-6r treated cells except that they increased glutamate and IL-6 release following extended exposure (72hrs). These observations indicate limited therapeutic benefit of sustained release NBQX encapsulated in nanoparticles which were associated with detrimental effects of raised lactate dehydrogenase and nitrite. These findings supported cell viability assays (MTS) indicating empty nanoparticles at high concentrations (100mg/ml) increased MTS release vs controls across all timepoints analysed (1, 3 and 7 days) by 2.6- ($p=0.012$), 3.9- ($p<0.0001$) and 2.9-fold ($p=0.048$) respectively. NBQX treatment after pathophysiological loading (5000μstrain) modulates the mRNA expression of bone turnover (*opg* 1.43-fold decrease; *alp*, 3.1-fold decrease ($p<0.0001$)), inflammation (*il-6*, 1.4-fold decrease, $p=0.033$) and glutamate signalling markers (*gria-1*, 3-fold decrease, $p=0.015$). NBQX treatment elicited a repressive effect on all inflammatory biomarkers analysed, as well as on glutamate and OPG release across all time points tested.

Two GluR antagonist sustained release delivery vehicles were developed with differing release properties. PLGA nanoparticles sustained release of low (49μg/ml from 20mM NBQX loaded freeze dried nanoparticles) GluR antagonist loads over 3-5 weeks whereas Pluronic-F-127/Carbopol-934 hydrogels sustained release over 27hrs of high (0.74mg/ml from 2.5mM DNQX loaded hydrogels) concentrations. This study also provides evidence of the capacity of NBQX to protect against changes to bone turnover and induce the release of anti-inflammatory cytokines following a pathological inflammatory stimulus and to decrease the expression of bone turnover markers and inflammation following pathological loading.

Acknowledgements

I do not feel that I can adequately express in words the gratitude I feel to all those who have encouraged and supported me throughout this PhD, but I will give it a shot.

First and foremost, I would like to acknowledge the unwavering guidance given to me throughout my PhD from my supervisors, Professor Debbie Mason, Dr Charles Heard and Professor James Birchall. Their support was invaluable to navigating the ups and downs of this PhD and they encouraged my scientific curiosity, nurtured my developing analytical skills and provided a safe space to communicate ideas and overcome hurdles. I am very aware that I stand on the shoulders of giants with regards to the work in this thesis. This PhD wouldn't even exist without the wealth of knowledge contributed to the fields of osteoarthritis, glutamate receptor signalling and drug delivery by my supervisors. I am grateful for the funding and support provided by Cardiff University and the Versus Arthritis Biomechanics and Bioengineering Centre and for the networking and collaboration opportunities the Centre provided.

A huge thank you has to go to Dr Sophie Gilbert, Dr Cleo Bonnet and Carole Elford who were patient teachers to a wet behind the ears academic and ensured I was equipped with the analytical skills I needed to carry out this PhD. No matter how many questions asked and regardless of their own commitments and stresses, Soph, Cleo and Carole were always available to provide hands on help or useful advice for which I am incredibly grateful. I'd like to also thank: Dave Houston for showing me the ropes in my first week in the School of Pharmacology and imparting many words of wisdom; Hannah Boostrom for showing me the ways of HPLC, the ticking of which still often reverberates within my dreams; Elen Everet for teaching me all things rheology and Dr Joel Alvez for providing me with some rather gruesome bovine joint anatomy lessons which memorably resulted in a blood soaked shirt for Joel (cow's blood, not his).

To my loving family, who have picked me up when I've struggled and encouraged me when things have been going well, I couldn't have got through this PhD without you. Mum and Dads words of comfort and wisdom in times of stress were a ballast in stormy waters and my sister Esther's positivity and encouragement never failed to pick me up. To my long-suffering girlfriend, Hannah, I cannot express what your limitless love and support has meant to me. Without you keeping me on track I would have struggled to keep going through some of the trials and tribulations of this PhD. Hannah may have earnt a Doctorate by proxy through patiently listening to me verbalise all my work over the last 4 years. To Hannah's family, Myles, Helen, Brin and Ella, thank you for being a reliable source of comfort and laughter (particularly Myles). To all the boys at CURFC and Pontypool RFC, having the outlet of rugby throughout the PhD helped me keep some perspective and let me blow off steam and beating Swansea at the Principality Stadium was a particular highlight of my university experience. A specific thank you to big Al 'Foley' Burrell, who made sure I never slipped out of the social world and who's friendship I value massively.

Finally, to quote my favourite author J.R.R. Tolkien "Few can foresee whither their road will lead them, till they come to its end". This has been an unforgettable journey in which I have had experiences that will shape me for the rest of my life.

Table of Contents

List of Abbreviations

ACL	Anterior Cruciate Ligament
ACLT	ACL Transection
ADAMTS-4/5	A Disintegrin and Metalloproteinase with Thrombospondin Motifs-4/5
AgNPs	Silver Nanoparticles
AIA	Antigen Induced Arthritis
ALP	Alkaline Phosphatase
AMPA	dl-α-amino-3-hydroxy-5-methylisoxasole-4-propionate
ANOVA	Analysis of Variance
ATP	Adenosine Tri-Phosphate
AuNPs	Gold Nanoparticles
BBR	Berberine
BCS	Biopharmaceutical Classification System
BLAST	The Basic Alignment Search Tool
BMU	Basic Multicellular Unit
BSA	Bovine Serum Albumin
BSP	Bone Sialoprotein
BSP	Betamethasone Sodium Phosphate
cAMP	Cyclic Adenosine Monophosphate
cDNA	Complementary DNA
CFA	Complete Freunds Adjuvant
cGMP	Cyclic Guanosine Monophosphate
ChS	Condroitin Sulphate
CI	Confidence Intervals
CIA	Collagen Induced Arthritis
CNS	Central Nervous System

COX-2	Cyclooxygenase -2
CRP	C-Reactive Protein
CSF-1	Colony Stimulating Factor-1
Ct	Cycle Threshold
DAMP	Damage Associated Molecular Pattern
DEX	Dexamethasone
dH_2O	Distilled Water
DKK	Dickkopf
DL	Drug Loading
DLS	Dynamic Light Scattering
DMOAD	Disease Modifying Osteoarthritis Drug
DMP-1	Dentine Matrix Protein-1
DNA	Deoxyribonucleic Acid
Dsh	Dishevelled
EAA	Excitatory Amino Acid
ECL	Electrochemiluminescence
ECM	Extracellular Matrix
EE	Encapsulation Efficiency
ELISA	Enzyme Linked Immunosorbent Assay
ELS	Electrophoretic Light Scattering
eNOS	Endothelial Nitric Oxide Synthase
ERK	Extracellular Signal-Regulated Kinase
FAK	Focal Adhesion Kinase
FBS	Fetal Bovine Serum
FDA	Food and Drug Administration
FGF	Fibroblast Growth Factor
FITC	Fluorescein Isothiocyante

FLS	Fibroblast Like Synoviocyte
FN	Fibronectin
G’	Elastic Modulus
G”	Viscous Modulus
GAG	Glycosaminoglycan
GI	Gastro-Intestinal
GluR	Glutamate Receptor
Gsk3	Glycogen Synthase Kinase-3
HA	Hyaluronic Acid
hOB	Primary Human Osteoblast
HPLC	High Performance Liquid Chromatography
IA	Intra-Articular
IFN	Interferon
IGF	Insulin Like-Growth Factor
IL-…	Interleukin-…
IL-1Ra	Interleukin 1 Receptor Antagonist
iNOS	Inducible Nitric Oxide Synthase
IP(3)	D-myo-inositol 1,4,5-trisphosphate
IV	Intra-Venous
JAK2	Janus Kinase-2
KA	Kainate
KAFAK	kinase-Activated Protein Kinase 2-Inhibiting Cell-Penetrating Peptide
KGN	Kartogenin
KMO	Kaiser-Meyer-Olkin
KOOS	Knee Injury and Osteoarthritis Outcome Score
LC	Loading Capacity
LDH	Lactate Dehydrogenase

LRP	Low Density Lipoprotein Receptor Related Protein
MAPK	Mitogen Activated Protein Kinase
mBSA	Methylated Bovine Serum Albumin
MEPE	Matrix Extracellular Phosphocycloprotein
MES	Minimum Effective Strain
MetS	Metabolic Syndrome
MIA	Monoiodoacetate
MIP-1b	Monocyte Inflammatory Protein-1b
MMP	Matrix Metalloproteinase
MNP	Melanin Nanopartilces
MNX	Meniscectomy
MSC	Mesenchymal Stem Cell
MSD	Mesoscale Discovery
MTP	Medial Tibial Plateau
MTT	(3-(4,5-Dimethylthiazol-2-yl)-2,5-Diphenyltetrazolium Bromide)
MTX	Methotrexate
NBF	Neutral Buffered Formalin
NCBI	National Centre for Biotechnology Information
NF-kb	Nuclear Factor Kappa Beta
NGF	Nerve growth factor
NICE	National institute for health and care excellence
NIH	National Institiute of Health
NIM	nanoparticles in microspheres
NMDA	N-methyl-d-aspartate
nNOS	neuronal nitric oxide synthase
NO	Nitric oxide
NSAID	non-steroidal anti-inflammatory drugs

OA	Osteoarthritis
OARSI	Osteoarthritis Research Society International
OARSI	Osteoarthritis Research Society International
OCN	Osteocalcin
OCT	Optimal Cutting Temperature Compound
OPG	Osteoprotegerin
OSM	Oncostatin M
Osx	Osterix
PBS	Phosphate Buffered Saline
PCA	Principal Component Analysis
PDI	Poly Dispersity Index
PEO	Poly(Ethylene Oxide)
PGE2	Prostaglandin E(2)
PHEX	Phosphate Regulating Endopeptidase Homologue, X-Linked
PLGA	Poly(Lactic-co-Gylcolic Acid)
PLL	Poly(L-Lysine)
pNIPAM	Poly(N-Isopropylacrylamide)
PPO	Poly(Propylene Oxide)
PTOA	Post Traumatic OA
QD	Quantum Dot
QoL	Quality of Life
RA	Rheumatoid Arthritis
RANK	Receptor Activator of Nuclear Factor Kappa-b
RANKL	Receptor Activator of Nuclear Factor Kappa- b Ligand
RANTES	Regulated on Activation, Normal T Cell Expressed and Secreted
RCT	Randomised Control Trial
RNA	Ribonucleic Acid

RT	Reverse Transcriptase
Runx2	Runt-Related Transcription Factor 2
SD rats	Sprague Dawley Rats
SEM	Scanning Electron Microscopy
SLN	Solid Lipid Nanoparticle
SOST	Sclerostin
SR	Systematic Review
Tg’	Glass Transition Temperature
TGF-b	Transforming Growth Factor-b
THR	Total Hip Replacement
TKR	Total Knee Replacement
T_m	Melting Temperatures
TMB	Tetramethylbenzidine
TMJ	Temporomandibular Joint
TNFa	Tumour Necrosis Factor-a
TRAP	Tartrate-Resistant Acid Phosphatase
Tris base	Tris(hydroxymethyl)aminomethane Base
VEGF	Vascular Endothelial Growth Factor
w/v	Weight/Volume
WHO	World Health Organisation
WOMAC	Western Ontario and McMaster Universities Osteoarthritis Index

Thesis Word Count: 65,702

Chapter 1

Introduction

1.1 Osteoarthritis

1.1.1 Disease Characteristics

Osteoarthritis (OA) is one of the most common diseases globally with 26.9 million US adults predicted to have had the condition in 2005 (Nüesch et al., 2011). Global Burden of Disease figures estimated that 242 million people were living with activity limiting knee or hip OA accounting for 13 million years lived with disability (Osteoarthritis Research Society International, 2016). It has been estimated that 10% of men and 18% of women over the age of 60 are affected (Woolf and Pfleger, 2003). The socio-economic burden of OA has been estimated to cost between 1 and 2.5% of gross domestic product in developed countries (Hiligsmann et al., 2013).

In 2016 the OA Research Society International (OARSI) released a white paper to the U.S. food and drug administration (FDA) reviewing the current OA literature. This supported the designation of OA as a serious disease that is currently without a cure and with no therapies that prevent disease progression or adequately manage loss of mobility and the pain associated with the disease (Osteoarthritis Research Society International, 2016). OA has been associated with multiple co-morbidities, which include cardiovascular disease, diabetes, lung disease, depression, obesity and hearing and visual impairments (Reeuwijk et al., 2010). People suffering from OA have a higher likelihood of having other chronic conditions. Stroke, metabolic syndrome and peptic ulcers have been identified as key co-morbidities (Swain et al., 2019). The presence of co-morbidities in adult OA sufferers is associated with increased pain and decreased daily activity (van Dijk et al., 2010). Psychological factors such as stress, anxiety and depression have been linked with OA (Hausmann et al., 2017). The physical, psychological and economic burden of OA represents a significant and growing issue in an aging society. The World Health Organisation (WHO) highlights OA as one of the 10 most disabling diseases in developed countries and indicates a need for research into the:

- Efficacy, safety and cost effectiveness of current therapeutics in the long-term management of OA.
- Development of diagnostics, biomarkers and new imaging technologies to better monitor OA progress.

- Effectiveness of potential therapies and the impact of risk factors in using new diagnostics and biomarkers.

Addressing one or all of these research aims is key for the development of more effective OA therapies to address the unmet clinical need (World Health Organisation, 2013).
OA is a degenerative joint disease that manifests as pain, inflammation and swelling in affected joints. It results in disability in progressed cases. The symptoms are the result of destructive changes to tissue in and around the joint. They involve changes in subchondral bone, synovial inflammation, damage to and loss of articular cartilage and weakening of periarticular muscle (Kim et al., 2018).

Changes to bone physiology play a central role in the development of OA and are closely linked to the alterations observed in articular cartilage during disease progression (Kim et al., 2018). The process of bone remodelling, the impact of mechanical loading on bone and the link to biomechanical signalling occurring in healthy bone are key in understanding the alterations that can take place due to the development of OA.

1.1.2 OA Risk Factors

The major risk factors in development of OA include age, prior joint injury, joint malalignment and systemic metabolic disorders, which collectively lead to altered cellular signalling and inflammatory responses (Reviewed in Appleton, 2018 and Mills et al., 2018)

1.1.2.1 Aging

Aging is a major risk factor to the development of OA. Multiple chronic conditions that have age as a major risk factor, such as Alzheimer's, OA and sarcopenia, exhibit similar cellular and molecular mechanisms (Ladislas, 2000). Cells can only undergo a limited number of population doublings in culture, a phenomenon known as the Hayflick limit (Hayflick and Moorhead, 1961). This is attributed to the shortening of telomeres during every round of cell division as a consequence of DNA polymerase activity (Ladislas, 2000). A common feature of the aforementioned chronic degenerative diseases is low grade systemic inflammation termed 'inflamm-aging' (Franceschi et al., 2000), that results in the release of inflammatory markers, that can drive the development of OA.

Systemic age related changes linked to OA include increased circulatory levels of IL-6, C-reactive protein (CRP) and TNFα (Strandberg and Tilvis, 2000, Bruunsgaard, 2002). Lower sex steroid hormones and increased levels of visceral fat are characteristics associated with aging and linked to greater levels of inflammatory markers, including IL-6 and TNFα (Bruunsgaard, 2002). A link between OA development and IL-6 levels has also been identified. In an epidemiological study by Singh and Newman, serum IL-6 levels were robustly associated with the incidence of age related disease and adverse outcomes such as disability and mortality (Singh and Newman, 2011). Serum IL-6 and CRP concentrations were increased in patients with knee OA and identified as predictive markers for risk of OA progression (Spector et al., 1997, Livshits et al., 2009). A study of 149 randomly selected subjects (46% female, mean age 63) by Stannus et al., (2013) measured the association between knee pain and inflammatory markers over 5 years. This study identified a positive association between change in total knee pain and serum levels of high sensitivity-CRP as well as serum levels of TNFα (Stannus et al., 2013). This study identified a link between specific inflammatory markers and OA associated pain as well as aging and progression of OA, highlighting the multifactorial nature of OA. The link between a wide range of inflammatory markers and aging was studied by Morrisette-Thomas et al., (2014). Release of IL-6, CRP, IL-15, IL-8 and macrophage inflammatory protein-1b were found to positively correlate with age and anti-inflammatory IL-10 was found to negatively correlate with age increase. The findings of this study also highlighted an age related increase in some anti-inflammatory markers (IL-1 receptor antagonist (IL-1Ra), soluble glycoprotein 130, soluble TNF receptors I and II) (Morrisette-Thomas et al., 2014). This study also postulates that the increase in inflammatory markers associated with age, stimulates the release of anti-inflammatory factors and that the ratios of these factors may indicate susceptibility to age related diseases.

The circadian, 'cellular clock' in mammals is controlled by the hypothalamus. Within the hypothalamus the suprachiasmatic nuclei reacts to inputs from external cues, mainly light, in order to transmit temporal information throughout the body and regulate genes controlling tissue physiology (Takahashi et al., 2008). Circadian rhythm affects chondrocyte proliferation (Stevenson et al., 1990) and bone formation (Igarashi et al., 2013) with a peak

in cellular activity (ECM component production) during the middle of the light period and a trough in the middle of the dark period. The effects of circadian rhythm on chondrocytes dampen with age and represent a contributory factor to the development of OA (Gossan et al., 2015). Circadian 'clock' genes are also downregulated due to mechanical stress in chondrocytes (Kanbe et al., 2006) and this has been further supported by evidence suggesting circadian rhythm is repressed in other joint tissue (synovium) (Haas and Straub, 2012). The identification of circadian rhythm within articular cartilage, which declines due to aging, presents a therapeutic target for age related OA by disrupting the natural rhythm to return to a younger phenotype.

1.1.2.2 Metabolic Syndrome

Another factor impacting systemic inflammation and associated with aging is metabolic syndrome (MetS). This condition lacks an accepted definition but consists of four central features: insulin resistance, visceral obesity, atherogenic dyslipidaemia and hypertension (Zhuo et al., 2012). Data from 7714 subjects, used as a representative sample of the general population in the USA from the National Health and Nutrition Examination Survey III, showed an increased prevalence of MetS in OA sufferers regardless of sex or race. MetS was demonstrated in 59% of individuals suffering from OA and 23% of patients without OA. 64.8% of OA sufferers aged 18-65 exhibited MetS whereas only 20.6% suffered from MetS in the non-OA population indicating a link between OA and MetS development in relatively young individuals (Puenpatom and Victor, 2009).

1.1.2.3 Joint trauma / Injury

Physical loading and prior joint injury are major contributors to OA progression. This is demonstrated in athletes where increased physical demands combined with potential for musculoskeletal injury result in a high prevalence of early onset OA. This was demonstrated in a systematic literature review of former professional football payers (aged 35-45) indicating a 80% prevalence of knee OA and 17% ankle OA (Kuijt et al., 2012). In a systematic review comparing elite athletes from a range of both individual and team sports it was concluded that, despite heterogeneity in their findings, the prevalence of OA is

increased in former athletes compared to the general population (Gouttebarge et al., 2015). Related to this, obesity has been shown to represent a significant risk factor in the development of OA, with every 5kg of weight gained representing a 36% increased risk in the development of knee OA (Lementowski and Zelicof, 2008). The joints of overweight patients are subject to increased loading, altered inflammatory signalling and relatively low muscle to fat ratios (Bliddal et al., 2014).

The evidence indicating that both elite athletes and those suffering from obesity are highly susceptible to the development and progression of OA suggests that altering joint biomechanics impacts joint health (Figure 1.1). In addition, joint malalignment is an independent risk factor in the development of OA (Puno et al., 1991, Tanamas et al., 2009) which can further increase the risk of OA development in obese individuals and following joint trauma (Beaver et al., 1992, Sharma et al., 2000).

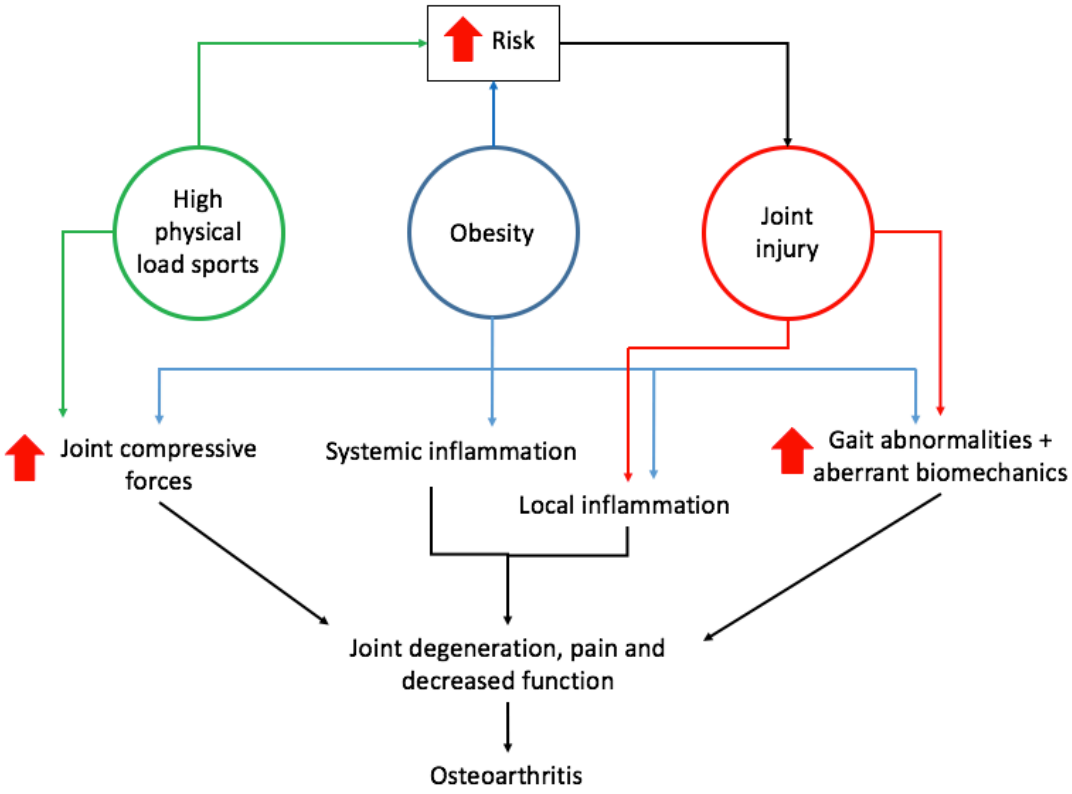

Figure 1.1: Flow diagram representing the link between obesity, high physical load sports and joint injuries with OA development and progression (designed by author, developed using information from:(Sharma et al., 2000, Anderson et al., 2011, Kuijt et al., 2012, Bliddal et al., 2014)).

With this in mind, PTOA is the development of OA following a joint injury. As Reviewed by Anderson et al. (2011), more than 40% of people who suffer articular cartilage injuries,

meniscus tears or ligament damage go on to develop knee OA (Anderson et al., 2011). Significant ligamentous or capsular injuries increase the risk of developing OA by up to 10 times. Most articular fractures increase OA risk by up to 20 times. PTOA represents at least 12% of all lower limb OA sufferers (Anderson et al., 2011). PTOA represents a potential therapeutic target over conventional OA as the point of OA induction can be tracked back to the initial joint trauma. This would allow for the application of preventative therapies and optimisation of drug delivery timing with regards to stage of PTOA development. PTOA is reviewed in further detail in section 1.1.4 as this pathology is a potential target for therapeutic interventions discussed in this thesis.

1.1.3 Pathology of OA

While OA is commonly referred to as non-inflammatory arthritis, as opposed to autoimmune 'inflammatory' RA, there is mounting evidence indicating inflammation plays a key role in OA pathology. Structural degeneration and pain are two additional significant contributors to OA pathology. Some evidence indicates that both peripheral and central pain sensitisation can occur in OA, resulting in normal joint function becoming painful (Bajaj et al., 2001, Melzack et al., 2001). This can be further exacerbated by social and psychological factors (Dieppe and Lohmander, 2005). Inflammation is a key feature to OA development. Pain is linked to neurogenic inflammation that can lead to joint damage (Kidd et al., 2003). Therefore, pain may not only be a symptom but also a factor in the propagation of OA. Pain, inflammation and degradation are key aspects in the development of OA and are interwoven to produce a complex pathology.

1.1.3.1 Cartilage

Cartilage provides smooth, hardwearing, load bearing functionality to healthy synovial joints. Cartilage provides a cushion to bone and can withstand decades of impact (Correa and Lietman, 2017). Chondrocytes sit within a matrix of collagen type II, IX and XI that provide strength and stiffness; proteoglycans, such as aggrecan, provide stiffness and durability against compressive forces, and non-collagenous proteins, such as Anchorin, help anchor chondrocytes within the cartilage matrix (Buckwalter and Mankin, 1998).

Structurally, articular cartilage can be sub-divided into 4 zones (Table 1.1) (Jeon et al., 2010). The maintenance of this cartilage is key to the function of a healthy joint.

Table 1.1: The characteristics of articular cartilage zones. Adapted from Jeon et al., 2010.

Zone	**Structure/layout**
A: Superficial	This is a thin zone composed of 2 layers. The lamina Splendens, composed of mainly collagen fibres in an acellular sheet below which is a layer of flattened, parallel chondrocytes. This is an ECM high in water fibronectin and collagen that thereby imparts high tensile strength to this zone (Buckwalter and Mankin, 1998, Temenoff and Mikos, 2000).
B: Transitional	This zone contains spherical chondrocytes and large collagen fibrils with less water and collagen than the superficial zone but more proteoglycans. In this zone, fibrils are arranged randomly with regards to the articular surface (Buckwalter and Mankin, 1998, Temenoff and Mikos, 2000).
C: Middle	This is the biggest zone with the largest diameter collagen fibrils, lowest water levels and most proteoglycan content. Collagen fibrils and Chondrocytes, which are stacked in columns, are orientated perpendicular to the articular surface. Cells have high levels of synthetic activity (Wong et al., 1996).
D: Calcified	This zone lies closest to subchondral bone and acts as a transitional layer from softer hyaline cartilage to calcified bone (Cohen et al., 1998). Chondrocytes are small and have low metabolic activity and calcified ECM begins to surround cells (Buckwalter and Mankin, 1998, Temenoff and Mikos, 2000).

Healthy cartilage is aneural and, therefore, may not be the primary source of pain in OA (Hunter et al., 2003). However, vascularisation of non-calcified articular cartilage has been identified across a wide range of histological severity scores in explants from Total Knee Replacement (TKR) and post-mortem articular surfaces (Suri et al., 2007). Perivascular innervation of cartilage has been identified in the same study. This indicates a source of pain

in OA is driven by cartilage vascularisation (Suri et al., 2007). Radiographic evidence clearly indicates loss of articular cartilage in OA pathogenesis and is used as a diagnostic tool. However, the radiographically observable loss of cartilage does not reflect the loss of function and pain experienced by OA sufferers (Pritzker, 2003, Arden and Nevitt, 2006, Altman and Gold, 2007) (Figure 1.2).

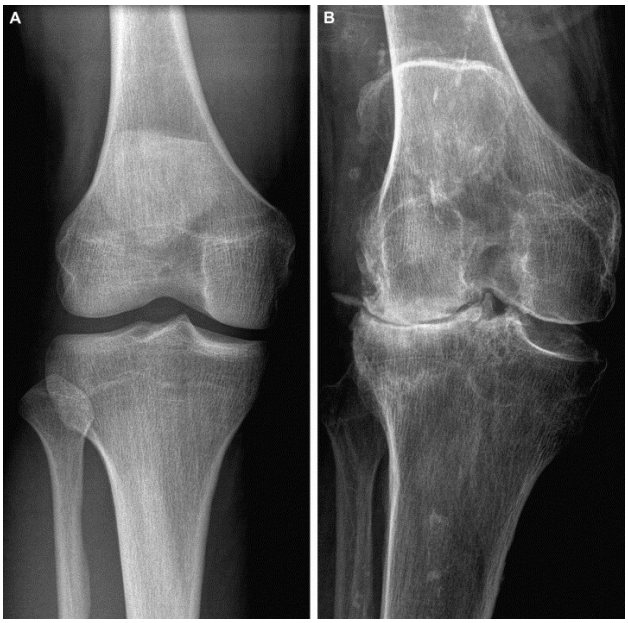

Figure 1.2: Radiograph from healthy (A) and osteoarthritic (B) knee joint radiographs. Taken from Altman and Gold, 2007 with permissions granted for use of this figure in this thesis. Tibial attrition visible across the medial region of the OA joint (B).

Human OA cartilage histopathology can be subdivided into 6 grades of increasing OA severity. Grade 0 represents healthy, intact cartilage progressing all the way to grade 5 and 6 where there is exposed sclerotic bone and the formation of fibrocartilage with the development of osteophytes and altered bone remodelling (Pritzker et al., 2006).

In OA the cartilage ECM is slowly degraded by proteolytic enzymes. Aggrecan is one of the key proteoglycans in cartilage ECM and is essential for the ability of cartilage to withstand compression. The proteolytic degradation of aggrecan is a major contributor to arthritis pathology (Troeberg and Nagase, 2012). Evidence of Aggrecan degrading enzymes, termed aggrecanases, was discovered by Sandy et al., following collection of synovial fluid from patients with knee injury, early and late stage OA (Sandy et al., 1992). The most active 'aggrecanases' that have been identified are A Disintegrin and Metalloproteinase with

Thrombospondin motifs -4 (ADAMTS-4) and ADAMTS-5 (Gendron et al., 2007). Both ADAMTS-4 and -5 have been shown to play significant roles within cartilage degradation. Inhibition of the activity of ADAMTS-5 has been shown to promote cartilage repair in mice *in vivo.* Blocking of the aggrecan immunoglobulin domain aggrecanase cleavage site results in a protection from ADAMTS-5 and inflammatory molecule (IL-1α) induced cartilage degradation (Sandy and Verscharen, 2001, Little et al., 2007). In healthy human cartilage explants, siRNA mediated inhibition of both ADAMTS-4 and ADAMTS-5 resulted in a reduced loss of aggrecan following TNFα and oncostatin M (OSM) inflammatory stimulation (Song et al., 2007). In the same study, ADAMTS-4 and ADAMTS-5 siRNA inhibition within OA cartilage explants also resulted in decreased aggrecan degradation (Song et al., 2007). Collagen type II is one of the key proteins imparting structure and tensile strength to cartilage ECM and its degradation is associated with the development of OA (Billinghurst et al., 1997). The activity of collagen degrading enzymes in cartilage has long been known (Ehrlich et al., 1977). A primary collagenase identified in OA cartilage is MMP-13. Studies demonstrate increased MMP-13 expression and activity in OA cartilage (Reboul et al., 1996, Kevorkian et al., 2004, Piecha et al., 2010). *In vivo* models demonstrate MMP-13 activity stimulating cartilage degradation (Neuhold et al., 2001), inhibition of which protects against a degradative state (Johnson et al., 2007, Piecha et al., 2010). In addition to ADAMTS-4/5 and MMP-13 multiple, other MMPs and aggrecanases have been identified in OA cartilage (Kevorkian et al., 2004).

Inflammation plays a key role in OA cartilage pathology. Inflammation has been linked with cartilage destruction (Kim et al., 2018) but cytokines play both protective and degradative roles. A wide range of cytokines and their corresponding receptors have been implicated in OA including IL-1β, TNF, IL-6, IL-15, IL-17, IL18 and IL-21 (Kapoor et al., 2011). Of these factors IL-1β and TNF control degeneration of articular cartilage (Kapoor et al., 2011, Larsson et al., 2015). It has been shown that fragments of cartilage components in the synovial fluid can further stimulate inflammation induced degradation resulting in a positive feedback loop of degradation (Homandberg et al., 1998, Pulai et al., 2005, Fichter et al., 2006). Activation of chondrocytes occurs in OA and results in overproduction of both ECM components and ECM degrading enzymes (Goldring and Marcu, 2009). Inflammatory stimuli

can result in chondrocyte activation via NF-κB and MAPK pathways (Goldring and Marcu, 2009).

Proteins released from the synovium (S100 proteins (alarmins) and damage-associated molecular pattern (DAMP) molecules, cytokines IL-1β, TNFα, and IL-15, chemokines (CCL19, monocyte chemotactic protein-1 and monocyte inflammatory protein (MIP-1β), and complement components) can activate toll like receptors that are expressed on chondrocytes and are present in OA cartilage lesions and drive inflammation associated matrix degradation (Yammani et al., 2006, Zreiqat et al., 2010, Geurts et al., 2011, Loeser et al., 2012). IL-6 is one the most elevated cytokines associated with OA inflammation (Malemud, 2015, Watt et al., 2016). Elevated levels of matrix degrading enzymes in OA joint synovial fluid is stimulated by the activity of inflammatory cytokines, including IL-6, IL-1β and TNFα, causing increased cartilage ECM degradation (Struglics et al., 2006, Malemud and Schult, 2008).

This wide range of signalling pathways and inflammatory molecules demonstrate the complex and intricate network of mechanisms that can lead to cartilage destruction and OA pathogenesis and highlight the interconnection between surrounding tissues (e.g. inflammatory markers in synovial fluid) in OA pathology.

1.1.3.2 **Bone**

Bone is a key structural and functional tissue within the joint. Bone development, mechanotransduction, maintenance and remodelling are controlled directly or indirectly through the synergistic action of different bone cells. Osteoblasts are the primary cells involved in the deposition of bone matrix, differentiating from mesenchymal stem cells (MSCs) (Fung Ling Chau et al., 2009, Capulli et al., 2014, Kenkre and Bassett, 2018). Mature osteoblasts face three fates: Become osteocytes, bone lining cells or undergo apoptosis (Capulli et al., 2014). Osteocytes differentiate from mature osteoblasts that have become buried within the mineralized bone matrix they lay down (Sawa et al., 2019). Osteocytes allow communication through the bone matrix to superficial bone lining cells and internal bone marrow cells via their interconnected dendrites that extend through canaliculi

(Bonewald, 2011, Prideaux et al., 2016). Osteoclasts form from the differentiation of precursor macrophage/monocyte cells near the surface of bone and drive bone resorption (Khosla, 2001, Boyle et al., 2003). Osteoclast and osteoblast differentiation is controlled by the osteocytes that are, therefore, responsible for the regulation of bone remodelling (Kenkre and Bassett, 2018).

Through the action of the bone remodelling cycle, bone has the capacity to add or remove bone mass in response to hormonal and mechanical stimuli (Wolff, 1892, Bodine et al., 1996, Lee et al., 2002, Hajati et al., 2009). A range of signalling molecules and pathways are implicated in response of bone to external physiological and pathological stimuli including extracellular signal-regulated kinase-1/2 (ERK-1/2), Focal Adhesion kinase (FAK), Mitogen activated protein kinase (MAPK), G-prtein mediated signalling, wnt signalling, prostaglandin signalling, Nitric Oxide (NO) signalling, Adenosine Tri-Phosphate (ATP) signalling, RANKL/RANK/OPG and oestrogen signalling (Somjen et al., 1980, Pitsillides et al., 1995, Ralston et al., 1995, Udagawa et al., 2000, Aguirre et al., 2001, Bord et al., 2003, Rubin et al., 2003, Norvell et al., 2004, Chatzizacharias et al., 2008, Robling et al., 2008, Callewaert et al., 2010, Kwon et al., 2010, Wang et al., 2011, Rumney et al., 2012, Cabahug-Zuckerman et al., 2016, Yavropoulou and Yovos, 2016)

Subchondral bone has been shown to impact the homeostasis of articular cartilage (Stupina et al., 2015). It is linked to cartilage via an osteochondral interface that provides a graduated transition from hyaline cartilage to subchondral bone, thereby, increasing capacity to resist mechanical compression (Seo et al., 2014). The subchondral bone contributes to joint repair by recruitment of bone marrow stem cells to sites of cartilage damage. Multiple techniques such as microfracture, drilling and abrasion have been investigated with the aim of stimulating this response to induce a therapeutic effect (Insall, 1974, Rae and Noble, 1989, Aglietti et al., 1994).

Bone structure and metabolism is altered in OA development and contributes to disease progression. Dysregulation of bone remodelling leads to physical changes in bone structure in OA. This is characterised by thickening of the subchondral plate, intraosseous cyst and osteophyte formation, which can occur in varied locations across the joint (Beuf et al.,

2002). Increased bone volume and decreased mineral density has been identified in the trabecular bone of OA patients (Li and Aspden, 1997, Karvonen et al., 1998, Day et al., 2001). A study observing patients' knees, longitudinally following ACL rupture, identified significant increases in subchondral bone trabecular thickness and osteophyte formation 4 years after injury, but no subchondral cortical bone thickening or change in joint space width (Buckland-Wright et al., 2000). These findings indicate that bone microstructure is altered prior to the detection of any cartilage defects and may be an early marker of OA development following joint trauma.

As cartilage is avascular, subchondral bone plays a role in the supply of nutrients to maintain healthy cartilage. After three years, in a long term non-human primate study, allografts, where the osteochondral interface was blocked, demonstrated increased cartilage degradation vs allographs in which the osteochondral interface remained intact. This suggests a role for interaction between cartilage and bone being key in the maintenance of healthy cartilage (Malinin and Ouellette, 2000).

The changes observed in local bone microstructure in OA is stimulated by a range of biomechanical and inflammatory factors (some of which are described in more detail in Appendix Table 9.3). In OA pathogenesis, increased turnover of collagen type 1 has been linked with increased TGF-β signalling. Matrix degradation is increased due to the increased activity of MMP-2, and ALP levels are increased leading to altered mineralization (Bailey and Mansell, 1997, Mansell and Bailey, 1998). Increased ALP and OCN release has been identified at the cellular level in primary human OA osteoblasts compared to 'normal' human osteoblasts *in vitro* (Hilal et al., 1998). Osteoblasts isolated from human OA sclerotic (thickened) subchondral bone have been shown to produce increased levels of IL-6, IL-8, OCN, osteopontin, TGF-β1 and collagen type I as well as exhibiting increased ALP activity vs non-sclerotic bone (Sanchez et al., 2008). This demonstrates a link with inflammatory mediators in OA bone pathogenesis. Additionally, SOST expression (a wnt signalling inhibitor) has been shown to be decreased in subchondral bone osteocytes following surgically induced joint damage in a sheep OA model. Conversely SOST expression was increased in areas of cartilage damage in the same model (Chan et al., 2011).

RANKL/RANK/OPG signalling plays a key role in bone homeostasis and is also linked to chondrocyte function (Kwan Tat et al., 2009, Bellido et al., 2010). RANKL, expressed in subchondral osteoblasts, plays a role in osteoclast recruitment in OA, hence, leading to a resorptive state in early OA bone (Jones et al., 2002, Tat et al., 2008). High levels of OPG in both OA patient serum and synovial fluid have been correlated with disease severity in knee OA (Pilichou et al., 2008). OPG was also associated with hand OA development (Pantsulaia et al., 2010).

Subchondral bone changes have been correlated with pain in OA (McCrae et al., 1992). Subchondral bone, in addition to synovium, periosteum and ligaments, contains nerve endings indicating a role in pain associated with OA. The generation of sympathetic and sensory nerves is accompanied by angiogenesis at the osteochondral interface (Suri et al., 2007, Walsh et al., 2007). Systemic injection of angiogenesis inhibitor PPI-2458 in a meniscal transectomy rat model resulted in reduced pain behaviour, joint damage and synovial inflammation as well as reduced osteochondral and synovial angiogenesis (Ashraf et al., 2011). Inflammatory cytokines released in OA have been associated with pain hypersensitivity with TNFα, IL-1β and IL-6 having been shown to induce heat (*in vivo* rat skin model) and mechanical hypersensitivity (Opree and Kress, 2000). IL-1β has been shown to increase levels of nerve growth factor (NGF) and inflammatory induced hyperalgesia in a complete Freund's adjuvant intra-plantar injection rat model (Safieh-Garabedian et al., 1995). NGF is involved in sympathetic and sensory neurone development (Patel et al., 2000). Increased levels of NGF have been identified in the synovial fluid of patients with RA and OA (Aloe et al., 1992). NGF has been shown to activate and sensitise bone *in vivo* (Nencini et al., 2017). Glutamate exposure has been linked with joint pain in humans (Alstergren et al., 2010) and antagonism of glutamate receptors within the joint has been shown to alleviate the symptomos of OA including pain, inflammation and bone pathology (Bonnet et al., 2015, Bonnet et al., 2019, Bonnet et al., 2020). The role of glutamate signalling in OA and PTOA is further discussed in section 1.4.

These studies highlight the link between inflammatory mediator release and pain propagation and further indicate the interlinked network of altered tissue production, inflammation and pain in OA pathogenesis.

1.1.3.3 **Synovium**

The synoviocytes present in the synovium of joints are responsible for the production of synovial fluid components and produce molecules that play a role in maintaining joint surface integrity such as hyaluronic acid (HA) and lubricin (Hui et al., 2012). Synovial fluid provides lubrication and regulatory functions within the joint, for example lubricin protects the articular joint surface from deposition of pathological proteins and contributes to synovial cell homeostasis (Rhee et al., 2005). The synovium removes by-products of chondrocyte metabolism from the joint space as it is a semipermeable membrane allowing controlled molecular trafficking. As cartilage is avascular the synovium plays a role in nutrient supply to chondrocytes (Pap et al., 2020). Populations of mesenchymal stem cells are present within the synovium with capacity to differentiate into cartilage, bone and fat cells (Yang et al., 2011), leading to suggestions that a synovial stem cell niche contributes to joint tissue maintenance and repair (Fox and Warnock, 2011). Changes in synovium permeability and synovial fluid content have been identified in OA pathogenesis.

Synovitis contributes to OA pathology. Increased synovial fluid levels of IL-6 and TNF-α have also been associated with increased risk for patient progression to radiographically observable OA (Kapoor et al., 2011, Larsson et al., 2015). IL-6 levels are elevated immediately after joint injury further linking this cytokine to injury related OA (Watt et al., 2016). Cell surface IL-1 receptor type 1 is involved in mediating the activation of cells by pro-inflammatory cytokine IL-1β and has been shown in increased levels on OA synovial fibroblasts vs healthy cells (Sadouk et al., 1995). Additionally, glutamate levels have been shown to be upregulated in the synovial fluid of both RA and OA patients (McNearney et al., 2004) along with the expression of various glutamate receptor signalling components within the joint, which is discussed in more detail in section 1.4.

As previously mentioned (section 1.1.3.3), a range of proteins released from the synovium (alarmins, DAMPs, cytokines and chemokines) stimulate articular chondrocytes causing matrix destruction (Benito et al., 2005). Activation of transcription factors by a range of signalling pathways (NF-kB, runt related transcription factor 2, Elf-3, CCAAT/enhancer

binding protein, activator protein 1 and hypoxia inducible factor 2a) regulates the expression of inflammatory mediators and matrix degrading enzymes (Loeser et al., 2012). This range of inflammatory molecules and proteins, present in synovial fluid, contributes to OA pathogenesis.

In OA, the synovium becomes more permeable allowing infiltration of inflammatory cells such as T and B-lymphocytes (Lindblad and Hedfors, 1987, Revell et al., 1988). Synovial membrane pathology has been defined in 4 patterns: Hyperplastic, defined by synovial lining hyperplasia seen in early OA synovium specimens ; fibrotic, defined by capsular fibrosis, identified in late OA ; detritus-rich, defined by the presence of bone and cartilage debris identified in late OA; and inflammatory, characterised by lymphocyte infiltration and present in early and late stage OA independent of the presence of debris in the synovial fluid (Oehler et al., 2002). These pathological patterns highlight the diverse nature of synovial pathology. Altered synovial membrane permeability in OA also results in decreased levels of large proteins such as HA, identified by increased blood plasma serum HA levels (Goldberg et al., 1991). The presence of synovitis has been indicated as a marker for active cartilage breakdown in a clinical study on patients with post-traumatic patellofemoral chondropathy (Ayral et al., 1999).

The synovium is well innervated and likely to be a source of the pain identified in OA pathology (Dieppe and Lohmander, 2005). Synovial thickening in older OA patients has been associated with knee pain (Hill et al., 2001). An increased concentration of CRP has been identified within synovium and has been associated with increased levels of IL-6 in the synovial fluid and increased infiltration of inflammatory cells (Pearle et al., 2007). Serum CRP levels in knee and hip OA patients has been significantly associated with pain, joint tenderness and functional disability (Wolfe, 1997). Additionally, the severity of OA related pain, but not the extent of OA progression, has been associated with serum CRP levels in patients with hip and knee OA (Sturmer et al., 2004). Chronic synovitis, present in OA, results in changes to sensory neurone central connections resulting in central sensitisation to pain (Pezet et al., 2001, Niissalo et al., 2002). Inflammatory mediators (TNFα, IL-6 and IL-1β), present in the synovial fluid of OA sufferers, can influence hyperalgesia via directly stimulating nociceptive neurones or indirectly through increasing prostaglandin release

(Kidd et al., 2004). NGF plays a role in pain transmission and hyperalgesia. Synoviocytes express NGF receptor and IL-1β and TNF stimulate production of NGF by the synovium (Raychaudhuri and Raychaudhuri, 2009, Seidel et al., 2010). Neurotransmitter substance P is found in the synovium as well as in osteophytes and areas of cartilage erosion (Sutton et al., 2009). It has been found to influence synoviocyte proliferation and the production of collagenases and prostaglandin (Lotz et al., 1987). This indicates a direct role for the nervous system in the pathogenesis of arthritis via synovial cells.

1.1.3.4 Meniscus

The meniscus provides stability to the knee joint in conjunction with ligaments (Levy et al., 1982). Structurally, the menisci are fibrocartilaginous semi-circular wedges that help distribute compressive joint loads (Ishihara et al., 2009a). The menisci can be damaged following joint trauma, often in conjunction with ligamentous rupture (Metcalf and Barrett, 2004). Meniscal damage is a risk factor for developing OA when left untreated (Englund et al., 2009) and following surgical intervention in the form of a meniscectomy to remove damaged tissue (Roos et al., 1998, Englund et al., 2003). Acute levels of inflammation have been observed in patients following meniscal trauma (Englund et al., 2009) and synovial inflammation was observed in a high proportion of patients (43%) at the time of meniscectomy, 15 weeks after traumatic joint injury (Scanzello et al., 2011). When comparing degenerative menisci vs intact menisci in late stage OA patients, upregulation of inflammatory and catabolic associated genes, such as ADAMTS-5, fibroblast growth factor-7 (FGF-7) and PGE synthase, was identified in the degenerative menisci (Sun et al., 2010). In addition to increased inflammation, meniscal damage and subsequent resection results in altered joint gait mechanics due to a loss of structural support (Allaire et al., 2008, Netravali et al., 2010). Also, the inflammation associated with joint injury has been associated with joint pain (Berenbaum, 2013) that in-turn is associated with modification of gait (Henriksen et al., 2010, Boyer et al., 2012). Altered joint loading through a change in gait due to pain or altered joint structure following surgery can increase medial cartilage loading (Yang et al., 2010). Altered cartilage loading because of altered gait mechanics can result in an increased risk of cartilage breakdown leading to increased inflammation and joint pain (Henriksen et al., 2010, Attur et al., 2011, Andriacchi et al., 2015). The structural changes and

inflammatory response following damage show that meniscus function is another factor in the pathogenesis of OA.

1.1.3.5 Ligamentous Tissue

The ligaments of joints help maintain joint stability and assist in normal joint motion (Bendjaballah et al., 1997). Injuries to the ACL of the knee occur most frequently in individuals with high levels of physical activity (Beynnon et al., 2005) and often coincide with damage to other tissue such as the meniscus (Lohmander et al., 2007). As many patients with acute ACL damage are young (<30 years old), injuries to this ligament are a major risk factor in the development of early onset OA symptoms such as pain, inflammation and decreased joint function (Lohmander et al., 2004, von Porat et al., 2004). With reported rates of OA, 10 to 20 years following ACL injury, ranging widely from 10% to 90% (Lohmander and Roos, 1994, Gillquist and Messner, 1999, Myklebust and Bahr, 2005), the range in OA prevalence following ligament (ACL) damage highlights the complex nature of disease pathogenesis. This may be associated with the fact that ACL injuries often coincide with damage to other joint tissue such as meniscal tears, damage to other ligaments, bone bruises, articular cartilage injury and fractures to intra-articular bone (Beynnon et al., 2005). Increased levels of inflammatory cytokines, glutamate, matrix fragments and proteases have all been identified in the synovial fluid of patients following joint injuries involving ligament damage (Lohmander et al., 1993, Lohmander et al., 1994, Lohmander et al., 2003, Nelson et al., 2006, Bonnet et al., 2020). These consequences highlight the function of ligamentous tissue on the maintenance of joint stability and, following injury, the propagation of inflammatory and degradative pathways in other joint tissue (cartilage, meniscus) that contribute to OA pathogenesis in young patients.

1.1.4 Post Traumatic Osteoarthritis

Individuals who develop OA following an injury represent a substantial proportion of OA sufferers (12% of all lower limb OA) and those that suffer a joint injury have a much higher chance of developing OA (Anderson et al., 2011). Additionally, PTOA can manifest in individuals at a younger age following joint injury (Kuijt et al., 2012). There are currently no

disease modifying therapeutics approved for the treatment of OA and there are challenges with treating developed OA due to the lack of concordance of disease symptoms (pain) with diagnostic tests (x-ray analysis of degradation) and the complex chronic multi-tissue development of the condition. The point at which pathological joint degeneration begins can be traced back to the time of injury in PTOA. This provides the potential to optimise the timing of therapeutic intervention and introduce preventative measures to reduce the risk of developing OA. Research into PTOA mechanisms is key in improving our understanding of OA and in the development of optimised and novel therapeutics.

Figure 1.3 depicts the short and long term catabolic and anabolic response to injury within joint tissue (Anderson et al., 2011). An initial acute catabolic phase follows joint injury and is characterised by the release of cytokines (IL-1, IL-6, IL-8 and TNF), MMPs (MMP-1, -3, -8, -9, -13, ADAMTS), raised levels of reactive oxygen species, chondrocyte death, recruitment of inflammatory cells and immediate glycosaminoglycan loss caused by collagen rupture (Punzi et al., 2016). The acute phase is followed by an intermediate phase where the catabolic processes of the acute phase are balanced by anabolic processes that then leads into a predominantly anabolic phase resulting in the potential for tissue repair (Anderson et al., 2011).

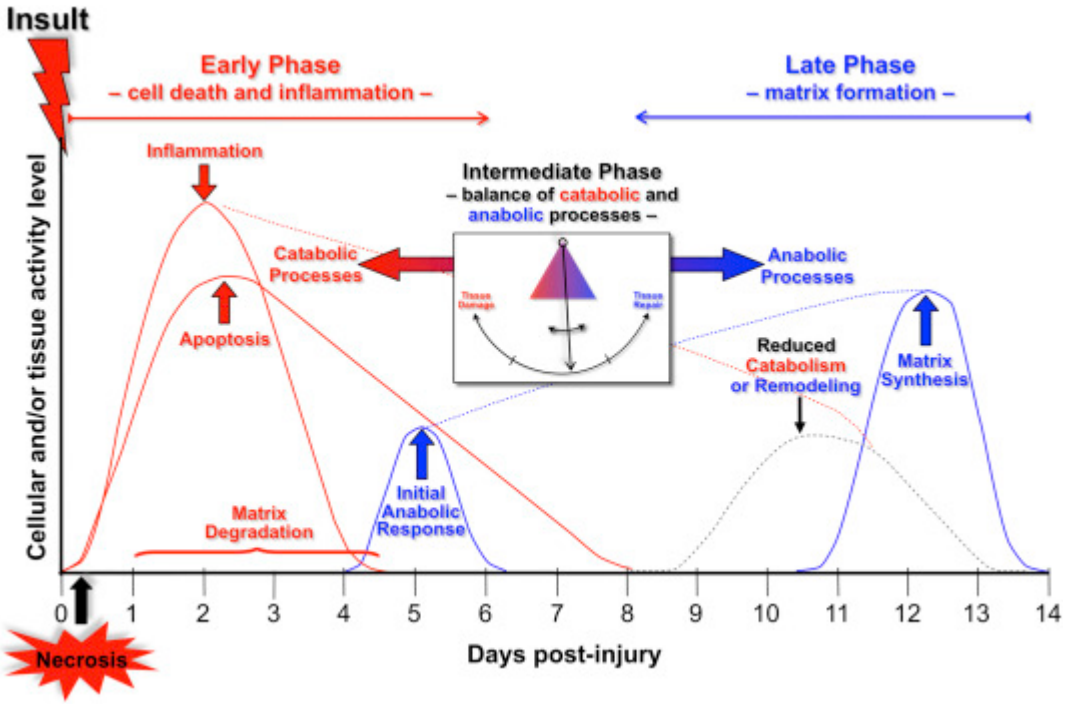

Figure 1.3: Diagrammatic representation of the overlap of cellular catabolic and anabolic responses to joint trauma from Anderson et al., 2011. (Permission to use this figure in this thesis granted).

This information can be utilised to tailor the timing of therapeutic intervention, the longevity of sustained drug release and the nature of the therapeutic employed to minimise the degradative imbalance created by traumatic joint injury.

1.2 Current OA Treatments

Joint degradation in OA affects multiple tissue types (articular cartilage, subchondral bone, synovium, surrounding ligaments) resulting in pain, inflammation and swelling of affected joints. Many of the physiotherapy, weight management and exercise interventions are effective non-pharmaceutical methods for managing the symptoms of OA (McAlindon et al., 2014).

1.2.1 Pharmacological Therapies

Pharmaceutical intervention is limited to management of OA symptoms and can improve the quality of life in the short term. However, this does not address the underlying pathology. The majority are targeted towards reducing arthritic pain and inflammation. However, long term usage is associated with increased risk of heart and renal damage as well as GI tract complications associated with oral administration (Hunter et al., 2011, Lanas et al., 2011). Analgesics such as paracetamol are often the first line of treatment for arthritic pain. However, a systematic review of paracetamols usage to treat OA has indicated that it has only minimal short term benefit, throwing its universal usage into question (Machado et al., 2015). Opioid analgesics are strong pain killers effective at treating chronic pain. However, side effects such as nausea and constipation, can reduce patient compliance to treatment (Furlan et al., 2006) and opioid abuse and dependence represent a severe health and socioeconomic burden to society. A 2013 study estimated the US economic burden of opioid abuse as $78.5 billion (Florence et al., 2016). Between 2005 and 2015 a 22.3% increase in global opioid use related disability adjusted life years was identified (Kassebaum et al., 2016) highlighting a growing global problem with opioid abuse and dependence (Rosner et al., 2019).

Steroid therapy is administered via IA injection for OA pain relief and anti-inflammation. Current findings suggest that evidence of the symptomatic relief and treatment efficacy is limited and, at best, that steroid injection to treat OA is a short-term treatment to a chronic problem (Bannuru et al., 2009, Hepper et al., 2009). IA injection is associated with increased risk of infection (Cancienne et al., 2015, Werner et al., 2016). Some evidence is coming to light that IA steroid injections can have a destructive effect on joint tissue (McAlindon et al., 2017, Tiwari et al., 2018, Kompel et al., 2019, Bonnet et al., 2020). Overall, the wide usage of IA corticosteroid injections to treat OA, as recommended by the National Institute for Health and Care Excellence (NICE), has little support in the literature for long term efficacy (Orchard, 2020). Appendix Table 9.4 provides a detailed insight into the main pharmaceutical options currently used clinically as treatments for OA.

1.2.2 Surgical Intervention

Despite a range of approved therapeutics for the treatment of OA symptoms, each comes with associated side effects and there are currently no approved 'disease modifying' pharmaceuticals for the treatment of the underlying degenerative condition (Philp et al., 2017). Ultimately, surgical intervention is the only treatment to restore joint function and reduce pain (Figure 1.4) (Bergschmidt et al., 2011, De l'Escalopier et al., 2016). Certain surgical procedures such as total hip replacements (THRs) have a more than 95% success rate and allow patients to have a pain free joint after only a few days (Learmonth et al., 2007). For late-stage knee OA a TKR can be performed (Figure 1.4) (Bergschmidt et al., 2011, De l'Escalopier et al., 2016).

Despite improvements in pain scores with TKR (Skou et al., 2015), pain and stiffness often remain after surgery resulting in a reduced likelihood of returning to full joint function and a need for long term rehabilitation (Parvizi et al., 2014). Up to 30% of patients have reported experiencing chronic pain in the months and years post TKR (Burns et al., 2015).

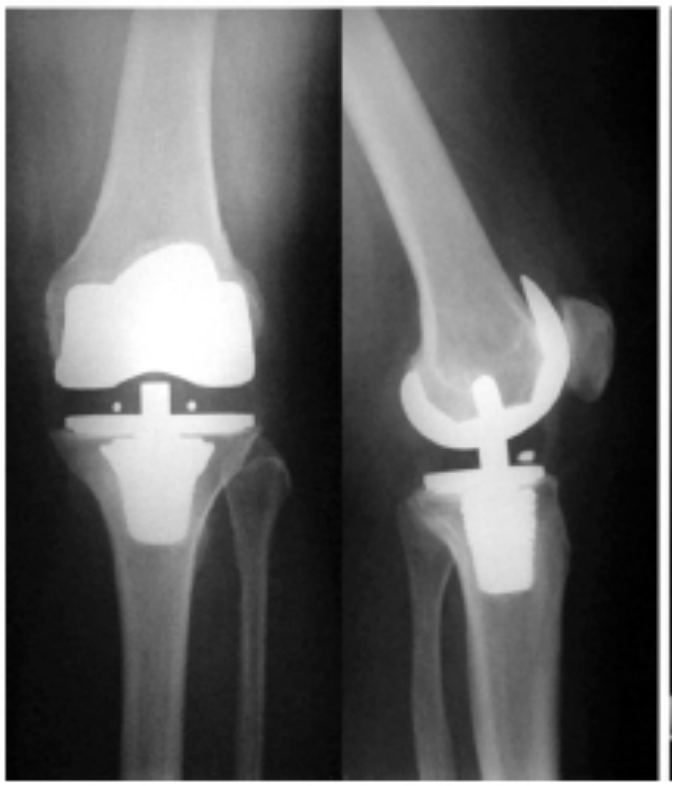

Figure 1.4: A radiograph of a TKR taken anterior-posterior and laterally of a TKR 25 months after implantation (73 year old female patient). Image taken and cropped from figure 2 of Bergschmidt et al., 2011 (http://creativecommons.org/licenses/by-nc/3.0/). Permission granted for use of this figure in this thesis

Although surgical intervention often improves the symptoms of OA, there are inherent risks of post-surgical infection (Kapadia et al., 2016). Both age and obesity are major risk factors for OA development. However, these two factors also impact the incidence of post-operative complications and morbidity from joint replacement surgery (Belmont Jr et al., 2014). Increased life expectancy coupled with a decrease in the average age of a primary joint replacing surgery mean that repeat surgeries to replace worn out implants are more regularly needed, placing increased risk to patients due to multiple surgeries required on aging patients (Weinstein et al., 2013). This represents a particular problem to individuals needing joint replacement surgery due to early onset OA, such as PTOA, as multiple replacement surgeries, constituting progressively increased risk, may be required due to the limited lifespan of artificial joints (Ghalme et al., 2016). A therapeutic that could target the pathology of OA while treating the symptoms would be more beneficial to patients than current symptom managing drugs, while reducing the need for invasive joint surgery.

1.2.3 New and Disease Modifying Treatments

In addition to established pharmacological, non-pharmacological and surgical therapeutic interventions, novel treatment pathways and strategies are being investigated. Colchicine and hydroxychloroquine have both been investigated as novel pharmaceutical interventions in the treatment of OA. Small clinical trials demonstrated some efficacy in the treatment of knee OA using Colchicine (Das et al., 2002) and hydroxychloroquine (Bryant et al., 1995). However, more recent double blind placebo controlled studies indicated that no significant improvement in pain scores occurred as a result of treatment with both Colchicine (Leung et al., 2018) and hydroxychloroquine (Kingsbury et al., 2018).

TNF inhibitors have shown efficacy as therapeutic agents in the treatment of RA (Rubbert-Roth and Finckh, 2009). However, a clinical trial observing the effect of 40mg subcutaneous administration of TNF inhibitor adalimumab every other week for 12 weeks compared with a placebo in the treatment of hand OA did not detect any improvement in joint pain, synovitis or bone marrow lesions (Aitken et al., 2018). In a 1-year double blind placebo controlled randomised study of patients with symptomatic hand OA, TNF inhibitor etanercept, administered at 50mg weekly did not deliver a significant improvement in pain scores at 24 weeks or synovitis after 1 year. However, a significant reduction in MRI detected bone marrow lesions was observed after 1 year in a small subgroup of patients (Kloppenburg et al., 2018).

Due to the lack of long term efficacy of IA corticosteroid injections (Arroll and Goodyear-Smith, 2004), sustained release formulations have been investigated to determine if they deliver an extended therapeutic benefit. Triamcinolone acetonide microsphere extended-release formulation FX006 was shown to have significant improvement in pain intensity scores over 5-10 weeks compared to immediate release triamcinolone in a phase IIa randomised, double blind controlled trial (Bodick et al., 2015). In a phase IIb study, FX006 did not deliver a significant improvement on daily life pain compared to a placebo at 12 weeks but did show a significant improvement at weeks 1-11 and 13 weeks (Conaghan et al., 2018b). In a phase III multicentre double-blind randomized control trial, a single IA injection of FX006 (32mg) was found to deliver a significant improvement to WOMAC pain,

physical function, stiffness scores and knee injury and OA outcome quality of life (KOOS-QoL) scores at 12 weeks compared to immediate release triamcinolone and a placebo. These studies have contributed to FX006 being licenced by the US FDA for use in the treatment of OA-knee pain and highlight the potential of extended-release formulations in maximising the therapeutic benefit of pharmacological interventions (Conaghan et al., 2018c).

Bone is a significant contributor to OA pathology. Use of bisphosphonates to modulate bone turnover have been investigated in the treatment of OA. A double-blind placebo-controlled trial on patients with magnetic resonance imaging (MRI) identified bone marrow lesions and knee pain demonstrated that treatment with a single 5mg/100ml infusion of zoledronic acid significantly improved pain scores (visual analogue scale) and reduced bone marrow lesions but did not affect joint function scores (KOOS) at 6 months (Laslett et al., 2012). However, in a longer term study of an annual 5mg zoledronic acid treatment for knee pain and bone marrow legions, no significant effect on bone marrow legions, pain or function (WOMAC) was identified at 24 months (Cai et al., 2018).

Treatment of arthritic pain using capsaicin (CNTX-4975) to target TRPV1-pain receptors has demonstrated some efficacy with a single IA dose of 1mg CNTX-4975. This delivered significant improvements to WOMAC pain scores at 12 and 24 weeks compared to a placebo in a double blind, randomised study (Stevens et al., 2017). Anti-NGF therapeutics have been developed to target OA pain. A phase III trial using subcutaneous administration of anti-NGF monoclonal antibody Tanezumab demonstrated that 2.5mg of treatment improved pain and function (WOMAC) and patient global assessment scores compared to a placebo at 16 weeks. This was further improved by increasing dosage at 8 weeks to 5mg (Stevens et al., 2017).

As OA is a degenerative condition, development of disease modifying OA drugs (DMOADs) to address tissue changes (e.g. cartilage loss and subchondral bone lesions) and to treat disease progression have been investigated. Recombinant fibroblast growth factor 18 (sprifermin) has been shown to stimulate cartilage growth in a rat meniscal damage model of injury induced OA (Moore et al., 2005). Patients given two cycles of weekly IA injections

of sprifermin (weeks 0-2 and 13-15) at doses of 10, 30 or 100μg demonstrated significant reductions of MRI, identified overall femorotibial cartilage loss and lateral femorotibial cartilage loss as well as a reduction in the loss of lateral joint space width after 12 months. However, this study did not identify significant cartilage reduction in the medial femorotibial compartment, which was the primary efficacy endpoint (Lohmander et al., 2014). In a long term (5 year) phase two randomized placebo-controlled trial, reduction in mean cartilage thickness in 100μg sprifermin treated patients compared to a placebo was significantly decreased in medial, lateral, central medial and central lateral regions over 3 years. However, this modulation of joint structural degradation did not manifest as a significant difference in OA symptoms between treatment and placebo groups (Hochberg et al., 2018).

Wnt signalling plays a role in cartilage turnover and OA pathogenesis through modulation of osteoblasts and chondrocytes (Deshmukh et al., 2018). SM04690 is a small molecule inhibitor of the wnt signalling pathway. In a phase II randomized double-blind placebo-controlled trial, 0.07mg of SM04690 significantly improved pain on walking scores (WOMAC A1) compared to a placebo at 39 and 52 weeks in unilateral symptomatic knee OA patients and improved at 26, 39 and 52 weeks in symptomatic knee OA patients. However, no significant effect to patient pain on walking was observed in the intention to treat population (Kennedy et al., 2018).

MIV-711 is a selective reversible inhibitor of cathepsin K, a cysteine protease linked with bone resorption and degradation of key cartilage matrix proteins (aggrecan and collagen type I and II) (Ghouri and Conaghan, 2019). In a 6-month placebo controlled randomised multicentre phase IIa trial on patients with knee OA, MIV-711 administered 4 times daily for 26 weeks at 100 and 200mg, significant reduction in cartilage loss on the medial femur was observed in the 100mg treatment group compared to placebo. Additionally, both MIV-711 concentrations used demonstrated a significant reduction in MRI quantified bone disease progression at 26 weeks compared to placebo. However, no significant reductions in pain or QoL scores were found in this trial (Conaghan et al., 2018a).

IL-1 is a key inflammatory cytokine involved in OA pathogenesis and the blockade of its receptor has been shown to modulate OA pathogenesis in dog ACL trauma models (Caron et

al., 1996, Pelletier et al., 1997), equine osteochondral fragment induced OA (Frisbie et al., 2002), rabbit meniscectomy model (Fernandes et al., 1999) and a mouse articular fracture model (Furman et al., 2014). These promising *in vivo* findings have been followed by clinical trials. A single IA injection of IL1-Receptor antagonist significantly improved mean pain score by 9.2 (KOOS scoring; p=0.0011) and mean QoL score by 18.4 (p=0.0048), over two weeks, for individuals suffering from an acute anterior cruciate ligament (ACL) knee injury and when administered within a month of injury compared to placebo controls (Kraus et al., 2012). A recombinant IL-1Ra, called anakinra, did not show any significant difference in WOMAC pain scores from placebo after 4 weeks in a randomised multicentre double-blind study (Chevalier et al., 2009). Additionally, in a phase II trial, 100mg lutikizumab, which inhibits the action of IL-1α and IL-1β, was shown to deliver a significant improvement in WOMAC pain scores at 16 weeks following bi-weekly subcutaneous injections in patients with knee OA. However, other lutikizumab concentrations used in this study (25 and 200mg) did not deliver any therapeutic benefit and no significant structural changes were observed compared to a placebo indicating that lutikizumab had limited disease modifying capacity in this trial (Kavanaugh et al., 2018). One clinical trial investigated the effects of a 3 monthly subcutaneous delivery of IL-1β monoclonal antibody canakinumab to treat patients with previous myocardial infarction and $\geq$2mg/l serum CRP. A 150mg dose of canakinumab was associated with a reduced reoccurrence of cardiovascular events compared to a placebo (Ridker et al., 2017). A sub-study from this trial identified reduced knee and hip replacements as well as decreased OA symptoms and OA related adverse events in patients treated with canakinumab compared to placebo (Schieker et al., 2018). A systematic review of autologous IL-1Ra blood-derived products concluded that there is some limited evidence that IA injection therapy could improve pain and functionality in knee OA with few adverse events (Ajrawat et al., 2019). Despite promising animal study findings, there is limited evidence from clinical trials that IL-1Ra can act as a novel DMOAD treating both symptoms and structure degradation associated with OA.

1.2.4 Current Unmet Needs

OA has a complex pathology affecting multiple tissue types via a range of pathways linked to pain, inflammation and degradation. Systematic reviews have shown a disparity between radiographically observable OA and the severity of symptoms (Bedson and Croft, 2008, Kinds et al., 2011). These highlights both the challenge in diagnosis but also the complex relationship between physical degeneration and symptom manifestation in OA sufferers. Delivering effective therapeutic intervention is, therefore, equally complex. Non-pharmaceutical approaches such as weight management, exercise and physiotherapy can manage symptoms but cannot prevent disease progression (McAlindon et al., 2014). Surgical intervention can drastically improve quality of life for some procedures, such as total hip replacement (Learmonth et al., 2007), but in the case of total knee replacement, 20% of patients are still in pain following surgery (Hofmann et al., 2011). Additionally, in the case of PTOA sufferers, who may develop OA at a younger age following joint injury, further revision surgery is more likely as implants only have a limited lifetime (Beard et al., 2019).

A gold standard therapy would be a DMOAD that also delivered symptomatic relief. Current approved pharmaceutical interventions for OA fall short of this standard. Commonly used corticosteroids have been shown to deliver only short-term benefit to OA symptoms (Bannuru et al., 2009, Hepper et al., 2009). Utilisation of sustained delivery vehicles has been shown to improve the therapeutic benefit of corticosteroids (Bodick et al., 2015). This demonstrates that the use of sustained release delivery may improve therapeutic potential of currently available OA drugs and that sustained delivery is key in the treatment of a chronic long-term conditions such as OA. Novel therapies described in section 1.2.3., such as: TNF inhibitors (etanercept), IL-1Ra (lutikizumab, canakinumab and anakinra), cathepsin K inhibitors (MIV-711), anti-NGF (Tanezumab) and recombinant FGF-18 (sprifermin), show some promise in managing either symptoms of OA such as pain and joint function or reducing cartilage degradation and bone marrow lesion formation. However, there is no therapeutic approved for use in humans or in clinical trials that has been shown to reduce the structural progression of OA and deliver symptom modifying relief. A therapy that delivers no significant symptomatic relief to the patient, despite modifying the joint structural degradation, is unlikely to achieve good patient compliance. As OA is now defined as a serious disease (Osteoarthritis Research Society International, 2016) development of a

DMOAD with capacity to manage OA symptoms as well as reduce or prevent disease progression is crucial to plug an unmet need in OA therapeutics.

OA represents a challenge to the design of clinical studies, the duration of a trial must take into consideration the biological mechanism under investigation and the outcome measure being quantified, which, for a slow developing chronic condition like OA, can lead to extended trial duration. OA has a complex multi-tissue pathology. Therefore, factors such as selection of study populations taking into account co-morbidities, origin of OA, and any pain or structural sub-phenotypes are important (McAlindon et al., 2015). A lack of correlation between patient reported symptoms and radiographically identifiable joint degeneration (Arden and Nevitt, 2006) highlights the importance and complexity in the selection of both pain and structural outcome measures and patient reported outcomes and physical performance measures (McAlindon et al., 2015). OA development following joint trauma (PTOA) represents a major sub-population within the overall OA cohort (Lohmander et al., 2007). Clinical trial design to investigate preventative interventions for PTOA has been addressed by Watt et al. (2019). PTOA provides a window for preventative OA therapeutics, however, clinical trials would be long term and there are no recommendations for how to measure the preventative effect of interventions in OA following injury (Emery et al., 2015). Watt et al. (2019) reviewed 37 studies of acute knee injury intervention and developed recommendations for patient eligibility criteria that takes into consideration the definition of acute knee injury, time since injury and age of patient to minimise the risk of already having developed OA. This study also addressed outcome measures with recommended timelines for: general outcome measure data collection; use of patient reported outcomes and functional outcomes; use of imaging techniques such as x-ray and MRI; assessment of biomarkers as exploratory outcome measures and collection of biomarkers (particularly synovial fluid) for identification of molecular changes following injury. Recommendations were provided for the timing of intervention and the selection of comparators. Finally, specific challenges and research questions were highlighted for further investigation including further work to define injury type populations for studies, optimal timeframe for intervention and identification of predictive biomarkers for OA development. Further use of pre-clinical animal models to support translation of interventions into clinical trials was recommended as well as obtaining patient and public involvement to assess study design

feasibility. In terms of outcomes, longer term trials were recommended to developed improved understanding of joint trauma history, biomarkers, relationship between early and late outcome scores and the relationship between patient reported outcomes and biomarker/imaging outcomes. Additionally, investigation into the best patient reported outcome measure to use in further PTOA trials was recommended (Watt et al., 2019).

This study addresses the complexity and difficulty in clinical trial design for preventing PTOA and delivers conclusions on study conduct with recommendations for further investigation highlighting PTOA as a target for future therapeutic intervention taking into consideration: timing of intervention; biomarker tracking; length of trial; and assessment of outcomes. Repurposing of therapeutics to target specific pathways may be a new avenue to explore in the treatment of PTOA.

1.3 Models for Investigation of Joint Pathologies

1.3.1 Overview

PTOA represents a unique therapeutic opportunity for OA treatment, as the event of OA initiation can be tracked from the point of Injury and treatment options tailored accordingly. This has beneficial implications for OA patients who have experienced joint injury such as ACL injuries, meniscal damage and ankle sprains. The development and application of both animal *in vivo* models and primary or cell line *in vitro* models that accurately represent clinical OA, PTOA or joint inflammation is essential to provide a platform for the early-stage investigation of potential arthritis therapeutics. OA has complex pathologies so there is little consensus on the most representative model for the human manifestation of the disease. However, the more closely a model represents the clinical OA phenotype the better the chance that *in vitro, ex vivo* and *in vivo* drug investigations will manifest in a clinically viable product and provide therapeutic benefit to millions of arthritis sufferers worldwide.

1.3.1.1 In Vitro OA Models

1.3.1.1.1 2D Cell Culture

2D cell culture allows for a large number of cells to be investigated that have been cultured, in easily controlled conditions, from a single primary or cell line source. However, the controlled and isolated nature of monolayer cell culture conditions removes the potential systemic influences that would apply *in vivo* and cells grow on a flat surface which does not represent the 3D environment found *in vivo* (Edmondson et al., 2014). Joint cells such as chondrocytes rely on contact with their extracellular environment to function (Johnson et al., 2016). Therefore, culture conditions that ensure cells are cultured as close to their *in vivo* function as possible are key to delivering a useful monolayer cell culture model. Chondrocyte monolayers have been utilised to study the impact of inflammatory cytokines (IL-1α, IL-6 and IL-8) present in OA on cells (Novakofski et al., 2012, Sylvester et al., 2012). Cytokine treatment (IL-6) and mechanical stimulation of osteocyte cell line monolayers has been investigated (Bakker et al., 2014).

The *in vivo* joint environment relies on crosstalk between multiple tissue types to function and dysregulation of this communication can occur in OA. Cell co-culture systems allow for modelling of cell-cell interactions key to joint tissue function (Hendriks et al., 2007). However, as with monolayer culture of single cell types, the 2D environment *in vitro* is not representative of the 3D *in vivo* environment that cells naturally reside within. Often cells will require differing cell culture media. This means that a compromise in conditions must be reached that could compromise cellular physiology. Monolayer cell culture provides a controlled environment but differences in systemic influence, 3D environment and culture conditions may limit alignment with *in vivo* functionality of cells.

1.3.1.1.2 3D Cell Culture

3D cell culture allows for closer mimicry of the 3D *in vivo* environment and matrix interactions in which cells reside. 3D conditions can also be adapted to provide structural support to mechanosensitive cells that is key to modelling load responsive joint tissue (Cope et al., 2019). However, the physical and biological properties of the 3D scaffold utilised may

not accurately reflect the 3D extracellular matrix *in vivo*. 3D cell culture models have been utilised to study mechanical loading of bone cells (Vazquez et al., 2014), mechanically stimulated (hydro-static, osmotic pressure and dynamic compression) chondrocytes (Mizuno and Ogawa, 2011, Bougault et al., 2012, Pingguan-Murphy and Nawi, 2012), osteogenic potential of bone marrow stem cells (Di Maggio et al., 2011), the chondrogenic potential of pellet cultured synoviocytes (Bilgen et al., 2007) and inflammatory treatment (TNFα) of joint capsule myofibroblasts (Mattyasovszky et al., 2010). Multiple 3D co-culture models have been employed to investigate joint cell interactions including: bone cell interactions following mechanical loading (Vazquez et al., 2014) and cytokine (IL-6) treatment (Wu et al., 2017); an osteoblast-chondrocyte co-culture to analyse the effect of mechanical loading on co-culture cell-cell interactions (Lin et al., 2010); and a synoviocyte and chondrocyte co-culture model developed to help improve understanding of synovium-cartilage interactions in OA (Blasioli et al., 2014).

Mesenchymal stem cells (MSCs) represent a useful tool for application in musculoskeletal *in vitro* models due to their capacity to differentiate into multiple different lineages (Wang et al., 2014). Y201 MSCs are an immortalised human stem cell population that has demonstrated osteogenic, chondrogenic and adipogenic differentiation potential while maintaining mechanoresponsive behaviour, making them an ideal cell line for the development co-culture *in vitro* human 'osteo-chondral' models (James et al., 2015, Galarza Torre et al., 2018). Mason et al (2018) adapted their 3D bone loading model (Vazquez et al., 2014) to use Y201 MSCs subjected to osteogenic and chondrogenic differentiation in 3D collagen type I gels (for osteogenic) and agarose gels (for chondrogenic). This model included interactions between these different cell populations in 3D culture to investigate the impact of mechanical loading onto osteogenically differentiated cells (Mason et al., 2018). Models such as this aim to more closely represent the *in vivo* OA to provide effective tools for therapeutic development.

1.3.1.2 Ex Vivo (explant) OA Models

Utilisation of tissue explant models allows for study of the natural extracellular structure of joint tissue with cellular physiological processes remaining intact (Zien et al., 2001). However, cell death often occurs at the edge of tissue explants and in relatively acellular tissue, such as cartilage, only a limited number of cells can be extracted for analysis (eg qRT-PCR). Due to the fact that tissue explants are taken from patient or animal tissue, samples may have limited availability and there is natural variability between explants due to the variance in mechanical forces at different locations on the joint especially in a pathologically complex condition such as OA (Johnson et al., 2016). Regarding human samples, obtaining healthy tissue explants for accurate control is restricted. Explant models have been used to study various processes within the joint, such as: the impact of mechanical loading on cartilage (human and bovine) (Fitzgerald et al., 2004, Bush et al., 2005, Jeffrey and Aspden, 2006); the effect of inflammatory stimulus on a human osteochondral explant model (Geurts et al., 2018); the impact of loading on cartilage and bone explants (Thibault et al., 2002); mechanobiological investigations using a bovine bone explant model seeded with osteoblasts (Chan et al., 2009); and the effect of synovium and cartilage interaction on cartilage ECM component production (Beekhuizen et al., 2011).

1.3.1.3 In Vivo OA Models

Modelling OA using different *in vivo* animal models is well established and multiple different animal models have been developed to aid investigation into different aspects of the disease without the limitations of compromised culture conditions (e.g. 3D structure, culture media) and a lack of systemic influence and altered cellular viability that can be present when using *in vitro* and *ex vivo* models (Cope et al., 2019). Use of animal models allows for assessment of a consistent OA phenotype and collection of tissue samples for analysis while controlling for the time of OA induction and tracking of disease progression (Lampropoulou-Adamidou et al., 2014). OA develops slowly over the course of many years in humans, animal models exhibit a wide range of OA development times. Depending on the animal used, drug dosage may vary in animal models compared to that used in humans. Genetic differences between animal models and humans as well as anatomical and mechanical differences within joints mean that *in vivo* model findings do not always translate to identification of a clinically viable outcome for humans (Lampropoulou-

Adamidou et al., 2014). However, utilising *in vivo* models to improve understanding of the complex mechanisms and pathological processes that take place in the joint and in OA aids the development of viable therapeutic interventions (Le Graverand-Gastineau, 2009, Mina-Osorio, 2015). Multiple animal models have been developed including mouse, rat, hamster, guinea pig, cat, rabbit, canine, caprine, ovine, equine, zebrafish, porcine, bovine and non-human primate (Cope et al., 2019). These have been employed to: improve understanding of OA mechanics and molecular biology; provide evidence of therapeutic outcomes for pre-clinical trials; assess novel therapeutic toxicity; and assess arthritis symptoms. Different models have been developed to investigate OA pathology from a range of initiating stimuli.

1.3.1.3.1 Spontaneous Models

Some animal models develop OA spontaneously such as guinea pig (Bendele and Hulman, 1991), STR/ORT Mice (Walton, 1977), rabbit (Arzi et al., 2012), dog (McDevitt and Muir, 1976, Moreau et al., 2014) and horses (Olive et al., 2009). These models can be used to provide a more accurate comparison to human degenerative OA as no intervention is required to induce OA pathology. These models can also be used to study mechanically or chemically induced OA allowing for comparison between traumatic/induced OA and spontaneous OA (Bendele, 1987, Little and Hunter, 2013). The major drawback of spontaneous models is the extended time for arthritis to develop, this extended time has associated costs for animal housing and maintenance but does more closely represent the slow pathogenesis of spontaneous OA in humans (Kuyinu et al., 2016).

In addition to naturally occurring spontaneous OA models, genetically modified animals can be used to breed strains susceptible to OA development. They can be used to investigate protective or contributing genes, thereby, aiding an understanding of the molecular basis of OA. Genetically modified mouse models have been commonly used to assess the impacts of knocking out a range of genes including those related to bone signalling (Matsui et al., 2009), matrix degradation (Majumdar et al., 2007), inflammation (Clements et al., 2003), matrix components (Kamekura et al., 2006) and transcription factors (Kamekura et al., 2006). OA is a multi-tissue condition with a complex pathogenesis. Therefore, the use of

genetic models to target one gene may be too reductive to produce a translatable clinical outcome (McCoy, 2015).

1.3.1.3.2 Surgical Models

Surgical models cause rapid OA development and allow for the induction of OA through reproducible trauma to the joint space (e.g. via meniscectomy). These models are most commonly used but have limitations as they are not representative of the pathogenesis of degenerative OA without traumatic origin (Lampropoulou-Adamidou et al., 2014) and have an associated increased risk of infection compared with less invasive models. Surgical models involve ACL transection (ACLT) and meniscectomy (MNX) where removal or transection of ligaments or meniscus destabilises the joint resulting in arthritis development in a range of animals, including: rat (Pickarski et al., 2011), mice (Lorenz and Grässel, 2014), dog (Berjon et al., 1991, Frost-Christensen et al., 2008) and rabbit (Batiste et al., 2004). ACLT cartilage lesions have been shown to develop more slowly than in MNX models allowing for a potentially more accurate representation of traumatic OA (Piskin et al., 2007). Surgical induction of a cartilage defect termed the 'articular groove' model has been applied to a range of animals including rats, dogs, sheep, pigs and horses (Ahern et al., 2009). A chondral defect dog model was shown to induce an OA phenotype after 3 weeks with low synovial inflammation and lower pain than ACLT models allowing for investigation into an OA phenotype with potential relevance to human OA (Frost-Christensen et al., 2008). A long-term dog model has been developed that allows for the investigation into the contribution of bone trauma alone to OA pathogenesis and said impact trauma has to surrounding cartilage (Mrosek et al., 2006). Surgical fracture models have been developed for investigation into the healing response of bone (Bonnarens and Einhorn, 1984). This includes sub-chondral drilling, where a several holes are drilled into the subchondral bone to elicit bone marrow stimulated cartilage repair via the release of stem cells and growth factors into the defect space (Orth et al., 2013). A rabbit drill hole defect model demonstrates chondrogenesis and bone repair originating from MSCs released from a full thickness drill defect. However, long term assessment (12-48 weeks) demonstrated progressive degeneration of the repaired cartilage, indicating newly synthesised cartilage failed to integrate with the healthy cartilage (Shapiro et al., 1993). A rat defect model

indicated that the timing of exercise following a full thickness defect could impact the reparative response with exercise 4 weeks post-surgery resulting in production of cartilage ECM components whereas, 2 weeks post-surgery, exercise hampered the repair process (Song et al., 2014).

1.3.1.3.3 Chemically Induced Models

Multiple methods have been developed to induce arthritis via injection of chemicals that can induce a toxic or inflammatory response resulting in arthritis development. This has the benefit of being less invasive than surgical models and, therefore, reducing the risk of surgical infection. Chemically induced OA models provide a platform to study pain and inflammation, two key symptoms of OA. However, unlike non-invasive ACLr or spontaneous OA models, the addition of chemical substances does not correlate with the pathogenesis of OA or PTOA in humans (Reviewed in Kuyinu et al., 2016) . Certain chemicals are commonly used to induce OA. This Includes IA injection of Monoiodoacetate (MIA) (Guzman et al., 2003, Marker and Pomonis, 2012); IA injection of collagenase (van Osch et al., 1996, Adaes et al., 2014); Papain (Lampropoulou-Adamidou et al., 2014); and Quinolone antibiotics (Ingham et al., 1977, Lozo et al., 2002, Sendzik et al., 2009). Furthermore, despite their usage as an arthritis therapeutic, multiple animal models investigate steroid induced arthroscopies and the impact of steroids on osteonecrosis (Silberberg et al., 1966, Nakazawa et al., 2002, Ichiseki et al., 2004, Little and Smith, 2008, Chen et al., 2019b).
AIA utilises the natural T-cell immune response to deliver an inflammatory arthritis phenotype. This follows the intra-articular injection of an antigen such as methylated bovine serum albumin (mBSA) into a Complete Freunds adjuvant (CFA) preimmunised animal resulting in a strong degradative and inflammatory phenotype. Inflammatory flairs can be induced by re-administration of low antigen doses to mimic human arthritic flairs (van den Berg et al., 2007, Bonnet et al., 2015).

1.3.1.3.4 Non-Surgical Injury Models

Non-surgical injury models were originally developed to study the effect of loading on bone mechanotransduction, while reducing the risk of infection and increased inflammatory response associated with surgical models (section 1.3.1.3.2) (Turner et al., 1991, Akhter et al., 1998, Hinton et al., 2018). These non-invasive models have been adapted to study the effects of loading on joint disease such as OA (Poulet et al., 2011). A model utilising a single compressive overload to rupture the ACL leading to OA development was developed in mice by Christiansen et al. as a model for PTOA (Christiansen et al., 2015) and in rats (Ramme et al., 2016). A mouse model utilising a single compressive force to rupture the ACL, leading to the development of PTOA, has been recently utilised for analysis of novel anti-arthritic therapeutics (Gilbert et al., 2018, Bonnet et al., 2020). Tibial fracture models allow for investigation into the reparative response of bone and surrounding tissue following traumatic injury as well as assessment of bones' mechanical properties. These models have been developed in mice, rats, rabbits, sheep, goats and dogs (Urist and McLean, 1941, Hsu and Robinson, 1969, White et al., 1977, Skirving et al., 1987, Heitemeyer et al., 1990, Schemitsch et al., 1996). Fractures are generated by a range of methods. Manual fracturing (Kernek and Wray, 1973), three point bending (Jackson et al., 1970) and guillotine-like fracturing (Bonnarens and Einhorn, 1984) aim to mimic non-surgical accidental fractures. *In vivo* injury models have provided a platform to study the effects of both physiological and pathophysiological loads and trauma on bone specifically and the joint as a whole. This has led to advances in the understanding of joint mechanosignalling and the mechanisms behind the development of certain joint diseases such as PTOA.

1.3.1.4 Osteoarthritis Model Summary

In vitro and *in vivo* models provide controlled and adaptable platforms by which investigation of the complex causes, mechanisms and potential therapeutic avenues for OA can be addressed. Choice of experimental model is not straightforward. It must relate to the focus of the investigation be that of primary degenerative OA or secondary injury induced PTOA; with a focus on inflammation or to target pain; to understand the mechanisms of cartilage generation or the contribution of bone to pathology. Choice of the most relevant model for each line of investigation is key to ensuring findings accurately translate to the human pathology.

1.4 Role of Glutamate Signalling in OA Pathogenesis

Glutamate is an excitatory amino acid essential for neurotransmission in the mammalian central nervous system (CNS) (Hinoi et al., 2004). GluRs are divided into two broad classes: metabotropic (mGluR) and ionotropic (iGluR) (Figure 1.5).

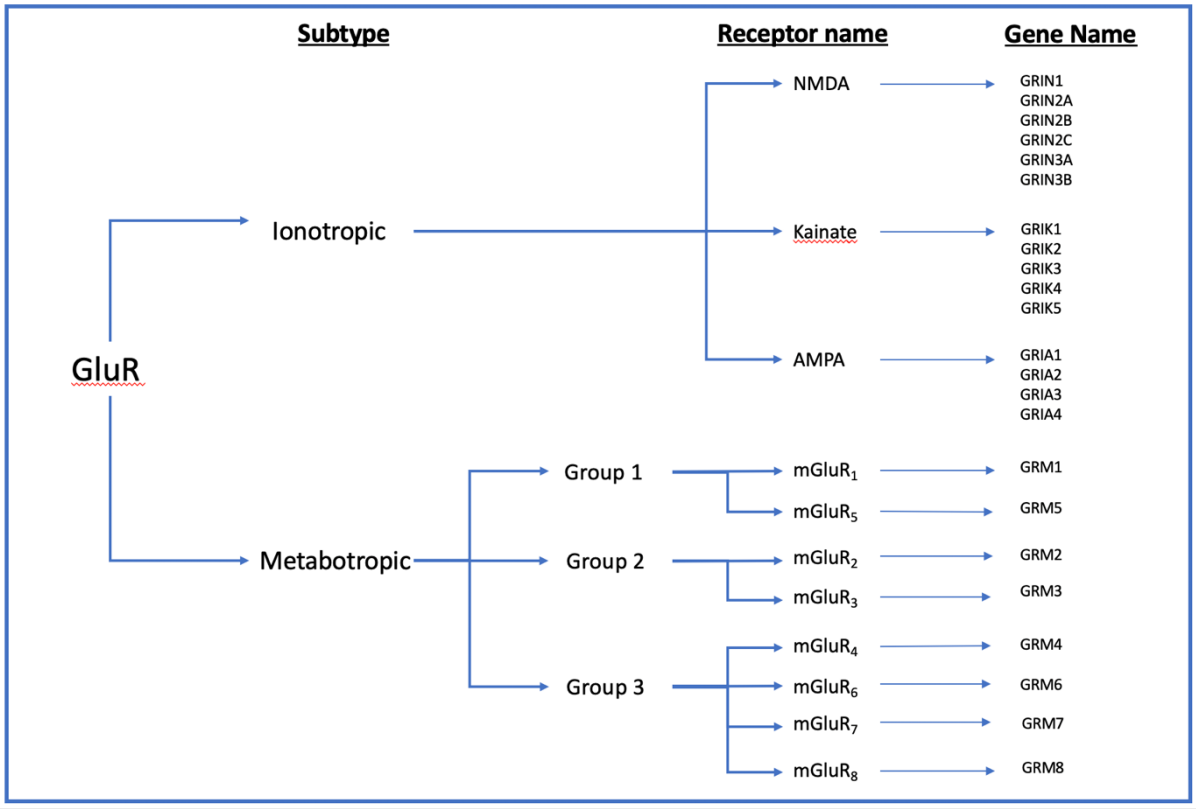

Figure 1.5: Glutamate receptor subdivisions and genes developed using information from Reiner and Levitz, 2018. Image designed by the Author.

These classes are further subdivided into mGluR types I, II and III and iGluR dl-α-amino-3-hydroxy-5-methylisoxasole-4-propionate (AMPA), Kainate (KA) and *N*-methyl-d-aspartate (NMDA) (Figure 1.7)(Reiner and Levitz, 2018).

Glutamate is released by a range of joint cells. In a rat model Kaolin and carrageenan induced knee inflammation increased glutamate release from local neurones (Lawand et al., 2000). Increased glutamate release was also identified in the synovial fluid of both OA and RA patients compared to healthy cadaveric controls (McNearney et al., 2000). Additionally,

glutamate levels in the synovial fluid of patients following ACL rupture and meniscal damage has been shown to be comparable to that of OA patient synovial fluid (Bonnet et al., 2020).

1.4.1 Glutamate Signalling Machinery Expression

Both metabotropic and ionotropic GluRs, are expressed in various joint tissues (Table 1.2).

Table 1.2: Localisation of GluR subtypes to specific joint cells or tissues. **+** *expressed in human healthy tissue;* **+** *expressed in human RA or OA tissue;* **+** *expressed in rat/mouse tissue. *MG-63 osteoblast like osteosarcoma cells.*

Joint Cell Type	iGluR AMPA	iGluR KA	iGluR NMDA	mGluR I	mGluR II	mGluR III	Ref
Chondrocytes	+ + +	+	+ +			+	(Salter et al., 2004, Wang et al., 2005, Flood et al., 2007, Bonnet et al., 2015, Bonnet et al., 2020)
Synoviocytes	+	+ +	+ + +	+	+	+ +	(Hinoi et al., 2005, Flood et al., 2007, Bonnet et al., 2015, Bonnet et al., 2020)
Meniscus	+ +	+				+	(Flood et al., 2007, Bonnet et al., 2020)
Osteocytes	+		+				(Chenu et al., 1998, Bonnet et al., 2015, Bonnet et al., 2020)
Osteoblasts	+	+	+ +	+*+		+	(Chenu et al., 1998, Patton et al., 1998, Gu and Publicover, 2000, Hinoi et al., 2001, Gu et al., 2002, Hinoi et al., 2002b, Hinoi et al., 2003, Kalariti et al.,

							2007, Bonnet et al., 2015, Bonnet et al., 2020)
Osteoclasts	+	+	+ +			+	(Chenu et al., 1998, Patton et al., 1998, Szczesniak et al., 2005, Bonnet et al., 2015)

Along with increased expression of TNFα and regulated on activation, normal T cell expressed and secreted (RANTES), upregulation of NMDA NR1 ionotropic glutamate receptor was observed *in vitro* on cultured human synoviocytes treated with glutamate receptor agonist NMDA (McNearney et al., 2010). Ionotropic glutamate receptor expression has been identified on menisci, fibroblast-like synoviocytes and fat pads as well as human normal fibroblast like synoviocytes and OA human chondrocytes (Flood et al., 2007). Ionotropic glutamate signalling machinery has been identified *in vitro* in both human cell line and rat articular chondrocytes (Piepoli et al., 2009). In an *in vivo* VGLUT1$^{(-/-)}$ KO mice model and in *in vitro* mouse osteoclast culture glutamate signalling has been observed (Morimoto et al., 2006). Ionotropic GluRs have been identified on human osteoclasts (Chenu, 2002). AMPAR2 and KA1 GluRs have been identified in multiple joint tissues (bone, cartilage, synovium and meniscus) in rat (AIA) and mouse (PTOA) *in vivo* models (Bonnet et al., 2015, Bonnet et al., 2020) as well as on human meniscal fibroblasts taken from meniscectomy patients (Bonnet et al., 2020).

1.4.2 Glutamate Signalling Function in OA

Factors regulated by GluRs include:

arthritic pain, through glutamate activation of iGluR and mGluR on peripheral nerve terminals and glutamate release from afferent peripheral nerve terminals due to tissue damage or inflammation (Miller et al., 2011). Inhibition of AMPA/KA glutamate receptors with NBQX has been shown to improve pain related behaviour in an inflammatory (AIA) model and two PTOA models (MNX and ACLr) (Bonnet et al., 2015, Bonnet et al., 2020);

immune response, NMDA receptor blockade has been shown to upregulate CD4+ T cells

and CD4+CD25+ regulatory T cells in an inflammatory model of arthritis (Lindblad et al., 2012); **synovial fibroblast proliferation**, that was repressed *in vitro* by kynurenic acid that is an iGluR antagonist (Parada-Turska et al., 2006); **inflammation**, by inhibition of KA/AMPA receptors, reducing levels of IL-6 release from human synoviocytes (Flood et al., 2007) and through modulation of meniscal *il-6* expression levels following AMPA/KA receptor inhibition with NBQX (Bonnet et al., 2015); and **degeneration** identified through the inhibition of NMDA resulting in increased proMMP-2 release from human synoviocytes and expression of AMPA receptors on human OA chondrocytes (Flood et al., 2007). The NMDA receptor has been shown to play a role in the mechanotransduction process in healthy chondrocytes. This is disrupted in OA chondrocytes indicating a role in the degradative response of cartilage in OA (Salter et al., 2004). Inhibition of AMPA/KA GluRs via intra-articular injection of NBQX has been shown to protect against joint degeneration in both inflammatory arthritis (AIA) and PTOA (ACLr, MNX) rodent models (Bonnet et al., 2015, Bonnet et al., 2017, Bonnet et al., 2020).

These factors highlight the influential role that glutamatergic signalling plays in multiple joint tissues in the propagation of OA pathogenesis.

1.4.3 There is no preventative therapeutic for Treating PTOA

Glutamate is an excitatory neurotransmitter that acts as a signalling molecule in peripheral neuronal and non-neuronal tissue. The potential for glutamate signalling in the joint was first discovered in bone in response to mechanical load (Mason 1997) and may represent a novel method of therapeutic opportunity.

Glutamate concentrations in the synovial fluid of RA and OA patients are elevated 52-fold and 42-fold respectively (McNearney et al., 2000) compared with Non OA/RA cadaveric synovial fluid. Increased glutamate levels are associated with an increase in inflammatory mediators in RA (McNearney et al., 2004). Glutamate levels in the synovial fluid of patients following ACL reconstruction and meniscal arthroscopy are comparable to those of OA patients and glutamate levels decrease significantly in the synovial fluid of patients between <20 weeks and >100 weeks after ACL injury ($p<0.05$) (Bonnet et al., 2020). Due to the

increased concentrations of glutamate in the joint in arthritis, and its correlation with inflammatory cytokines, and as well as the range of effects GluRs have on the joint, GluR antagonists have been investigated as potential disease modifying therapeutics (Flood et al., 2007, Lam and Ng, 2010, Vijayan Gangadharan et al., 2011, Lindblad et al., 2012, Bonnet et al., 2015, Bonnet et al., 2017, Bonnet et al., 2020).

The body of evidence using GluR antagonists in animal models of arthritis indicates that these drugs alleviate both symptoms and pathology (described in more detail in Appendix table 9.5). This sets the tone for the development of novel therapeutics that target GluRs and through this, successfully treat arthritis.

Intra-articular injection of 2.5mM of ionotropic AMPA/KA glutamate receptor specific antagonist NBQX at the point of AIA induction reduced end stage histological joint severity score by 28.8$\pm$1.7%, swelling by 33% and improved early weight-bearing (days 1 and 2) in AIA rats (Bonnet et al., 2015). Additionally, reduced expression of *il-6* mRNA was identified in the meniscus of AIA+NBQX treated rats compared to controls ($p<0.05$) and inflammation scores were significantly reduced in NBQX treatment groups compared to vehicle controls ($p<0.001$).

NBQX (25mM) has been shown to deliver significant reductions in swelling (7 and 8 days; $p<0.05$ and $p<0.01$), pain ($p<0.05$), inflammation (day 21, $p<0.05$) and joint severity scores in a surgical MNX model (Bonnet et al., 2017). These surgical model findings reflect those of the inflammatory (AIA) model.

More specifically to PTOA, in a non-invasive, mouse, ACL rupture injury model, NBQX intervention (20mM), immediately following injury, delivered a significant reduction in swelling (1 and 2 days; $p<0.05$ and $p<0.01$), maintained inflammation at naive control levels and reduced bone and cartilage defects significantly ($p<0.001$). Administration of a second NBQX dose at 24hrs post ACL rupture resulted in significantly improved joint scores compared to single dose groups ($p<0.05$) highlighting the potential for sustained NBQX dosage delivering improved therapeutic output (Bonnet et al., 2017, Bonnet et al., 2020). This model demonstrates the preventative benefit that NBQX administration may have

towards PTOA specifically, in addition the therapeutic effects shown in inflammatory (AIA) arthritis (Bonnet et al., 2015).

In addition to NBQX, multiple anonymised AMPA/KA specific glutamate receptor antagonists have been investigated for their therapeutic potential using the ACLr model. These molecules have the additional benefit of having passed phase 1 clinical trials allowing for accelerated approval for use in humans. 4 molecules, termed drug A, B, C and D, were compared to HA or steroid (Depo-Medrone) injected immediately following injury, contralateral knees were used as controls (Bonnet et al., 2019, Bonnet et al., 2020). Drug A significantly reduced knee swelling to day 0 levels (day 2, $p<0.01$) as well as drug C (day 2, $p<0.05$). Steroid injections reduced swelling significantly compared to vehicle ($p<0.001$) and HA ($p<0.05$) but only on a short-term basis with no effects observed after day 2. All GluR antagonists, but not steroids or HA, reduced lameness scores compared to vehicle controls by 3 days (Drug B, $p<0.001$; drug C, $p<0.05$; drug D, $p<0.05$). Drug A reduced mean degradation scores by 40% (day 21) whereas HA had no effect and steroid injections increased degeneration by 50% ($p<0.05$).

The findings of these studies indicate that the targeting of AMPA/kainate iGluR through IA administration of antagonists, such as NBQX, represents a viable anti-arthritic intervention in AIA, surgical and PTOA models, with protective effects on bone. The effect of a single IA injection of AMPA/KA receptor antagonists appears to demonstrate efficacy above and beyond that delivered by steroid or HA intervention (PTOA model) (Bonnet et al., 2019, Bonnet et al., 2020) or glucocorticoid, Methotrexate, anti-TNF, anti-IL-6 and anti-IL-1 in animal models as outlined below.

1.4.3.1 Therapeutic Effect of Non-glutamate Receptor Antagonist Therapeutics in Comparable Models.

AIA mice treated with 1.25mg/kg intra-venous (IV) dexamethasone had significantly reduced ($p<0.01$) knee joint swelling over 5 days and demonstrated short term (day 1) improvements in joint histology scores ($p<0.01$) (Baschant et al., 2011). In a rabbit surgical drill injury model involving the creation of drill holes in the femoral notch, IA administration of

dexamethasone (0.5mg/kg) resulted in significantly lower synovial histological scores compared to vehicle controls at 48hrs and 9 weeks post-surgery ($p<0.05$), significantly lower cartilage damage scores at 9 weeks post-surgery compared to vehicle controls on samples from the femoral condyle and tibial plateau ($p<0.05$) and significant reductions in synovial mRNA levels of IL-1 β, IL-6 and IL-8 after 48hrs ($p<0.05$) (Heard et al., 2015).

Whilst free methotrexate (MTX) (500μg), administered IA at arthritis induction in mouse AIA, did not affect knee swelling or joint degeneration. Liposome conjugated MTX reduced knee swelling by 1.94+/-0.12mm ($p<0.0001$; 1-day, vs unconjugated MTX). Conjugated MTX also significantly inhibited synovial thickening on days 3 and 7 ($p<0.007$ vs unconjugated MTX; $P<0.03$ vs saline controls) and arthritis index ($p<0.01$ vs unconjugated MTX and 0.0002 vs saline controls) (Williams et al., 2001).

Etanercept (5.5mg/kg) and infliximab (7mg/kg) administered intra-peritoneally in AIA mouse at 6hrs, 1 day, 4 days, 8 days, 11 days and 15 days after arthritis induction revealed no effect on joint pathology after 21 days and an approximately 20% reduction in swelling in the first week (Boettger et al., 2008). Continuous intrathecal administration of etanercept (6.6μg/hr) significantly reduced pain (primary mechanical hyperalgesia; day 3; $p<0.001$), swelling ($p<0.033$) inflammation (day 3; $p<0.05$) and bone and cartilage destruction (day 3; $p<0.05$) (Boettger et al., 2010).

Recombinant humanised monoclonal antibody for IL-6 Tocilizumab (1$\beta\mu$g/mL) was administered intrathecally into the cerebrospinal space in an MIA inflammatory rat model of arthritis. Tocilizumab treatment resulted in significantly attenuate centralised pain signalling ($p<0.01$), reduced expression of GluR1 and NR2B in the dorsal horn and improved OA pain behaviour (hindlimb weight bearing) ($p<0.01$) (Lin et al., 2017).

Novel OA drugs have delivered some efficacy. IL-1 receptor antagonists have been identified as potential DMOADs. However, in a CIA mouse model 37.5μg/hour IL-1Ra delivered intraperitoneally via an osmotic pump for two weeks did not reduce cartilage destruction or synovial inflammation (van Dalen et al., 2017). Additionally, IL-1$\alpha^{-/-}$ and IL-1$\beta^{-/-}$ mice were

not protected in a murine meniscectomy model of OA (Nasi et al., 2017). In a mouse ligamentous/meniscal injury model of PTOA, 3 injections of 500ng IL-1Ra for 1 week immediately following injury resulted in a significant reduction in cartilage degradation compared to sham operated PBS controls ($p<0.05$) and a complete prevention of cartilage MMP13 increase (Bollmann et al., 2020). In a rat PTOA model (ACLT) IL-1RA encapsulated in PLGA microparticles significantly reduced cartilage degeneration and synovial histopathology scores ($p<0.001$) compared to controls while delivering cumulative IL-1Ra release over 72hrs to extend the therapeutic window (Elsaid et al., 2016). The differences in therapeutic efficacy of IL-1Ra, depending on which animal model is used, highlight the complex nature of arthritis pathology and the need for careful study design.

These studies showcase some of the investigations that highlight anti-arthritic effects of a range of therapeutics in either AIA or PTOA models. NBQX IA intervention has demonstrated therapeutic effects towards pain, swelling, inflammation (*il-6* expression and histological inflammation scores) and joint degeneration across three separate models for arthritis including both inflammatory and post-traumatic pathologies (Bonnet et al., 2015, Bonnet et al., 2017, Bonnet et al., 2020). Additional evidence suggests sustained (24hr) administration of NBQX delivers further therapeutic benefits in PTOA compared to single administration and that other AMPA/KA glutamate receptor antagonists have shown therapeutic effects in the same model (Bonnet et al., 2017, Bonnet et al., 2019, Bonnet et al., 2020). Further investigation into the therapeutic benefits of sustained AMPA/KA glutamate receptor antagonist intervention in PTOA would build on these initial findings.

1.5 Drug Delivery and Sustained Release

Multiple methods have been developed for sustained delivery of therapeutics to treat a range of conditions, from breast cancer to multiple sclerosis (Zhang et al., 2008). Delivery vehicles can take a wide range of forms including thermoresponsive hydrogels, micro-particles, liposomes and nanoparticles each allowing for sustained drug delivery.

1.5.1 Drug Delivery Options to Treat OA

1.5.1.1 Oral Drug Delivery

Oral drug delivery is the most commonly used form of drug delivery (Reviewed by Ensign et al., 2012) and allows for easy self-administration of drugs in solid or liquid form. Orally administered drugs are absorbed through the GI tract which has a very high surface area due to the villi covering the surface (Schenk and Mueller, 2008). However, there are multiple factors to consider in the development of oral drug delivery systems. The stomach has a low pH (1-2) and contains digestive enzymes, ensuring drugs are not metabolised prior to GI tract absorption is essential and macromolecular drug products such as insulin have poor oral bioavailability due to proteolytic degradation (Goldberg and Gomez-Orellana, 2003). To protect drug products against degradation and optimise absorption, protective enteric coatings have been developed to reduce the exposure of the active ingredient to the acidic and enzymatic conditions of the stomach (Tomlinson, 1987). The stomach is covered in a mucosal epithelium that forms a constantly secreted protective barrier against the harsh pH and enzymatic environment but also may act as a barrier to the diffusion of certain therapeutic delivery systems (Cone, 2009).

The biopharmaceutical classification system (BCS) was developed to help define a drug product's bioavailability via application of Ficks laws of diffusion (Fick, 1855) applied to gastrointestinal membranes. The BCS is split into four classes: Class 1 – high solubility and high permeability; this is where the drug is well absorbed and the rate limiting step is the drug dissolution or the rate at which the stomach empties. Class 2 – low solubility and high permeability drugs; For drugs of this class absorption is slower than Class 1, therefore, the dissolution profile must be defined at a range of pHs representative of a longer stretch of the GI tract. Class 3 – high solubility and low permeability drugs. For these drugs, the rate limiting step is membrane permeability which can result in variability in drug absorption levels. Class 4 – low solubility and low permeability. Drugs within this class represent a challenge to oral drug delivery as the amount of absorption will rely on the limits of permeability and solubility (Amidon et al., 1995).

Even products of BCS Class 1 may not deliver high systemic availability due to first pass metabolism within the liver, meaning that much higher doses are required to deliver equivalent plasma concentrations as IV administration (Pond and Tozer, 1984). In patients with impaired liver function, oral drug delivery may put additional strain on the liver and altered drug metabolism resulting in a variance in systemically available drug concentrations compared to patients with fully functioning livers (Shakya et al., 2018).

All these factors highlight some of the challenges that need to be overcome to ensure therapeutic bioavailability of an oral drug formulation. Regarding OA therapeutics, multiple oral drug formulations are available. NSAIDs are commonly used to treat OA pain and come in oral formulations (van Walsem et al., 2015) and have been shown to deliver improved reductions in OA pain over paracetamol (Zhang et al., 2004). Several studies have demonstrated efficacy of NSAIDs in delivering pain relief such as Celecoxib (Deeks et al., 2002), Diclofenac (Pavelka, 2012), Meloxicam, Etodolac, Rofecoxib, Etoricoxib, Lumiracoxib and valdecoxib (Chen et al., 2008). However, chronic NSAID administration has been linked with an increased risk of cardiovascular events and GI tract bleeds (Bhala et al., 2013). The adverse events associated with chronic oral NSAID administration in combination with poor oral bioavailability of many drugs due to low membrane permeability and drug metabolism make targeted administration of therapeutics to treat OA an attractive line of investigation as higher drug loads can be delivered locally with a reduced risk of systemic toxicity while removing a risk of potential GI tract complications.

1.5.1.2 Topical Drug Delivery

Topical drug delivery formulations are widely used for the local delivery of drugs to the skin or underlying tissue or systemically via the barrier of the skin (Williams, 2015). The skin represents a multilayer barrier comprising different cells and appendages. The layers of the skin represent different barriers to drug delivery. The outer layer of the skin, called the epidermis, is represented by multiple sublayers of terminally differentiating keratinocytes from the stratum basale to the stratum corneum. This consists of multiple flattened layers of anucleated corneocytes stacked upon each other within a lipid bilayer to provide the primary barrier properties of human skin (Reviewed by (Fuchs and Raghavan, 2002,

Wikramanayake et al., 2014)). Below the epidermis is the deepest layer of skin (3-5mm thick) called the dermis. This is mainly composed of an extracellular network of elastin and collagen in a primarily aqueous environment. The Dermis is metabolically active and contains blood vessels reaching to below the Dermal-epidermal junction. This means that drug removal from the dermis is rapid as blood flow maintains a high concentration gradient between the external environment and the internal layers of the skin (Williams, 2015). Within the skin are different appendages such as hair follicles that can act as shunts routes or 'shortcuts' for drug delivery through the stratum corneum. However, these only occupy a small proportion of the overall skin surface (Essa et al., 2002).

Drug delivery through the skin occurs via transcellular or intercellular delivery through the stratum corneum. In transcellular drug delivery, the molecule is transported through the aqueous intracellular environment of the stratum corneum corneocytes and through the lipoidal intercellular regions. Intercellular drug delivery occurs through the lipid bilayers between corneocytes in the stratum corneum. Once through the stratum corneum, molecules diffuse down to the concentration gradient and are transported away via capillaries within the dermis (Reviewed by Barry, 2001).

Topical drug delivery provides a non-invasive route that can bypass first pass effect drug metabolism, allow for patient self-administration and can provide sustained drug delivery options (Prausnitz and Langer, 2008). However, to diffuse through the skin, drug products must be able to transfer through multiple lipid and aqueous layers. Drugs with low lipophilicity (low positive log partition coefficient values) are often selected, as high lipophilicity may inhibit drug clearance through the vasculature in the dermis (Prausnitz and Langer, 2008). As the skin acts as a barrier to large molecules, transdermal drugs ideally have a low molecular weight (<600Da). A low effective dosage is needed for transdermal drugs to limit the volume of drug delivery formulation that has to be applied to the skin to an acceptable size (Barry, 2001, Williams, 2015). The stratum corneum can be bypassed using microneedles. This is a delivery device that allows for the use of a wider range of therapeutics in transdermal drug delivery while avoiding stimulation of pain receptors and damage to blood vessels that can occur with more invasive delivery forms (Birchall et al., 2011). In addition to this, drug encapsulation into vesicles and particles, physical or chemical

modification of the stratum corneum and electrically assisted drug delivery all provide platforms from which to optimise transdermal drug delivery (Barry, 2001).

Multiple formulations have been developed for the topical drug delivery of therapeutics to treat OA symptoms. These include delivery of NSAIDs and Capsaicin (Rodriguez-Merchan, 2018). Mixed findings have been identified in two systematic reviews by Derry et al. It was found that topical NSAIDs diclofenac and ketoprofen provide OA knee pain relief in one review (Derry et al., 2016) whereas limited efficacy was identified from the same products in a later review over 6 to 12 weeks (Derry et al., 2017). Although Topical delivery allows for avoidance of potential GI complications associated with oral NSAID delivery, there is still variation in the findings for efficacy in the treatment of OA symptoms (Rodriguez-Merchan, 2018). Clinical trials and systematic reviews have indicated that topical capsaicin treatment is efficacious at treating OA pain compared to a placebo (Deal et al., 1991, Kosuwon et al., 2010, Laslett and Jones, 2014).

To summarise, therapies for topical drug delivery in arthritis have shown some efficacy in the management of OA symptoms and provide a non-invasive delivery option. However, the skin represents a barrier to drug delivery of certain therapeutics (hydrophilic/very lipophilic, larger molecular weight and high efficacious dose drugs) and localised delivery of drugs to target joints may be compromised via uptake into local dermis vasculature resulting in systemic delivery.

1.5.1.3 Subcutaneous Drug Delivery

Subcutaneous tissue is mostly adipose and provides blood vessel and neuronal innervation to the skin while providing mechanical protection. Drug delivery into the subcutaneous layer diffuses slowly and allows for a sustained rate of absorption making it the preferred route of delivery for drugs such as insulin that require low level sustained dosage (Kim et al., 2017).

Subcutaneous delivery of biopharmaceuticals enables patient self-administration thereby reducing the need for travel for clinical administration and improving the quality of life for patients with reduced mobility such as those suffering from arthritis (Bittner et al., 2018). In

comparison to systemic IV administration, subcutaneous drug delivery leads to reduced administration time and hence reduced burden to hospitals and patients (Bittner et al., 2018). In the case of trastuzumab, a breast cancer therapeutic, both patients and healthcare professionals preferred subcutaneous drug delivery over IV in hospital and this improved further when administration was carried out at home (Tjalma et al., 2017). An algorithm developed by Tetteh and Morris in 2014, indicated that the cost of administration for intra-muscular and subcutaneous biologics is lower than that of biologics delivered intravenously (Tetteh and Morris, 2014). These findings, in combination with the improved impact to patient quality of life, make subcutaneous delivery an attractive candidate for therapeutic delivery. For self-administration of a subcutaneous therapy, patients must be carefully trained to ensure they are competent to deliver a consistent therapeutic dose and minimise the risk to their own safety through overdosing. Adjusting the concentrations of formulations to reduce volume for administration and the inclusion of dispersion enhancers to aid the spreading of drug into the interstitial space are two methods of adapting subcutaneous drug formulations to improve the ease of self-administration (Frost, 2007, Bittner et al., 2018).

Multiple subcutaneous formulations have been developed for the treatment of RA. Etanercept, adalimumab, certolizumab pegol and golimumab are anti-TNFα therapeutics; Tocilizumab and sarilumab are both IL-6 receptor antagonists and anakinra is an IL-1 receptor antagonist, all of which have been developed for subcutaneous administration (Bittner et al., 2018, FDA, 2019b). Tocilizumab delivered in both IV and subcutaneous formulations has been shown to have similar long and short term efficacy in a RCT for the treatment of RA (Scott, 2017). With this in mind, compared to IV administration, the potential patient quality of life benefits of self-administration and reduced risk of injection site infection make subcutaneous formulations an attractive delivery option in the treatment of RA.

Due to the systemic nature of RA the location subcutaneous delivery is selected to ensure effective systemic dosing of therapeutics. In the case of OA, the pathology is localised to affected joints so therapeutic intervention may be of increased benefit when targeted to effected tissue. Targeted localised delivery has the added benefit of reducing the risk of

adverse side effects due to systemic exposure and allows for the use of therapeutics with low oral bioavailability in the case of IA delivery to treat OA. IA is a commonly used drug delivery form to ensure a therapeutic is targeted to the site of OA pathology. The incidence of adverse events remains low (Nguyen and Rannou, 2017). However, there are potential risks associated with IA drug delivery as described in section 1.5.1.4. Subcutaneous delivery of OA therapeutics localised to the site of pathology represents a patient self-administration delivery method that confers the therapeutic benefits of localised OA treatment, whilst minimising the risk of adverse events due to IA or IV injection. Ensuring effective therapeutic delivery from the site of subcutaneous application into the articular space, guaranteeing consistency of dose following self-administration and reducing the risk of systemic adverse events would all be factors requiring consideration in the development of a subcutaneous delivery vehicle for the localised treatment of OA.

1.5.1.4 Intra-articular Drug Delivery

Due to the localised nature of OA, administration of therapeutics locally via IA Injection is a logical delivery option. IA Injection reduces the risk of side-effects associated with systemic exposure due to oral drug administration (Nguyen and Rannou, 2017). Additionally, drugs with low oral bioavailability can be administered locally via IA injection. Direct IA delivery allows for control of initial drug dosage to the precise location affected by OA. The benefits of IA injection come with inherent risks, in the case of knee injections: synovial inflammation (Chen et al., 2002), nerve damage (Iizuka et al., 2005), septic and aseptic arthritis (Bernardeau et al., 2001, Charalambous et al., 2003) have all been observed following treatment. Side effects have also been observed in hip (necrotizing fasciitis) and shoulder (osteomyelitis, necrotising fasciitis and gas gangrene) IA injections (Cheng and Abdi, 2007).

Timing of IA injection is crucial in PTOA, and the correct intervention timing, combined with sustained drug release, could maximise the therapeutic effect during the acute post-traumatic phase (Punzi et al., 2016). Synovial fluid turnover occurs within joints resulting in the rapid clearance of suspensions injected into the synovial space. Suspensions of naproxen, cortisone and ketoprofen have half-lives of between 1 and 2 hours while HA has a

half-life of 22 to 26 hours (Butoescu et al., 2009). Small molecules like GluR antagonists have been shown to clear rapidly from the joint space via lymphatic drainage, synovial microvasculature and drug metabolism (Levick, 1980) and, as reviewed by Larsen et al. (2008), small molecules have been shown to have a short-lived joint retention half-life ranging between 0.5-6hrs (Larsen et al., 2008). Although no nanoparticle therapies have been approved for the treatment of OA, a triamcinolone acetonide microsphere sustained release formulation (FX006) has been approved for use in the treatment of OA by the FDA. This followed trials indicating improved joint residence time, reduced systemic exposure and WOMAC pain, physical function and stiffness scores and KOOS-QoL at 12 weeks compared to immediate release triamcinolone and a placebo (Conaghan et al., 2018c, Kraus et al., 2018). FX006 microsphere therapy highlights the capacity for sustained release formulations to improve and extend the therapeutic benefits of immediate release therapies. This could be useful in preventative PTOA intervention by extending the timeframe of drug exposure, potentially allowing for improved therapeutic benefits

1.5.2 Nanoparticles

Nanoparticles have a wide range of applications within medicine such as fluorescent labelling, tissue engineering, MRI contrast enhancement, protein detection and drug delivery (Salata, 2004). In the area of drug delivery, nanoparticles provide a vehicle for poorly water-soluble drug encapsulation, controlled release, drug targeting and the minimisation of systemic drug levels which reduces the risk of any related side effects. Various mechanisms of drug release can take place from nanoparticles and are affected by the nature of the drug encapsulated, the type of nanoparticle and the formulation methodology (Son et al., 2017). Where the drug is dispersed or dissolved in the core of a nanoparticle, diffusion-controlled release occurs across the membrane of the nanoparticle down the concentration gradient (Cauchetier et al., 2003). Matrix type nanoparticle delivery systems do not have a barrier to diffusions. They, therefore, often demonstrate high initial drug delivery which reduces over time as the diffusion distance from inside the carrier increases (Son et al., 2017). Solvent controlled release can occur from nanoparticles following the influx of water (osmotic controlled release) causing a concentration gradient for drug release to be maintained via zero order release kinetics (Reviewed by Langer and

Peppas, 1983). Additionally, swelling controlled release can occur in delivery vehicles in which mesh size controls drug release (can occur in hydrogels) (Lin and Metters, 2006). Nanoparticles composed of biodegradable polymers (e.g. Poly(lactic-co-glycolic acid) (PLGA)) release drug following enzymatic degradation or hydrolysis of the overall polymer matrix or from the surface to the centre of the particle (Lee and Chu, 2008). Some nanoparticle delivery systems have been developed that release in response to external stimuli such as pH, ionic strength, temperature, electricity or magnetism (Min et al., 2010, Li et al., 2011). This allows for targeted drug release in specific environments within the body or following application of an external stimulus. Various mathematical models have been developed to describe the release kinetics from controlled drug delivery systems (Reviewed by Dash et al., 2010). These include: zero order, first order, Higuchi model, Hixson-Crowell and Korsmeyer-Peppas model (Hixson and Crowell, 1931, Higuchi, 1962, Gibaldi and Feldman, 1967, Costa and Sousa Lobo, 2001). There are now a range of nanoparticle based drug delivery therapeutics approved for clinical use in humans, the majority of which comprises liposomal or polymer based vehicles (Zhang et al., 2008). However, none of the approved nanoparticles have been developed to target OA.

1.5.2.1 Nanoparticles and the Treatment of OA

Although currently not approved for use in the clinical setting, multiple groups are investigating nanoparticles for the sustained delivery of OA therapeutics. When developing drug delivery vehicles to treat OA, the environment into which these vehicles are being injected must be taken into consideration. Control of nanoparticle size (<1000nm) can result in delivery vehicles that have reduced immune cell detection resulting in reduced phagocytosis and deliver an enhanced tissue permeability. (Reviewed by Holyoak et al., 2016). These properties would be beneficial in a sustained release delivery vehicle designed to be delivered via IA injection into the joint space in the treatment of OA.

Even within the nanoscale there are a wide range of particle sizes under investigation, from 7nm QDs to 900nm self-assembling complexes (Bajpayee et al., 2014, Singh et al., 2014). The QDs were shown to have maximum cartilage penetration at sizes bellow 10nm allowing for delivery of therapeutics deep into the articular cartilage (Bajpayee et al., 2014).

Regarding the larger nanoparticles, 900nm self-assembling pHEMA-pyridine protein tethered nanoparticles demonstrated significantly higher joint retention into male Lewis rat stifle joints than small nanoparticles of the same type and free protein, indicating larger nanoparticles are more resistant to clearance from the joint space (Singh et al., 2014). Nanoparticles have been developed to deliver a wide range of therapeutics including bioactive proteins (Whitmire et al., 2012, Singh et al., 2014), NSAIDs (Arias et al., 2009, Bishnoi et al., 2014), synthetic binding peptides (Rothenfluh et al., 2008), DNA (Lu et al., 2011) and compounds to induce cellular differentiation (Kang et al., 2014). A combination of materials and synthesis methods have been utilised to formulate nanoparticles for application in arthritis including synthetic polymers (PLGA), natural polymers (chondroitin sulphate, HA), gold, silver, magnetic metals, liposomes and QDs (Arias et al., 2009, Pascarelli et al., 2013, Jain et al., 2014, Riffault et al., 2015, Wang et al., 2018). Due to the range of particle types, sizes and drug loads a variety of effects have been observed both *in vitro* and *in vivo* as a result of nanoparticle application. Appendix table 9.6 summarises a wide range of in vitro and in vivo studies focused on the development of nanoparticles to aid in the treatment of joint disease.

Combined, these studies highlight the broad spectrum of work investigating the effect of nanoparticles in the treatment of OA. The results from these studies indicate the potential to improve the effects of currently approved therapeutics and investigate alternate delivery options for novel disease modifying anti-osteoarthritic drugs.

1.5.3 Thermoresponsive Hydrogels

Thermoresponsive hydrogels represent a sustained release delivery vehicle for arthritis therapeutics. Stimuli-sensitive hydrogels can undergo a reversible sol-gel phase transition in response to certain stimuli such as temperature, pH, light, electromagnetic radiation, ionic strength and biomolecules. These hydrogels can be adapted to function as *in situ* forming hydrogels (He et al., 2008), existing in an aqueous 'sol state' before administration into an *in vivo* environment, at which point they transition into a solid gel. These properties make *in situ* forming hydrogels an ideal candidate for localised sustained drug delivery in the treatment of joint disease via IA injection or subcutaneous injection. The gelation of the

hydrogel under physiological conditions greatly reduces drug clearance (Venkatesh et al., 2013). Additionally, these hydrogels can be easily formulated, sterilised and encapsulate both hydrophilic and hydrophobic drugs with no encapsulation losses. The capacity to inject *in situ* forming hydrogels subcutaneously, for controlled local drug delivery, provides a less invasive platform for OA therapeutic delivery than IA injection with ramifications for patient compliance and reduced infection risk while bypassing the barrier of the stratum corneum. Localised subcutaneous delivery has been investigated in the treatment of tumours (Reviewed in Larsen et al. 2013).

Pluronic's or poloxamers are a group of non-ionic surface-active agents (Figure 1.6)(Ruel-Gariépy and Leroux, 2004). These polymers, consisting of blocks of poly(ethylene oxide) (PEO) and poly(propylene oxide) (PPO), can form into reversible thermosetting hydrogels when dissolved in high concentrations in aqueous solutions and are listed on the FDA's inactive ingredients database as 'generally regarded as safe' (Venkatesh et al., 2013).

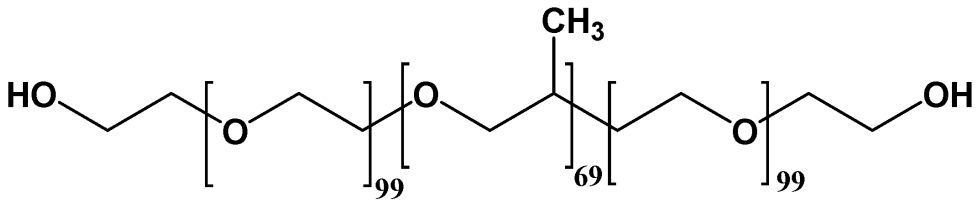

Figure 1.6: Chemical Structure of Pluronic F-127 (Donato et al. 2020). Permissions granted for use of this figure in this thesis.

Pluronic F127 (poloxamer 407) can form into semi-solid gels at body temperature (37°C) (Ruel-Gariépy and Leroux, 2004) and toxicity data indicates that it is well tolerated *in vivo* (Liu et al., 2007). Due to its low toxicity and favourable gelation characteristics, Pluronic F-127 has been investigated for use in multiple medical applications, such as, treating burns, topical anticancer drug delivery, and sustained injectable drug delivery (Ruel-Gariépy and Leroux, 2004).

1.5.3.1 Thermoresponsive Hydrogels and the Treatment of OA

Multiple Pluronic F127 based formulations have been developed for the delivery of anti-inflammatory drugs and analgesics used in the treatment of OA (Choi et al., 1998, Paavola et al., 2000, Shin et al., 2000a, Venkatesh et al., 2013). IL-1Ra, delivered subcutaneously in male Wistar rats via a sustained release Pluronic F-127 based hydrogel, exhibited prolonged release compared to an aqueous IL-1Ra solution, resulting in greater efficacy to inhibit plasma IL-1β stimulated production of IL-6 (Akash et al., 2012). MTX, loaded into pluronic-F127 hydrogels, exhibited sustained release *in vitro* over 120 hours into PBS (pH7.4) resulting in a reliable delivery vehicle for prolonged delivery of an anti-arthritic agent (Venkatesh et al., 2013). Following subcutaneous injection into nude mice, dexamethasone, loaded into PLGA microspheres and encapsulated in a HA and pluronic-F127 based hydrogel, was shown to increase the expression of chondrogenic markers from encapsulated rabbit MSCs (Bae et al., 2010). Piroxicam, encapsulated in a Pluronic F127 and HA-based hydrogel, was shown to deliver both a sustained release (over 200 hours) of drug and improved bioavailability compared to a drug in aqueous solution after articular cavity injection in beagle dogs *in vivo*. These studies demonstrate a range of Pluronic F-127 hydrogel formulations have been utilised to investigate the optimisation of anti-arthritic therapeutics.

1.5.4 Sustained GluR Antagonist Delivery to Treat PTOA

PLGA nanoparticles represent a viable vehicle for sustained release of IA injected arthritis therapeutics. They both extend drug effects through decreased clearance and reduce infection risk through decreased need for multiple injections. Thermosetting *in situ* hydrogels can be injected subcutaneously to provide localised sustained release delivery to target tissue. Sustained delivery of arthritis therapeutics from Pluronic F-127 based hydrogels has been shown to extend therapeutic effects and subcutaneous delivery could reduce infection risk associated with IA drug application and facilitate patient self-application.

There is evidence to suggest that sustained application of GluR antagonist NBQX application in a PTOA model (ACL rupture) enhances the anti-arthritic effects already identified by Bonnet et al., (2015) in an AIA model. Two injections of NBQX delivered at days 0 and 1 post

arthritic induction are more effective than a single injection at day 0 (Bonnet et al., 2020). This thesis investigates extending AMPA/kainate GluR antagonist joint residence time and reducing the need for invasive applications through development of novel drug delivery vehicles with the aim of enhancing the therapeutic effect of these antagonists while improving the ease of application and reducing the risk of infection to the patient.

1.6 Hypothesis and Aims

Thesis Hypothesis:

AMPA and kainate glutamate receptor (GluR) antagonists can be incorporated into sustained release delivery systems that can protect against inflammatory or mechanically driven pathways in bone *in vitro.*

Each experimental chapter contributes to the overarching hypothesis via a series of aims as follows:

Chapter 3:

To synthesise and characterise PLGA nanoparticles for delivery of GluR antagonists; determine the GluR sustained release characteristics and investigate freeze drying as a long term nanoparticle storage option.

Chapter 4:

To synthesise and characterise a thermoresponsive hydrogel for delivery vehicle for GluR antagonists; determine GluR sustained release characteristics and investigate GluR antagonist permeation through the synovial membrane.

Chapter 5:

To determine whether pathological levels of pro-inflammatory IL-6/sIL-6r exposure followed by short term AMPA/KA GluR antagonist application with or without sustained release of AMPA/KA GluR antagonist from PLGA nanoparticles influences bone remodelling, glutamate and inflammatory signals.

Chapter 6:

To determine whether mechanically induced bone remodelling of Y201 derived osteocyte-like cells in 3D induces pathological markers of bone remodelling and inflammation and is affected by short term treatments with AMPA/KA GluR antagonist NBQX.

Chapter 2

Materials and Methods

2.1 Materials

All cell culture plasticware was purchased from Sigma unless otherwise stated; Folded Capillary Zeta Cells and disposable plastic cuvettes for dynamic light scattering measurements were purchased from Malvern Panalytical; DNQX disodium salt and NBQX disodium salt were purchased from HelloBio; Poly-Vinyl Alcohol, Poly(lactic-co-glycolic acid; 50:50 lactide to glycolide), Pluronic F-68, Ethyl Acetate, Pluronic F-127, Trehalose, Carbopol 934, Trifluoroacetic acid, HPLC grade H_2O, HPLC grade Acetonitrile, β-glycerophosphate, Ascorbic acid-2-phosphate, Dexamethasone, 10% Neutral Buffered Formalin solution, Alizarin red, Cetylpyridinium chloride, Rat tail type I collagen, Glacial acetic acid, sodium bicarbonate, Tris base and paraformaldehyde were purchased form Sigma-Aldrich unless otherwise stated; 1X Phosphate buffered saline (pH7.4), DMEM +glutaMAX, αMEM, Fetal Bovine Serum, Penicillin (10000U/ml) and Streptomycin (10000U/ml), Ethanol, TripleE express (tripsin), 10XMEM, TRIzol, DNase free kit, DEPC treated RNase free H_2O, Superscript IV and Sybr green were all purchased from ThermoFisher Scientific unless otherwise stated; CytoTox 96® Non-radioactive Cytotoxicity Assay (LDH assay), Griess Reagent System (nitrite detection assay), CellTiter 96® Aqueous One Solution Cell Proliferation Assay (MTS assay), deoxynucleotide triphosphate (dNTP) mix, Random primers and RNasin® (RNase Inhibitor) were all purchased from Promega unless otherwise stated; Optimal cutting temperature compound (OCT) was purchased from SciGen Ltd.; Phalloidin-iFluor 488 reagent was purchased from Abcam; human IL-6 and soluble IL-6 receptor were purchased from PeproTech; human glutamate ELISA kits were purchased form Abnova; V-PLEX Proinflammatory Panel 1 Human Kit was purchased from Mesoscale Discovery.

2.1 Equipment

All nanoparticle centrifugation was carried out in a Heraeus Fresco 17 Centrifuge (Thermo Scientific) unless otherwise stated. All RNA prep centrifugation was carried out on a PrismR Centrifuge (Labnet International inc.) unless otherwise stated.

2.2 PLGA Nanoparticles.

2.2.1 PLGA Nanoparticles Synthesis.

2.2.1.1 Microfluidic Nanoparticle Synthesis

Initial studies synthesised PLGA nanoparticles in a microfluidic channel by mixing a solution of acetonitrile containing 25mg/ml PLGA (50:50 lactide to glycolide) with distilled water containing 2% PVA using hydrodynamic flow focusing in a Nanoasemblr™ benchtop apparatus. PLGA nanoparticles were formulated according to Precision Nanosystems PLGA Nanoparticle protocol. The Nanoasemblr™ Benchtop software was set to the parameters shown in Table 2.1.

Table 2.1: PLGA nanoparticle synthesis process parameters for Nanoasemblr ™ Benchtop software

Volume	2ml
Flow Rate Ratio	1:1 (aqueous to solvent)
Total Flow Rate	8ml/min
Left Syringe Size / Right Syringe Size	1ml/1ml
Autoswitch	ON
Start Waste Volume / End Waste Volume	0.25ml / 0.05ml

One blunt syringe was filled with 1ml of 20mg/ml PLGA/acetonitrile solution and one with 2% PVA solution and DNQX disodium salt concentrations of 0, 10, 30 and 50mM respectively. The 2% PVA syringes, containing DNQX disodium salt, was loaded into the left position within the Nanoasemblr™ block and the PLGA/Acetonitrile syringe was loaded into the right. A nanoparticle collection tube was placed in the left collection tube clip and a waste tube was clipped in the right. The Nanoasemblr™ was then closed and the system run according to the parameters in Table 2.1. Once the Nanoasemblr™ had returned to its original position the nanoparticle collection tube was removed and nanoparticles assessed immediately for size, zeta potential and Poly dispersity index (PDI) using a Malvern Zetasizer (Malvern Panalytical Ltd) (section 2.2.3). 200μl aliquots of PLGA nanoparticles were pipetted onto SuperFrost® Plus (Thermo Scientific) slides and covered with a coverslip coated in

Vectashield® mounting medium with DAPI for imaging using an Olympus BX61 upright fluorescent microscope (section 2.8.4).

2.2.1.2 Double Emulsion Nanoparticle Synthesis

PLGA nanoparticles were synthesized via an adapted double emulsion method for the encapsulation of water soluble compounds (Cohen-Sela et al., 2009). DNQX disodium salt or NBQX disodium salt was dissolved in 1ml 3% w/v PVA in distilled H_2O (dH_2O) to a concentration of 2.5 or 20mM according to effective doses in rodent models of arthritis (Bonnet et al., 2015, Bonnet et al., 2020). This solution was then pipetted into 3mls solvent solution comprising 30mg/ml PLGA and 30mg/ml Pluronic F-68 dissolved in ethyl acetate. This mix was sonicated over ice at an amplitude of 20 microns for 90 seconds using a Soniprep 150 probe sonicator (Sanyo Electric Co., Ltd.). The resulting emulsion (4ml) was then pipetted into 10ml of 2% w/v PVA. This mix was then sonicated over ice at an amplitude of 10 microns for 90 seconds as previously. The emulsion was then placed on a temperature controlled magnetic stirrer (Fisher Scientific) at 1200rpm and 25°C for 2 hours to evaporate the ethyl acetate solvent. Nanoparticles were then isolated via centrifugation at 10,000g for 3 hours. Supernatant was pipetted off and isolated particles were resuspended in 20ml PBS or 10ml of bovine synovial fluid for release studies (section 2.2.6.) or split into 4ml aliquots suspended in bovine synovial fluid, DMEM or PBS for dynamic light scattering analysis (section 2.2.3).

2.2.2 Bovine Synovial Fluid Extraction

Bovine lower legs were purchased from Maddock Kembrey Meats (Maesteg, Wales, UK) within 2hrs of death and skinned. Dr Joel Alves (veterinary surgeon) directed dissections. To extract the synovial fluid, the carpal joint was rotated to 45° and a short 30-gauge needle inserted anteriorly into both the lateral and medial joint compartments (Figure 2.1). Approximately 2.5ml of synovial fluid was then extracted from each compartment (5ml synovial fluid/joint) and centrifuged for 15 minutes at 1000g to remove cells and debris.

Synovial fluid samples were stored in a sealed 50ml centrifuge tube at -20°C for use in nanoparticle suspension (section 2.2.3.) and GluR antagonist release studies (section 2.2.6.).

Figure 2.1: Synovial fluid extraction from the medial compartment of a bovine fetlock carpal joint

2.2.3 Nanoparticle Size, PDI and Zeta Potential

After PLGA nanoparticles were synthesized, isolated and resuspended (sections 2.2.1.1 and 2.2.1.2), a 1ml aliquot was taken for dynamic light scattering (DLS) analysis using a Malvern Zetasizer (Malvern Panalytical Ltd). Plastic cuvettes were used to quantify particle size and PDI. Folded capillary zeta cells (Malvern Panalytical Ltd) were used to quantify zeta potential. Table 2.2 outlines the refractive index and viscosity values used to define synovial fluid, PBS and DMEM as well as the main nanoparticle material, PLGA.

Table 2.2: The factors inputted into the Malvern Zetasizer software for quantification of size, PDI and zeta potential of PLGA nanoparticles in different suspensions.

Material/Dispersant	Refractive Index	Viscosity (mPa.s / cP)	Reference
PLGA	1.460	N/A	(Wu et al., 2014)
PBS	1.330	0.8882 (cP)	(Malvern, 2007, Diéguez et al., 2009)
DMEM	1.345	3 (cP)	(Curl et al., 2005, Diéguez et al., 2009, Alwani et al., 2015)
Synovial fluid	1.34	500 (mPa.S)	(Nuki and Ferguson, 1971, Rinaudo et al., 2009, Banquy et al., 2014, Bortel et al., 2015, Thompson et al., 2015)
Water	1.330	0.8872 (cP)	(Malvern, 2007, Diéguez et al., 2009, Alwani et al., 2015)

2.2.4 Calculation of Encapsulation Efficiency and Loading Capacity

Following PLGA nanoparticle isolation (section 2.2.1.2), the supernatant was pipetted off and stored at -20°C for HPLC analysis (section 2.4). By quantifying the GluR antagonist concentration within this supernatant, the concentration of 'free' unencapsulated drug was determined and encapsulation efficiency (EE) was quantified via the following equation: [(Drug added - 'Free' unencapsulated drug)/Drug added]*100. This defines the percentage of the original drug encapsulated into the nanoparticles. Loading capacity (LC) is the amount

of drug loaded per unit weight of nanoparticle and was calculated as: [(amount of entrapped drug/total nanoparticle weight)]*100.

2.2.5 Freeze Drying PLGA Nanoparticles

After PLGA nanoparticle synthesis (section 2.2.1.2), the nanoparticle pellet was resuspended in 4.5ml of 5% w/v trehalose in distilled water solution and analyzed for size, PDI and zeta potential (section 2.2.3). The nanoparticle suspension was snap frozen in liquid nitrogen for 10 minutes and rapidly transferred to a reduced pressure freeze drying chamber on a CoolSafe Freeze drier (ScanVac) at -106°C for 18 hours. The freeze-dried nanoparticle 'cake' was either stored at -80°C, resuspended in 4.5ml dH_2O, before reanalysis for size, PDI and zeta potential (section 2.2.3), resuspended for GluR antagonist release assays (section 2.2.6) or resuspended for MTS assays (section 2.12.2.1) and 3D Y201 MSC culture studies (section 2.7).

2.2.6 GluR Antagonist Release from PLGA Nanoparticles

After PLGA nanoparticle synthesis and centrifugation (section 2.2.1.2), the nanoparticle pellet was resuspended in 20ml of PBS or resuspended in 10ml of bovine synovial fluid (section 2.2.2) and placed on a temperature controlled magnetic stirrer (ThermoFisher) at 37°C and 125rpm and covered to prevent evaporation.

Drug release studies were also carried out with PLGA nanoparticles following freeze drying (section 2.2.5) in 20ml PBS as above.

For all GluR antagonist release studies, 1ml aliquots were taken at 1, 3, 24, 48, 72, 148, 172, 336, 504, 672 and 840 hours and centrifuged at 15,000g for 1 hour. The supernatants from these samples were then analyzed via HPLC and the drug content quantified (section 2.4). GluR antagonist concentration as well as percentage release was plotted against time to determine the drug release over time from fresh and freeze dried PLGA nanoparticles.

2.2.7 Scanning Electron Microscopy (SEM)

2.2.7.1 Fresh Filtered Nanoparticles

PLGA nanoparticles were synthesized (section 2.2.1.2) and either used immediately (within 1 hour) or suspended in 37°C PBS for 3 weeks on a magnetic stirrer (ThermoFisher). Nanoparticles were isolated via centrifugation (10,000g, 3 hours), resuspended in 2ml dH_2O and filtered onto 50nm Nuclepore track-etch polycarbonate filter membranes (Whatman®) using a KNF Laboport® vacuum pump (KNF Neuberger Inc., USA) pressurized filtration system. Filters were then washed through with 5ml of increasingly high concentrations of ethanol (50%, 70%, 90% and 100%) using the same Laboport® vacuum pump pressurized filtration system. The entirety of each ethanol wash was allowed to pass through the filter prior to the application of the next wash (approximately 15 minutes). Dr Christopher Von Ruhland (Facility Lead, Electron and Light Microscopy, Central Biotechnology Services, School of Medicine, Cardiff University) sectioned, gold coated and collected SEM images of nanoparticle coated filters.

2.2.7.2 Freeze Dried Nanoparticles

Following freeze drying (section 2.2.5), nanoparticles were fixed to a stub, gold coated and SEM imaged on the day of freeze drying and following 4 weeks storage at -80°C by Dr Christopher Von Ruhland (Facility Lead, Electron and Light Microscopy, Central Biotechnology Services, School of Medicine, Cardiff University).

2.3 Thermoresponsive Hydrogels

2.3.1 Thermoresponsive Hydrogel Synthesis

Thermoresponsive hydrogel synthesis was adapted from Venkatesh et al., (2013). To enable investigation into a range of hydrogel rheological properties for application in this thesis, Pluronic F-127 was slowly added to distilled water over ice while mixing at 250rpm on a magnetic stirrer to result in a range of Pluronic F-127 concentrations (19%, 22%, 25% and

28% w/v) in distilled water. Following this, Carbopol 934 was added to the Pluronic F-127 solution over ice to a concentration of 0.5% w/v. This mixture was homogenized for 90 seconds over ice with an SHM1 homogenizer (Stuart-Equipment) and then allowed to settle at 5°C for 24 hours in a sealed 50ml centrifuge tube for rheological analysis (section 2.3.2) or drug release studies (section 2.3.3 and 2.3.5).

2.3.2 Thermoresponsive Hydrogel Rheological Testing

Pluronic F-127 based hydrogels (19%, 22%, 25% and 28% concentrations, section 2.3.1) viscosity and viscoelastic properties were measured using a Bohlin CVOR200 rheometer (Bohlin Instruments, UK) with a PP-20, 20mm insert and gap set to 750μm. Rheological methods were developed with the assistance of Elen Everett (PhD student, Cardiff University School of Dentistry (Everett, 2018)). Within 2 minutes of removal from 5°C, 1ml of hydrogel was pipetted onto the rheometer plate for each test and allowed to equilibrate to the plate temperature (5, 25 or 37°C) for 2 minutes. Bohlin CVOR200 Software was utilized to operate the rheometer, record data and convert data for graphical analysis and statistical analysis.

2.3.2.1 Thermoresponsive Hydrogel Viscosity Measurement

The temperature flow curve of thermoresponsive Pluronic F-127 hydrogels was established between 5°C and 40°C to assess the impact of temperature to sample viscosity with a temperature change of 2°C/minute and a fixed shear value of $1s^{-1}$. Shear rate ramp tests were performed between a range of 0.1 to $1000s^{-1}$.

2.3.2.2 Thermoresponsive Hydrogel Viscoelastic Measurement

Viscoelastic properties of thermoresponsive hydrogels were quantified by measurement of the elastic (storage) modulus (G') and viscous (loss) modulus (G"). Oscillation measurement was carried out in the linear region of the viscoelastic curve as quantified by an amplitude

sweep carried out between 0.01 and 0.1 strain at a constant frequency of 1Hz. Frequency sweep tests were carried out between 0.1 and 10Hz at a constant stress of 0.1Pa.

In order to evaluate the change in viscoelastic properties of thermoresponsive Pluronic F-127 hydrogels in response to temperature, a temperature sweep was carried out at a stress of 0.1Pa and a constant frequency of 1Hz. Temperature ranged from 5°C to 45°C increasing at 2°C/ minute. The juncture of G' and G" over the temperature gradient represented the sol/gel transition temperature at which point the thermoresponsive hydrogel transitions from a liquid into a gel.

2.3.3 DNQX release from Thermoresponsive Hydrogels

2.5mM DNQX was dissolved in both 22% and 25% Pluronic F127 hydrogels (section 2.3.1) by adding 0.74mg DNQX disodium salt per ml of hydrogel. These concentrations were selected to deliver optimal gelling and viscosity characteristics, (see chapter 4 of this thesis). DNQX was added to the water component of the hydrogel and dissolved by vortexing prior to the addition of Pluronic F-127 and Carbopol-934 (section 2.3.1). The delivery of DNQX from hydrogels into 250ml PBS at 37°C across a dialysis membrane (molecular weight cut off 10KDa) was utilized to determine drug release over time. The Slide-A-Lyzer® dialysis cassette (3ml capacity, Thermo Scientific) was hydrated in PBS for 2 minutes before 2ml of 2.5mM DNQX loaded 22% or 25% w/v Pluronic F127 hydrogels were injected into the cassette and incubated at 37°C for 5 minutes to allow hydrogels to gel. The hydrogel-loaded cassette was then suspended in PBS at 37°C on a magnetic stirrer for 48 hours. At 1, 5, 15, 30 minutes and 1, 2, 4, 6, 22 and 27 hours, 1ml samples of PBS were extracted and stored at -20°C for HPLC quantification of DNQX (section 2.4) and an equal volume of fresh PBS added to maintain sink conditions. DNQX concentration was calculated at each time point to determine the sustained release from hydrogels over time. Positive control release studies with 2ml of 2.5mM DNQX injected directly into the dialysis cassette were carried out to determine if any GluR antagonist release curves obtained via this method was from hydrogel sustained release as opposed just diffusion through the dialysis cassette membrane.

2.3.4 Bovine Synovial Membrane Isolation

Bovine lower legs were purchased from Maddock Kembrey Meats (Maesteg, Wales, UK) within 2hrs of death and skinned. Dr Joel Alves (veterinary surgeon) directed dissections. Using a scalpel, subcutaneous tissue and tendons were removed to expose the carpal joint synovial membrane. Approximately 2cm diameter discs of synovial membrane and joint capsule were dissected using a scalpel from the anterior medial and lateral joint compartments (Figure 2.2). These were stored at 4°C and used within 1 hour in Franz Diffusion Cell studies of DNQX delivery from hydrogels (section 2.3.5) through the bovine synovial membranes and joint capsule sections.

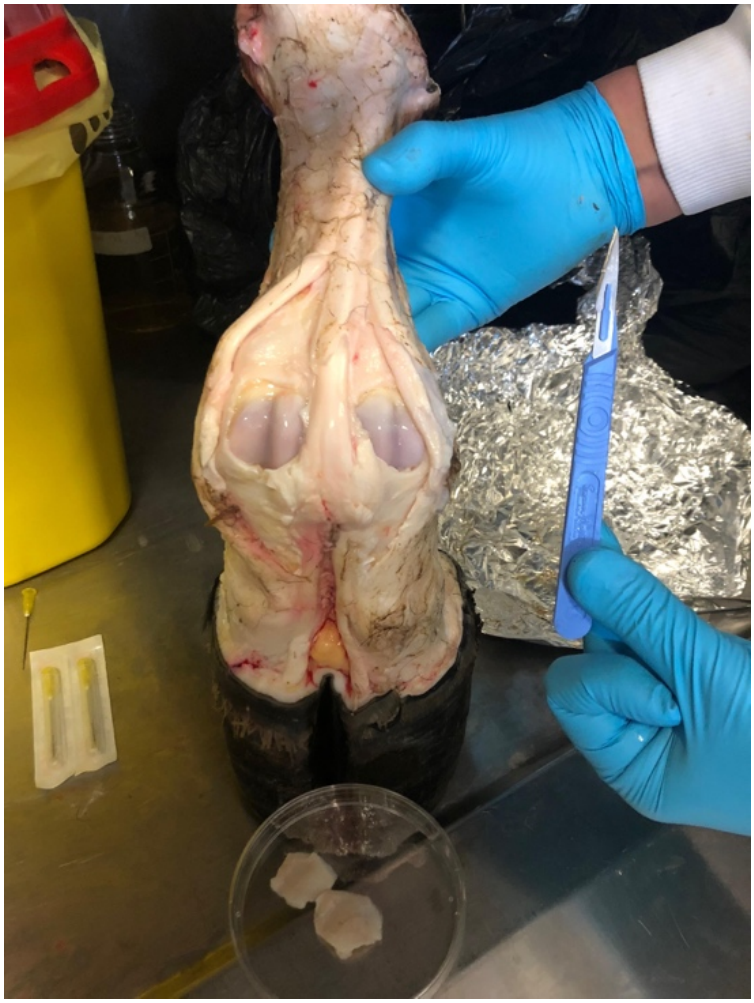

Figure 2.2: Synovial membrane extraction from anterior medial and lateral compartments of a skinned bovine joint.

2.3.5 Franz Diffusion Cell Studies of DNQX Delivery from Thermoresponsive Hydrogels Through the Bovine Synovial Membrane and Joint Capsule.

For membrane permeation studies, all-glass Franz Diffusion Cells were used with a diffusion area of 0.88cm^2 (1cm diameter). Synovial membrane sections (section 2.3.4) were mounted on the pre-greased flanges of the receptor compartment. The donor chamber was placed on top of the membrane and clamped in place. A micro-stirrer bar was added to the receptor compartment that was then filled with a receptor phase of 3ml PBS, equilibrated to 37°C, and capped. The Franz Diffusion Cells were placed on a multiple stirrer plate in a thermostatically controlled water bath set to 37°C for 15 minutes to allow temperature to reach equilibrium.

1ml of 2.5mM DNQX loaded thermoresponsive hydrogel (25% w/v Pluronic F-127, sections 2.3.1 and 2.3.3), was injected onto the synovial membrane in the Franz Diffusion Cell donor compartment in direct contact with the synovial membrane. The donor compartment was then sealed to prevent evaporation. At 15 minutes, 1, 2, 4, 6, 24 and 48 hours, the 3ml PBS receptor phase was removed and stored at -20°C and the extracted phase replaced with 3mls of fresh, temperature equilibrated (37°C), receptor phase (PBS). DNQX concentration in the receptor phase was measured by HPLC at each time point to quantify diffusion though the synovial membrane over 48 hours (section 2.4).

2.4 High Performance Liquid Chromatography

2.4.1 DNQX Quantification

Samples, stored at -20°C, obtained from PLGA nanoparticle (section 2.2.6) and thermoresponsive hydrogel release studies (section 2.3.3. and 2.3.5.) were thawed at room temperature and filtered through Sartorious™ Minisart™ 20μm syringe filters (Fisher Scientific, UK) into glass screwtop autosampler 1.5ml HPLC vials (Merck, Germany). HPLC analysis was performed using an Agilent series 1100 HPLC system (Agilent Technologies, Hewlett Packard, USA), at 276nm fitted with a Kinetex® C18, 100A, 5μm, 150x4.6mm

column (Phenomenex®, USA). Fixed elution was used involving 87.5% HPLC grade H_2O with 0.1% trifluoroacetic acid (TFA) and 12.5% HPLC grade acetonitrile with 0.1% TFA.
Each sample was run for 10 minutes to ensure sample retention time was reached (see Appendix Section 9.2.) and the peak area was quantified using the data analysis section of the Agilent series 1100 ChemStation Software in comparison to DNQX calibration curve (See Appendix section 9.1).

2.4.2 NBQX Quantification

Samples, stored at -20°C, obtained from PLGA nanoparticle (section 2.2.6) and thermoresponsive hydrogel release studies (section 2.3.3 and 2.3.5) were thawed at room temperature and filtered through Sartorious™ Minisart™ 20μm syringe filters (Fisher Scientific, UK) into glass screwtop autosampler 1.5ml HPLC vials (Merck, Germany). HLPC analysis was performed under the same conditions as with DNQX in section 2.4.1. However, each sample was only run for 7 minutes to ensure sample retention time was reached (see Appendix section 9.2) and the peak area was quantified using the data analysis section of the Agilent series 1100 ChemStation Software in comparison to NBQX calibration curve (See Appendix section 9.1).

2.5 2D Cell Culture

2.5.1 Y201 Mesenchymal Stem Cell Culture

Y201 MSCs are a stable human MSC cell line (kindly provided by Paul Genever (James et al., 2015, Kay et al., 2018)). Undifferentiated Y201 MSCs (used between passage 60-90 (Kay et al., 2018)) were removed from liquid nitrogen, thawed at room temperature, added to 10ml of pre-incubated (37°C, 5% CO_2) Y201 MSC maintenance culture media (DMEM, 10% FBS and 100U/ml Streptomycin-Penicillin) in a 50ml centrifuge vial and centrifuged for 5 minutes at 395g. The supernatant was removed, and the cell pellet gently resuspended in 5ml of Y201 culture media at 37°C. The cell suspension was added to a T225 culture flask containing 25ml of Y201 culture media at 37°C. Cells were incubated (37°C, 5% CO_2), media was changed every 2 days and cells split every 5 days at 90% confluency.

2.5.2 Primary Human Osteoblast Culture

Bone samples were obtained from TKR surgeries. Written, informed consent was obtained from participants prior to sample collection as per the Biomechanics and Bioengineering Research Centre Versus Arthritis Research Protocol, which has been reviewed and approved by the Health and Care Research Wales ethics committee, Wales REC 3, reference 10/MRE09/28, IRAS project number 51853. Samples were taken from two female patients aged 57 (patient ID number 2635) and 75 (patient ID number 2513) with TKRs performed on 11/10/2018 and the 04/04/2018 respectively. Bone processing and hOB isolation was performed by Carole Elford. 1cm diameter Bone cores were drilled from the tibial plateau, cut up as small as possible using a scalpel, then washed with 20ml PBS repeatedly (5 times) until only clean bone remained. Bone was then placed in a T75 culture flask in hOB culture media (αMEM, 10% FBS and 100U/ml Strept/pen). Flasks were left for 1 week to allow hOBs to grow from bone samples, media was refreshed every 3 days and hOBs isolated from bone cores were passaged at 90% confluency into fresh T75 flasks to separate cells from the processed bone. The original T75 flasks containing processed bone were cultured with fresh media and utilised as a source of fresh, passage 1, hOBs for multiple (up to 5) passages into fresh T75 flasks. hOBs were then used at passage 2 or 3 to prevent cells undergoing phenotypic and genotypic changes associated with senescence of primary human cells at high passage numbers (Hayflick, 1965).

2.5.3 Y201 MSC and hOB Mineralisation Assays

For mineralization assays, cells were cultured at 20,000 cells/well for hOBs and 16,000 cells/well for Y201s in 24 well plates with an osteogenic media (37°C, 5% CO_2). Y201 MSC osteogenic media consisted of DMEM, 10% FBS, Strept/Pen, 10mM β-glycerophosphate, 50μg/ml ascorbic acid and 10^{-7}M dexamethasone. hOB osteogenic media consisted of αMEM, 10%FBS, Strept/Pen, 2mM β-glycerophosphate, 50μg/ml ascorbic acid, and 10^{-7}M dexamethasone (Bonnet et al., 2015, Mason et al., 2018).

At 7 and 14 days following culture in osteogenic media, media was removed and stored at -20°C, and cells washed with 0.5ml PBS, fixed in 0.5ml of neutral buffered formalin (NBF) (15 minutes at room temp), washed with 0.5ml of dH_2O and stained with 0.3ml of alizarin red (5 minutes at room temperature). Stained cells were washed with 0.5ml of 50% ethanol 5 times to remove excess alizarin red, left to air dry (20 minutes at room temp) and photographed with a digital camera (Canon, UK) attached to an Eclipse TS100 light microscope (Nikon, UK) at 10x magnification. For quantification alizarin red staining, 0.5ml of cetylpyridinium chloride solution (10% w/v in dH_2O) was added per well, plates were sealed with autoclave tape and left for 12 hours at room temperature (approximately 20°C) to allow for the alizarin red affixed to cells to transfer into the cetylpyridinium chloride solution. 200µl aliquots were then taken from each well, transferred to a 96 well plate and absorbance read at 540nm in a FLUOstar OPTIMA plate reader (BMG Labtech).

2.6 3D Y201 MSC Culture for Mechanical Loading

2.6.1 3D Y201 MSC Culture for Loading

Recently Mason et al. has adapted their 3D bone model (Vazquez, 2013) to incorporate osteogenically differentiated Y201 cells (Gilbert et al., 2020).

2.6.2 Silicon Plate Preparation

Custom made 16 well silicone plates (Vazquez, 2013) were soaked for 24 hours in Chemgene disinfectant (StarLab, UK) then rinsed four times with an excess of distilled water (approximately 1l per rinse) and left to soak for a further 24hrs in distilled water, after which they were autoclaved. Each well in the silicone plates was coated with 500µl rat tail type I collagen (corning cat. No. 354236, 0.15mg/ml in 0.2N glacial acetic acid) and left in the tissue culture fume hood for 12 hours to allow collagen to adhere to plate surfaces. Excess coating collagen was removed and stored at 4°C for reuse up to 4 times. Coated plates were left to air dry in the tissue culture fume hood for 12 hours. Prepared plates were then ready for immediate use or were stored for up to one week at 4°C in sterile conditions.

2.6.3 Y201 MSC 3D Collagen Gels

Prior to gel preparation all solutions and reagents were placed on ice and pipette tips stored at 4°C for 12 hours, to reduce the risk of premature collagen setting. Rat tail tendon type I collagen (Sigma, Lot number SLBV2852), dissolved to 2.5mg/ml in 7mM glacial acetic acid was mixed with 5X MEM containing 11g/l sodium bicarbonate ($NaHCO_3$) at a 4:1 ratio to produce a 2mg/ml collagen solution.

The collagen mix was neutralized to pH 7.4 with a 1M tris(hydroxymethyl)aminomethane (Tris) base on ice. A 5µl aliquot of Tris base was pipetted into the collagen mix and gently mixed with a pipette tip. The collagen mix was then tested for pH test strips (pH range 6.0-7.7) (Merck, Germany) by pipetting 10µl directly onto the strip. This process was repeated until the desired pH (7.4) was achieved.

Y201 MSC Maintenance media (section 2.5.1) was removed from 90% confluent Y201 MSCs in T225 culture flasks, and cells washed with 10ml PBS, trypsinised with 1.5ml of TripleE express for 5 minutes at room temperature, resuspended in 10ml of Y201 MSC maintenance media per T225 flask and centrifuged at 395g for 5 minutes. Supernatant was removed and cell pellet was resuspended in 10ml of Y201 MSC maintenance media. To calculate cell number, 10ul of cell suspension was pipetted onto a hemacytometer and viewed at 10X magnification under an Eclipse TS100 light microscope (Nikon, UK). Cells were manually counted in each of 4, 4x4 grids and an average cell number generated. The cells calculated on the hemacytometer from the 10ul aliquot were multiplied by 10^5 to obtain the number of cells in the 10ml cell suspension.

The required amount of cell suspension ($0.125x10^6$ cells per 250µl gel) was centrifuged at 395g for 5 minutes, the supernatant removed, and cell pellet resuspended in cold maintenance media at a volume of less than 10% of the total volume required for gels.

This cell suspension was then gently added to the collagen mix on ice, and pipette mixed ensuring that no bubbles were created. 250μl of the cell/gel suspension was then added to each coated well of the silicon plate and incubated at 37°C at 5% CO_2 for 1 hour to allow the gels to set. Y201 maintenance media (section 2.5.1.; 800μl/well) was then added and cells incubated for 24 hours at 37°C at 5% CO_2.

2.6.4 Y201 3D Collagen Gel Loading

Following incubation for 24 hours in Y201 maintenance media (section 2.5.1), media was replaced with 800μl per well of Y201 osteogenic media (section 2.5.3). Media was replaced every 3 days and gels loaded after 7 days treatment with osteogenic media. 48 hours prior to loading, 3D cultures in silicone plates were transferred to the incubator (37°C at 5% CO_2) located within the mechanical loading laboratory and media changed 24 hours before loading. 1 hour prior to loading, media was removed and stored at -20°C (t=-1hr) and 200μM NBQX in dH_2O or dH_2O vehicle controls added to fresh osteogenic media to a final volume of 800μL. An hour following this (t=0), silicone plates were either unloaded or subjected to physiological (500μstrain) and pathophysiological (5000μstrain) loads via a displacement of 0.07mm and 0.7mm respectively (Mason personal communication) for 5 minutes at 10Hz using a Bose ElectroForce® 3200 instrument (Kent, UK), controlled with WinTest® Software 4.1 with TuneIQ control optimization (BOSE). Media was removed 1hr and 24hrs post loading, split into 200μl aliquots and stored at -20°C for LDH (section 2.12.1.), Nitrite (section 2.11.) and ELISA (section 2.10.) analysis. Gels were prepared for imaging (section 2.8.) or mRNA extraction for qRT-PCR gene expression analysis (section 2.9.). The silicon plate layout for this study can be found in Appendix section 9.4.1.

2.7 3D Y201 Culture for IL-6 and Soluble IL-6 Receptor (sIL-6r) Treatment Unencapsulated vs Sustained NBQX Treatment

The 3D rat tail type 1 collagen gel culture model was used in plastic plates to study the impact of an inflammatory stimulus on osteogenically differentiated Y201 MSCs and to develop understanding of how both short term (1hr) and sustained (PLGA nanoparticle)

NBQX delivery might modulate inflammatory response. IL-6 and its soluble receptor (sIL-6r) were used as inflammatory stimuli at concentrations found present in human synovial fluid following joint injury or with developed OA (Kotake et al., 1996, Higuchi et al., 2006, Swärd et al., 2012, Watt et al., 2016) and utilised in previous inflammatory cell culture studies (Bakker et al., 2014, Wu et al., 2017).

2.7.1 Plastic Plate Preparation and Y201 MSC 3D Collagen Gel Preparation

48 well plastic cell culture plates were used with identical well volume to those of the silicone plates used in the Y201 MSC loading study. Collagen plate coating and Y201 3D collagen gel preparation was identical to that carried out in sections 2.6.2 and 2.6.3 with the only difference being the use of 48 well plastic cell culture plates in the place of silicone plates.

2.7.2 Il-6 and IL-6 Soluble Receptor Treatment

Following 24 hours incubation of 3D cultures in Y201 MSC maintenance media (section 2.5.1.; 37°C, 5% CO_2), media was replaced with Y201 MSC osteogenic media (section 2.5.3) at 800µl per well and cells were cultured for 7 days with media changes every 3 days. For plate experimental layout see Appendix section 9.4.2. After 7 days, the media was removed and replaced with 800µl Y201 osteogenic media containing IL-6 (5ng/ml) and sIL-6r (40ng/ml) in all but the control wells (Kotake et al., 1996, Bakker et al., 2014, Watt et al., 2016). After 1-hour, free NBQX was added to both 'NBQX' and 'NBQX+Nanoparticle' wells to a final concentration of 200µM. After 1 hour of NBQX treatment, all media was replaced with 800µl fresh Y201 MSC osteogenic media incorporating IL-6/sIL-6r as before, except for controls, which had no IL-6/sIL-6r. In addition, NBQX loaded PLGA nanoparticles (section 2.2.1.2) were added at 10mg/ml to the 'NBQX+Nanoparticle' wells. At 24 and 72 hours, media was removed and stored in 200µl aliquots at -20°C for LDH (section 2.12.1), nitrite (section 2.11) and ELISA (section 2.10) analysis. Gels were removed and RNA extracted for qRT-PCR gene expression analysis (section 2.9) or cryosectioning and fluorescent imaging (section 2.8). The plate layout for this study can be found in Appendix section 9.4.2.

This treatment regime allowed for comparison between short term NBQX treatment (1 hour) and sustained NBQX application through PLGA nanoparticle delivery on the impact of an inflammatory stimulus to osteogenically differentiated Y201 MSCs. The addition of 200μM of free NBQX for 1 hour prior to the application of NBQX loaded PLGA nanoparticles in the sustained group was to mimic the effect of free drug clearance that occurs *in vivo* within the joint space.

2.8 Fluorescent Imaging Cells from 3D Collagen Type I Gels

2.8.1 Gel Extraction and Infiltration

3D cells in rat tail type I collagen gels (sections 2.6 and 2.7) were lifted from silicone wells using a sterilized spatula. Following which, gels were washed once with 1ml PBS and fixed in 500μl of paraformaldehyde (diluted in 1X PBS from 8% paraformaldehyde stock stored in -20°C) and incubated at 4°C for 30 minutes. Paraformaldehyde was removed, gels washed twice in 1mls PBS, incubated in 500μl of PBS overnight at 4°C and then infiltrated with a 1:1 mix of OCT compound and stored at 4°C ready for sectioning.

2.8.2 Cryosectioning

Following infiltration with OCT (section 2.8.1), gels were cut in half using a scalpel (Figure 2.3A). Plastic gel section containers were half filled with OCT and semi-circular gels were added in an orientation that ensured the planar section of the gel lay parallel to the sectioning blade of the cryostat once mounted to the cryostat chuck (Figure 2.3B) (Adapted from Vasquez (2013)).

Once orientated correctly, the plastic gel section containers were filled with OCT and OCT-gels were frozen over isopropanol that was chilled over dry ice. At this stage, frozen OCT-gel blocks were either immediately transferred to the OTF5000 cryostat (Bright instruments) for sectioning or stored at -20°C for future sectioning.

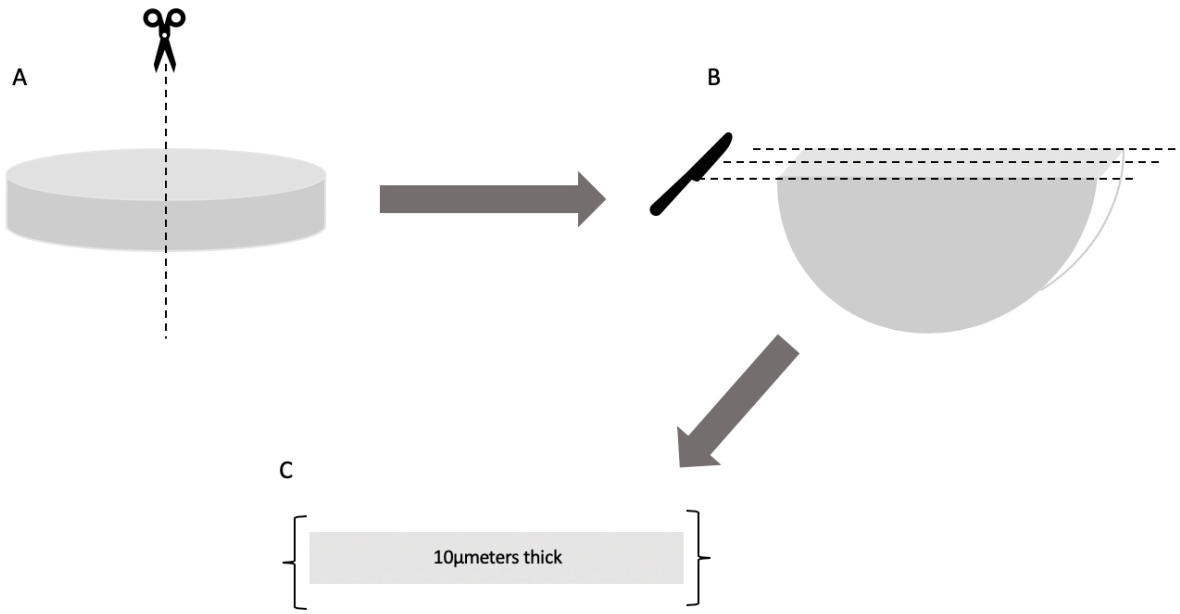

Figure 2.3: A diagrammatic representation of the sectioning process for 3D collagen gels containing Y201 MSCs. A) gels sliced in half prior to freezing and sectioning; B) gels were orientated to ensure cryosectioning along the planar surface of the gel; C) 10µm thickness sections were sliced from the gels (image designed by Author).

To proceed with cryosectioning, frozen OCT-gel blocks were mounted onto cryostat chucks in an orientation that ensured gels were sectioned along the flat surface of the semi-circle (Figure 2.3B). A small amount of OCT was dispensed onto the chuck and the OCT-gel block was affixed by freezing in contact with the OCT on the chuck when placed onto the 'specimen' shelf of the OTF5000 Cryostat (Bright instruments). This was set to a working temperature of -21°C. Once frozen, chucks with attached gels were placed into the cryostat and fixed in place in an orientation that ensured the sectioning blade cut through the gel as depicted in Figure 2.3B. To ensure samples remained frozen, cryosectioning was only carried out when the 'chamber temp' was below -20°C, and this temperature was monitored throughout. Initially, the cryostat was set to take 20µm sections. These were placed on SuperFrost® Plus Section slides (Thermo Scientific, UK) and were checked for the presence of Y201 MSCs cultured in the 3D collagen gels using an Eclipse TS100 light microscope

(Nikon, UK) at 10x magnification. Once cells/gels were visually detected, the cryostat was set to take 10μm sections (Figure 2.3C). 3 sections were affixed per slide and 10 slides were taken per gel. For each specific morphology 3 slides were stained per gel (section 2.8.3). Slides were then stored at -20°C ready for staining. Any remaining gel was removed from the chuck using a scalpel and stored at -20°C for future sectioning.

2.8.3 Phalloidin Staining

CytoPainter Phalloidin-iFluor 488 Reagent (Abcam, UK) is a phalloidin conjugate that selectively binds to actin filaments (F-actin). The iFluor 488 dye can be detected with a fluorescent microscope at Excitation wavelength/Emission wavelength=493/517nm. Actin participates in many cell processes such as cell division and motility. Staining for actin is useful in determining cell shape of osteocytes (Vazquez et al., 2014).

Phalloidin-iFluor conjugate staining was carried out according to manufacturer's protocol. Slides (section 2.8.2.) were removed from -20°C and allowed to equilibrate to room temperature then hydrated with 2ml of PBS per section. PBS was aspirated off and sections treated with 0.1% Triton X-100 in PBS for 5 minutes to permeabilise cells. Sections were then washed 3 times with PBS and treated with 100μl of 1X phalloidin conjugate (1μl per 1ml of PBS + 1% BSA) per section. Sections were left to stain for 60 minutes at room temperature whilst protected from light. Excess stain was removed by washing sections 3 times with an excess volume of PBS (approximately 5ml/section), then removing excess PBS and mounting in a Vectashield® mounting medium containing DAPI (approx. 1ml/ coverslip inverted and placed on stained sections). Stained sections were then immediately taken for fluorescent imaging.

2.8.4 Fluorescent Imaging

Stained sections (section 2.8.3) and microfluidically synthesised PLGA nanoparticles (section 2.2.1.1) were imaged using an Olympus BX61 upright fluorescent microscope. Images were processed using AnalySIS software (Vazquez et al., 2014) and were taken with autoexposure

parameters to obtain the maximum dynamic range. Within the BX61 microscope were three fluorescent filter set options. U/MNU2 filter set allowed ultraviolet excitation and a broad emission range (Ex360-37010nm, Em420nm (long pass), Dichroic mirror 400nm (long pass)).This is used for observation of DAPI staining (nuclear staining) (Olympus, 2020). U/MNIB2 filter set is used for 'GREEN' probes, such as FITC and iFluor-488, with Ex470-490nm, Em510nm (long pass) and dichroic mirror 505nm (long pass) (Olympus, 2020). Finally, U/MNG2 filter set was used for 'RED' probes, such as Alexa 594, with an Ex530-550nm, Em590nm (long pass) and dichroic mirror 570nm (long pass)(Olympus, 2020).

To visualise the phalloidin-iFluor-488 stained sections, images were taken with the U/MNU2 filter set to identify cellular nuclei and the U/MNIB2 filter set to Identify iFluor-488 stained actin. Having identified cells for imaging, the 'Acquire' function on the Analysis software was used to optimise exposure time and capture an image of sections with both the U/MNU2 and U/MNIB2 filters. Each image was assigned a colour (blue for DAPI staining, green for phalloidin staining). The 'create composite image' function merged the two images to produce a single image containing both the green actin (phalloidin) stain and the blue nuclear (DAPI) stain. Scale bars were then added to each image.

To visualise micro fluidically synthesised PLGA 'nanoparticles', images were taken at 20X magnification. If easily identifiable using the magnification available on this fluorescent microscope then particles are unlikely to be within the nanoscale range. As no nuclei are present within the PLGA particles, fluorescent microscopy was used primarily as a means of identifying large particle agglomerates indicated in the DLS analysis of microfluidically synthesised PLGA nanoparticles.

2.9 Gene Expression Analysis

2.9.1 RNA Extraction from 3D Gels

Total Y201 RNA was extracted from 3D gels using TRIzol reagent according to the manufacturer's protocol (Thermofisher, UK). 500μl of TRIzol reagent was added to each gel,

pipetted repeatedly to dissolve the gels and lyse the cells, and TRIzol suspension stored at -80°C until RNA was extracted.

For RNA extraction, samples were thawed on ice and 0.1ml of chloroform added. They were then incubated at room temperature for 2-3 minutes, and centrifuged at 12,000g for 15 minutes at 4°C. The aqueous upper phase containing the RNA was transferred to a fresh DNAse/RNAse free centrifuge tube and 0.25ml of isopropanol added to precipitate the RNA at room temperature for 10 minutes. After centrifugation for 10 minutes (12,000g, 4°C), RNA pellets were washed with 0.5ml of 75% ethanol (cooled to 4°C) then centrifuged at 7500g for 5 minutes at 4°C. Supernatant was then carefully discarded and pellets left to dry in a fume hood for 15 minutes or until no liquid was visible with the naked eye. Dried pellets were resuspended in 40μl RNase free water and then incubated at 55°C for 15 minutes to solubilize the RNA ready for downstream applications.

2.9.2 DNAse Treatment of Isolated RNA

RNA (section 2.9.1) was DNase treated to remove any DNA contamination using a DNA-free™ kit (Thermofisher, UK) following manufacturer's instructions. 0.1 volume of 10X DNase I Buffer and 1μl of recombinant DNase I were added to each RNA sample, mixed gently and incubated at 37°C for 30 minutes. Following incubation, 0.1 volume of DNase inactivation reagent was mixed into the RNA suspension and incubated for 2 minutes at room temperature. Samples were then centrifuged for 1.5 minutes at 10,000g and RNA transferred to a fresh tube for estimation of RNA concentration and purity.

2.9.3 RNA Concentration and Purity

Total RNA was quantified using a NanoDrop 2000 with Nanodrop 2000/2000c software (Thermo scientific, UK). All measurements were compared with a blank of DEPC treated RNAse free water. 1μl of RNA was pipetted onto the receiver. RNA concentration was displayed as μg/μl. RNA purity was indicated by the 260nm/230nm (A_{260}/A_{230}) absorbance ratio for the presence of phenol, salts and carbohydrates and the 260nm/280nm (A_{260}/A_{280})

absorbance ratio for the presence of protein contamination. Samples with A_{260}/A_{230} and A_{260}/A_{280} approximately 2 were deemed good quality. Samples were excluded below a value of 1.8.

2.9.4 Reverse Transcription

Total RNA was reverse transcribed to complementary DNA (cDNA) using a SuperScript® IV reverse transcriptase kit according to the manufacturer's protocol (Thermofisher). Total RNA (150ng) was combined with DEPC-treated (DNAse and RNAse free) water to a volume of 11.9µl. Following which, 0.1µl of 500ng/µl of random hexamers and a 1µl of 10mM dNTP mix was added. This 13µl RNA-primer mix was heated at 60°C for 5 minutes then incubated on ice for 1 minute to anneal to the primers. A 7µl reverse transcriptase (RT) reaction mix was prepared per sample, comprising 4µl of vortexed 5X SuperScript® IV Buffer, 1µl 100mM dithiothreitol, 1µl Ribonuclease Inhibitor and 1µl SuperScript® IV Reverse Transcriptase (200U/µl). This RT mix was then added to the annealed RNA samples, resulting in a total reaction volume of 20µl. The reverse transcription reaction was then carried out (23°C for 10 minutes, 52.5°C for 10 minutes and 80°C for 10 minutes) and held at 4°C using a Prime TC-312 thermal cycler (Techne, Cambridge, UK). cDNA was then stored at -20°C.

2.9.5 Quantitative PCR (qPCR)

Platinum® SYBR® Green qPCR SuperMix-UDG (ThermoFisher) was used to carry out all qPCR reactions. The fluorescent signal emitted by the dye increases in proportion to double stranded DNA accumulating during PCR amplification (Promega, 2020). The increase threshold was automatically set as the midpoint of the logarithmic phase of the amplification curve. Consequently, a cycle threshold value (Ct), corresponding to the point at which the fluorescence crosses the threshold, was generated as sample cDNA was run (Bustin et al., 2009, Vazquez, 2013). The Platinum SYBR Green SuperMix contained Magnesium Chloride at a final concentration of 3mM, which was the concentration then used in all RT-qPCR reactions.

qPCR was carried out on a Stratagene Mx3000P cycler and amplifications monitored using MxPro RT-qPCR software (Agilent Technologies). Polypropylene RT-qPCR plates were used with optical strip caps (Applied Biosystems, ThermoFisher UK) and amplification reactions were carried out in a reaction volume of 20μl. Before each amplification, a master mix was made up containing, per sample: 10μl of Platinum® SYBR® Green qPCR SuperMix-UDG; 0.2μl of 10μM forward primer and 0.2μl of 10μM reverse primer and 8.6μL of DEPC-treated DNase and RNase free water. This makes up a master mix volume of 19μl per sample to which 1μl of cDNA was added to provide the final reaction volume of 20μl. Thermocycling was then carried out, consisting of an initial denaturation step for 10 minutes at 95°C followed by 40x cycles of 95°C for 30 seconds (denaturation), 60°C for 30 seconds (annealing) and 72°C for 30 seconds (extension). The cycle was then finalised with a dissociation cycle at 95°C for 1 minute, 55°C for 1 minute and 95°C for 30 seconds before holding at 4°C. The results from the thermocycler were stored and analysed using MxPro RT-qPCR software (Agilent Technologies, USA). Melting curves generated for genes from loading studies (section 2.6) and IL-6/sIL-6r inflammatory studies (section 2.7) are displayed in Appendix section 9.3.2.

2.9.5.1 cDNA Standard Curves

To assess the linear range and efficiency of detection for all primers and allow for optimisation of reaction conditions, cDNA standard curves were performed using stock Y201 cDNA from 3D collagen cell culture (500ng reverse transcribed). cDNA was serially diluted 1:10 with DEPC treated water to give a concentration range from 10^1 (stock) to $1x10^{-8}$. Each standard curve was performed with Platinum® SYBR® Green qPCR SuperMix-UDG ($MgCl_2$ 3mM) and 0.1μM forward and reverse primer concentration. For standard curves to be considered successful, an R^2 value $\geq$0.99 and an efficiency of 90-110% were required (Bustin et al., 2009). cDNA standard curves generated by the MxPro RT-qPCR software for gene expression identified from RNA extracted in cell culture experiments can be found in Appendix section 9.3.3.

2.9.5.2 Reference Genes

Reference genes act as internal controls for performing qRT-PCR. An optimal reference gene would have consistent stable expression levels regardless of experimental intervention or design and be universally recognised. However, several studies have reported variation of reference gene expression levels (Bemeur et al., 2004, Chi et al., 2012, Powell et al., 2014, Jo et al., 2019).

Therefore, to ensure stable reference genes were selected for each experiment, qRT-PCR was carried out on several candidate reference genes on all samples across each experiment (*18s, ywhaz, eef2* and *rpl13a*). The most stable combination of reference genes was then determined using RefFinder software (https://www.heartcure.com.au/for-researchers/; (Xie et al., 2012)). This software utilises outputs from multiple gene stability algorithms to determine the most stable reference genes or the combination of reference genes for use in each experiment in the form of a recommended comprehensive ranking. The most stable genes were assigned the lowest numerical value and the least stable the highest.

Algorithms compared within RefFinder were: BestKeeper (Pfaffl et al., 2004); NormFinder (Andersen et al., 2004); geNorm (Vandesompele et al., 2002); and the comparative delta Ct method (Silver et al., 2006). These mathematical algorithms calculate best reference gene or reference gene combination for an individual experimental design by ranking reference genes according to expression stability.

Using geNorm software for each experiment (loading and IL-6 inflammatory) described in sections 2.6 and 2.7, the most stable reference gene or reference gene combination, as calculated by determining the geometric mean of the two most stable reference genes, is stated in the Appendix (section 9.3.1).

2.9.5.3 Relative RT-qPCR

Quantifying, via the relative quantification method, requires normalising the expression of a gene of interest to the stable reference gene (as section 2.9.5.2) within that specific sample and then calibrating this expression to a reference sample (commonly an untreated control).

Within the experimental chapters of this thesis the reference group used as a calibrator is clearly stated in the methods. The $2^{(-\Delta\Delta Ct)}$ method (Livak and Schmittgen, 2001) was utilised to quantify relative expression of genes of interest from RT-qPCR reactions. Selected stable reference gene Ct values were subtracted from their corresponding gene of interest Ct value delivering a normalised value known as delta Ct (ΔCt). The ΔCt for each experimental sample was then taken away from the ΔCt of the selected Calibrator (e.g. negative control samples) resulting in a delta-delta Ct value ($\Delta\Delta$Ct). These Experimental $\Delta\Delta$Ct values are now expressed relative to the calibrator. To conclude this process, all $\Delta\Delta$Ct values were converted to Relative Expression Units by making the negative of the $\Delta\Delta$Ct values an exponent of 2 ($2^{(-\Delta\Delta Ct)}$).

2.9.5.3.1 Primer Design

Primers sequences were designed for known human gene sequences using the National Centre for Biotechnology Information (NCBI) website Primer-BLAST toolkit (https://www.ncbi.nlm.nih.gov/tools/primer-blast/) to deliver 100% sequence homology and span an intron. Primer-BLAST uses the Primer3 programme (https://sourceforge.net/projects/primer3/) to design primers. The Basic Alignment Search Tool (BLAST) ensures similar reaction melting temperatures (T_m), GC% content, while avoiding non-specific gene amplifications, minimising the risk of primer-dimer formations and excluding 3' end complementation. Table 2.3 contains primer sequences, accession numbers where available, amplicon size, melting temperature and source. Regarding primer source, where available primers were provided by colleagues, Dr Sophie Gilbert, Dr Cleo Bonnet (Cardiff University, School of Bioscience) and Carole Elford (Cardiff University School of Medicine and Cardiff University School of Bioscience), *eaat-1* and *eaat-3* Primer sequences were obtained from Dr Karen Brakespear's thesis (Brakspear, 2011). Primers were synthesised and purchased from Eurofins Genomics, Germany.

Table 2.3: Primer details for reference genes (18s, ywhaz, eef2 and rpl13a), bone markers (opg, rankl, dmp-1, sost, ocn, col-1a1), inflammatory markers (il-6 and tnfα) and glutamate signalling components (grik-1, gria-1, eaat-1 and eaat-3).

Gene	Primers (5'-3')	Amplicon size (bp)	T_m (°C)	Intron spanning	Source / Reference
***18s* Ribosomal RNA** NR_146119	Fwd: GCAATTATTCCCCATGAACG Rev: GGCCTCACTAAACCATCCAA	123	58	No	Dr. Sophie Gilbert (Frye et al., 2005)
Ywhaz NM_001135701	Fwd: AACTTGACATTGTGGACATC Rev: AAAACTATTTGTGGGACAGC	152	55	No	Dr. Sophie Gilbert
eef2 NM_001961.4	Fwd: GTGGTGGTGGACTGTGTGTC Rev: CGCTGGAAGGTCTGGTAGAG	161	61	No	Dr. Sophie Gilbert
rpl13a NM_012423.4	Fwd: GGATGGTGGTTCCTGCTG Rev: TGGTACTTCCAGCCAACCTC	100	60	No	Carole Elford (Scully, 2015)
rankl NM_003701	Fwd: CAGAAGATGGCACTCACTGCA Rev: CACCATCGCTTTCTCTGCTCT	203	60	No	Carole Elford (Boukhechba et al., 2009)
opg NM_002546.4	Fwd: GAGATAGAGTTCTGCTTGAAACA Rev: CCATCTGGACATCTTTTGCAAA	104	58	No	Carole Elford
alp NM_000478.3	Fwd: GTACGAGCTGAACAGGAACAACG Rev: CTTGGCTTTTCCTTCATGGTG	151	62	No	Carole Elford (Boukhechba et al., 2009)
dmp-1 NM_004407.4	Fwd: AGCATCCTGCTCATGTTCCTTT Rev: GAGCCAAATGACCCTTCCATT	106	61	No	Carole Elford (Boukhechba et al., 2009, Scully, 2015)
sost NM_025237.3	Fwd: AGAGTACCCCGAGCCTCC Rev: AGCTGTACTCGGACACGTCTTTG	116	63	No	Carole Elford (Boukhechba et al., 2009, Scully, 2015)
ocn NM_199173.6	Fwd: CTTTGTGTCCAAGCAGGAGG Rev: CTGAAAGCCGATGTGGTCAG	166	59	No	Carole Elford
col-1a1 NM_000088.4	Fwd: CTCCTGACGCACGGCC Rev: CCGTTCTGTACGCAGGTGATT	80	61	No	Carole Elford (Boukhechba et al., 2009)
tnfα NM_000594.4	Fwd: CTCTTCTGCCTGCTGCACTTTG Rev: ATGGGCTACAGGCTTGTCACTC	135	63	No	Dr. Sophie Gilbert. Designed by Origene http://www.origene.com/catalog/
il-6 NM_000600.5	Fwd: AGACAGCCACTCACCTCTTCAG Rev: TTCTGCCAGTGCCTCTTTGCTG	132	64	No	Dr. Sophie Gilbert. Designed by Origene http://www.origene.com/catalog/

***grik-1* (Kainate)** NM_000830.1	Fwd: CATTGCCTCGCACCGGGCAT Rev: GTCAAGCCATCCCACCGGGC	123	70	No	Dr. Cleo Bonnet (unpublished)
***gria-1* (AMPA)** NM_001364167.2	Fwd: ACACCCAAGGGGTCTGCCCT Rev: CGTACCACCATTTGCTTTTCAGCTTGT	100	66	No	Dr. Cleo Bonnet (unpublished)
***eaat-1* (+1ex9skip)** NM_004172.5	Fwd: ACCGCTGTCATTGTGGGTA Rev: GTTCCCCAGGAAAGGAGAAG	94	59	No	Dr. Karen Brakspear (Brakspear, 2011)
eaat-3 NM_004170.6	Fwd: AATTCTACTTTGCTTTTCCTGGAG Rev: CCAGTGCAGCAACACCTGTA	102	61	No	Dr. Karen Brakspear (Brakspear, 2011)

2.10 Immunoassays: Multiplex Electrochemiluminescence and Enzyme Linked Immunosorbent Assays

A multiplex electrochemiluminescence (ECL) kit and single-plex ELISAs were utilised to measure levels of several protein biomarkers the relevance of which to bone signalling is described in the introduction Table 1.1.

Multiplex ECLs were carried out in the Central Biotechnological Services (Cardiff University), with the guidance of Dr. Ann Kift-Morgan utilising a Mesoscale discovery (MSD) plate reader (Meso Scale Diagnostics, Maryland, USA) to determine chemiluminescence measurements. For all ELISA and ECL studies aliquoted media samples from both 3D Y201 MSC loading studies (section 2.6) and 3D IL-6/sIL-6r studies (section 2.7) were centrifuged to remove cells, frozen 1x and thawed for analysis to avoid analyte concentration variability due to repeat freeze-thaw cycles. Once thawed, media samples were vortexed briefly before commencement of the ELISA/ECL. Table 2.4 summarises the immunoassays utilised and the ranges of detection.

Table 2.4: Immunoassay details and standard curve detection ranges.

Biomarker	**Immunoassay**	**Assay kit name**	**Assay kit source**	**Standard curve lower limit of quantification (LLOQ) and upper limit of quantification (ULOQ)**
INF-γ				1.76-938 pg/ml

IL-10	ECL	U-Plex Pro-inflam Combo 1 Human	K15049 MSD	0.298-233 pg/ml
IL-12p70				1.22-315 pg/ml
IL-13				4.12-353 pg/ml
IL-1β				0.646-375 pg/ml
IL-2				0.890-938 pg/ml
IL-4				0.218-158 pg/ml
IL-6				0.633-488 pg/ml
IL-8				0.591-375 pg/ml
TNFα				0.690-248 pg/ml
Glutamate	ELISA	Human Glutamate ELISA kit	KA 1909 Abnova	0.6-60 μg/ml
SOST	ELISA	Human SOST Quantikine® ELISA kit	DSST00 RandD Systems® (Biotechne®)	31.3-2000 pg/ml
OPG	ELISA	Human OPG ELISA kit	RDR-OPG-Hu 2bScientific	0.156-10ng/ml

All Assays were run on a 96 well plate layout with standards run in duplicate. Where possible, samples were run in duplicate. For all ELISA kits a dilution range experiment was run prior to the full assay to determine if the media required dilution to fit within the standard curve. Samples were left undiluted and diluted 1:2, 1:4 and 1:8 and compared against standards 1, 4 and 7 of the standard curve range along with a blank control. Plate layouts for ELISAs and ECL assays can be found in the Appendix (section 9.5).

2.10.1 Biomarker Concentration Calculation

Standards were used within the same microplate as the test media to generate a standard curve of absorbance readings compared to known analyte concentrations. 5-parameter logistic regression curve fitting with interpolation was then used to determine the exact

concentration of analytes within the experimental media. The equation for 5PL regression is:

$$F(x) = d + \frac{a - d}{(1 + (\frac{x}{c})^b)^g}$$

5-parameter logistic regression can be applied to determine the equation of non-linear, asymmetrical sigmoidal curves, where *a* is the minimum asymptote (the value at 0 standard concentration), *b* is the slope of the curve, *c* is the inflection point, *d* is the maximum asymptote (value for infinite standard concentration) and *g* is the asymmetry factor (Khatib, 2018). Upon quantification of analytes within the experimental media, ELISA and ECL datasheets provided recommended maximum and minimum ranges of detection within the range of the standard curve. Samples exceeding this range were only utilised if the coefficient of variance between duplicate wells fell below 20% (Khatib, 2018) and samples were still within the lowest/highest standard. Samples with readings completely outside of the range of the standard curve were not used in analysis. For ELISAs, a test calibration assay was carried out to optimise dilutions of media to detect analytes within the linear range of the standard curve. Dilution tests were not possible with the ECL multiplex assays due to the reaction required to read signals.

Having established the optimal sample dilution and following interpolation from 5-parameter logistic regression, quantified concentrations were multiplied by their dilution factor to obtain the true analyte concentration. Following dilution tests, ELISAs for glutamate and OPG required media to be diluted 1:2 to ensure reliable analyte quantification, whereas SOST was undiluted.

2.10.2 ELISAs

ELISA kits were used to quantify Y201 cell culture media levels of glutamate, SOST and OPG (Table 2.4) from the cell loading (section 2.6) and IL-6/sIL-6r inflammatory studies (section 2.7). Each of these test kits came with 96 detachable wells. Prior to the testing of experimental samples one column of wells (8 wells) were used to optimise the dilutions required to fit outputs within the standard curve for each ELISA (Table 2.4).

2.10.2.1 Glutamate

The glutamate ELISA contained an extraction and derivatisation step prior to the quantitative determination of glutamate via competitive sandwich ELISA. The derivatisation step is the chemical transformation of glutamate into a derivative product to increase detectability and stability. The protocol was followed according to manufacturer's instructions. The solid phase of the 96 well microtiter plate had the glutamate bound to it. This competed for antibody binding sites with the derivatized samples, standards and controls. Once the system reached equilibrium, free antigen and antigen-antibody complexes were washed off. The solid phase bound antibody was detected by an anti-rabbit IgG-peroxidase conjugate with tetramethylbenzidine (TMB) as a substrate. A stop solution halted the reaction causing the solution to turn from blue to yellow. This was monitored at an absorbance of 450nm on a FLOUstar® OPTIMA plate reader (BMG Labtech, UK). Unknown sample quantification was then achieved by comparison with a standard curve (section 2.10.1).

2.10.2.2 SOST

The SOST ELISA was a quantitative sandwich enzyme immunoassay. The ELISA procedure was carried out according to manufacturer's instructions. A human specific SOST monoclonal antibody was precoated on a 96 well microplate. Standards and samples were pipetted onto wells and SOST binds to the coating antibody. Unbound substance was then washed off and the solid phase bound antibody detected by a SOST specific enzyme-linked (horseradish peroxidase) polyclonal antibody with TMB as a substrate. A stop solution halted the reaction causing the solution to turn from blue to yellow. This was monitored at an absorbance of 450nm on a FLOUstar® OPTIMA plate reader (BMG Labtech, UK). Unknown sample quantification was then achieved by comparison with a standard curve (section 2.10.1).

2.10.2.3 OPG

The quantitative OPG sandwich ELISA was carried out according to manufacturer's instructions. The microtiter plate with this kit was precoated with an OPG specific antibody. Samples and standards were then added to appropriate microtiter plate wells with a biotin conjugated OPG specific antibody preparation. Any unbound biotin-conjugate antibody was washed off. Following this, Avidin conjugated to horseradish peroxidase was added with TMB as a substrate. A stop solution halted the reaction causing the solution to turn from blue to yellow. This was monitored at an absorbance of 450nm on a FLOUstar® OPTIMA plate reader (BMG Labtech, UK). Unknown sample quantification was then achieved by comparison with a standard curve (section 2.10.1). Following dilution standard testing, it was determined that media samples required a 1:2 dilution to ensure OPG levels fitted within the range of the standard curve.

2.10.3 Electrochemiluminescence Assays

MSD (Meso scale Diagnostics, USA) was developed to facilitate the execution of multiplex ECL assays for the detection of multiple proteins simultaneously within one sample. Compared to ELISAs and other immunoassay types, MSD multiplex ECLs typically exhibit broader detection ranges and higher sensitivity (V-PLEX White paper, MSD). For the purposes of this thesis, a V-plex MSD assay for the detection of inflammatory mediators in the form of a 10-plex inflammatory combo kit (IFN-γ, IL-10, IL-12p70, IL-13, IL-1β, IL-2, IL-4, IL-6, IL-8, TNF-α) was utilized (Table 2.4).

MSD microplates were read using a Sector Imager 6000 MSD plate reader and analysed with Discovery Workbench v3 (Meso Scale Discovery, USA). The principal of MSD assays is utilising high binding affinity carbon electrodes attached to the bottom of multiplot plates. Attached to these plates were the antibodies of choice in combination with ECL labels linked with detection antibodies. The MSD plate reader then applied electricity to the plate electrodes inducing light emission by ECL labels. The light emission was then quantified by a photometer. The MSD Workbench software generated an automatic standard curve using 5-parameter logistic regression and generated absolute concentrations after having adjusted for dilutions using built in algorithms.

2.10.3.1 Pro-inflammatory Multiplex (MSD)

For the MSD proinflammatory-1 10-plex kit, the assay procedure was followed according to manufacturer's instructions. It was not possible to carry out dilution tests with the MSD kit as the fixed 96 well plate could only face plate reader exposure once. Media samples were, therefore, prediluted at 1:2 ratio, in accordance with glutamate and OPG ELISA dilution experiments (section 2.10.2.1 and 2.10.2.3), in order to maximise the chance of obtaining results within the range of the standard curves. Media samples from the IL-6/sIL-6r inflammatory study (section 2.7) and the pathophysiologically loaded Y201 MSCs from the cell loading study (section 2.6) were assayed according to the plate layout in Appendix section 9.5.

2.11 Griess Assay

A Griess Reagent System assay (Promega) was utilised to quantify the levels of nitrite (NO_2-) released into cell culture media from osteogenically differentiated Y201 MSCs cultured in 3D. This followed exposure to loading and treatment with free NBQX (section 2.6) and followed exposure to IL-6/sIL-6r and treatment with either free NBQX or NBQX encapsulated in PLGA nanoparticles (section 2.7). Nitrite is a stable product formed from the breakdown of NO a messenger molecule found in multiple biological systems. The protocol was followed according to manufacturer's instructions with plate layouts shown in Appendix section 9.5.1 using a nitrite standard curve made up in the same media used in experiments (Appendix section 9.1).

To prepare the nitrite standard curve, 100μl of 100μM of nitrite solution suspended in osteogenic Y201 MSC culture media (section 2.5.1.) was pipetted in triplicate to the top row (row A) of a 96 well plate. 50μl of blank osteogenic Y201 MSC culture media was then added to the remaining 7 rows (rows B-H) of the standard column (Appendix section 9.5.1), 6 two-fold serial dilutions (50μl/well) were performed to generate a standard curve (100, 50, 25, 12.5, 6.25, 3.13, 1.56μM). The final row of wells (row H) was left with 50μl blank media (0μM). 50μl of experimental sample media was added to each plate (Appendix section 9.5).

50µl of Sulfanilamide solution (1% sulphanilamide in 5% phosphoric acid) was added to all samples and incubated for 7.5 minutes at room temperature and protected from light. 50µl of NED (0.1% N-1-napthylethylenediamine dihydrochloride in water) solution was then added and incubated for 7.5 minutes at room temperature and protected from light. Absorbance was measured immediately using a 96 well FLUOstar® OPTIMA (BMG Labtech, UK) plate reader with a filter set at 540nm. The absorbance values of each experimental sample were quantified as a concentration by comparison with the standard curve plotted from each experiment (Appendix, section 9.1).

2.12 Toxicity/Cell Viability Assays

2.12.1 Lactate Dehydrogenase Assays

LDH is a stable enzyme released from most cell types following cell wall rupture. LDH is quantified in cell culture media to assess the level of plasma membrane damage and is a common cytotoxicity marker.

Media samples aliquoted from 2D mineralization assays (section 2.5.3.), 3D Y201 MSC loading studies (section 2.6) and 3D Y201 MSC inflammatory studies (section 2.7), were removed from storage at -20°C and thawed at room temperature. 50µl samples were mixed with 50µl of LDH substrate mix and incubated at room temperature for 30 minutes in the dark in a 96 well plate before adding 50µl of stop solution to halt the reaction. The LDH levels were colorimetrically quantified at 490nm absorbance using a FLUOstar® OPTIMA (BMG Labtech, UK) Plate reader.

2.12.2 MTS Assays

All MTS assays were carried out using a CellTiter 96® AQ_{ueous} One Solution Cell Proliferation Assay (Promega) for the colorimetric quantification of metabolically active cells. All Assays were carried out on hOBS cultured at $4x10^4$ cells per well in 96 well plates with 100µl per well of hOB culture media (section 2.5.2.) with the addition of PLGA nanoparticles (section

2.12.2.1.) or following addition of conditioned medium from 25% Pluronic F-127 hydrogels (section 2.12.2.2.) compared to treatment free controls.

All assays were carried out according to the manufacturer's protocol. The CellTiter 96® AQ_{ueous} One Solution reagent was thawed at room temperature for 90 minutes. 20µl of CellTiter 96® AQ_{ueous} One Solution reagent was pipetted into each well containing hOBs in 100µl of hOB cell culture media. The plates were then incubated for 4 hours (37°C, 5% CO_2). Immediately following incubation, absorbance was recorded at 490nm, using a FLUOstar® OPTIMA (BMG Labtech, UK) 96 well plate reader.

2.12.2.1 MTS Assay Timeline with PLGA Nanoparticles

To determine the metabolic impact of PLGA nanoparticles on hOBs in monolayer, an MTS assay was carried out following exposure of hOBs to a range of blank PLGA nanoparticle concentrations (0.1, 1, 10 and 100mg/ml) suspended in hOB cell culture media at different time points (1, 3 and 7 days). Figure 2.4 demonstrates the experimental timeline for MTS assays on hOBs following PLGA nanoparticle exposure.

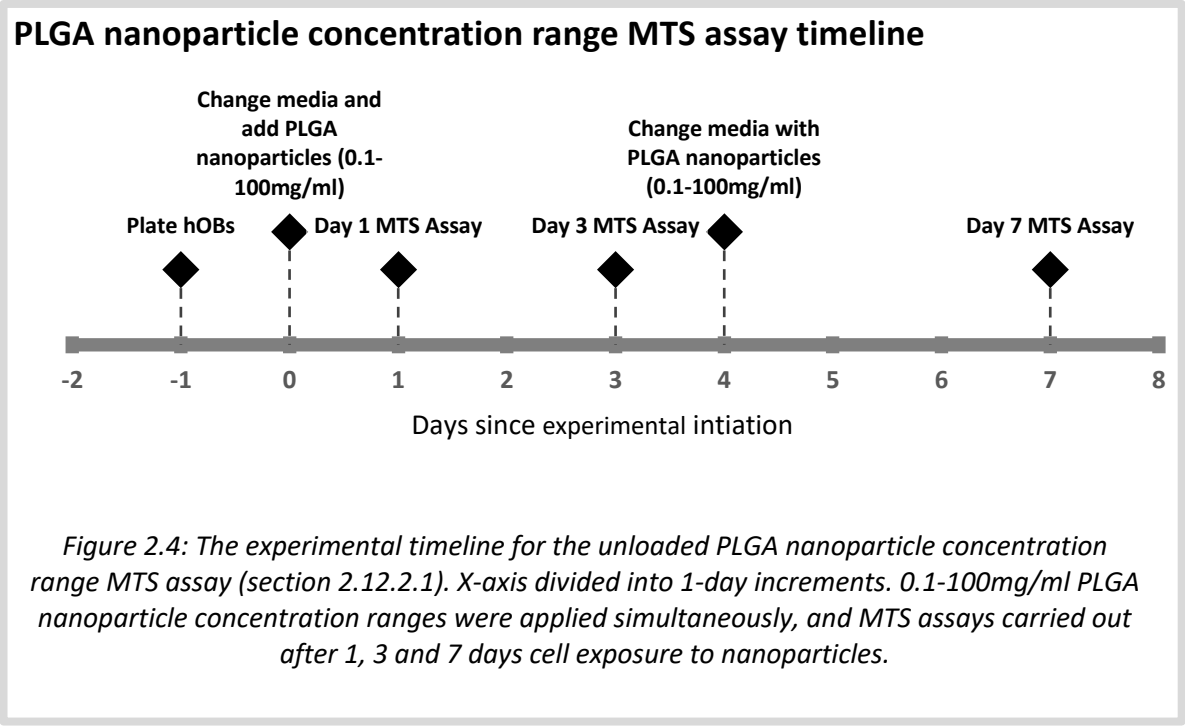

Figure 2.4: The experimental timeline for the unloaded PLGA nanoparticle concentration range MTS assay (section 2.12.2.1). X-axis divided into 1-day increments. 0.1-100mg/ml PLGA nanoparticle concentration ranges were applied simultaneously, and MTS assays carried out after 1, 3 and 7 days cell exposure to nanoparticles.

2.12.2.2 MTS Assay Timeline with 25% Pluronic F-127 Thermoresponsive Hydrogels

To determine the metabolic impact of 25% Pluronic F-127 thermoresponsive hydrogels on hOBs in monolayer, hOB cell culture media was conditioned with a range of Hydrogel to cell culture media ratios (1:1, 1:2, 1:4, 1:8) for differing lengths of time (1, 3 and 7 days). The thermoresponsive hydrogels were set for 5 minutes at 37°C prior to the addition of media for conditioning. This media was then used to culture the hOBs for 3 days and an MTS assay carried out. Using conditioned media allowed for quantification of the effects of products released from Pluronic F-127 hydrogels into culture media over time and aid understanding of how these hydrogels might affect their immediate biological environment (Smith et al., 2006, Darnell et al., 2013). Figure 2.5 demonstrates the timeline of hOB cell culture for the MTS assay following exposure to 25% Pluronic F-127 hydrogel conditioned media.

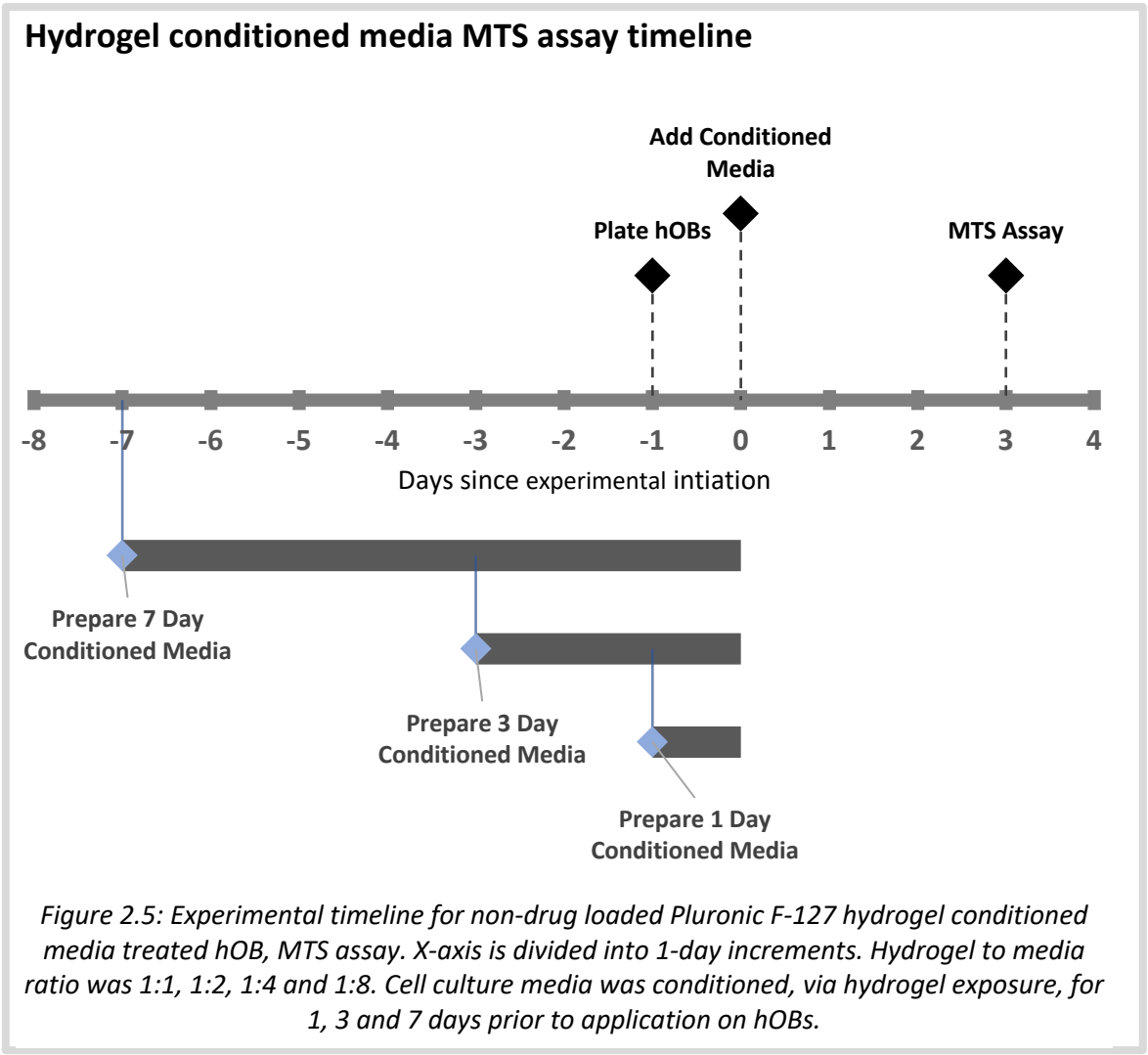

Figure 2.5: Experimental timeline for non-drug loaded Pluronic F-127 hydrogel conditioned media treated hOB, MTS assay. X-axis is divided into 1-day increments. Hydrogel to media ratio was 1:1, 1:2, 1:4 and 1:8. Cell culture media was conditioned, via hydrogel exposure, for 1, 3 and 7 days prior to application on hOBs.

2.12.2.3 Cell Free Treatments to Negate the Effect of Anomalous Background Absorbance.

To remove any anomalies in absorbance due to treatment, PLGA nanoparticle loaded media (0.1, 1, 10 and 100 mg/ml) and Pluronic F-127 hydrogel conditioned media (1:1, 1:2, 1:4, 1:8 hydrogel: media) were applied to cell free wells (100μl/well). They underwent identical assay procedure as to that carried out on hOBs. The absorbance readings from cell free media were then taken away from those obtained from treated cells to negate any anomalous readings due to background absorbance from treatment.

2.13 Data Analysis

All graphical analysis and production were performed on Microsoft Excel® and data plotted as mean ± Standard error, aside from gene expression data which was plotted with 95% confidence intervals. All statistical analysis was carried out using SPSS statistics package version 25.0.0.1. Significance was at the 95% level ($p<0.05$). Where data was found to be normally distributed (Shapiro-Wilk test) and of equal variance (Levenes test), parametric comparisons were utilised (1-way and 2-way Analysis of Variance (ANOVAs)). Data was transformed to conform to the requirements of parametric testing if required. If, following transformation, data was still not of equal variance (as determined by Levenes test), nonparametric testing alternatives were carried out (Mann-Whitney U test, Kruskal-Wallis H test and Friedman test). In 2 factor ANOVA, pairwise post-hoc comparisons (Tukeys and Bonferroni) were carried out if either factor or their interaction was significant.
For ELISA, ECL and qRT-PCR data from IL-6/sIL-6r (section 2.7) and loading (section 2.6) studies Spearman's correlations were carried out as opposed to Pearson's as relationships between variables were not always linear. As data was continuous, variables represent paired observations and the relationship between variables was monotonic (either positive or negative correlation but not necessarily linear) Spearman's correlations were deemed appropriate.

For multivariate data, principal component analysis (PCA) was performed on continuous data. To ensure variables met the test assumptions for PCA all variables must have: at least

1 correlation value of $r \geq 0.3$, as determined via a correlation matrix table generated using SPSS, to ensure linearity between all variables; sampling adequacy, measured using Kaiser-Meyer-Olkin (KMO) test for individual variables, must be passed (KMO value ≥ 0.5 but ideally >0.6)(Kaiser, 1974) and Bartlett's test for sphericity must be passed, which runs on the null hypothesis that there are no correlations between variables. A Bartlett's score of $p<0.05$ is, therefore, required to continue PCA. If any of these tests were failed, variables causing the failure were removed from the data set and the analysis was re-run.

Chapter 3

The Development and Characterisation of GluR Antagonist Loaded PLGA Nanoparticles for the Treatment of Joint Disease

3.1 Introduction

In the treatment of OA, reducing the risk of systemic exposure and optimising localised drug delivery to the area of disease by IA drug delivery is common in the clinic (Wehling et al., 2017), and allows for the delivery of therapeutics with poor oral bioavailability. However, drug clearance from the joint space is rapid (Brown et al., 2019a). For the treatment of a chronic degenerative condition such as OA, sustained delivery options would be of great clinical benefit extending the therapeutic effects of a treatment, while reducing the need for multiple and painful injections. A sustained release microparticle formulation of triamcinolone acetonide, called FX006, has been approved by the FDA for use in humans to treat OA (more on this can be found in section 1.2.3). This has been shown to significantly improve joint pain, physical function, quality of life and stiffness scores in phase III clinical studies compared to immediate release triamcinolone and a placebo (Conaghan et al., 2018c). This highlights the potential benefit of sustained release formulations in optimising the therapeutic potential of new and established drugs to treat a long term, chronic condition such as OA.

Nanoscale drug delivery vehicles can be formulated to slow drug clearance from the joint, improving residence time and potentially extending therapeutic effects (Jin et al., 2017, Niazvand et al., 2017). Additionally, nanoscale materials have been shown to have the capacity to penetrate the ECM and cell barriers, therefore, improving the biodistribution of therapeutics (Zhao et al., 2011, Brown et al., 2019a). With this in mind, several studies have investigated the use of nanoparticles in the treatment of arthritis, utilising a wide range of synthesis techniques, materials and nanoparticle sizes (Zille et al., 2010, Cho et al., 2014, Riffault et al., 2015, Bottini et al., 2016) (see Appendix Table 9.6).

Multiple nanoparticle delivery formulations have now been FDA approved (Bobo et al., 2016). PLGA is a biocompatible biodegradable polymer which has been FDA approved for use in humans in multiple drug product formulations (Makadia and Siegel, 2011). PLGA based nanoparticles have been developed for the delivery of several different therapeutics for the treatment of a range of conditions (Danhier et al., 2012) including inflammatory conditions such as arthritis. In a study by Higaki et al., it was observed that a hydrophilic

glucocorticoid (betamethasone sodium phosphate (BSP)) was targeted to joint inflammation when encapsulated within PLGA nanoparticles and delivered IV in an inflammatory *in vivo* rat model and exhibited enhanced resolution of joint inflammation compared to free-BSP (Higaki et al., 2005).

PLGA nanoparticles can be developed using a range of formulation methods, allowing for both hydrophobic (oil-in-water) and hydrophilic (double emulsion) drug encapsulation. Modification of surface properties (e.g. PEGylation) can also be exploited to specifically target cell and tissue types in the treatment of different conditions such as: prostate cancer (Soppimath et al., 2001, Dhar et al., 2008); the brain (Olivier, 2005); and RA (Nogueira et al., 2016). Additionally, a wide range of studies demonstrate the sustained release capabilities of PLGA nanoparticles (Danhier et al., 2012). With this in mind, PLGA nanoparticles represent a viable potential delivery vehicle for the sustained release of GluR antagonists via IA injection in the treatment of joint disease (detailed in section 1.5.2). This chapter focuses on the first part of the thesis hypothesis to determine whether AMPA and kainate glutamate receptor (GluR) antagonists can be incorporated into the sustained release nanoparticles. DNQX has demonstrated increased receptor specificity to kainate receptors over NBQX (Nordholm et al., 1997). There is evidence to suggest that kainate receptor activation is involved in the propagation of joint degradation via increasing IL-6 release (Flood et al., 2007). Therefore, in addition to NBQX, which has been shown to deliver anti-arthritic therapeutic effects *in vivo* (Bonnet et al., 2015, Bonnet et al., 2020), AMPA/KA specific GluR antagonist DNQX was also investigated for sustained delivery.

3.1.1 Hypothesis, Aims and Objectives

Thesis Hypothesis: AMPA and kainate glutamate receptor (GluR) antagonists can be incorporated into sustained release delivery systems that can protect against inflammatory or mechanically driven pathways in bone *in vitro.*

This chapter contributes towards the thesis hypothesis via the overarching aim below, which has been further subdivided into a series of aims and objects:

Overarching Aim: To synthesise and characterise PLGA nanoparticles for delivery of GluR antagonists; determine the GluR sustained release characteristics and investigate freeze drying as a long term nanoparticle storage option.

Aim 1: To synthesise and characterise nanoparticles encapsulating DNQX and NBQX.

Objective 1.1: To develop a double emulsion PLGA nanoparticle synthesis method for the encapsulation of DNQX and NBQX.
Objective 1.2: To determine DNQX and NBQX loaded PLGA nanoparticle size, PDI and zeta potential using a Malvern Zetasizer.
Objective 1.3: To establish the shape, uniformity and agglomeration of freshly synthesised DNQX loaded PLGA nanoparticles using scanning electron microscopy.
Objective 1.4: To determine the effect of synovial fluid on the particle size, PDI and zeta potential of drug-loaded nanoparticles.

Aim 2: To determine the effect of freeze drying on DNQX loaded PLGA nanoparticles.

Objective 2.1: To determine the effect of freeze drying on DNQX loaded nanoparticles size, PDI and zeta potential using a Malvern Zetasizer.
Objective 2.2: To compare the shape, uniformity and agglomeration of freeze dried DNQX loaded PLGA nanoparticles using scanning electron microscopy.

Aim 3: To quantify drug release profiles of DNQX and NBQX loaded into PLGA nanoparticles at concentrations shown to be effective *in vivo* in PBS at 37°C over 35 days.

Objective 3.1: To measure encapsulation efficiency and drug release of 2.5-20mM DNQX encapsulated in PLGA nanoparticles.
Objective 3.2: To measure encapsulation efficiency and drug release of 2.5mM DNQX encapsulated in PLGA nanoparticles into synovial fluid.
Objective 3.3: To measure encapsulation efficiency and drug release of 20mM NBQX encapsulated in PLGA nanoparticles at concentrations shown to be effective *in vivo*.

Aim 4: To investigate the toxicity of PLGA nanoparticles.

Objective 4.1: To expose hOBs to a concentration range of empty PLGA nanoparticles and test cell viability over 1, 3 and 7 days using an MTS assay.

3.2 Results

3.2.1 Physical Characterisation of GluR Antagonist Loaded PLGA Nanoparticles.

Nanoparticles developed using microfluidic synthesis technique (section 2.2.1.1.) exhibited GluR antagonist load dependant increases in size and major, visually detectable, agglomerates that formed immediately after synthesis. The results from this synthesis methodology are documented in Appendix section 9.6. However, the persistent agglomeration meant stable nanoscale particles could not be synthesised, so a double emulsion synthesis methodology for the encapsulation of water-soluble drugs was utilised over microfluidics throughout this chapter.

3.2.1.1 PLGA nanoparticle size, PDI and charge.

DLS was utilised to quantify freshly synthesised PLGA nanoparticles size and PDI and electrophoretic light scattering (ELS) to measure zeta potential with a range of GluR antagonist loads (Figure 3.1A-C).

Incorporating GluR into PLGA nanoparticles significantly reduced particle size vs controls for 2.5mM DNQX loaded Nanoparticles (t-test, $p=0.001$); 20mM DNQX loaded nanoparticles (t-test, $p=0.023$) and 20mM NBQX loaded nanoparticles (t-test, $p<0.0001$). 2.5mM DNQX loading reduced mean nanoparticle size 1.26-fold compared to unloaded controls, this change was corrected by freeze drying. 20mM DNQX loading reduced mean nanoparticle size 1.25-fold. 20mM NBQX loaded freeze dried nanoparticles had a 1.38-fold mean reduction in nanoparticle size vs control (Figure 3.1A).

Incorporating GluR into PLGA nanoparticles significantly increased (1.39-fold) PDI in 2.5mM loaded PLGA nanoparticles vs controls (Mann-Whitney U test, $p=0.0495$) and there was a significant reduction (1.53-fold) in PDI in 20mM NBQX loaded nanoparticles vs controls (t-test, $p=0.030$) (Figure 3.1B).

There were significant effects of GluR load of PLGA nanoparticles on zeta potential. 2.5mM DNQX loaded nanoparticles had a significant, 4.33-fold reduction in zeta potential compared to unloaded particles (t test, $p=0.001$). Freeze dried 2.5mM DNQX loaded nanoparticles had a significant 4.25-fold reduction compared to unloaded nanoparticles (t-test, $p=0.006$). 20mM DNQX loaded nanoparticles had a significant 5.06-fold reduction compared to unloaded nanoparticles (Mann Whitney U test, $p=0.0495$). Freeze dried 20mM NBQX loaded nanoparticles had a 4.90-fold reduction vs unloaded nanoparticles (t test, $p<0.001$) (Figure 3.1C).

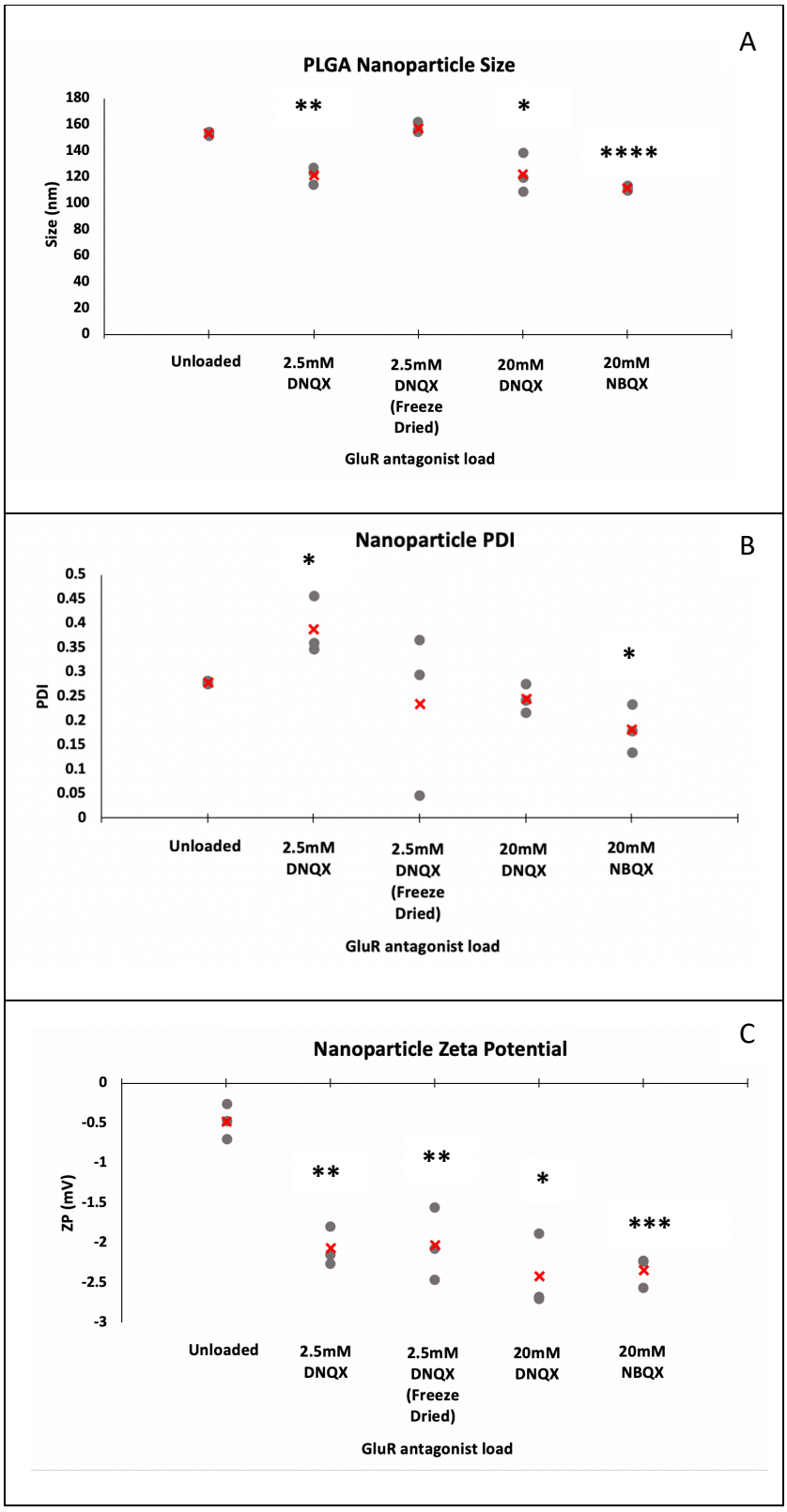

*Figure 3.1: DLS quantification of PLGA nanoparticles synthesised via double emulsion methodology (section 2.2.1.2) using a Malvern Zetasizer. Nanoparticles were suspended in PBS immediately following synthesis or freeze drying for DLS and ZP quantification (section 2.2.3). Red 'x' indicates the mean value of independent repeats. A) nanoparticle size; B) nanoparticle polydispersity index; C) nanoparticle zeta potential. (n=3; independent experimental replicates). *p<0.05, **p<0.01, ***p<0.001, ****p<0.0001 vs unloaded nanoparticles (T-tests).*

DNQX loaded nanoparticles were assessed via DLS in various fluids: PBS (release study fluid and physiological pH), DMEM+10%FBS (Y201 *in vitro* culture media) and bovine synovial fluid (representative of the *in vivo* environment nanoparticles would be subjected to) (Figure 3.2A-C).

There was a significant main effect of dispersant on nanoparticle size (1-way ANOVA; $p<0.0001$). Suspension in DMEM+10% FBS resulted in a 1.20-fold increase in nanoparticle size compared to PBS suspended particles ($p=0.001$). Suspension in bovine synovial fluid resulted in a 5.06-fold reduction in size compared to PBS suspended nanoparticles and a 6.09-fold reduction compared to DMEM+10%FBS suspension ($p<0.0001$ vs both other suspensions) (Figure 3.2A).
There was a significant main effect of dispersant on nanoparticle PDI (1-way ANOVA; $p<0.001$). A 1.03-fold change in PDI between nanoparticles suspended in PBS and in DMEM+10%FBS was not a significant difference ($p=0.865$). The PDI of nanoparticle suspended in bovine synovial fluid was 1.26-fold increased vs PBS suspension ($p<0.001$) and 1.22-fold increase compared to DMEM+10%FBS suspension ($p=0.001$) (Figure 3.2B).
There was a significant main effect of dispersant on nanoparticle zeta potential (Kruskal-Wallis test; $p<0.0001$). The 1.35-fold decrease in DMEM+10%FBS suspended nanoparticle zeta potential compared to PBS suspended nanoparticles was not found to be significant ($p=0.670$). Bovine synovial fluid suspended nanoparticles were shown to deliver 5723-fold reduction compared to PBS suspended nanoparticles ($p<0.0001$) and a 4244-fold reduction compared to DMEM+10%FBS suspended nanoparticles ($p=0.008$) (Figure 3.2C).

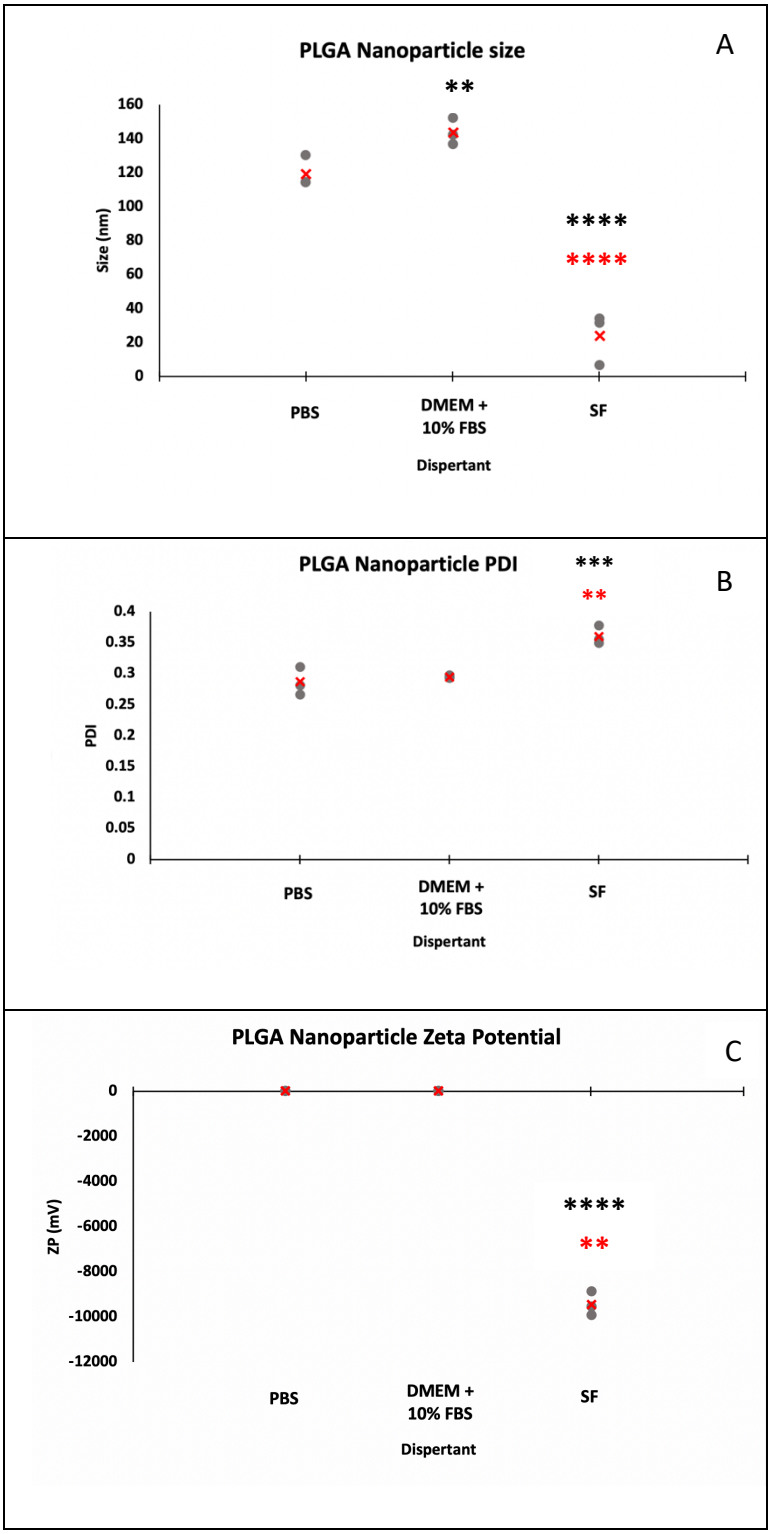

Figure 3.2: DLS and ZP measurements comparing blank PLGA nanoparticles suspended in three different dispersants immediately following double emulsion nanoparticle synthesis (section 2.2.1.2). The dispersants were PBS, DMEM + 10% FBS and Bovine synovial fluid (SF) to represent release study media; in vitro cell culture media and the biological joint environment for IA injection respectively. Red 'x' indicates the mean value of independent repeats *A) Nanoparticle size; B) Nanoparticle polydispersity index; C) Nanoparticle zeta potential (n=3; independent repeat experiments). **p<0.01, ***p<0.001, ****p<0.0001 vs PBS (T-Tests)*

3.2.1.2 Scanning Electron Microscopy Nanoparticle Characterisation

To validate sizing measurements taken using DLS, DNQX loaded nanoparticles were also isolated and imaged using SEM, to visually assess particle size. This was done on fresh nanoparticles and 3-week-old particles isolated from a DNQX release study, with PBS as the release media, to identify any visual differences that might occur over time (Figure 3.3). SEM micrographs of fresh PLGA nanoparticles exhibit smooth spherical morphology at a size range of between 100-300nm which visually correlates to sizes detected by DLS measurement (Figure 3.3A-B and Figure 3.1A). After three weeks in PBS at 37°C nanoparticles have increased in size to the 1-3µm diameter range and developed a non-uniform morphology. No large particle agglomerates were visible on SEM micrographs.

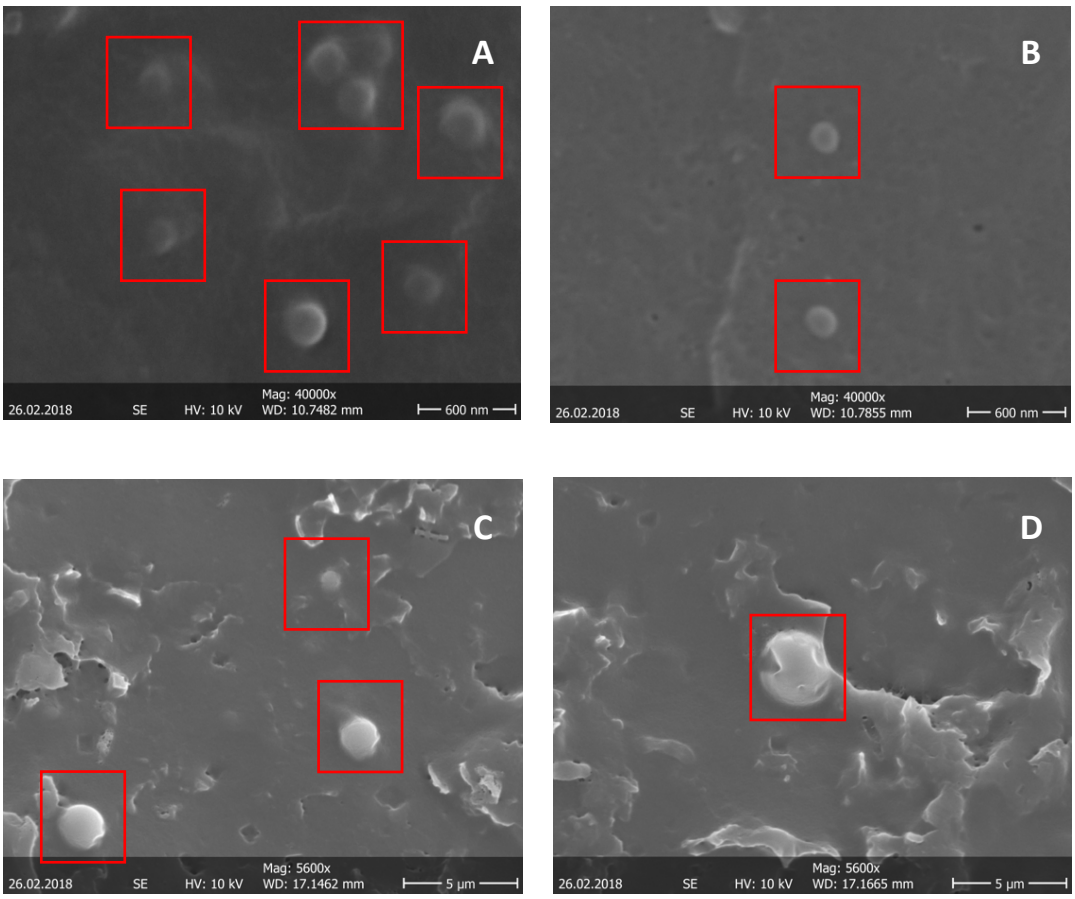

Figure 3.3: SEM micrograph of PLGA nanoparticles isolated via filtration onto 50nm Nuclepore track-etch polycarbonate filter membranes (Whatman®) prior to gold coating and imaging (methods section 2.2.7.1). A+B images taken less than 24hrs after synthesis, scale bar at 600nm; C+D images taken three weeks after synthesis, scale bar at 5µm. Red boxes on images applied to aid with nanoparticle identification.

3.2.2 Physical Characterisation of Freeze Dried GluR Antagonist Loaded PLGA Nanoparticles

To allow for long term nanoparticle storage and ease of use via resuspension in delivery fluid (e.g., water) a freeze-drying method was utilised to preserve nanoparticles.

3.2.2.1 DLS Characterisation of PLGA Nanoparticles Before and After Freeze Drying

To determine the impact of freeze drying on nanoparticle characteristics, nanoparticles were examined by DLS before and after freeze drying (Figure 3.4A-C).

Freeze drying PLGA nanoparticles did not significantly affect size (t-test, $p=0.244$) and PDI (t-test, $p=0.656$) but significantly increased zeta potential by 1.87-fold (t-test, $p<0.001$) (Figure 3.4A-C). The 'after freeze drying' DLS and zeta potential data were also displayed in comparison to other GluR loaded PLGA nanoparticles in Figure 3.1A-C.

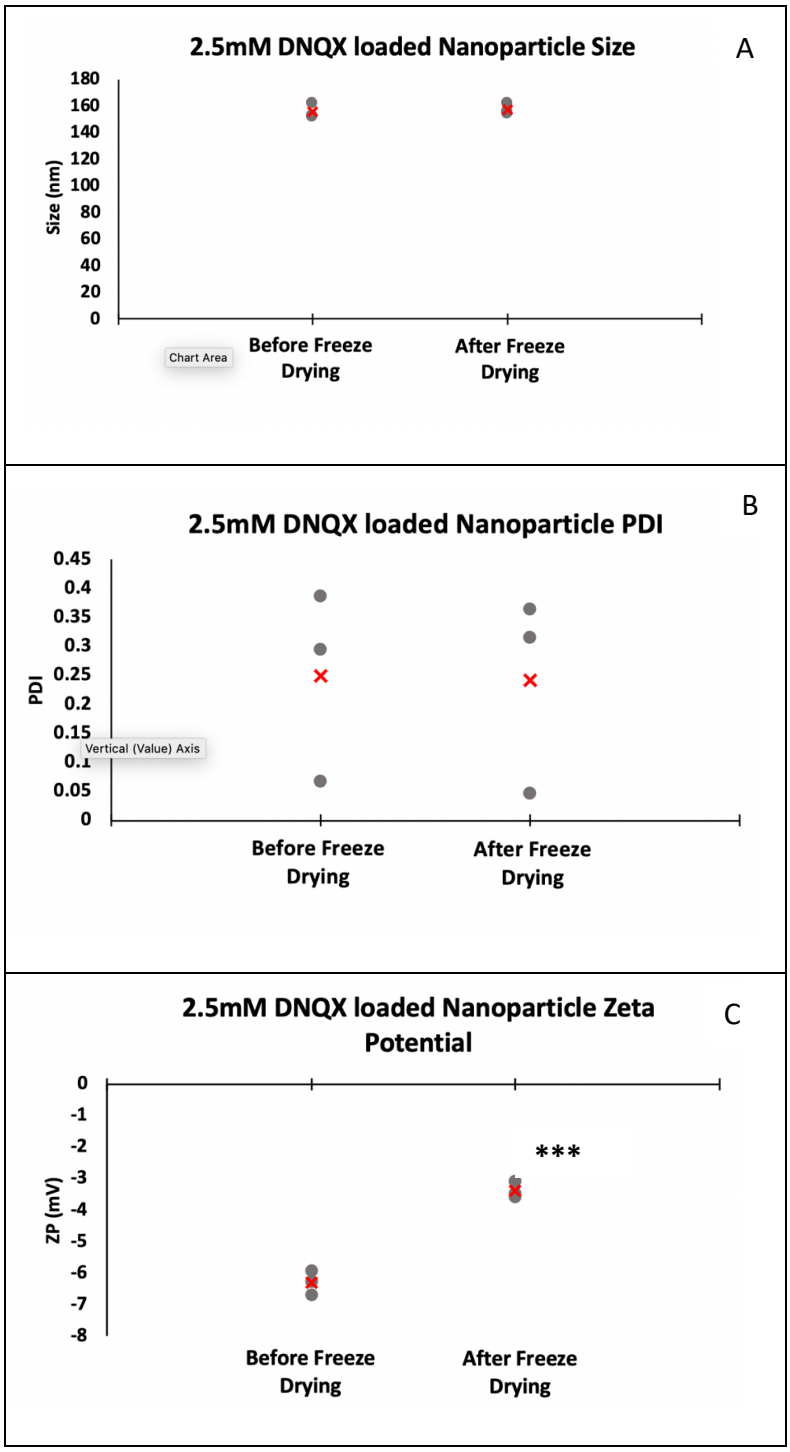

Figure 3.4: DLS and ZP measurements comparing PLGA nanoparticle characteristics before and after freeze drying (section 2.2.5). 'Before Freeze Drying' analysis was carried out immediately following double emulsion nanoparticle synthesis (section 2.2.1.2); 'After Freeze Drying' analysis took place immediately following resuspension after freeze drying. Red 'x' indicates the mean value of independent repeats *A) Nanoparticle size; B) Nanoparticle PDI; C) Nanoparticle zeta potential (n=3; independent repeat experiments). ***p<0.001 (T-Test)*

3.2.2.2 SEM Characterisation of Freeze Dried PLGA Nanoparticles.

To visually determine the presence of nanoscale particles following freeze drying, SEM images were taken (Figure 3.5).

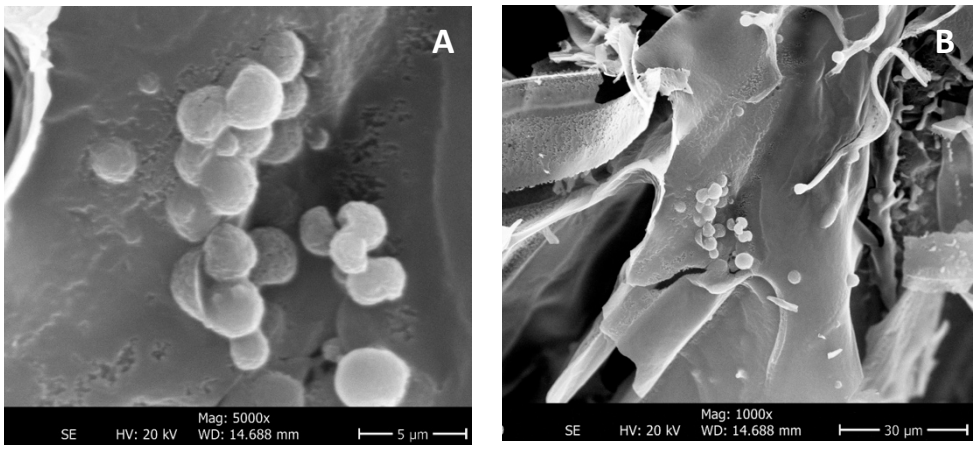

Figure 3.5: SEM micrographs of freeze dried PLGA imaged less than 24 hours after synthesis (section 2.2.1.2) and subsequent freeze drying (section 2.2.5). A) scale bar: 5 microns. B) scale bar: 30 microns.

SEM micrographs confirm the presence of spherical nanoscale particles (400nm to 3µm range) following freeze drying (Figure 3.5A-B).

3.2.3 GluR Antagonist Release from PLGA Nanoparticles

3.2.3.1 DNQX Release into PBS

Drug release from PLGA nanoparticles into PBS was quantified following the load of differing concentrations of DNQX (Figure 3.6A-B).

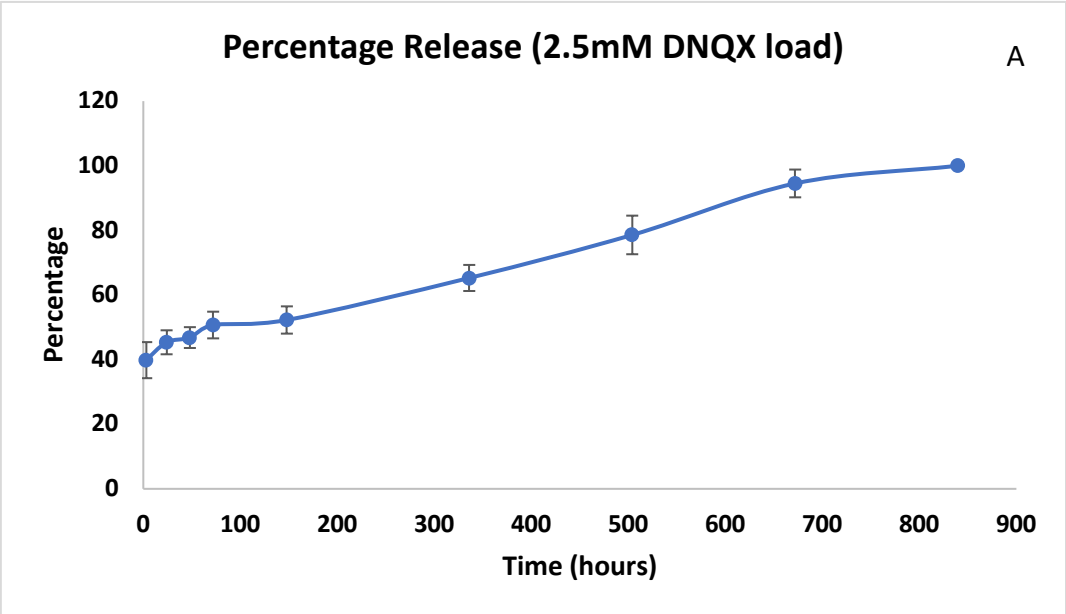

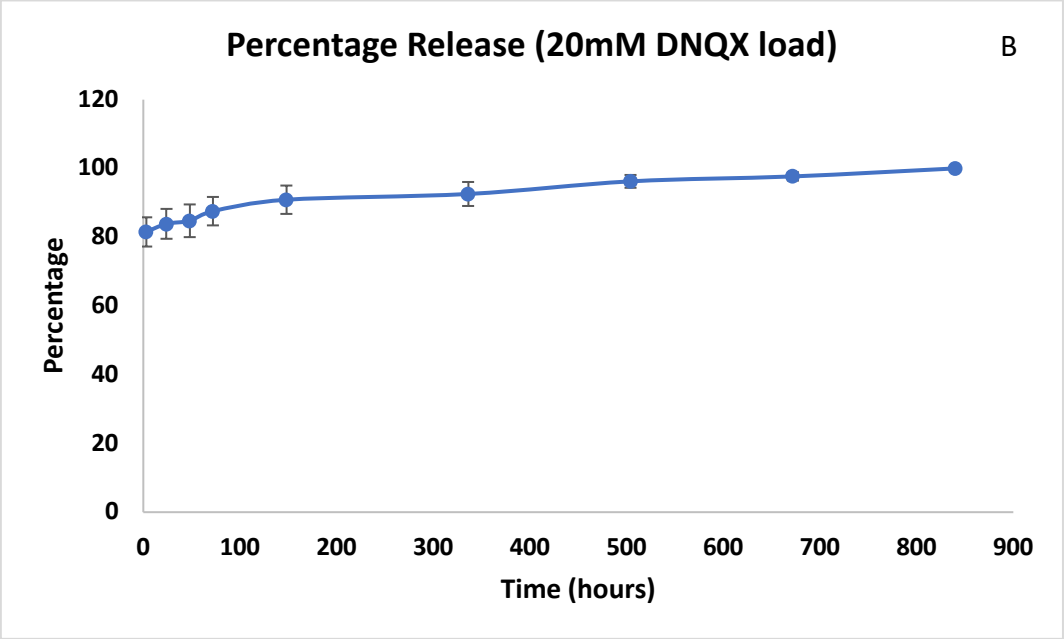

Figure 3.6: DNQX released into 20ml PBS at 37℃ over time from double emulsion synthesised PLGA nanoparticles loaded with an original DNQX concentration of 2.5 and 20mM. Using the synthesis method described in methods section 2.1.1.2. (n=3; independent experimental repeats). A) Release displayed as percentage release from 2.5mM DNQX loaded nanoparticles, EE: 29.3±11.4%, LC: 0.241±0.094%. B) Release displayed as percentage release from 20mM DNQX loaded nanoparticles, EE: 26.5±11.2%, LC: 1.741±0.736.

An average of 39.8%±5.58% of DNQX was released immediately from 2.5mM DNQX loaded PLGA nanoparticles. This was followed by sustained release of the remaining encapsulated drug for the next 840 hours. 94.5%±4.30% of DNQX release took place by 672 hours. Given

the EE, a total of 216.7±84.7μg was encapsulated for sustained DNQX delivery from these nanoparticles.

An average of 81.1%±4.10% of DNQX was released immediately from 20mM loaded PLGA nanoparticles. This was followed by a sustained release of the remaining encapsulated drug over the next 840 hours. 96.2%±1.86% of DNQX release had occurred by 504 hours. Given the EE, a total of 1567.3±662.5μg was encapsulated for sustained DNQX delivery from these nanoparticles.

3.2.3.2 DNQX Release into Bovine Synovial Fluid

With the proposed application of GluR loaded PLGA nanoparticles being via IA injection, the effect of synovial fluid (bovine) on DNQX release from 2.5mM DNQX loaded PLGA nanoparticles was quantified (Figure 3.7).

.

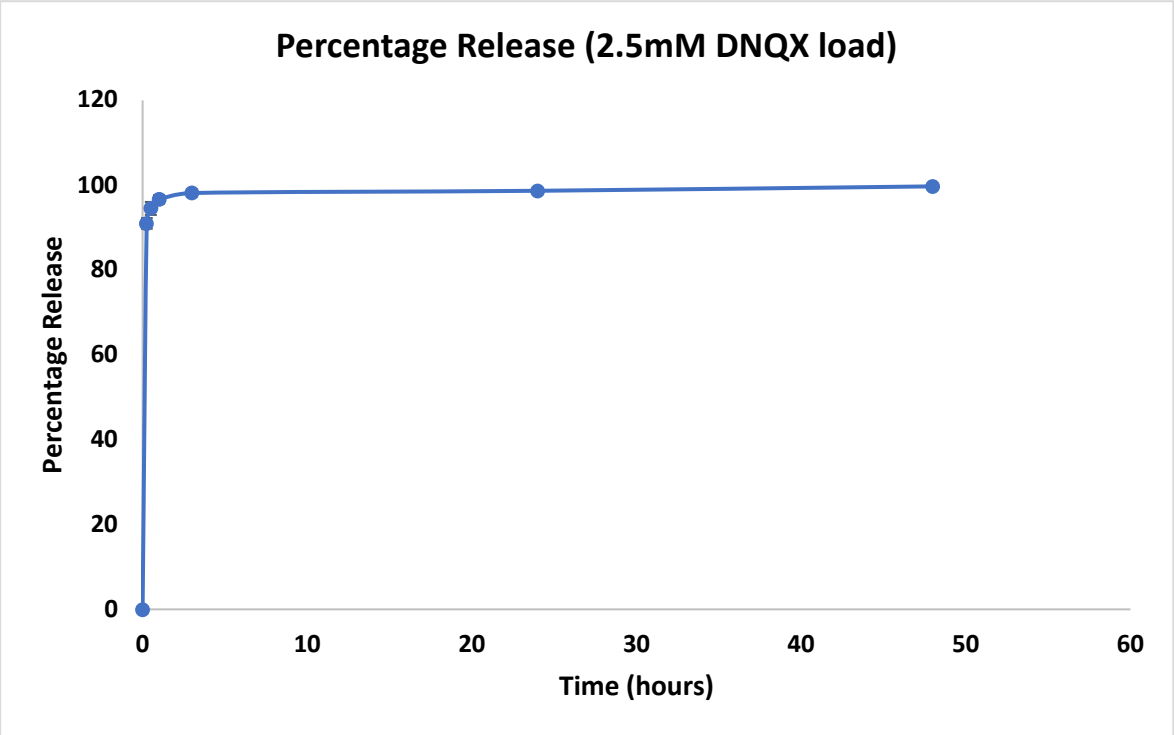

Figure 3.7: DNQX Released into bovine synovial fluid (SF) at 37℃ from PLGA nanoparticles loaded with an original DNQX concentration of 2.5mM via double emulsion synthesis described in methods section 2.2.1.2. (n=3; independent experimental replicates). Release displayed as DNQX percentage release into bovine synovial fluid, EE 30.9±3.7%, LC: 0.254±0.031%.

An average of 91.0%±1.26% of DNQX was released immediately from PLGA nanoparticles into bovine synovial fluid. With 98.7%±0.30% being delivered by 24 hours and 99.7%±0.40% delivered by 48 hours. Given the EE, a total of 1827.5±220.4µg was encapsulated for sustained DNQX delivery from these nanoparticles.

3.2.3.3 NBQX Release into PBS from Freeze Dried Nanoparticles

Development of a sustained NBQX release delivery vehicle for comparison against free NBQX arthritis studies (Bonnet et al., 2015, Bonnet et al., 2020) and application in *in vitro* models (chapter 5 of this thesis) was investigated. Delivery from freeze dried NBQX nanoparticles was quantified (Figure 3.8). 20mM of NBQX was loaded into nanoparticles at the start of synthesis (section 2.2.1.2.) and the drug released into PBS.

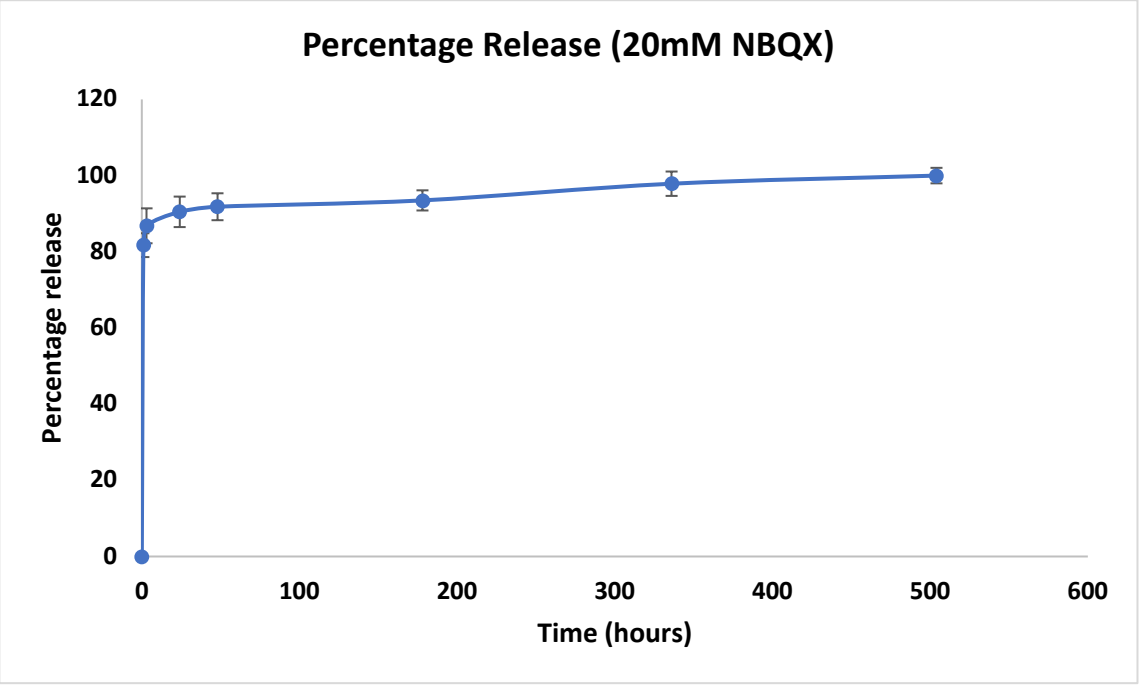

Figure 3.8: NBQX released into 20ml PBS at 37℃ over time from freeze dried PLGA nanoparticles loaded with an original NBQX concentration of 20mM using the double emulsion synthesis method described in methods section 2.2.1.2 (n=3; independent experimental replicates). Release displayed as percentage release from freeze dried 20mM NBQX PLGA nanoparticles, EE: 12.9±3.8%, LC: 0.850±0.248%.

An average of 81.7%±3.13% of NBQX was immediately released from PLGA nanoparticles followed by a sustained release of the remaining encapsulated drug over 504 hours.

97.9%±3.20% of NBQX was released after 336 hours. Immediate release of NBQX from PLGA nanoparticles closely correlates to that from 20mM loaded DNQX loaded nanoparticles (Figure 3.6B). Sustained release from PLGA nanoparticles is retained following freeze drying. Given the EE, a total of 982.8±286.9μg was encapsulated for sustained NBQX delivery from these nanoparticles.

3.2.4 Effect of PLGA Nanoparticles on Primary Human Osteoblast Viability

MTS assays are used to quantify mitochondrial activity which is an indicator of cell viability. To determine the impact of PLGA nanoparticles on cell viability, a 0.1-100mg/ml concentration range of blank PLGA nanoparticles were applied over 1, 3 and 7 days to human primary osteoblasts, as these cells are thought to mediate protective effects of GluR antagonists in OA (Figure 3.9) (Bonnet et al., 2015).

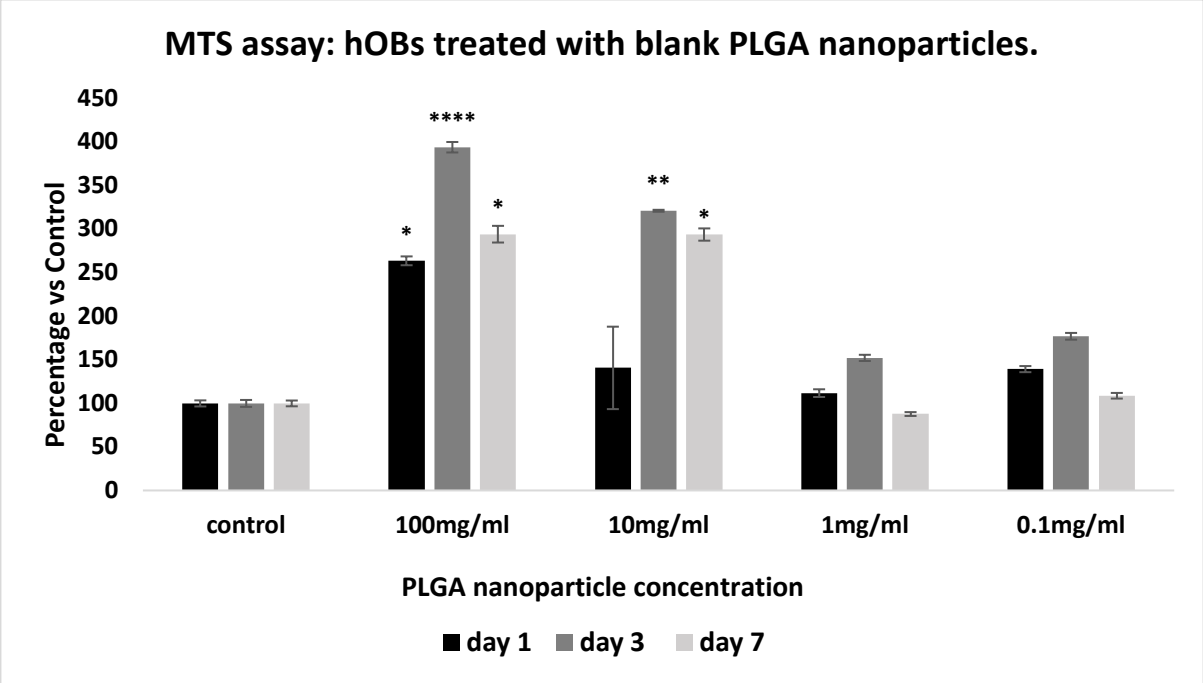

*Figure 3.9: The percentage release of MTS from primary human osteoblasts (hOBs) following exposure to a range of concentrations of unloaded PLGA nanoparticles vs untreated controls (n=6; Cell culture well replicates). Following 24hrs in hOB cell culture media (section 2.5.2), hOBs were cultured for either 1, 3 or 7 days in hOB cell culture media containing a range of blank PLGA nanoparticle concentrations (0.1-100mg/ml) at which point an MTS assay was carried out (Section 2.12.2) to determine the level of MTS release vs untreated hOB controls as a representation of cellular proliferation. To remove any anomalies in absorbance due to treatment, PLGA nanoparticle loaded media (0.1, 1, 10 and 100 mg/ml) was applied to cell free wells and taken away from the from the values obtained from the cellular (hOB) assay (Section 2.12.2.3). These underwent identical assay procedure as to that carried out on wells containing hOBs. *p<0.05, **p<0.01, ****p<0.0001 vs control (Kruskal Wallis test) .*

For MTS release, there was a significant effect of nanoparticle concentration ($p=0.006$), time ($p=0.001$) and interaction of nanoparticle concentration and time ($p<0.0001$) (Kruskal-Wallis test, Figure 3.9). Pairwise comparison with Bonferroni corrections for multiple comparisons revealed that, following 1 day of 100mg/ml nanoparticle exposure, MTS was significantly increased 2.64-fold vs controls ($p=0.012$). 10mg/ml, 1mg/ml and 0.1mg/ml exposure did not significantly affect MTS release at 1-day compared to controls. At 3 days 100mg/ml nanoparticle exposed cells demonstrated a significant 3.94-fold increase in MTS release compared to controls ($p<0.0001$) and 10mg/ml exposed cells demonstrated a significant 3.21-fold increase in MTS release compared to controls ($p=0.001$). At 7 days 100mg/ml nanoparticle exposed cells demonstrated a significant 2.94-fold increase in MTS release compared to controls ($p=0.048$) and 10mg/ml exposed cells demonstrated a significant 2.94-fold increase in MTS release compared to controls ($p=0.032$).

3.3 Discussion

3.3.1 GluR Antagonist Loading Influences PLGA Nanoparticle size, PDI and Zeta Potential

The purpose of aim 1 was to synthesise nanoparticles capable of encapsulating DNQX and NBQX and analyse resulting nanoparticle physical characteristics using DLS and SEM imaging. The effects of DMEM+10% FBS (*in vitro* culture media) and bovine synovial fluid on particle characteristics was also investigated to determine the potential effects of experimental or clinical conditions on drug release.

Particle size is one of the key characteristics of nanoparticles that can provide increased benefits over microparticles. The very high surface area to volume ratio of nanoparticles provides a large interface with their environment meaning increased reactive potential. In this case, this would indicate an increased exposure of GluR antagonist released from or attached to the surface of these nanoparticles to surrounding tissue. As confirmed by both DLS and SEM imaging, PLGA nanoparticles were successfully synthesised in the nanoscale range (Figure 3.1A and 3.3). *In vivo* IV polymeric nanoparticle delivery in an inflammatory rat and mouse arthritis model have demonstrated that nanoparticles accumulate within inflamed joints with accumulation correlating to severity of inflammation (Ishihara et al., 2009b). The capacity to passively target areas of joint inflammation has been proposed as a consequence of the increased vascular permeability as reviewed by Durymanov et al. (2017) (Boerman et al., 1997, Metselaar et al., 2003, Durymanov et al., 2017). Nanoparticles have been shown to have an increased capacity for intra-cellular uptake compared to microparticles (Desai et al., 1997, Zauner et al., 2001, Panyam and Labhasetwar, 2012). Nanoparticles of <200nm size have been predominantly investigated as they are smaller than the width of a microcapillary. This allows for enhanced tissue penetration through the micro vasculature when injected into the bloodstream and has the capacity to cross epithelial lining (Vinogradov et al., 2002, Singh and Lillard, 2009). Nanoparticles of this size have been shown to have enhanced cellular uptake (Desai et al., 1997). Additionally, it has been demonstrated that particles bellow 200nm do not activate the lymphatic system, hence have a reduced removal rate from circulation (Prokop and Davidson, 2008, Rizvi and Saleh, 2018). Based on this evidence, nanoparticles synthesised in this chapter have

demonstrated favourable size characteristics for use in a biological system as the consistent formulation of <200nm nanoparticles was achieved (Figure 3.1A).

Nanoparticle size is significantly reduced when loaded with GluR antagonists in all but the 2.5mM DNQX loaded freeze dried batches (Figure 3.1A). Studies have indicated that drug loading can have a significant effect on particle size (Adebileje and Amani, 2018, Massella et al., 2018), a factor that takes place following GluR antagonist loading. However, all GluR antagonist loaded nanoparticles tested remained below 200nm, indicating the passive targeting and permeability properties resulting from nanoparticle size would be maintained. The lack of size reduction in 2.5mM DNQX loaded freeze dried batches could be due to the freeze-drying process removing excess GluR antagonist, a characteristic not observed in the 20mM NBQX freeze dried batches potentially due to the greater initial drug load. Alternatively, studies have demonstrated that freeze drying can degrade nanoparticles and cause leakage of their encapsulated contents leading to a change in nanoparticle size detected (Choi et al., 2004). During freeze drying, the cryoprotectant (in this case 5% w/v Trehalose) forms a protective coating around the nanoparticles when dropped below its glass transition temperature, thereby, protecting them against mechanical stress and preventing aggregation. However, when insufficient cryoprotectant is used, or too high a nanoparticle concentration is present, nanoparticle agglomeration can occur due to an incomplete protective effect. In a study by Date et al., 20% w/v trehalose demonstrated an increased protective capacity on nanoparticle size compared to 20% w/v fructose, this effect was reduced at increasing nanoparticle concentrations (Date et al., 2010). This may indicate that either the cryoprotectant concentration was low or nanoparticle concentration high in this study leading to the detected nanoparticle size changes following freeze drying. However, as previously mentioned, these changes still resulted in nanoparticles of <200nm with sizes of 111.3nm for 2.5mM DNQX loaded freeze dried nanoparticles and 157.1nm 20mM NBQX loaded freeze dried nanoparticles (Figure 3.1A). Therefore, freeze-dried nanoparticles were deemed still within acceptable size ranges for further investigation.

Key factors to consider when developing nanoparticle delivery systems are PDI and zeta potential which have been quantified via DLS and electrophoretic light scattering respectively.

Nanoparticle PDI is a unitless value representing the size distribution of nanoparticles analysed. Nanoparticle PDI between the range of 0.1 to 0.3 indicates a monodisperse suspension. This would represent a homogenous population of nanoparticles which is key in controlled drug delivery systems (Chen et al., 2011). A poly disperse suspension (PDI>0.3) would indicate uncontrolled particle size and possible particle agglomeration. Particle size and size distribution are noted as a critical quality attributes by the FDA for liposomal delivery vehicles (FDA, 2018), highlighting the importance of these attributes in nanoparticle development. Unloaded PLGA nanoparticles were found to have an average PDI of 0.278. This was not significantly impacted by GluR antagonist loading.

Drug loading has been shown to reduce PDI (Azevedo et al., 2014) and nanoparticle freeze drying conditions have been shown to alter sample PDI (Choi et al., 2004). A reduction in 20mM NBQX loaded freeze dried nanoparticle PDI could have been influenced by these factors and indicates increased particle monodispersity (Figure 3.1B).

Negative surface charge of formulated nanoparticles ensures good particle stability and low particle dispersion with a charge of $\pm$30mV thought to ensure good nanoparticle stability (Ahsan et al., 2002). The small negative zeta potential observed on all GluR antagonist loaded PLGA nanoparticles, ranging between -2.07 and -2.42mV, would be expected to be insufficient to confer stability and reduce the chances of nanoparticle agglomeration (Figure 3.1C). Despite this, a lack of agglomeration was identified in SEM imaging of nanoparticles and PDI indicated particle monodispersity (<0.3) at sub 200nm size ranges (Figure 3.3).

Due to the comparatively large surface area of nanoparticles, aggregation can be a problem. Zeta potential represents the potential difference between a stationary layer of fluid attached to the surface of a particle (termed electric double layer) and that of the media the particles are dispersed within (Delgado et al., 2007). A negative zeta potential can act as a high energy barrier and stabilise nanosuspensions (Musumeci et al., 2006). Additionally, the

increase in zeta potential negativity following GluR antagonist load may indicate that drug loading contributes to particle stability (Figure 3.1C). However, due to the low magnitude of the zeta potential value for these nanoparticles, it is unlikely that there would be any stabilising effect from these charges. Additionally, studies have demonstrated that changes in ionic salt concentration and pH can change the value of quantified zeta potential (Pavlin and Bregar, 2012) and that the suspension media of nanoparticles can have a great effect on zeta potential and, thereby, on particle stability (Kaasalainen et al., 2012). This has significant implications for biological application of nanoparticles, where the *in vitro* media and *in vivo* environment protein content, ionic strength and pH could dramatically effect particle agglomeration and stability through altering zeta potential (investigated in Figure 3.2C).

To gain some understanding into the impact of the *in vitro* culture environment and the *in vivo* joint space environment on nanoparticle characteristics, PLGA nanoparticles were suspended in PBS (pH7.4), cell culture media (DMEM+10% FBS) and bovine synovial fluid. No significant difference for nanoparticle PDI and zeta potential between PBS and DMEM+10%FBS was identified (Figure 3.2B-C). This would indicate that particle dispersion and surface charge remain consistent when exposed to *in vitro* culture conditions supporting the application of sustained GluR antagonist delivery from these nanoparticles in cell culture models for investigating arthritis. However, the lack of difference in nanoparticle zeta potential between PBS and DMEM is inconsistent with the literature, which indicates biological culture media has a significant effect on calculated zeta potential and can lead to nanoparticles becoming cytotoxic (Maiorano et al., 2010, Lordan and Higginbotham, 2012, Pavlin and Bregar, 2012). The small value (<5mV) for zeta potential calculated in PBS and DMEM for these nanoparticles may explain this inconsistency, as a lack of particle charge would mean that a change in the charge of the media, in which the particles were suspended, would have little impact (Figure 3.2C). The increase (1.2-fold) in nanoparticle size in DMEM+10% FBS compared with PBS suspension could be due to the presence of serum proteins from the 10% FBS inducing agglomeration as reported by others (Bantz et al., 2014). Strojan et al., also reported particle size increases detected by DLS when FBS was added to RPMI cell culture media (Gibco Laboratories) (Strojan et al., 2017). PLGA nanoparticles of sub 200nm size have been shown to mitigate the effects of TNFα induced

inflammation *in vitro* in a human chondrocyte cell model via sustained dexamethasone delivery. Cells were cultured in DMEM+10% FBS (Park et al., 2012). Additionally, PLGA nanoparticles have been shown to successfully infiltrate chondrocytes (DMEM+15% FCS), synoviocytes (DMEM+10% FCS) and MSC (DMEM+10% FCS) without eliciting any clear pathological response following particle degradation *in vitro* (Riffault et al., 2015). These findings support the statement that the nanoparticles developed in this chapter could act as a sustained delivery vehicle for *in vitro* application in DMEM+10% FBS treated joint cell culture systems.

Suspension in bovine synovial fluid reduced the size and zeta potential of nanoparticles and increased PDI, indicating aggregation of particles. Synovial fluid is viscous and cloudy and is a complex combination of proteins and other molecules such as HA, lubricin and proteinases. DLS is based on light scattering and hence the use of a cloudy media may skew size results (Bhattacharjee, 2016). Additionally, particulates and charged proteins within the synovial fluid may deliver unreliable zeta potential results following quantification by electrophoretic light scattering (Bhattacharjee, 2016). Therefore, despite centrifuging to remove any major particulates prior to DLS analysis, synovial fluid may not be an optimal media in which to accurately quantify particle characteristics using DLS or electrophoretic light scattering. Diluting synovial fluid with PBS or using an alternate biologically representative fluid may elicit more reliable findings and allow development of an understanding of particle behaviour in the joint environment prior to the initiation of any *in vivo* testing. Understanding the propensity for nanoparticles to aggregate in the joint environment is useful as studies have shown particle aggregation alters *in vivo* biodistribution and propensity for phagocytosis (Mohr et al., 2014). Significant increases to PLGA nanoparticle size and decreases in zeta potential were identified following suspension in bovine synovial fluid and saline (0.5%w/v) (Brown et al., 2019b). In this study, nanoparticles were suspended in bovine synovial fluid for 30mins at 37°C then washed and suspended in water for DLS and zeta potential quantification. This methodology would be useful for further investigation into the effect of synovial fluid on PLGA nanoparticle characteristics from this chapter.

These findings contribute towards the overarching aim of this chapter by confirming synthesis of PLGA nanoparticles (<200nm) (Figure 3.1A and Figure 3.3) and Identifying an impact of GluR loading to particle size. Additionally, PDI of <0.3 indicating a monodisperse particle size distribution with and without NBQX and DNQX loading (Figure 3.1B). Nanoparticle characteristic (PDI and ZP) remained consistent when suspended in an *in vitro* culture media (Figure 3.3B-C) allowing for further investigation into potential *in vitro* applications of GluR sustained delivery from these nanoparticles. However, suspension in synovial fluid indicated that this nanoparticle formulation may have a destabilising effect on particle physical characteristics (Figure 3.3A-C) and improved stability would be required to ensure a more robust formulation for in vivo delivery.

3.3.2 Freeze Drying Impacts GluR Antagonist Loaded PLGA Nanoparticles Zeta Potential but not Size or PDI.

To determine the effect of freeze drying on DNQX loaded PLGA nanoparticles, physical properties of PLGA nanoparticles before and after freeze drying were assessed through DLS and SEM imaging (Figure 3.4 and 3.5). Freeze drying allows for increased long-term nanoparticle storage capability while maintaining nanoparticle properties. Freeze drying removes water from a sample through a process called sublimation. With nanoparticles made of biodegradable polymers, such as PLGA, removal of water can enhance particle chemical stability by removing the risk of hydrolysis of chemical bonds which is a major factor contributing to PLGA degradation (Lemoine et al., 1996). To protect particles from ice crystallisation stress and the risk of aggregation during the freeze-drying process, cryoprotectants are added. The most commonly used freeze drying cryoprotectants are sugars which are known to convert to a glass like form at a particular temperature (Tg'). Nanoparticles trapped within this glassy sugar matrix can be protected from the stresses of freeze dying. Trehalose was the cryoprotectant utilised in this study due to its repeated use in the literature owing to its high Tg', low chemical reactivity and low hygroscopicity (Abdelwahed et al., 2006). A concentration of 5% has been shown to be necessary to maintain PLGA nanoparticle size following freeze drying (Chacón et al., 1999). Additionally, visualisation of particles using SEM becomes very difficult above a cryoprotectant concentration of 5% (Fonte et al., 2012).

A nanoparticle's ability to return to its original size from a freeze-dried powder following reconstitution in an aqueous system has been termed its "redispersibility" (Lee et al., 2009). Following freeze-drying, nanoparticles in this thesis exhibited good redispersibility (Figure 3.4A). The nanoparticle characteristics are also maintained for PDI (Figure 3.4B). However, zeta potential was significantly less negative following freeze drying (Figure 3.4C). This could result in decreased particle stability in suspension, although the magnitude of zeta potential values is small, so this difference is likely to have little impact. The change in zeta potential could be a consequence of the loss of some encapsulated DNQX following the freeze-drying process. Additionally, this change could be attributed to the presence of cryoprotectant in the nanoparticle suspension media. It has been shown that sorbitol, fructose and glucose all increase the negative zeta potential of nanoparticles (Soares et al., 2013). A study investigating cryoprotectant effects on insulin loaded PLGA nanoparticles demonstrated that 10% w/v trehalose caused the greatest increase in negative zeta potential compared to sucrose, glucose, fructose and sorbitol and when compared to blank nanoparticles (Fonte et al., 2012). The reduced zeta potential magnitude observed between nanoparticles in a 5% w/v trehalose solution before and after freeze drying could be attributed to a reduction in the cryoprotectant concentration following freeze drying that has been reported to effect nanoparticle size and zeta potential properties (Lee et al., 2009).

SEM imaging was used to visually verify particle characteristics following freeze drying. SEM images show PLGA nanoparticles affixed to cryoprotectant within the nanoscale range, although some particles were visually closer to 1μm (Figure 3.5). DLS data of freeze-dried nanoparticles indicated that the average nanoparticle size is well below 1μm. However, PDI values indicate that there is some variability in particle size dispersion so there may be a few particles close to the microscale range that would be more easily identifiable via SEM imaging. With regards to the overarching aim of this chapter (Section 3.1.1), these visual SEM findings in combination with the DLS results (Figures 3.4 and 3.5), indicate that the freeze-drying methodology developed for the long-term storage of GluR antagonist loaded PLGA nanoparticles is capable of maintaining nanoparticle dispersibility and morphology with no impact to size and PDI of DNQX loaded PLGA nanoparticles as a consequence of

freeze drying. This then allows for investigation into GluR antagonist sustained delivery from freeze dried nanoparticles and applications *in vitro.*

3.3.3 PLGA Nanoparticles Sustain Release of GluR Antagonists

Having quantified size and physical properties of PLGA nanoparticles loaded with GluR antagonists, aim 3 of this chapter was to investigate the sustained release capabilities of these formulations. Drug release was assessed at different drug loading concentrations in PBS and synovial fluid, and the impact of freeze drying on the sustained release investigated to contribute towards the overarching aim of this results chapter (Section 3.1.1).

DNQX has been shown to have an increased kainate receptor specificity over NBQX (Nordholm et al., 1997). There is evidence to suggest that kainate receptor activation is involved in the propagation of joint degradation via increasing IL-6 release (Flood et al., 2007). Development of DNQX sustained release nanoparticles allows for a comparator to NBQX sustained delivery in *in vitro* and *in vivo* models of arthritis, providing a platform for progressing the understanding of the mechanisms by which AMPA/KA glutamate receptor antagonists deliver an anti-arthritic therapeutic effect. Release of DNQX from PLGA nanoparticles was achieved over 840 hours (5 weeks) (Figure 3.6). EE is a measure of the percentage of the drug that is incorporated into the nanoparticles following synthesis. LC is the percentage of drug by weight as a component of the overall weight of the nanoparticles. EE and LC were low for both 2.5mM and 20mM DNQX load (Figure 3.6), as reported by others for water soluble drugs (Kumari et al., 2010). This has been proposed to be due to the leakage of the hydrophilic drug into the aqueous external phase during double emulsion nanoparticle synthesis (Huang et al., 2018). In this chapter, use of stabilisers (PVA and Pluronic F-68) were incorporated into the methodology upfront to maximise EE and LC. DNQX load did not affect EE being 29.3% for 2.5mM DNQX and 26.5% for 20mM DNQX loaded nanoparticles. However, LC showed a 7-fold increase (0.241 to 1.741%) from 2.5mM to 20mM DNQX load showing that increased DNQX loading results correlate with the amount of drug available for sustained delivery. Concentrations of GluR antagonist shown to elicit an anti-arthritic effect *in vivo* have ranged from 2.5mM to 20mM of free drug dissolved

in water for direct IA injection and 200μM used *in vitro* (Bonnet et al., 2015, Bonnet et al., 2020). These concentrations have been much higher than those shown to be encapsulated in PLGA nanoparticles in this study. However, the binding affinity (ic50) of the GluR antagonists loaded onto the nanoparticles in this study is much lower than the concentrations that have been delivered *in vivo*, with NBQX ic50 for kainate receptor at 4.8μM and AMPA receptor at 0.15μM and DNQX ic50 at 2μM for kainate receptor and 0.5μM for AMPA receptor (Reviewed by Nordholm et al., 1997). However, these values were obtained via *in vitro* studies on chicken retina cells and, therefore, may not be representative of the inhibitory capacity of these AMPA/KA GluR antagonists in joint cells. Regarding the ic50 values reviewed by Nordholm et al., (1997), there is enough NBQX and DNQX loaded onto PLGA nanoparticles to deliver a potential inhibitory effect through AMPA/KA inhibition. A potential avenue of investigation would be to combine the high free drug concentrations used *in vivo* (2.5/20mM) or *in vitro* (200μM) with the low but sustained dosage from PLGA nanoparticles in this study and thereby observe any additional effects to bulk free NBQX application (Bonnet et al., 2015, Bonnet et al., 2020) delivered by low sustained PLGA nanoparticle NBQX application. The effects of this combination of low PLGA nanoparticle drug release with an immediate high concentration application of GluR antagonist on inflammatory marker stimulated bone cells is investigated in Chapter 5 of this thesis *in vitro*.

Another characteristic indicative of drug release from PLGA nanoparticles is the biphasic release curve. This is due to the burst release of drug attached to the particle surface followed by sustained release of encapsulated drug as the particle breaks down though hydrolysis or biodegradation (Makadia and Siegel, 2011). All release curves using these nanoparticles in this chapter demonstrate a burst release of surface attached GluR antagonist (86μg out of 217μg for 2.5mM DNQX load; 1277μg out of 1567μg for 20mM DNQX load and 803μg out of 983μg for 20mM NBQX load)(Figures 3.6 to 3.8), followed by sustained release of the remaining drug over varying periods of time depending on drug loading and the release environment. With evidence to showing that high concentrations (20mM) of free GluR antagonist (NBQX) have a protective effect on the joint *in vivo* (Bonnet et al., 2015, Bonnet et al., 2020), bulk burst release of GluR antagonists from these

nanoparticles could allow for an initial high drug load and subsequent sustained low concentration delivery. However, even the burst release concentrations delivered from these nanoparticles remain substantially lower than that shown to deliver anti-arthritic effects *in vivo* (Bonnet et al., 2015, Bonnet et al., 2020). It has been shown that IA administration of NBQX at two points over 24hrs following PTOA induction (ACLr) delivered an increased protective effect to joint destruction, particularly in bone, compared to 1 NBQX injection (20mM) (Bonnet et al., 2020). These findings indicate a role for sustained NBQX delivery to traumatic arthritis development and highlight the potential benefits of sustained release and reduced joint clearance provided by the PLGA nanoparticles.

2.5mM DNQX loaded PLGA nanoparticles were assessed for drug delivery in bovine synovial fluid to provide evidence of the effect of a joint environment on sustained release from the PLGA nanoparticles (Figure 3.7). Nanoparticles EE (30.9%) and LC (0.254%) were similar to that of nanoparticles delivering into PBS. However, the vast majority of encapsulated drug was released rapidly from nanoparticles (91.0%). This indicates that the environment nanoparticles are subjected to within the synovial fluid has a destabilising effect supported by evidence from nanoparticle physical property characterisation in synovial fluid (Figure 3.2). It has been demonstrated that microscale particle isolation via centrifugation is reduced in biological media of higher viscosity (Momen-Heravi et al., 2012). Therefore, the high suspension viscosity of synovial fluid in this study could have affected the ability to collect nanoparticles via centrifugation and hence retrieve accurate values for drug release. In an attempt to address this, synovial fluid release study samples were diluted 1:5 in PBS prior to centrifugation. However, a potential step could have been to perform release studies in a range of synovial fluid dilutions in order to ascertain the impacts of synovial fluid properties on GluR antagonist release. Alternatively, the methods developed by Thing et al., (2019) could have been used to carry out release studies from a donor media of GluR antagonist loaded nanoparticles suspended in synovial fluid across a dialysis membrane into PBS release media (Thing et al., 2019).

To allow for storage and ease of use, freeze dried nanoparticles have been routinely used. Sustained release of NBQX from freeze dried PLGA nanoparticles was achieved (Figure 3.8). Following the burst release of 81.7% of encapsulated drug, which is slightly lower than that

from 20mM DNQX loaded nanoparticles (87.7%), the remaining NBQX was delivered over the course of 3 weeks (504hrs). However, EE and LC of 20mM NBQX loaded freeze dried nanoparticles (EE 12.9%, LC 0.850%) are reduced compared with 20mM DNQX loaded nanoparticles (EE 26.5% LC 1.741) that have not been freeze dried (Figure 3.6B and 3.8). The potential impact of freeze drying on GluR antagonist load and particle stability has been discussed in section 3.4.2. To provide more a direct comparison, drug release studies with 20mM DNQX loaded freeze dried nanoparticles would need to be carried out thereby removing the variation in GluR antagonist type.

The freeze-drying method used in this thesis provided good nanoparticle redispersibility and retained nanoparticle sustained drug delivery capacity, despite a reduced delivery time frame (from 5 weeks to 3 weeks) (Figures 3.4 and 3.8). This method has revealed nanoparticles with characteristics allowing for investigation into the effects of low concentration sustained NBQX release compared to and in combination with free NBQX (chapter 5) and thereby addressing the sustained release delivery system component of the thesis hypothesis.

3.3.4 PLGA Nanoparticle Concentration Impacts Bone Cell Viability

The purpose of aim 4 was to test the toxicity of PLGA nanoparticles to support *in vitro* application for investigation into the effects of sustained GluR antagonist release systems and address the thesis hypothesis (section 3.1.1). PLGA is a recognised biocompatible and biodegradable polymer (Bobo et al., 2016). Therefore, in selecting PLGA as the major nanoparticle component, while utilising a lower toxicity solvent such as ethyl acetate (NCBI, 2019) in preparing the formulation, there is a reduced risk of cellular toxicity. To confirm this, PLGA nanoparticles were applied to hOBs. This is a cell type within the joint shown to be effected by GluR application (Bonnet et al., 2015, Bonnet et al., 2020) and, therefore, of interest to therapeutic intervention through sustained GluR delivery. To ascertain the effect of nanoparticle constituents alone (and not GluR antagonists), blank PLGA nanoparticles were applied to hOBs for differing time points (1, 3 and 7 days) at a concentration range of 0.1 to 100mg/ml (Figure 3.9). Effects on cellular activity were determined via an MTS assay for the quantification of mitochondrial activity in viable cells. MTS assays work by

calorimetrically quantifying levels of formazan that is produced from the conversion of tetrazolium salt by cell mitochondrial activity. None of the applied nanoparticle concentrations had an effect on decreasing MTS production compared to untreated controls, which reinforces the evidence that PLGA is not toxic. However, at all-time points the 100mg/ml treated cells showed significantly increased mitochondrial activity compared to controls. 10mg/ml treated cells demonstrated a less pronounced but significant increase compared to controls at days 3 and 7. This effect was not likely due to high particle concentrations influencing the 96 well plate reader absorbance readings as this was accounted for by normalising results to readings from cell free media containing the same nanoparticle concentration as used on cells. There is some evidence that PLGA, when in scaffold form, can display MTT formazan dye sorption and hence cause false negative results. This could be the case with these very high nanoparticle concentrations (Qi et al., 2011). Multiple cell culture studies have indicated that PLGA nanoparticles have no significant effect on cytotoxicity determined by MTS assays (Destache et al., 2009, Amjadi et al., 2013, Wang et al., 2015). The nanoparticles formulated in this chapter did not effect cell viability at concentrations of 1 or 0.1mg/ml (Figure 3.9). However, high particle concentrations (100mg/ml) have not delivered reliable findings hence present a potential risk to cell viability. To optimise GluR antagonist drug delivery from these PLGA nanoparticles, a balance must be struck between delivering a therapeutic GluR antagonist load and minimising the risk of affecting cellular viability though high PLGA concentration.

The purpose of aim 4 was to test the cytotoxicity of PLGA nanoparticles to then support in vitro application in cells culture studies (Chapter 5) and address the thesis hypothesis (section 3.1.1). Significant increases in MTS release following applications of high nanoparticle concentrations could be due to a potentially uncontrolled increase in mitochondrial activity. Therefore, for further *in vitro* testing, a PLGA nanoparticle concentration in the middle of this range will be selected (10mg/ml) to maximise the amount of GluR antagonist available (as GluR load is limited; section 3.4.3) for delivery while managing any potential effects to cell viability.

3.3.5 Conclusions and Future Objectives

The overarching aim of this chapter was to synthesise and characterise sustained release PLGA nanoparticles for delivery of GluR antagonists and investigate options for long term nanoparticle storage and thereby contribute to the thesis hypothesis by providing a platform for sustained GluR antagonist delivery for investigation into protective effects on inflammatory or mechanically driven pathways in bone *in vitro.* This chapter demonstrated the synthesis of nanoscale particles with good size dispersion (Figures 3.1A+B) which delivered a sustained release of low concentrations of GluR antagonists over 3 to 5 weeks (Figures 3.6 and 3.8). Development of a hydrogel delivery vehicle allowing for shorter term sustained release but with higher concentrations of GluR was investigated in chapter 4 of this thesis to provide additional sustained delivery platforms with differing release characteristics.

Low zeta potential values (Figure 3.1C) indicated a potential lack of particle stability which was further supported by altered nanoparticle physical properties in synovial fluid (Figure 3.2) and a lack of sustained GluR antagonist release in the same biological suspension (Figure 3.7), these findings indicated that this nanoparticle formulation may not be suitable for *in vivo* investigations into sustained release. However, GluR loaded PLGA nanoparticles maintained their physical properties in *in vitro* cell culture media (Figure 3.2) indicating potential to utilise this delivery vehicle in further *in vitro* investigations.

To allow for nanoparticle storage and ease of use (e.g. dilutions to varying nanoparticle concentrations), a freeze-drying methodology was investigated. Results indicated that freeze-dried nanoparticles redispersed with only small non-significant changes to size, PDI and physical appearance (Figures 3.4 and 3.5). Following freeze drying, sustained drug delivery was still possible at a reduced timeline from 5 down to 3 weeks (Figure 3.8). Additionally, results from zeta potential quantification and drug release studies may point to a loss of GluR antagonist loading correlating with a less negative zeta potential and a reduced EE and LC. Freeze drying capability allows for a GluR antagonist loaded sustained delivery vehicle that can be stored at low temperatures (4°C) to improve shelf life by reducing encapsulated drug losses (Gürsoy et al., 1989).

Blank PLGA nanoparticles were applied to hOBs and an MTS assay carried out to help determine suitability for *in vitro* application. PLGA nanoparticles did not decrease bone cell (hOB) MTS release at any concentration but did induce an increase in MTS release when high concentrations were applied (100mg/ml) (Figure 3.9). Nanoparticle concentration must, therefore, be taken into consideration when planning application *in vitro* to maximise GluR delivery while avoiding any potential cytotoxic effects. Future work could carry out a range of toxicity tests using nanoparticles at concentrations required to deliver a therapeutic dose to further explore the cellular impact of applying these nanoparticles. This would provide a wider set of evidence as to their toxicity. This final perspective as been partially addressed in chapter 5 of this thesis which indicates increased LDH release from NBQX loaded nanoparticle (10mg/ml) treated cells compared to all other treatment groups (control, free NBQX and IL-6 treated; Figure 5.5).

Chapter 4

Development of a Thermoresponsive Hydrogel for Localised Subcutaneous Delivery of GluR Antagonist

4.1 Introduction

IA injection is the most common route to locally administer therapeutics in the management of OA. However, this comes with accompanied risk of infection and requires administration by a healthcare professional (Glyn-Jones et al., 2015) (detailed in section 1.5.1.4). Subcutaneous drug delivery relies on the delivery of drug doses into the vasculature or lymph system via a deep layer of the dermis called the subcutis and provides a delivery option that bypasses the GI tract (Figure 4.1; detailed in section 1.5.1.3) (Jones et al., 2017). Subcutaneous drug delivery can allow for increased ease of application by patients with the added benefit of being less invasive than IA injection while bypassing the barrier of the stratum corneum (Dietrich et al., 2014, Freundlich et al., 2014, Bansback et al., 2015).

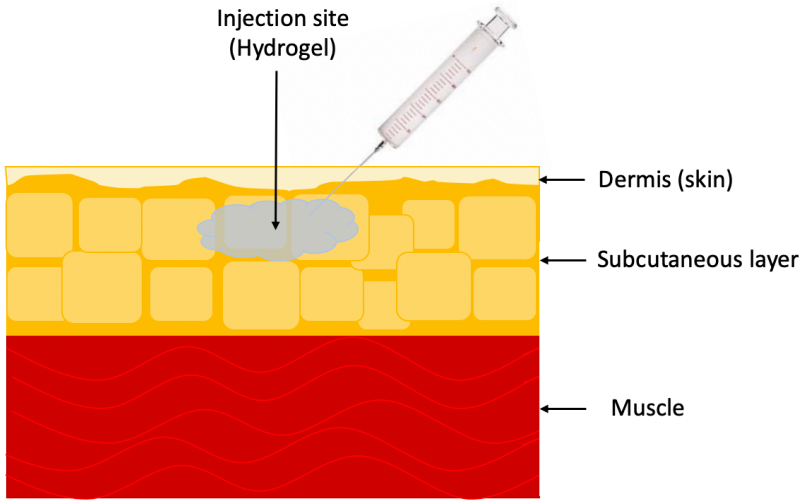

Figure 4.1: Diagrammatic representation of subcutaneous injection. Subcutaneous injections are reviewed in more detail in Section 1.5.1.3 (image designed by Author).

Thermoresponsive hydrogels can deliver a sustained drug dose while protecting drugs from clearance and improving half-life (detailed in section 1.5.3). It has been shown that IA injection of GluR antagonist NBQX on two consecutive days results in an improved therapeutic effect compared to a single injection (Bonnet et al., 2020). Therefore, investigating a short term (2 day) sustained NBQX delivery via a less invasive subcutaneous administration in the form of an injectable thermoresponsive hydrogel could be of

therapeutic benefit. This establishes a semisolid monolith of GluR antagonist below the skin that will provide slow sustained drug release to the joint area. This would add to the evidence indicating that GluR antagonists could represent a novel arthritic disease modifying therapeutic at concentrations of 2.5 and 20mM (Bonnet et al., 2015, Bonnet et al., 2020).

Hydrogels have been extensively investigated for a range of applications. These include: encapsulation of cells (Sefton et al., 2000); scaffolds to aid in the repair and regeneration of organs or tissue, key in the field of tissue engineering (Naahidi et al., 2017); and as drug delivery systems (Chatterjee et al., 2018). Of specific interest for this chapter are thermosetting hydrogels that utilise a range of natural polymers such as chitosan, gelatin and cellulose and synthetic polymers such as Pluronic's, Poloxamers and pNIPAM (Klouda, 2015) to change physical characteristics in response to a temperature stimulus. This is of particular interest to biomedical applications, allowing for a minimally invasive injectable liquid to be delivered and be induced to gel once raised to body temperature (Klouda, 2015). A common characteristic of thermoresponsive polymers utilised in hydrogels is a lower critical solution temperature. This is the temperature above which the hydrogel undergoes a transition from a liquid to a gel (sol-gel) which can be quantified experimentally using rheology (Ward and Georgiou, 2010).

A common synthetic polymer utilised in thermoresponsive hydrogels is Pluronic-F-127. Pluronic's are triblock copolymers consisting of poly(ethylene oxide)-*b*-poly(propylene oxide)-*b*-poly(ethylene oxide) (PEO-PPO-PEO). PEO is polar and PPO is non-polar. The presence of hydrophobic and hydrophilic monomers organised into block copolymers means Pluronic's can form ordered structures in solutions (Russo and Villa, 2019). Pluronic's follow a two-step gelling process involving the formation of spherical micelles followed by stacking of micelles to form a gel as temperature increases (Figure 4.2) (Klouda, 2015).

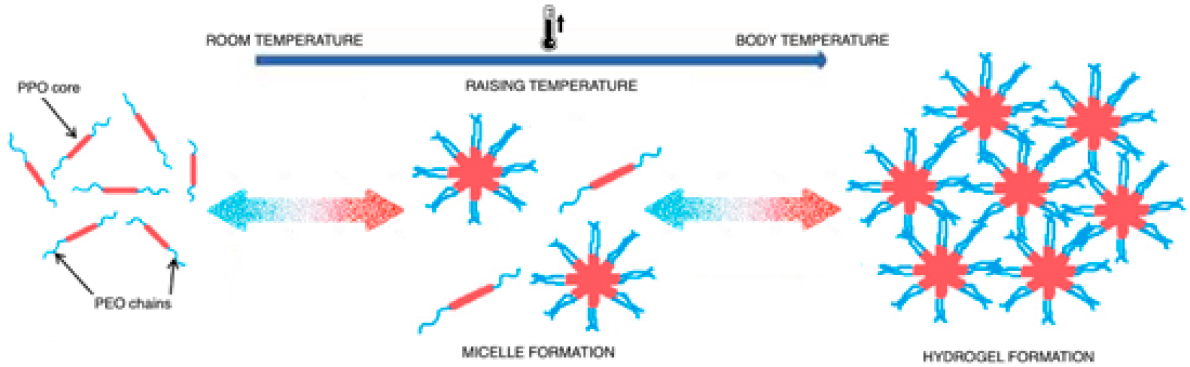

Figure 4.2: A diagrammatic representation of the mechanism of Pluronic hydrogel formation over a change in temperature, taken from Russo and Villa, 2019. Permissions granted for use of this fiaure in this thesis.

Pluronic F-127 (Poloxamer 407) is the most extensively studied of the Pluronic's used in drug delivery due to its lower critical gelation concentration, the concentration required to form a gel at a specified temperature, and it having the lowest toxicity of the Pluronic range (Gong et al., 2013). Additionally, Pluronic F-127 has been utilised in the sustained delivery of several therapeutics (Kabanov et al., 2002, Guo et al., 2009, Jung et al., 2017) and allows for simple incorporation of water-soluble drugs, such as the GluR antagonists utilised in this study. Pluronic F-127 hydrogels have exhibited low mechanical strength and have stability issues such as rapid dissolution in biological fluids (Akash and Rehman, 2015). To overcome these problems Pluronic F-127 hydrogels have been combined with other components to optimise physical properties. For example, Pluronic F-127 and HA-based hydrogels were shown to elicit enhanced mechanical strength compared to Pluronic alone, while providing sustained release of the NSAID, piroxicam, to treat arthritis *in vivo* (Jung et al., 2017).

Carbopol's have been shown to exhibit high viscosity at low concentrations and low toxicity making them a useful component for hydrogel drug delivery vehicles in combination with the thermoresponsive properties of Pluronic F-127. Additionally, Carbopol 934 based gels have been investigated as a bioadhesive drug delivery system (Craig et al., 1994) to enhance localised drug delivery. Carbopol 934 has been demonstrated to contain hydrogel mucoadhesive properties in multiple studies (Sahoo et al., 2011, Ahmed and Bhaduri, 2017, Ali et al., 2019, Nagar et al., 2019) and has been shown to increase viscosity and bioadhesiveness of gels when incorporated (Shin et al., 2000b). The bioadhesive and viscous

properties of Carbopol 934 containing gels could be utilised to enhance the thermoresponsive drug delivery properties of Pluronic F-127 hydrogels.

In a Pluronic F-127 based hydrogel, the addition of mucoadhesive Carbopol 934 reduced the gelation temperature of hydrogels under investigation (Gaikwad, 2010). Combined Pluronic F-127 and Carbopol 934 containing hydrogels provide sustained drug delivery (12 hours) and optimum gelation time, viscosity and bioadhesive strength compared to Carbopol free formulations without altering gel stability (25°C/60% relative humidity) for 3 months (Hani and Shivakumar, 2013). Sustained drug delivery of an anti-arthritic agent (Aceclofenac) has been demonstrated in Pluronic F-127 and Carbopol 934 hydrogels (Fathalla et al., 2014). Drug released from these vehicles occurs from a combination of spontaneous release and surface erosion by local fluids. More details on drug delivery from thermoresponsive Pluronic F-127 based hydrogels can be found in Section 1.5.3 in the introduction of this thesis.

Utilisation of Pluronic F-127 with Carbopol-934 has been investigated in this chapter in the development of a bioadhesive thermoresponsive hydrogel for the subcutaneous delivery of GluR antagonists to treat arthritis. The gel would be injected as a liquid under the skin over the affected join, to allow thermosetting in situ. The released drug would then passively diffuse across the synovial membrane and into the synovial fluid. This would provide an advantage over IA injection in that there would be no physical trauma and a risk of infection to the joint capsule. This chapter focuses on the first part of the thesis hypothesis to determine whether AMPA and kainate glutamate receptor (GluR) antagonists can be incorporated into the sustained release hydrogels

4.1.1 Hypothesis, Aims and Objectives

Thesis Hypothesis: AMPA and kainate glutamate receptor (GluR) antagonists can be incorporated into sustained release delivery systems that can protect against inflammatory or mechanically driven pathways in bone *in vitro.*

This chapter contributes towards the thesis hypothesis via the overarching aim below, which has been further subdivided into a series of aims and objects:

Overarching Aim: To synthesise and characterise a thermoresponsive hydrogel for delivery vehicle for GluR antagonists; determine GluR sustained release characteristics and investigate GluR antagonist permeation through the synovial membrane.

Aim 1: To synthesise Pluronic F-127 based thermoresponsive hydrogels loaded with DNQX and test physical responses to temperature change.

Objective 1.1: To synthesise hydrogels over a range of Pluronic F-127 concentrations (19%, 22%, 25%, 28%) incorporating 2.5mM DNQX.

Objective 1.2: To evaluate hydrogel viscosity and viscoelastic and elastic moduli when exposed to a linear temperature increase (5 to 45°C) over time (2°C/minutes).

Objective 1.3: Quantify sol-gel transition temperature and use it to select optimal Pluronic F-127 concentration for hydrogel injection and subcutaneous gel formation.

Aim 2: To investigate DNQX release rate from thermoresponsive hydrogels.

Objective 2.1: To inject hydrogels loaded with 2.5mM DNQX at optimal Pluronic F-127 concentration into dialysis cassette and measure the release of DNQX into PBS at 37°C over 27 hours using HPLC.

Objective 2.2: To inject hydrogels loaded with 2.5mM DNQX at optimal Pluronic F-127 concentration into a Franz diffusion chamber containing bovine synovial membrane and measure the release of DNQX into PBS at 37°C over 48 hours using HPLC.

Aim 3: To test toxicity of Pluronic F-127 thermoresponsive hydrogels.

Objective 3.1: To expose human primary osteoblast to a range of vehicle loaded thermoresponsive hydrogel concentrations and test cell viability over 1-7 days using MTS assay.

4.2 Results

4.2.1 Thermoresponsive Hydrogel Rheology

4.2.1.1 Temperature Change Effects of Pluronic F-127 and Carbopol 934 Hydrogel Viscosity

Pluronic F-127 concentration significantly affected gel viscosity upon exposure to increased temperature (1-way ANOVA, P<0.0001; Figure 4.3).

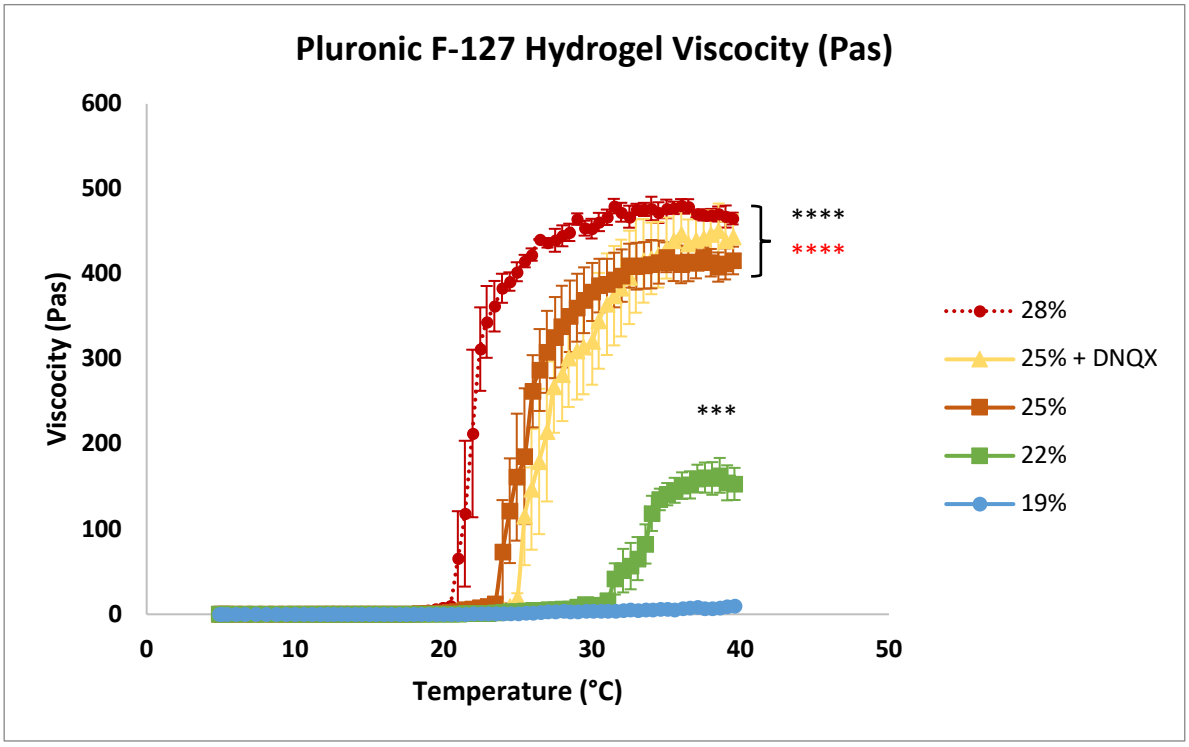

*Figure 4.3: Pluronic F-127 based hydrogel viscosity changes measured over a temperature gradient of 5 to 40 ℃. Within 2 minutes of removal from storage at 5 ℃, the hydrogel under investigation (1ml) was added to the rheometer plate for testing (PP-20, 20mm insert with 750μm gap width), temperature increase set to 2 ℃/min and a fixed shear value of $1s^{-1}$ applied (section 2.3.2). Percentages in this figures' legend refer to percentage w/v of Pluronic F-127 in hydrogel. 2.5mM DNQX was used in 25% w/v hydrogel. (n=3; independent repeat experiments). ***P<0.001 / ****P<0.0001 vs 19% w/v Pluronic F-127 hydrogels, ****P<0.0001 vs 22% w/v Pluronic F-127 hydrogels (1-way ANOVA).*

19% w/v Pluronic F-127 hydrogels did not increase in viscosity at higher temperatures, indicating a failure to set. 22% w/v F-127 hydrogels steeply increased in viscosity with a sol-gel transition from 31.1 to 37.1°C and a maximum viscosity of 163±20.5Pa. 25% w/v

Pluronic F-127 steeply increased in viscosity with a sol-gel transition from 23.5 to 30.5°C and a maximum viscosity of 420±17.5Pa. 25% w/v Pluronic F-127 hydrogels with the inclusion of 2.5mM DNQX increased steeply in viscosity with a sol-gel transition between 24.9 and 33.5°C and a maximum viscosity of 451±31.4Pa. 28% w/v Pluronic F-127 hydrogels demonstrated a rapid increase in viscosity with a sol-gel transition between 20.4 to 26.5°C and maximum viscosity of 480±7.8Pa. At 37.1°C, close to human core body temperature, the viscosity of all other Pluronic F-127 concentrations were significantly higher than 19% w/v ($p<0.0001$ for 28%, 25% and 25%+DNQX; $P<0.001$ for 22%). The viscosity of 25%, 25% +DNQX and 28% w/v Pluronic F-127 hydrogels was significantly ($p<0.0001$) higher than that of 22% at 37.1°C. No significant difference was found between, 25%, 25% +DNQX and 28% w/v Pluronic F-127 hydrogels ($p>0.05$).

4.2.1.2 Temperature Change Effects on Pluronic F-127 and Carbopol 934 Hydrogel Viscous and Elastic Moduli

The crossover point where G'>G" indicates the temperature at which a sol-gel transition has taken place, where the hydrogel has transferred from a liquid to a gel like state (Figure 4.4). 19% w/v Pluronic F-127 hydrogels sol-gel transition takes place between 22.7 and 23.2°C at values of 3.97±1.88Pa for G' and 3.53±0.94Pa for G" (Figure 4.4A). In 19% w/v gels, viscosity did not exhibit a dramatic increase at greater temperatures (Figure 4.3). In the 22% w/v Pluronic F-127 hydrogel sol-gel transition takes place between 19.7 and 20.2°C with G'=5.04±1.29Pa and G"=4.20±1.00Pa (Figure 4.4B) with an increase in viscosity initiating at 31.1°C (Figure 4.3). 25% w/v Pluronic F-127 hydrogels show a sol-gel transition temperature between 19.2 and 19.7°C, with G'=13.9±6.43Pa and G"=11.09±1.91Pa (Figure 4.4C). An increase in viscosity from 23.5°C was observed for this gel (Figure 4.3). 25% w/v Pluronic F-127 hydrogels loaded with 2.5mM DNQX show a sol-gel transition temperature between 21.2 and 21.8°C with G'=29.91±11.07Pa and G"=27.23±11.43Pa (Figure 4.4D). For this gel an increase in viscosity from 24.9°C was observed (Figure 4.3). 28% w/v Pluronic F-127 hydrogels exhibit a sol-gel transition at between 18.8 and 19.3°C with G'=21.04±7.51 Pa and G"=19.03±2.52Pa (Figure 4.4E). An increase in viscosity for this gel was observed from 20.4°C (Figure 4.3). For 19%, 22% and 28% w/v Pluronic F-127 G'<G" at higher

temperatures. 19% Pluronic hydrogels demonstrate a transition to G'< G" between 36.7 and 37.2°C where G'=98.62±13.75Pa and G"=100.56±16.27Pa (Figure 4.4A). 22% Pluronic F-127 hydrogels demonstrate a transition to G'<G" between 40.7 and 41.2°C where G'=2056.67±151.33Pa and G"=2086.67±229.73Pa (Figure 4.4B). 28% Pluronic F-127 hydrogels demonstrate a transition to G'< G" between 37.2 and 37.7°C where G'=4735±304.5Pa and G" =4753±223.3Pa (Figure 4.4E).

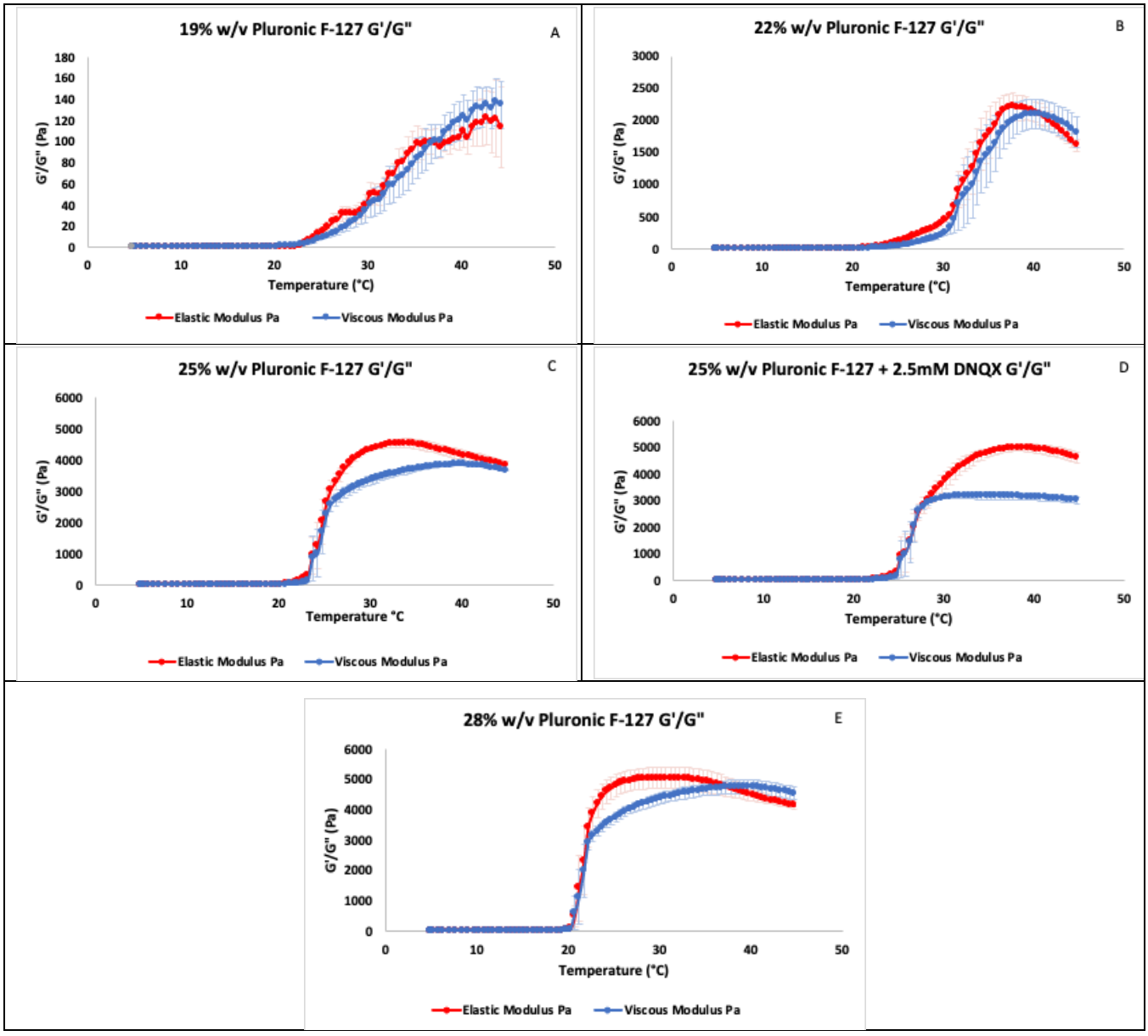

Figure 4.4A-E: Elastic (G') and viscous (G") moduli changes over a temperature gradient of 5-45 ℃ (temperature increase of 2 ℃/min). Viscoelastic quantification was carried within 2 minutes of removal from storage at 5°C, the hydrogel under investigation (1ml) was added to the rheometer plate for testing. A stress of 0.1Pa at a constant frequency of 1Hz was applied using a PP-20, 20mm insert with a gap width of 750μm (Section 2.3.2). A) 19% w/v Pluronic F-127 content hydrogels. B) 22% w/v Pluronic F-127 content hydrogels. C) 25% w/v Pluronic F-127 content hydrogels. D) 25% + 2.5mM DNQX w/v Pluronic F-127 content hydrogels. E) 28% w/v Pluronic F-127 content hydrogels. (n=3; independent repeat experiments).

4.2.2 DNQX Release from Thermoset Hydrogels at 37°C

There was no significant main effect for Pluronic F-127 concentration on DNQX release ($p=0.936$) (2-way ANOVA, Figure 4.5). Free DNQX positive controls demonstrated a lag of 1hr until 100% release was detected. This lag would, therefore, also apply to the release rate from hydrogels. Hydrogel sustained release was maintained for up to 27 hours (1620 minutes). DNQX concentration in release media (PBS) was significantly greater at 1hr than at 5 minutes (7.1-fold increase for 22% Pluronic hydrogels; 4.83-fold increase for 25% Pluronic hydrogels ($p=0.001$ and $p=0.003$ respectively). At 4hrs DNQX release was significantly greater than at 1hr (2.3-fold for 22% Pluronic and 2.2-fold for 25% Pluronic hydrogels, $p=0.0499$). DNQX release at 22hrs was significantly greater than at 4 (1.6-fold for 22% Pluronic and 1.6-fold for 25% Pluronic hydrogels, $p<0.0001$) and 6hrs (1.3-fold for 22% Pluronic and 1.3-fold for 25% Pluronic hydrogels, $p=0.014$). Positive controls of free DNQX released 100% of encapsulated drug after 1 hour.

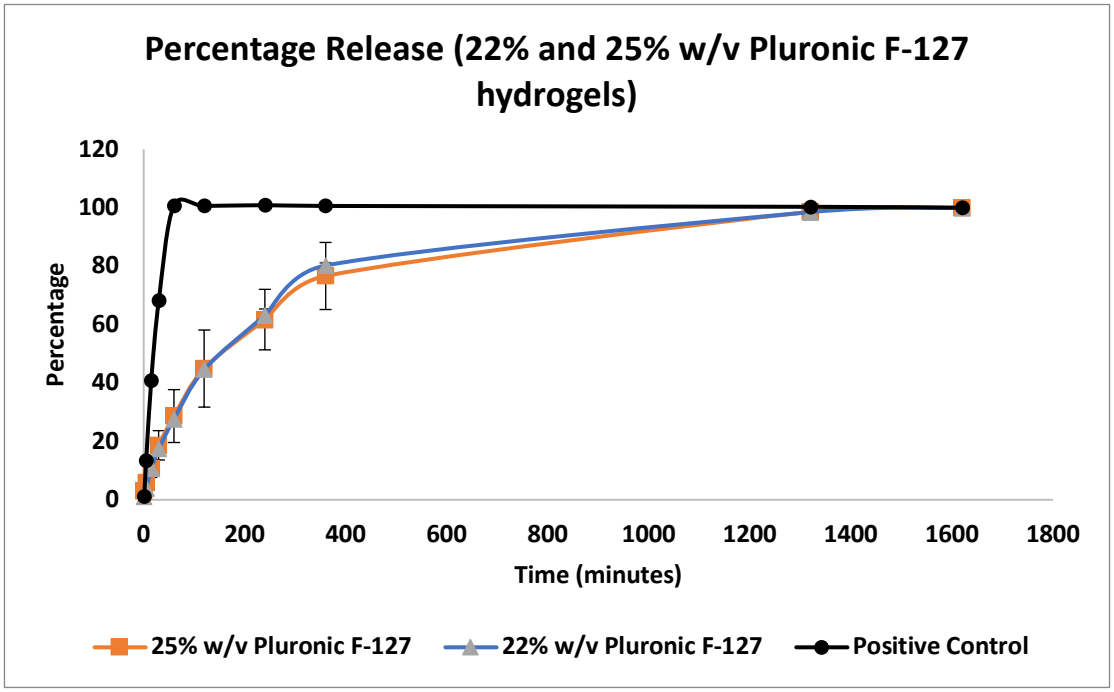

Figure 4.5: Percentage DNQX release from 22% and 25% w/v Pluronic F-127 hydrogels (2ml) across a 10KDa Mw cut off Slide-A-Lyzer® dialysis cassette membrane (3ml capacity, Thermo Scientific) into 37°C PBS (pH7.4). Each gel was loaded with 2.5mM DNQX and compared to positive control of 2.5mM unencapsulated (free; 2ml) DNQX permeating the dialysis cassette membrane (section 2.3.3). Gels were set at 37°C for 5 minutes in dialysis cassettes prior to release studies (n=3; independent repeat experiments).

4.2.3 Synovial Membrane Diffusion of DNQX from Thermosetting Hydrogel

DNQX release from a 25% w/v Pluronic F-127 hydrogel through a bovine synovial membrane was sustained for up to 24 hours (Figure 4.6). 97.8±10.37μM/cm^2 DNQX diffused through the synovial membrane representing a total amount of 76.8±8.1μM. The steady state flux representing the amount of DNQX to flow through the synovial membrane area over time was calculated between 0.25 and 6 hours to be 5.92±0.57J (μM/cm^2/hr) and between 4 to 24hrs to be 3.69±0.37J. The flux between 24 and 48hrs was 0 (Figure 4.6).

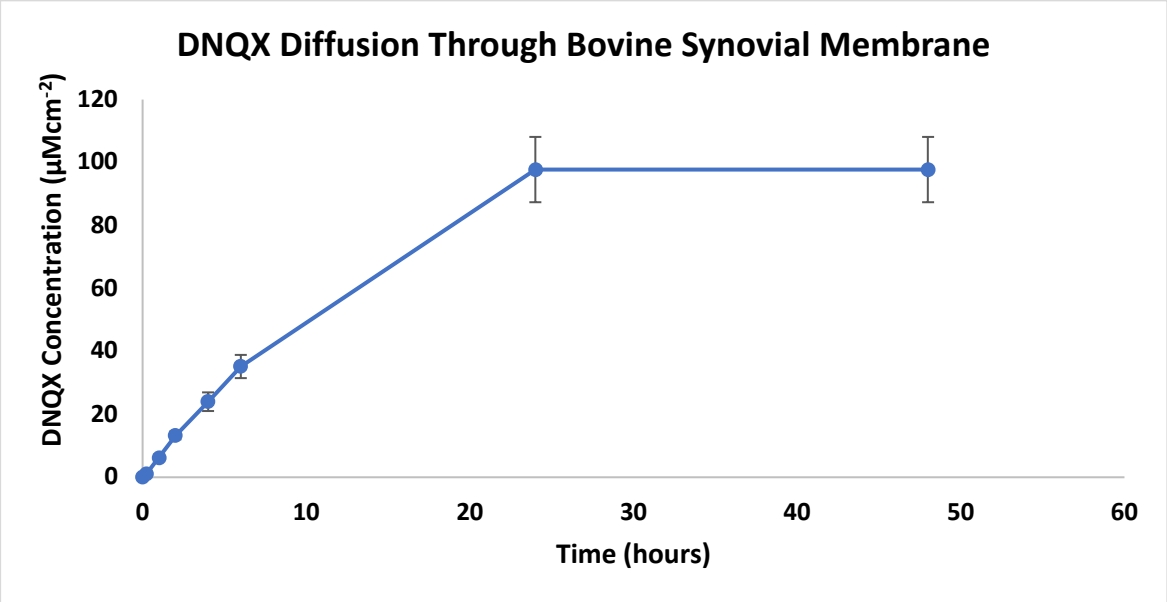

Figure 4.6: FDC study quantifying DNQX diffusion, through bovine synovial membrane explants (Section 2.3.4), from 25% w/v Pluronic F-127 hydrogels synthesised according to methods in Section 2.3.1. Hydrogels were loaded with 2.5mM DNQX and diffusion apparatus set up according to methods section 2.3.5. A PBS receptor phase (pH 7.4, 37°C) was used, from which DNQX concentration diffusing from hydrogels through the bovine synovial membranes was quantified over time (Section 2.3.5) (n=3; independent repeat experiments).

4.2.4 Thermosetting Hydrogel Toxicity on Primary Human Osteoblast Cells

Media was conditioned with various amounts of 25% w/v Pluronic F-127 hydrogels (1:1 to 1:8 hydrogel:media) for 1,3 or 7 days and the effects on hOB viability over 3 days assessed by MTS assay (Figure 4.7). For MTS release, the impact of conditioning ratio and time was assessed via comparison on individual treatment groups with controls. This revealed that a 1:1 hydrogel to media ratio resulted in a significantly decreased MTS release compared to controls at day 1 (3.7-fold decrease, p=0.004, Mann Whitney U), 3 (4.7-fold, p<0.0001, t-

test) and 7 (8-fold, p=0.04, Mann Whitney U). For 1:2 hydrogel to media ratio MTS release decreased on days 1 (3.1-fold, p=0.004, Mann Whitney U), 3 (3.8-fold, p=0.004, Mann Whitney U) and 7 (3.5-fold, p=0.004, Mann Whitney U). For 1:4 hydrogel to media ratio MTS release decreased on days 1 (2.4-fold, p<0.0001, t-test), 3 (2.5-fold, p=0.004, Mann Whitney U) and 7 (2.3-fold, p<0.0001, t test). For 1:8 hydrogel to media ratio MTS release increase compared to controls at day 1 (1.2-fold, p=0.031, t-test) and decrease at day 7 (1.5-fold, p<0.0001, t-test). There was no significant difference in 1:8 hydrogel to media cells at day 3 vs controls.

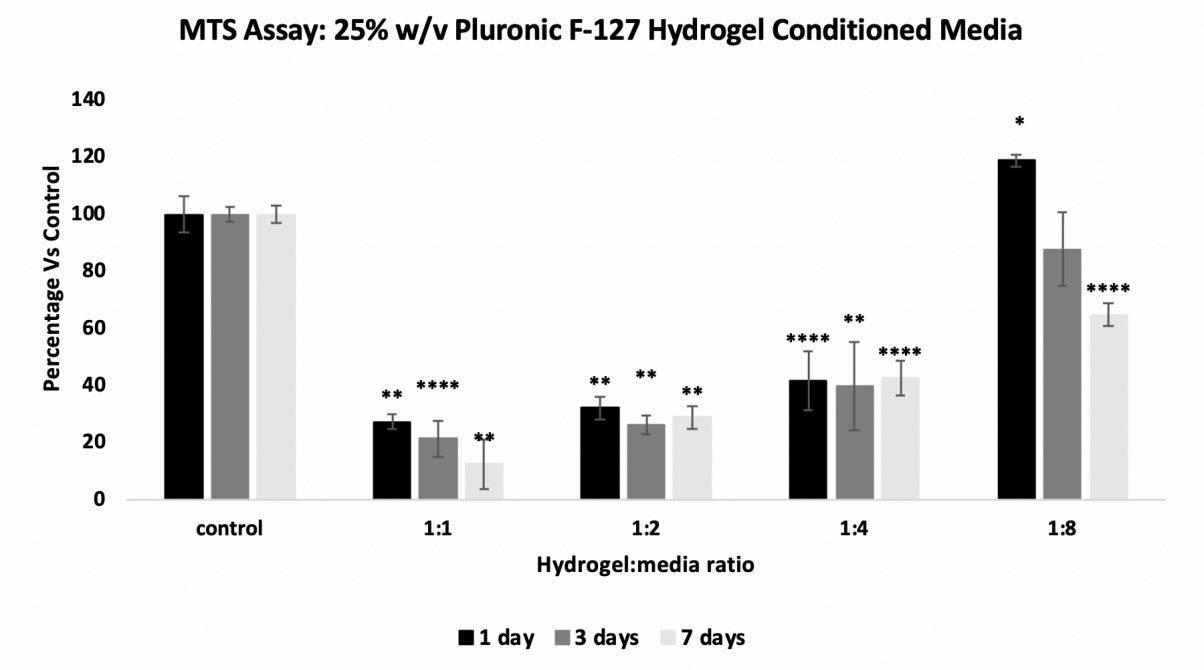

*Figure 4.7: The percentage release of MTS from primary human osteoblasts (hOBs) following 72hrs exposure hOB cell culture media (Section 2.5.2) conditioned with 25% w/v Pluronic F-127 hydrogels at a range of ratios (Hydrogel:media ratios: 1:1, 1:2, 1:4 and 1:8) vs untreated controls (n=6; cell culture well replicates). Hydrogels were set for 5 minutes at 37°C prior to conditioning with media and media conditioning lasted for 1, 3 or 7 days prior to application on hOBs (Section 2.12.2.2). *p<0.05, **p<0.01, ****p<0.0001 vs control.*

4.3 Discussion

The overarching aim of this chapter was to develop and test a sustained release thermoresponsive hydrogel for delivery of GluR antagonists and thereby contribute to the sustained delivery system development component of the thesis hypothesis (section 4.1.1) along investigations into nanoparticle delivery vehicles developed in chapter 3 of this thesis.

4.3.1 Pluronic F-127 Concentration in Hydrogels Alters their Rheological Properties

Aim 1 of this chapter investigated Pluronic F-127 based formulations rheological properties in response to temperature with and without DNQX loading to gain an understanding of the thermoresponsive properties of this formulation and contribute to the overarching aim (section 4.1.1).

Rheological investigation compared the increase in hydrogel viscosity over a temperature gradient of 5 to 40°C to encompass both storage conditions and physiological core body temperature. Aside from 19% w/v Pluronic content, all hydrogels exhibited an increase in viscosity ranging between 20 and 37°C consistent with the literature which indicates 20% w/v concentrations or higher are thermally gelling (Figure 4.3) (Derakhshandeh et al., 2010). Viscosity increases with temperature have been shown in the literature for Pluronic F-127 aqueous solutions (Jalaal et al., 2017) and in a 20% w/v Pluronic F-127 and 0.5% w/v Carbopol 934 hydrogel formulation a 35-fold increase in viscosity was observed between 8 and 37°C (Venkatesh et al., 2013). Due its lack of viscosity changes with increases in temperature, 19% w/v Pluronic F-127 hydrogels were not suitable for further investigation into drug delivery applications (Figure 4.3).

As reported by others, the temperature range at which viscosity changes occurred was inversely proportional to the Pluronic F-127 concentration (Klouda, 2015). 25% and 28% Pluronic F-127 hydrogels have a significantly higher viscosity at human core body temperature (37°C) than both 19% and 22% w/v Pluronic F-127 hydrogels (Figure 4.3).

22% w/v F-127 hydrogels exhibited a steep increase in viscosity from 31.1 to 37.1°C. Comparison of 22% w/v Pluronic F-127 elastic and viscous moduli demonstrates that G'>G", indicating a transition from a solution into a gel like material (Mayol et al., 2008), from between 19.7 and 20.2°C. However, a dramatic increase in G' and G" values occurred between 30.7 and 38.2, consistent with the observed increases in viscosity at similar temperatures (Figure 4.4B). 22% w/v Pluronic F-127 hydrogels are gel-like at physiological temperature (37°C) with a less rapid change in viscosity than 25% and 28% Pluronic hydrogels. External loading and physical movement would result in shear forces applied to the hydrogel at the site of injection. These forces are reduced in subcutaneous tissue compared to the skin surface (Ohura et al., 2008). However, a less viscous gel would have a potentially reduced capacity to withstand physiological shear forces and erosion (Gioffredi et al., 2016, Deliormanlı and Türk, 2019). Selection of an injection site less exposed to movement or impact, as well as application of protective dressings may reduce the impact of shear forces to subcutaneously injected hydrogels (Ohura et al., 2008).

25% w/v Pluronic F-127 hydrogels sharply increase in viscosity between 23.5 and 30.5°C for unloaded hydrogels and between 24.9 and 33.5°C for 2.5mM DNQX loaded hydrogels indicating that DNQX increases the temperature required to induce a sol-gel transition. This is supported by elastic and viscous moduli that indicate unloaded hydrogels undergo a sol-gel transition between 19.2 and 19.7°C whereas DNQX loaded hydrogels undergo a sol-gel transition between 21.2 and 21.8°C (Figures 4.4C and D). DNQX is in the form of a disodium salt and salt concentration is known to influence the transition temperature of thermoresponsive polymer hydrogels (Gandhi et al., 2015) with increased concentrations of salt content having been shown to increase hydrogel sol-gel transition temperature (Kundu et al., 2010). This information indicates that control of drug loading is required to ensure consistency of hydrogel thermoresponsive characteristics. Drug free hydrogels at this Pluronic F-127 concentration have a rapid increase in G'/G" between 23.6 and 25.6°C which fits within the temperature range for increase in viscosity (Figure 4.4C). With the addition of DNQX these hydrogels demonstrated a rapid increase in G'/G" between 24.7 and 27.7°C (Figure 4.4D). This also aligns closely with the temperature range shown to induce a rapid increase in DNQX loaded hydrogel viscosity (Figure 4.3). As Sol-gel transition still occurs

below human body temperature but above so low a temperature as to impede injectability. 2.5mM DNQX loading does not influence the compatibility of these hydrogels for clinical application.

28% w/v Pluronic F-127 hydrogels show a sharp increase in viscosity between 20.4 to 26.5°C and a sol-gel transition between 18.8 and 19.3°C. A rapid increase in G'/G" was identified between 20.2 and 22.2°C which aligns with the rapid increase in viscosity (Figure 4.4E). 28% w/v Pluronic F-127 hydrogels were not selected for further investigation because, despite clear thermoresponsive characteristics, the sol-gel transition temperature was the lowest of all tested Pluronic F-127 concentrations (18.8-19.3°C) making it the highest risk of gelation prior to injection. To further support this decision, G' transitioned to <G" at between 37.2 and 37.7°C. There is little evidence in the literature to explain this transition (Derakhshandeh et al., 2010, Nie et al., 2011, Chatterjee et al., 2018). However, a change in the gel properties at physiological temperature and a potential lack of stability would make 28% w/v Pluronic F-127 hydrogel a less optimal drug delivery vehicle candidate.

Due to their higher sol-gel transition temperatures and sharp increases in viscosity over temperature 22% and 25% w/v Pluronic F-127 hydrogels were analysed for GluR antagonist delivery capacity (section 4.3.2.). One of the objectives of this study was to identify hydrogels suitable for subcutaneous delivery. A study by Webb measured subcutaneous temperature of human male subjects at a range of external temperatures. At an external temperature of 27°C, mean±standard deviation of subject's subcutaneous temperature was calculated as 33.5±1.3°C (Webb, 1992). Ambient or room temperature, as defined by the WHO and European and Japanese Pharmacopoeia regulatory guidelines for pharmaceutical products, is between 15 and 25°C (E.C.A., 2017). 22% w/v Pluronic F-127 hydrogels are still in the process of increasing in viscosity (31.1 to 37.1°C) at a 33.5°C subcutaneous skin temperature. 25% w/v Pluronic F-127 hydrogels have the benefit of gelation below subcutaneous temperature, while remaining liquid at room temperature (20°C). Having reached peak viscosity when loaded with 2.5mM DNQX between 24.9 and 33.5°C. 25% w/v Pluronic F-127 hydrogels were selected for further FDC (Section 4.3.3) and MTS assay hOB cell viability (Section 4.3.4) studies due to the steeper increase in viscosity and G'/G" at sub

physiological temperature vs 22% w/v Pluronic F-127 hydrogels and the use of this Pluronic concentration for release studies in the literature (Derakhshandeh et al., 2010).

Drug diffusion coefficients decrease with an increase in hydrogel viscosity and Pluronic F-127 content (Gilbert et al., 1986, Pandit and Wang, 1998). Using the highest concentration and viscosity of Pluronic F-127 hydrogel investigated in this study (28% w/v) may provide the longest sustained release of GluR antagonist through slower diffusion, which would be optimal in the treatment of a chronic condition such as OA. However, at this concentration, hydrogels are likely to gel prior to injection into the patient and, therefore, are not practical. 25% w/v Pluronic F-127 hydrogels provided the next highest concentration and viscosity levels that are not significantly different to that of 28% w/v hydrogels. Therefore, 25% Pluronic F-127 hydrogels provide the most useful rheological characteristics to be injectable as a liquid and gel *in situ* while optimising the Pluronic F-127 content to deliver extended sustained GluR antagonist delivery. These findings (Figure 4.3 and 4.4) indicate clear thermoresponsive characteristics of these hydrogel formulations and utilisation of a range of Pluronic F-127 concentrations allowed for selection of optimal rheological properties for carrying forward into further *in vitro* testing.

4.3.2 Sustained DNQX Release is Demonstrated from Pluronic F-127 Thermoresponsive Hydrogels *In Vitro* and Shown to Permeate through Biological Joint Membranes.

The second aim of this chapter was to investigate the DNQX release from thermoresponsive hydrogels to understand the sustained release capacity of these formulations for delivery of GluR antagonists (section 4.1.1).

Drug delivery from thermoresponsive hydrogels occurs as a combination of diffusion through the gel and dissolution as the gel dissolves (Ricci et al., 2005). Drug release from Pluronic F-127 hydrogels follow Higuchi's root square law (Barichello et al., 1999, Kim et al., 2000), which describes drug release as a diffusion process of the amount of drug released against the square root of time (Higuchi, 1962). Both 22% and 25% w/v Pluronic F-127 hydrogels deliver a 2.5mM DNQX load over 27 hours into PBS under physiological conditions

(37°C, pH7.4) with no differences in release rates between hydrogels (Figure 4.5). Positive controls of free DNQX release through the semi-permeable membrane indicate 1hr is required for the complete diffusion of a drug without encapsulation in hydrogels in this release study set up (Figure 4.5). This delay in release will also impact the hydrogel release data. However, comparison of 22 and 25% w/v Pluronic F-127 hydrogel release curves with the positive control curve does still indicate sustained delivery was achieved due to drug release from hydrogels. The release profile demonstrates that it follows closely Higuchi's square root law for the first 6 hours of release, consistent with drug release study investigations using other Pluronic F-127 formulations (Figure 4.5)(Jung et al., 2017, Deliormanlı and Türk, 2019). In comparison to the nanoparticles developed in chapter 3, hydrogels deliver only a short term sustained release (Figure 3.6 vs Figure 4.5). However, sustained GluR antagonist delivery over 24hrs from these hydrogels provides a platform to investigate the findings that demonstrate GluR antagonist IA injection on two consecutive days has a significantly increased anti-arthritic effect compared to a single injection *in vivo* using a PTOA model (Bonnet et al., 2020) but with the added benefit of removing the need for multiple injections and extending half-life by protecting the drug from clearance within the hydrogel.

Large increases in Pluronic F-127 concentration have been shown to reduce cumulative drug release (20% vs 30% w/v Pluronic F-127) (Derakhshandeh et al., 2010). However, the relatively small difference in Pluronic F-127 concentration between 22 and 25% Pluronic F-127 hydrogels may explain the lack of a significant release profile difference. Due to the synthesis methodology for these hydrogels, no GluR antagonist is lost through processing ensuring a consistent drug load can be obtained which differs from the low encapsulation efficiency and loading capacity of nanoparticles identified in chapter 3. However, this should be balanced with the effects of drug load on hydrogel rheological properties (see section 4.4.1). When delivering *in situ*, DNQX delivery from hydrogels can diffuse down across the synovial membrane to the target tissue but also diffuse laterally into surrounding tissue. This could mean that the dose of GluR antagonist delivered from these hydrogels into the joint is variable and that surrounding tissue would also be impacted. It is worth considering that in addition to bone (Chenu et al., 1998, Hinoi et al., 2003) and cartilage (Salter et al., 2004, Wang et al., 2005), glutamate signalling has been shown to present on synovial cells

(Flood et al., 2007, McNearney et al., 2010), nerves (Lawand et al., 2000), Schwann cells (Parpura et al., 1995), mast cells (Aniksztejn et al., 1990) and platelets (Vasta et al., 1993). Additionally, glutamate signalling has shown to play a role in peripheral nociception in inflammatory induced pain (Carlton and Coggeshall, 1999). Thus, glutamate receptor antagonist release from hydrogels into surrounding tissue could have multifactorial effects on a range of joint cells and neuronal signalling. This could have the capacity to further mitigate OA symptoms such as pain. However, there is also a risk of non-target tissue effects and studies to investigate potential side effects, following joint localised subcutaneous administration of these hydrogels to treat OA, should be carried out.

25% w/v Pluronic F-127 hydrogels are capable of delivering a sustained drug load through a bovine synovial membrane into PBS at physiological pH and temperature (pH7.4 and 37°C) (Figure 4.6). The steady state flux from 15 minutes to 24hrs was greater than the concentration at which a DNQX inhibits receptor binding (IC_{50}) at AMPA GluR binding sites (0.50±0.10μM) and kainite binding sites (2.0±0.1μM) in rat cortical membranes (Figure 4.6) (Honoré et al., 1988). With this in mind, sufficient DNQX is capable of passing through the bovine synovial membrane to elicit GluR receptor antagonism and potential deliver an antiarthritic therapeutic effect. The synovial membrane has no tight junctions or basement membrane providing an extracellular configuration that allows the passage of the majority of small molecules (<10KDa) (van Weeren, 2014). Therefore, despite the clear difference in size between human and bovine anatomy, these diffusion results suggest that sustained DNQX release from 25% w/v Pluronic F-127 hydrogels would be able to penetrate the human synovial membrane.

Rheological investigations (discussed in section 4.4.1), highlight the capacity for this hydrogel (25% Pluronic F-127 loaded with 2.5mM DNQX) to be handled as a liquid outside the body and injected using a hypodermic needle either subcutaneously or directly into the joint to the site of trauma (Anderson et al., 2011). Upon injection, the hydrogel sets *in situ* upon reaching physiological temperature where it acts as a large reservoir of GluR antagonist capable of delivering a sustained DNQX dosage (Figures 4.5 and 4.6) and thereby elicit potential preventative effects on the development of OA. However, care must be taken to avoid toxic levels of systemic GluR antagonist when administering via a less

targeted method, as these could have off target effects on GluR receptors located within other tissues and organs such as the central nervous system.

Inflamed joints have increased synovial membrane permeability to large molecules (Pejovic et al., 1995), with severity of inflammation positively correlating with increased permeability to larger proteins (Kushner and Somerville, 1971). Pluronic F-127 has a molecular weight of 12,500Da and Carbopol 934 has a molecular weight of 72Da and it has been shown that synovial membrane is permeable to large proteins (200kDa) (Sterner et al., 2016). Despite the proposed subcutaneous application of the hydrogel synthesised in this study, there may be scope for hydrogel excipients, in addition to GluR antagonist, to enter an inflamed joint space via an increased synovium permeability. Therefore, investigation into the cellular viability impact of these hydrogels on target tissue is required (discussed in section 4.4.3).

Studies have been carried out where nanoparticles are suspended in hydrogels to improve delivery characteristics (Yin et al., 2009, Pelegrino et al., 2018). A potential future investigation could look at combining the nanoparticle delivery vehicles developed in chapter 3 of this thesis with the hydrogels developed in this chapter, this could provide the benefit of longer term sustained delivery from nanoparticles (up to 5 weeks; Figure 3.6) of small quantities of GluR antagonist while utilising a shorter term (27 hours) release of larger (mM) concentrations of GluR antagonist (Figures 4.5 and 4.6). This delivery process could target both the initial inflammatory spike following joint trauma (Anderson et al., 2011) and sustain release begin to target longer-term chronic inflammation leading to PTOA.

4.3.3 Pluronic F-127/Carbopol 934 Hydrogel Conditioned Media Impacts Bone Cell Viability.

The final aim of this chapter looked to test the toxicity of thermoresponsive hydrogels to improve understanding of any potential adverse impacts of this delivery vehicle prior to any *in vitro* or *in vivo* applications (Section 4.1.1).

Pluronic F-127 and Carbopol 934 do not induce a cytotoxic response on multiple cell types including chondrocytes (Park et al., 2009), hepatic cells (Liu et al., 2017), fibroblasts (Demirci

et al., 2015, Rajeshwari et al., 2017), synovial fibroblasts (Boddu et al., 2015) and nasal mucosal membrane (Majithiya et al., 2006). Therefore, the major components of this hydrogel are generally accepted to be biocompatible and not cytotoxic. Any potential IA injection applications for this hydrogel (for example as a comparator to free drug *in vivo* studies (Bonnet et al., 2020)) would bring it into contact with synovium, ligaments, meniscus, cartilage and bone. Bone is the main target tissue for investigation into the effects of GluR antagonists in this thesis. Therefore, in this study, hOBs were used to investigate the impact to cell viability of the hydrogel GluR antagonist delivery vehicle developed in this chapter. There is conflicting evidence as to the cytotoxic effect of Pluronic F-127 on osteoblasts. Cell line osteoblasts (MG-63) have been shown to have reduced cellular viability (determined via MTT assay) following encapsulation in 20% w/v Pluronic F-127 hydrogels over 6 days (Brunet-Maheu et al., 2008). Whereas in a MC3T3-E1 osteoblast cell line cell viability study (MTS assay), coating cells that were cultured in plastic with 25%, 20% and 17.5% w/v Pluronic F-127 hydrogels did not cause a significant reduction to cell viability over 4 and 24hrs (Lippens et al., 2011). However, in the same study, encapsulation of MC3T3-E1 cells into 20% w/v Pluronic hydrogels resulted in a reduction in cell viability at 3 and 5 days (not at 1 day) as determined by the percentage of viable fluorescent stained cells (Lippens et al., 2011).

Treatment of hOBs with media conditioned in contact with a thermo-set 25% w/v Pluronic F-127 hydrogel for 1, 3 and 7 days caused a decrease in MTS release for 1:1 (3.7-, 4.7- and 8-fold respectively), 1:2 (3.1-, 3.8- and 3.5-fold respectively) and 1:4 (2.4-, 2.5- and 2.3-fold respectively) hydrogel to media ratios compared to unconditioned media controls (Figure 4.7). These findings indicate a cytotoxic response of hOBs to hydrogels in high concentrations. However, as hydrogel to media ratio is decreased, MTS decrease is smaller (Figure 4.7). 1:8 hydrogel to media treated cells increase MTS release compared to controls at day 1 and only reduced MTS release 1.5-fold by day 7 which is a smaller impact than all other ratios used. These findings demonstrate that reducing hydrogel concentration can mitigate a decreased cell viability response to hOBs.

There has been a large variance identified in knee joint synovial fluid volume in OA patients (Chen et al., 2017a), with one study aspirating an average of 18.74$\pm$4.67ml of synovial fluid

from patients and another calculating knee synovial fluid volumes between 0.56 and 71.71ml (Kraus et al., 2007). Cytotoxic 1:1 hydrogel to media samples correlate to a Pluronic F-127 concentration of 12.5% w/v and a Carbopol 934 concentration of 0.25% w/v in the total sample volume and non-cytotoxic 1:8 hydrogel to media concentrations relate to a Pluronic F-127 concentrations of 1.56% w/v and Carbopol 934 concertation of 0.031% (Figure 4.7). If considering IA injection of hydrogels for treatment in OA and assuming a synovial fluid volume of approximately 19ml in the knee (Chen et al., 2017a), an injection volume of 2.4ml of 25% Pluronic F-127 hydrogel would result in a ratio of 1:8 hydrogel to synovial fluid and reduce the risk of a cytotoxic response. However, the aforementioned variance in synovial fluid volume in OA sufferers means that injection volume may have to be varied according to patient synovial fluid volume.

The decrease in cell viability observed in 1:8 hydrogel to media treated cells as conditioning time increases (1, 3 and 7 days) may indicate some effects on cell viability could be due to the breakdown of the hydrogel over time. This would correlate with the literature indicating that Pluronic F-127 hydrogels lack stability and are easily eroded (Abdi et al., 2012, Diniz et al., 2015). This also ties in with release data demonstrating hydrogels finish releasing GluR antagonist by 27 hours (Figure 4.5 and 4.6). Therefore, after this timepoint hydrogels may have fully degraded. For the intended short-term release application, this degradation still allows for a sustained application of GluR antagonist while extending the physiological half-life and improving the opportunity for localised joint therapeutic activity. Pluronic F-127 is FDA approved for use in drug formulations and evidence in the literature indicates that Pluronic F-127 based gels are generally well tolerated *in vitro* (Abdi et al., 2012, Diniz et al., 2015, Gioffredi et al., 2016, Zhang et al., 2017). However, there is evidence suggesting the degradation of Pluronic F-127 via sonication is potentially cytotoxic (Wang et al., 2012). There is, therefore, a risk that ultra-sound therapy, which can be used to manage arthritis symptoms (Falconer et al., 1992), could induce a toxic effect if combined with application of these hydrogels.

Carbopol 934 is commonly used in the pharmaceutical and cosmetics industries as a thickening agent and emulsion stabiliser. It is on the list of inactive ingredients approved for use in drug products by the FDA (FDA, 2019a). Therefore, as Carbopol 934 is present in

hydrogels at only a small percentage (0.5% w/v) comparative to Pluronic F-127, it is unlikely to contribute to cytotoxic effects observed in MTS assays.

The evidence from the MTS assay findings in combination with the literature would indicate that, when used at a suitable concentration, the potential effects to cell viability of this 25% w/v Pluronic F-127 hydrogel formulation can be nullified. However, the concentration and duration of application must be considered prior to any further *in vitro* studies.

4.3.4 Conclusions and future objectives

The hydrogel formulations investigated in this chapter were shown to deliver sol-gel transitions at sub physiological temperatures (Figures 4.3 and 4.4), deliver sustained release over 24hrs (Figures 4.5 and 4.6) and, when used at a reduced exposure concentration, have controllable cytotoxic properties in vitro when applied to osteoblasts (Figure 4.7). These findings address the overarching aim of this chapter (section 4.1.1) and provide a shorter term (24hrs) sustained release delivery system with highly controllable drug loading for comparison with the low drug load, longer term (up to 5 weeks) GluR antagonist PLGA nanoparticle delivery system investigated in chapter 3. These two delivery systems allow for differential investigation into the impacts of sustained GluR antagonist delivery in the treatment of OA thereby contributing to the thesis hypothesis.

Future work in this area could investigate the impact of pH on hydrogel rheological characteristics as there is evidence that a change in pH alters drug release rate from Pluronic F-127 based hydrogels (Derakhshandeh et al., 2010). This would also be useful in optimising these hydrogels for use within the joint as the joint microenvironment pH is weakly acidic in those suffering from OA (Chen et al., 2019a). Additionally, a wider range of GluR antagonists could be tested for sustained release (e.g. NBQX) to aid in development of this delivery vehicle for the OA joint environment. Further diffusion studies could be conducted on human synovial membrane samples isolated from both healthy and arthritic joints to advance understanding of the capability of GluR antagonists to diffuse into the joint space when considering a subcutaneous route of administration. Assessment of hydrogel cytotoxicity on cell types present in tissue surrounding the proposed subcutaneous implant

site (e.g. the dermis) would provide more information on the potential off target effects of these hydrogels. Progression to *in vivo*, hydrogel implant experiments to assess toxicity and GluR antagonist drug delivery in physiological and pathophysiological (ACL rupture, AIA and meniscal transection models) environments would further progress the understanding of this delivery system.

Chapter 5

The Effects of Sustained GluR Antagonist Application on Pathological Signals *In Vitro* in 2D and 3D

5.1 Introduction

OA is a heterogenous chronic and degenerative condition (Deveza et al., 2019) that involves all tissues in the joint. There are multiple risk factors contributing to OA development, one of which, representing approximately 12% of all OA cases, is prior joint injury leading to PTOA 5-15 years later (Xia et al., 2014). PTOA can result in early onset of OA if trauma occurs at a young age. However, PTOA provides a timeline for OA development that can be tracked to the point of injury and, therefore, allows for investigation into the optimal timing for therapeutic intervention to mitigate or prevent OA development (discussed in more detail in sections 1.1.2.3 and 1.1.4). One of the key factors linked to OA is inflammation. In PTOA an immediate inflammatory spike at the time of injury is then followed by a slow chronic increase in inflammation as OA develops (PTOA is further reviewed in section 1.1.4) (Anderson et al., 2011). PTOA has been modelled *in vivo* using a non-surgical ACL rupture mouse model developed by Gilbert et al. This model mimicked PTOA via application of a single 12N load that ruptured the ACL without damaging surrounding tissue. This allows a known point of injury from which to map disease progression, develop therapeutics to target PTOA and identify novel early stage disease biomarkers, such as inflammatory marker profiles in early PTOA (Figure 5.1) (Gilbert et al., 2018).

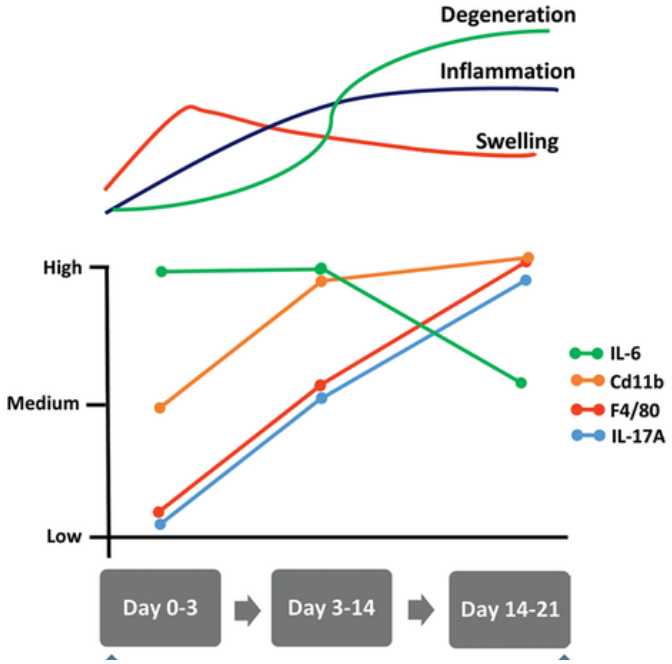

Figure 5.1: Disease progression and inflammatory marker release from the point of ACLr in mouse model PTOA (taken from Gilbert et al., 2018; Permission granted for the use of this figure in this thesis).

This study highlighted an upregulation of inflammatory markers (IL-6, iNOS) and degrading enzymes (ADAMTS-4, MMP-3) soon after joint injury (4hrs) in cartilage (Gilbert et al., 2018). Disease progression was rapid and severe which may not mimic the decades PTOA takes to develop in humans but allows for quicker controlled observation of PTOA development to build understanding and develop therapeutic interventions (further review of animal models in section 1.3.1.3). Bonnet et al, have demonstrated potential therapeutic benefits of GluR antagonists in the aforementioned ACLr model, an AIA model and an MNX rodent. Model of arthritis (detailed in section 1.4.3). These studies highlight the importance of inflammation to OA development and the potential for GluR antagonist NBQX to act as a disease modifying therapeutic.

The combination of both pro- and anti-inflammatory mediators produced at the early stages of joint injury may influence the development of OA and therapeutic intervention at this stage with IA inflammatory antagonists, such as IL-1Ra, has been investigated in both animal models (Lieberthal et al., 2015) and human trials (Kraus et al., 2012, Ajrawat et al., 2019). Several inflammatory molecules have been identified as significantly upregulated in human synovial fluid immediately following joint injury (MMP-3, IL-6, TIMP-1, activin A, monocyte chemotactic protein 1 and tumour necrosis factor stimulated gene-6). Of the main inflammatory molecules identified as significantly elevated within the synovial fluid of PTOA patients, IL-6 alone was shown to significantly contribute to baseline knee injury and OA outcome score ($KOOS_4$) baseline and was independently associated with $KOOS_4$ change over 3 months. On average, the highest quartile IL-6 at baseline had a 10-point increased $KOOS_4$ compared to the lowest IL-6 quartile (Swärd et al., 2012, Watt et al., 2016). *In vivo* investigations indicate that IL-6 is key in inflammatory arthritis progression, with IL-6 knockout mice being completely protected from developing CIA (Alonzi et al., 1998). Activation of KA GluRs on human fibroblast like synoviocytes leads to increased IL-6 release (Flood et al., 2007), IA injection of the AMPA/KA receptor antagonist NBQX (2.5mM), reduced IL-6 expression, joint swelling and joint degradation over 21 days in an AIA model (Bonnet et al., 2015) (detailed in section 1.4.2). Therefore, the reduction in IL-6 levels following NBQX treatment could be a mechanism by which GluR antagonist treatment mitigates joint destruction (further review of novel therapies and current unmet therapeutic

need for the treatment of OA in sections 1.2.3 and 1.2.4). Additionally, IA injection of NBQX on two consecutive days, compared with one day treatment free controls, elicited an increased capacity to protect bone and cartilage degradation scores after ACL rupture in mice *in vivo* indicating that a sustained delivery of NBQX may be therapeutically beneficial (Gilbert et al., 2018, Bonnet et al., 2020).

In AIA and ACL rupture *in vivo* models, IA NBQX administration protected against bone changes and modulated inflammation (Bonnet et al., 2015, Bonnet et al., 2020). Inflammation is key to the bones' response to injury and influences bone turnover (Reviewed by Mountziaris and Mikos (2008)) and alterations in the release of inflammatory molecules is a contributor to OA development (Sokolove and Lepus, 2013) (further detailed in section 1.1.3.2). IL-6 regulates osteoblast and osteoclast differentiation in bone and has been shown to be influential in the early stages of fracture healing (Yang et al., 2007). IL-6 is produced by osteoblasts via stimulation by IL-1, increased levels of IL-6 and IL-1 are coupled with RANKL expression leading to a bone resorptive state (Gerstenfeld et al., 2003). IL-6 trans signalling via its soluble receptor has been shown to promote osteoclastogenesis via the activity of RANKL in osteoblasts (Palmqvist et al., 2002). Blockade of trans IL-6 signalling using soluble gp130 resulted in reduced arthritis severity in an AIA mouse model (Nowell et al., 2003). IL-6 deficient mice have been shown to have decreased bone loss following oral infection (Baker et al., 1999). In hip fracture patients, increased serum levels of IL-6 have been negatively associated with lower extremity functional score (Lower Extremity Gain Scale) (Miller et al., 2006). These studies demonstrate that bone is responsive to inflammation, particularly IL-6, which plays a role in bone turnover and pathology.
In this chapter, to determine whether sustained delivery of AMPA/KA GluR antagonists might affect bone turnover, mineralisation assays with both NBQX and DNQX treated primary human osteoblasts and osteogenically differentiated Y201 MSCs were carried out. Additionally, LDH assays on cell culture media assessed any cytotoxic effect due to GluR antagonist application.

This chapter focuses on the second part of the thesis hypothesis investigating the protective effects of GluR antagonists on inflammatory driven pathways in bone. This is addressed through developing a 3D cell culture model (see cell culture layout Appendix Figure 9.7) that

allows for investigation into the impact of pathological levels of IL-6 induced inflammation to bone over 24 and 72hrs. Y201 MSCs were exposed to osteogenic media (section 2.7) to stimulate osteogenic differentiation and a range of bone, inflammatory and glutamate signalling markers were quantified by both qRT-PCR and immunossay to determine the phenotype of these cells and allow for understanding of the impact of inflammatory stimulus, following IL-6 stimulation, to said phenotype. Following inflammatory stimulation, this model was utilised to investigate the impact of free GluR antagonist NBQX treatment in the short term (1hr) as well as a combinatorial treatment of free NBQX (for 1hr) and NBQX loaded Nanoparticles developed in chapter 3 of this thesis. Each cell culture well was treated as an individual biological replicate for the purposes of this study to allow for statistical comparisons. This is a pilot study which looks to define the baseline of this cell set upon which to build an understanding of the impact of inflammatory (IL-6) and GluR antagonist (NBQX) intervention. This work has potential downstream applications as a novel drug screening tool.

5.1.1 Hypothesis, Aims and Objectives

Thesis Hypothesis: AMPA and kainate glutamate receptor (GluR) antagonists can be incorporated into sustained release delivery systems that can protect against inflammatory or mechanically driven pathways in bone *in vitro.*

This chapter contributes towards the thesis hypothesis via the overarching aim below, which has been further subdivided into a series of aims and objects:

Overarching aim: To determine whether pathological levels of IL-6/sIL-6r exposure followed by short term AMPA/KA GluR antagonist application with or without sustained release of AMPA/KA GluR antagonist from PLGA nanoparticles influences bone remodelling, glutamate and inflammatory signals.

Aim 1: To determine whether sustained DNQX and NBQX affects osteoblast viability.

Objective 1.1: To measure the effect of sustained application (7-14 days) of a dose range (1μM to 200μM) of DNQX and NBQX on viability of osteogenically differentiated Y201 human MSC cells and hOBs cultured in 2D utilising an LDH assay.

Aim 2: To determine whether sustained DNQX and NBQX affects osteoblast mineralisation.

Objective 2.1: To measure the effect of sustained application (1-14 days) of a dose range (1μM to 200μM) of DNQX and NBQX on mineralisation of osteogenically differentiated Y201 human MSC cells and hOBs cultured in 2D utilising an alizarin red mineralisation assay.

Aim 3: To determine whether IL-6 treatment of Y201 MSC derived osteocyte-like cells in 3D induces pathological markers of bone remodelling and inflammation, and whether this is affected by sustained delivery of NBQX encapsulated in PLGA nanoparticles.

Y201 human MSCs were differentiated to osteocyte like cells in 3D in collagen type 1 gels, stimulated with IL-6 and sIL-6r receptor to 'mimic' PTOA, and treated with either unencapsulated NBQX (200μM) or unencapsulated NBQX (200μM) + NBQX loaded PLGA nanoparticles. Measurements were taken after 1 and 3 days.

Objective 3.1: To test the effect of IL-6 stimulus and short term versus sustained NBQX application on cell viability via LDH assay and observing cell morphology through cryosectioning, actin staining and fluorescent imaging.

Objective 3.2: To test the effect of IL-6 stimulus and short term versus sustained NBQX application on markers of bone remodelling by measuring mRNA expression of *sost, dmp1, opg, rankl, col1a1, ocn* and *alp* by RTqPCR and protein release of OPG and sclerostin by enzyme linked immunosorbent assays.

Objective 3.3: To test the effect of IL-6 stimulus and short term versus sustained NBQX application on markers of inflammation by measuring mRNA expression of *il-6* by RTqPCR, protein release of IL-1β, IL-2, IL-6, IL-8, TNF-α, IL-12p70, IFN-γ IL-10, IL-13, IL-4 by enzyme linked immunosorbent assays and NO release via a Griess assay.

Objective 3.3: To test the effect of IL-6 stimulus and short term versus sustained NBQX application on glutamate signalling by measuring mRNA expression of *gria1*, *grik1, eaat1* and *eaat3* and release of the amino acid glutamate detected by ELISA.

5.2 Results

5.2.1 The Effect of GluR Antagonists on 2D Osteoblasts LDH Release

There was no effect of DNQX or NBQX on Y201 MSC or hOBs at any timepoint tested (7 or 14 days) when comparing treatment groups to untreated controls (multiple t-tests; $p>0.05$) (Figures 5.2A to 5.2F).

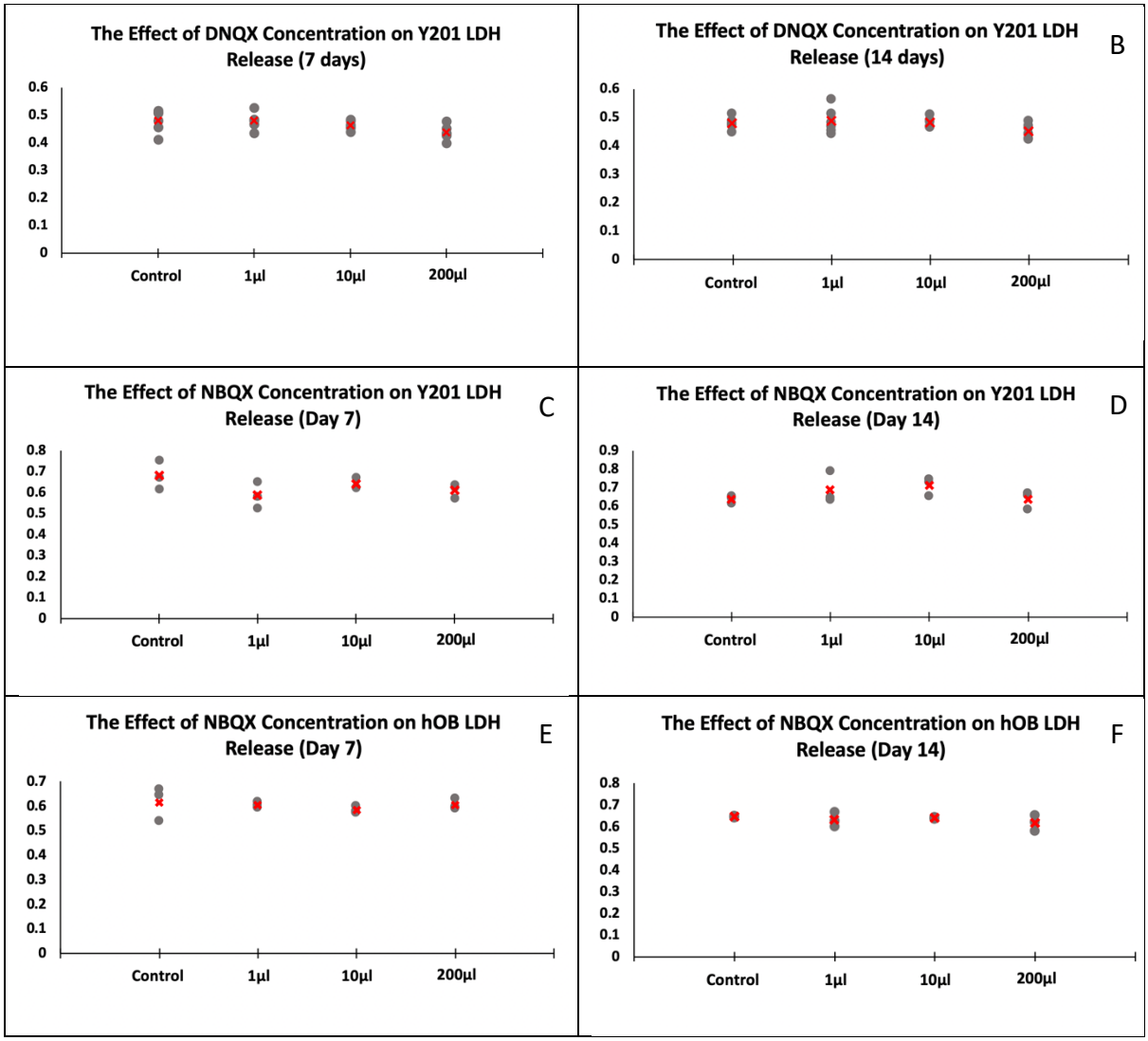

Figure 5.2: Absorbance (490nm) reflecting LDH released (Section 2.12.1) into osteogenic cell culture media (section 2.5.3) from 2D cell culture studies (Y201 Cell culture described in section 2.5.1 and hOB cell culture in section 2.5.2). NBQX/DNQX treatment was applied at the point of osteogenic media application. A+B) Osteogenically differentiated Y201 MSCs treated with a DNQX concentration range vs untreated control after 7 (A) and 14 (B) days in cell culture (n=6; cell culture well replicates); C+D) Osteogenically differentiated Y201 MSCs treated with a NBQX concentration range vs untreated control after 7 (C) and 14 (D) days in cell culture (n=3; cell culture well replicates). E+F) Primary human osteoblasts treated with an NBQX concentration range vs untreated control after 7 (E) and 14 (F) days in cell culture (n=3; cell culture well replicates). Red x in all graphs indicates the mean average for that treatment group.

5.2.2 GluR Antagonists Reduced Osteoblast Mineralisation

Regarding hOBs, comparison of NBQX/DNQX treatment groups with untreated controls revealed that 200μM NBQX treatment decreased mean absorbance compared to untreated controls 1.06-fold but this was not significant ($p>0.05$; t-test) whereas 200μM DNQX significantly decreased absorbance 1.15-fold ($p=0.021$; t-test) and 400μM DNQX significantly decreased absorbance 1.14-fold ($p=0.005$; t-test) compared to controls (Figure 5.3A). Regarding Y201s, comparison of NBQX/DNQX treatment groups with untreated controls revealed that Y201 mean absorbance was reduced 1.07-fold by 200μM NBQX treatment but this was not significant ($p>0.05$; Mann-Whitney U test) whereas 200μM DNQX significantly decreased Y201 mean absorbance 1.14-fold ($p<0.0001$; Mann-Whitney U test) and 400μM DNQX significantly reduced Y201 mean absorbance 1.13-fold ($p<0.0001$; Mann-Whitney U test) (Figure 5.3B).

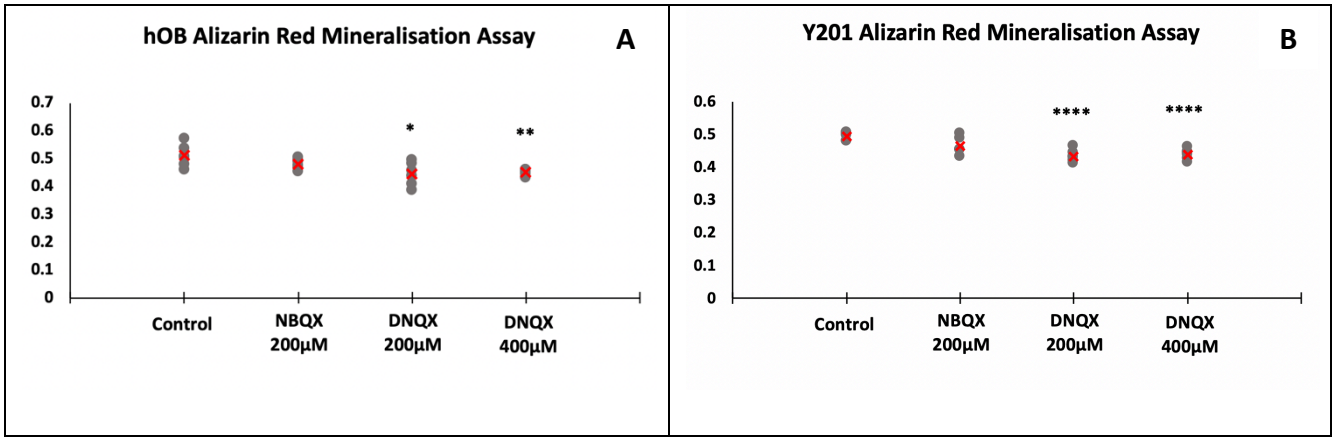

*Figure 5.3: Absorbance values (540nm) obtained from alizarin red mineralisation assay following GluR antagonist treatment on cell culture monolayers for 14 days (section 2.5.3 for methods): A) primary human osteoblasts with a sustained application of NBQX (200μM) and DNQX (200 and 400μM). B) osteogenically differentiated Y201 MSCs with a sustained application of NBQX (200μM) and DNQX (200 and 400μM). *p<0.05, **p<0.01, ****p<0.0001 vs untreated controls (t-test/Mann Whitney U). (n=6; cell culture well replicates).*

Regarding Y201s, comparison of DNQX treatment groups with untreated controls revealed that 1μM (p=0.238, t-test) and 10μM (p=0.087; t-test) treatment did not affect Y201 absorbance compared to controls but 200μM DNQX treatment caused a significant 1.22-fold decrease in Y201 mean absorbance compared to controls (p=0.003; t-test) (Figure 5.4A). Comparison of NBQX treatment groups with untreated controls revealed that 1μM (p=0.263; t-test) and 10μM (p=0.651; t-test) did not affect Y201 absorbance compared to controls, 200μM NBQX treatment caused a significant 1.81-fold decrease in Y201 mean absorbance compared to controls (p=0.001; t-test) (Figure 5.4B). Regarding hOBs, comparison of NBQX treatment groups with untreated controls revealed that there was no significant effect of 1μM (p=0.543; t-test) or 10μM (p=0.058; t-test) treatment but there was a significant 1.28-fold decrease for 200μM NBQX treatment compared to controls (p=0.006; t-test) (Figure 5.4C).

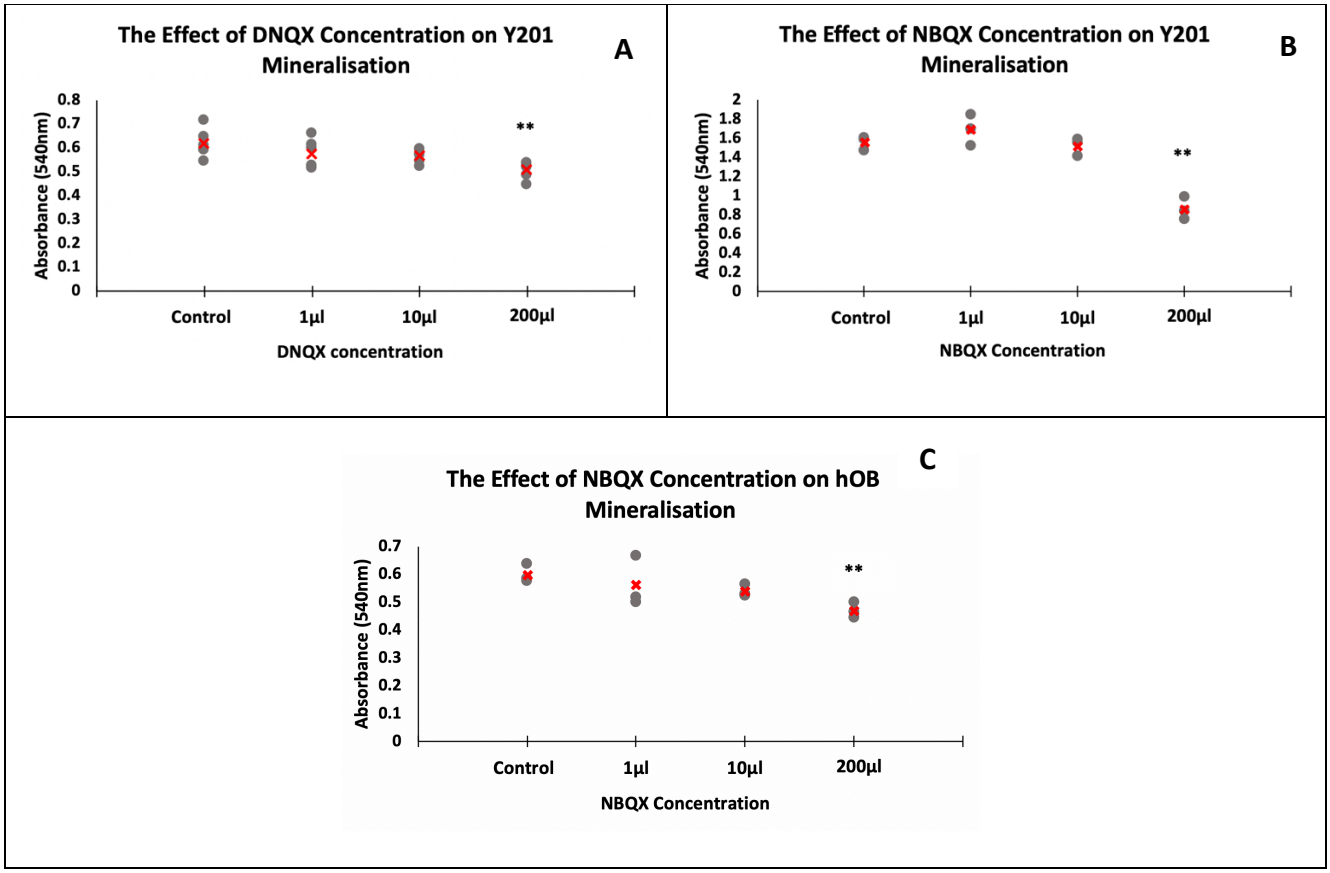

*Figure 5.4: Absorbance values (540nm) obtained from alizarin red mineralisation assay (section 2.5.3) following sustained exposure to GluR antagonist concentration ranges. A) Osteogenically differentiated Y201 MSC mineralisation assay with a sustained application of a range of DNQX concentrations for 14 days (n=6; cell culture well replicates). B) Osteogenically differentiated Y201 MSC mineralisation assay with a sustained application of a range of NBQX concentrations for 14 days (n=3; cell culture well replicates). C) hOB mineralisation assay with a sustained application of a range of NBQX concentrations for 14 days (n=3; cell culture well replicates). **p<0.01 vs control (t-test).*

5.2.3 The Effect of Short Term and Sustained Treatment with NBQX on IL-6/sIL-6r Stimulated Y201 Derived Osteocytes in 3D

Regarding results for this study, treatment groups will be abbreviated to allow for more concise graphical outputs. Controls were entitled 'control'; IL-6/sIL-6r inflammatory treated cells were entitled 'IL-6'; free NBQX treated cells were entitled 'NBQX' and free NBQX (1hr) + NBQX loaded nanoparticle treated cells were entitled 'NP'.

5.2.3.1 IL-6 Treatment and NBQX (Short Term and Sustained) Treatment Influences LDH Release.

For LDH release by osteocyte-like Y201 cells in 3D, there was no significant interaction of treatment and time ($p>0.05$) but there was a significant effect of time ($p<0.0001$) and treatment ($p<0.0001$) (2 factor ANOVA) (Figure 5.5). Pairwise comparisons with Bonferroni corrections for multiple comparisons revealed that, at 24hrs, there was an increase in LDH release in nanoparticle treatment groups compared to all other groups (1.17, $p<0.001$; 1.18-fold, $p<0.001$ and 1.17-fold $p<0.001$ for controls, IL-6 and NBQX treatment groups respectively). At 72hrs there was an increase in LDH release in nanoparticle treatment group compared to controls and all other treatment groups (1.19-fold, $p<0.0001$; 1.17-fold, $p<0.0001$ and 1.21-fold, $p<0.0001$ for controls, IL-6 and NBQX treatment groups respectively). There was an increase in LDH release between 24 and 72hrs for controls and all treatment groups (1.24-fold, 1.28-fold, 1.22-fold and 1.26-fold for controls, IL-6, NBQX and nanoparticle treatment groups respectively, $p<0.0001$ for all groups).

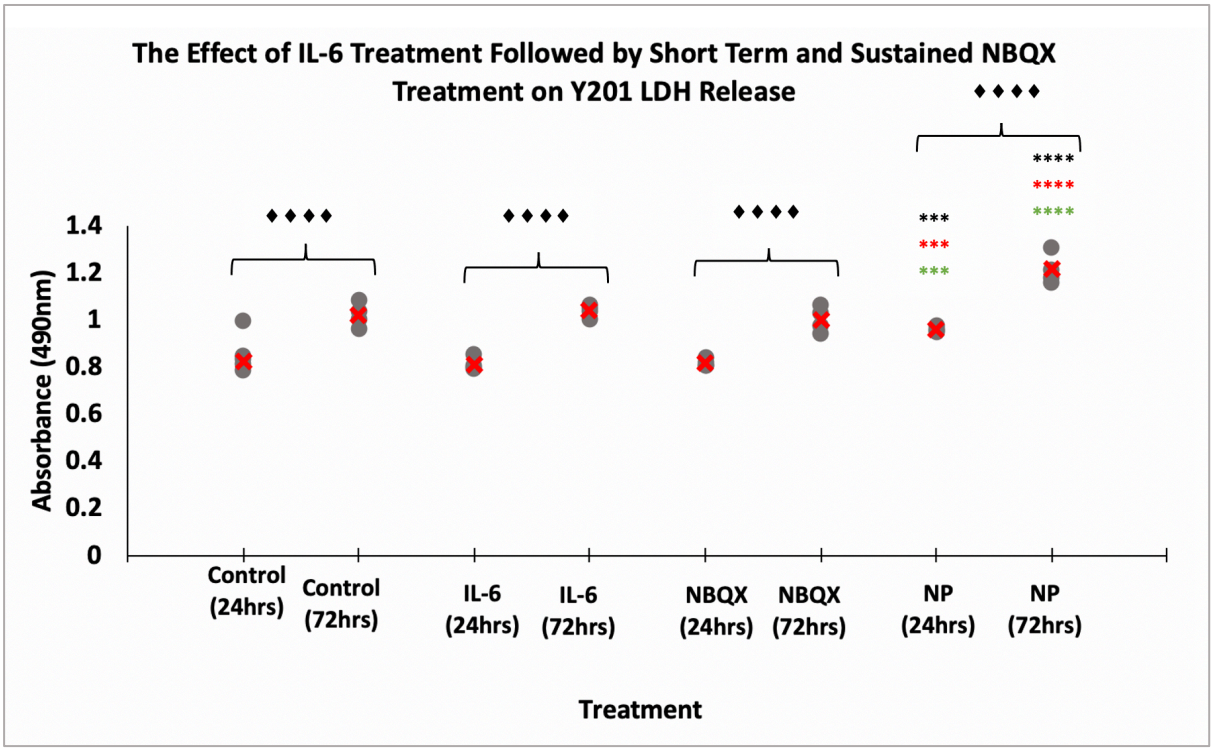

*Figure 5.5: Effect of IL-6/sIL-6r treatment and NBQX or NBQX+NBQX loaded nanoparticle intervention on absorbance (490nm), reflecting LDH released (Section 2.12.1) into cell culture media by osteogenically differentiated Y201 MSCs from IL-6/sIL-6r cell culture study (section 2.7) after 24 and 72hrs. (n=4; cell culture well replicates) Red **x** represents the mean value of replicates for each treatment group. ***p<0.001, ****p<0.0001 vs control, ***p<0.001, ****p<0.0001 vs IL-6/ sIL-6r treatment, ***p<0.001, ****p<0.0001 vs free NBQX treatment. ♦♦♦♦p<0.0001 24hrs vs 72hrs (statistical significance determined by 2-factor ANOVA).*

5.2.3.2 IL-6/sIL-6r Treatment and Intervention with Short Term or Sustained Nanoparticle Loaded NBQX Does not Affect Y201 Morphology

Representative images were taken of osteogenically differentiated Y201 MSCs in 3D type 1 collagen gels after IL-6/sIL-6r treatment and NBQX intervention study. Randomly selected fields of view from each treatment group revealed that cells were dispersed throughout gel sections and formed dendritic extensions, visually identifiable via phalloidin staining of the major cytoskeletal component actin (Figure 5.6). All treatment groups were not visually different from controls at both time points.

	Time	
Treatment	**24hrs**	**72hrs**
Control	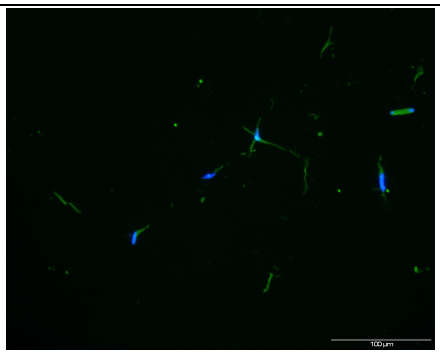	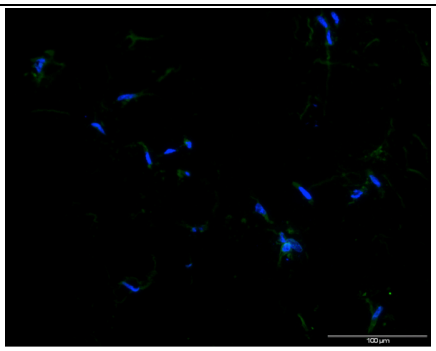
IL-6	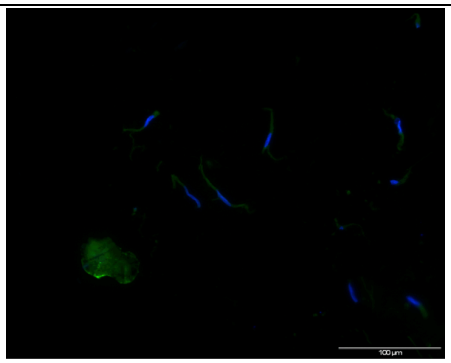	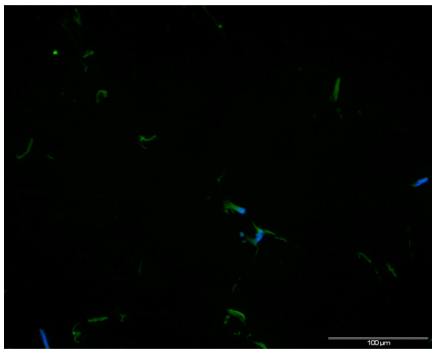
NBQX	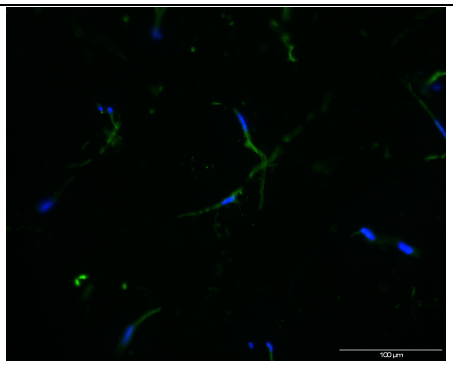	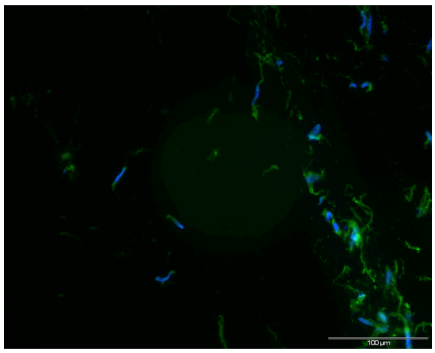
NP	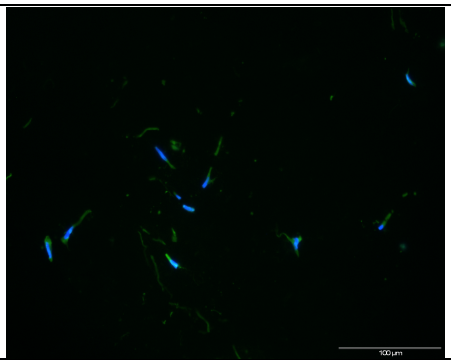	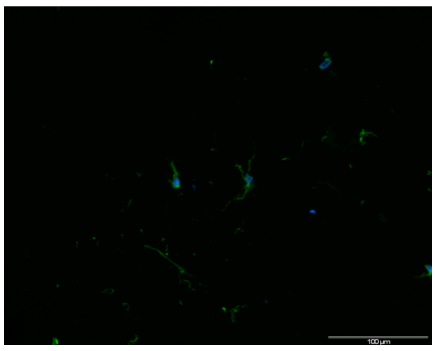

Figure 5.6: Effect of IL-6/sIL-6r treatment and NBQX or NBQX+NBQX loaded nanoparticle intervention on fluorescent microscopy images (section 2.8.4) of osteogenically differentiated Y201 MSCs stained with DAPI (blue) nuclear stain and Phalloidin (green) actin cytoskeletal stain. 10μM cryosectioned gels were isolated from each treatment group of IL-6/sIL-6r study at each time point (24 and 72hrs) (sections 2.8.1 to 2.8.3). 100μm scale bar in bottom right corner of each image.

5.2.3.3 Sustained NBQX Increased Nitric Oxide Release After IL-6/IL-6r Treatment

For nitrite release there was no significant interaction of treatment and time but there was a main effect of time ($p<0.0001$) and treatment ($P<0.0001$) (2 factor ANOVA) (Figure 5.7). Pairwise comparisons, with Bonferroni corrections for multiple comparisons, revealed that, at 24hrs, nitrite release increased in NP treatment groups compared to all other groups (2.92-fold, $p<0.001$; 2.65-fold, $p<0.001$ and 3.60-fold, $p<0.0001$ compared to controls, IL-6 and NBQX treatment groups respectively). NBQX treated cells had a 1.23-fold non-significant decrease in nitrite release compared to controls at 24hrs. At 72hrs, nitrite release was increased in NP treatment group compared to all other treatments (2.99, $p<0.0001$; 1.69-fold, $p<0.001$ and 1.67-fold, $p<0.001$ compared to controls, IL-6 and NBQX treatment groups respectively). There was an increase in nitrite release in IL-6 (1.77-fold, $p=0.030$) and NBQX (1.79-fold, $p=0.023$) treatment groups compared to controls at 72hrs. There was an increase in nitrite release in all IL-6/sIL-6r treated groups (IL-6, NBQX, NP) between 24 and 72hrs (2.40-fold, $p<0.001$; 3.32-fold, $p<0.0001$ and 1.54-fold, $p<0.001$ for IL-6, NBQX and NP treatment groups respectively).

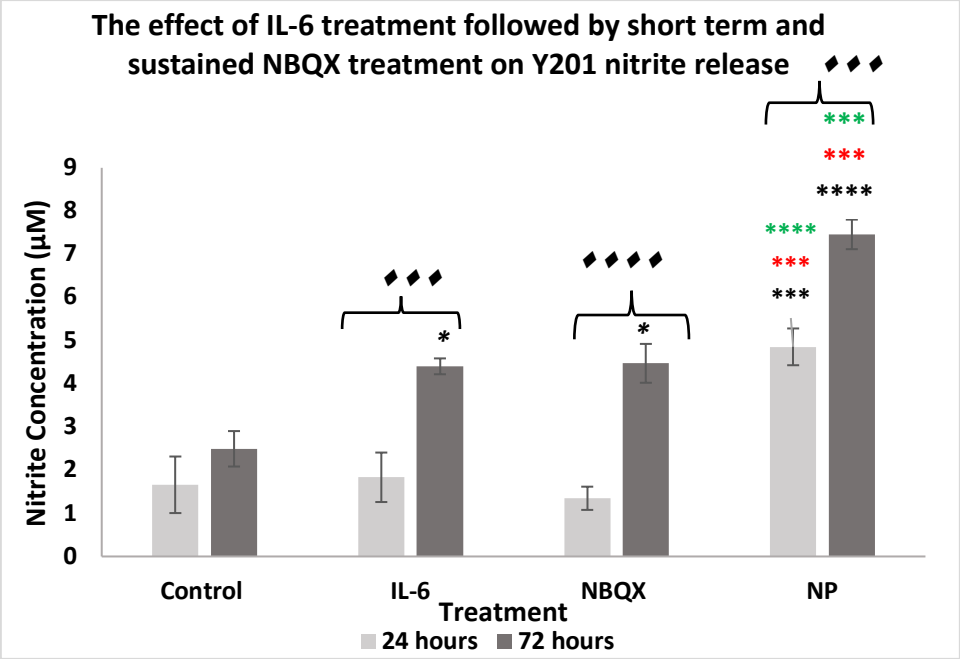

*Figure 5.7: Effect of IL-6/sIL-6r treatment and NBQX or NBQX+NBQX loaded nanoparticle intervention on nitrite release concentration into media (Griess assay section 2.11) from osteogenically differentiated Y201 MSCs from IL-6/sIL-6r cell culture study (section 2.7) after 24 and 72hrs (n=4; cell culture well replicates). Error bars representing standard error of the mean. *p<0.05, ***p<0.001, ****p<0.0001 vs control. ***p<0.001, ****p<0.0001 vs IL-6/sIL-6r treatment. *** p<0.001, ****p<0.0001 vs NBQX loaded nanoparticle treatment. ♦♦♦p<0.001, ♦♦♦♦p<0.0001 24hrs vs 72hrs (2-factor ANOVA was used to determine statistical significance across treatment and time).*

5.2.3.4 Short Term and Sustained NBQX Treatment Alter mRNA Expression After IL-6/IL-6r Treatment

The effect of IL-6/sIL-6r treatment on mRNA expression by Y201-derived osteocyte-like cells in 3D, and the subsequent treatment with free NBQX or NBQX in PLGA nanoparticles is shown in Figure 5.8 to Figure 5.16 and summarised in Table 5.1. Reference genes of *eef2* combined with *rpl13a* gave a stability factor of 0.375 and efficiencies of qPCR fall between 90 and 110% (Appendix section 9.3). Gene expression data are summarised according to bone signalling related genes (blue), inflammatory marker genes (red) and glutamate signalling related genes (green) (Table 5.1). *rankl, tnfα, sost* and *dmp1* were not detected under any treatment conditions in this study.

The expression ***opg*** was not significantly affected by treatment but was affected by time ($p<0.0001$) with no interaction between treatment and time (2-factor ANOVA) (Figure 5.8). Pairwise comparisons, with Bonferroni corrections for multiple comparisons, revealed that there was a decrease in mean *opg* expression between 24 and 72hrs in control (4.34-fold, $p<0.001$) IL-6/sIL-6r treatment (2.42-fold, $p=0.019$) and short term NBQX treatment groups (3.25, $p=0.004$) but not after nanoparticle treatment. At 24hrs, all IL-6/sIL-6r treated cells (IL-6, NBQX and NP) demonstrated between 1.63 and 1.94-fold decreases in mean *opg* expression compared to controls although this was not significant and at 72hrs there was a non-significant increase in NP treated groups compared to all other groups (1.82-fold vs IL-6).

The expression of ***il-6*** was not significantly affected by treatment but there was a significant main effect of time ($p<0.0001$) and a significant interaction of treatment and time ($p=0.001$) (2-factor ANOVA) (Figure 5.9). Pairwise comparisons, with Bonferroni corrections for multiple comparisons, revealed that there was a decrease in mean *il-6* expression between 24 and 72hrs in controls (6.66-fold, $p<0.0001$), this decrease was also observed in NBQX treatment groups (1.92-fold, $p=0.014$) and a non-significant decrease observed in IL-6/sIL-6r treatment groups (1.56-fold, $p=0.054$). At 24hrs all IL-6/sIL-6r treated groups (IL-6, NBQX, NP) demonstrated between a 2.46 and 2.58-fold reduction in *il-6* expression ($p=0.017$,

p=0.012 and p=0.019 for IL-6, NBQX and NP respectively vs controls). At 72hrs, NBQX loaded nanoparticle treated cells demonstrated an increase in *il-6* expression compared to controls (2.18-fold, p=0.029).

The expression of ***col-1a1*** was not significantly affected by time or treatment but there was a significant interaction of treatment and time (p=0.035) (2-factor ANOVA) (Figure 5.10). Pairwise comparison, with Bonferroni corrections for multiple comparisons, revealed that at 24hrs, nanoparticle treatment groups demonstrated between 2.36 and 3.31-fold increased *col-1a1* expression compared to all other treatment groups (p=0.042, p=0.014, p=0.010 for control, IL-6/sIL-6r and NBQX treatment groups vs NP respectively).

The expression of ***ocn*** was not significantly affected by treatment or interaction of treatment and time but there was a significant main effect of time (p<0.001) (2-factor ANOVA) (Figure 5.11). Pairwise comparisons, with Bonferroni corrections for multiple comparisons, revealed that, between 24 and 72hrs, there was a decrease in the expression of *ocn* in controls cells (2.51-fold, p=0.005) and in NBQX treated cells (1.86-fold, p=0.047). There was a decrease in *ocn* expression in IL-6 treated cells between 24 and 72hrs but this was not found to be significant (1.77-fold, p=0.056). At 24hrs, there was a non-significant decrease in *ocn* expression between 1.46 and 1.89-fold for all cells exposed to IL-6/sIL-6r treatment (IL-6, NBQX, NP).

The expression of ***alp*** did not demonstrate a significant interaction of treatment and time but there was a significant main effect of time (p<0.001) and treatment (p=0.029) (2-factor ANOVA) (Figure 5.12). Pairwise comparisons, with Bonferroni corrections for multiple comparisons, revealed a decreased in *alp* expression between 24 and 72hrs in control groups (2.41-fold, p=0.002) and in NBQX treatment groups (2.41-fold, p=0.002). At 24hrs, there was a non-significant decrease in *alp* expression in il-6 treatment group compared to both controls (1.99-fold, p=0.061) and NBQX treated cells (2.08-fold, p=0.054). At 72hrs, there was a non-significant increase in *alp* expression in NP treatment groups compared to all other treatment groups (1.59-fold vs IL-6 treatment).

The expression of ***gria-1*** did not demonstrate a significant interaction of treatment and time but there was a significant main effect of time (p=0.022) and treatment (p=0.049) (2-factor ANOVA) (Figure 5.13). Pairwise comparison with Bonferroni corrections for multiple comparisons revealed that there was a decrease in *gria-1* expression between 24 and 72hrs in controls (2.33-fold, p=0.0098). At 24hrs, there was a decrease in *gria-1* expression in il-6 treatment group compared to controls (3.08-fold, p=0.019). There was also a non-significant decrease in *gria-1* expression in NBQX and NP treatment groups at 24hrs (1.80-fold and 2.05-fold respectively).

The expression of ***grik-1*** did not demonstrate any significant main effects of treatment, time or interaction of treatment and time (2-factor ANOVA) (Figure 5.14).

The expression of ***eaat-1*** did not demonstrate any significant main effects of treatment, time or interaction of treatment and time (2-factor ANOVA) (Figure 5.15). There was a non-significant decrease in *eaat-1* expression between 24 and 72hrs in IL-6 treated cells (2.65-fold).

The expression of ***eaat-3*** was not significantly affected by treatment or interaction of treatment and time but there was a significant main effect of time (p=0.007) (Figure 5.16). Pairwise comparisons with Bonferroni corrections for multiple comparisons revealed that between 24 and 72hrs *eaat-3* expression decreased in controls (2.75-fold, p=0.0099) and decreased non significantly in NBQX treatment groups (2.07-fold, p=0.051). At 24hrs, there was a non-significant decrease in *eaat-3* expression in all treatment groups (IL-6, NBQX, NP) compared to controls ranging between 1.49 and 1.64-fold. At 72hrs, there was a non-significant decrease in *eaat-3* expression in NBQX treatment groups compared to IL-6.

Table 5.1: Summary of 2-way ANOVA findings from gene expression analysis. ***P values in black*** *vs control.* ***P values in Orange*** *vs IL-6 group.* ***P values in dark green*** *vs NBQX treatment group.* ***P values in yellow*** *represent 24 vs 72hr time points.* ***P values in grey*** *represent main effects of treatment or time. Arrows indicate an increase or a decrease in expression.*

Activity	Analyte	Treatment							Time (24 to72hrs)				
		Main effect	IL-6		NBQX		NP		Main effect	Controls	IL-6	NBQX	NP
			24hrs	72hrs	24hrs	72hrs	24hr	72hrs					
Bone signalling	*opg*	None							P<0.0001	p<0.001 ↓	P=0.019 ↓	P=0.004 ↓	
	ocn	None							P<0.001	p=0.005 ↓		P=0.047 ↓	
	Col-1a1	None					P=0.042 P=0.014 P=0.010 ↑		None				
	alp	P=0.029							P<0.001	p=0.002 ↓		P=0.002 ↓	
pro-inflammatory	*il-6*	None	P=0.017 ↓		P=0.012 ↓		P=0.019 ↓	P=0.029 ↑	P<0.0001	P<0.0001 ↓		P=0.014 ↓	
Glutamate signalling.	*grik-1*	None							None				
	gria-1	P=0.049	P=0.019 ↓						P=0.022	P<0.001 ↓			
	eaat-1	None							None				
	eaat-3	None							P=0.007	P<0.001 ↓			

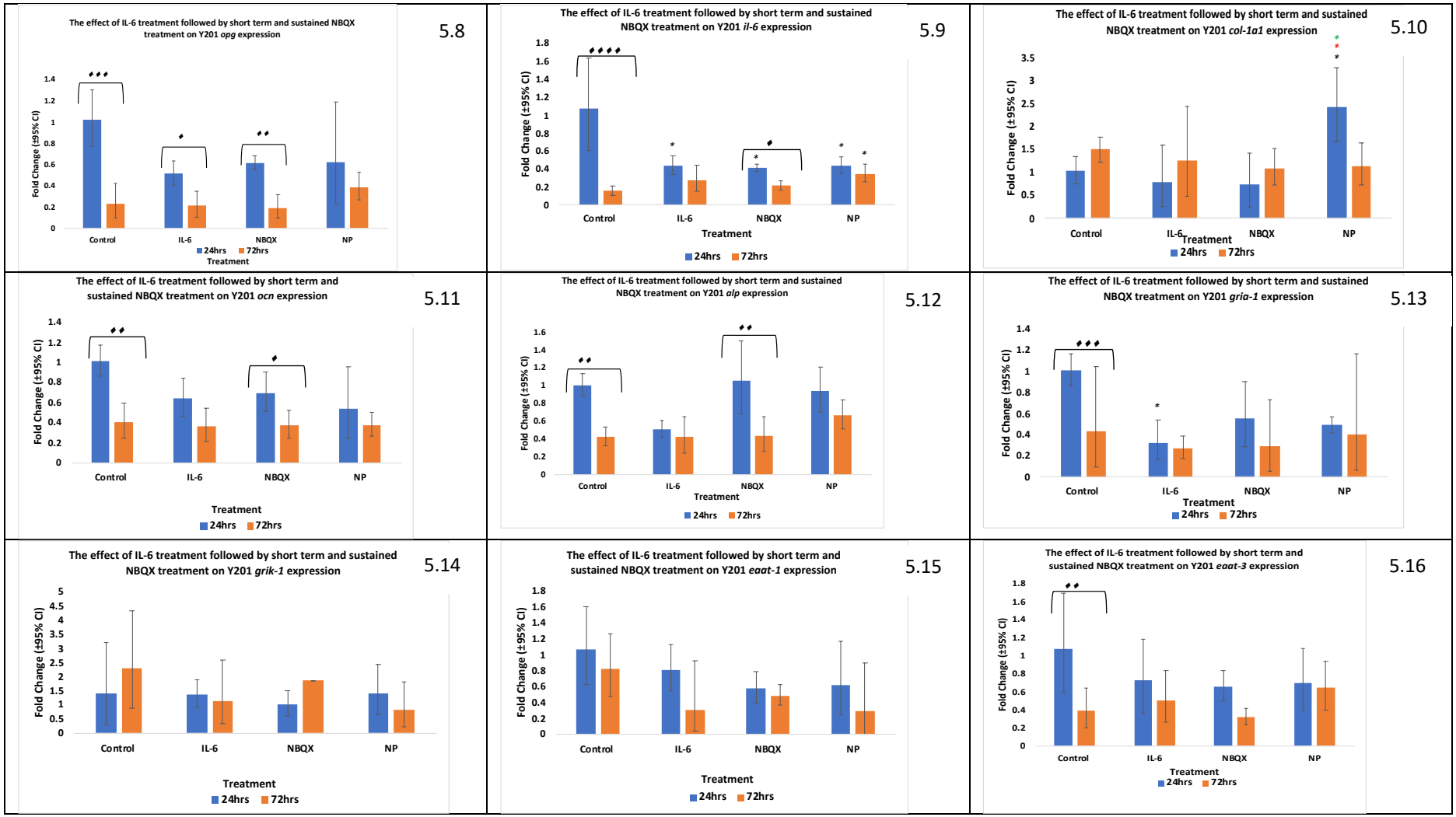

*Figures 5.8-5.16: Effect of IL-6/sIL-6r treatment and NBQX or NBQX+NBQX loaded nanoparticle intervention on gene expression of bone markers, inflammatory molecules and glutamate signalling components. qRT-PCR analysis on RNA extracted from Y201 MSCS (section 2.9) and relative expression quantified of opg (Figure 5.8), il-6 (Figure 5.9), col1a1 (Figure 5.10), ocn (Figure 5.11), alp (Figure 5.12), gria-1 (Figure 5.13), grik-1 (Figure 5.14), eaat-1 (Figure 5.15) and eaat-3 (Figure 5.16). Expression was normalised to the geometric mean of eef2 and rpl13a and fold change calculated using the $2^{-\Delta\Delta Ct}$ method. Data displayed as mean fold change with 95% confidence intervals. Statistical significance was determined using 2-factor ANOVA with Bonferroni comparisons *p<0.05 vs controls, *p<0.05 vs IL-6, *p<0.05 vs NBQX. ♦♦♦♦p<0.0001, ♦♦♦p<0.001, ♦♦p<0.01, ♦p<0.05 for 24 vs 72hrs (n=3; cell culture well replicates).*

5.3.3.4.1. Gene Expression Correlations After IL-6/sIL-6r Treatment

All Spearman's rho correlations met the specified assumptions (section 2.13) (Table 5.2). Regarding bone related genes, significant positive correlations were found between *opg* and *ocn, alp, il-6, gria1, eaat-1* and *eaat-3*. Significant positive association was identified between *ocn* and *alp, il-6* and *gria-1. Col-1a1* was significantly positively associated with *grik-1. alp* was significantly positively associated with *il-6, gria-1* and *eaat-3*. Regarding Inflammatory genes, *il-6* was positively associated with *gria-1* and *eaat-3* as well as the previously mentioned bone related genes *alp, ocn* and *opg.* Regarding glutamate signalling related genes, *grik-1* was significantly positively associated with *col-1a1* as previously mentioned. *Gria-1* was significantly positively associated with *eaat-1* and *eaat-3* and, as previously mentioned, significantly positively associated with inflammatory gene *il-6* and bone related genes *alp, ocn* and *opg. eaat-1* was significantly positively associated with *eaat-3* and *gria-1* glutamate signalling genes while also being significantly positively associated with *opg. eaat-3* was significantly positively associated with *eaat-1* and *gria-1,* as mentioned previously, as well as *il-6, alp* and *opg*.

Negative but not significant correlations were identified between *col-1a1* and *ocn* and *col-1a1* and *opg*. As well as *grik-1* and *opg*. Particularly strong positive correlations (>0.700, p<0.001) were identified between *opg* and *il-6*; *eaat-3* and *il-6* and *eaat-3* and *opg* and shown in scatter plots subdivided into treatment according to marker colour and time according to marker shape (Figure 5.17 to Figure 5.19).

Positive correlations shown between *il-6, eaat-3* and *opg* (Figure 5.17 to Figure 5.19) all show that all groups treated with IL-6/sIL-6r (IL-6, NBQX, NP) have generally higher delta Ct values than controls at 24hrs. For each pair of correlations, at 72hrs all values are generally higher than their 24hr equivalent, aside from nanoparticle treatment groups, contributing to the positive correlation identified in Table 5.2 and visually demonstrating the significant main effect of time identified between treatment groups (Table 5.1). The difference between IL-6/sIL-6r treatment groups and controls is less clear at 72hrs than at 24hrs for all pairs of correlations analysed (Figures 5.17, 5.18 and 5.19).

*Table 5.2: Spearman's rho correlation matrix heatmap for genes of interest from IL-6/sIL-6r inflammatory study. Bold white letters indicate a significant correlation. Gene of interest colour coding: **Red**= pro-inflammatory; **Blue**= Bone signalling; **Green**= Glutamate signalling. Positive correlation shading: 0.001-0.399=( ); 0.400-0.699=( ); 0.700-0.899=( ). Negative correlation shading: 0.001-0.399=( ).*

OPG	0.537 0.003	-0.173 0.209	0.680 <0.001	**0.817** **<0.001**	-0.241 0.146	0.646 <0.001	0.445 0.015	**0.730** **<0.001**	ρ Sig.
	OCN	-0.127 0.277	0.479 0.009	0.624 <0.001	-0.032 0.446	0.532 0.004	0.154 0.236	0.263 0.107	ρ Sig.
		COL-I	0.229 0.141	-0.011 0.480	0.416 0.030	0.171 0.212	0.060 0.389	0.157 0.232	ρ Sig.
			ALP	0.671 <0.001	-0.103 0.328	0.501 0.006	0.098 0.324	0.650 <0.001	ρ Sig.
				IL-6	-0.013 0.478	0.595 0.001	0.030 0.444	**0.739** **<0.001**	ρ Sig.
					GRIK-1	0.240 0.147	0.345 0.063	0.238 0.149	ρ Sig.
						GRIA-1	0.406 0.024	0.630 <0.001	ρ Sig.
							EAAT-1	0.404 0.025	ρ Sig.
								EAAT-3	ρ Sig.

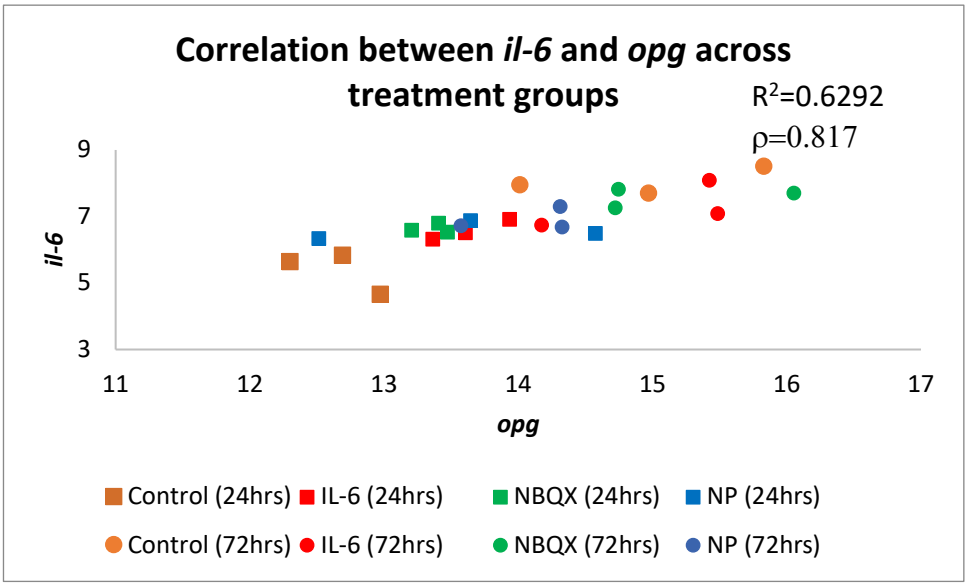

Figure 5.17: Scatterplot of opg vs il-6 delta Ct values for gene expression for all treatment groups (Control, IL-6/sIL-6r, short term NBQX and sustained NBQX loaded PLGA nanoparticles) across all time points (24 and 72hrs). R squared and Spearman's rho values displayed on chart.

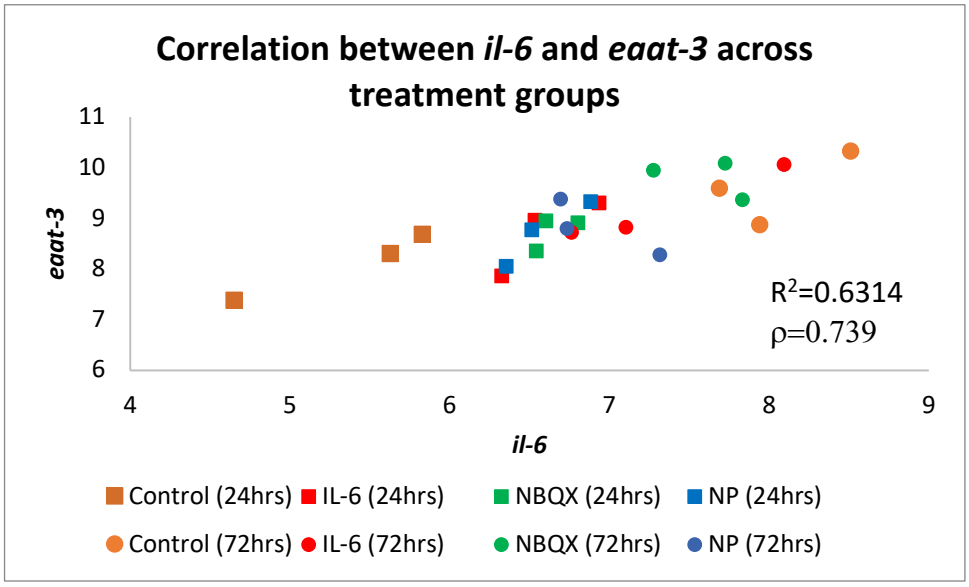

Figure 5.18: scatterplot of il-6 vs eaat-3 delta Ct values for gene expression for all treatment groups (Control, IL-6/sIL-6r, short term NBQX and sustained NBQX loaded PLGA nanoparticles) across all time points (24 and 72hrs). R squared and Spearman's rho values displayed on chart.

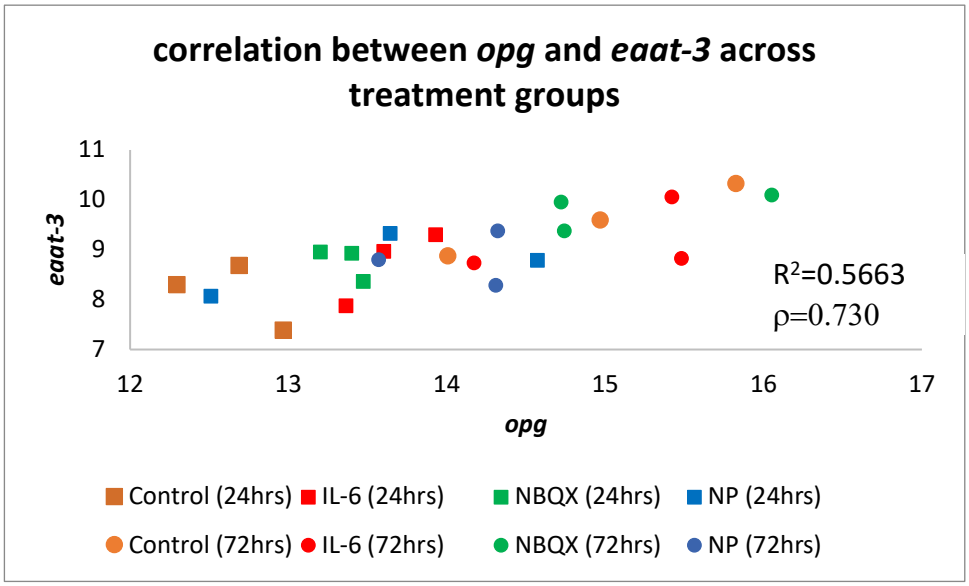

Figure 5.19: Scatterplot of opg vs eaat-3 delta Ct values for gene expression for all treatment groups (Control, IL-6/sIL-6r, short term NBQX and sustained NBQX loaded PLGA nanoparticles) across all time points (24 and 72hrs). R squared and Spearman's rho values displayed on chart.

The complex interactions between different gene expression levels in this study was investigated using multivariate analysis to determine the variance within the gene expression data and group into principal components.

5.3.3.4.2. Multivariate Analysis of Gene Expression After IL-6/sIL-6r Treatment with NBQX or Nanoparticles

PCA was applied to determine treatment group affects from linear combinations of genes of interest from IL-6/sIL-6r inflammatory study. The data was split and PCA applied at each time point of data collection (24 and 72hrs) and all assumptions satisfied (section 2.13). At 24 hours, two components were generated accounting for 76.5% of the variance (Figure 5.20) with principal component (PC) 1 explaining 49.8% and PC2 explaining 26.7%. The eigenvalue scores for PC1 were Glutamate signalling components (*eaat-1, eaat-3* and *gria-1*) as well as inflammatory markers and bone turnover markers (*il-6* and *opg*). These genes were associated with positive PC1 eigenvalue scores. Positive PC2 eigenvalue scores were most pronounced with bone markers *alp* and *col-1a1* with *eaat-1* having a high negative score (Figure 5.20A).

Visual analysis indicates the PCA score space can be subdivided into two clusters (Figure 5.20B). Cluster 1 contains controls which have not been treated with IL-6/sIL-6 and have negative PC1 scores. Cluster two represents IL-6/sIL-6r treated cells which account for both positive PC1 and PC2 scores but spread across a wide range. Free NBQX and NBQX loaded nanoparticle treated cells are spread in between these two clusters most of which lie within the positive PC1 and the positive and negative PC2 quadrants.

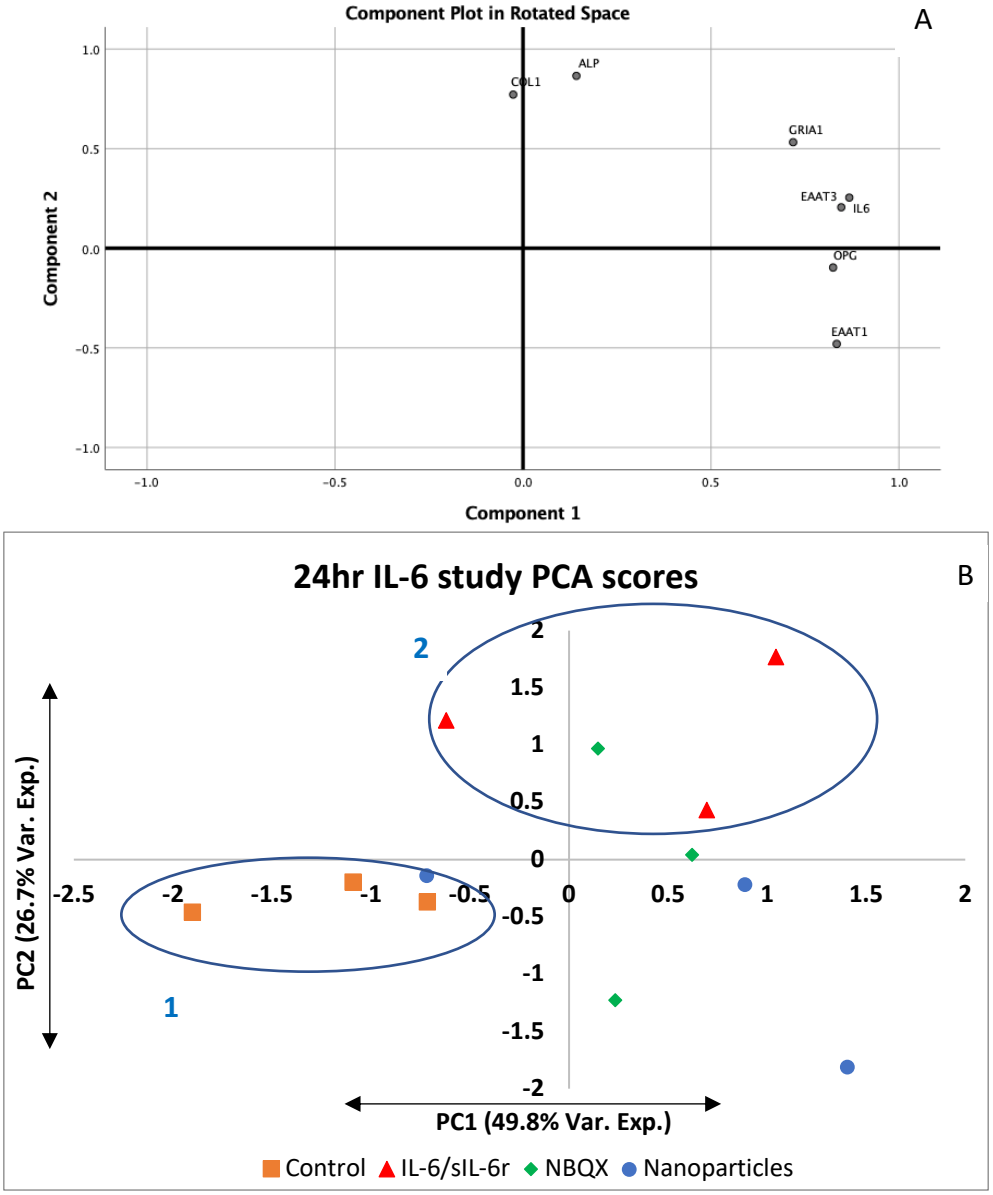

Figure 5.20: PCA based on components at 24hrs to determine treatment group affects from linear combinations of genes of interest from IL-6/sIL-6r inflammatory study (section 2.7). 76.5% of variance explained (PC1=49.8%, PC2=26.7%). A) gene of interest weightings for PC1 and PC2. B) Variable score plot for PC1 and PC2, subdivided into treatments. Score clusters are highlighted by circles. ocn and grik1 were excluded from analysis as they to satisfy the value of KMO sampling adequacy to acceptable levels (>0.5)(section 2.13). Eigenvalue scores were 0.868, 0.846, 0.834, 0.825, 0.718 for PC1 for IL-6, eaat-3, eaat-1, opg and gria-1 respectively and -0.480, 0.532, 0.865 and 0.772 for PC2 for eaat-1, gria-1, alp and col-1a1 respectively.

PCA of Genes of interest at 72hrs from IL-6/sIL-6r inflammatory study produced two principal components accounting for 75.6% of variance (Figure 5.21). PC1 explained 56.9% and PC2 explained 18.7%. Analysis of the principal components revealed that positive eigenvalue scores of PC1 were attributed to a combination of *eaat-3, alp, opg* and *il-6.* Large PC2 positive eigenvalue scores were represented by *col-1a1* and *gria-1* with small positive eigenvalue scores for *eaat-3* and *alp* (Figure 5.21A).

Two clusters were visually identified from PCA scores. Cluster 1 was represented by NBQX loaded nanoparticle treated cells accounted for negative PC1 scores and a range of negative to positive PC2 scores. Cluster two was consisted of a mix of control, IL-6/sIL-6r and NBQX treatment groups and represented slightly negative PC2 scores (Figure 5.21B). Additionally, control cells were shown to consistently represent negative PC2 values.

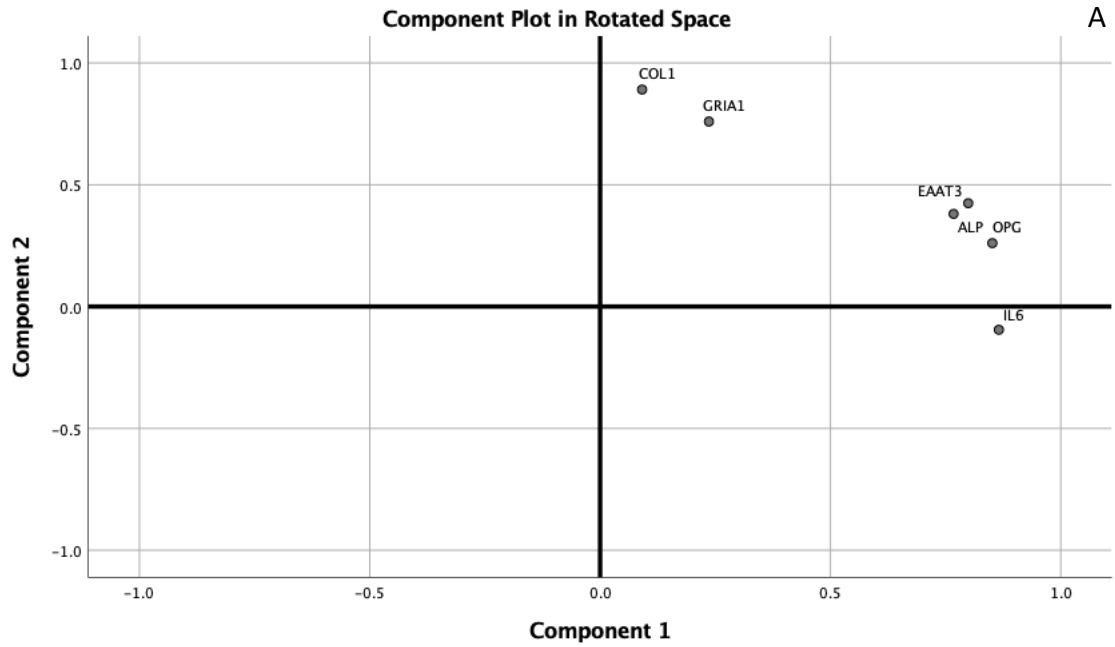

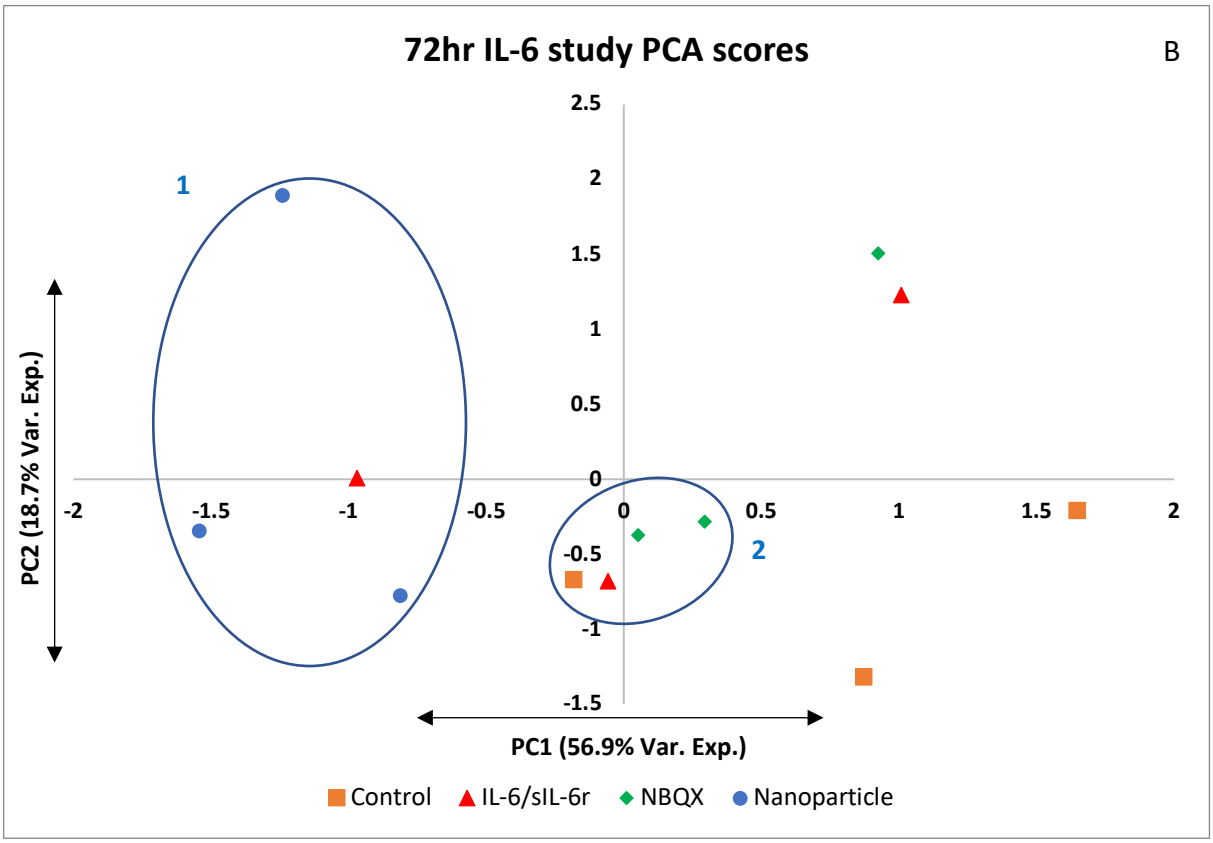

Figure 5.21: PCA based on components at 72hrs to determine treatment group affects from linear combinations of genes of interest from IL-6/sIL-6r inflammatory study (section 2.7). 75.6% of variance explained (PC1=56.9%, PC2=18.7%). A) gene of interest weightings for PC1 and PC2 B) Variable score plot for PC1 and PC2, subdivided into time and treatment. eaat1, ocn and grik1 were removed from analysis to satisfy value of KMO sampling adequacy to acceptable levels (>0.5) (section 2.13). Eigenvalue scores were 0.866, 0.851, 0.799 and 0.767 for PC1 for il-6, opg, eaat-3 and alp respectively and 0.424, 0.380, 0.891, 0.760 for PC2 for eaat-3, alp, col-1a1 and gria-1 respectively.

5.2.3.5 Short-Term and Sustained NBQX Treatment Alters Protein Expression After IL-6/IL-6r Treatment

The effects of NBQX and NP treatment on IL-6/sIL-6r stimulated 3D bone model on release of proteins (Figure 5.22 to Figure 5.33) are summarised and grouped into, bone signalling, glutamate, pro-inflammatory, anti and pro-inflammatory and anti-inflammatory markers (Table 5.3). Sclerostin levels were found to be below the limit of quantification for the standard curve for all conditions.

For **IFN-gamma** release, there was no main effect of treatment at 72hrs ($p>0.05$) (1-way ANOVA) (Figure 5.22). Samples at 24hrs were below the range of quantification, therefore, effectively zero. There was a non-significant increase in IFN-gamma release compared to controls in IL-6/sIL-6r treatment groups (2.45-fold). Short term NBQX treatment and NBQX loaded nanoparticle treatment groups demonstrated non-significant decreases compared to IL-6/sIL-6r (1.12-fold and 1.86-fold respectively).

For **IL-8** release, there was no main effect of treatment at 24hrs ($p>0.05$) (1-way ANOVA) (Figure 5.23). Values at 72hrs were above the range of quantification, therefore, not taken into account for analysis. There was a non-significant reduction in IL-8 release in the NBQX loaded nanoparticle treatment group compared to controls (1.28-fold).

For **IL-10** release, there was no main effect of treatment ($P>0.05$) (Kruskal-Wallis test) but there was a significant effect of time on IL-10 release ($p<0.0001$) (Mann-Whitney U test) and a significant effect of the interaction of treatment and time ($p=0.026$) (Kruskal Wallis test) (Figure 5.24). Pairwise comparisons, with Bonferroni corrections for multiple comparisons, revealed that, at 24hrs there was an increase in IL-10 release in short term NBQX treatment groups compared to controls (2.19-fold non-significant) and IL-6/sIL-6r treatment (3.24-fold, $p=0.045$). There was a non-significant increase in IL-10 release in control (3.03-fold), IL-6/sIL-6r (4.28-fold, $p=0.072$) and NP (3.35-fold) treatment groups between 24 and 72hrs.

For **IL-12p70** release, there was no main effect of time or interaction of treatment and time ($p>0.05$) but there was a significant effect of treatment ($p<0.001$) (2 factor ANOVA) (Figure 5.25). Pairwise comparisons, with Bonferroni corrections for multiple comparisons, revealed that at 24hrs there was an increase in IL-12p70 for NBQX and NP treated groups compared to controls (15.52-fold, $p=0.004$ and 14.48-fold $p=0.008$ respectively). There was also a non-significant increase in IL-12p70 in IL-6 treatment group (11.30-folg, $p=0.062$). At 72hrs, there was an increase in IL-12p70 release for all treatment groups compared to controls (3.03-fold, $p=0.040$;3.31-fold, $p=0.015$ and 3.06-fold, $p=0.036$ for IL-6, NBQX and NP groups respectively). There was a non-significant increase in IL-12p70 for control groups between 24 and 72hrs (5.02-fold)

For **IL-13** release, there was no main effect of treatment ($p>0.05$) (Kruskal-Wallis test) but there was a main effect of time ($p<0.0001$) (Mann-Whitney U test) and there was an interaction of treatment and time ($p=0.036$) (Kruskal-Wallis test) (Figure 5.26). Pairwise comparisons with Bonferroni corrections for multiple comparisons revealed that at 24hrs, there was an increase in IL-13 for short term NBQX treated cells compared to IL-6/sIL-6r treated cells (2.64-fold, $p=0.029$). There was an increase in IL-13 expression in IL-6 treatment groups between 24 and 72hrs (3.88-fold, $p=0.015$). There was a non-significant increase in IL-13 release in control and NP treatment groups between 24 and 72hrs (2.17-fold and 2.59-fold respectively).

For **IL-1β** release, there was no effect of treatment or interaction of treatment and time ($p>0.05$) but there was a significant effect of time ($p=0.001$) (2 factor ANOVA) (Figure 5.27). Pairwise comparisons, with Bonferroni corrections for multiple comparisons, revealed that there was an increase in IL-1β release between 24 and 72hrs for controls (2.02-fold, $p=0.009$) and IL-6 treatment groups (2.59-fold, $p=0.004$). At 24hrs, there was a non-significant increase in IL-1β release in NBQX groups compared to IL-6 treatment group (2.18-fold).

For **IL-2** release, there was no main effect of treatment or of interaction of treatment and time ($p>0.05$) (Kruskal Wallis test). There was a significant effect of time on IL-2 release ($p<0.0001$) (Mann-Whitney U test) (Figure 5.28). Pairwise comparisons, with Bonferroni

corrections for multiple comparisons, revealed that there was a non-significant increase in IL-2 release in all treatment groups and controls between 24 and 72hrs (4.56-fold, p=0.092; 2.26-fold, p=0.807; 1.76-fold, p=1.000 and 2.62-fold, p=1.000 for controls, IL-6, NBQX and NP treatment groups respectively). At 24hrs, there was a non-significant decrease in IL-2 release in NBQX loaded nanoparticle treated cells compared to IL-6/sIL-6r (1.64-fold) returning IL-2 release close to control levels.

For **IL-4** release, there was no main effect of time ($p>0.05$) but there was a significant effect of treatment ($p<0.0001$) and of the interaction of treatment and time ($p<0.0001$) (2 factor ANOVA) (Figure 5.29). Pairwise comparisons, with Bonferroni corrections for multiple comparisons, revealed that, at 24hrs, there was an increase in IL-4 release for all treatment groups compared to controls (10.87-fold, $p<0.0001$;13.84-fold, $p<0.0001$ and 12.95-fold, $p<0.0001$ for IL-6, NBQX and NP treatment groups respectively). There was a non-significant increase in IL-4 release in NBQX treatment group compared to IL-6 at 24hrs (1.27-fold). At 72hrs there was an increase in IL-4 release in all treatment groups compared to controls (4.57-fold, $p<0.0001$; 4.92-fold, $p<0.0001$ and 4.83-fold, $p<0.0001$ for IL-6, NBQX and NP treatment groups respectively).

For **IL-6** release, there was not an interaction of treatment and time ($p>0.05$) but there was a significant effect of treatment ($p<0.0001$) and time ($p<0.001$) (2 factor ANOVA) (Figure 5.30). Pairwise comparisons, with Bonferroni corrections for multiple comparisons, revealed that, at 24hrs, there was an increase in IL-6 release for all treatment groups exposed to IL-6/sIL-6r (IL-6, NBQX, NP) (7.94-fold, $p<0.0001$; 8.08-fold, $p<0.0001$ and 8.96-fold, $p<0.0001$ for IL-6, NBQX and NP treatment groups respectively). There was also an increase in NP treatment group compared to IL-6 and NBQX treatment groups at 24hrs (1.13-fold, p=0.003 and 1.11-fold p=0.013 respectively). At 72hrs, there was an increase in IL-6 release in all IL-6/sIL-6r treated groups (IL-6, NBQX, NP) compared to controls (4.70-fold, $p<0.0001$; 4.78-fold, $p<0.0001$ and 5.15-fold, $p<0.0001$ for IL-6, NBQX and NP treatment groups respectively). There was also an increase in IL-6 release in NP treatment group compared to IL-6 at 72hrs (1.10-fold, p=0.023). There was an increase in IL-6 release for control cells, IL-6 and NBQX treatment groups between 24 and 72hrs (1.81-fold, p=0.004; 1.07-fold, p=0.035 and 1.07-fold, p=0.034 for controls, IL-6 and NBQX respectively).

For **TNFα** release, there was no significant effect of treatment or interaction of treatment and time ($p>0.05$) (Kruskal-Wallis test) but there was a significant effect of time on TNFα release ($p<0.0001$, Mann-Whitney U test) (Figure 5.31). Pairwise comparisons, with Bonferroni corrections for multiple comparisons, revealed that there was an increase in TNFα release between 24hrs and 72hrs in IL-6 treatment groups (6.78-fold, $p=0.015$). At 24hrs, there was a non-significant increase in TNFα release in NBQX treatment groups compared to IL-6 treatment group (3.81-fold). At 72hrs, there was a non-significant increase in TNFα release in IL-6/sIL-6r treated cells compared to control (1.60-fold) and a non-significant decrease in short term NBQX treated cells compared to IL-6/sIL-6r treated cells (1.37-fold).

For **glutamate** release, there was no interaction of treatment and time ($p>0.05$) but there was a significant effect of treatment ($p=0.012$) and time ($p<0.0001$) (2 factor ANOVA) (Figure 5.32). Pairwise comparisons, with Bonferroni corrections for multiple comparisons, revealed that, at 24hrs, there was a decrease in glutamate release in NBQX treatment groups compared to controls (1.15-fold, $p=0.030$). At 72hrs, there was an increase in glutamate release in NP treatment groups vs IL-6 treatment (1.12-fold, $p=0.018$). There was an increase in glutamate release in between 24hrs and 72hrs for all treatment groups and controls (1.20, $p<0.0001$; 1.22-fold, $p<0.0001$; 1.34-fold, $p<0.0001$ and 1.35-fold, $p<0.0001$ for controls, IL-6, NBQX and NP treatment respectively).

For **OPG** release, there was no significant effect of treatment ($p>0.05$) or interaction of treatment and time ($p>0.05$) but there was a significant effect of time ($p<0.0001$ (2 factor ANOVA) (Figure 5.33). Pairwise comparisons, with Bonferroni corrections for multiple comparisons, revealed that there was an increase in OPG release between 24 and 72hrs across controls and all treatment groups (3.81-fold, $p<0.0001$; 3.59-fold, $p<0.0001$; 4.10-fold, $p<0.0001$ and 4.38-fold, $p<0.0001$).

Table 5.3: A summary of statistically significant findings for analyst concentrations determined from IL-6/sIL-6r inflammatory study (section 2.7) relating to figures 5.22 to 5.33. ***Black P values*** *vs control;* ***Orange P values*** *vs IL-6/sIL-6r treatment;* ***Dark green P values*** *vs Free NBQX treatment;* ***Grey P values****, main effect of treatment or time;* ***Yellow P values****, significant change between 24 and 72hrs; Arrow direction indicates whether significant findings relate to an increase or a decrease.*

	Analyte	Treatment							Time (24 to 72hrs)				
		Main effect	IL-6		NBQX		NP		Main effect	Control	IL-6	NBQX	NP
			24hrs	72hrs	24hrs	72hrs	24hrs	72hrs					
Bone marker	OPG	None							P<0.0001	P<0.0001 ↑	P<0.0001 ↑	P<0.0001 ↑	P<0.0001 ↑
Glutamate signalling	Glutamate	P=0.012			P=0.030 ↓			P=0.018 ↑	P<0.0001	P<0.0001 ↑	P<0.0001 ↑	P<0.0001 ↑	P<0.0001 ↑
Pro-inflammatory	IL-1β	None							P=0.001	P=0.009 ↑	P=0.004 ↑		
	IL-2	None							P<0.0001				
	IL-6	P<0.0001	P<0.0001 ↑	P<0.0001 ↑	P<0.0001 ↑	P<0.0001 ↑	P<0.0001 P=0.003 P=0.013 ↑	P<0.0001 P=0.023 ↑	P<0.001	P=0.004 ↑	P=0.035 ↑	P=0.034 ↑	
	IL-8	None							N/A				
	TNF-α	None							P<0.0001		P=0.015 ↑		
	IL-12p70	P<0.001		P=0.04 ↑	P=0.004 ↑	P=0.015 ↑	P<0.008 ↑	P=0.036 ↑	None	No main effect	No main effect		
Pro/anti-inflammatory	INF-γ	None							N/A				
Anti-inflammatory	IL-10	None			P=0.045 ↑				P<0.0001				
	IL-13	None			P=0.029 ↑				P<0.0001		P=0.015 ↑		
	IL-4	P<0.0001	P<0.0001 ↑	P<0.0001 ↑	P<0.0001 ↑	P<0.0001 ↑	P<0.0001 ↑	P<0.0001 ↑	None				

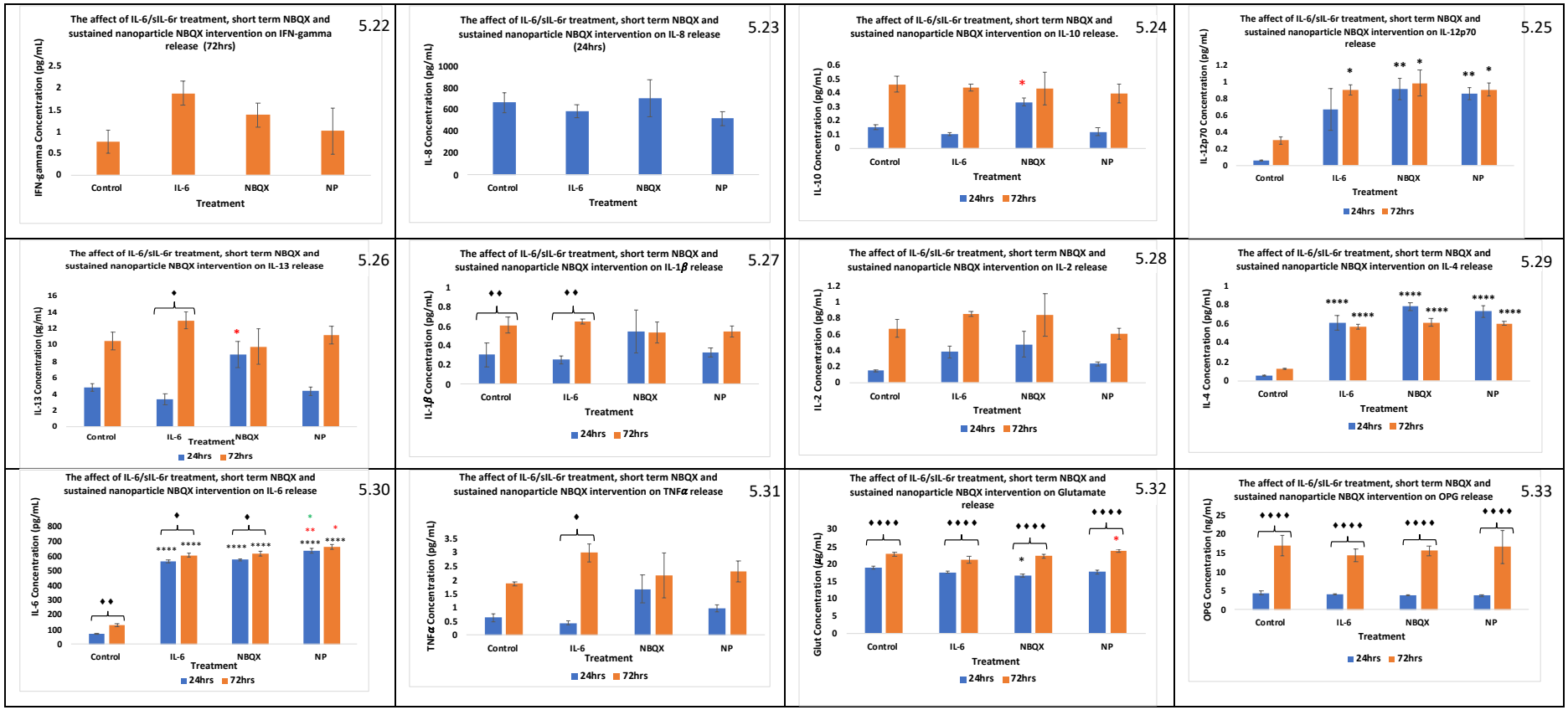

*Figures 5.22 to 5.33: Effect of IL-6/sIL-6r treatment and NBQX or NBQX+NBQX loaded nanoparticle intervention on Immunoassay quantified release of inflammatory markers, glutamate and OPG from cell culture media at 24 and 72hrs (section 2.10). Markers quantified by electrochemiluminescence multiplex assay were IFN-γ (figure 5.22), IL-8 (figure 5.23), IL-10 (figure 5.24), IL-12p70 (figure 5.25), IL-13 (figure 5.26), IL-1β (figure 5.27), IL-2 (figure 5.28), IL-4 (figure 5.29), IL-6 (figure 5.30) and TNFα (figure 5.31). ELISA quantified markers were glutamate (figure 5.32) and OPG (figure 5.33). IFN-γ (figure 5.22) and IL-8 (figure 5.23) contained values outside the limits of quantification which were not included in analysis. Data displayed as analyte concentration (pg/ml, ng/ml or µg/ml) with error bars representing standard error of the mean. Statistical significance was determined using 2-factor ANOVA with Bonferroni post hoc tests. *p<0.05, **p<0.01,****p<0.0001 vs control. *p<0.05, **p<0.01 vs IL-6. *p<0.05 vs NBQX. ♦p<0.05, ♦♦p<0.01, ♦♦♦♦p<0.0001 for 24 vs 72hrs (n=4; cell culture well replicates).*

5.2.3.5.1 Analyte Release Correlations After IL-6/sIL-6r Treatment

Table 5.4 demonstrates the Spearman's rho correlation results of analysis comparing all immunoassay data grouped into 4 sections: glutamate and OPG, pro-inflammatory, anti and pro-inflammatory and anti-inflammatory. The majority of analyte correlations were positive. However, significant negative correlation was identified between Glutamate and IL-4 (-0.299; P=0.048).

Particularly strong positive correlations (>0.700, p<0.001) were identified between IL-1β and IL-2, TNFα, IL-10 and IL-13; between IL-2 and TNFα, INF-γ, IL-10 and IL-13; between TNFα and IL-10 and IL-13; between IL-12p70 and IL-4; between INF-γ and IL-13 and finally between IL-10 and IL-13. The strongest positive correlation identified was between TNF-α and IL-13 (>0.901; p<0.001). To better visualise the strongest of these correlations as well as the single significant negative correlation identified, scatterplots subdivided into treatment groups were plotted. The strong positive correlation between TNFα and IL-13 is broadly grouped into 24hr treatment groups with low IL-13 and TNFα release increasing to 72hr treatment groups with increased release with the exception of free NBQX treatment group that appears more spread between time points. This observation ties in with significant main effect of time seen for both these markers (P<0.0001; Table 5.3). All groups treated with IL-6/sIL-6r (IL-6, NBQX, NP) are broadly overlapping for IL-13 compared to TNFα but control groups for TNFα are observed to have lower values at 72hrs than other treatment groups (Figure 5.34). Regarding the significant negative correlation observed between glutamate and IL-4 (Figure 5.35), a clear split between control groups at both time points and all other treatment groups is observable, this ties in with the significant main effect of treatment observed for both glutamate and treatment*time for IL-4 where treatment groups were identified as being significantly different from control groups (Table 5.3). The wide range of significant positive correlations and complex interactions between the release of different markers in this study was investigated using multivariate analysis to explain the variance within the marker release data and grouped into principal components.

*Table 5.4: Spearman's rho Correlation matrix heatmap of immunoassay analytes from IL-6 inflammatory study. Bold and white letters indicate a significant correlation. Red background indicates a positive correlation, blue background indicates a negative correlation. Analyte colour coding: **Black**= glutamate and OPG; **Red**= pro-inflammatory; **Blue**= anti and pro-inflammatory; **Green**= anti-inflammatory. Positive correlation shading: 0.001-0.399=( ); 0.400-0.699=( ); 0.700-0.899=( ); 0.900-1=( ). Negative correlation shading: 0.001-0.399=( ); 0.400-0.699=( ); 0.700-0.899=( ) .*

ρ Sig.p	OPG											
ρ Sig.p	**0.800** **<0.001**	Glut										
ρ Sig.p	0.399 0.014	**0.424** **0.008**	IL-1β									
ρ Sig.p	**0.535** **0.001**	**0.440** **0.006**	**0.782** **<0.001**	IL-2								
ρ Sig.p	0.155 0.207	0.207 0.128	0.202 0.134	0.330 0.033	IL-6							
ρ Sig.p	-0.290 0.457	0.221 0.206	-0.088 0.373	-0.403 0.061	-0.244 0.181	IL-8						
ρ Sig.p	**0.499** **0.002**	**0.518** **0.001**	**0.850** **<0.001**	**0.790** **<0.001**	**0.409** **0.010**	0.335 0.102	TNF-α					
ρ Sig.p	0.010 0.479	-0.027 0.443	0.319 0.040	0.294 0.054	**0.640** **<0.001**	0.104 0.357	**0.520** **0.001**	IL-12p70				
ρ Sig.p	-0.071 0.408	-0.239 0.195	0.407 0.066	**0.736** **0.001**	0.354 0.098	**-0.800** **0.100**	**0.646** **0.005**	**0.450** **0.046**	INF-γ			
ρ Sig.p	**0.606** **<0.001**	**0.517** **0.001**	**0.776** **<0.001**	**0.757** **<0.001**	0.228 0.105	**0.609** **0.006**	**0.872** **<0.001**	0.257 0.082	**0.693** **0.002**	IL-10		
ρ Sig.p	**0.596** **<0.001**	**0.508** **0.002**	**0.768** **<0.001**	**0.790** **<0.001**	0.262 0.074	-0.018 0.474	**0.901** **<0.001**	0.319 0.040	**0.754** **0.001**	**0.878** **<0.001**	IL-13	
ρ Sig.p	-0.098 0.303	**-0.299** **0.048**	0.023 0.451	0.074 0.344	**0.519** **0.001**	0.074 0.393	0.208 0.126	**0.821** **<0.001**	0.136 0.315	0.021 0.456	0.105 0.283	IL-4

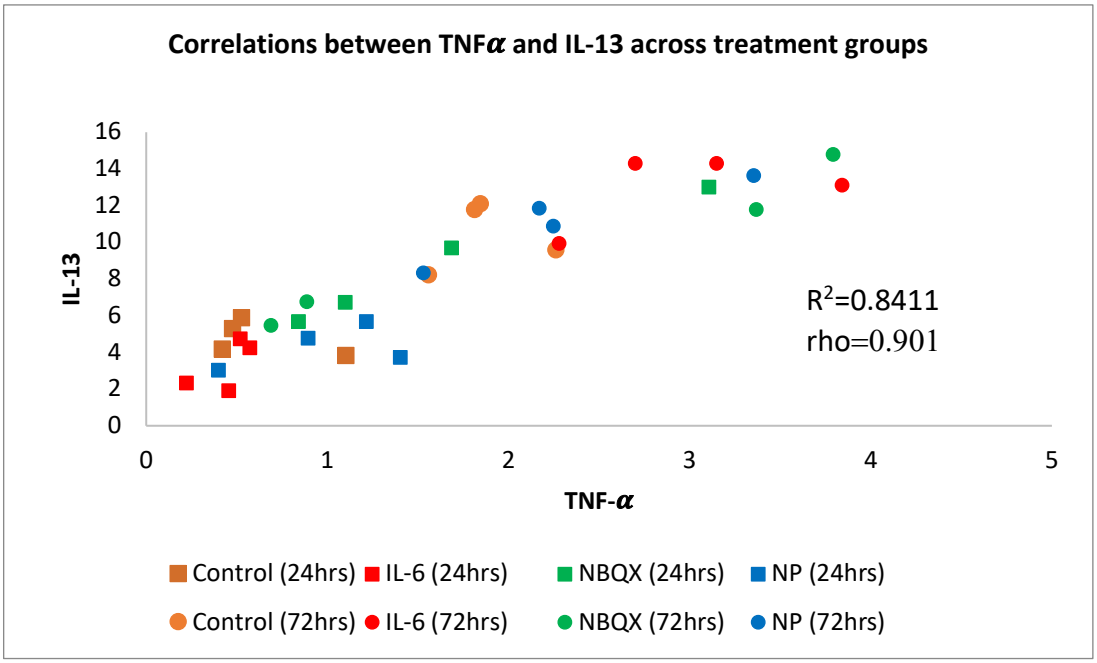

Figure 5.34: Scatterplot of TNFa vs IL-13 concentration values for protein release for all treatment groups (Control, IL-6/sIL-6r, short term NBQX and sustained NBQX loaded PLGA nanoparticles) across all time points (24 and 72hrs). R squared and Spearman's rho values displayed on chart.

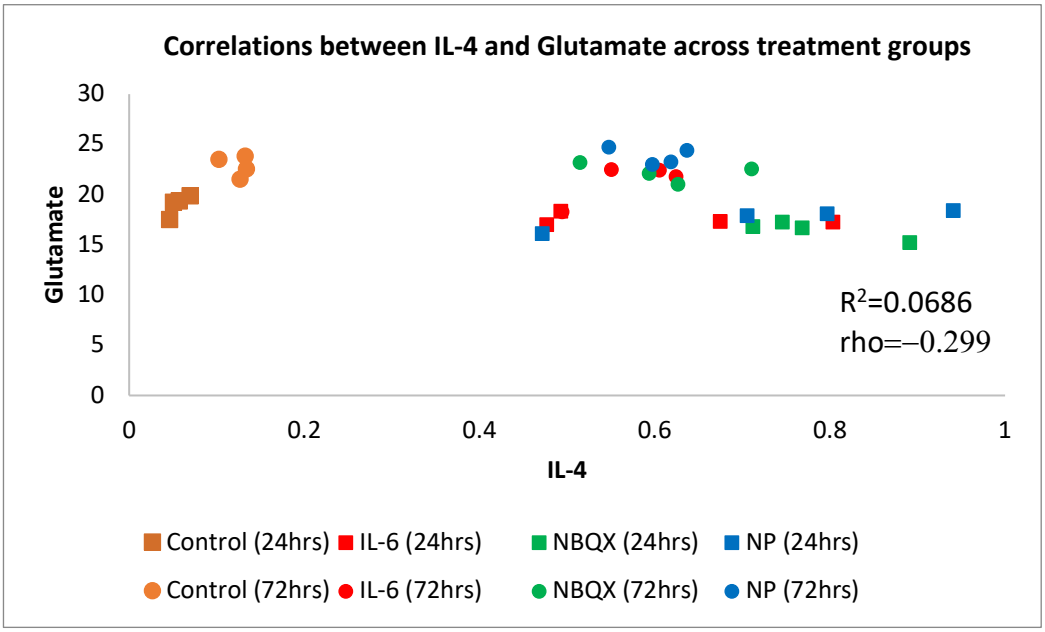

Figure 5.35: Scatterplot of IL-4 vs Glutamate concentration values for protein release for all treatment groups (Control, IL-6/sIL-6r, short term NBQX and sustained NBQX loaded PLGA nanoparticles) across all time points (24 and 72hrs). R squared and Spearman's rho values displayed on chart.

5.2.3.5.2 Multivariate Analysis of Analyte Release After IL-6/sIL-6r Treatment with Short-Term NBQX or Nanoparticles

PCA was applied to determine treatment group affects from linear combinations of protein markers from IL-6/sIL-6r inflammatory study. The data was split and PCA applied at each time point of data collection (24 and 72hrs) and all PCA assumptions satisfied (linear relationship between variables with no outliers and large sample sizes).

Two principal components were identified that account for 72.8% of variance. PC1 explains 49.6% and PC2 explains 23.2% (Figure 5.36). Positive large eigenvalue scores for PC1 were identified for pro-inflammatory markers IL-2 and TNFα and anti-inflammatory markers IL-10 and IL-13. Positive large eigenvalue scores for PC2 were identified for pro-inflammatory marker IL-6 and anti-inflammatory marker IL-4. Negative eigenvalue scores for PC2 were identified for OPG and glutamate (Figure 5.36A).

Principal component scores visual analysis revealed 3 clusters. Cluster 1 was represented by control cells and associated with negative PC2 scores and neutral PC1 scores, whereas all cells treated with IL-6/sIL-6r had positive PC2 scores. Cluster 2 represented NBQX loaded nanoparticle and IL-6/sIL-6r inflammatory treatments which were associated with negative PC1 and positive PC2 scores, whereas short term NBQX treated cells in cluster 3 had positive PC1 and positive PC2 scores (Figure 5.36B).

A

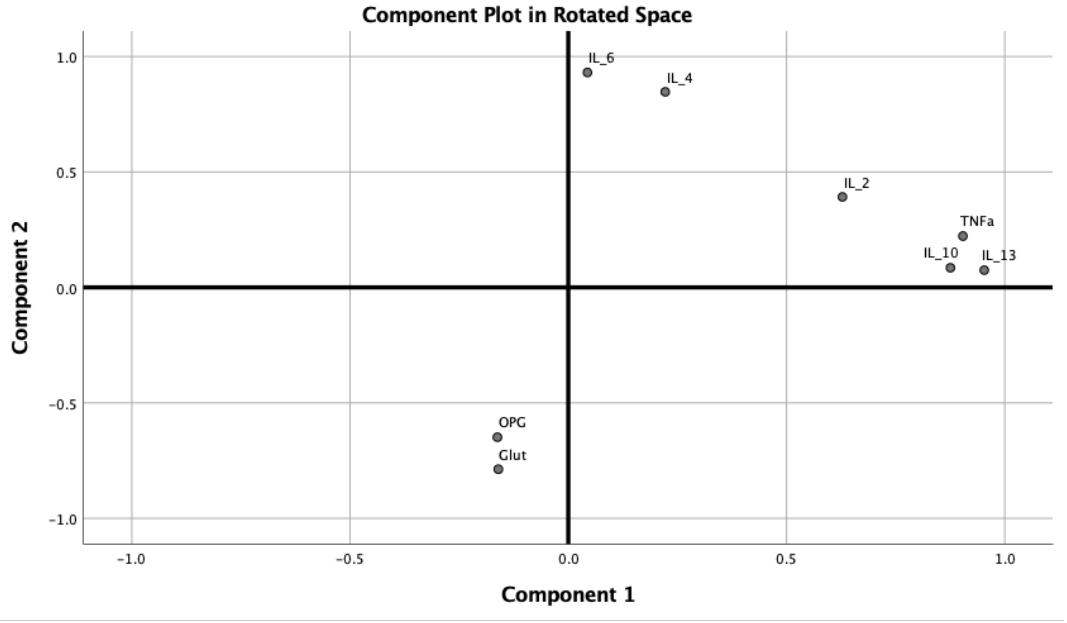

B

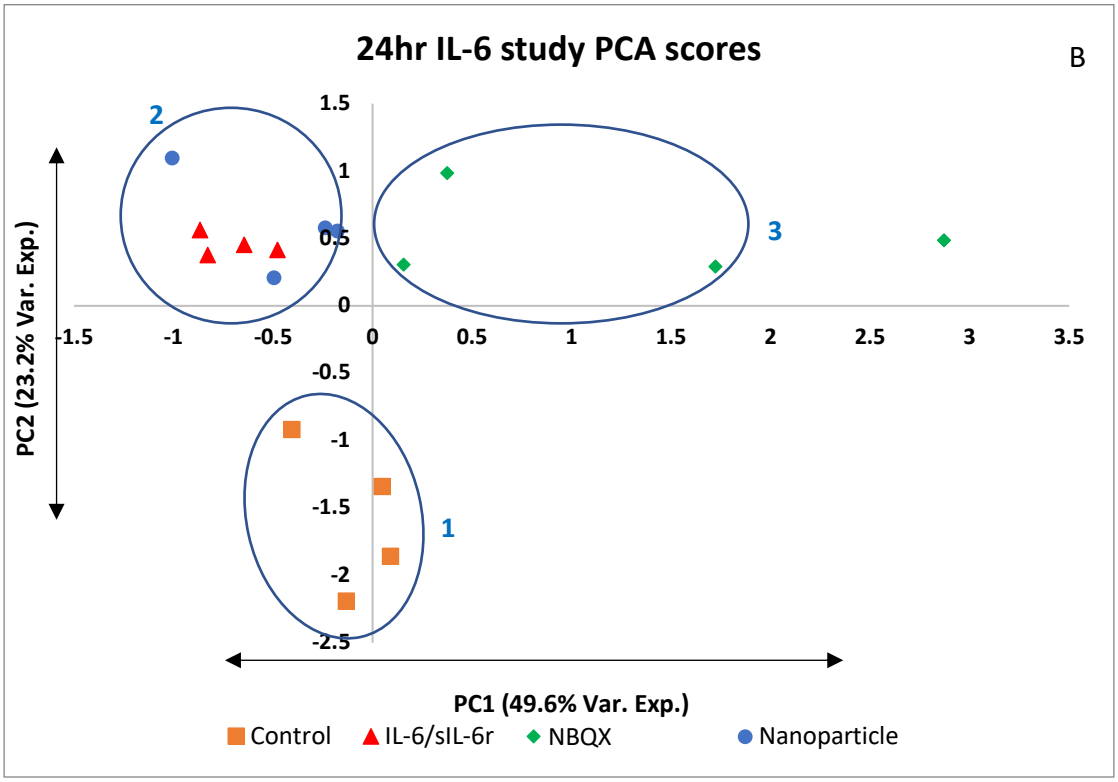

Figure 5.36: PCA based on components at 24hrs to determine treatment group affects from linear combinations of analyte concentrations released from IL-6/sIL-6r inflammatory study (section 2.7). 72.8% of variance explained (PC1=49.6%, PC2=23.2%). A) analyte weightings for PC1 and PC2. B) Variable score plot for PC1 and PC2, subdivided into time and treatment. INF-γ, IL-8, IL12p70 and IL-1β were removed from analysis to satisfy value of KMO sampling adequacy and achieve KMO value acceptable levels (>0.5)(Section 2.13). Eigenvalue scores were 0.875, 0.953, 0.628 and 0.904 for PC1 for IL-10, IL-13, IL-2 and TNFα respectively and 0.392, 0.847, 0.932, -0.787 and -0.649 for PC2 for IL-2, IL-4, IL-6, glutamate and OPG respectively.

Two principal components explained 79.3% of variance. PC1 explained 50.0% and PC2 explained 29.3% (Figure 5.37). Analysis of the principal component weightings highlighted that large positive eigenvalue scores for PC1 were identified for pro-inflammatory markers (IL-2, IL-1β and TNFα) and anti-inflammatory markers (IL-10 and IL-13). Small positive eigenvalue scores were shown for IL-12p70, IL-4 and IL-6. Positive large PC2 eigenvalue scores were demonstrated by pro-inflammatory markers IL-6 and IL12p70 and anti-inflammatory marker IL-4. Negative PC2 eigenvalue scores were shown for IL-10 and IL-1β. Glutamate did not contribute substantially to either PC1 or PC2 (Figure 5.37A).

Visual analysis of PC score plots revealed 2 clusters. Cluster 1 was mainly represented by IL-6/sIL-6r treated cells and was associated with positive PC1 and PC2 scores. Cluster 2 was represented by control cells and associated with negative PC2 scores and a broad spread of negative to positive PC1 scores. Free NBQX and NBQX loaded nanoparticles did not conform to these clusters although some NBQX loaded nanoparticle groups were located close to cluster 1 and all treatment groups were positive for PC2 compared to negative PC2 for controls (cluster 2) (Figure 5.37B).

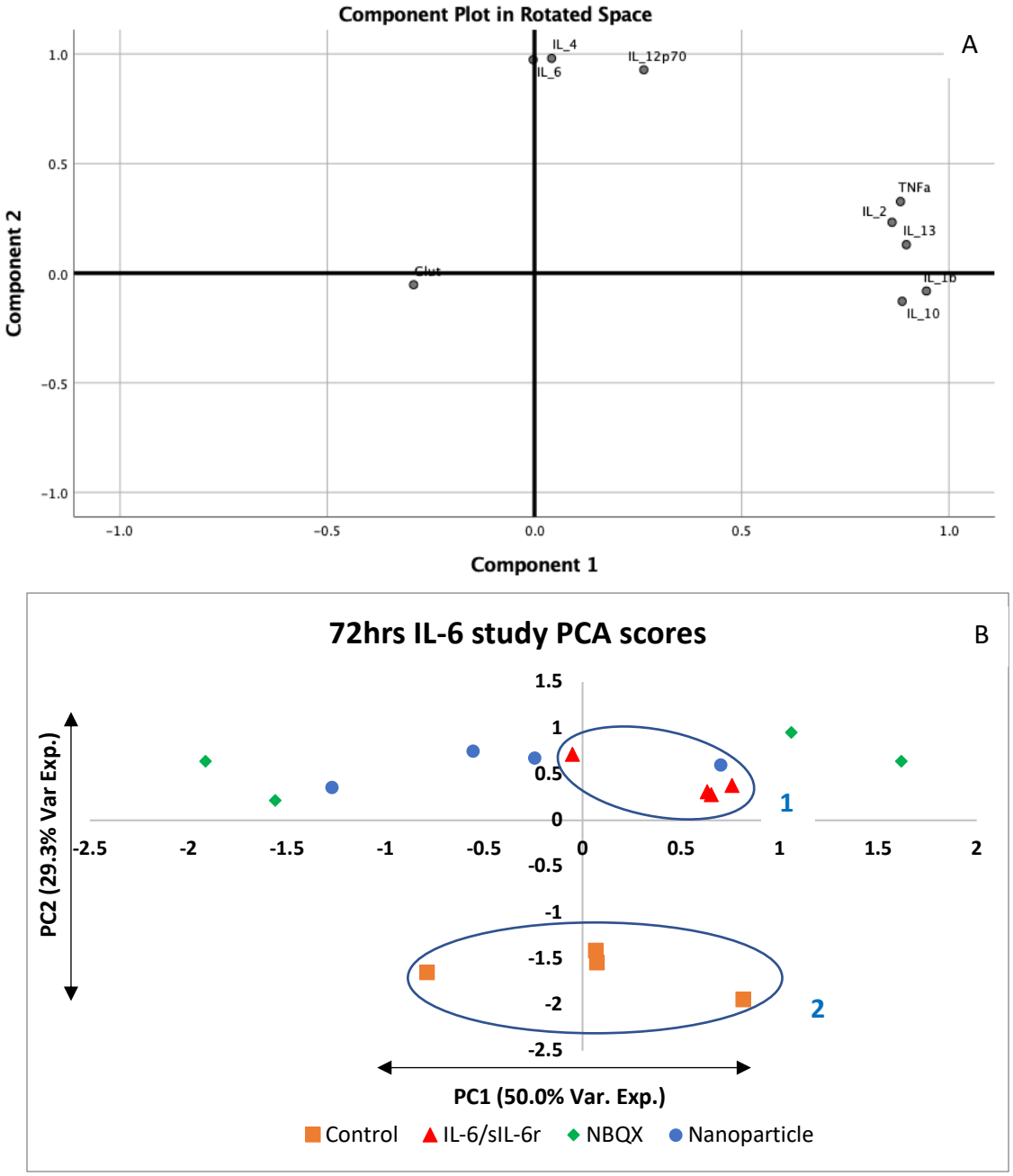

Figure 5.37: PCA based on components at 24hrs, explaining72hrs to determine treatment group affects from linear combinations of analyte concentrations released from IL-6/sIL-6r inflammatory study (section 2.7). 79.3% of variance explained (PC1=50.0%, PC2=29.3%. A) gene of interestanalyte weightings for PC1 and PC2. B) Variable score plot for PC1 and PC2 subdivided into time and treatment. INF-γ, IL-8 and OPG were removed from analysis to optimise value of KMO sampling adequacy and achieve KMO value acceptable levels (>0.5) (Section 2.13). Eigenvalue scores were 0.750, 0.631, 0.868, 0.822, 0.452,0.409, 0.938 and 0.880 for PC1 for IL-10, IL-12p70, IL-13, IL-1β, IL-4, IL-6, TNFα and IL-2 respectively and -0.491, 0.729, -0.474, 0.871 and 0.884 for PC2 for IL-10, IL-12p70, IL-1β, IL-4 and IL-6 respectively.

5.3 Discussion

5.3.1 DNQX and NBQX Effect on Bone Cell Viability

Addressing Aim 1 of this chapter (section 5.1.1), the application of DNQX or NBQX did not increase LDH release from Y201 MSCs or hOBs at any concentration, indicating that this family of GluR antagonists are not toxic to osteogenically differentiated Y201 MSCs over 2 weeks (Figure 5.2A-F). This is consistent with Flood et al. who demonstrated that application of 150μM GluR antagonist NBQX for 15 hours on human fibroblast-like synoviocytes had no significant effect on LDH release compared to controls (Flood et al., 2007). Application of either glutamate receptor antagonist CNQX (AMPA/KA specific) or MK801 (NMDA specific) did not induce any cytotoxic response (MTT assay) to rat primary osteoblast cultures at concentrations up to 100μM (Lin et al., 2008). Additionally, Glutamate treatment has been shown to have no significant effect of LDH release and MTT reduction when exposed to primary mouse osteoclasts (Hinoi et al., 2007). These *in vitro* findings in combination with *in vivo* application of AMPA/KA GluR antagonists (Lin et al., 2008, Bonnet et al., 2015, Bonnet et al., 2020) contribute to aim 1 of this chapter (section 5.1.1) by indicating that AMPA/KA glutamate receptor antagonism in this study is unlikely to be cytotoxic in osteoblasts and supports the usage of these GluR antagonists for further *in vitro* testing in the inflammatory model utilised in this chapter and the loading model in chapter 6 of this thesis.

Future work would look to directly assess the effects of DNQX and NBQX application on bone cell proliferation by quantifying cellular proliferation in comparison to controls via use of an MTT assay. Understanding changes in osteoblast (hOB) proliferation would be helpful in assessing the mechanisms by which GluR antagonists regulate bone turnover via altering osteoblast proliferation.

5.3.2 DNQX and NBQX Decreases Bone Cell Mineralisation.

Aim 2 of this chapter was to determine whether sustained DNQX and NBQX affects osteoblast mineralisation (section 5.1.1). The effect of DNQX and NBQX on osteoblast mineralisation was investigated by exposing osteogenically differentiated Y201 MSCs and

hOBs to either NBQX and DNQX in osteogenic cell culture media and quantifying mineralisation using an alizarin red staining.

DNQX and NBQX application over 14 days reduced mineralisation in both hOBs and Y201 MSC cells at greater than or equal to 200μM (Figures 5.3 and 5.4). These data are consistent with others showing that NBQX and other ionotropic glutamate receptor antagonists (CNQX, MK801) significantly reduces osteoblast mineralisation in osteoblasts *in vitro* (Dobson and Skerry, 2001, Lin et al., 2008, Bonnet et al., 2015).

Increased subchondral bone formation is a characteristic of the development of late-stage OA (Karsdal et al., 2008, Kwan Tat et al., 2010). The inhibitory effect of NBQX and DNQX on osteoblast mineralisation *in vitro* indicates that these antagonists may offer a protection against bone changes in OA, through modulating osteogenesis quantified by alizarin red staining of calcium ions as a determinant of mineralised matrix output. Additionally, the alizarin red mineralisation assay detects all osteogenic processes, therefore, would be impacted by changes in bone cell proliferation in addition to bone turnover.

Table 5.5: NBQX and DNQX binding affinity to ionotropic glutamate receptors as described by Nordholm et al. 1997.

GluR antagonist	Binding site	IC50
DNQX	Kainate	2μM
	AMPA	0.5μM
	NMDA (glycine site)	9.5μM
NBQX	Kainate	4.8μM
	AMPA	0.15μM
	NMDA (glycine site)	>90μM
CNQX	Kainate	1.5μM
	AMPA	0.3μM
	NMDA (glycine site)	14μM

In osteogenically differentiated Y201 MSCs, both NBQX and DNQX showed no significant effects on mineralisation at low concentrations (1 and 10μM) but a significant reduction in mineralisation compared with controls at 200μM (1.22-fold for DNQX, 1.88-fold for NBQX)

(Figure 5.4A and 5.4B). NBQX elicited a similar pattern in hOBs with a significant 1.28-fold reduction in mineralisation being observed at the 200μM treatment group compared with controls (Figure 5.4C). In direct comparison on both hOBs and Y201s, DNQX reduced mineralisation more than NBQX at 200μM (1.06-fold compared to 1.15-fold for hOBs and 1.07-fold and 1.14-fold for Y201 MSCs for NBQX and DNQX respectively). These findings indicate that high concentration (200μM) of sustained GluR antagonist is required to reduce bone cell mineralisation. DNQX is a more potent inhibitor of the kainate GluR than NBQX. Additionally, DNQX exhibits binding affinity for the NMDA receptor through affinity for the NMDA associate glycine site which NBQX does not (Nordholm et al., 1997). This would indicate that NMDA receptor inhibition in combination with AMPA/KA inhibition (DNQX) has a greater effect on bone mineralisation than AMPA/KA inhibition alone (NBQX). However, 200μM of DNQX would be high enough to inhibit all three ionotropic glutamate receptors (>ic50 for NMDA, AMPA and KA, Table 5.5). Further to this, binding studies comparing NMDA receptor antagonist MK-801 in primary rat chondrocytes and rat brain membranes highlighted a large difference in binding affinity between cell sources (IC_{50} of 1.7μM for chondrocytes 0.0023μM for brain membranes) (Piepoli et al., 2009). With this in mind it must be noted that ic50 values for these glutamate receptor antagonists were supported by binding studies following NMDA, AMPA and KA stimulation in the chicken retina and, therefore, inhibitory specificity may be different in bone (Nordholm et al., 1997). These findings mean we cannot determine which specific ionotropic glutamate receptor antagonism is responsible for altering mineralisation from this study.

In conclusion, sustained treatment with high dose (200μM) NBQX and DNQX reduces human osteoblast mineralisation. These NBQX and DNQX concentrations are far higher than the AMPA/KA specific ic50 values. Thus, their effect may be via NMDA/AMPA/KA GluRs due to regulation of differentiation, proliferation, matrix synthesis or mineralisation.

5.3.3 IL-6 Treatment of Y201 MSC Derived Osteocyte-like Cells in 3D Induces Pathological Markers of Bone Remodelling and Inflammation and is Affected by Short Term NBQX Application and Sustained Delivery of NBQX Encapsulated in PLGA Nanoparticles

OA is accompanied by bone changes that manifest prior to cartilage destruction (Brandt et al., 1991, Kwan Tat et al., 2010). Notably, early stage bone resorption occurs (Bettica et al., 2002) followed by sclerotic subchondral bone formation and thickening in developed OA (Buckland-Wright et al., 1990, Buckland-Wright et al., 1996). Bone resorption is a characteristic of inflammatory arthritis, driven by pro-inflammatory cytokines including TNFα, IL-6, IL-1β and IL-17 (Koenders et al., 2005, Sawa et al., 2006, Binder et al., 2013). Raised levels of IL-6 have been identified in synovial fluid of OA patients (Pozgan et al., 2010). Additionally, increased inflammatory and degradative markers have been identified in synovial fluid of patients within one month following acute knee injury (Catterall et al., 2010) with IL-6 levels in knee synovial fluid samples <8 weeks post injury significantly associated with $KOOS_4$ outcome scores (Watt et al., 2016). NBQX, AMPA/KA specific ionotropic GluR antagonism significantly reduced the release of inflammatory marker IL-6 in human fibroblast-like synoviocytes *in* vitro (Flood et al., 2007) and IA NBQX reduced inflammation and bone changes in both AIA (Bonnet et al., 2015) and PTOA (Bonnet et al., 2020) models of arthritis.

Aim 3 of this chapter investigates the impact of short-term compared to sustained NBQX application on a novel inflammatory 3D *in vitro* bone cell model to reveal potential mechanisms underlying its protective effects *in vivo* and provide a pathological *in vitro* model from which to further analyse the impacts of inflammation to bone and determine the potential of therapeutic intervention. Inflammation was stimulated by treatment with IL-6 in combination with its soluble receptor (IL-6/sIL-6r) following which, short term or sustained treatment given using free NBQX or free NBQX in combination with NBQX encapsulated in PLGA nanoparticles was applied and investigated for any potential therapeutic impact. This novel model was utilised as a pilot study with results providing a baseline to establish the use of this model in future experimentation and as such n numbers were defined as cell culture well replicates from one study. The limitations of this approach are discussed in more detail in section 7.6.2.1.

5.3.3.1 IL-6 Treatment and NBQX Intervention of Y201 MSC Derived Osteocyte-like cells in 3D Effects LDH Release but not Cell Morphology

To test any toxic effects of short term as well as short term in combination with sustained NBQX application after IL-6/sIL-6r stimulation of Y201 derived osteocyte like Y201 MSCs, LDH assays and cell morphology were assessed. Neither short term NBQX (1hr, 200μM) or IL-6/sIL-6r treatment (5ng/ml IL- 6 and 40ng/ml sIL-6r) altered LDH release at 24 and 72hrs. This is consistent with the data showing that 200μM NBQX is not cytotoxic (Figure 5.5). Free NBQX + NBQX loaded PLGA nanoparticle treated cells significantly increased LDH release compared with all other treatments (Figure 5.5). Given that free NBQX alone does not significantly affect LDH release on osteogenically differentiated Y201 MSCs after IL-6/sIL-6r stimulation, the toxic effect of nanoparticle treatment is either due to the application of PLGA nanoparticles, or the sustained release of NBQX or a combination of the two. High concentrations of unloaded PLGA nanoparticles (100mg/ml) significantly altered hOB cell viability across all time points tested (MTS assay; section 3.3.4.; Figure 3.9). To maximise the load of NBQX available for sustained delivery (as NBQX concentrations encapsulated in PLGA nanoparticles were low, see chapter 3) while mitigating the risk of impacting cellular viability, 10mg/ml NBQX loaded PLGA nanoparticle concentrations were used in this study. However, this PLGA concentration alone, or in combination with NBQX, may have induced a cytotoxic response and, therefore, may mask any therapeutic effects of sustained NBQX release. PLGA nanoparticle treatment (0.05 to 5mg/cm^2) of osteosarcoma cell line MG-63 cells *in vitro* caused a cytotoxic response due to cellular uptake of nanoparticles in a concentration dependent manner (Altındal and Gümüşderelioğlu, 2016) and blank PLGA nanoparticles at concentrations greater than 500μg/ml have been shown to reduce macrophage viability (MTT assay) (Derman et al., 2015). Therefore, it may be that the 10mg/ml concentration of nanoparticles used in this study is high enough to cause a cytotoxic response. Despite these findings, PLGA nanoparticles are generally accepted as being biocompatible and of low toxicity, with PLGA having been approved for use in humans in drug delivery systems by the US FDA and the European Medicine Agency (Danhier et al., 2012). Several PLGA nanoparticle formulations have shown no cytotoxicity (MTT assays) *in vitro* when applied to various cells sources including osteoblasts (Destache et al., 2009, Amjadi et al., 2013, Wang et al., 2015). However, the nanoparticle concentrations applied in

these studies were in the μg/ml to low mg/ml concentration which is much lower than that applied in MTS assays in chapter 3 of this thesis and that used in this chapter.

Multiple PLGA nanoparticle formulations having been approved for use in humans. Nevertheless, there are no PLGA nanoparticle formulations approved for the treatment of OA (Zhong et al., 2018, Kou et al., 2019), although a PLGA microsphere formulation for the sustained delivery of corticosteroid triamcinolone acetonide (FX006) has been approved for use in the treatment of OA knee pain (Bodick et al., 2015, Conaghan et al., 2018a, Conaghan et al., 2018b).

Finally, LDH levels significantly increase over time (24 vs 72hrs; Figure 5.5). Although LDH levels increase, the proportion of LDH per cell may have remained consistent if the cell population in this study has increased between 24 and 72 hours. Cell number was not quantified at each time point so we cannot normalize this data to confirm this theory. Large changes in cell number is unlikely with terminally differentiated osteocytes but may be the case with Y201 MSCs in a pre-osteogenic state (Zhang et al., 2019). The significant increase in LDH is possibly due to increase in cell numbers over time, as it occurred in controls as well as IL-6 and NBQX treated cells. Future work in identifying cell numbers at each time point via a live/dead assay could be used to normalize LDH release assay findings for cell number. However, this is a destructive test and therefore findings would only be indirectly related to the LDH released from cell culture wells of the same treatment group.

To summarise, quantification of LDH release revealed that the concentrations of IL-6/sIL-6r used in this study, although relating to pathological concentrations found in the joint following injury (Kotake et al., 1996, Watt et al., 2016), were not cytotoxic vs controls and therefore represent a viable application of inflammatory stimulus moving forwards for further investigation and allow for determination of the impacts of therapeutic interventions (such as NBQX) without alterations to cell viability.

All treatment groups at all timepoints have phalloidin stained cytoplasmic extensions beginning to form (Figure 5.6). This is characteristic of healthy osteocyte-like cells cultured in 3D that behave more like cells *in vivo* and interact via cell extensions within an

extracellular matrix (Justice et al., 2009, Breslin and O'Driscoll, 2013, Vazquez, 2013). The images indicate the beginnings of osteocyte like phenotype, as osteocytes form an interlinked network through the bone ECM *in vivo* via cell extensions (Gu et al., 2005, Vazquez, 2013, Scully, 2015). No obvious differences were observed in cell morphology, although, changes in cell shape and extension length were not quantified. Osteocyte specific genes (*sost, dmp-1*) were not found to be expressed from cells in this study, but the expression of late osteoblast markers (*ocn*) was identified. This indicates that the cells in this study are representative of a late osteoblast/early osteocyte as opposed to a fully differentiated osteocyte.

These findings show that this culture system provides a 3D type I collagen scaffold in which Y201 MSCs can remain viable and differentiate to dendritic phenotypically osteocyte-like cells providing a more accurate representation of the *in vivo* environment than an equivalent 2D cell culture study (Edmondson et al., 2014).

Together these findings address objective 3.1 contributing towards aim 3 of this chapter (section 5.1.1) which builds the understanding of the impacts of IL-6/sIL-6r, NBQX and the PLGA nanoparticles developed in chapter 3 of this thesis within the context of this novel 3D osteogenically differentiated Y201 MSC model.

5.3.3.2 IL-6 Treatment and NBQX Intervention on Y201 MSC Derived Osteocyte-like Cells in 3D Affects Nitric Oxide Release.

To test the effects of short term and sustained NBQX application after IL-6/sIL-6r stimulation of Y201 derived osteocyte like cells on nitrite release, a Griess assay was performed.

Nitrite levels were not significantly changed following IL-6/sIL-6r with or without free NBQX application at 24hrs (Figure 5.7). After 72 hours, both IL-6/sIL-6r treated cells and IL-6/sIL-6r+NBQX treated cells had significantly increased nitrite levels compared to controls and vs equivalent 24hr treatment groups.

NO signalling plays a role in bone homeostasis, with reduced bone mass observed in endothelial NOS knockout mice as a consequence of reduced osteoblastic function (Yavropoulou and Yovos, 2016). Additionally, NO acts as neurotransmitter, which has been linked to glutamatergic signalling within the CNS, where increased NO has correlated with an increase in glutamate release (Lourenço et al., 2011).

In OA joints dysregulation NO plays a destructive and proinflammatory role (Jin et al., 2017). NO signalling is regulated by endothelial NOS (eNOS) in osteoblasts, causing low NO levels and, inducible NOS (iNOS) in activated osteocytes, resulting in high levels of NO production (Hamilton et al., 2013). eNOS deficient mice have been shown to have slowed postnatal bone formation and defective osteoblast proliferation and differentiation that can be restored by exogenous NO administration (Aguirre et al., 2001). Elevated levels of NO have been identified on bone cyst lining cells in addition to raised levels of IL-6 and IL-1β (Komiya et al., 2000) highlighting an association of these molecules in pathological bone. In OA, NO is found in elevated levels and has been shown to mediate the destructive effects of IL-1β and TNF-α in cartilage (Vuolteenaho et al., 2007). NOS activation in rats increased osteophyte formation and cartilage degradation while selective nNOS inhibition mitigated the severity of the joint damage (Gokay et al., 2016). In Synovium, NO signalling has been shown to mediate apoptosis of cells in synovial explants with NOS inhibitors reducing this impact (van't Hof et al., 2000). In an oestrogen knockout mouse model, systemic increases in IL-6, TNFα and IL-1β were linked with increased NO release and bone resorption (Cuzzocrea et al., 2003). The effect of NO release following IL-6/sIL-6r exposure in bone has not been previously demonstrated to our knowledge in an equivalent culture system. It may be the case that the exposure to pathological concentrations of IL-6/sIL-6r in this study induced NO release via the upregulation of other pro-inflammatory cytokines such as TNFα and IL-1β. Both cytokines demonstrate increased release over time following IL-6/sIL-6r treatment in this study and both of these cytokines have been linked to pathological phenotypes caused by NO release in cartilage and synovium (Stefanovic-Racic et al., 1994, Vuolteenaho et al., 2007). These studies highlight that, NO signalling plays a role in bone, cartilage and synovium and has been shown to be linked with inflammation and degradation in the joint.

The significant increase over 72hrs in NO release vs controls in IL-6/sIL-6r treatment groups highlights a novel characteristic of this model. Subsequently the NO release profile identified in this model would allow for investigation into the impact of various interventions (such as GluR antagonists) and thereby support understanding of inflammatory signalling in bone and pathways by which novel interventions may be beneficial.

In the 3D osteocyte-like culture, IL-6/sIL-6r treatment induced a NO signal after 72 hours that was not inhibited by short term NBQX treatment (Figure 5.7). Glutamate signalling in bone has been linked to NO release with L-glutamate treatment of bone marrow stromal cells reducing NO production via down regulation of Ca^{2+} signalling (Foreman et al., 2005). This effect was found to be mediated via metabotropic GluRs and may explain why, in this study, there is a lack of effect on NO release following NBQX mediated ionotropic glutamate receptor antagonism. The 2.65-fold NO increase at 24hrs and 1.69-fold NO increase at 72hrs vs IL-6/sIL-6r treatment groups following NBQX loaded nanoparticle application indicates a potential pathological phenotype with this concentration of nanoparticles over that seen with IL-6/sIL-6r stimulation alone (Figure 5.7). Since, NO signalling regulates bone formation and resorption, significant NO increases following NBQX loaded PLGA nanoparticle application could have a pathological impact on bone homeostasis (Hamilton et al., 2013).

Future work delivering unencapsulated NBQX for sustained periods of time (greater than 1hr) would reveal whether NBQX treatment could inhibit IL-6/sIL-6r stimulated NO release from Y201 MSC differentiated bone cells in the absence of the cellular response to the nanoparticles themselves. Alternatively, to directly determine if the nanoparticle concentration (10mg/ml) used in this study induces NO release, a range of nanoparticle concentrations could be applied, and the effects investigated.

5.3.3.3 IL-6 Treatment and NBQX Intervention of Y201 MSC Derived Osteocyte-like cells in 3D Influences Bone Turnover, Inflammatory and Glutamate Signalling.

The effect of short-term and sustained nanoparticle NBQX application on IL-6/sIL-6r stimulated Y201 3D cultures on bone turnover, inflammatory and glutamatergic signals was

addressed through qRT-PCR and immunoassay analysis. Individual gene and protein analysis across treatments as well as multivariate correlation and principal component analysis were performed to investigate the data. This pilot study will be used to determine a baseline for control measurements as well as to investigate the effects of inflammatory treatment and subsequent NBQX intervention to the turnover/release of the aforementioned molecules.

5.3.3.3.1 Bone Turnover

The expression of bone turnover markers *opg, ocn, col-1a1* and *alp* was identified in this study along with the release of OPG (table 5.1 and figures 5.8, 5.10, 5.11, 5.12 and 5.33). The complete lack of quantifiable levels of *sost* and *dmp-1* expression and release of SOST by osteogenically differentiated Y201 MSCs, combined with the expression of osteoblast markers *col1a1* and *alp* and late stage osteoblast marker *ocn* in control and treatment groups indicates cells are in a late osteoblast / early osteocyte stage of differentiation (Franz-Odendaal et al., 2006, Capulli et al., 2014) as cells were dendritic (figure 5.6), which is a morphological characteristic of osteocytes. Expression of all bone turnover markers, other than *col-1a1,* significantly decreased between 24 and 72hrs in control groups. This possibly indicates that cells are progressing towards osteocyte terminal differentiation by reducing markers such as *ocn*, *alp* and *opg,* which are associated with osteoblast phenotype (Abe et al., 2019, Sawa et al., 2019). This significant decrease in these markers in control groups over time highlights a characteristic of the cells in this model that, when focusing on *alp,* differs with the application of IL-6/sIL-6r indicating an impact to the bone turnover phenotype of cells in this model following inflammatory molecule exposure (figure 5.12). This characteristic then highlighted the potential therapeutic impact of short term NBQX and nanoparticle treatment mitigating the effect of IL-6/sIL-6r on *alp* expression by returning levels to that of controls at 24hrs (Figure 5.12). This is consistent with evidence to suggest that IL-6 may reduce bone mass by modulating communication between osteocytes and osteoblasts and reducing *alp* activity (Bakker et al., 2014)

There was a significant increase in OPG release across all treatment groups as a factor of time. These findings could be the result of a build-up of OPG released from cells in a closed

culture environment that did not receive a media change between 24 and 72hrs meaning that OPG release was measured per 24hrs then per 72hrs.

Particularly strong positive correlations (>0.7) were observed between *opg, il-6* and *eaat-3* expression (Figures 5.17-5.19), highlighting the link between glutamate signalling, bone turnover and inflammation in this study. When plotting these correlations, across all comparisons made (*il-6* vs *opg, il-6* vs *eaat-3* and *opg* vs *eaat-3*), it is evident that all groups treated with IL-6/sIL-6r (IL-6, NBQX, NP) at 24 hours differ in expression from control groups but that this difference is not observed at 72hrs. This evidence, considering that IL-6/sIL-6r treatment is consistent across all group's vs control, may indicate a role of IL-6 inflammatory application in the turnover of these markers providing a baseline for the observation of future interventions.

qRT-PCR PCA revealed that, at 24hrs, *opg* is regulated alongside *il-6, gria-1, eaat-1* and *eaat-3* contributing positively to PC1 and *alp* and *col-1a1* positively contribute to PC2 alongside *gria-1* (figure 5.20). All IL-6/sIL-6r treated groups are clearly separated by PCA from controls and have broadly positive PC1 and PC2 scores compared to controls that have negative PC1 and PC2 scores, indicating bone turnover markers (*opg, alp, col-1a1*) in combination with AMPA GluR, glutamate transporter and *il-6* expression drive the changes seen at 24hrs (figure 5.20). When observing the graphical outputs for these groupings, we see that, at 24hrs, there is a reduction (although not significant) in all IL-6/sIL-6r treatment groups vs controls for *opg, il-6, eaat-1, eaat-3 and gria-1* (Figures 5.8, 5.9, 5.13, 5.15 and 5.16). As with correlation plots (Figures 5.17-5.19), PCA has revealed a consistent impact to the variance of glutamate signalling and bone turnover markers in this model as a consequence of IL-6/sIL-6r pathological inflammatory application at 24hrs. Additionally, this evidence indicates that this effect is not sustained to 72hrs where variance caused by IL-6/sIL-6r treatment is not a factor in PCA groupings (figure 5.21). This interpretation highlights a characteristic of this novel cell culture model that may be compared against for investigation into future impacts of therapeutic interventions. However, no effects were identified as a consequence of short term NBQX treatment or nanoparticle treatment for these markers (*opg, il-6, eaat-1, eaat-3 and gria-1*) in this study. As previously mentioned, IL-6/sIL-6r induced changes to *alp* expression were mitigated in short term NBQX and

Nanoparticle treatment groups (figure 5.12), PCA also groups *alp* variance with *col-1a1* at 24hrs (Figure 5.20A). When investigating the graphical outputs we see that NBQX loaded nanoparticle application at 24 hours caused an increase in *col-1a1* expression, which codes for type-I collagen, the most abundant structural protein in bone (Hronik-Tupaj et al., 2011). The short term (24hr) increase in *col-1a1* mRNA levels could indicate a pro-osteoblastic differentiation effect of nanoparticle application. *Col-1a1* is expressed throughout osteoblast differentiation and especially in late stage mature osteoblasts (Capulli et al., 2014) as well as throughout osteocyte differentiation (Compton and Lee, 2014). Increased *col-1a1* expression in response to nanoparticle treatment indicates a bone forming response of osteogenically differentiated Y201 MSCs that, in combination with PCA groupings with *alp* (Figure 5.20) would indicate a bone forming response to NBQX loaded nanoparticle treatment (Yang et al., 2013). In addition to these findings, PCA analysis at 72hrs separates nanoparticle treatment groups from all other groups primarily via PC1 scores which are a factor of variance in *alp* and *opg (*as well as *eaat-3* and *il-6)* (figure 5.21). When investigating the graphical outputs for these markers we see that the variance is due to increases in turnover as a consequence of nanoparticle application (figure 5.8, 5.9, 5.12 and 5.16), although only significantly so for il-6 vs controls (figure 5.9). These PCA findings indicate a nanoparticle treatment group impact to bone turnover (as well as inflammation and glutamate signalling) that is sustained over 72hrs but may be pathological as differs from untreated controls as well as IL-6/sIL-6r treatment groups.

IL-6/sIL-6r treatment has previously been shown to increase the RANKL signalling in osteocytes resulting in a pro-osteoclastogenesis phenotype and increased RANKL/OPG ratio (Wu et al., 2017). The results from this study indicate that IL-6/sIL-6r treatment may also promote this phenotype through reduction of *opg* expression (Highlighted in PCA at 24hrs figure 5.20). The RANKL/OPG signalling axis is key in the communication of osteocytes, osteoclasts and osteoblasts in controlling bone turnover. RANKL is an osteoblast membrane bound protein that binds to a RANK receptor on the surface of osteoclasts and promotes osteoclast activity. However, *rankl* was not detected in quantifiable levels in this study. OPG acts as a decoy receptor for RANK and inhibits osteoclast formation (Martin and Sims, 2015). *Opg* expression from osteocytes has been identified as a factor in the osteocytic control of bone homeostasis (Kramer et al., 2010) and that bone loss is driven by a

reduction in *opg* levels expressed from osteocytes (Bellido, 2014, Piemontese et al., 2016). PGE_2 mediated decreases in *opg* expression have been linked with IL-6 secretion in osteoblasts (Liu et al., 2005), highlighting a negative correlation between OPG and IL-6 in bone.

Regarding bone turnover markers investigated from this model, correlation (figure 5.17 and 5.19) and PCA analysis (figures 5.20) have demonstrated that the inflammatory stimulus utilised (IL-6/sIL-6r) results in a 24hr reduction to bone turnover markers (*opg, alp*) as well as *il-6* and glutamate signalling components (*eaat-3, gria-1*). This finding may potentially reflect a pro-resorptive phenotype in bone and allows for identification of any potential therapeutic effects of interventions (as was the case with NBQX to *alp* turnover). These findings have helped to build an understanding of the bone phenotype within this model as well as the impact of IL-6/sIL-6r pathological stimulus to these cells. This foundation now allows for future investigation into alternate interventions (such as DNQX) and sustained applications (such as from the hydrogels in chapter 4 of this thesis) thereby addressing the thesis hypothesis (section 5.1.1) by allowing for investigation into the protective effects of delivery systems on inflammatory driven pathways in bone *in vitro*.

5.3.3.3.2 Inflammatory Markers

At 24 hours, IL-6/sIL6r treatment increased the release of IL-12p70 (15.52-fold; Figure 5.25) and, unsurprisingly, considering the inflammatory stimulus, increased IL-6 release (7.94-fold; Figure 5.30) compared to controls. This was also the case at 72hrs (3.03-fold and 4.70-fold respectively). There was a significant increase in TNFα release between 24 and 72hrs in IL-6/sIL-6r treated cells (6.78-fold; Figure 5.31). There was a significant increase in IL-1β release in both control and IL-6/sIL-6r treatment groups between 24 and 72hrs (2.02-fold and 2.59-fold respectively; Figure 5.27) The anti-inflammatory marker IL-4 was significantly increased compared with controls for all treatment groups at all time points (Figure 5.29). IL-10 and IL-13 were significantly increased (3.24-fold and 2.64-fold respectively; Figures 5.24 and 5.26) by short term NBQX treatment after 24hrs compared with IL-6/sIL-6r alone treated cells.

Il-6 expression was significantly reduced for all treatment groups compared to control at 24hrs indicating that the Y201 osteocyte like cells reduce *il-6* expression due to the external experimental addition of pathophysiological IL-6 levels (Kotake et al., 1996, Watt et al., 2016). The IL-6/sIL-6r treatment in this study will influence the effect on bone turnover as trans (soluble IL-6 receptor) IL-6 signalling has been shown to be the primary influence on bone formation and osteoclastogenesis over cis (membrane bound IL-6 receptor) signalling (McGregor et al., 2019). IL-6 treatment of primary human osteocytes has been shown not to impact *il-6* expression but this wasn't in the presence of sIL-6r (Pathak et al., 2016) which further implicates trans il-6 signalling in bone cell function. There is some evidence that IL-6/sIL-6r treatment of MLO-Y4 osteocytes results in an upregulation of *il-6* expression along with *tnf*α (Bakker et al., 2014), which is not consistent with this study. Additionally, this consistent decrease in *il-6* turnover represents a characteristic of this model that can be used to baseline the impact of any therapeutic interventions during future testing.

TNFα release was strongly positively correlated with anti-inflammatory marker IL-13 release (>0.900; Table 5.4) and PCA grouped TNFα with anti-inflammatory IL-10 and IL-13 and strongly positively contributing to PC1 at 24hrs (Figure 5.36A). All IL-6/sIL-6r treated cells (IL-6, NBQX, NP) were separated from controls indicating an impact of inflammatory intervention to the immunoassay markers quantified in this chapter at 24hrs (Figure 5.36B)

Nanoparticle and IL-6 treatment groups were clustered together at 24hrs and represented negative PC1 scores whereas NBQX treated cells were separated with positive PC1 scores, a result of TNFα, IL-10 and IL-13 variance influenced by short term NBQX treatment vs the nanoparticle and IL-6 treatment groups and controls (Figure 5.36B). The impact of NBQX to these markers at 24hrs can be visualised in figures 5.31 (TNFα), 5.26 (IL-13) and 5.24 (IL-10) and demonstrates a short term (24hr) inflammatory response as a consequence of NBQX application with potential therapeutic implications due to the increase in anti-inflammatory cytokines not previously identified as a consequence of GluR antagonism in bone.

At 72hrs there was an association of IL-6 and IL-4 as positive factors for PC2 along with IL-12p70 (Figure 5.37A). Additionally, TNFα, IL-1β and IL-2 were shown to be factors that

strongly positively contribute to PC1 scores in combination with IL-10 and IL-13 (Figure 5.37A). As with 24hrs, all IL-6/sIL-6r treated cells (IL-6, NBQX, NP) at 72hrs had positive scores for PC2 and controls had negative scores (Figure 5.37B). Although none of the short term NBQX treated cells conformed to the IL-6/sIL-6r alone cluster, there was no clear separation between short-term NBQX treatment scores and IL-6/sIL-6r treatment at 72hrs. This highlights the short-term impact of this NBQX intervention, and the lack of a clear sustained therapeutic effect delivered by nanoparticles.

As with bone markers, PCA of immunoassay inflammatory markers has revealed that at both 24 and 72hrs (Figures 5.36 and 5.37) IL-6/sIL-6r treatment variance can be distinguished from controls as a consequence of biomarkers, in this case IL-4 and IL-12p70 increases (Figures 5.25 and 5.29) (in combination with significant decreases in *il-6* turnover). Variance in these markers can be tracked to determine any impact of therapeutic intervention during future analysis and further establishes the phenotype of this model combining with variance to *opg* and *alp* identified at 24hrs (section 5.4.3.3.1).

Regarding the biological impact of upregulation of these markers in response to L-6/sIL-6r treatment, IL-12p70 has been shown to protect against osteoclastogenesis *in vitro* (Moreira et al., 2004) and acts as a stimulatory factor for T cells (Gee et al., 2009). In immune responses to conditions such as malaria, increased IL-6 release has been correlated with increased IL-12p70 release (Lyke et al., 2004). Higher plasma levels IL-12 have been identified in osteoporotic patients and the same study identified increased plasma IL-6 levels in patients with lower bone mineral density (Ilesanmi-Oyelere et al., 2019). Although raised IL-12p70 levels have been identified within arthritic joints, along with raised IL-6 levels (Vangsness et al., 2011, Vincent et al., 2013) a mechanism by which IL-6 induces increased IL-12p70 levels in bone has not been identified. The strong association of IL-4 identified in IL-6/sIL-6r treatment groups in this study provides evidence for an anti-inflammatory response to pathological pro-inflammatory stimulus in bone. This study provides evidence that IL-12p70, a conventionally pro-inflammatory mediator, is strongly associated with IL-6/sIL-6r exposure within bone *in vitro*, the release of which has not previously been directly linked to IL-6 in this tissue type. In bone, IL-4 treatment on *ex vivo* bone samples has been shown to have a protective effect on bone maintenance associated

with a 70% reduction in IL-6 levels (Miossec et al., 1994). This experiment demonstrates the reverse of Miossec et al., (1994), in which IL-6/sIL-6r exposure induces an increase in IL-4, an affect that has not previously been identified in bone *in vitro* to our knowledge. This release in anti-inflammatory markers could be in response to pathological inflammation and IL-4 has been detected alongside pro-inflammatory cytokines including IL-6 in both OA and RA patient synovial fluid (Schlaak et al., 1996). IL-4 has been shown to deliver protective effects to joints in an ACL+MCL transection rat model of OA, in which IA injection of recombinant rat IL-4 ameliorated joint destruction, reduced loss of aggrecan and decreased NO production in chondrocytes (Yorimitsu et al., 2008). IL-4 treatment, with or without IL-10 has been shown to reduce the production of IL-1β and TNFα in healthy human cartilage explants (van Meegeren et al., 2012). IL-4 has been shown to increase *alp* expression in osteoblast like cells (MG63 cell line) (Riancho et al., 1993). IL-4 and IL-13 have been shown to induce OPG production by primary mouse osteoblasts and inhibit osteoclast differentiation (Yamada et al., 2007). Recombinant IL-4 administration in an osteonecrosis mouse model inhibited osteocyte mediated osteonecrosis and reduced osteoclast accumulation (Wu et al., 2016) further supporting a protective role of this cytokine in bone.

Significantly increased detection of IL-6 release in this study at all time points following IL-6/sIL-6r treatment is to be expected due to the pathological levels of this cytokine added to the cell culture media (Figure 5.30). The concentration detected across all treatment groups was between 550 and 560pg/ml this was close to ten-fold less than the 5ng/ml added at the initiation of the study. The *in vivo* half-life of IL-6 is between 2-4hrs (Marino and Giotta, 2008). However, due to the closed culture system used in this study, IL-6 clearance is not a factor in the *in vitro* IL-6 half-life so this may vary from that determined *in vivo*. Soluble IL-6 receptor was added along with IL-6 and the formation of an IL-6/sIL-6r complex would have reduced detection of free un-complexed IL-6 (Montero-Julian et al., 1994). The lack of IL-6 release reduction following short term (1hr) NBQX treatment could indicate that sustained increased NBQX concentrations may be necessary to induce a significant IL-6 release reduction. Further to this, it may be that in addition to bone, alternate joint tissues are responsible for the reduction in *il-6* expression following NBQX treatment *in vivo,* as NBQX treatment reduced *il-6* mRNA expression in meniscus (Bonnet et al., 2015) and synovial fibroblasts (Flood et al., 2007). The increase in IL-6 release in NBQX loaded nanoparticle

treated cells ties is consistent with increased *il-6* expression compared to controls (2.18-fold; Figure 5.9) at 72hrs in the same treatment group. IL-6 detected in synovial fluid is associated with knee injury and osteoarthritis ($KOOS_4$) scores following acute injury (Watt et al., 2016) and increased likelihood of developing radiographic knee OA (Livshits et al., 2009). Over expression of IL-6 is associated with bone resorption and osteoclast activation (Palmqvist et al., 2002, Li et al., 2016). Increased IL-6 release following nanoparticle treatment is likely to be pathological and ties in with gene expression, LDH release (Figure 5.5) and NO release (Figure 5.7) assay findings in this study.

In inflammatory arthritis, such as RA, there is an upregulation of anti-inflammatory markers in response to raised levels of inflammatory markers (Choy, 2012, Mateen et al., 2017). The association of pro-inflammatory cytokines (TNFα and IL-1β) with anti-inflammatory cytokines (IL-10 and IL-13), identified in immunoassay PCA (Figures 5.36 and 5.37), highlights a coordinated pro-and anti-inflammatory response to IL-6/sIL-6r stimulus due to short term NBQX intervention at 24hrs (Figure 5.36). This finding indicates that this novel model has potential to highlight the impact of therapeutic intervention on biomarker release and thereby act as a drug screening tool for future studies, while building understanding of the impact of inflammatory driven pathways in bone thereby addressing the thesis hypothesis (section 5.1.1.).

From a biological perspective the impact of short term NBQX treatment on inflammatory marker release may have therapeutic implications. IL-10 can down-regulate the production of pro-inflammatory cytokines such as IL-6, TNFα and IL-1 through repressing expression from activated macrophages (Zhang and An, 2007). In a study examining Lipopolysaccharide stimulation of *ex vivo* synovium samples from multiple OA sites, low IL-10 production was associated with an increased risk of OA (Miossec et al., 1992). In RA patients, IL-10 has been negatively correlated with disease severity (scored by DAS28) while IL-6 and TNFα were positively correlated (Shrivastava et al., 2015). Cultured human RA synovial fibroblasts were shown to constitutively express IL-10 mRNA and IL-1β and TNFα upregulated IL-10 *in vitro* (Ritchlin and Haas-Smith, 2001). This association of IL-10 with pro-inflammatory IL-1β and TNFα was identified in immunoassay PCA in this study indicating a similar process may occur

in osteogenically differentiated cells following pro-inflammatory stimulus while being reflective of a therapeutic intervention effect (Figure 5.36). However, IL-10 treated human cartilage explants demonstrated reduced IL-1β and TNFα production in a blood induced *in vitro* degradation model indicating that the action of IL-10 differs depending on tissue type and external conditions. IL-10 deficient mice develop osteoporosis symptoms including reduced bone mass and suppressed bone formation with reduced generation of osteoblasts (Dresner-Pollak et al., 2004). Additionally, IL-10 is known to inhibit osteoclastogenesis at the early stage of osteoclast differentiation (Xu et al., 1995). In a rat spinal cord injury model, osteocytes, positive for multiple inflammatory markers, were observed including TNFα, IL-6, IL-17 and IL-10 with inflammatory markers being associated with changes in bone turnover leading to a resorptive phenotype (Metzger et al., 2019). The association of Pro- and anti-inflammatory molecules release by osteocytes following injury identified by Metzger et al., (2019) correlates with the Pro and anti-inflammatory cytokine release association identified in this study following both IL-6/sIL-6r treatment (IL-6 and IL-4) and short term NBQX treatment (IL-10, IL-13, IL-1β and TNFα). Following inflammatory stimulation with lipopolysaccharide and IL-13 treatment, synovial membranes extracted from OA patients undergoing total knee replacement surgery demonstrated decreased synthesis of IL-1β and TNFα. Both IL-13 and IL-4 have been shown to inhibit bone resorbing activity in foetal mouse long bones (Onoe et al., 1996). Additionally, IL-13 and IL-4 were shown to suppress IL-1 induced COX-2 mediated prostaglandin synthesis (Onoe et al., 1996) indicating a potential mechanism by which these anti-inflammatory cytokines reduce bone resorption via osteoblasts. Based on the protective and anti-resorptive effects of IL-10 and IL-13 identified in the literature on bone, synovium and cartilage, the short term NBQX induced increase in IL-10 and IL-13 at 24hrs (Figures 5.24 and 5.26), identified in this study would have the potential to deliver therapeutic benefit. The impact of short term NBQX intervention in this study may indicate a mechanism of action via the regulation of anti-inflammatory cytokines in bone and could be a potential path by which NBQX intervention has demonstrated therapeutic effects in inflammatory arthritis and joint injury models *in vivo* (Bonnet et al., 2015, Bonnet et al., 2020). This anti-inflammatory property of NBQX via upregulation of IL-10 and IL-13 has not been previously identified in bone (osteocytes or

osteoblasts) and represents an insight into the potential drug screening capability of this model.

Addition of TNFα, IL-1β and IL-6 has been shown to synergistically enhance the expression of *il-6, il-8, tnfα* and *il-1β* in primary human osteocytes indicating that pro-inflammatory signalling is coordinated (Pathak et al., 2016). However, the impact of pro-inflammatory stimuli on anti-inflammatory marker release was not investigated in this study. Therefore, the association of TNFα, IL-1β with anti-inflammatory cytokines following stimulation of osteocyte-like Y201 MSCs with IL-6/sIL-6r and subsequent treatment with NBQX in this study delivers a novel insight into the response of osteocyte-like cells to inflammatory insult. An alternate interpretation could be that the upregulation of TNFα and IL-1β represents a pro-inflammatory response to NBQX withdrawal as NBQX (200μM) cell culture media was replaced with NBQX free media after 1hr of exposure in short term 'NBQX' treatment groups, with the aim of reflecting joint clearance rates of the drug. This is not an effect that has been previously observed in bone following NBQX administration. However, increases in joint inflammation following NSAID withdrawal have been identified in inflammatory arthritis patients (Thompson et al., 1988) and disease flares are common in juvenile idiopathic arthritis follow treatment withdrawal, particularly from biological therapies (Halyabar et al., 2019).

No increase compared to IL-6/sIL-6r treatment groups for TNFα, IL-1β, IL-10 and IL-13 release was observed in nanoparticle treated cells at 24hrs, differing from short term NBQX treatment (Figures 5.24, 5.26, 5.27 and 5.31). The increase in IL-6 release and expression in NBQX loaded nanoparticle treatment groups may represent a pathological pro-inflammatory response following sustained exposure to 10mg/ml PLGA nanoparticles (Figures 5.30 and 5.9). This is consistent with the increased levels of LDH and nitrite release observed in the same treatment group in this study (Figures 5.5 and 5.6). The increase in *il-6* expression may indicate an apoptotic phenotype induced by nanoparticle treatment since apoptotic MLO-Y4 osteocyte media has been shown to contain more IL-6 and sIL-6r than non-apoptotic (Cheung et al., 2012). An inflammatory phenotype after nanoparticle treatment is consistent with the increased LDH release (cellular toxicity) and level of

oxidative stress (NO release) observed after this treatment and demonstrates a capability of this model to detect potentially deleterious impacts of interventions.

5.3.3.3.3 Glutamate Signalling

There was no significant effect of treatment or time on *grik-1* and *eaat-1* expression (Figures 5.14 and 5.15). *Gria-1* expression was significantly reduced in IL-6/sIL-6r treatment groups compared to controls (3.08-fold) (Figure 5.13). Short term NBQX treatment groups reduced glutamate release compared with controls at 24hrs (1.15-fold, p=0.03; Figure 5.31) although not compared to IL-6/sIL-6r treatment groups. These findings highlight the potential for NBQX treatment to reduce glutamate release as demonstrated in both RA and OA patients and joint injury (ACLr, meniscal tear) patient synovium (McNearney et al., 2000, McNearney et al., 2004, Bonnet et al., 2020). At 72hrs PCA identified an association of glutamate release with nanoparticle treatment groups (Figure 5.37). This ties in with the significant increase in glutamate release in nanoparticle treatment groups compared to IL-6/sIL-6r treatment groups at 72hrs (1.12-fold, p=0.018; Figure 5.31).

Glutamate release has been linked with the release of increased inflammatory markers *in vivo* and *in vitro* (McNearney et al., 2004). PCA analysis may, therefore, indicate nanoparticle application is inducing glutamate linked pathological response as short term NBQX treatment did not increase glutamate levels. However, the increase in glutamate may be a consequence of sustained NBQX exposure from PLGA nanoparticles and not the nanoparticles themselves. Glutamate release has been shown to depend on the stage of osteoblast differentiation with an increase in glutamate release correlating with ALP release in MC3T3-E1 cells cultured over 7 days in a pro-differentiation environment (Bhangu et al., 2001). Intra-cellular glutamate levels are regulated by glutamine synthetase during osteoblast differentiation (Olkku and Mahonen, 2008). In rat MSCs, glutamine synthetase activity is rapidly reduced at the point of cellular mineralisation in osteogenic culture conditions resulting in increased intra-cellular glutamate concentrations (Olkku and Mahonen, 2008). These studies may indicate that nanoparticle intervention is inducing a pro-resorptive phenotype to osteogenically differentiated Y201 MSCs over 72hrs. Short term NQBX treatment reductions in glutamate release supports *In vivo* studies that highlight

the role of NBQX intervention in reducing joint pathology and IL-6 levels in both inflammatory and mechanical trauma animal models (Bonnet et al., 2015, Bonnet et al., 2020). The association of IL-6 with joint pathology (Watt et al., 2016) in addition to evidence linking glutamate to synovial fluid inflammatory cytokine levels from RA and OA (McNearney et al., 2004) and NBQX inhibition of IL-6 release in RA human fibroblast-like synoviocytes (Flood et al., 2007) highlight regulation of glutamate signalling in the joint as important to OA pathology and this study indicates this regulation is extended to osteogenically differentiated cells exposed to inflammatory stimulus *in vitro*. However, a lack of variance in glutamate release between the IL-6/sIL-6r treatment group and controls indicates that IL-6 trans signalling is not a driver for glutamate release and that any changes in release (such as those identified by short term NBQX and Nanoparticle application in this study; Figure 5.32) may be having impacts independently of the inflammation induced changes.

Ionotropic GluR expression has been shown to vary between healthy and diseased joint tissue. mRNA for AMPAGluR2 expressed in OA cartilage but not in a primary human chondrocyte. cDNA library and KA1 receptor mRNA was expressed in RA but not in healthy fibroblast-like synoviocytes (Flood et al., 2007). AMPAR2 and KA1 receptors have been shown to be localised to areas of bone remodelling in human OA samples (medial tibial plateaux, (MTP)) with AMPAR2 identified in some osteocytes but not osteoclasts and KA1 identified in osteoclasts and osteoblasts. Additionally, AMPAR2 and KA1 have been identified in OA cartilage primarily in the middle section of the MTP and less so in the severely degraded areas (Bonnet et al., 2015). In an AIA model AMPAR2 and KA1 were localised to areas of bone remodelling and NBQX treatment reduced bone remodelling with a concurrent decrease in GluR positive cells (Bonnet et al., 2015). In an ACL rupture model of PTOA, there was an increase in the expression of AMPAR2 on mouse stifle joint osteocytes, osteoblasts, synovial lining cells and ligaments in ACL rupture groups compared to groups where the ACL is intact. NBQX treatment reduced the expression of AMPAR2 on ligaments and bone cells (osteocytes and osteoblasts) in this model. In the same model, KA1 receptor expression was lost following ACL rupture on chondrocytes and returned with NBQX treatment. KA1 expression was increased in ligament and synovial lining cells following ACL rupture and reduced in NBQX treatment groups (Bonnet et al., 2020). The

effect of IL-6/sIL-6r treatment observed in this study reduces both *gria-1* and bone turnover marker (*alp, opg, ocn*) expression at 24hrs, along with the association of *gria-1, il-6* and *opg* expression in PC1 contributing to IL-6 treatment cluster in PCA (Figure 5.20; discussed with regards to bone in section 5.4.3.3.1). Aside from highlighting a potential marker by which to phenotypically characterise this model and allow for investigation into therapeutic interventions, this finding provides evidence that down regulation of this AMPA GluR occurs in response to inflammation in osteocyte-like cells. This may point towards an IL-6 signalling mediated mechanism by which down regulation of this AMPA specific GluR occurs following pathological joint trauma, as synovial IL-6 and histological inflammation have been shown to increase following traumatic joint injury (Watt et al., 2016, Bonnet et al., 2020).

qRT-PCR PCA analysis indicated an association of *eaat-3* with *il-6* expression at 24hrs in PC1 for all IL-6/sIL-6r treated groups (IL-6, NBQX, NP; Figure 5.20) and correlation analysis revealed a strong positive correlation (rho=0.739) between *il-6* and *eaat-3* expression that was driven by IL-6/sIL-6r treatment at 24hrs (Figure 5.18). These results indicate a potential IL-6 association with glutamate transporter expression. Glutamate transporters such as EAAT-3 are responsible for removing glutamate from the synaptic cleft and thereby terminating signalling events (Brakspear and Mason, 2012). *Eaat-3* is expressed in osteoblasts (Takarada et al., 2004) and the inhibition of EAATs in primary osteoblasts has been shown to induce an upregulation of *alp* activity . GLAST-1 (EAAT-1) has been shown to be expressed in the plasma membrane of osteocytes and expression has been shown to be internalised in response to low extracellular glutamate levels (Huggett et al., 2002). The results of this study demonstrate that glutamate transporter EAAT-3 expression is transiently regulated in response to IL-6 induced inflammation in osteocyte-like cells providing another biomarker characterising this model to build understanding of inflammatory driven pathways in bone and investigate potential therapeutic impacts.

5.3.4 Conclusions

The overarching aim of this chapter was to determine whether pathological levels of IL-6/sIL-6r exposure followed by short term AMPA/KA GluR antagonist application with or without sustained release of AMPA/KA GluR antagonist from PLGA nanoparticles influences

bone remodelling, glutamate and inflammatory signals. NBQX and DNQX do not elicit a cytotoxic response on both hOB and osteogenically differentiated Y201 MSCs at 7 and 14 days when applied as part of cell culture media up to concentrations substantially higher than the ic50 values for NBQX and DNQX (Figure 5.2). Both NBQX and DNQX reduce bone cell mineralisation (Figures 5.3 and 5.4), highlighting the capacity of these GluR antagonists to modulate mineralisation of osteoblasts and supporting the *in vivo* evidence indicating NBQX intervention reduces inflammation and trauma induced bone pathology.

The main component of this chapter was a pilot study which looked to build an understanding of the impact of pathological inflammation (Kotake et al., 1996, Bakker et al., 2014, Watt et al., 2016)(IL-6/siL-6r) and GluR antagonist (NBQX) intervention to bone, glutamate signalling and inflammation with potential downstream applications as a novel drug screening tool.

Y201 MSCs displayed osteocytic morphology in all treatment groups (Figure 5.6) but did not express *dmp-1* and *sost* indicating a late osteoblast/early osteocyte state of differentiation of the cells in this model. A phenotype of IL-6/sIL-6r treatment was identified which included down regulation of *alp, opg, eaat-3* and *gria-1* at 24hrs and increased release of IL-4 and IL-12p70 vs controls (figure 5.20, table 5.1, figure 5.36, table 5.3). This model also highlighted some potential therapeutic impacts of NBQX treatment: *alp* expression levels were corrected by short term NBQX treatment (Figure 5.12) and there was a significant increase in anti-inflammatory marker release (IL-10 and IL-13) at 24hrs (Figures 5.24 and 5.26). This represents a novel insight into a potential anti-inflammatory mechanism by which NBQX intervention elicits the therapeutic effects observed in *in vivo* models of arthritis.

This pilot study utilised cell well replicates for comparison between treatment groups which, repeats of this study on multiple occasions would allow for more robust insights into the impact of both IL-6/sIL-6r and any future therapeutic interventions (discussed more in the limitations section 7.6.2.1 of the discussion chapter of this thesis).

Overall, an IL-6/sIL-6r *in vitro* inflammatory model was investigated and shown to elicit inflammatory, glutamatergic and bone signalling responses from osteogenically differentiated Y201 MSCs compared to controls. This platform then identified some potential therapeutic efficacy of short-term NBQX treatment against inflammatory, glutamate and bone signalling and represents the first steps towards the development of a novel drug screening tool for PTOA. This chapter contributes to the thesis hypothesis by providing a platform for the investigation into protective effects of therapeutic interventions on inflammatory driven pathways in bone.

Chapter 6

Elucidating the Effects Sustained GluR Antagonist Application on Osteocyte-like Cell Responses to Pathophysiological Loading *in vitro* in 3D

6.1 Introduction

Mechanical loading is known to be a key driver of bone remodelling (Christen et al., 2014). Frosts mechanostat theory attempts to demonstrate how bone adapts to its mechanical environment through the addition/loss of matrix to optimise strain, linking strain with bone remodelling (Frost, 1996). As described by Frost and further developed by Bailey et al., (1996), different levels of mechanical strain have varied impacts on bone remodelling and can be defined by 4 levels. The minimum effective strain (MES) thresholds define the loading thresholds at which a change in osteogenic response occurs. Below the MES of 50-200μstrain lies the 'trivial loading zone' in which bone remodelling is predominantly resorptive. The 'physiological loading zone' lying between a lower MES of 50-200μstrain and an upper of 2000-3000μstrain is characterised by a balance of osteoblast and osteoclast function resulting in bone maintenance. The 'overload zone' above the MES of 2000-3000 results in organised addition of bone matrix. Very high loads push bone into the 'pathological loading zone' (>4000μstrain) in which unorganised bone matrix is laid down to respond to the high mechanical demands, this is then replaced by organised bone over time (Bailey et al., 1996, Frost, 1996).

Mechanical signalling in bone is regulated through the coordinated action of osteoblast and osteoclasts via osteocytes (Hill, 1998, Christen et al., 2014). Osteocytes organise the anabolic deposition of bone mineral through interaction with osteoblasts and via the release of a range of molecules with the capacity to inhibit (ANK, Decorin, MEPE, NPP1, PPi, Sclerostin) or promote (BSP-1, biglycan, DMP1, PHEX, Pit-1, tissue non-specific ALP, type 1 collagen) mineralisation (Atkins and Findlay, 2012). Sclerostin, in particular, is made almost exclusively by osteocytes in bone and a key negative regulator of bone mass, as highlighted in Van Buchem's disease, where down-regulation of SOST (sclerostin coding gene) results in a high bone mass phenotype (Balemans et al., 2002). Osteocytes are also essential to osteoclast mediated breakdown of bone matrix via expression of RANKL which stimulates osteoclast differentiation and subsequent bone resorption (Nakashima et al., 2011, Xiong et al., 2011). The response of bone to mechanical stimuli, or a lack thereof, is controlled by the interactions between osteocytes, osteoblasts and osteoclasts. Osteocyte viability is reliant

on bone loading with unloading having been shown to induce osteocyte hypoxia (Dodd et al., 1999), high mechanical loading inducing osteocyte apoptosis and matrix damage and low level loading protecting osteocyte viability *in vivo* (Noble et al., 2003). Osteocyte ablation removes the bone remodelling response to mechanical load in an unloading mouse model (Tatsumi et al., 2007) demonstrating that osteocytes are essential to the mechanical regulation of bone turnover.

Following unloading mice limbs *in vivo*, trabecular bone mass decreased. This was found to be associated with upregulation of RANKL in osteoblasts and SOST in osteocytes via the osteocyte network in bone (Moriishi et al., 2012). The unloading, resorptive response of bone relates to the region below the minimum effective strain threshold in Frost's mechanostat theory (Frost, 1996).

Physiological mechanical loading is key to osteocyte survival and cellular metabolism (Zhang et al., 2018). The accepted mechanism by which osteocytes translate mechanical stimulus into molecular signals is via mechanically induced interstitial fluid flow in the lacuna-canicular system that interconnects osteocytes and more distant bone cells (Martin, 2000). NO, PGE_2 and ATP are early molecular signals released from osteocytes following mechanical loading and shown to play a role in mechanotransduction in bone (Turner et al., 1996, Ajubi et al., 1999, Bonewald, 2011, Delgado-Calle et al., 2014, Kringelbach et al., 2015). Mechanical loading can enhance osteoblast differentiation via Wnt/β-catenin pathway activation (Chen et al., 2017b). Loading induces inhibition of SOST expression from osteocytes which promotes bone formation via decreasing inhibition of wnt signalling in osteoblasts which in turn increases the release of OPG (Robling et al., 2008, Delgado-Calle et al., 2017). Mechanical loading reduces the osteocyte produced RANKL/OPG ratio resulting in reduced osteoclastogenesis (You et al., 2008). Low level mechanical loading is key to the controlled maintenance of healthy bone mass and representative of the physiological loading in Frost's mechanostat theory (Frost, 1996).

In an osteocyte *in vitro* joint injury model, the RANKL/OPG ratio was shown to increase dependant on the size of injury (Mulcahy et al., 2011). High mechanical loading results in bone microdamage, leading to apoptosis of the adjacent osteocytes and an increase in

osteoclastogenesis to remove damaged bone (Cardoso et al., 2009, Kennedy et al., 2014). In response to supra-physiological loading, bone matrix is rapidly laid down in a woven, as opposed to lamellar, morphology (McBride and Silva, 2012). Woven bone formation is a clear response to macro-damage in bone (e.g. fracture) (Tami et al., 2003, Kidd et al., 2010) and is induced when there is a requirement for rapid bone formation over the organised slower formation of lamellar bone and relates to the pathological loading zone of Frost's mechanostat theory (Frost, 1996).

In PTOA, OA develops as the consequence of historical mechanical trauma to the joint and is thought to represent between 13% and 48% of knee OA cases following ACL or ACL and meniscal injury (at least 10 years post-injury) (Øiestad et al., 2009, Thomas et al., 2017). 12% of patients with lower extremity OA present with a history of joint injury (Described in more detail in introduction section 1.1.4) (Anderson et al., 2011). Pathophysiological levels of loading resulting in injury to the joint induces an acute inflammatory response at the site of injury that perpetuates alongside mechanical instability and rapid unorganised deposition of woven bone (Tami et al., 2003, Anderson et al., 2011). Inflammation also impacts bone homeostasis with IL-6 released from mechanically stimulated osteocytes being shown to regulate osteoblast function (Bakker et al., 2014) and IL-1β and TNFα having been shown to induce osteocyte apoptosis and inhibit mechanical loading stimulated osteocyte NO production (Tan et al., 2006, Bakker et al., 2009).

Glutamatergic signalling has been identified within bone (Mason et al., 1997) and is associated with OA (Described with more detail in introduction section 1.4) (McNearney et al., 2000). Glutamate levels increase dramatically in mechanically stimulated (ACL transection) OA models (Jean et al., 2005). Additionally, levels of glutamate in the synovial fluid of patients following ACL rupture and meniscus damage repair were found to be comparable to that of OA patients (Bonnet et al., 2020). Following mechanical loading of rat bone *in vivo*, the glutamate transporter GLAST-1, homologous to human EAAT-1, was down regulated in osteocytes (Mason et al., 1997). Osteoblasts release glutamate spontaneously *in vitro* (Genever and Skerry, 2001) that is increased following stimulation with ionotropic GluR agonist AMPA (Hinoi et al., 2002a). Direct administration of AMPA *in vivo* has been shown to increase bone formation, an effect inhibited by co-administration of AMPA

receptor antagonist CNQX (Lin et al., 2008). It has been proposed by Mason (2004) that glutamate is released following the mechanical load induced opening of stretch sensitive calcium channels in osteocytes stimulating osteoblast mediated glutamate signalling.

GluRs have been identified on multiple joint cell types in addition to osteocytes, including chondrocytes (Piepoli et al., 2009), synoviocytes (Flood et al., 2007), osteoclasts (Morimoto et al., 2006) and osteoblasts (Chenu et al., 1998). Antagonism of ionotropic GluR NMDA in osteoclasts inhibited bone resorption *in vitro* implicated a role of glutamate signalling in bone homeostasis (Chenu et al., 1998). IA injection of glutamate receptor antagonists have been shown to inhibit arthritic pain in a carrageenan induced arthritis model (MK801, NBQX) (Zhang et al., 2003) and improve the effect of dexamethasone in treating joint pain and swelling in a Freund's Complete Adjuvant rat model (substance P and CNQX) (Lam and Ng, 2010). Sustained systemic administration of NMDA receptor antagonist memantine in a CIA mouse model resulted in reduced synovitis and joint destruction (Lindblad et al., 2012). Inhibition of AMPA and KA ionotropic GluRs with NBQX has been shown to modulate arthritis symptoms (pain, swelling and inflammation) as well as reduce joint damage when injected at the point of arthritis induction in inflammatory (AIA), PTOA (ACL rupture) and surgical (Meniscal transection) *in vivo* models of arthritis (Bonnet et al., 2015, Bonnet et al., 2019, Bonnet et al., 2020). Additionally, *in vitro* application of NBQX has been shown to modulate human osteoblast mineralisation (Bonnet et al., 2015), further indicating a role of glutamate signalling in the regulation of bone.

This chapter focuses on the second part of the thesis hypothesis investigating the protective effects of GluR antagonists on mechanically driven pathways in bone. The studies in this chapter utilised a 3D cell culture system that allowed for the application of varied levels of loading to cells (Vazquez, 2013) seeded with osteogenically differentiated Y201 MSCs allows for investigation into the impact of select levels of loading (reflective of Frosts Mechanostat theory) as well as study of therapeutic intervention. Addressing the thesis hypothesis, the impact of load and AMPA/KA GluR antagonism (200μM NBQX) intervention on immunoassay and qRT-PCR outputs of bone turnover markers, inflammatory markers and glutamate signalling components was quantified thereby contributing towards the understanding of mechanically driven pathways in bone while delivering evidence towards

another potential drug screening tool in addition to the inflammatory 3D system investigated in chapter 5 of this thesis.

6.1.1 Hypothesis, Aims and Objectives

Thesis Hypothesis: AMPA and kainate glutamate receptor (GluR) antagonists can be incorporated into sustained release delivery systems that can protect against inflammatory or mechanically driven pathways in bone *in vitro.*

This chapter contributes towards the thesis hypothesis via the overarching aim below, which has been further subdivided into a series of aims and objects:

Overarching aim: To determine whether mechanically induced bone remodelling of Y201 derived osteocyte-like cells in 3D induces pathological markers of bone remodelling and inflammation and is affected by short term treatments with AMPA/KA GluR antagonist NBQX.

Objective 1.1: To test the effect of pathophysiological loading and short term NBQX application on cell viability via LDH assay and observing cell morphology through cryosectioning, actin staining and fluorescent imaging.

Objective 1.2: To test the effect of pathophysiological loading and short term NBQX application on markers of bone remodelling by measuring mRNA expression of *opg, rankl, col-1a1, ocn, alp* and *sost* by RTqPCR and protein release of OPG and sclerostin by enzyme linked immunosorbent assays.

Objective 1.3: To test the effect of pathophysiological loading and short term NBQX application on markers of inflammation by measuring mRNA expression of *il-6* by RTqPCR, protein release of IL-1β, IL-2, IL-6, IL-8, TNF-α, IL-12p70, IFN-γ IL-10, IL-13, IL-4 by enzyme linked immunosorbent assays and nitric oxide release via a Griess assay.

Objective 1.4: To test the effect of pathophysiological loading and short term NBQX application on glutamate signalling by measuring mRNA expression of *gria-1, grik-1*, *eaat-1* and *eaat-3* and release of the amino acid glutamate detected by ELISA.

6.2 Results

6.2.1 Mechanical Loading but not NBQX Treatment Effects Y201 Morphology

Physiologically loaded cells, regardless of time or treatment with NBQX, demonstrate a lack of clear dendritic morphology with no DAPI stained nuclei and no phalloidin stained cell extensions. Pathophysiologically loaded Y201s, regardless of time or treatment with NBQX, display phalloidin stained dendritic extensions and consistently identifiable nuclei (Figure 6.1). All subsequent experiments focused on pathophysiological loading samples.

	Time	
Treatment / Loading	**1hr**	**24hrs**
Control / Physiological load	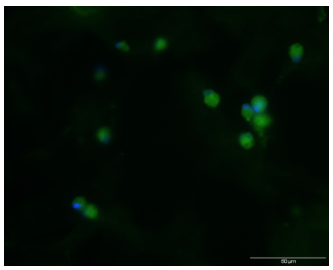	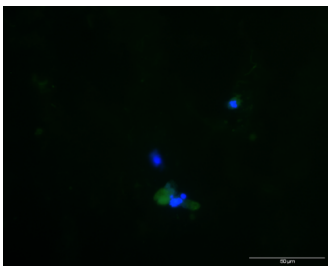
NBQX / Physiological load	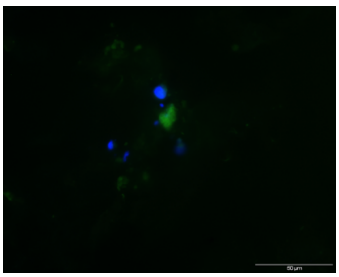	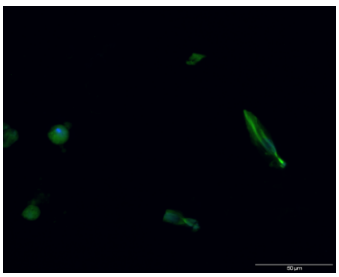
Control / Patho-physiological load	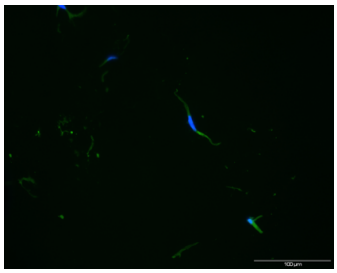	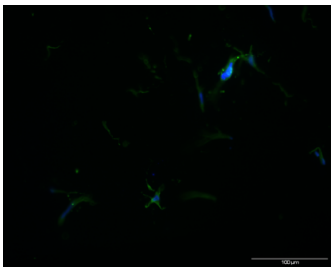
NBQX / Patho-physiological load	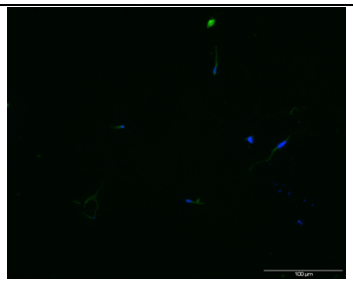	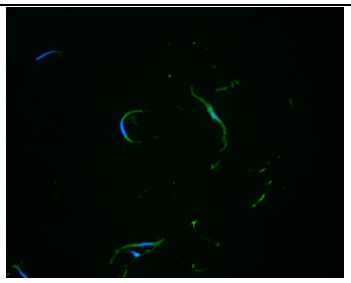

Figure 6.1: Effect of physiological loading (500μstrain) or pathophysiological loading (5000μstrain) (+/- NBQX) on fluorescent microscopy images (section 2.8.4) of osteogenically differentiated Y201 MSCs stained with DAPI (blue) nuclear stain and Phalloidin (green) actin cytoskeletal stain. 10μM cryosectioned gels were isolated from each treatment group of the loading study at each time point tested (1 and 24hrs) (sections 2.8.1 to 2.8.3). Autoexposure applied to obtain the maximum dynamic range. 50/100μm scale bar in bottom right corner of each image.

6.2.2 The Effect of Pathophysiological Loading and NBQX Treatment on LDH Release

The release of LDH was not affected by NBQX treatment but there was a significant effect of time ($p<0.0001$) (2-factor ANOVA) (Figure 6.2). Pairwise comparisons, with Bonferroni corrections for multiple comparisons, revealed that between 1 and 24hrs there was an increase in LDH release in both controls (1.14-fold, $p=0.001$) and NBQX treatment groups (1.11-fold, $p=0.003$).

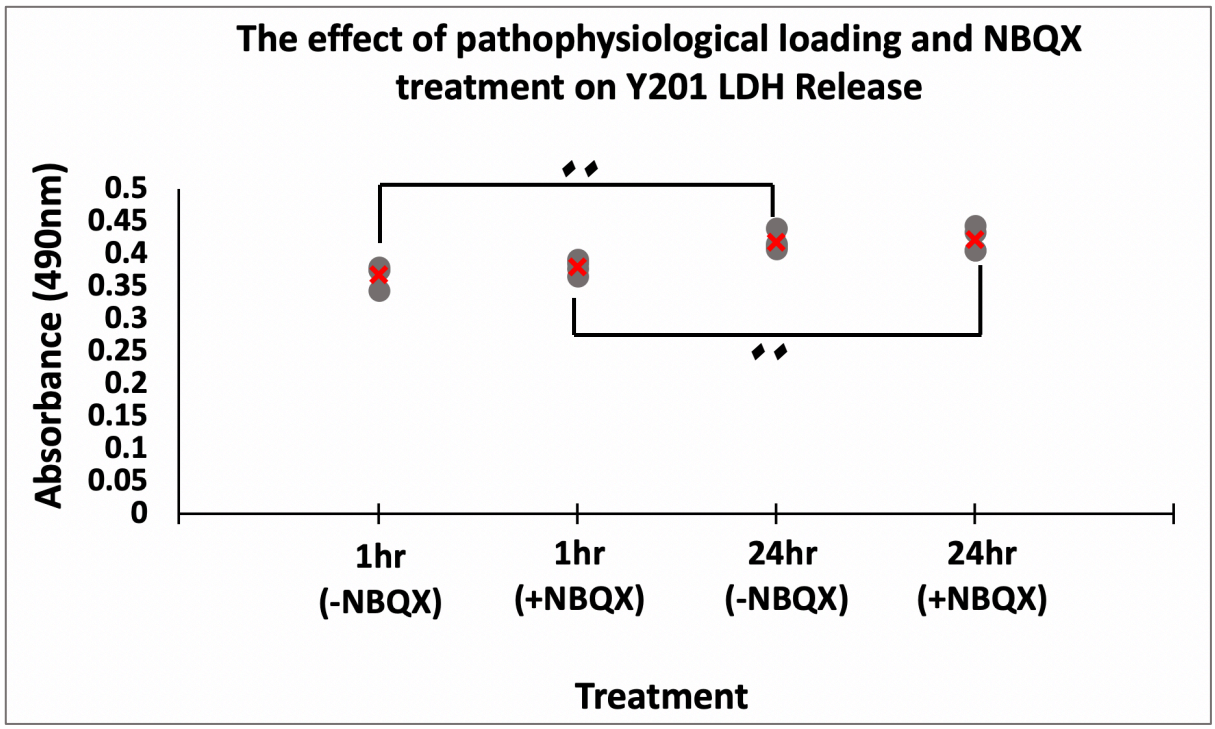

Figure 6.2: *Effect NBQX treatment following 1 and 24hrs from pathophysiological loading stimulus (5000μstrain) on absorbance (490nm), reflecting LDH released (Section 2.12.1) into cell culture media by osteogenically differentiated Y201 MSCs 3D loading cell culture study (section 2.6) (n=4; cell culture well replicates). Red x represents the mean value of replicates for each treatment group* (♦♦ $p<0.01$ between 1 and 24hrs; *statistical significance determined by 2-factor ANOVA).*

6.2.3 NBQX Treatment Does Not Significantly Affect Nitric Oxide Release Following Pathophysiological Loading

At 1hr NBQX treatment caused a 1.67-fold reduction in nitrite release. At 24hrs, nitrite release increased from 0 in control groups to 0.61±0.26μM in NBQX treatment groups. Between 1 and 24hrs, nitrite release from control cells reduced from 0.76±0.38μM to zero. (Figure 6.3).

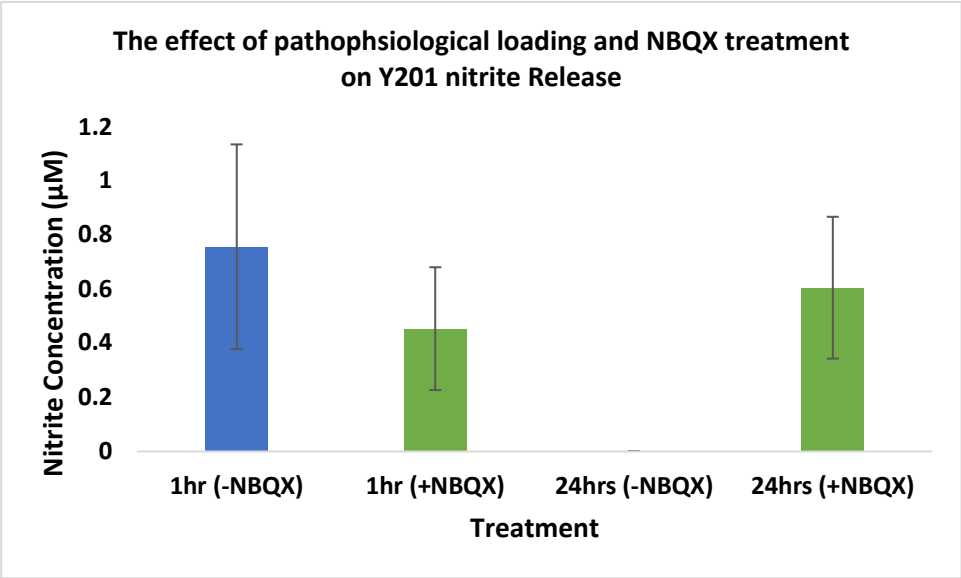

Figure 6.3: Effect of NBQX treatment following 1 and 24hrs from pathophysiological loading stimulus (5000μstrain) on nitrite release concentration into media (Griess assay section 2.11) from osteogenically differentiated Y201 MSCs from loading cell culture study (section 2.6 (n=4; cell culture well replicates). Error bars representing standard error of the mean.

6.2.4 Time After Load and NBQX Treatment Alters mRNA Expression Following Pathophysiological Loading.

Expression of genes of interest following pathophysiological loading and NBQX treatment were analysed by qRT-PCR (Figure 6.4 to Figure 6.12) and significant differences summarised (Table 6.1). The geometric mean of reference genes *18s* and *rpl13a* gave a stability factor of 1.117 using GeNorm stability analysis. Gene expression data are summarised according to bone signalling related genes (blue), inflammatory marker genes (red) and glutamate signalling related genes (green). *rankl, sost* and *tnfα* expression was not detected under any treatment conditions in this study.

The expression of ***opg*** expression was not affected by treatment but was affected over time (p=0.020) (2-factor ANOVA) (Figure 6.4). Pairwise comparisons, with Bonferroni corrections for multiple comparisons, revealed that there was an increase in *opg* expression between 1 and 24hrs in NBQX treated cells (1.59-fold, p=0.023) but not in control cells. At 1hr, there

was a non-significant decrease in mean *opg* expression in NBQX treatment group vs controls (1.43-fold).

The expression ***il-6*** expression was significantly affected by treatment (p=0.01) and time (p=0.0001) (2-factor ANOVA) (Figure 6.5). Pairwise comparisons, with Bonferroni corrections for multiple comparisons, revealed that, at 1hr, there was a decrease in *il-6* expression in NBQX treatment groups compared to controls (1.42-fold, p=0.033). There was a decrease in *il-6* expression between 1 and 24hrs in both control (5.07-fold, p<0.0001) and NBQX treatment groups (7.16-fold, p<0.0001).

The expression ***alp*** expression was significantly affected by treatment (p<0.0001) and time (p=0.004) and there was an interaction between treatment and time (p=0.028) (2-factor ANOVA) (Figure 6.6). Pairwise comparisons, with Bonferroni corrections for multiple comparisons, revealed that, at 1hr, there was a decrease in *alp* expression in NBQX treated cells compared to controls (3.06-fold, p<0.0001). This was also the case at 24hrs (2.51-fold, p=0.001). There was a significant decrease in *alp* expression between 1 and 24hrs in control groups (1.59-fold, p=0.001) but not NBQX treated groups.

The expression ***col-1a1*** (2-factor ANOVA) (Figure 6.7) and ***ocn*** (Kruskal-Wallis test) (Figure 6.8) expression was not significantly affected by treatment and showed no interaction of these factors.

The expression ***gria-1*** expression was not significantly affected by time (p=0.058) but there was a significant effect of treatment (p=0.014) (2-factor ANOVA) (Figure 6.9). Pairwise comparisons, with Bonferroni corrections for multiple comparisons, revealed that, at 1hr, there was a decrease in gria-1 expression in NBQX treated cells compared to controls (2.99-fold, p=0.015).

The expression ***grik-1*** and ***eaat-1*** expression were not significantly affected by treatment or time and showed no interaction between these factors (2-factor ANOVA) (Figure 6.10 and Figure 6.11).

The expression ***eaat-3*** expression was not significantly affected by treatment but there was a significant effect of time (p=0.022) (2-factor ANOVA) (Figure 6.12). Pairwise comparisons with Bonferroni corrections for multiple comparisons revealed that there were non-significant increases in *eaat-3* expression between 1 and 24hrs for both controls (1.62-fold, p=0.068) and NBQX treatment groups (1.46-fold, p=0.095).

*Table 6.1: Summary of 2-way ANOVA findings from loading study gene expression analysis (Figures 6.4-6.12). **P values in dark grey** represent significant main effects of treatment or time. **P values in black** represent NBQX vs control. **P values in yellow** represent 1hr vs 24hr time points.*

Activity	Analyte	NBQX Treatment			Time (1 to 24hrs)		
		Main effect of NBQX treatment	1hr	24hrs	Main effect of time after loading	Controls	NBQX
Bone signalling	*opg*	None			P=0.020		P=0.023 ↑
	ocn	None			None		
	col-1a1	None			None		
	alp	p<0.0001	P<0.0001 ↓	P=0.001 ↓	P=0.004	P=0.001 ↓	
Pro-inflammatory	*il-6*	P=0.01	P=0.033 ↓		p<0.0001	P<0.0001 ↓	P<0.0001 ↓
Glutamate signalling	*grik-1*	None			None		
	gria-1	P=0.014	P=0.015 ↓		None		
	eaat-1	None			None		
	eaat-3	None			P=0.022		

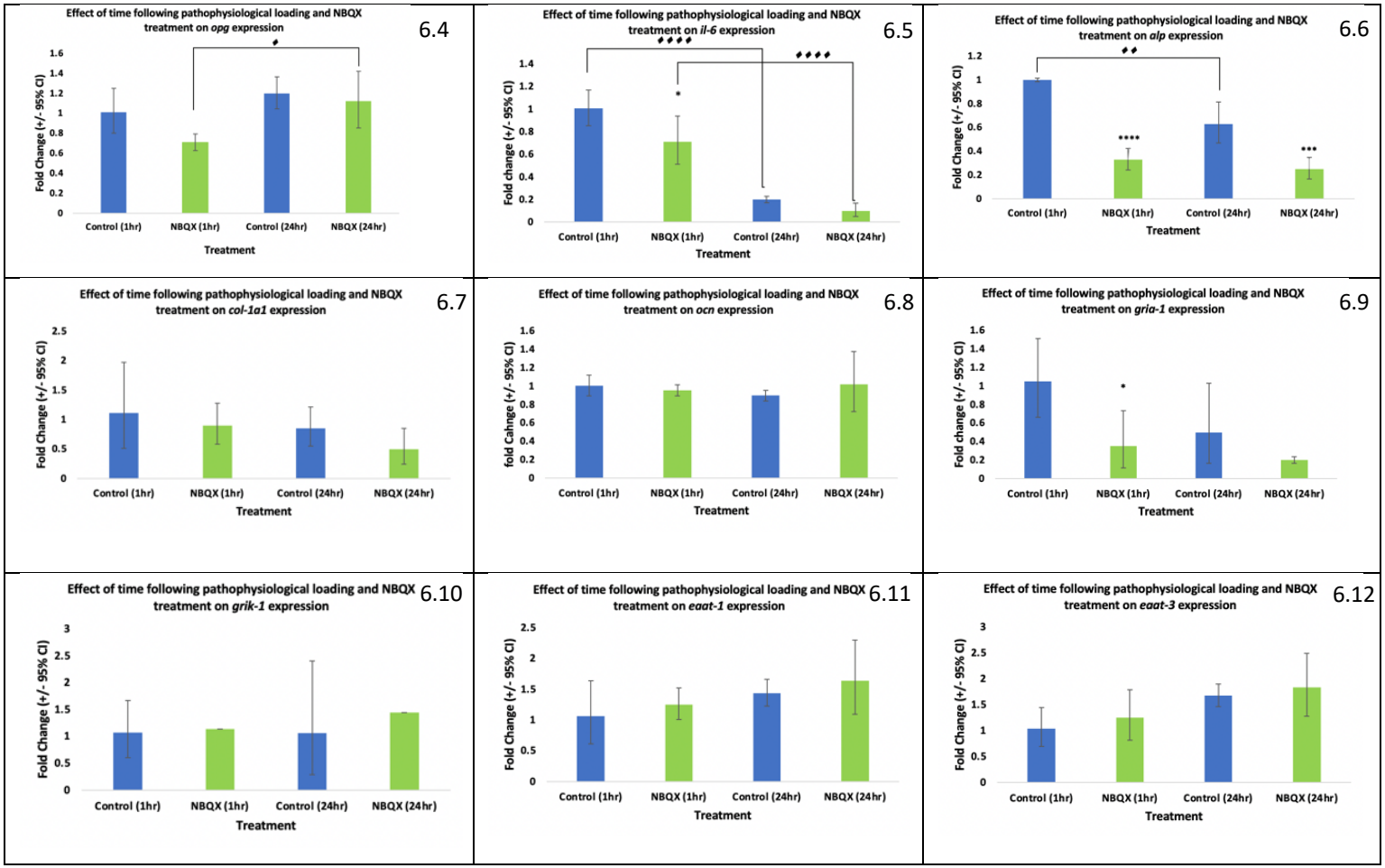

*Figures 6.4-6.12: Effect of NBQX treatment following 1 and 24hrs from pathophysiological loading stimulus (5000μstrain) on gene expression of bone markers, inflammatory molecules and glutamate signalling components. qRT-PCR analysis on RNA extracted from Y201 MSCS (section 2.9) and relative expression quantified of opg (Figure 6.4), il-6 (Figure 6.5), alp (Figure 6.6), col1a1 (Figure 6.7), ocn (Figure 6.8), gria-1 (Figure 6.9), grik-1 (Figure 6.10), eaat-1 (Figure 6.11) and eaat-3 (Figure 6.12). Expression was normalised to the geometric mean of 18s and rpl13a and fold change calculated using the $2^{-\Delta\Delta Ct}$ method. Data displayed as mean fold change with 95% confidence intervals. Statistical significance was determined using 2-factor ANOVA with Bonferroni comparisons ****p<0.0001, *p<0.05 vs treatment free controls; ♦♦♦♦p<0.0001, ♦♦p<0.01, ♦p<0.05 for 1 vs 24hrs post pathophysiological loading (n=3; cell culture well replicates).*

6.2.4.1 Gene Expression Correlations After Pathophysiological Loading

All Spearman's rho correlations met the specified assumptions (section 2.13) (Table 6.2). Regarding osteogenic markers, both *col-1a1* and *alp* were positively correlated with *il-6* and *gria-1*. In addition to osteogenic correlations, *il-6* mRNA expression positively correlated with *gria-1* and negatively correlated with *eaat-1* and *eaat-3*. In addition to correlations with *il-6* and osteogenic markers, a strong (>0.900) positive glutamatergic signalling correlation was identified between *eaat-1* and *eaat-3.*

The strong significant positive correlations between *gria-1* and *alp* as well as between *eaat-1* and *eaat-3* and the significant negative correlations between *eaat-1, eaat-3* and *il-6* have been plotted in scatter plots and subdivided into treatment groups to provide more information as to the nature of these correlations.

The positive correlation between *eaat-1* and *eaat-3* is primarily the result of differences between time points at 1 and 24hrs with NBQX treatment groups overlapping (Figure 6.13). The positive correlation between *alp* and *gria-1* is a clear consequence of NBQX treatment. However, there is an increase in values as a consequence of time within each treatment group (Figure 6.14). both *eaat-1* vs *il-6* and *eaat-3* vs *il-6* demonstrate negative correlations that are a consequence of time (Figure 6.15 and Figure 6.16).

*Table 6.2: Spearman's ρ Correlation matrix heatmap of gene expression markers (Figures 6.4-6.12) following pathophysiological load. Bold and white letters indicate a significant correlation. Red background indicates a positive correlation, blue background indicates a negative correlation. Gene of interest colour coding: **Red**= pro-inflammatory; **Blue**= Bone signalling; **Green**= Glutamate signalling. Positive correlation shading: 0.001-0.399=( ); 0.400-0.699=( ); 0.700-0.899=( ); 0.900-1=( ).*
Negative correlation shading: 0.001-0.399=( ); 0.400-0.699=( ).

OPG	0.175 0.293	0.301 0.171	0.175 0.293	-0.203 0.264	0.429 0.145	0.133 0.340	0.371 0.118	0.441 0.076	ρ Sig.
	OCN	0.295 0.176	0.004 0.496	0.021 0.474	0.084 0.422	0.039 0.453	0.453 0.070	0.425 0.084	ρ Sig.
		COL-I	0.483 0.056	**0.601** **0.019**	0.143 0.368	**0.503** **0.048**	-0.042 0.448	-0.063 0.423	ρ Sig.
			ALP	**0.587** **0.022**	-0.381 0.176	**0.713** **0.005**	-0.091 0.389	-0.266 0.202	ρ Sig.
				IL-6	0.024 0.478	**0.566** **0.027**	**-0.497** **0.050**	**-0.678** **0.008**	ρ Sig.
					GRIK-1	-0.571 0.069	0.119 0.389	0.000 0.500	ρ Sig.
						GRIA-1	-0.455 0.069	-0.441 0.076	ρ Sig.
							EAAT-1	**0.916** **<0.001**	ρ Sig.
								EAAT-3	ρ Sig.

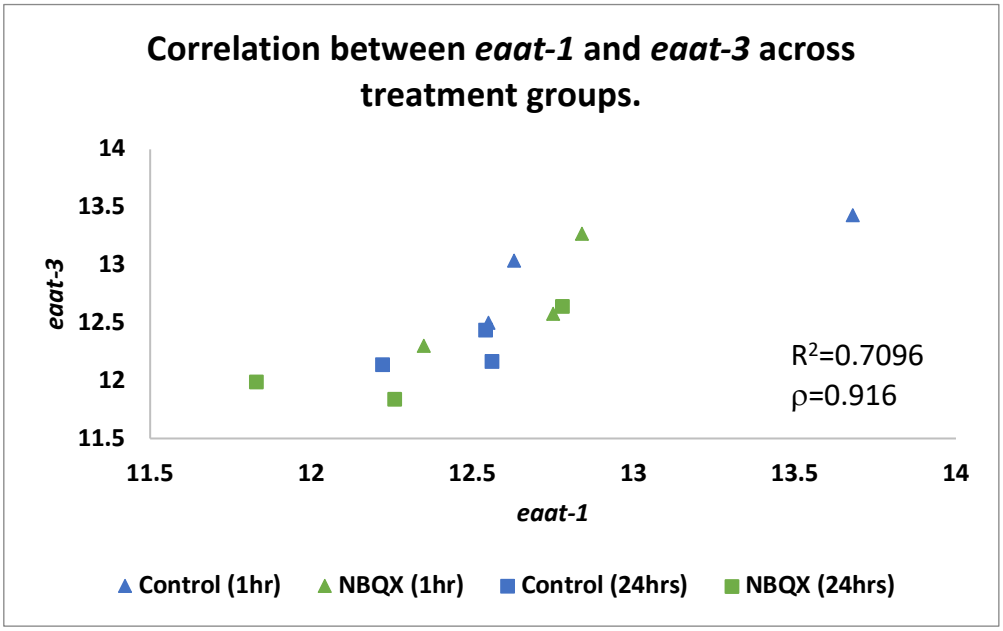

Figure 6.13: Scatterplot of eaat-1 vs eaat-3 for delta Ct gene expression values for all treatment groups (control and NBQX) across all time points tested (1 and 24hrs). R squared and Spearman's rho values displayed on chart.

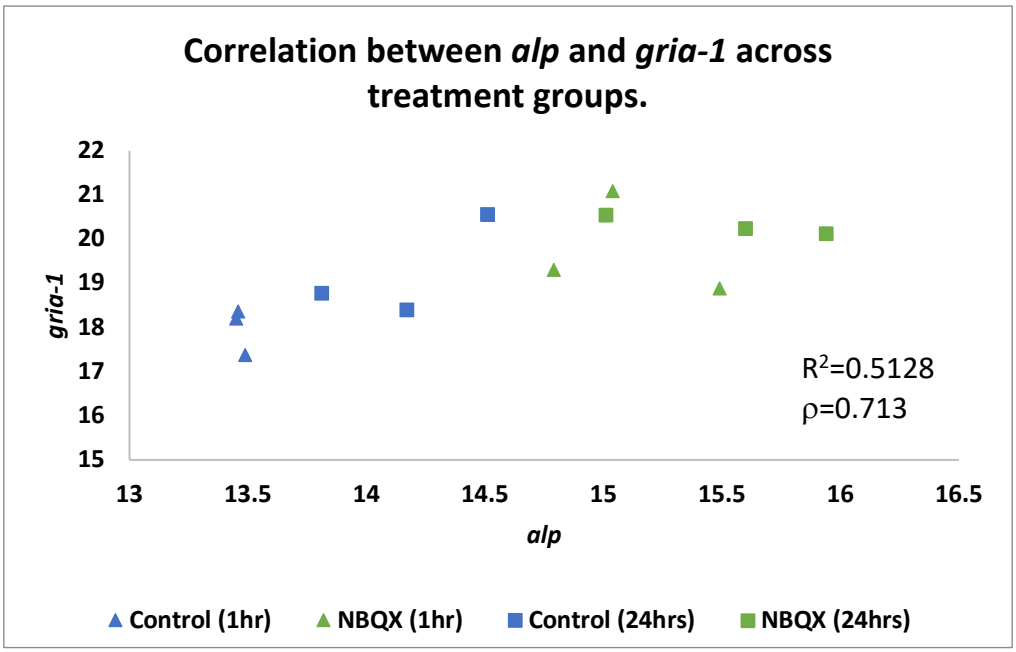

Figure 6.14: Scatterplot of alp vs gria-1 for delta Ct gene expression values for all treatment groups (control and NBQX) across all time points tested (1 and 24hrs). R squared and Spearman's rho values displayed on chart.

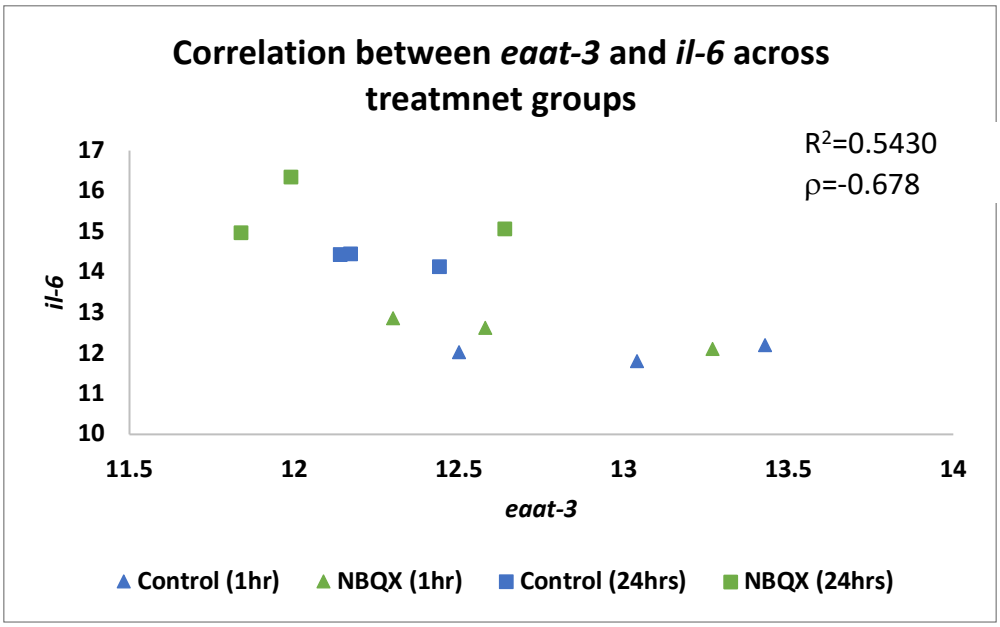

Figure 6.15: Scatterplot of eaat-3 vs il-6 for delta Ct gene expression values for all treatment groups (control and NBQX) across all time points tested (1 and 24hrs). R squared and Spearman's rho values displayed on chart.

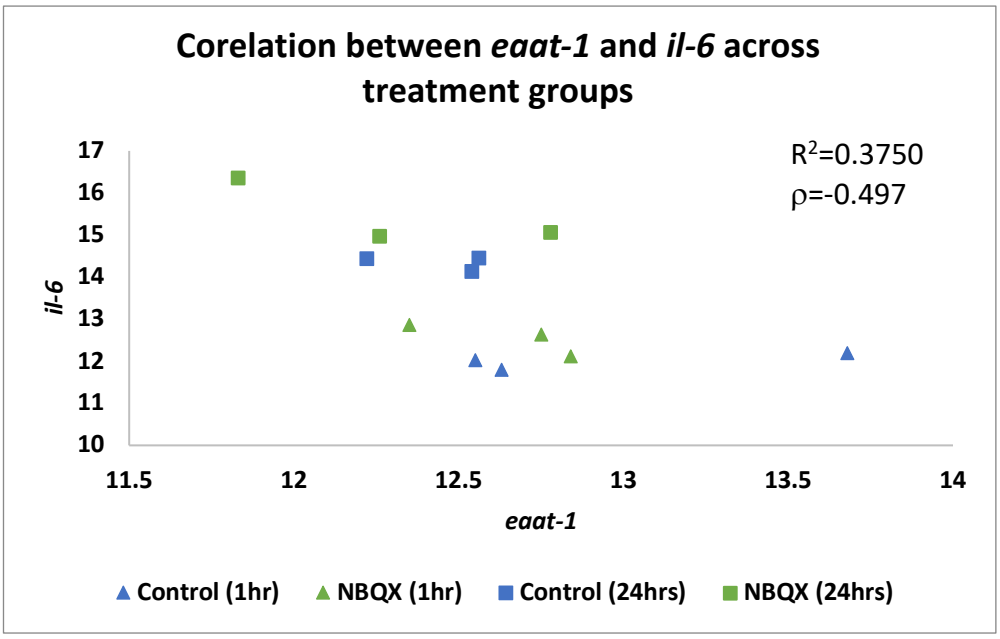

Figure 6.16: Scatterplot of eaat-1 vs il-6 for delta Ct gene expression values for all treatment groups (control and NBQX) across all time points tested (1 and 24hrs). R squared and Spearman's rho values displayed on chart.

6.2.4.2 Multivariate Analysis of Gene Expression After Pathophysiological Loading and NBQX Treatment

PCA was applied to determine treatment group and time affects from linear combinations of genes of interest from pathophysiological loading study. All assumptions of PCA were satisfied (section 2.13). Two components were generated, accounting for 72.1% of the variance (Figure 6.17) with PC1 explaining 50.3% and PC2 explaining 21.8%. The eigenvalue scores of PC1 were positive for glutamate signalling component *gria-1* and inflammatory markers and bone turnover markers (*il-6* and *alp*) with negative eigenvalue scores for *eaat-1* and *eaat-3.* The eigenvalue scores of PC2 were positive for bone markers (*alp* and *ocn*) and glutamate signalling components (*eaat-1* and *eaat-3*) as well as a negative eigenvalue score for inflammatory marker *il-6*. Visual analysis indicates the score space can be divided into 4 clusters broadly representative of each treatment group at each time point (Figure 6.17B). Cluster 1 contains control groups at 1hr and represents negative PC1 scores with PC2 scores ranging from positive to negative. Cluster 2 contains control groups at 24hrs and resides close to the zero point of PC1 with slightly negative PC2 scores. Cluster 3 contains NBQX treatment groups at 1hr and represents positive PC2 scores with generally positive PC1

scores. Cluster 4 contains NBQX treatment groups at 24hrs and represents positive PC1 scores with positive to negative PC2 scores with some overlap with cluster 3.

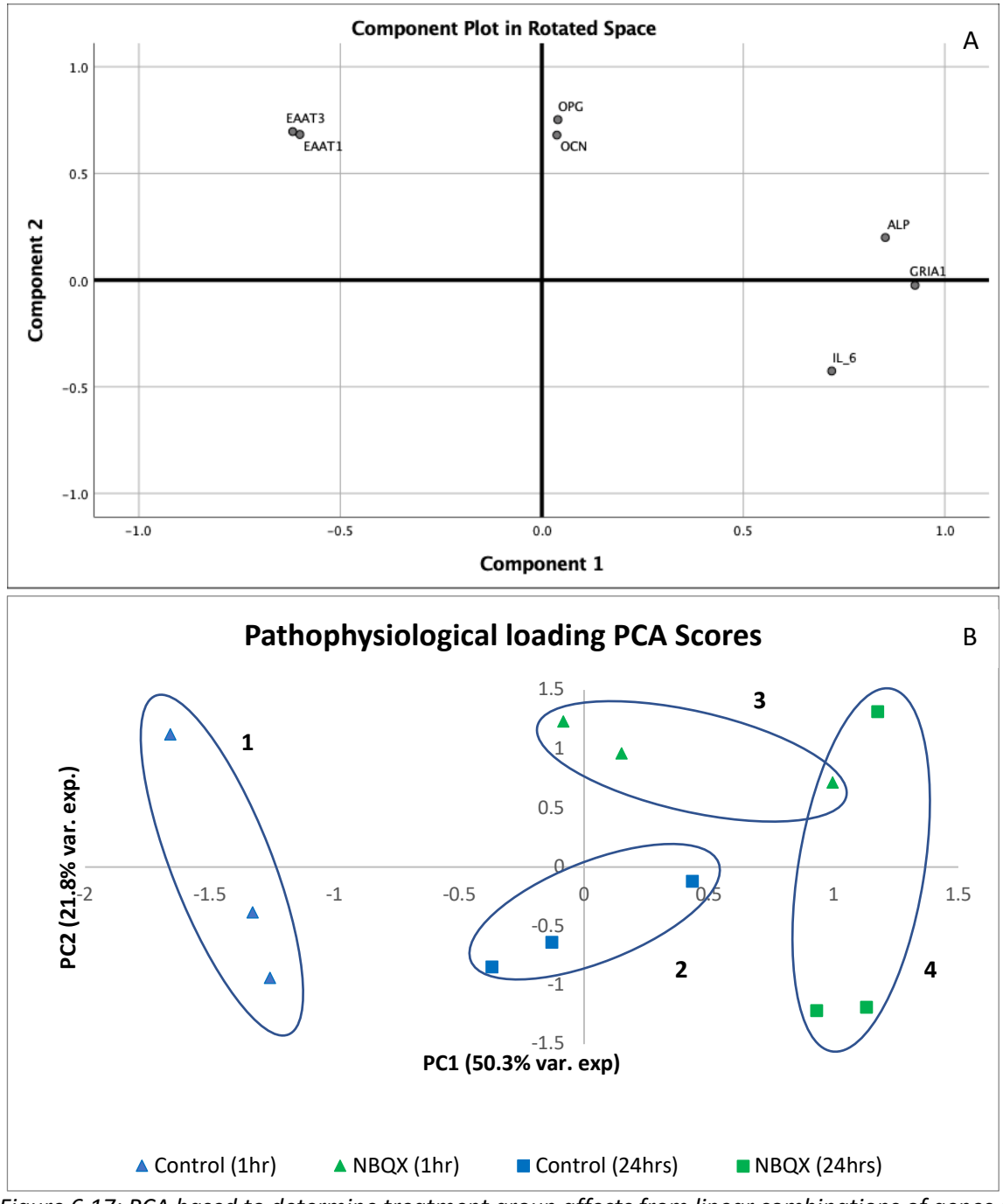

Figure 6.17: PCA based to determine treatment group affects from linear combinations of genes of interest from loading study (section 2.6). 72.1% of variance explained (PC1=50.3%, PC2=21.8%). A) gene of interest weightings for PC1 and PC2. B) Variable score plot for PC1 and PC2, subdivided into time and treatment. Col1a1 and grik1 were excluded from analysis to return KMO sampling adequacy to acceptable levels (>0.5)(section 2.13). The eigenvalue scores were 0.926, 0.852, 0.719, -0.618 and -0.601 for PC1 for gria-1, alp, il-6, eaat-3 and eaat-1 respectively and -0.426, 0.752, 0.696, 0.683 and 0.680 for PC2 for il-6, opg, eaat-3, eaat-1 and ocn respectively.

6.2.5 Time Post-Loading and NBQX Treatment Alters Protein Expression Following Pathophysiological Loading

Immunoassay markers (Figure 6.18 to Figure 6.29) were grouped into OPG and glutamate, pro-inflammatory cytokines, anti and pro-inflammatory cytokines and anti-inflammatory cytokines (Table 6.3).

For **IFN-gamma** release, there was a significant effect of NBQX treatment ($p=0.012$) and time after loading ($p<0.0001$) and interaction of treatment and time ($p=0.015$) (2-factor ANOVA) (Figure 6.18). Pairwise comparisons, with Bonferroni corrections for multiple comparisons, revealed that, NBQX treatment decreased IFN-gamma release compared to controls (2.25-fold, $p=0.002$) at 24hrs, and IFN-gamma release increased between 1 and 24hrs in both controls (12.99-fold, $p<0.0001$) and NBQX treatment groups (8.01-fold, $p=0.0096$).

For **IL-10** release there was a significant effect of NBQX treatment ($p=0.007$), time after loading ($p<0.0001$) and interaction of treatment and time ($p=0.029$) (2-factor ANOVA) (Figure 6.19). Pairwise comparisons, with Bonferroni corrections for multiple comparisons, revealed that, NBQX treatment decreased IL-10 release compared to controls (2.00-fold, $p=0.002$) at 24hrs and IL-10 release increased between 1 and 24hrs in both controls (7.12-fold, $p<0.0001$) and NBQX treatment groups (4.67-fold, $p<0.001$).

For **IL-12p70** release, there was no interaction of treatment and time ($p>0.05$) but there was a significant effect of NBQX treatment ($p<0.001$) and time after loading ($p<0.0001$) (2-factor ANOVA) (Figure 6.20). Pairwise comparisons, with Bonferroni corrections for multiple comparisons, revealed that, NBQX treatment decreased IL-12p70 release compared to controls at 1hr (4.63-fold, $p<0.001$) and 24hrs, (2.39-fold, $p=0.006$) and IL-12p70 release increased between 1 and 24hrs in both controls (5.91-fold, $p<0.001$) and NBQX treatment groups (11.44-fold, $p<0.0001$).

For **IL-13** release, there was no interaction of treatment and time ($p=0.070$) but there was a significant effect of NBQX treatment ($p<0.001$) and time after loading ($p<0.0001$) (2-factor

ANOVA) (Figure 6.21). Pairwise comparisons, with Bonferroni corrections for multiple comparisons, revealed that, NBQX treatment decreased IL-13 release compared to controls at 1hr (which was not significant) (1.73-fold, $p=0.087$) and 24hrs (1.76-fold, $p<0.001$). IL-13 release increased between 1 and 24hrs for both control (2.45-fold, $p<0.0001$) and NBQX treatment groups (2.40-fold, $p=0.004$).

For **IL-1β** release, there was no significant effect of NBQX treatment ($p>0.05$), time after loading ($p>0.05$) or interaction of treatment and time ($p>0.05$) (Mann-Whitney U and Kruskal Wallis tests) (Figure 6.22). NBQX treatment decreased IL-1β compared to controls, (2.18-fold) at 1hr, which was not significant. IL-1β release decreased between 1 and 24hrs in control groups (1.76-fold), which was not significant.

For **IL-2** release, there was no significant effect of NBQX treatment ($p=0.072$) but a significant main effect of time after loading ($p<0.0001$) and an interaction of treatment and time ($p=0.020$) (2-factor ANOVA) (Figure 6.23). Pairwise comparisons, with Bonferroni corrections for multiple comparisons, revealed that, NBQX treatment decreased IL-2 release compared to controls (1.99-fold, $p=0.006$) at 24hrs and IL-2 release increased between 1 and 24hrs for both controls (19.69-fold, $p<0.0001$) and NBQX treatment groups (6.88-fold, $p<0.001$).

For **IL-4** release, there was a significant effect of NBQX treatment ($p=0.012$), time after loading ($p<0.0001$) and interaction of treatment and time ($p=0.015$) (2-factor ANOVA) (Figure 6.24). Pairwise comparisons, with Bonferroni corrections for multiple comparisons, revealed that, NBQX treatment decreased IL-4 release compared to controls (2.48-fold, $p=0.001$) at 24hrs and IL-4 release increased between 1 and 24hrs for both control (21.25-fold, $p<0.0001$) and NBQX treatment groups (9.19-fold, $p<0.001$).

For **IL-6** release, there was no significant effect of NBQX treatment ($p>0.05$) or interaction of treatment and time ($p>0.05$) but there was a significant effect of time after loading ($p<0.0001$) (2-factor ANOVA) (Figure 6.25). Pairwise comparisons, with Bonferroni corrections for multiple comparisons, revealed that there was an increase in IL-6 release between 1 and 24hrs in both control (4.54-fold, $p<0.0001$) and NBQX treatment groups

(3.62-fold, p<0.0001). NBQX treatment decreased IL-6 release compared to controls (1.25-fold) at 24hrs, which was not found to be significant.

For **IL-8** release, there was no significant interaction of treatment and time but there was a significant effect of NBQX treatment (p=0.0098) and of time after loading (p<0.0001) (2-factor ANOVA) (Figure 6.26). Pairwise comparisons, with Bonferroni corrections for multiple comparisons, revealed that, NBQX treatment decreased IL-8 release compared to controls (1.53-fold, p=0.008) at 1hr and IL-8 release increased between 1 and 24hrs in both control (1.68-fold, p<0.0001) and NBQX treatment groups (2.37-fold, p<0.0001).

For **TNFα** release, there was a significant effect for NBQX treatment (p<0.001), time after loading (p<0.0001) and interaction of treatment and time (p=0.001) (2-factor ANOVA) (Figure 6.27). Pairwise comparisons, with Bonferroni corrections for multiple comparisons, revealed that, NBQX treatment decreased TNFα release compared to controls (2.20-fold, p<0.0001) at 24hrs and TNFα release increased between 1 and 24hrs in both control (4.09-fold, p<0.0001) and NBQX treatment groups (2.54-fold, p=0.005).

For **glutamate** release, there was not an interaction of treatment and time but there was a significant effect of NBQX treatment (p<0.001) and time after loading (p<0.0001) (2-factor ANOVA) (Figure 6.28). Pairwise comparisons ,with Bonferroni corrections for multiple comparisons, revealed that, NBQX treatment decreased glutamate release compared to controls at 1 (1.24-fold, p=0.004) and 24hrs (1.18-fold, p=0.004) and glutamate release increased between 1 and 24hrs in both control (1.24-fold, p<0.001) and NBQX treatment groups (1.31-fold, p<0.001).

For **OPG** release, there was no significant effect of NBQX treatment (p>0.05) or significant interaction of treatment and time (p>0.05) but there was a significant effect of time after loading (p<0.0001) (2-factor ANOVA) (Figure 6.29). Pairwise comparisons, with Bonferroni corrections for multiple comparisons, revealed that, OPG release increased between 1 and 24hrs for both controls (5.07-fold, p<0.0001) and NBQX treated cells (4.01-fold, p<0.0001). NBQX treatment decreased OPG release compared to controls (1.49-fold) at 24hrs which was not found to be significant.

*Table 6.3: A summary of significant findings for analyte concentrations determined from pathophysiological loading study (Figures 6.18-6.29). **Dark grey p values** indicate a significant main effect of treatment or time. **Black P values** NBQX treatment vs control; **Yellow p values**= significant effect of time 1 vs 24hrs; Direction of arrow indicates whether significant findings relate to an increase or decrease.*

Activity	Analyte	NBQX Treatment			Time (1 to 24hrs)		
		Main Effect	1hr	24hrs	Main effect	Control	NBQX
Bone Marker	OPG	None			p<0.0001	P<0.0001 ↑	P<0.0001 ↑
Glutamate signalling	Glutamate	p<0.001	P=0.004 ↓	P=0.004 ↓	p<0.0001	P<0.001 ↑	P<0.001 ↑
Pro-inflammatory	IL-1β	None			None		
	IL-2	None		P=0.006 ↓	p<0.0001	P<0.0001 ↑	P<0.001 ↑
	IL-6	None			P<0.0001	P<0.0001 ↑	P<0.0001 ↑
	IL-8	P<0.001	P=0.008 ↓		p<0.0001	P<0.0001 ↑	P<0.0001 ↑
	TNF-α	P<0.001		P<0.0001 ↓	p<0.0001	P<0.0001 ↑	P=0.005 ↑
	IL-12p70	P<0.001	P<0.001 ↓	P=0.006 ↓	p<0.0001	P<0.001 ↑	P<0.0001 ↑
Pro/anti-inflammatory	IFN-γ	P=0.012		P=0.002 ↓	p<0.0001	P<0.0001 ↑	P<0.001 ↑
Anti-inflammatory	IL-10	P=0.007		P=0.002 ↓	p<0.0001	P<0.0001 ↑	P<0.001 ↑
	IL-13	P<0.001		P<0.001 ↓	p<0.0001	P<0.0001 ↑	P=0.004 ↑
	IL-4	P=0.012		P=0.001 ↓	p<0.0001	P<0.0001 ↑	P<0.001 ↑

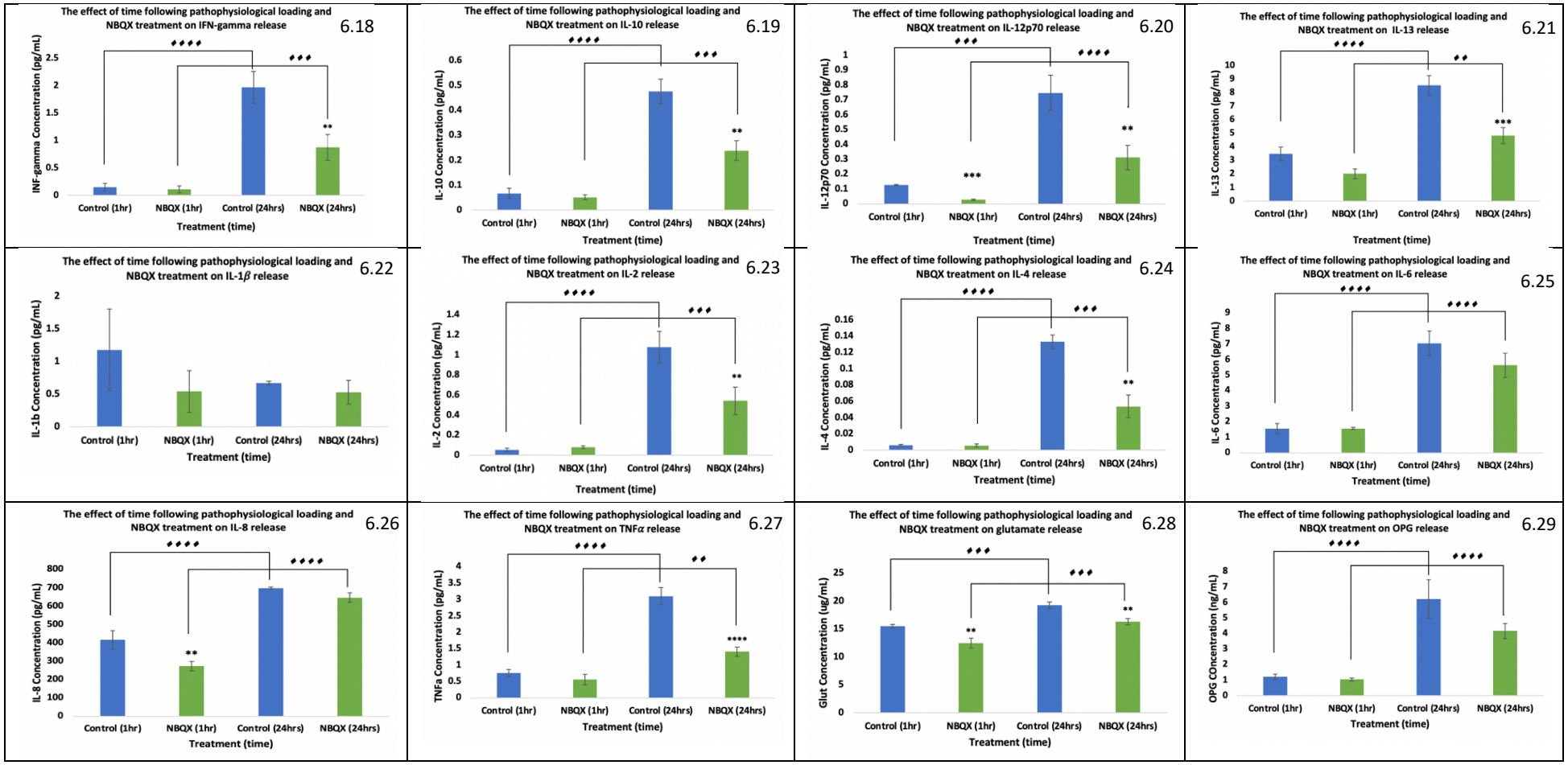

Figures 6.18-6.29: Effect of NBQX *treatment* following 1 and 24hrs from pathophysiological loading stimulus (5000µstrain) *on Immunoassay quantified release of inflammatory markers, glutamate and OPG from cell culture media (section 2.10). Markers quantified by electrochemiluminescence multiplex assay were IFN-γ (figure 6.18), IL-10 (figure 6.19), IL-12p70 (figure 6.20), IL-13 (figure 6.21), IL-1β (figure 6.22), IL-2 (figure 6.23), IL-4 (figure 6.24), IL-6 (figure 6.25), IL-8 (figure 6.26) and TNFα (figure 6.27). ELISA quantified markers were glutamate (figure 6.28) and OPG (figure 6.29). Data displayed as analyte concentration (pg/ml, ng/ml or µg/ml) with error bars representing standard error of the mean. Statistical significance was determined using 2-factor ANOVA with Bonferroni post hoc tests. *p<0.05, **p<0.01,***p<0.001, ****p<0.0001 vs untreated controls. ♦♦p<0.01, ♦♦♦p<0.001, ♦♦♦♦p<0.0001 for 1 vs 24hrs (n=4; cell culture well replicates).*

6.2.5.1 Analyte Release Correlations Following Pathophysiological Loading

No significant negative correlations were identified (Table 6.4). All markers were found to be significantly positively correlated, aside from IL-1β, that only had a significant positive correlation with TNFα and glutamate. Correlations of IL-1β with glutamate and TNFα, positive correlations between pro and anti-inflammatory cytokines IL-6 with IL-13 and positive correlations between OPG and glutamate were displayed in correlation scatterplots to highlight the impact of short term NBQX treatment and time on correlations (Figures 6.30-6.33).

Visual interpretation of scatterplots indicates that, for comparisons of IL-1β with TNFα (Figure 6.30) and glutamate (Figure 6.31), time is the most prevalent factor contributing to positive correlations with 24hr control and NBQX treatment values scoring higher. This is also more clearly the case for IL-6 vs IL-13 (Figure 6.32) and OPG compared to glutamate (Figure 6.33) scatterplots.

*Table 6.4: Spearman's ρ Correlation matrix heatmap of immunoassay analytes (Figures 6.18-6.29) from loading study following pathophysiological load. Bold and white letters indicate a significant correlation. Red background indicates a positive correlation, blue background indicates a negative correlation. Analyte colour coding: **Black**= glutamate and OPG **Red**= pro-inflammatory; **Blue**= anti and pro-inflammatory; **Green**= anti-inflammatory. Positive correlation shading: 0.001-0.399=( ); 0.400-0.699=( ); 0.700-0.899=( ); 0.900-1=( ). Negative correlation shading: 0.001-0.399=( ).*

ρ Sig.p	OPG											
ρ Sig.p	0.742 <0.001	Glut										
ρ Sig.p	0.331 0.105	0.547 0.014	IL-1β									
ρ Sig.p	0.848 <0.001	0.744 <0.001	0.159 0.278	IL-2								
ρ Sig.p	0.868 <0.001	0.829 <0.001	0.244 0.181	0.915 <0.001	IL-6							
ρ Sig.p	0.802 <0.001	0.903 <0.001	0.282 0.145	0.853 <0.001	0.891 <0.001	IL-8						
ρ Sig.p	0.871 <0.001	0.915 <0.001	0.435 0.046	0.874 <0.001	0.894 <0.001	0.924 <0.001	TNF-α					
ρ Sig.p	0.878 <0.001	0.846 <0.001	0.301 0.148	0.824 <0.001	0.837 <0.001	0.903 <0.001	0.903 <0.001	IL-12p70				
ρ Sig.p	0.858 <0.001	0.853 <0.001	-0.217 0.249	0.986 <0.001	0.902 <0.001	0.965 <0.001	0.965 <0.001	0.855 <0.001	INF-γ			
ρ Sig.p	0.773 <0.001	0.850 <0.001	0.215 0.212	0.841 <0.001	0.859 <0.001	0.900 <0.001	0.912 <0.001	0.868 <0.001	0.923 <0.001	IL-10		
ρ Sig.p	0.806 <0.001	0.856 <0.001	0.300 0.129	0.826 <0.001	0.853 <0.001	0.921 <0.001	0.941 <0.001	0.877 <0.001	0.944 <0.001	0.882 <0.001	IL-13	
ρ Sig.p	0.818 <0.001	-0.902 <0.001	0.441 0.076	0.902 <0.001	0.895 <0.001	0.930 <0.001	0.902 <0.001	0.937 <0.001	0.883 <0.001	0.909 <0.001	0.874 <0.001	IL-4

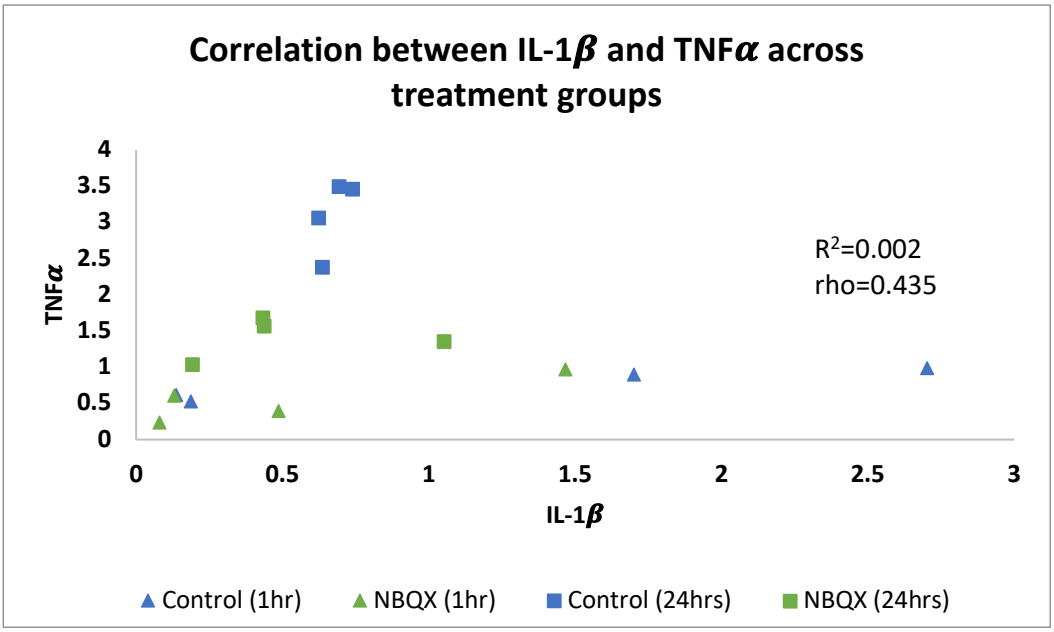

Figure 6.30: Scatterplot of IL-1β vs TNFα release from immunoassay analysis. Concentration values for protein release for all treatment groups (control and NBQX) at each timepoint analysed (1 and 24hrs). R squared and Spearman's rho values displayed on chart.

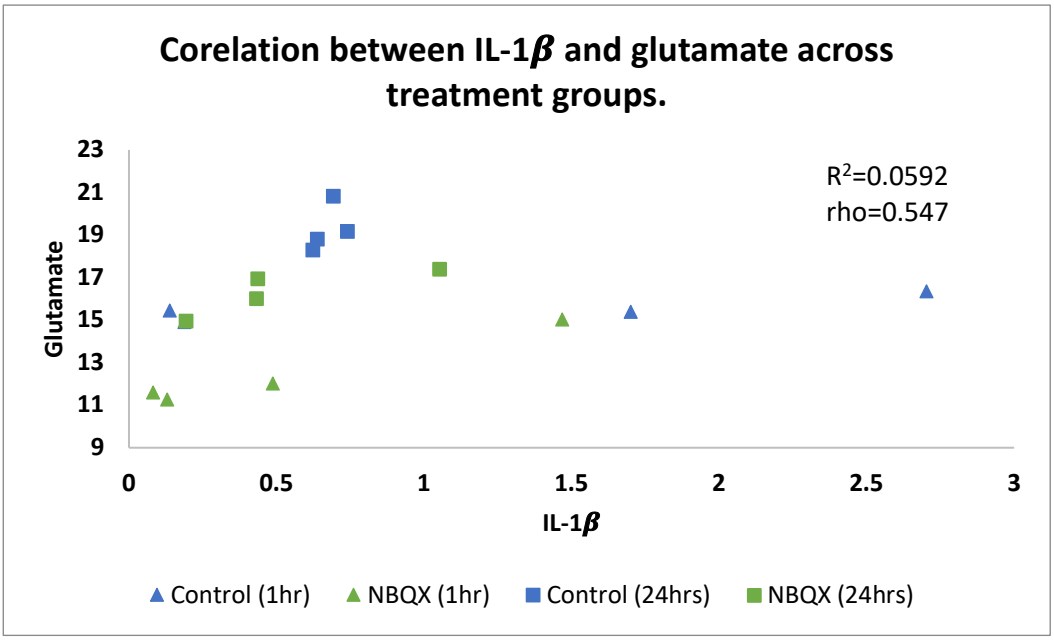

Figure 6.31: Scatterplot of IL-1β vs Glutamate release from immunoassay analysis. Concentration values for protein release for all treatment groups (control and NBQX) at each timepoint analysed (1 and 24hrs). R squared and Spearman's rho values displayed on chart.

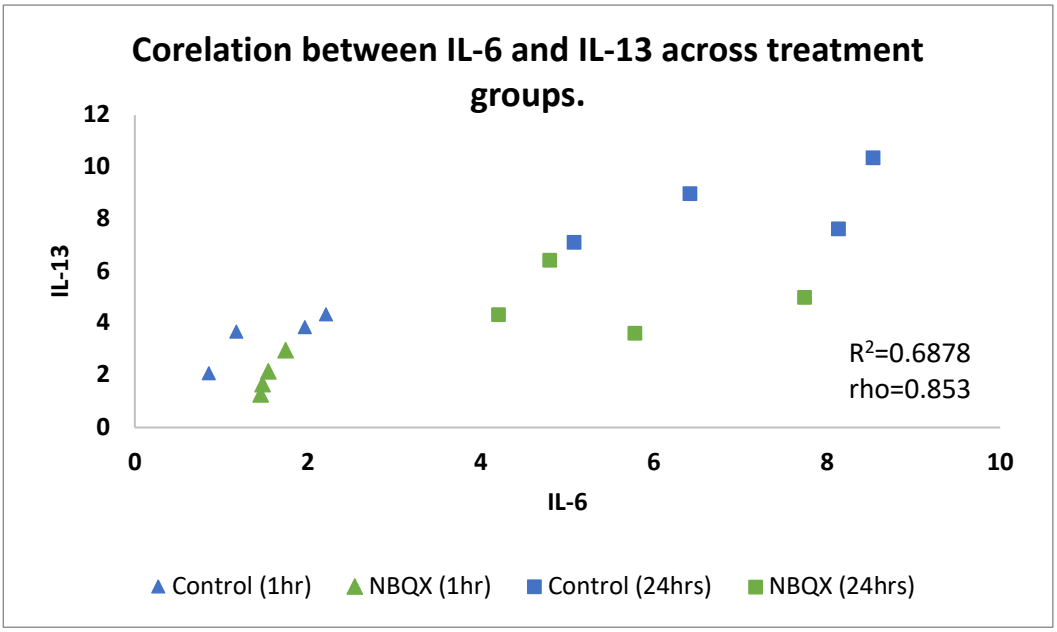

Figure 6.32: Scatterplot of IL-6 vs IL-13 release from immunoassay analysis. Concentration values for protein release for all treatment groups (control and NBQX) at each timepoint analysed (1 and 24hrs). R squared and Spearman's rho values displayed on chart.

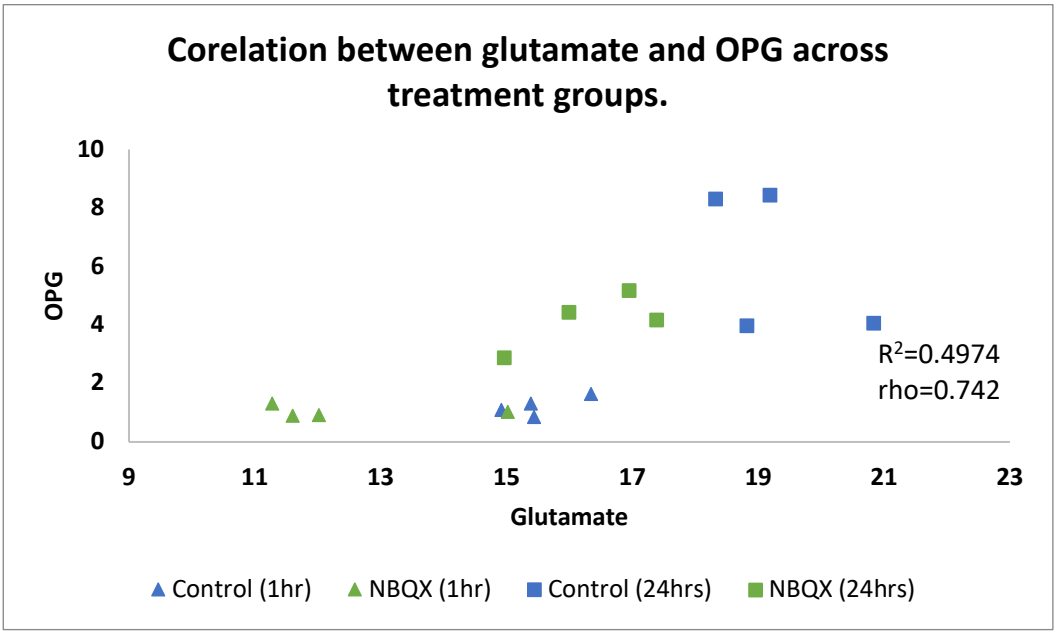

Figure 6.33: Scatterplot of glutamate vs OPG release from immunoassay analysis. Concentration values for protein release for all treatment groups (control and NBQX) at each timepoint analysed (1 and 24hrs). R squared and Spearman's rho values displayed on chart.

6.2.5.2 Multivariate Analysis of Analyte Release After Pathophysiological Loading and NBQX Treatment

PCA was applied to determine treatment group affects from linear combinations of protein markers from the pathophysiological loading study. All assumptions were satisfied (linear relationship between variables with no outliers and large sample sizes). Due to inadequate correlation scores (<0.3 for all comparisons) produced in PCA IL-1β data was removed from analysis. Only 1 principal component was extracted from the data accounting for 88.2% of the variance. Due to this an analyte weightings table and score plot could not be generated. PC1 was composed of all remaining markers bar IL-1β (Glutamate, TNFα, OPG, IL-6, IL-2, IL-12p70, IL-10, IL-13, IL-4 and IFNγ; **Error! Reference source not found.** 6.5).

Table 6.5: Principal component eigenvalue table resulting from linear combinations of analyte concentrations obtained from loading study (section 2.6). Scores for each marker represented in PC1 accounting for 88.2% of variance. IL-1β was removed from analysis to optimise value of KMO sampling adequacy and achieve KMO value acceptable levels (>0.5) (Section 2.13).

Analyte	PC1 eigenvalue score
IFNγ	0.965
IL_10	0.975
IL_12p70	0.910
IL_13	0.952
IL_2	0.969
IL_4	0.963
IL_6	0.937
IL_8	0.887
TNFα	0.965
Glut	0.869
OPG	0.930

6.3 Discussion

The overarching aim of this chapter was to determine whether mechanically induced bone remodelling of Y201 derived osteocyte-like cells in 3D induces pathological markers of bone remodelling and inflammation and is affected by short term treatments with AMPA/KA GluR antagonist NBQX. Loading was applied to 3D cell cultures at μstrain values reflecting loading zones within Frosts mechanostat theory (discussed in the introduction of this chapter) (Frost, 1996) and NBQX applied 1hr prior to loading and left on cells for the duration of the study to investigated any therapeutic impact. The data generated from this study was used to identify potential mechnoresponsive biomarkers that can be used to screen for the effectiveness of GluR antagonist therapeutic interventions. n numbers were defined as cell culture well replicates from one pilot study. The limitations of this study utilising cell culture well replicates as opposed to independent repeat experiments to define n numbers are discussed in detail in section 7.6.2.1.

6.3.1 Mechanical Loading and NBQX Intervention of Y201 Derived Osteocyte-like Cells Effects Cell Morphology

A lack of cytoplasmic extensions and viable nuclei in the physiological loading cells indicated cells were unsuitable for analysis (Figure 6.1). This was further confirmed as RNA extraction was not achievable from unloaded and physiological loaded cells. Therefore, the analysis in this chapter focuses on the pathophysiologically loaded cells with cytoplasmic extensions indicating improved cellular viability compared to unloaded and physiologically loaded cells. Cell extensions are a characteristic of osteocytic cells (Gu et al., 2005). Therefore, the phenotype observed, following pathophysiological loading, could indicate the osteogenic differentiation of Y201 MSCs in an culture environment more representative of *in vivo* conditions than 2D *in vitro* cell culture models (Figure 6.1) (Edmondson et al., 2014).

6.3.2 Pathophysiological Mechanical Loading and NBQX Intervention on Y201 MSC Derived Osteocyte-Like Cells Affects LDH Release

LDH release was determined as a measure of cell viability. There was no significant effect on LDH release following NBQX application at both time points (Figure 6.2). This is consistent with LDH findings in chapter 5 of this thesis (Figures 5.2 and 5.5), that indicate the concentration of NBQX used (200μM) is not cytotoxic. There is a significant increase with respect to time, some of this may be due to the increased time cells have spent in culture meaning an increased time in which LDH may increase in a close culture environment (1hr vs 24hrs). This would correlate with significantly increased levels of inflammatory biomarkers released over time found in this study. However, these findings may also be a consequence of the loading stimulus to which cells were exposed resulting in an increase in cellular proliferation. 5000μstrain was determined to be representative of a pathophysiological load, at which bone is stimulated into a 'reparative state' in which unorganised bone matrix is laid down (Bailey et al., 1996). Mechanical loading has been demonstrated to stimulate osteogenic differentiation and bone matrix production (Tanaka et al., 2003, Sittichokechaiwut et al., 2010). Finally, the increase in LDH may reflect an increase in cell proliferation that has been shown to occur in osteoblasts cultured in 3D type I collagen gels in response to mechanical stimuli (Ignatius et al., 2005). If this were the case, LDH levels may increase but remain proportional to cell number. However, as LDH release was not normalised to cell number in this study this effect was not quantifiable.

6.3.3 Pathophysiological Mechanical Loading and NBQX Intervention of Y201 MSC Derived Osteocyte-like Cells Affects Nitric Oxide Release.

Nitrite, the stable metabolite of NO, quantified from pathophysiologically loaded cells was below the assay limits of quantification for all 24hr control replicates, three-quarters of 1hr control replicates, three-quarters of 1hr NBQX replicates and half of 24hr NBQX replicates (Figure 6.3). Therefore, no significant effect of treatment or time on NO release was identified. Since NO release from bone cells following mechanical stimulus occurs rapidly and is transient and returns to control levels within 1 hour (Pitsillides et al., 1995, Klein-Nulend et al., 1998, McAllister and Frangos, 1999), the time points at which data was analysed may have been too far from the time of stimulus to determine any load induced effects upon nitrite levels. These findings indicate that, with the experimental set up used in

this chapter, nitrite levels determined via Griess assay cannot be used as an output to determine the impact of mechanical loading or therapeutic intervention.

Despite the findings in this loading model, multiple studies highlight a role of NO signalling in mechanical bone signalling and indicate pathological loading induced changes to bone turnover are mediated by NO signalling (Turner et al., 1996, Delgado-Calle et al., 2014, Fahlgren et al., 2018). Therefore, future investigations with assessment of immediate (<1hr) nitrite release following load may be useful in determining more about the involvement of NO signalling in this bone loading study with the additional benefit of providing another analyte for baselining control cells to determine any impact of load or therapeutic intervention.

6.3.4 Pathophysiological Loading and NBQX Intervention on Y201 MSC Derived Osteocyte-like Cells Affects the mRNA Expression and Protein Release of Bone Turnover, Inflammatory and Glutamate Signalling Markers

The effect of pathophysiological loading and NBQX treated Y201 3D cultures on bone turnover (*ocn, rankl, col-1a1, opg,* OPG*, alp* and *sost*), pro- and anti-inflammatory markers (IL-1β, IL-2, IL-6, IL-8, TNFα, IL-12p70, IFN-gamma, IL-10, IL13, IL-4 and *il-6*) and glutamate signalling components (*grik-1, gria-1, eaat-1* and *eaat-3* and glutamate) protein release and mRNA expression was addressed through ELISA/multiplex ECL assay analysis and qRT-PCR respectively. Regarding mRNA quantification, unloaded and Physiologically loaded samples did not produce quantifiable RNA. In pathophysiologically loaded samples *rankl, sost* and *tnfα* were not identified at quantifiable levels. Due to the bulk of data produced, correlation analysis and PCA was applied to visualise any trends in data correlation and variation.

6.3.4.1 Bone Turnover

Levels of *sost* and *dmp-1* produced by osteogenically differentiated Y201 MSCs were not high enough to be quantified. This, in combination with the expression of osteoblastic markers *col-1a1, alp* and *ocn* (Figures 6.6, 6.6 and 6.8 respectively), could imply that cells are in a late osteoblastic / early osteocytic stage of differentiation and not late stage

osteocytes (characterised by *sost* and *dmp-1* expression) (Franz-Odendaal et al., 2006, Capulli et al., 2014).

PCA reduced data to two principal components (PC1 and PC2) (Figure 6.17). When observing PC scores, outputs can be grouped into 4 clusters broadly contributing to the 2 treatment groups across two time points. All clusters were separate apart from some slight overlap between the 1 and 24hr NBQX treatment group clusters at positive PC1 and PC2 scores.

Short term NBQX treatment decreased *alp* expression at 1 (3.06-fold) and 24hrs (2.51-fold) compared to controls (figure 6.6). In bone, ALP plays a key role in the differentiation of osteoblasts from mesenchymal progenitors and its expression has been linked to degradation of mineralisation inhibitors (specifically mineralisation pyrophosphate) (Greenblatt et al., 2017) and bone mineralisation (Golub and Boesze-Battaglia, 2007). Under physiological or low-level loading of bone marrow MSCs *in vitro* and osteoblasts extracted from mice tibia following *in vivo* loading, ALP is upregulated and contributes to osteogenesis (Scott et al., 2008, Lu et al., 2018, Lionikaite et al., 2019). In a study investigating the periosteal bone response to external mechanical loading *in vivo* a decrease in *alp* mRNA was observed in periosteal tissue (Raab-Cullen et al., 1994). Overall *alp* expression can be varied depending on the type and magnitude of mechanical stimulus, however the significant decrease due to NBQX application following pathological loading may indicate therapeutic effect towards bone identifiable in this model.

Alp was grouped with *gria-1* and *il-6* with variance associated with NBQX treatment (Figure 6.17). When looking into more detail, all these markers show a decrease in turnover when exposed to NBQX (Figures 6.6, 6.9 and 6.5 respectively). IL-6 has been shown to be elevated in the synovial fluid of patients following acute knee injury and was associated with worsened $KOOS_4$ scores (Watt et al., 2016). This indicates a pathological role in the joint's response to traumatic loading. NBQX treatment has been shown to decrease IL-6 release in synoviocytes (Flood et al., 2007) and this study indicates this effect occurs following NBQX treatment in osteocyte-like cells in this model and is associated with a reduction in bone turnover marker expression (*alp*) and AMPA receptor expression (*gria-1*). AMPA receptors have been identified on osteoblasts, osteoclasts and osteocytes and have been shown to be

regulated by loading in bone (Chenu et al., 1998, Szczesniak et al., 2005, Bonnet et al., 2020). Inhibition of NMDA receptors (MK-801) on rat primary osteoblasts reduced ALP activity and *ocn* expression (Hinoi et al., 2003) highlighting an association with ionotropic GluR signalling and bone turnover within the literature. Following pathological loading of mouse knees (ACL rupture) *in vivo,* NBQX injection at the point of injury reduced bone and joint severity scores (Bonnet et al., 2020) and CNQX has been shown to prevent an AMPA induced increase in bone volume in rat tibia (Lin et al., 2008). This study supports the literature indicating that AMPA/KA GluR antagonists, such as NBQX, downregulates bone markers *in vitro* within the context of mechanical loading. Additionally, the findings of this study demonstrate a role of AMPA receptor subunit GluR1 (*gria-1*) in responding to NBQX treatment following pathological loading associated with decreased bone turnover and inflammation.

opg was associated with the NBQX treatment group cluster 1hr after loading which reflects the short-term impact of NBQX in decreasing *opg* turnover mentioned earlier in this section (Figure 6.17 and Figure 6.4). *Opg* expression increased between 1 and 24hrs in NBQX treatment groups (1.59-fold) (Figure 6.4) indicating that any changes to expression of this marker were short-lived (1hr) and not maintained to 24hrs where expression returned to control levels. No significant change in OPG release was observed due to NBQX treatment (Figure 6.29). OPG protein release did significantly increase as an effect of time in both control and NBQX treatment groups (5.07-fold and 4.01-fold respectively). Early upregulation of OPG, as well as IL-6, has been identified in the bone repair process so the increase over time following loading may indicate that this marker can be used to track the impact of pathophysiological load in this model (Fazzalari, 2011). Increase in OPG release (figure 6.29) and *opg* expression (figure 6.4) from 1 to 24hrs and is consistent with findings by Gilbert et al. (2020) that indicate *opg* expression increases in both physiologically and pathophysiological loaded osteocyte like Y201 MSCs between 1 and 24hrs (Gilbert et al., 2020). Bone remodelling occurs in response to physiological loading induced microdamage and is coordinated by the osteocyte (Raggatt and Partridge, 2010). *Opg* expression is upregulated following mechanical loading and represses resorption *in vitro* in an osteoblasts-osteoclast co-culture system (Li et al., 2013). The findings in this study would suggest an NBQX induced transient repression of *opg* expression, and subsequent release,

with potential to deliver a bone remodelling response in the *in vivo* bone tissue setting. This is in agreement with studies that indicate NBQX administration mitigates bone turnover following pathological loading (ACL rupture) (Bonnet et al., 2020) and may deliver preventative benefit towards developing PTOA. This study identifies OPG as a bone marker for tracking the effect of therapeutic intervention following pathophysiological loading in this model.

The down regulation of *alp* (figure 6.6) following NBQX treatment along with the short term down regulation in *opg* (figure 6.4), may reflect a repression of osteoblast activity induced by NBQX treatment and a reduction of load induced bone remodelling. This could represent therapeutic effect as unorganised bone overgrowth is associated with pathological loading (Frost, 1996) and subchondral bone remodelling is an early indicator of OA pathology and precedes cartilage destruction commonly associated with OA (Mansell et al., 1997, Hayami et al., 2006). Therefore, the decreased bone remodelling markers (*opg* and *alp;* Figures 6.4, 6.6 and 6.17) seen in NBQX treatment groups in this study following pathological loading indicates this model can be used to investigate potential novel antiarthritic therapeutics in the context of bone loading and supports the evidence demonstrating the protective effect of NBQX seen *in vivo* in both inflammatory and PTOA models of arthritis (Bonnet et al., 2015, Bonnet et al., 2020).

This model highlights a potential bone focused mechanism by which NBQX delivers a therapeutic benefit following joint injury and identifies associations of *alp, il-6* and *gria-1* turnover which may be used as a baseline to assess the impact of alternate interventions (e.g. sustained release NBQX) in future studies with this model.

6.3.4.2 Inflammation

NBQX treatment decreased IL-8 (1.53-fold, at 1hr; Figure 6.26), IL-12p70 (4.63-fold, at 1hr and 2.39-fold at 24hrs; Figure 6.20), IL-2 (1.99-fold, at 24hrs; Figure 6.23) and TNFα (2.20-fold at 24hrs; Figure 6.27). Release of all pro-inflammatory cytokines, bar IL-1β, significantly increased as a consequence of time for both control and NBQX treatment groups (see Figures 6.18-6.29). *Il-6* expression was decreased post loading in NBQX treatment groups

compared to controls at 1hr (1.42-fold) and non-significantly at 24hrs (2-fold) (figure 6.5). There was a decrease in *il-6* expression from 1 to 24hrs in both control (5.07-fold) and NBQX (7.16-fold) treatment groups (Figure 6.5). Regarding pro- and anti-inflammatory cytokines, IFN-γ release was too low to be detected within the range of quantification at 1 hour. However, at 24hrs, levels were significantly reduced in NBQX treatment groups compared to controls (2.25-fold) (Figure 6.18). IFN-γ release significantly increased over time in both control (12.99-fold) and NBQX (8.01-fold) treatment groups (Figure 6.18). IL-4, IL-10 and IL-13 significantly decreased in NBQX treatment groups compared to control post pathophysiological loading (Figures 6.24, 6.19 and 6.21 respectively). PCA grouping of all inflammatory markers into one principal component (Table 6.5) as well as scatterplots where IL-6 compared to IL-13 (Figure 6.32) and OPG compared to glutamate (Figure 6.33) indicate that time is the most prevalent factor contributing to positive correlation with the additional observation that control treatment groups also contribute to higher scores compared to NBQX treatment groups. This evidence corroborates the consistent variance detailed in Figures 6.18 to 6.29, highlighting the trend of increased marker release over time following pathophysiological loading and decreases as a consequence of NBQX treatment in this study.

Pathological load universally increased (bar IL-1β) the protein release of inflammatory markers. In human trabecular bone chips expressing osteocyte specific markers (SOST, DMP1, MEPE), gene expression of pro-inflammatory markers IL-6, IL-8, IL-1β and TNFα was identified (Pathak et al., 2016). It has been shown that mechanically loaded osteocytes produced pro-inflammatory markers (IL-6) that may impact bone turnover (Bakker et al., 2014) and that TNFα and IL-1β meditate the osteocyte response to mechanical loading (Kulkarni et al., 2012, Liao et al., 2017). This is consistent with the acute inflammatory response identified in synovial fluid following joint injury, highlighted particularly by TNFα, IL-6 and IL-8 release at 1 day post injury (Anderson et al., 2011, Lieberthal et al., 2015).
In a study measuring the effect of extended (4hrs) cyclic loading on subchondral osteoblasts *in vitro* (sclerotic vs non-sclerotic), both IL-8 and IL-6 gene expression was upregulated (Sanchez et al., 2012). TNFα expression has been linked with OA development and promotion of osteoclastogenesis (Rigoglou and Papavassiliou, 2013). IL-6 isolated from knee

injury patient synovial fluid has been highlighted as a key inflammatory marker associated with patient reported outcomes ($KOOS_4$ scores). Highest IL-6 level patients reported significantly lower $KOOS_4$ scores compared to low IL-6 level patients (Watt et al., 2016). IL-12p70 has been shown to be a stimulatory factor for T-cells (Gee et al., 2009). A potential role for IL-12 in the inhibition of TNFα mediated osteoclastogenesis has been identified (Nagata et al., 2003, Yoshimatsu et al., 2009, Morita et al., 2010). These factors indicate that certain pro-inflammatory cytokines (IL-12) repress osteoclast induced bone resorption. IFN-γ (and TNFα) treatment has been shown to decrease glutamate released from primary human osteoblasts *in vitro* (Genever and Skerry, 2001). The decrease in glutamate release identified in NBQX treatment groups in this study may (figure 6.28), therefore, link with the observed decrease in IFN-γ. Increases in anti-inflammatory cytokines (IL-4, IL-10, IL-13 and IL-1Ra) have been identified following joint injury and in early stage OA (compared with late OA) (Barker et al., 2014, Lieberthal et al., 2015). Additional studies highlight that IL-4, IL-10 and IL-13 contribute to the in joint inflammatory response to load (Onoe et al., 1996, Araujo-Pires et al., 2015). When taken together, these studies highlight a complex and multifaceted inflammatory response to mechanical loading in the joint. This model is shown to release these markers following pathological load while providing a platform for the study of interventions (in this case NBQX).

The current understanding of PTOA indicates an inflammatory and apoptotic catabolic response of joint localised cells to trauma within the first 4 days post injury (Anderson et al., 2011). The osteochondral interface has been shown to be closely linked, not only physically, but via biomolecular crosstalk (Yuan et al., 2014). Early inflammatory response following joint injury has been shown to contribute to PTOA development but a full understanding of the complex inflammatory mechanisms by which this occurs has yet to be developed (Lieberthal et al., 2015). The capacity of NBQX to modulate inflammatory markers at the early stages following pathological loading of osteogenically differentiated Y201 MSCs, indicates a therapeutic role for this GluR antagonist in treating the long-term chronic effects of joint injury that can result in PTOA development. However, it is worth noting that NBQX induced reduction of anti-inflammatory markers which may contribute to bone resorption and that further understanding of the interlinked and intricate inflammatory mechanisms

that take place following pathological loading of bone would be key in optimising the therapeutic timing and delivery.

PCA of mRNA expression indicates that *il-6* is associated with *gria-1* and *alp* linked to NBQX treatment at 24hrs (Figure 6.17). As discussed in the previous section (6.4.4.1), this association highlights a role of AMPA/KA GluR antagonism in modulating inflammation, bone turnover and AMPA glutamate signalling following pathological mechanical loading. *Il-6* expression is negatively correlated with *eaat-1* and *eaat-3* expression (Table 6.2) and although correlation is not causation, this does highlight the opposing outcome on gene expression of the markers following pathological loading and represents a biomarker characteristic of this model that may be used to investigate the impact of future interventions. *Il-6* expression reduces between 1 and 24hrs (Figure 6.5) whereas both *eaat-1* and *eaat-3* expression increases (non-significantly) over time after loading (Figures 6.11 and 6.12 respectively). High glutamate is detected in synovial fluid following traumatic loading (ACLr/Meniscal tear) in humans (Bonnet et al., 2020) and increased IL-6 has been identified in synovial joints following injury (Watt et al., 2016). Therefore, the IL-6 levels identified post pathological loading in this study may coincide with increased glutamate release although comparisons with unloaded controls would be needed to confirm this. With this in mind, increased glutamate exposure increases *eaat* expression (Mason and Huggett, 2002) and GLAST-1 (*eaat-1*) has been shown to be upregulated in osteoblasts and downregulated in osteocytes in response to mechanical load *in vivo* (Mason et al., 1997) highlighting a glutamate exposure and mechanical load induced modulation of glutamate transporters in bone that supports the findings of this study. A later section will discuss the impact of glutamate signalling markers identified in this study (section 6.4.4.3).

An increase in glutamate, bone turnover (OPG) and inflammatory markers following pathological loading of bone has been demonstrated in various studies both *in vivo* and *in vitro* (Anderson et al., 2011, Fazzalari, 2011, Barker et al., 2014, Lieberthal et al., 2015, Hao et al., 2017). Additionally, NBQX intervention has been demonstrated to influence bone turnover and inflammatory signalling (Bonnet et al., 2015, Bonnet et al., 2019, Bonnet et al., 2020). This data indicates a capacity for this concentration of NBQX (200μM), to impact multiple aspects of the inflammatory response following a pathological level of loading in

osteogenically differentiated Y201 MSCs and provides evidence that this model may be a useful drug screening tool to highlight the impact of prospective interventions to loaded bone. This model further highlights that the release of pro- and anti-inflammatory markers are linked via feedback loops meaning that reductions in pro-inflammatory signalling may result in a reduced anti-inflammatory response.

The *in vitro* loading study in this chapter provides a platform to specifically investigate the impact of mechanical loading and NBQX intervention on bone cells and does indicate a capacity for this compound to influence bone cell inflammation and glutamate release consistent with *in vivo* findings. Additionally, this universal increase in all inflammatory markers following pathophysiological load (bar Il-1β) represents a characteristic of this model by which the impact of future therapeutic intervention can be gauged and compared to NBQX in this study.

6.3.4.3 Glutamate Signalling

Glutamate release significantly decreased at both 1hr and 24hrs post load in NBQX treatment groups compared to controls (1.24-fold and 1.18-fold respectively; Figure 6.28). Glutamate levels still increased over time following pathological loading in both control (1.24-fold) and NBQX (1.31-fold) treatment groups (Figure 6.28). This highlights the capacity of osteogenically differentiated cells to release glutamate in response to pathological loading (Mason, 2004) and indicates this model reflects this capacity. Decreases in glutamate following NBQX treatment at both 1 and 24 hours indicate a sustained effect is delivered with potential to impact inflammation and bone repair as highlighted by *in vivo* studies (Bonnet et al., 2015, Bonnet et al., 2019, Bonnet et al., 2020). High levels of glutamate in both OA and RA patient's synovial fluid as well as in the synovial fluid of patients following ACL rupture and meniscal damage repair (McNearney et al., 2000, Bonnet et al., 2020) indicate a role of glutamate in joint pathology with a potential load induced mechanism of release. The capacity of NBQX to mitigate glutamate release from osteogenically differentiated cells in this study associated with modulation of bone turnover (via OPG release) and inflammation (all inflammatory markers investigated), highlighted by protein release PCA (Table 6.5), identifies a potential therapeutic mechanism of action in

the treatment of joint injury and in turn provides further evidence towards the use of NBQX as a preventative therapeutic in the treatment of PTOA.

gria-1 expression was significantly reduced post loading in NBQX treatment groups compared to controls at 1hr (2.99-fold; Figure 6.9). GRIA-1 is the ionotropic glutamate receptor AMPA sub-unit 1 and has been shown to be expressed in osteoblasts, osteoclasts and osteocytes (Chenu et al., 1998, Szczesniak et al., 2005, Brakspear and Mason, 2012). NBQX specifically antagonises AMPA receptors (and KA receptors) (Libbey et al., 2016) and GluR signalling has been shown to be regulated by load *in vivo* (Szczesniak et al., 2005, Bonnet et al., 2020). The modulation of *gria-1* expression by NBQX treatment of pathophyiologically loaded osteocytes in 3D in this study is consistent with the ability of this drug to regulate glutamate signalling within bone and supports the evidence that this GluR is involved in bones' response to loading (Chenu et al., 1998, Hinoi et al., 2001, Hinoi et al., 2002b, Szczesniak et al., 2005, Brakspear and Mason, 2012, Bonnet et al., 2020). PCA of mRNA expression data associating bone turnover (*alp*), *il-6* and *gria-1* with NBQX treatment in this study (Figure 6.17) supports the *in vivo* evidence indicating NBQX administration can modulate bone turnover and inflammation with an associated effect on AMPA glutamate signalling machinery. The evidence from this study indicates NBQX treatment may provide a therapeutic benefit via downregulation inflammation and bone turnover with associated regulation of AMPA GluR signalling. Additionally, this model highlights *gria-1* as a potential biomarker to use as a baseline for the understanding of the impact of future interventions when compared to these findings.

Eaat-3 demonstrated a significant increase with respect to time post pathological loading (Figure 6.12). Additionally, *eaat-3* positively correlates with *eaat-1* (Figure 6.13) and is grouped closely with regards to variance in PCA (Figure 6.17).

Glutamate concentrations are raised in the synovial fluid of OA and RA patients (McNearney et al., 2000, McNearney et al., 2004) and following ACL rupture and meniscal tear (Bonnet et al., 2020), demonstrating a glutamate release response following injury. With this in mind, glutamate exposure increases *eaat* expression and translocation to the cell membrane to remove extracellular glutamate (Huggett et al., 2000, Mason and Huggett,

2002). Therefore, the increase of *eaat-3*/*eaat-1* expression may be in response to a pathological load induced release of glutamate identified in protein release studies (Figure 6.28). Glutamate transporters move glutamate against its concentration gradient and *eaat-1* and *eaat-3* expression has been demonstrated in osteoblasts (Takarada et al., 2004) and *eaat-1* expression in osteocytes (Mason et al., 1997). EAAT inhibition can influence osteoblast-like cell bone forming capacity *in vitro* via upregulation of ALP activity (following TBOA inhibition) and upregulation of OCN and osteonectin (t-PDC inhibition) (Brakspear et al., 2009). Upregulation of *eaat-1* and *eaat-3* expression over time following pathological loading, in this thesis, indicates a mechanically regulated response of glutamate signalling in bone that was not influenced by NBQX inhibition of the AMPA/KA GluRs.

This model further demonstrates a link between glutamatergic signalling and bone turnover in response to pathological loading, while highlighting NBQX as a potential modulator for this signalling via AMPA GluRs and direct down regulation of glutamate release. The increase of glutamate transporter gene expression over time following pathophysiological load may be used in future as a biomarker to understand the impact of various loads and interventions when using this model.

6.3.5 Conclusions

The overarching aim of this chapter was to determine whether mechanically induced bone remodelling of Y201 MSC derived osteocyte-like cells in 3D induces pathological markers of bone remodelling and inflammation and is affected by treatment with NBQX. Addressing this aim contributes to the thesis hypothesis by providing an *in vitro* platform to build understanding of the protective effects of AMPA/Kainate GluR antagonism on mechanically driven pathways in bone.

This chapter characterised the Y201 MSC used as a potential late osteoblastic/early-osteocytic phenotype (section 6.4.1 and 6.4.4.1)

Gene expression analysis demonstrated a capacity for short term sustained NBQX treatment, following application of a pathophysiological level of loading, to reduce

expression of bone markers (*alp* and *opg;* Figures 6.4, 6.6 and 6.17), inflammatory markers (*il-6;* Figure 6.5) and glutamatergic signalling components (*gria-1;* Figure 6.9) and highlighted a potential pathological load induced increase in glutamate transporter expression (*eaat-1* and *eaat-3*). (discussed in section 6.4.4; Figures 6.11, 6.12, 6.13 and 6.17). Future work focusing on the mechanisms by which these markers may interact, the potential therapeutic intervention supplied by GluR antagonists with differing receptor specificities (e.g. DNQX and CNQX) and the timing and duration of intervention in this model (e.g. sustained release) could add to the insights from this gene expression analysis by comparing against the biomarker outputs established in this study.

Immunoassay analysis supported gene expression findings, indicating a role of NBQX treatment in decreasing release of a range of pro- and anti-inflammatory markers following pathological loading as well as in the levels of glutamate and OPG released by cells (discussed in section 6.4.4; Table 6.3, Table 6.5 and Figures 6.18-6.29). These findings highlight the interwoven nature of inflammatory, bone turnover and glutamatergic signalling in pathologically loaded bone cells *in vitro* and demonstrate a capacity for NBQX treatment to influence these markers shortly after mechanical stimulus.

This study supports the therapeutic effects of NBQX treatment identified *in vivo*, by demonstrating that NBQX directly impacts bone independent of other joint tissues. This model demonstrates the application of a 3D cell culture loading system that could provide data more representative of that produced by cells *in vivo* than of that produced in a 2D culture environment and begins to establish a range of biomarkers within this model (*il-6, gria-1, alp, opg, eaat-1, eaat-3* and inflammatory markers) by which the impact of load and therapeutic intervention could be investigated thereby improving understanding of mechanically driven pathways in bone and providing an animal free platform in which to screen potential anti-arthritic therapies.

Chapter 7

Conclusions and Future Work

7.1. Results Summary

The overarching hypothesis of this thesis was that AMPA and kainate glutamate receptor (GluR) antagonists can be incorporated into sustained release delivery systems to allow for investigation into their protective effects on inflammatory or mechanically driven pathways in bone *in vitro.* The overarching aims of the 4 results chapters described in this thesis were established to address the overarching hypothesis:

- **Overarching aim 1:** *To synthesise and characterise sustained release PLGA nanoparticles for delivery of GluR antagonists and investigate options for long term nanoparticle storage.*
- **Overarching aim 2:** *To develop and test a sustained release thermoresponsive hydrogel for delivery of GluR antagonists.*
- **Overarching aim 3:** *To determine whether pathological levels of IL-6/sIL-6r exposure followed by short term AMPA/KA GluR antagonist application with or without sustained release of AMPA/KA GluR antagonist from PLGA nanoparticles influences bone remodelling, glutamate and inflammatory signals.*
- **Overarching aim 4:** *To determine whether mechanically induced bone remodelling of Y201 derived osteocyte-like cells in 3D induces pathological markers of bone remodelling and inflammation and is affected by short term treatments with AMPA/KA GluR antagonist NBQX.*

This chapter brings together the findings of each results chapter with recommendations for future work and discusses the limitations of experimental approaches adopted in this thesis.

7.2. GluR Antagonists Were Encapsulated into PLGA Nanoparticles

There is some *in vivo* evidence to suggest that sustaining the delivery period of GluR antagonists can improve upon the anti-inflammatory and joint protective benefits observed in inflammatory and traumatic models of arthritis (Bonnet et al., 2015, Bonnet et al., 2020). Sustained drug delivery using PLGA nanoparticles for IA injection in the treatment of OA allows for: direct delivery to the diseased tissue; reduced risk of systemic drug exposure;

improved delivery of drugs with poor oral bioavailability; reduced drug clearance from the joint space and decreased need for multiple, painful injections with an associated risk of infection (Wehling et al., 2017, Brown et al., 2019a). PLGA is biocompatible, biodegradable and approved for use in multiple drug delivery formulations by the FDA (Makadia and Siegel, 2011) and a range of studies have demonstrated PLGA nanoparticles can be tailored to provided optimal drug delivery for the target tissue (Soppimath et al., 2001, Olivier, 2005, Danhier et al., 2012, Nogueira et al., 2016).

Table 7.1: Summary of GluR antagonist loaded PLGA nanoparticle characteristics and release properties extracted from data in chapter 3 of this thesis (figures 3.6, 3.7 and 3.8).

Delivery Vehicle (release media)	Size (nm; PDI)	Zeta Potential (mV)	EE (%) and LC (%)	Percentage immediate release (%)	Delivery duration
2.5mM DNQX loaded PLGA NPs (PBS)	121 (0.39)	-2.1	29.3 and 0.24	39.8	5 weeks
20mM DNQX loaded PLGA NPs (PBS)	122 (0.24)	-2.4	26.5 and 1.74	81.1%	5 weeks
2.5mM DNQX loaded PLGA NPs (Bovine synovial fluid)	121 (0.39)	-2.1	30.9 and 0.254	91.0%	48hrs
Freeze dried 20mM NBQX loaded PLGA NPs (PBS)	111 (0.18)	-2.3	12.9 and 0.850	81.7%	2 weeks

All nanoparticles formulated in chapter 3 were within the nanoscale range with low poly dispersity, indicating a narrow size distribution (Table 7.1). Delivering a sustained GluR antagonist load using particles in the nanoscale range ensures a large surface area to volume ratio which has been linked with reduced systemic clearance, increased cellular permeability and passive targeting to areas of inflammation in the literature (Desai et al., 1997, Ishihara et al., 2009b, Durymanov et al., 2017). The sub 200nm size of nanoparticles formulated in this chapter has also been linked to an enhanced capacity to cross epithelial linings and penetrate microvasculature (Vinogradov et al., 2002, Singh and Lillard, 2009). Although negative, the small values for zeta potential that were identified for nanoparticles in these formulations (Table 7.1), highlight an avenue for future investigation into

nanoparticle surface modification with charged species to create a more robust formulation for *in vivo* testing (Table 7.1). Freeze dried PLGA nanoparticles were easily resuspended for drug delivery studies and did not exhibit altered size or PDI (Figure 3.4). Additionally, sustained GluR antagonist (NBQX) delivery was still maintained (over 2 weeks, Table 7.1) indicating the freeze-drying methods used may provide a mechanism for the long-term storage of sustained GluR antagonist release nanoparticles. The GluR antagonist loaded PLGA nanoparticles developed in this study exhibited low EE (between 12% and 29%; Figures 3.6-3.8) resulting in low amounts of drug available for sustained delivery (1.57mg in 20mM DNQX loaded nanoparticles (78.5μg/ml in release studies) and 0.98mg in freeze dried 20mM NBQX loaded nanoparticles (49μg/ml in release studies). However, this study demonstrated development of a delivery vehicle for use in investigating the effect of sustained, low concentrations, of GluR antagonists. High nanoparticle concentrations (100mg/ml) delivered significantly increased levels of hOB MTS release at all timepoints tested (figure 3.9) suggesting that nanoparticle concentration needs to be balanced to reduce the risk of a cytotoxic response while maximising GluR antagonist available for sustained delivery.

0.98mg of NBQX was released over 14 days from freeze dried nanoparticles (97.9% released) in PBS (Figure 3.8). These PLGA nanoparticles provide a platform for the investigation into the sustained delivery of GluR antagonists at very low but potentially still therapeutic concentrations. Higher EE may be achieved through increasing nanoparticle size or changing emulsifying solvent (McCall and Sirianni, 2013). However, this may come at the expense of nanoparticle toxicity and tissue penetrative capacity of sub 200nm nanoparticles formulated in this study. Recommended future work would be to increase the negativity of nanoparticle zeta potential for improved stability when delivering *in vivo*. This chapter addresses its overarching aim and contributes to the thesis hypothesis by demonstrating incorporation of GluR antagonists into a sustained release delivery system thereby providing a platform to investigate the effects on pathways in bone (as is carried out in chapter 5 of this thesis).

7.3. Thermoresponsive Hydrogels Were Developed for Localised Subcutaneous GluR Antagonist Delivery.

IA injection of GluR antagonists on two consecutive days has been shown to improve therapeutic effect compared with one single injection in a mouse ACL rupture model (Bonnet et al., 2020). This indicates 2-day sustained GluR antagonist delivery may be of benefit over immediate release delivery. Utilising a Pluronic F-127 and Carbopol-934 based formulation allowed for the preparation of thermoresponsive hydrogels with low toxicity components that have the capacity for sustained delivery of water-soluble compounds such as GluR antagonists (Craig et al., 1994, Gong et al., 2013). A localised subcutaneous route of administration for these hydrogels would mean reduced invasiveness of drug delivery compared to IA injection and potential for patient self-administration although, with its widespread usage in OA treatment, IA injection would still clearly be an option (Bansback et al., 2015). The thermoresponsive properties of hydrogel formulations would allow for a liquid injection that gels *in situ* and forms a localised reservoir of therapeutic GluR antagonists for sustained delivery.

Table 7.2: Summary of GluR antagonist loaded Pluronic F-127 based hydrogel characteristics and sustained delivery properties. Data extracted from figures in chapter 4 of this thesis (figures 4.4, 4.5 and 4.6).

Delivery Vehicle (delivery media)	Sol gel transition temperature (°C)	Membrane type	Delivery duration
2.5mM DNQX loaded 22% Pluronic F-127 w/v hydrogel (PBS)	20 (identified in formulation with no GluR antagonist load)	Semi-permeable dialysis cassette (10KDa Mw cut-off)	27hrs
2.5mM DNQX loaded 25% Pluronic F-127 w/v hydrogel (PBS)	22	Semi-permeable dialysis cassette (10KDa Mw cut-off)	27hrs
2.5mM DNQX loaded 25% Pluronic F-127 w/v hydrogel (PBS)	22	Bovine synovial membrane	24hrs

Pluronic F-127 concentrations were optimised to ensure sol-gel transitions below subcutaneous temperature while remaining injectable at close to room temperature (Table 7.2; Figure 4.3 and 4.4). Due to the nature of hydrogel formulation methodology, there were no encapsulation losses of GluR antagonist allowing for a highly controllable sustained

drug delivery in the μM to mM range over 27hrs (Figure 4.5 and 4.6). Addition of 2.5mM GluR antagonist did slightly alter the rheological properties of hydrogels (Figures 4.3 and 4.4), this would, therefore, need to be taken into consideration when altering drug load, as up to 20mM NBQX has been shown to be an effective direct delivery formulations *in vivo* (Bonnet et al., 2020). In addition to semi permeable membrane diffusion, hydrogels sustained delivery through isolated bovine synovial membranes indicating a less invasive *in vivo* form of GluR antagonist delivery, may be viable with this delivery vehicle (Figure 4.6). Hydrogels were shown to be toxic *in vitro* (MTS assay) when exposed to hOBs at ratios greater than 1:8 (hydrogel: cell culture media; Figure 4.7). Therefore, low localised volumes of hydrogel would reduce the risk of a toxic response.

Overall, hydrogels formulated in this chapter exhibited thermosetting characteristics and sustained GluR antagonist delivery at 2.5mM AMPA/KA GluR antagonist (DNQX) load. The GluR antagonist concentrations used in this investigation have been shown to deliver therapeutic effects towards the treatment of OA *in vivo* (Bonnet et al., 2015, Bonnet et al., 2020). As synovial membrane permeability has been demonstrated to alter with inflammation (Kushner and Somerville, 1971, Hartjen et al., 2018), further testing of diffusion through human synovial membranes with a comparison of healthy and arthritic membranes would be useful future work. This would help to clarify the diffusion properties of GluR antagonists from this hydrogel formulation in the patient. *In vivo* hydrogel implant experiments would be a useful future line of investigation to understand toxicity and drug delivery characteristics when applied *in vivo* to a pathophysiological joint environment such as PTOA (ACL rupture) or AIA (inflammatory joint model). This would allow for comparison with the protective therapeutic findings of immediate release GluR antagonist formulations in these models (Bonnet et al., 2015, Bonnet et al., 2020). Additionally, encapsulation of GluR antagonist loaded PLGA nanoparticles, formulated in Chapter 3 of this thesis, within these thermoresponsive hydrogels would be an interesting next step in developing a delivery vehicle. This would provide a high concentration (mM) short term (up to 27hrs) release of GluR antagonist (from hydrogels), followed by longer term (2-5 weeks), sustained low amounts (2mg), GluR antagonist delivery from PLGA nanoparticles. This combined sustained release formulation may be useful in addressing the inflammatory spike that follows joint trauma while modulating the slow chronic joint degeneration that precedes the

development of PTOA (Anderson et al., 2011). The findings of this chapter address the thesis hypothesis and the chapter overarching aim by providing an alternate sustained delivery vehicle to the nanoparticles developed in chapter 3 which demonstrates very different sustained release properties and improved drug loading controllability. This provides a broader range of delivery vehicles from which to investigate the impact of sustained AMPA/KA GluR antagonism to treat OA in future.

7.4. Elucidating the Effects of Sustained GluR Antagonist Application on Pathological Signals *in vitro* in 2D and 3D

In an ACL rupture mouse model of PTOA (Gilbert et al., 2018) an upregulation of inflammatory markers, specifically IL-6, was identified soon after joint injury along with degradative enzymes (ADAMTS-4 and MMP-3). IA injection of NBQX delivered at the point of arthritic induction in this model delivered anti-degradative and anti-inflammatory therapeutic intervention (Bonnet et al., 2020). In the same way NBQX intervention delivered significant therapeutic benefit in an AIA model (Bonnet et al., 2015). IL-6 has been shown to significantly contribute to knee injury OA outcome scores (Watt et al., 2016). IL-6 release has been linked with OA development and glutamate signalling in *in vivo* models of arthritis (Alonzi et al., 1998, Bonnet et al., 2015, Bonnet et al., 2020) as well as in investigations into joint tissue (synovium, bone and cartilage) (Palmqvist et al., 2002, Wong et al., 2006, Flood et al., 2007, Tsuchida et al., 2012, Wu et al., 2017). Low numbers of membrane bound 'cis-signalling' IL-6 receptors are present on bone cells (osteoblasts) and, therefore, IL-6 trans signalling via a soluble receptor (sIL-6r) has been proposed as the primary IL-6 signalling mechanism in bone (Jones and Rose-John, 2002). Trans signalling is primarily responsible for the pro-inflammatory activity of IL-6 (Rose-John, 2012, Wu et al., 2017). This chapter developed a 3D *in vitro* osteocyte model, differentiated from Y201 MSCs, to provide a platform for investigation into the impact of pathological concentrations of IL-6 and its soluble receptor (sIL-6r) (Bakker et al., 2014, Watt et al., 2016, Wu et al., 2017). The effects on bone turnover, inflammation and glutamate signalling were then investigated following short term (1hr) NBQX exposure, mimicking the *in vivo* clearance of NBQX that would occur in the joint and sustained NBQX exposure from PLGA nanoparticles to investigate longer term effects of low concentrations of sustained NBQX.

Mineralisation assays on hOBs and osteogenically differentiated Y201 MSCs in 2D indicated that DNQX and NBQX inhibited mineralisation *in vitro* at concentrations of 200μM to 400μM (Figures 5.3 and 5.4). This is consistent with Bonnet et al. (2015) and highlights the capacity of other ionotropic GluR antagonists to modulate bone turnover via AMPA/KA inhibition in addition to NBQX. LDH release was not affected by GluR antagonists which corroborates the evidence, indicating these drugs are well tolerated *in vivo* (Figure 5.2)(Ingwersen et al., 1994, Herrling, 1997, Bonnet et al., 2015, Bonnet et al., 2019, Bonnet et al., 2020). In the 3D osteocyte, osteogenically differentiated Y201 MSC model, IL-6/sIL-6r treatment did not affect LDH levels (Figure 5.5) but did increase nitrite release after 72 hours (Figure 5.6), indicating oxidative stress and highlighting a potential marker from which to track the impact of therapeutic intervention in this model.

Alp and *opg* expression was reduced following IL-6/sIL-6r treatment and *alp* corrected by short term NBQX exposure at 24hrs (Figures 5.8, 5.12 and 5.20). Multivariate analysis highlighted, IL-4, IL-12p70 and IL-6 release were correlated following IL-6/sIL-6r treatment (Figures 5.36, 5.25, 5.29 and 5.30) indicating a cohort of pro and anti-inflammatory cytokines were upregulated following pathological inflammatory exposure providing a further cohort of biomarkers within this model from which the impact of therapeutic intervention on inflammation (IL-6/sIL-6r) induced marker upregulation could be investigated in future studies. As well as correcting bone turnover alterations from inflammatory exposure, short term NBQX treatment increased release of anti-inflammatory markers (IL-10 and IL-13) compared to IL-6/sIL-6r treatment groups (Figures 5.24 and 5.26), indicating an anti-inflammatory mechanism by which NBQX elicits a therapeutic benefit in inflammatory joint disease. Multivariate analysis highlighted an association of IL-1β and TNFα with anti-inflammatory molecules (IL-10 and IL-13) in NBQX treatment groups at 24hrs (Figure 5.36). This indicated that, under the pro-inflammatory conditions in this study, NBQX not only delivered an anti-inflammatory effect but also delivered a short-term increase in release of pro-inflammatory cytokines commonly associated with bone resorption. Multivariate analysis also was also useful in defining groups of biomarkers impacted by IL-6/sIL-6r inflammatory exposure *alp, opg, eaat-3* and *gria-1* were grouped by variance indicating down regulation vs controls at 24hrs in IL-6/sIL-6r treated cells (Figure 5.20).

Through beginning to define the impact of IL-6 signalling on a range of biomarkers (*alp, opg, eaat-3* and *gria-1* down regulated vs controls at 24hrs and increased release of IL-4 and IL-12p70 vs controls), this model provides an *in vitro* platform for the study of the effects of trans signalling IL-6 induced inflammation in human osteocyte-like cells and allows for focused investigation into the mechanisms by which AMPA/KA GluR antagonists (specifically NBQX in this instance) deliver therapeutic effects observed *in vivo* (Bonnet et al., 2015, Bonnet et al., 2020). This pilot study provides the foundations on which a drug screen tool may be developed to further understand the therapeutic effects of prospective interventions to an inflammatory bone environment thereby optimising drug selection prior to *in vivo* and clinical studies.

Although not demonstrating any clear therapeutic benefits, NBQX loaded PLGA nanoparticle treatment was shown to induce an inflammatory state where glutamate (Figure 5.32) and IL-6 (Figure 5.30) were both raised when bone cells were under stress (indicated by raised LDH and nitrite levels; Figures 5.5 and 5.7). This evidence ties together findings that glutamate and IL-6 levels are raised in the synovial fluid of joints following injury (ACL rupture) (Watt et al., 2016, Bonnet et al., 2020) and indicates that this process occurs in bone having been exposed to pathological levels of inflammation. These results also highlight that the biomarkers investigated in this model can be utilised to detect a potential non-therapeutic impact as well as therapeutic benefits of interventions.

This study demonstrated that NBQX regulates inflammatory and bone turnover markers in human osteocyte like cells in 3D, following IL-6/sIL-6r stimulation. Future work applying sustained NBQX delivery in this model from thermosetting hydrogels synthesised in Chapter 4 of this thesis may reveal more about the sustained release impact of NBQX in high concentrations (200μM+) which have been shown to impact bone cell mineralisation. Additionally, utilising a lower PLGA nanoparticle concentration in this study may mitigate the pro-inflammatory effects and allow for investigation into the sustained release of low NBQX amounts (μg range) without interference from the delivery vehicle itself. Changing the timing of NBQX application would be useful future work to help further understand the

inflammatory-modulatory capacity of NBQX using this *in vitro* model and indicate what may be the optimal timing for therapeutic intervention for *in vivo* testing.

This chapter addresses its overarching aim and contributes to the thesis hypothesis through the development of a model with biomarker outputs for bone, inflammation and glutamate signalling that can be used to define the impact of a pathological inflammatory stimulus (IL-6/sIL-6r) and investigates subsequent therapeutic intervention in the form of NBQX and NBQX loaded nanoparticles. This study provides a platform on which inflammatory driven pathways in bone may be investigated and the impact of interventions screened.

7.5. Elucidating the Effects of GluR Antagonist Application on Osteocyte-like Cellular Responses to Pathophysiological Loading *in vitro* in 3D.

Mechanical loading is a key factor in bone remodelling with the magnitude of loading eliciting different effects on bone synthesis (Bailey et al., 1996, Frost, 1996, Christen et al., 2014). The osteocyte coordination of osteoblasts and osteoclasts activity is central to the response of bone to mechanical stimuli and acts via a range of signalling pathways to activate bone resorption or deposition (Atkins and Findlay, 2012). Osteocyte apoptosis occurs following unloading of bone resulting in bone resorption via RANKL/RANK/OPG and SOST signalling (Moriishi et al., 2012). Osteocytes coordinate the production of lamellar bone matrix under physiological loading via reduction of SOST release and the RANKL/OPG ratio (Robling et al., 2008, Bonewald, 2011, Yan et al., 2020). Pathological levels of loading (>4000μstrain) induce the rapid laying down of unorganised bone matrix (Bailey et al., 1996, Frost, 1996, McBride and Silva, 2012). Following joint injury, the development of PTOA is common, representing 12% of all lower limb OA cases (Anderson et al., 2011), often manifesting at a younger age and increasing the likelihood of multiple joint replacement surgeries being required over a patient's lifetime (Thomas et al., 2017). Along with the rapid deposition of woven bone following joint injury, an acute inflammatory response manifests (Anderson et al., 2011) which in turn has been shown to impact bone homeostasis via an osteocyte mediated response (Tan et al., 2006, Bakker et al., 2009, Bakker et al., 2014). Glutamatergic signalling machinery has been identified in bone (Mason et al., 1997) and shown to play a role in bone homeostasis and response to joint injury (Chenu et al., 1998,

Chenu, 2002). Glutamate levels are increased in both OA and RA patients synovial fluid compared to cadaveric controls (McNearney et al., 2000) with levels of glutamate in the synovial fluid of patients following ACL rupture or meniscal damage similar to that of OA (Bonnet et al., 2020). The use of ionotropic GluR antagonists has been shown to protect against joint damage, inflammation and swelling in a post-traumatic (ACL rupture) model of arthritis (Bonnet et al., 2020) and it has been proposed that the glutamate response to bone loading is mediated by osteocytes (Mason, 2004).

This chapter utilised osteocyte-like, osteogenically differentiated Y201 MSCs cultured in 3D in custom silicon loading plates to expose cells to pathological levels of loading (5000μstrain) and to investigate the impact of NBQX intervention over 24hrs to bone turnover, glutamate signalling and inflammatory signalling. NBQX (200μM) application to 3D osteocyte-like cells was not cytotoxic (LDH) after pathophysiological loading, consistent with findings in chapter 5 of this thesis and literature (Figure 6.2), indicating NBQX is well tolerated *in vivo* and *in vitro* (Ingwersen et al., 1994, Herrling, 1997, Bonnet et al., 2020). However, LDH release did increase between 1 and 24hrs post loading indicating a potential cytotoxic response to pathological load. NBQX treatment downregulated the gene expression of bone turnover (*alp* and *opg;* Figures 6.4 and 6.6), inflammation (*il-6;* Figure 6.5) and glutamate signalling (*gria-1;* Figure 6.9) markers following pathological loading of osteocyte like Y201 MSCs with multivariate analysis indicating a link between glutamate, inflammation and bone signalling in NBQX treatment groups (Figure 6.17). These findings support the *in vivo* evidence that IA NBQX administration improves swelling and joints scores (particularly bone) in a PTOA model (Bonnet et al., 2020) while directly highlighting bone as a target for NBQX intervention. This chapter provides more evidence as to the repressive effect of NBQX intervention to IL-6 inflammation, as observed in chapter 5 of this thesis and in separate *in vitro* and *in vivo* studies (Flood et al., 2007, Bonnet et al., 2015). Independent of NBQX intervention, this study demonstrated a potential pathological load induced increase in glutamate transporter expression (*eaat-1* and *eaat-3*; Figures 6.11, 6.12 and 6.17). This builds upon findings by Brakspear et al. (2009) indicating a role of glutamate transporters in bone signalling and mechanical loading.

NBQX intervention had a consistent repressive effect on the release of all pro- and anti-inflammatory markers analysed as well as OPG and glutamate release following pathological loading (Figures 6.18 to 6.29). This supports the anti-inflammatory, bone modulatory capacity indicated by gene expression analysis and represents a potential therapeutic impact of AMPA/KA receptor antagonism follow pathological loading. As identified by multivariate analysis (Table 6.5), the consistent trend across all immunoassay quantified biomarkers (bar IL-1β) of increased release over time after pathophysiological loadings (1 to 24hrs) and decrease in NBQX treatment groups compared to controls highlights both a load induced response in this model which can be used for comparison with different loading levels in future work and that these biomarkers can be used to detect the impact of a therapeutic intervention which, again, can be used to compare against future interventions (such as sustained release GluR antagonists).

Future work using this model to compare pathological loading and NBQX intervention to different loading levels (unloaded, physiological loading) would help further understanding of the role of osteocyte-like cell mediated glutamate signalling with inflammation and bone turnover. Additionally, this model could be used to deliver more evidence as to the impact of the timing and duration of NBQX intervention. The effects of a range of glutamate receptor antagonists with different receptor specificities could be investigated to identify which glutamate receptor subtype (ionotropic (AMPA, KA, NMDA) or metabotropic ($mGluR_{1-8}$) delivers the most potential as a therapeutic to target bone following traumatic loading.

This chapter addresses its overarching aim and contributes to the thesis hypothesis by defining a series of inflammatory, bone turnover and glutamate signalling biomarkers that increase over time following pathological levels of mechanical loading while responding to AMPA/KA GluR antagonist intervention. This model provides a platform to further investigate mechanically driven pathways in bone *in vitro.*

7.6. Limitations

7.6.1. GluR Antagonist Delivery Vehicles

7.6.1.1. Nanoparticle Characteristics

PLGA nanoparticle characteristics for size and PDI were quantified using DLS which is an indirect quantification method relying on refraction of particles through a suspension media. The heterogenous nature of synovial fluid as a suspension medium limits the accuracy of quantification of nanoparticles suspended within this fluid. Utilisation of filtered and centrifuged synovial fluid may have reduced this effect. The measurement of nanoparticles in more conventional suspension media (such as PBS) following exposure to synovial fluid, as carried out by Brown et al. (2019), could be utilised in future studies as an alternate method determining the impact of synovial fluid on nanoparticle physical properties. Fluorescent tagging of nanoparticles would have been another means of more direct nanoparticle quantification and allows for the possibility of monitoring nanoparticle cellular uptake via confocal microscopy (Xu et al., 2009). Nanoparticle toxicity was only measured with blank nanoparticles with the focus on determining the toxic effects of the delivery vehicle itself. However, any combinatorial toxic effects of PLGA nanoparticles and GluR antagonists were not determined. Additionally, toxic effects were only determined via an MTS assay which is a determination of cellular metabolic activity (Malich et al., 1997), use of additional cell viability quantification techniques such as LDH assays (measuring plasma membrane damage (Han et al., 2011)) or trypan blue staining (selectively stains dead cells with disrupted membranes (Strober, 1997)) would provide a measure of the number of dead cells as opposed to a quantification of cellular viability alone. Sustained GluR antagonist release from nanoparticles was not determined directly in an *in vivo* environment. Studies quantifying levels of GluR antagonist across multiple timepoints in synovial fluid following GluR antagonist loaded PLGA nanoparticle IA administration would be useful in determining *in vivo* sustained release characteristics.

7.6.1.2. Hydrogel Characteristics

Although the impact of 2.5mM DNQX drug loading on hydrogel rheological properties was determined, the effect of increased concentrations of GluR antagonist, such as 20mM used by Bonnet et al. (2020) or differing types of GluR antagonist (e.g. NBQX) was not quantified. DNQX release was only determined in PBS and not in *in vitro* and *ex-vivo* release media

(such as cell culture media or synovial fluid). Therefore, it is unknown whether sustained release will be affected by the environment into which hydrogels are delivering GluR antagonist. Additionally, release studies were only performed with DNQX, which may have differing release properties to NBQX. This would require quantification prior to any *in-vitro/in vivo* application. Future work utilising human membrane samples to quantify the diffusion properties of GluR antagonists from hydrogels would be more representative of clinical applications of this delivery vehicle. As with PLGA nanoparticles, hydrogel toxicity was only determined via MTS assay, additional cell viability techniques (e.g. Trypan blue, LDH assays) may be useful in determining more about the nature of any cytotoxic interactions with hydrogels. Hydrogel cytotoxicity was also determined indirectly by conditioning cell culture media with differing amounts of hydrogel across a range of timepoints. Direct application of hydrogels to cells in future studies may highlight differing cytotoxic effects.

7.6.1.3. Experimental Variability

The double emulsion PLGA nanoparticle synthesis methodology is a multistep process with various stages that could introduce variation within particle size characteristics, EE and drug release rates. The sonication stages of synthesis took place using a probe sonicator with the nanoparticle solution on ice. Efforts were made to ensure the nanoparticle solution beaker was consistently at the same depth within ice and that the probe sonicator was inserted into the solution at the same depth for each replicate. However, some variance due to the manual handling nature of this technique could be introduced, resulting in changes to the sonication mixing intensity to which nanoparticle replicates were exposed. Development of a rig to hold nanoparticle suspension over ice at consistently the same height would remove the human handling limitation from this process in future work. The evaporation stage of this process, to remove excess solvent (ethyl acetate), took place on a temperature-controlled plate. However, room temperature would have varied based on environmental conditions resulting in differing rates of solvent removal. Use of a temperature-controlled room for solvent evaporation would mitigate this risk.

The initial mixture of Pluronic F-127 and Carbopol-934 for hydrogels was homogenised over ice for 90 seconds. Efforts were made to ensure that the depth of the hydrogel mixture in ice and the position of the homogenizer blades were consistent between replicates. The use of a scaffold to hold samples in exactly the same position for each replicate would have removed any risk of manual handling variability. For rheological analysis, the rheometer itself was temperature controlled but the laboratory environment was not. Variance in laboratory temperature may; therefore, have introduced variance to rheological results. Using the rheometer in a temperature-controlled room would address this risk. For Franz Diffusion Cell studies through bovine synovial membranes, each membrane was extracted from a different carpal joint sample. It would be expected that there would be some variance in tissue properties as a consequence of the differences in age and size of the cow's that samples were extracted from. To minimise this limitation, samples could be requested from cows of the same age, breed, size and living conditions.

7.6.2. Limitations of 3D Cell Culture Assays

7.6.2.1. Cell Culture Replicates

A notable limitation of the cell culture studies carried out in this thesis is that n numbers were defined by cell culture well replicates for statistical comparison as opposed to repeat independent experiments. These studies were utilised as pilot studies with potential future applications as drug screening tools, where initially statistical significance is inferred from cell culture well replicates within one run as opposed to combinations of equivalent treatment group wells across multiple studies (Kitaeva et al., 2020, Larsson et al., 2020). However, with this approach any human error in experimental set up will not be captured and the variance of the effects observed in the cell culture models cannot be defined across multiple experimental runs (Lazic et al., 2018, Larsson et al., 2020). Carrying out repeat experiments with identical set ups would be a key future step in increasing the robustness of the interpretations derived from the models within this thesis and improving upon the understanding of biomarker variance following inflammatory stimulus, mechanical loading and GluR antagonist intervention.

7.6.2.2. Cellular Phenotype

Fluorescent imagery did indicate osteogenically differentiated Y201 MSCs, in both the loading and inflammatory studies, had osteocyte like dendritic morphology. There was a lack of *sost mRNA* expression identified in both *in vitro* models which is not representative of the osteocyte phenotype, although these cells did express *ocn* and *opg* which are both expressed in osteocytes phenotype, however, expression of primarily osteoblast markers *alp* and *col-1a1* was also detected (Dallas et al., 2013, Bellido, 2014, Prideaux et al., 2014). S*ost* a key regulator of bone formation (Winkler et al., 2003, Ten Dijke et al., 2008) is mechanically regulated (Robling et al., 2008, Tu et al., 2012) and regulated by inflammation (Heiland et al., 2010, Pathak et al., 2016). Y201 MSCs differentiated under these conditions have previously been shown to express osteocyte markers *sost, dmp-1* and *e11* in 3D collagen gels (Gilbert et al., 2020). The lack of *sost* mRNA expression in the 3D Y201 MSC studies in this thesis (chapters 5 and 6) may reflect low RNA yields/quality and require confirmation using immunological staining (Gilbert et al., (2020). If the lack of Sost is confirmed, there may be a requirement for extended culture time in future work to allow for full Y201 MSC differentiation into mature osteocytes. Replacing Y201 MSCs with primary osteocytes could address this limitation (Boukhechba et al., 2009, Nakashima et al., 2011, Prideaux et al., 2016) and primary human osteocytes have been shown to express osteocyte markers (*sost, dmp-1* and *e11*) when embedded in collagen gels in 3D (Bernhardt et al., 2020) so may provide a viable replacement for Y201 MSCs in these studies. However, this cell source is limited by sample availability and requires ethical consent to acquire.
The ocy 454 cell line has been shown to express SOST *in vitro* (Wein et al., 2015) and IDG-SW3 cell line has been shown to express SOST when cultured in 3D collagen type I gels (Woo et al., 2011). However, these are both maurine cell lines so not as representative of human genotypic and phenotypic heterogeneity as human sourced cells. Pre-osteocyte cell line HOB-01-C1 are human sourced, however, do not express mature osteocyte markers (e.g. SOST) when cultured *in vitro* (Bodine et al., 1996) so may not be a viable replacement for Y201 MSCs in this study. Multiple cell sources are available for 3D osteocyte-like cell culture, but each comes with its own limitations that need to be taken into consideration when planning further *in vitro* studies.

7.6.2.3. Mineralisation

The 3D cell culture system used in both the loading study and the inflammatory study was not mineralised and, therefore, not representative of mineralised bone *in vivo*. Mineralisation of collagen gels has been shown in previous studies (Woo et al., 2011, Scully et al., 2013, Scully, 2015). Mineralisation of collagen type I gels would make gels gradually stiffer, affecting the mechanical properties *in vitro* and has been associated with changes in IL-6 expression (Scully et al., 2013) and osteocyte differentiation, with increased mineralisation coinciding with increased levels of *sost* and *e11* osteocyte markers (Prideaux et al., 2012). Inhibition of mineralisation increases osteoblast markers (*ocn* and *col-1α1*) and decreases osteocyte markers (*sost, e11, dmp1, cd44*) (Prideaux et al., 2012). Mineralised 3D matrix would be more representative of the load bearing and inflammatory response of bone *in vivo* and impact the differentiation potential of osteocyte-like cells cultured in 3D. Further work investigating the impact of pathological, mechanical and inflammatory stimuli on mineralised 3D collagen type I matrices would be required to identify the impact of mineralisation to bone, glutamate and inflammatory signalling markers investigated in this thesis.

7.6.2.4. Experimental Variability

Some variability was identified across replicates in cell culture studies. This may be due to variability in model set up. The incorporation of Y201 MSCs within collagen gels, to ensure good cellular distribution but without introducing bubbles, must be performed consistently to prevent variance in cell number between replicates. Such variance could result in altered differentiation and signalling responses to inflammation and loading between replicates. Increasing cell number would be a potential solution, thereby, decreasing the risk of cell number variance between replicates. However, investigation into the 3D culture of multiple different osteocyte-like cells lines (MLO-Y4, IDGSW3, hOBs and Y201 MSCs) (Vazquez, 2013, Scully, 2015, Gilbert et al., 2020) means that cell numbers used in this study have been previously optimised and too many cells could result in constriction of collagen type I 3D gels. Additionally, any further changes in cell number would need to be monitored for phenotypic and signalling effects. An area that could result in experimental variability,

specific to the inflammatory study, could manifest from differences in the NBQX loaded PLGA nanoparticle treatment group. Nanoparticles were added to cells at a concentration of 10mg/ml. This assumes a uniform suspension of nanoparticles in the media. Any differences in suspension or nanoparticle sedimentation would result in variability in treatment concentrations between replicates. Ensuring adequate suspension immediately prior to cellular application of this treatment groups would be a method to minimise this potential effect.

7.6.2.5. Inflammatory Stimulus

The concentrations of the inflammatory IL-6 stimulus used in the inflammatory bone model in chapter 5 was justified based on patient IL-6 levels quantified in synovial fluid following joint injury (Watt et al., 2016) (5ng/ml). However, there is a large amount of variance in IL-6 release between patients (100-10,000pg/ml) given differences in patient age, physiology and injury forces. To our knowledge, a study quantifying levels of sIL-6r in synovial fluid of patients following joint injury has not been carried out. However, prior experiments applying an IL-6 signalling inflammatory stimulus on osteocytes have used 40ng/ml of sIL-6r (Bakker et al., 2014). This falls within the range of sIL-6r concentrations that has been shown to be present in OA patient synovial fluid (approximately 45±10 ng/ml (mean±SEM)) (Kotake et al., 1996). Therefore, this concentration was used in the IL-6 inflammatory study in this thesis (chapter 5). However, other studies have demonstrated lower levels of sIL-6r in the synovial fluid of OA patients (10.5±5ng/ml) (Desgeorges et al., 1997). Therefore, as with IL-6, sIL-6r levels have been shown to vary within the synovial fluid of OA and RA patients (Kotake et al., 1996, Desgeorges et al., 1997) possibly representing the variability in disease pathology. To account for the range of IL-6 and sIL-6r concentrations seen *in vivo*, experiments utilising a range of IL-6 concentrations in this model could be carried out. Following this, investigations into the differences in data output (e.g. mRNA and protein) would allow for greater understanding of the impact of the natural variability of this inflammatory marker. To our knowledge, studies on the levels of sIL-6r in the synovial fluid of patients following joint injury have not been carried out but significantly increased levels of sIL-6r have been identified in inflammatory arthropathies (RA and gout) compared to OA (Kotake et al., 1996, Desgeorges et al., 1997). This indicates differing joint pathologies result

in changes to sIL-6s production in the joint. This then indicates that the acute inflammation and damage caused by joint injury may result in changes to sIL-6r release compared to healthy joints. Studies quantifying the sIL-6r levels in the synovial fluid of patients following joint injury would be useful in further understanding the inflammatory impact of trauma to the joint.

7.6.2.6. Loading Device

The mechanical loading apparatus has some limitations. The impact of repeated usage on silicon plate elastic properties was not measured and could account for experimental variation. Visual inspection of silicon plates did reveal some variability in colour and texture, this may have manifested in changes to the mechanical properties of the plate. The generation of a new batch of silicon loading plates and consistent monitoring of their mechanical properties would be useful in mitigating any risk of variation due to the plates. Additionally, the aforementioned potential for variability in cell number in 3D type I collagen gels (section 7.6.2.3) could result in different impacts of strain across replicates. The strain applied by the loading device was not directly measured in each replicate well within the silicon plate. Therefore, there could also have been variability in the strain applied to cells across replicates. Application of speckle patterns to measure strain caused by mechanical loading in each well could be a method of tracking the magnitude of strain across each replicate.

7.7. Final Conclusions

To address the hypothesis of this thesis, sustained delivery vehicles were developed and shown to be capable of delivery of both low concentrations of sustained GluR antagonist over weeks via PLGA nanoparticles (chapter 3) and high concentrations over hours via thermo responsive Pluronic F-127/Carbopol 934 hydrogels (chapter 4). Application of both pathological inflammation (chapter 5) and mechanical loading (chapter 6) stimuli in 3D *in vitro* osteogenically differentiated Y201 MSC models highlighted the interconnected role glutamate signalling plays with both inflammation and bone turnover and provided evidence of potential biomarkers for the investigation of future therapeutic interventions in

both *in vitro* pathological inflammation or load exposed 3D environments. Sustained NBQX release from nanoparticles did not elicit a beneficial effect but did highlight a correlation between upregulation of both IL-6 signalling and glutamate in bone.

In terms of the potential of models investigated in this thesis as drug screening tools, NBQX treatment of osteogenically differentiated Y201 MSCs for 24hrs after loading did decrease bone turnover, inflammation, and glutamate signalling. There was also a protective effect on bone turnover, an increase in anti-inflammatory marker release and decrease in glutamate release following 1hr NBQX exposure in the inflammatory model. Future work may look to compare the data generated with NBQX application in this thesis against alternate intervention timings, delivery durations (potentially from sustained vehicles investigated in this thesis) or GluR antagonist specificities to build a robust understanding of the impact of GluR antagonism towards inflammatory or mechanically driven pathways in bone.

As there was no clearance of NBQX in the loading model, this may point towards a therapeutic benefit of sustained high concentrations of NBQX, a capacity which the hydrogels in chapter 4 of this thesis would be able to deliver. Therefore, future application of the GluR antagonist loaded hydrogels developed in this thesis to supply a high concentration (mM), easily controllable (no encapsulation losses), sustained delivery (up to 27hrs) of NBQX to *in vitro* and *in vivo* models of PTOA (Bonnet et al., 2020) has the potential to improve upon the promising therapeutic potential of ionotropic GluR antagonists in the treatment of joint disease.

Having provided an initial understanding into the protective effects of AMPA/KA GluR antagonism (via NBQX) in both inflammatory and pathological loading 3D bone *in vitro* models (chapters 5 and 6) and demonstrating the development of two GluR antagonist loaded sustained delivery systems from which GluR sustained release may now be further investigated (chapters 3 and 4) the work of this thesis addresses the hypothesis and provides an insight against which future analysis may be compared to improve the understanding of inflammatory and mechanically driven pathways in bone.

Chapter 8

References

ABDELWAHED, W., DEGOBERT, G., STAINMESSE, S. & FESSI, H. 2006. Freeze-drying of nanoparticles: Formulation, process and storage considerations. *Advanced Drug Delivery Reviews,* 58**,** 1688-1713.

ABDI, S. I. H., CHOI, J. Y., LEE, J. S., LEE, H. J., LEE, C., KIM, J. & CHUNG, H. Y. 2012. In Vivo study of a blended hydrogel composed of pluronic F-127-alginate-hyaluronic acid for its cell injection application. *Tissue Engineering and Regenerative Medicine* 9**,** 1-9.

ABE, Y., CHIBA, M., YAKLAI, S., PECHAYCO, R. S., SUZUKI, H. & TAKAHASHI, T. 2019. Increase in bone metabolic markers and circulating osteoblast-lineage cells after orthognathic surgery. *Scientific Reports,* 9**,** 20106.

ADAES, S., MENDONCA, M., SANTOS, T. N., CASTRO-LOPES, J. M., FERREIRA-GOMES, J. & NETO, F. L. 2014. Intra-articular injection of collagenase in the knee of rats as an alternative model to study nociception associated with osteoarthritis. *Arthritis Res Ther,* 16**,** R10.

ADEBILEJE, T. & AMANI, A. 2018. Modelling particle size, drug loading and release of BSA encapsulated into PLGA nanoparticles *J Material Sci Eng,* 7.

AGLIETTI, P., BUZZI, R., BASSI, P. B. & FIORITI, M. 1994. Arthroscopic drilling in juvenile osteochondritis dissecans of the medial femoral condyle. *Arthroscopy: The Journal of Arthroscopic & Related Surgery,* 10**,** 286-291.

AGUIRRE, J., BUTTERY, L., O'SHAUGHNESSY, M., AFZAL, F., FERNANDEZ DE MARTICORENA, I., HUKKANEN, M., HUANG, P., MACINTYRE, I. & POLAK, J. 2001. Endothelial Nitric Oxide Synthase Gene-Deficient Mice Demonstrate Marked Retardation in Postnatal Bone Formation, Reduced Bone Volume, and Defects in Osteoblast Maturation and Activity. *Am J Pathol,* 158**,** 247-57.

AHERN, B. J., PARVIZI, J., BOSTON, R. & SCHAER, T. P. 2009. Preclinical animal models in single site cartilage defect testing: a systematic review. *Osteoarthritis Cartilage,* 17**,** 705-13.

AHMED, A. B. & BHADURI, I. 2017. Development and Evaluation of Assam Bora Rice Starch-Carbopol Based Oral Mucoadhesive Gel of Irinotecan for Mouth Cancer. *Journal of Pharmacetical Sciences and Research,* 9**,** 1139-1146.

AHSAN, F., RIVAS, I. P., KHAN, M. A. & TORRES SUÁREZ, A. I. 2002. Targeting to macrophages: role of physicochemical properties of particulate carriers—liposomes and microspheres—on the phagocytosis by macrophages. *Journal of Controlled Release,* 79**,** 29-40.

AITKEN, D., LASLETT, L. L., PAN, F., HAUGEN, I. K., OTAHAL, P., BELLAMY, N., BIRD, P. & JONES, G. 2018. A randomised double-blind placebo-controlled crossover trial of HUMira (adalimumab) for erosive hand OsteoaRthritis - the HUMOR trial. *Osteoarthritis Cartilage,* 26**,** 880-887.

AJRAWAT, P., DWYER, T. & CHAHAL, J. 2019. Autologous Interleukin 1 Receptor Antagonist Blood-Derived Products for Knee Osteoarthritis: A Systematic Review. *Arthroscopy: The Journal of Arthroscopic & Related Surgery,* 35**,** 2211-2221.

AJUBI, N. E., KLEIN-NULEND, J., ALBLAS, M. J., BURGER, E. H. & NIJWEIDE, P. J. 1999. Signal transduction pathways involved in fluid flow-induced PGE2 production by cultured osteocytes. *American Journal of Physiology-Endocrinology and Metabolism,* 276**,** E171-E178.

AKASH, M. S. H., REHMAN, K., LI, N., GAO, J.-Q., SUN, H. & CHEN, S. 2012. Sustained Delivery of IL-1Ra from Pluronic F127-Based Thermosensitive Gel Prolongs its Therapeutic Potentials. *Pharm Res,* 29**,** 3475-3485.

AKASH, M. S. H. & REHMAN, K. 2015. Recent progress in biomedical applications of Pluronic (PF127): Pharmaceutical perspectives. *J Control Release,* 209**,** 120-38.

AKHTER, M. P., CULLEN, D. M., PEDERSEN, E. A., KIMMEL, D. B. & RECKER, R. R. 1998. Bone response to in vivo mechanical loading in two breeds of mice. *Calcif Tissue Int,* 63**,** 442-9.

ALI, A., KHALID, I., USMAN MINHAS, M., BARKAT, K., KHAN, I. U., SYED, H. K. & UMAR, A. 2019. Preparation and in vitro evaluation of Chondroitin sulfate and carbopol based mucoadhesive controlled release polymeric composites of Loxoprofen using factorial design. *European Polymer Journal,* 121**,** 109312.

ALLAIRE, R., MURIUKI, M., GILBERTSON, L. & HARNER, C. D. 2008. Biomechanical Consequences of a Tear of the Posterior Root of the Medial Meniscus: Similar to Total Meniscectomy. *JBJS,* 90**,** 1922-1931.

ALOE, L., TUVERI, M. A., CARCASSI, U. & LEVI-MONTALCINI, R. 1992. Nerve growth factor in the synovial fluid of patients with chronic arthritis. *Arthritis & Rheumatism,* 35**,** 351-355.

ALONZI, T., FATTORI, E., LAZZARO, D., COSTA, P., PROBERT, L., KOLLIAS, G., DE BENEDETTI, F., POLI, V. & CILIBERTO, G. 1998. Interleukin 6 Is Required for the Development of Collagen-induced Arthritis. *The Journal of Experimental Medicine,* 187**,** 461.

ALSTERGREN, P., ERNBERG, M., NILSSON, M., HAJATI, A. K., SESSLE, B. J. & KOPP, S. 2010. Glutamate-induced temporomandibular joint pain in healthy individuals is partially mediated by peripheral NMDA receptors. *J Orofac Pain,* 24**,** 172-80.

ALTINDAL, D. Ç. & GÜMÜŞDERELIOĞLU, M. 2016. Melatonin releasing PLGA micro/nanoparticles and their effect on osteosarcoma cells. *Journal of Microencapsulation,* 33**,** 53-63.

ALTMAN, R. D. & GOLD, G. E. 2007. Atlas of individual radiographic features in osteoarthritis, revised. *Osteoarthritis and Cartilage,* 15**,** A1-A56.

ALWANI, S., KAUR, R., MICHEL, D., CHITANDA, J., VERRALL, R. & KARUNAKARAN, C. 2015. Lysine-functionalized nanodiamonds as gene carriers: development of stable colloidal dispersion for in vitro cellular uptake studies and siRNA delivery application. *International Journal of Nanomedicine* 2016:11**,** 687-702.

AMIDON, G. L., LENNERNÄS, H., SHAH, V. P. & CRISON, J. R. 1995. A theoretical basis for a biopharmaceutic drug classification: the correlation of in vitro drug product dissolution and in vivo bioavailability. *Pharm Res,* 12**,** 413-20.

AMJADI, I., RABIEE, M. & HOSSEINI, M.-S. 2013. Anticancer Activity of Nanoparticles Based on PLGA and its Co-polymer: In-vitro Evaluation. *Iranian journal of pharmaceutical research : IJPR,* 12**,** 623-634.

AMORNDOLJAI, P., TANEEPANICHSKUL, S., NIEMPOOG, S. & NIMMANNIT, U. 2015. Improving of Knee Osteoarthritic Symptom by the Local Application of Ginger Extract Nanoparticles: A Preliminary Report with Short Term Follow-Up. *J Med Assoc Thai,* 98**,** 871-7.

ANDERSEN, C. L., JENSEN, J. L. & ORNTOFT, T. F. 2004. Normalization of real-time quantitative reverse transcription-PCR data: a model-based variance estimation approach to identify genes suited for normalization, applied to bladder and colon cancer data sets. . *Cancer Research* 64**,** 5245-5250.

ANDERSON, D. D., CHUBINSKAYA, S., GUILAK, F., MARTIN, J. A., OEGEMA, T. R., OLSON, S. A. & BUCKWALTER, J. A. 2011. Post-traumatic osteoarthritis: Improved understanding

and opportunities for early intervention. *Journal of Orthopaedic Research,* 29**,** 802-809.

ANDRIACCHI, T. P., FAVRE, J., ERHART-HLEDIK, J. C. & CHU, C. R. 2015. A Systems View of Risk Factors for Knee Osteoarthritis Reveals Insights into the Pathogenesis of the Disease. *Annals of Biomedical Engineering,* 43**,** 376-387.

ANIKSZTEJN, L., CHARRIAUT-MARLANGUE, C., ROISIN, M. P. & BEN-ARI, Y. 1990. Long-term potentiation in the rat hippocampus induced by the mast cell degranulating peptide: Analysis of the release of endogenous excitatory amino acids and proteins. *Neuroscience,* 35**,** 63-70.

ARAUJO-PIRES, A. C., VIEIRA, A. E., FRANCISCONI, C. F., BIGUETTI, C. C., GLOWACKI, A., YOSHIZAWA, S., CAMPANELLI, A. P., TROMBONE, A. P. F., SFEIR, C. S., LITTLE, S. R. & GARLET, G. P. 2015. IL-4/CCL22/CCR4 Axis Controls Regulatory T-Cell Migration That Suppresses Inflammatory Bone Loss in Murine Experimental Periodontitis. *Journal of Bone and Mineral Research,* 30**,** 412-422.

ARDEN, N. & NEVITT, M. C. 2006. Osteoarthritis: Epidemiology. *Best Practice & Research Clinical Rheumatology,* 20**,** 3-25.

ARIAS, J. L., LÓPEZ-VIOTA, M., LÓPEZ-VIOTA, J. & DELGADO, Á. V. 2009. Development of iron/ethylcellulose (core/shell) nanoparticles loaded with diclofenac sodium for arthritis treatment. *International Journal of Pharmaceutics,* 382**,** 270-276.

ARRICH, J., PIRIBAUER, F., MAD, P., SCHMID, D., KLAUSHOFER, K. & MÜLLNER, M. 2005. Intra-articular hyaluronic acid for the treatment of osteoarthritis of the knee: systematic review and meta-analysis. *Canadian Medical Association Journal,* 172**,** 1039-1043.

ARROLL, B. & GOODYEAR-SMITH, F. 2004. Corticosteroid injections for osteoarthritis of the knee: meta-analysis. *BMJ,* 328**,** 869.

ARZI, B., WISNER, E. R., HUEY, D. J., KASS, P. H., HU, J. & ATHANASIOU, K. A. 2012. A proposed model of naturally occurring osteoarthritis in the domestic rabbit. *Lab Animal,* 41**,** 20-25.

ASHRAF, S., MAPP, P. I. & WALSH, D. A. 2011. Contributions of angiogenesis to inflammation, joint damage, and pain in a rat model of osteoarthritis. *Arthritis & Rheumatism,* 63**,** 2700-2710.

ATKINS, G. J. & FINDLAY, D. M. 2012. Osteocyte regulation of bone mineral: a little give and take. *Osteoporosis International,* 23**,** 2067-2079.

ATTUR, M., BELITSKAYA-LÉVY, I., OH, C., KRASNOKUTSKY, S., GREENBERG, J., SAMUELS, J., SMILES, S., LEE, S., PATEL, J., AL-MUSSAWIR, H., MCDANIEL, G., KRAUS, V. B. & ABRAMSON, S. B. 2011. Increased interleukin-1β gene expression in peripheral blood leukocytes is associated with increased pain and predicts risk for progression of symptomatic knee osteoarthritis. *Arthritis & Rheumatism,* 63**,** 1908-1917.

AYRAL, X., RAVAUD, P., BONVARLET, J. P., SIMONNET, J., LECURIEUX, R., NGUYEN, M., SAUVAGE, E. & DOUGADOS, M. 1999. Arthroscopic evaluation of post-traumatic patellofemoral chondropathy. *J Rheumatol,* 26**,** 1140-7.

AZEVEDO, M. A., BOURBON, A. I., VICENTE, A. A. & CERQUEIRA, M. A. 2014. Alginate/chitosan nanoparticles for encapsulation and controlled release of vitamin B2. *International Journal of Biological Macromolecules,* 71**,** 141-146.

AZUMA, Y., KAJI, K., KATOGI, R., TAKESHITA, S. & KUDO, A. 2000. Tumor necrosis factor-alpha induces differentiation of and bone resorption by osteoclasts. *J Biol Chem,* 275**,** 4858-64.

BAE, S. E., CHOI, D. H., HAN, K. H. & PARK, P. 2010. Effect of temporally controlled release of dexamethasone on in vivo chondrogenic differentiation of mesenchymal stromal cells. *Journal of Controlled Release,* 143**,** 23-30.

BAILEY, A. J. & MANSELL, J. P. 1997. Do subchondral bone changes exacerbate or precede articular cartilage destruction in osteoarthritis of the elderly? *Gerontology,* 43**,** 296-304.

BAILEY, D. A., FAULKNER, R. A. & MCKAY, H. A. 1996. Growth, Physical Activity, and Bone Mineral Acquisition. *Exercise and Sport Sciences Reviews,* 24**,** 233-266.

BAJAJ, P., BAJAJ, P., GRAVEN-NIELSEN, T. & ARENDT-NIELSEN, L. 2001. Osteoarthritis and its association with muscle hyperalgesia: an experimental controlled study. *Pain,* 93**,** 107-114.

BAJPAYEE, A. G., WONG, C. R., BAWENDI, M. G., FRANK, E. H. & GRODZINSKY, A. J. 2014. Avidin as a model for charge driven transport into cartilage and drug delivery for treating early stage post-traumatic osteoarthritis. *Biomaterials,* 35**,** 538-549.

BAJPAYEE, A. G., QUADIR, M. A., HAMMOND, P. T. & GRODZINSKY, A. J. 2016. Charge based intra-cartilage delivery of single dose dexamethasone using Avidin nano-carriers suppresses cytokine-induced catabolism long term. *Osteoarthritis Cartilage,* 24**,** 71-81.

BAKER, P. J., DIXON, M., EVANS, R. T., DUFOUR, L., JOHNSON, E. & ROOPENIAN, D. C. 1999. CD4(+) T cells and the proinflammatory cytokines gamma interferon and interleukin-6 contribute to alveolar bone loss in mice. *Infect Immun,* 67**,** 2804-9.

BAKKER, A. D., SILVA, V. C., KRISHNAN, R., BACABAC, R. G., BLAAUBOER, M. E., LIN, Y. C., MARCANTONIO, R. A., CIRELLI, J. A. & KLEIN-NULEND, J. 2009. Tumor necrosis factor alpha and interleukin-1beta modulate calcium and nitric oxide signaling in mechanically stimulated osteocytes. *Arthritis Rheum,* 60**,** 3336-45.

BAKKER, A. D., KULKARNI, R. N., KLEIN-NULEND, J. & LEMS, W. F. 2014. IL-6 alters osteocyte signaling toward osteoblasts but not osteoclasts. *J Dent Res,* 93**,** 394-9.

BALEMANS, W., PATEL, N., EBELING, M., VAN HUL, E., WUYTS, W., LACZA, C., DIOSZEGI, M., DIKKERS, F. G., HILDERING, P., WILLEMS, P. J., VERHEIJ, J. B. G. M., LINDPAINTNER, K., VICKERY, B., FOERNZLER, D. & VAN HUL, W. 2002. Identification of a 52 kb deletion downstream of the SOST gene in patients with van Buchem disease. *Journal of Medical Genetics,* 39**,** 91-97.

BANNURU, R., DASI, U. R. & MCALINDON, T. E. 2010. Reassessing the role of acetaminophen in osteoarthritis: systematic review and meta-analysis. *Osteoarthritis and Cartilage,* 18**,** S250.

BANNURU, R. R., NATOV, S. N., OBADAN, I. E., PRICE, L. L., SCHMID, C. H. & MCALINDON, T. E. 2009. Therapeutic trajectory of hyaluronic acid versus corticosteroids in the treatment of knee osteoarthritis: a systematic review and meta-analysis. *Arthritis Rheum,* 61**,** 1704-11.

BANNURU, R. R., NATOV, N. S., DASI, U. R., SCHMID, C. H. & MCALINDON, T. E. 2011. Therapeutic trajectory following intra-articular hyaluronic acid injection in knee osteoarthritis-meta-analysis. *Osteoarthritis Cartilage,* 19**,** 611-9.

BANQUY, X., LEE, D. W., DAS, S., HOGAN, J. & ISRAELACHVILI, J. N. 2014. Shear-induced aggregation of mammalian synovial fluid components under boundary lubrication conditions. *Advanced Functional Materials* 24**,** 3152-3161.

BANSBACK, N., TRENAMAN, L. & HARRISON, M. 2015. How Important Is Mode of Administration in Treatments for Rheumatic Diseases and Related Conditions? *Current Rheumatology Reports* 17.

BANTZ, C., KOSHKINA, O., LANG, T., GALLA, H.-J., KIRKPATRICK, C. J., STAUBER, R. H. & MASKOS, M. 2014. The surface properties of nanoparticles determine the agglomeration state and the size of the particles under physiological conditions. *Beilstein J. Nanotechnology* 5**,** 1774-1786.

BARICHELLO, J. M., MORISHITA, M., TAKAYAMA, K. & NAGAI, T. 1999. Absorption of insulin from Pluronic F-127 gels following subcutaneous administration in rats. *International Journal of Pharmaceutics,* 184**,** 189-198.

BARKER, T., ROGERS, V. E., HENRIKSEN, V. T., AGUIRRE, D., TRAWICK, R. H., RASMUSSEN, G. L. & MOMBERGER, N. G. 2014. Serum cytokines are increased and circulating micronutrients are not altered in subjects with early compared to advanced knee osteoarthritis. *Cytokine,* 68**,** 133-136.

BARON, R. & KNEISSEL, M. 2013. WNT signaling in bone homeostasis and disease: from human mutations to treatments. *Nat Med,* 19**,** 179-92.

BARRY, B. W. 2001. Novel mechanisms and devices to enable successful transdermal drug delivery. *European Journal of Pharmaceutical Sciences,* 14**,** 101-114.

BAŞARAN, G., ÖZER, T., KAYA, F. A. & HAMAMCI, O. 2006. Interleukins 2, 6, and 8 levels in human gingival sulcus during orthodontic treatment. *American Journal of Orthodontics and Dentofacial Orthopedics,* 130**,** 7.e1-7.e6.

BASCHANT, U., FRAPPART, L., RAUCHHAUS, U., BRUNS, L., REICHARDT, H. M., KAMRADT, T., BRÄUER, R. & TUCKERMANN, J. P. 2011. Glucocorticoid therapy of antigen-induced arthritis depends on the dimerized glucocorticoid receptor in T cells. *Proceedings of the National Academy of Sciences,* 108**,** 19317-19322.

BATISTE, D. L., KIRKLEY, A., LAVERTY, S., THAIN, L. M. F., SPOUGE, A. R. & HOLDSWORTH, D. W. 2004. Ex vivo characterization of articular cartilage and bone lesions in a rabbit ACL transection model of osteoarthritis using MRI and micro-CT. *Osteoarthritis and Cartilage,* 12**,** 986-996.

BEARD, D. J., DAVIES, L. J., COOK, J. A., MACLENNAN, G., PRICE, A., KENT, S., HUDSON, J., CARR, A., LEAL, J., CAMPBELL, H., FITZPATRICK, R., ARDEN, N., MURRAY, D., CAMPBELL, M. K., BARKER, K., MURRAY, G., SIMPSON, H., DODWELL, D., DONELL, S., WAITE, J., ARDEN, N., BEARD, D., CAMPBELL, H., CARR, A., COOPER, C., DAVIES, L., DOLL, H., KENT, S., LEAL, J., FITZPATRICK, R., MURRAY, D., PRICE, A., COOK, J., CAMPBELL, M., FERNIE, G., MCDONALD, A., DUNCAN, A., CASTILLO, M., FUSCO, F., GRESHON, A., HOLLAND, K., LI, J., RABAIOTTI, E., REGAN, S., STALKER, V., FORREST, M., MACLENNAN, G., MCPHERSON, G., BOACHIE, C., COLLINS, D., CRUDEN, J., HALPIN, S., SMITH, B., TORGERSON, D., MAHER, C., BROWNSON, P., MULLINS, M. M., BLAZEBY, J., JENKINS, R., LEWIS, M., MINTOWT-CZYZ, W., BEVERLAND, B., BRYCE, L., CATNEY, J., DOBIE, I., DORAN, E., O'BRIEN, S., ALI, F., CRIPPS, H., WHILEMAN, A., WILLIAMS, P., TOMS, J., BROWN, E., HORNER, G., JENNINGS, A., ROSE, G., BAMFORD, F., GODDARD, W., MARYNISSEN, H., PEEL, H., RICHARDS, L., BELL, A., DEO, S., GRAYLAND, S., HOLLINGHURST, D., PEGLER, S., SATISH, V., WOODRUFFE, C., LONDON, N., DUFFY, D., BENNETT, C., FEATHERSTONE, J., COOK, J., DEARNLEY, K., MUTHUKUMAR, N., ONUOHA, L., WILSON, S., BANHER, S., EMEAKAROHA, E., HOROHAN, J., et al. 2019. The clinical and cost-effectiveness of total versus partial

knee replacement in patients with medial compartment osteoarthritis (TOPKAT): 5-year outcomes of a randomised controlled trial. *The Lancet,* 394**,** 746-756.
BEAVER, R. J., MAHOMED, M., BACKSTEIN, D., DAVIS, A., ZUKOR, D. J. & GROSS, A. E. 1992. Fresh osteochondral allografts for post-traumatic defects in the knee. A survivorship analysis. *The Journal of Bone and Joint Surgery. British volume,* 74-B**,** 105-110.
BEDSON, J. & CROFT, P. R. 2008. The discordance between clinical and radiographic knee osteoarthritis: A systematic search and summary of the literature. *BMC Musculoskeletal Disorders,* 9**,** 116.
BEEKHUIZEN, M., BASTIAANSEN-JENNISKENS, Y. M., KOEVOET, W., SARIS, D. B. F., DHERT, W. J. A., CREEMERS, L. B. & VAN OSCH, G. J. V. M. 2011. Osteoarthritic synovial tissue inhibition of proteoglycan production in human osteoarthritic knee cartilage: Establishment and characterization of a long-term cartilage–synovium coculture. *Arthritis & Rheumatism,* 63**,** 1918-1927.
BELLIDO, M., LUGO, L., ROMAN-BLAS, J. A., CASTAÑEDA, S., CAEIRO, J. R., DAPIA, S., CALVO, E., LARGO, R. & HERRERO-BEAUMONT, G. 2010. Subchondral bone microstructural damage by increased remodelling aggravates experimental osteoarthritis preceded by osteoporosis. *Arthritis Research & Therapy,* 12**,** R152.
BELLIDO, T. 2014. Osteocyte-Driven Bone Remodeling. *Calcified Tissue International,* 94**,** 25-34.
BELMONT JR, P. J., GOODMAN, G. P., WATERMAN, B. R., BADER, J. O. & SCHOENFELD, A. J. 2014. Thirty-Day Postoperative Complications and Mortality Following Total Knee Arthroplasty: Incidence and Risk Factors Among a National Sample of 15,321 Patients. *Am J of Bone and Joint Surgery* 96**,** 20-26.
BEMEUR, C., STE-MARIE, L., DESJARDINS, P., HAZELL, A. S., VACHON, L., BUTTERWORTH, R. & MONTGOMERY, J. 2004. Decreased beta-actin mRNA expression in hyperglycemic focal cerebral ischemia in the rat. *Neurosci Lett,* 357**,** 211-4.
BENDELE, A. M. 1987. Progressive chronic osteoarthritis in femorotibial joints of partial medial meniscectomized guinea pigs. *Vet Pathol,* 24**,** 444-8.
BENDELE, A. M. & HULMAN, J. F. 1991. Effects of Body Weight Restriction on the Development and Progression of Spontaneous Osteoarthritis in Guinea Pigs. *Arthritis & Rheumatism,* 34**,** 1180-1184.
BENDJABALLAH, M. Z., SHIRAZI-ADL, A. & ZUKOR, D. J. 1997. Finite element analysis of human knee joint in varus-valgus. *Clinical Biomechanics,* 12**,** 139-148.
BENDRE, M. S., MONTAGUE, D. C., PEERY, T., AKEL, N. S., GADDY, D. & SUVA, L. J. 2003. Interleukin-8 stimulation of osteoclastogenesis and bone resorption is a mechanism for the increased osteolysis of metastatic bone disease. *Bone,* 33**,** 28-37.
BENITO, M. J., VEALE, D. J., FITZGERALD, O., VAN DEN BERG, W. B. & BRESNIHAN, B. 2005. Synovial tissue inflammation in early and late osteoarthritis. *Annals of the Rheumatic Diseases,* 64**,** 1263-1267.
BERENBAUM, F. 2013. Osteoarthritis as an inflammatory disease (osteoarthritis is not osteoarthrosis!). *Osteoarthritis and Cartilage,* 21**,** 16-21.
BERGSCHMIDT, P., BADER, R., FINZE, S., SCHULZE, C., KUNDT, G. & MITTELMEIER, W. 2011. Comparative Study of Clinical and Radiological Outcomes of Unconstrained Bicondylar Total Knee Endoprostheses with Anti-allergic Coating. *Open Orthop J,* 5**,** 354-360.

BERJON, J. J., MUNUERA, L. & CALVO, M. 1991. Degenerative lesions in the articular cartilage after meniscectomy: preliminary experimental study in dogs. *J Trauma,* 31**,** 342-50.

BERNARDEAU, C., BUCKI, B. & LIOTE, F. 2001. Acute arthritis after intra-articular hyaluronate injection: onset of effusions without crystal. *Ann Rheum Dis,* 60**,** 518-20.

BERNHARDT, A., ÖSTERREICH, V. & GELINSKY, M. 2020. Three-Dimensional Co-culture of Primary Human Osteocytes and Mature Human Osteoclasts in Collagen Gels. *Tissue Engineering Part A,* 26**,** 647-655.

BETTICA, P., CLINE, G., HART, D. J., MEYER, J. & SPECTOR, T. D. 2002. Evidence for increased bone resorption in patients with progressive knee osteoarthritis: longitudinal results from the Chingford study. *Arthritis Rheum,* 46**,** 3178-84.

BEUF, O., GHOSH, S., NEWITT, D. C., LINK, T. M., STEINBACH, L., RIES, M., LANE, N. & MAJUMDAR, S. 2002. Magnetic resonance imaging of normal and osteoarthritic trabecular bone structure in the human knee. *Arthritis Rheum,* 46**,** 385-93.

BEYNNON, B. D., JOHNSON, R. J., ABATE, J. A., FLEMING, B. C. & NICHOLS, C. E. 2005. Treatment of Anterior Cruciate Ligament Injuries, Part I. *The American Journal of Sports Medicine,* 33**,** 1579-1602.

BHALA, N., EMBERSON, J., MERHI, A., ABRAMSON, S., ARBER, N., BARON, J. A., BOMBARDIER, C., CANNON, C., FARKOUH, M. E., FITZGERALD, G. A., GOSS, P., HALLS, H., HAWK, E., HAWKEY, C., HENNEKENS, C., HOCHBERG, M., HOLLAND, L. E., KEARNEY, P. M., LAINE, L., LANAS, A., LANCE, P., LAUPACIS, A., OATES, J., PATRONO, C., SCHNITZER, T. J., SOLOMON, S., TUGWELL, P., WILSON, K., WITTES, J. & BAIGENT, C. 2013. Vascular and upper gastrointestinal effects of non-steroidal anti-inflammatory drugs: meta-analyses of individual participant data from randomised trials. *Lancet,* 382**,** 769-79.

BHANGU, P. S., GENEVER, P. G., SPENCER, G. J., GREWAL, T. S. & SKERRY, T. M. 2001. Evidence for targeted vesicular glutamate exocytosis in osteoblasts. *Bone,* 29**,** 16-23.

BHATTACHARJEE, A., SHUKLA, M., YAKUBENKO, V. P., MULYA, A., KUNDU, S. & CATHCART, M. K. 2013. IL-4 and IL-13 employ discrete signaling pathways for target gene expression in alternatively activated monocytes/macrophages. *Free Radic Biol Med,* 54**,** 1-16.

BHATTACHARJEE, S. 2016. DLS and zeta potential – What they are and what they are not? *Journal of Controlled Release,* 235**,** 337-351.

BILGEN, B., ORSINI, E., AARON, R. K. & CIOMBOR, D. M. 2007. FBS suppresses TGF-β1-induced chondrogenesis in synoviocyte pellet cultures while dexamethasone and dynamic stimuli are beneficial. *Journal of Tissue Engineering and Regenerative Medicine,* 1**,** 436-442.

BILLINGHURST, R. C., DAHLBERG, L., IONESCU, M., REINER, A., BOURNE, R., RORABECK, C., MITCHELL, P., HAMBOR, J., DIEKMANN, O., TSCHESCHE, H., CHEN, J., VAN WART, H. & POOLE, A. R. 1997. Enhanced cleavage of type II collagen by collagenases in osteoarthritic articular cartilage. *The Journal of Clinical Investigation,* 99**,** 1534-1545.

BINDER, N. B., PUCHNER, A., NIEDERREITER, B., HAYER, S., LEISS, H., BLÜML, S., KREINDL, R., SMOLEN, J. S. & REDLICH, K. 2013. Tumor necrosis factor-inhibiting therapy preferentially targets bone destruction but not synovial inflammation in a tumor necrosis factor-driven model of rheumatoid arthritis. *Arthritis Rheum,* 65**,** 608-17.

BIRCHALL, J. C., CLEMO, R., ANSTEY, A. & JOHN, D. N. 2011. Microneedles in Clinical Practice–An Exploratory Study Into the Opinions of Healthcare Professionals and the Public. *Pharmaceutical Research,* 28**,** 95-106.

BISHNOI, M., JAIN, A., HURKAT, P. & JAIN, S. K. 2014. Aceclofenac-loaded chondroitin sulfate conjugated SLNs for effective management of osteoarthritis. *J Drug Target,* 22**,** 805-12.

BITTNER, B., RICHTER, W. & SCHMIDT, J. 2018. Subcutaneous Administration of Biotherapeutics: An Overview of Current Challenges and Opportunities. *BioDrugs : clinical immunotherapeutics, biopharmaceuticals and gene therapy,* 32**,** 425-440.

BLASIOLI, D. J., MATTHEWS, G. L. & KAPLAN, D. L. 2014. The degradation of chondrogenic pellets using cocultures of synovial fibroblasts and U937 cells. *Biomaterials,* 35**,** 1185-1191.

BLIDDAL, H., LEEDS, A. R. & CHRISTENSEN, R. 2014. Osteoarthritis, obesity and weight loss: evidence, hypotheses and horizons – a scoping review. *Obesity Reviews,* 15**,** 578-586.

BOBO, D., ROBINSON, K. J., ISLAM, J. & AL., E. 2016. Nanoparticle-Based Medicines: A Review of FDA-Approved Materials and Clinical Trials to Date. *Pharmaceutical Research,* 33**,** 2373-2387.

BODDU, S. H. S., ALSAAB, H., UMAR, S., BONAM, S. P., GUPTA, H. & AHMED, S. 2015. Anti-inflammatory effects of a novel ricinoleic acid poloxamer gel system for transdermal delivery. *International Journal of Pharmaceutics,* 479**,** 207-211.

BODICK, N., LUFKIN, J., WILLWERTH, C., KUMAR, A., BOLOGNESE, J., SCHOONMAKER, C., BALLAL, R., HUNTER, D. & CLAYMAN, M. 2015. An intra-articular, extended-release formulation of triamcinolone acetonide prolongs and amplifies analgesic effect in patients with osteoarthritis of the knee: a randomized clinical trial. *J Bone Joint Surg Am,* 97**,** 877-88.

BODINE, P. V., VERNON, S. K. & KOMM, B. S. 1996. Establishment and hormonal regulation of a conditionally transformed preosteocytic cell line from adult human bone. *Endocrinology,* 137**,** 4592-604.

BODMER, J. L., SCHNEIDER, P. & TSCHOPP, J. 2002. The molecular architecture of the TNF superfamily. *Trends Biochem Sci,* 27**,** 19-26.

BOERMAN, O. C., OYEN, W. J. G., STORM, G., CORVO, M. L., VAN BLOOIS, L., VAN DER MEER, J. W. M. & CORSTENS, F. H. M. 1997. Technetium-99m labelled liposomes to image experimental arthritis. *Annals of the Rheumatic Diseases,* 56**,** 369.

BOETTGER, M. K., HENSELLEK, S., RICHTER, F., GAJDA, M., STOCKIGT, R., VON BANCHET, G. S., BRAUER, R. & SCHAIBLE, H. G. 2008. Antinociceptive effects of tumor necrosis factor alpha neutralization in a rat model of antigen-induced arthritis: evidence of a neuronal target. *Arthritis Rheum,* 58**,** 2368-78.

BOETTGER, M. K., WEBER, K., GROSSMANN, D., GAJDA, M., BAUER, R., BAR, K. J., SCHULZ, S., VOSS, A., GEIS, C., BRAUER, R. & SCHAIBLE, H. G. 2010. Spinal tumor necrosis factor alpha neutralization reduces peripheral inflammation and hyperalgesia and suppresses autonomic responses in experimental arthritis: a role for spinal tumor necrosis factor alpha during induction and maintenance of peripheral inflammation. *Arthritis Rheum,* 62**,** 1308-18.

BOLLMANN, M., BRINKEMA, H., PIATEK, S., WALCHER, F., ALVAREZ, M., ELDRIDGE, S., DELL'ACCIO, F. & BERTRAND, J. 2020. Short term il1ra treatment reduces post-traumatic OA in mouse in vivo and, in vitro, in human cartilage [Abstract]. *Osteoarthritis and Cartilage,* 28.

BONEWALD, L. F. 2011. The amazing osteocyte. *Journal of Bone and Mineral Research,* 26**,** 229-238.
BONNARENS, F. & EINHORN, T. A. 1984. Production of a standard closed fracture in laboratory animal bone. *J Orthop Res,* 2**,** 97-101.
BONNET, C. S., WILLIAMS, A. S., GILBERT, S. J., HARVEY, A. K., EVANS, B. A. & MASON, D. J. 2015. AMPA/kainate glutamate receptors contribute to inflammation, degeneration and pain related behaviour in inflammatory stages of arthritis. *Annals of the Rheumatic Diseases,* 74**,** 242-251.
BONNET, C. S., GILBERT, S. J., WILLIAMS, A. S., BLAIN, E., WALSH, D. A. & MASON, D. J. 2017. NBQX, an AMPA-kainate glutamate receptor antagonist, alleviates inflammation, degeneration and pain related behaviour in two models of osteoarthritis [abstract]. *J. Orthop Res,* 35.
BONNET, C. S., GILBERT, S. J. & MASON, D. J. 2019. Repurposing glutamate receptor antagonists to prevent post-traumatic osteoarthritis [Abstract]. *Osteoarthritis and Cartilage,* 27**,** S170-S171.
BONNET, C. S., GILBERT, S. J., BLAIN, E., WILLIAMS, A. S. & MASON, D. J. 2020. AMPA and Kainate glutamate receptor antagonists prevent post-traumatic osteoarthritis. *JCI Insights* 5.
BORD, S., IRELAND, D. C., BEAVAN, S. R. & COMPSTON, J. E. 2003. The effects of estrogen on osteoprotegerin, RANKL, and estrogen receptor expression in human osteoblasts. *Bone,* 32**,** 136-141.
BORTEL, E. L., CHARBONNIER, B. & HEUGERGER, R. 2015. Development of a Synthetic Synovial Fluid for Tribological Testing. *Lubricants,* 3**,** 664-686.
BOSHTAM, M., ASGARY, S., KOUHPAYEH, S., SHARIATI, L. & KHANAHMAD, H. 2017. Aptamers Against Pro- and Anti-Inflammatory Cytokines: A Review. *Inflammation,* 40**,** 340-349.
BOTTINI, M., BHATTACHARYA, K., FADEEL, B., MAGRINI, A., BOTTINI, N. & ROSATO, N. 2016. Nanodrugs to target articular cartilage: An emerging platform for osteoarthritis therapy. *Nanomedicine,* 12**,** 255-68.
BOUGAULT, C., AUBERT-FOUCHER, E., PAUMIER, A., PERRIER-GROULT, E., HUOT, L., HOT, D., DUTERQUE-COQUILLAUD, M. & MALLEIN-GERIN, F. 2012. Dynamic compression of chondrocyte-agarose constructs reveals new candidate mechanosensitive genes. *PloS one,* 7**,** e36964-e36964.
BOUKHECHBA, F., BALAGUER, T., MICHIELS, J.-F., ACKERMANN, K., QUINCEY, D., BOULER, J.-M., PYERIN, W., CARLE, G. F. & ROCHET, N. 2009. Human Primary Osteocyte Differentiation in a 3D Culture System. *Journal of Bone and Mineral Research,* 24**,** 1927-1935.
BOYER, K. A., ANGST, M. S., ASAY, J., GIORI, N. J. & ANDRIACCHI, T. P. 2012. Sensitivity of gait parameters to the effects of anti-inflammatory and opioid treatments in knee osteoarthritis patients. *Journal of Orthopaedic Research,* 30**,** 1118-1124.
BOYLE, W. J., SIMONET, W. S. & LACEY, D. L. 2003. Osteoclast differentiation and activation. *Nature,* 423**,** 337.
BRAKSPEAR, K. S., PARSONS, P. & MASON, D. J. 2009. Cartilage metabolism and cell based therapiesfor tissue regeneration. *International Journal of Experimental Pathology,* 90**,** A85-A139.
BRAKSPEAR, K. S. 2011. *Glutamate regulation for bone repair* PhD, Cardiff University

BRAKSPEAR, K. S. & MASON, D. J. 2012. Glutamate signalling in bone. *Frontiers in Endocrinology,* 3.
BRANDT, K. D., MYERS, S. L., BURR, D. & ALBRECHT, M. 1991. Osteoarthritic changes in canine articular cartilage, subchondral bone, and synovium fifty-four months after transection of the anterior cruciate ligament. *Arthritis Rheum,* 34**,** 1560-70.
BRESLIN, S. & O'DRISCOLL, L. 2013. Three-dimensional cell culture: the missing link in drug discovery. *Drug Discovery Today,* 18**,** 240-249.
BROWN, S., KUMAR, S. & SHARMA, B. 2019a. Intra-articular targeting of nanomaterials for the treatment of osteoarthritis. *Acta Biomater,* 93**,** 239-257.
BROWN, S., PISTINER, J., ADJEI, I. M. & SHARMA, B. 2019b. Nanoparticle Properties for Delivery to Cartilage: The Implications of Disease State, Synovial Fluid, and Off-Target Uptake. *Molecular Pharmaceutics,* 16**,** 469-479.
BRUNET-MAHEU, J.-M., FERNANDES, J. C., DE LACERDA, C. A. V., SHI, Q., BENDERDOUR, M. & LAVIGNE, P. 2008. Pluronic F-127 as a Cell Carrier for Bone Tissue Engineering. *Journal of Biomaterials Applications,* 24**,** 275-287.
BRUUNSGAARD, H. 2002. Effects of tumor necrosis factor-alpha and interleukin-6 in elderly populations *Eyropean Cytokine Network* 13**,** 389-391.
BRYANT, L. R., DES ROSIER, K. F. & CARPENTER, M. T. 1995. Hydroxychloroquine in the treatment of erosive osteoarthritis. *The Journal of rheumatology,* 22**,** 1527-1531.
BUCHWALD, Z. S., KIESEL, J. R., DIPAOLO, R., PAGADALA, M. S. & AURORA, R. 2012. Osteoclast activated FoxP3+ CD8+ T-cells suppress bone resorption in vitro. *PloS one,* 7**,** e38199-e38199.
BUCKLAND-WRIGHT, J. C., MACFARLANE, D. G., LYNCH, J. A. & CLARK, B. 1990. Quantitative microfocal radiographic assessment of progression in osteoarthritis of the hand. *Arthritis Rheum,* 33**,** 57-65.
BUCKLAND-WRIGHT, J. C., LYNCH, J. A. & MACFARLANE, D. G. 1996. Fractal signature analysis measures cancellous bone organisation in macroradiographs of patients with knee osteoarthritis. *Ann Rheum Dis,* 55**,** 749-55.
BUCKLAND-WRIGHT, J. C., LYNCH, J. A. & DAVE, B. 2000. Early radiographic features in patients with anterior cruciate ligament rupture. *Annals of the Rheumatic Diseases,* 59**,** 641-646.
BUCKWALTER, J. A. & MANKIN, H. J. 1998. Articular cartilage: tissue design and chondrocyte-matrix interactions. *Instructional course lectures,* 47**,** 477-486.
BURNS, L. C., RITVO, S. E., FERGUSON, M. K., CLARKE, H., SELTZER, Z. & KATZ, J. 2015. Pain catastrophizing as a risk factor for chronic pain after total knee arthroplasty: a systematic review. *Journal of Pain Research,* 8**,** 21-32.
BUSH, P. G., HODKINSON, P. D., HAMILTON, G. L. & HALL, A. C. 2005. Viability and volume of in situ bovine articular chondrocytes—changes following a single impact and effects of medium osmolarity. *Osteoarthritis and Cartilage,* 13**,** 54-65.
BUSTIN, S. A., BENES, V., GARSON, J. A., HELLEMANS, J., HUGGETT, J., KUBISTA, M., MUELLER, R., NOLAN, T., PFAFFL, M. W., SHIPLEY, G. L., VANDESOMPELE, J. & WITTWER, C. T. 2009. The MIQE guidelines: minimum information for publication of quantitative real-time PCR experiments. *Clin Chem,* 55**,** 611-22.
BUTOESCU, N., JORDAN, O. & DOELKER, E. 2009. Intra-articular drug delivery systems for the treatment of rheumatic diseases: A review of the factors influencing their performance. *European Journal of Pharmaceutics and Biopharmaceutics,* 73**,** 205-218.

CABAHUG-ZUCKERMAN, P., FRIKHA-BENAYED, D., MAJESKA, R. J., TUTHILL, A., YAKAR, S., JUDEX, S. & SCHAFFLER, M. B. 2016. Osteocyte Apoptosis Caused by Hindlimb Unloading is Required to Trigger Osteocyte RANKL Production and Subsequent Resorption of Cortical and Trabecular Bone in Mice Femurs. *J Bone Miner Res,* 31**,** 1356-65.

CAI, G., AITKEN, D., LASLETT, L., HILL, C., MARCH, L., WLUKA, A. E., WANG, Y., BLIZZARD, L., CICUTTINI, F., WINZENBERG, T. & JONES, G. 2018. OP0016 A multicentre randomised controlled trial of zoledronic acid for osteoarthritis of the knee with bone marrow lesions [abstract]. *Annals of the Rheumatic Diseases,* 77**,** 57-58.

CALLEWAERT, F., BAKKER, A., SCHROOTEN, J., MEERBEEK, B. V., VERHOEVEN, G., BOONEN, S. & VANDERSCHUEREN, D. 2010. Androgen receptor disruption increases the osteogenic response to mechanical loading in male mice. *Journal of Bone and Mineral Research,* 25**,** 124-131.

CANCIENNE, J. M., WERNER, B. C., LUETKEMEYER, L. M. & BROWNE, J. A. 2015. Does Timing of Previous Intra-Articular Steroid Injection Affect the Post-Operative Rate of Infection in Total Knee Arthroplasty? *The Journal of Arthroplasty,* 30**,** 1879-1882.

CAPULLI, M., PAONE, R. & RUCCI, N. 2014. Osteoblast and osteocyte: games without frontiers. *Arch Biochem Biophys,* 561**,** 3-12.

CARDOSO, L., HERMAN, B. C., VERBORGT, O., LAUDIER, D., MAJESKA, R. J. & SCHAFFLER, M. B. 2009. Osteocyte Apoptosis Controls Activation of Intracortical Resorption in Response to Bone Fatigue. *Journal of Bone and Mineral Research,* 24**,** 597-605.

CARLTON, S. M. & COGGESHALL, R. E. 1999. Inflammation-induced changes in peripheral glutamate receptor populations. *Brain Research,* 820**,** 63-70.

CARON, J. P., FERNANDES, J. C., MARTEL-PELLETIER, J., TARDIF, G., MINEAU, F., GENG, C. & PELLETIER, J. P. 1996. Chondroprotective effect of intraarticular injections of interleukin-1 receptor antagonist in experimental osteoarthritis. Suppression of collagenase-1 expression. *Arthritis Rheum,* 39**,** 1535-44.

CATTERALL, J. B., STABLER, T. V., FLANNERY, C. R. & KRAUS, V. B. 2010. Changes in serum and synovial fluid biomarkers after acute injury (NCT00332254). *Arthritis Res Ther,* 12**,** R229.

CAUCHETIER, E., DENIAU, M., FESSI, H., ASTIER, A. & PAUL, M. 2003. Atovaquone-loaded nanocapsules: influence of the nature of the polymer on their in vitro characteristics. *International Journal of Pharmaceutics,* 250**,** 273-281.

CHACÓN, M., MOLPECERES, J., BERGES, L., GUZMÁN, M. & ABERTURAS, M. R. 1999. Stability and freeze-drying of cyclosporine loaded poly(d,l lactide–glycolide) carriers. *European Journal of Pharmaceutical Sciences,* 8**,** 99-107.

CHAN, B. Y., FULLER, E. S., RUSSELL, A. K., SMITH, S. M., SMITH, M. M., JACKSON, M. T., CAKE, M. A., READ, R. A., BATEMAN, J. F., SAMBROOK, P. N. & LITTLE, C. B. 2011. Increased chondrocyte sclerostin may protect against cartilage degradation in osteoarthritis. *Osteoarthritis Cartilage,* 19**,** 874-85.

CHAN, M. E., LU, X. L., HUO, B., BAIK, A. D., CHIANG, V., GULDBERG, R. E., LU, H. H. & GUO, X. E. 2009. A Trabecular Bone Explant Model of Osteocyte–Osteoblast Co-Culture for Bone Mechanobiology. *Cellular and Molecular Bioengineering,* 2**,** 405-415.

CHARALAMBOUS, C. P., TRYFONIDIS, M., SADIQ, S., HIRST, P. & PAUL, A. 2003. Septic arthritis following intra-articular steroid injection of the knee - A survey of current practice regarding antiseptic technique used during intra-articular steroid injection of the knee. *Clinical Rheumatology,* 22**,** 386-390.

CHATTERJEE, S., HUI, P. C.-L. & KAN, C.-W. 2018. Thermoresponsive Hydrogels and Their Biomedical Applications: Special Insight into Their Applications in Textile Based Transdermal Therapy. *Polymers,* 10**,** 480.

CHATZIZACHARIAS, N. A., KOURAKLIS, G. P. & THEOCHARIS, S. E. 2008. Disruption of FAK signaling: a side mechanism in cytotoxicity. *Toxicology,* 245**,** 1-10.

CHEN, A. L., DESAI, P., ADLER, E. M. & DI CESARE, P. E. 2002. Granulomatous inflammation after Hylan G-F 20 viscosupplementation of the knee: a report of six cases. *J Bone Joint Surg* 1142-1147.

CHEN, C. P. C., CHENG, C.-H., HSU, C.-C., LIN, H.-C., TSAI, Y.-R. & CHEN, J.-L. 2017a. The influence of platelet rich plasma on synovial fluid volumes, protein concentrations, and severity of pain in patients with knee osteoarthritis. *Experimental Gerontology,* 93**,** 68-72.

CHEN, H., QIN, Z., ZHAO, J., HE, Y., REN, E., ZHU, Y., LIU, G., MAO, C. & ZHENG, L. 2019a. Cartilage-targeting and dual MMP-13/pH responsive theranostic nanoprobes for osteoarthritis imaging and precision therapy. *Biomaterials,* 225**,** 119520.

CHEN, L., JI, Y., HU, X., CUI, C., LIU, H., TANG, Y., QI, B., NIU, Y., HU, X., YU, A. & FAN, Q. 2018. Cationic poly-l-lysine-encapsulated melanin nanoparticles as efficient photoacoustic agents targeting to glycosaminoglycans for the early diagnosis of articular cartilage degeneration in osteoarthritis. *Nanoscale,* 10**,** 13471-13484.

CHEN, M., LIU, X. & FAHR, A. 2011. Skin penetration and deposition of carboxyfluorescein and temoporfin from different lipid vesicular systems: In vitro study with finite and infinite dosage application. *Int J Pharm,* 408**,** 223-34.

CHEN, X., GUO, J., YUAN, Y., SUN, Z., CHEN, B., TONG, X., ZHANG, L., SHEN, C. & ZOU, J. 2017b. Cyclic compression stimulates osteoblast differentiation via activation of the Wnt/beta-catenin signaling pathway. *Mol Med Rep,* 15**,** 2890-2896.

CHEN, Y.-Y., WU, X.-S., TIAN, Y.-Y., ZHAO, P., SUN, S.-W. & YANG, C.-B. 2019b. Evaluation of Femoral Head Perfusion by Contrast-Enhanced Ultrasound in a Rabbit Model of Steroid-Induced Osteonecrosis. *Journal of Ultrasound in Medicine,* 39**,** 987-995.

CHEN, Y. F., JOBANPUTRA, P., BARTON, P., BRYAN, S., FRY-SMITH, A., HARRIS, G. & TAYLOR, R. S. 2008. Cyclooxygenase-2 selective non-steroidal anti-inflammatory drugs (etodolac, meloxicam, celecoxib, rofecoxib, etoricoxib, valdecoxib and lumiracoxib) for osteoarthritis and rheumatoid arthritis: a systematic review and economic evaluation. *Health Technol Assess,* 12**,** 1-278, iii.

CHEN, Z., CHEN, J., WU, L., LI, W., CHEN, J., CHENG, H., PAN, J. & CAI, B. 2013. Hyaluronic acid-coated bovine serum albumin nanoparticles loaded with brucine as selective nanovectors for intra-articular injection. *International Journal of Nanomedicine,* 8**,** 3843-3853.

CHEN, Z., LIU, D., WANG, J., WU, L., LI, W., CHEN, J., CAI, B.-C. & CHENG, H. 2014. Development of nanoparticles-in-microparticles system for improved local retention after intra-articular injection. *Drug Delivery,* 21**,** 342-350.

CHENG, J. & ABDI, S. 2007. Complications of joint, tendon, and muscle injections. *Techniques in Regional Anesthesia and Pain Management,* 11**,** 141-147.

CHENOUFI, H. L., DIAMANT, M., RIENECK, K., LUND, B., STEIN, G. S. & LIAN, J. B. 2001. Increased mRNA expression and protein secretion of interleukin-6 in primary human osteoblasts differentiated in vitro from rheumatoid and osteoarthritic bone. *J Cell Biochem,* 81**,** 666-78.

CHENU, C., SERRE, C. M., RAYNAL, C., BURT-PICHAT, B. & DELMAS, P. D. 1998. Glutamate Receptors Are Expressed by Bone Cells and Are Involved in Bone Resorption. *Bone,* 22**,** 295-299.

CHENU, C. 2002. Glutamatergic regulation of bone resorption. *Journal of musculoskeletal & neuronal interactions,* 2**,** 423-431.

CHEUNG, W.-Y., SIMMONS, C. A. & YOU, L. 2012. Osteocyte apoptosis regulates osteoclast precursor adhesion via osteocytic IL-6 secretion and endothelial ICAM-1 expression. *Bone,* 50**,** 104-110.

CHEVALIER, X., GOUPILLE, P., BEAULIEU, A. D., BURCH, F. X., BENSEN, W. G., CONROZIER, T., LOEUILLE, D., KIVITZ, A. J., SILVER, D. & APPLETON, B. E. 2009. Intraarticular injection of anakinra in osteoarthritis of the knee: a multicenter, randomized, double-blind, placebo-controlled study. *Arthritis Rheum,* 61**,** 344-52.

CHI, X., HU, R., YANG, Q., ZHANG, X., PAN, L., CHEN, N., CHEN, M., YANG, Z., WANG, T., HE, Y. & YU, S. 2012. Validation of reference genes for gene expression studies in peanut by quantitative real-time RT-PCR. *Mol Genet Genomics,* 287**,** 167-76.

CHO, H., STUART, J. M., MAGID, R., DANILA, D. C., HUNSAKER, T., PINKHASSIK, E. & HASTY, K. A. 2014. Theranostic immunoliposomes for osteoarthritis. *Nanomedicine: Nanotechnology, Biology and Medicine,* 10**,** 619-627.

CHOI, H.-G., JUNG, J.-H., RYU, J.-M., YOON, S.-J., OH, Y.-K. & KIM, C.-K. 1998. Development of in situ-gelling and mucoadhesive acetaminophen liquid suppository. *International Journal of Pharmaceutics,* 165**,** 33-44.

CHOI, M. J., BRIANÇON, S., ANDRIEU, J., MIN, S. G. & FESSI, H. 2004. Effect of Freeze-Drying Process Conditions on the Stability of Nanoparticles. *Drying Technology,* 22**,** 335-346.

CHOU, R., MCDONAGH, M. S., NAKAMOTO, E. & GRIFFIN, J. 2011. AHRQ Comparative Effectiveness Reviews: Analgesics for Osteoarthritis: An Update of the 2006 Comparative Effectiveness Review [internet]. Rockville (MD): Agency for Healthcare Research and Quality (US).

CHOY, E. 2012. Understanding the dynamics: pathways involved in the pathogenesis of rheumatoid arthritis. *Rheumatology (Oxford),* 51 Suppl 5**,** v3-11.

CHRISTEN, P., ITO, K., ELLOUZ, R., BOUTROY, S., SORNAY-RENDU, E., CHAPURLAT, R. D. & VAN RIETBERGEN, B. 2014. Bone remodelling in humans is load-driven but not lazy. *Nature Communications,* 5**,** 4855.

CHRISTIANSEN, B. A., GUILAK, F., LOCKWOOD, K. A., OLSON, S. A., PITSILLIDES, A. A., SANDELL, L. J., SILVA, M. J., VAN DER MEULEN, M. C. & HAUDENSCHILD, D. R. 2015. Non-invasive mouse models of post-traumatic osteoarthritis. *Osteoarthritis Cartilage,* 23**,** 1627-38.

CLAUDINO, M., GARLET, T. P., CARDOSO, C. R., DE ASSIS, G. F., TAGA, R., CUNHA, F. Q., SILVA, J. S. & GARLET, G. P. 2010. Down-regulation of expression of osteoblast and osteocyte markers in periodontal tissues associated with the spontaneous alveolar bone loss of interleukin-10 knockout mice. *Eur J Oral Sci,* 118**,** 19-28.

CLEMENTS, K. M., PRICE, J. S., CHAMBERS, M. G., VISCO, D. M., POOLE, A. R. & MASON, R. M. 2003. Gene deletion of either interleukin-1beta, interleukin-1beta-converting enzyme, inducible nitric oxide synthase, or stromelysin 1 accelerates the development of knee osteoarthritis in mice after surgical transection of the medial collateral ligament and partial medial meniscectomy. *Arthritis Rheum,* 48**,** 3452-63.

COHEN, N. P., FOSTER, R. J. & MOW, V. C. 1998. Composition and Dynamics of Articular Cartilage: Structure, Function, and Maintaining Healthy State. *Journal of Orthopaedic & Sports Physical Therapy,* 28**,** 203-215.

COHEN-SELA, E., CHORNY, M., KOROUKHOV, N., DANENBERG, H. D. & GOLOMB, G. 2009. A new double emulsion solvent diffusion technique for encapsulating hydrophilic molecules in PLGA nanoparticles. *Journal of Controlled Release,* 133**,** 90-95.

COLE, B. J. & SCHUMACHER, R. H. J. 2005. Injectable Corticosteroids in Modern Practice. *JAAOS - Journal of the American Academy of Orthopaedic Surgeons,* 13**,** 37-46.

COMPTON, J. T. & LEE, F. Y. 2014. A review of osteocyte function and the emerging importance of sclerostin. *The Journal of bone and joint surgery. American volume,* 96**,** 1659-1668.

CONAGHAN, P. G., BOWES, M. A., KINGSBURY, S. R., BRETT, A., GUILLARD, G., TUNBLAD, K., RIZOSKA, B., LARSSON, T., HOLMGREN, Å., MANNINEN, A., GÖHLIN, K., HEBER, W., GRAHAM, P., JANSSON, Å., WADELL, C., BETHELL, R. & ÖHD, J. 2018a. Six months' treatment with MIV-711, a novel Cathepsin K inhibitor induces osteoarthritis structure modification: results from a randomized double-blind placebo-controlled phase IIA trial [abstract]. *Osteoarthritis and Cartilage,* 26**,** S25-S26.

CONAGHAN, P. G., COHEN, S. B., BERENBAUM, F., LUFKIN, J., JOHNSON, J. R. & BODICK, N. 2018b. Brief Report: A Phase IIb Trial of a Novel Extended-Release Microsphere Formulation of Triamcinolone Acetonide for Intraarticular Injection in Knee Osteoarthritis. *Arthritis Rheumatol,* 70**,** 204-211.

CONAGHAN, P. G., HUNTER, D. J., COHEN, S. B., KRAUS, V. B., BERENBAUM, F., LIEBERMAN, J. R., JONES, D. G., SPITZER, A. I., JEVSEVAR, D. S., KATZ, N. P., BURGESS, D. J., LUFKIN, J., JOHNSON, J. R., BODICK, N. & INVESTIGATORS, F. X. P. 2018c. Effects of a Single Intra-Articular Injection of a Microsphere Formulation of Triamcinolone Acetonide on Knee Osteoarthritis Pain: A Double-Blinded, Randomized, Placebo-Controlled, Multinational Study. *The Journal of bone and joint surgery. American volume,* 100**,** 666-677.

CONE, R. A. 2009. Barrier properties of mucus. *Advanced Drug Delivery Reviews,* 61**,** 75-85.

COPE, P. J., OURRADI, K., LI, Y. & SHARIF, M. 2019. Models of osteoarthritis: the good, the bad and the promising. *Osteoarthritis and Cartilage,* 27**,** 230-239.

CORREA, D. & LIETMAN, S. A. 2017. Articular cartilage repair: Current needs, methods and research directions. *Seminars in Cell & Developmental Biology,* 62**,** 67-77.

COSTA, P. & SOUSA LOBO, J. M. 2001. Modeling and comparison of dissolution profiles. *European Journal of Pharmaceutical Sciences,* 13**,** 123-133.

CRAIG, D. Q. M., TAMBURIC, S., BUCKTON, G. & NEWTON, J. M. 1994. An investigation into the structure and properties of Carbopol 934 gels using dielectric spectroscopy and oscillatory rheometry. *Journal of Controlled Release,* 30**,** 213-223.

CURL, C. L., BELLAIR, C. J., HARRIS, T., ALLMAN, B. E., HARRIS, P. J., STEWART, A. G., ROBERTS, A., NUGENT, K. A. & DELBRIDGE, K. A. 2005. Refractive index measurement in viable cells using quantitative phase-amplitude microscopy and confocal microscopy *Cytometry part A,* 65A**,** 88-92.

CUZZOCREA, S., MAZZON, E., DUGO, L., GENOVESE, T., DI PAOLA, R., RUGGERI, Z., VEGETO, E., CAPUTI, A. P., VAN DE LOO, F. A. J., PUZZOLO, D. & MAGGI, A. 2003. Inducible Nitric Oxide Synthase Mediates Bone Loss in Ovariectomized Mice. *Endocrinology,* 144**,** 1098-1107.

DA COSTA, B. R., NUESCH, E., KASTELER, R., HUSNI, E., WELCH, V., RUTJES, A. W. S. & JUNI, P. 2014. Oral or transdermal opioids for osteoarthritis of the knee or hip. *Cochrane Database Syst Rev,* 9**,** Cd003115.

DALLAS, S. L., PRIDEAUX, M. & BONEWALD, L. F. 2013. The Osteocyte: An Endocrine Cell … and More. *Endocrine Reviews,* 34**,** 658-690.

DANHIER, F., ANSORENA, E., SILVA, J. M., COCO, R., LE BRETON, A. & PREAT, V. 2012. PLGA-based nanoparticles: an overview of biomedical applications. *J Control Release,* 161**,** 505-22.

DARNELL, M. C., SUN, J.-Y., MEHTA, M., JOHNSON, C., ARANY, P. R., SUO, Z. & MOONEY, D. J. 2013. Performance and biocompatibility of extremely tough alginate/polyacrylamide hydrogels. *Biomaterials,* 34**,** 8042-8048.

DAS, S. K., MISHRA, K., RAMAKRISHNAN, S., SRIVASTAVA, R., AGARWAL, G. G., SINGH, R. & SIRCAR, A. R. 2002. A randomized controlled trial to evaluate the slow-acting symptom modifying effects of a regimen containing colchicine in a subset of patients with osteoarthritis of the knee. *Osteoarthritis and Cartilage,* 10**,** 247-252.

DASH, S., MURTHY, P. N., NATH, L. & CHOWDHURY, P. 2010. Kinetic modeling on drug release from controlled drug delivery systems. *Acta Poloniae Pharmaceutica - Drug Research* 67**,** 217-223.

DATE, P. V., SAMAD, A. & DEVARAJAN, P. V. 2010. Freeze thaw: a simple approach for prediction of optimal cryoprotectant for freeze drying. *AAPS PharmSciTech,* 11**,** 304-313.

DAVIDSON, D. & PATEL, H. 2014. Cytokine-induced neutrophil chemotaxis assay. *Methods Mol Biol,* 1172**,** 107-13.

DAY, J. S., DING, M., VAN DER LINDEN, J. C., HVID, I., SUMNER, D. R. & WEINANS, H. 2001. A decreased subchondral trabecular bone tissue elastic modulus is associated with pre-arthritic cartilage damage. *Journal of Orthopaedic Research,* 19**,** 914-918.

DE L'ESCALOPIER, N., ANRACT, P. & BIAU, D. 2016. Surgical treatments for osteoarthritis. *Annals of Physical and Rehabilitation Medicine,* 59**,** 227-233.

DEAL, C. L., SCHNITZER, T. J., LIPSTEIN, E., SEIBOLD, J. R., STEVENS, R. M., LEVY, M. D., ALBERT, D. & RENOLD, F. 1991. Treatment of arthritis with topical capsaicin: a double-blind trial. *Clin Ther,* 13**,** 383-95.

DEEKS, J. J., SMITH, L. A. & BRADLEY, M. D. 2002. Efficacy, tolerability, and upper gastrointestinal safety of celecoxib for treatment of osteoarthritis and rheumatoid arthritis: systematic review of randomised controlled trials. *BMJ,* 325**,** 619.

DELGADO, A. V., GONZÁLEZ-CABALLERO, F., HUNTER, R. J., KOOPAL, L. K. & LYKLEMA, J. 2007. Measurement and interpretation of electrokinetic phenomena. *Journal of Colloid and Interface Science,* 309**,** 194-224.

DELGADO-CALLE, J., RIANCHO, J. A. & KLEIN-NULEND, J. 2014. Nitric oxide is involved in the down-regulation of SOST expression induced by mechanical loading. *Calcif Tissue Int,* 94**,** 414-22.

DELGADO-CALLE, J., SATO, A. Y. & BELLIDO, T. 2017. Role and mechanism of action of sclerostin in bone. *Bone,* 96**,** 29-37.

DELIORMANLI, A. M. & TÜRK, M. 2019. Flow Behavior and Drug Release Study of Injectable Pluronic F-127 Hydrogels containing Bioactive Glass and Carbon-Based Nanopowders. *Journal of Inorganic and Organometallic Polymers and Materials,* 30**,** 1184-1196.

DEMIRCI, S., DOĞAN, A., KARAKUŞ, E., HALICI, Z., TOPÇU, A., DEMIRCI, E. & SAHIN, F. 2015. Boron and Poloxamer (F68 and F127) Containing Hydrogel Formulation for Burn Wound Healing. *Biological Trace Element Research,* 168**,** 169-180.

DENG, R. H., QIU, B. & ZHOU, P. H. 2018. Chitosan/hyaluronic acid/plasmid-DNA nanoparticles encoding interleukin-1 receptor antagonist attenuate inflammation in synoviocytes induced by interleukin-1 beta. *J Mater Sci Mater Med,* 29**,** 155.

DERAKHSHANDEH, K., FASHI, M. & SEIFOLESLAMI, S. 2010. Thermosensitive Pluronic hydrogel: prolonged injectable formulation for drug abuse. *Drug design, development and therapy,* 4**,** 255-262.

DERMAN, S., MUSTAFAEVA, Z. A., ABAMOR, E. S., BAGIROVA, M. & ALLAHVERDIYEV, A. 2015. Preparation, characterization and immunological evaluation: canine parvovirus synthetic peptide loaded PLGA nanoparticles. *Journal of biomedical science,* 22**,** 89.

DERRY, S., CONAGHAN, P., DA SILVA, J. A. P., WIFFEN, P. J. & MOORE, R. A. 2016. Topical NSAIDs for chronic musculoskeletal pain in adults. *Cochrane Database of Systematic Reviews,* 4**,** CD007400.

DERRY, S., WIFFEN, P. J., KALSO, E. A., BELL, R. F., ALDINGTON, D., PHILLIPS, T., GASKELL, H. & MOORE, R. A. 2017. Topical analgesics for acute and chronic pain in adults - an overview of Cochrane Reviews. *Cochrane Database of Systematic Reviews,* 5.

DESAI, M. P., LABHASETWAR, V., WALTER, E., LEVY, R. J. & AMIDON, G. L. 1997. The Mechanism of Uptake of Biodegradable Microparticles in Caco-2 Cells Is Size Dependent. *Pharmaceutical Research,* 14**,** 1568-1573.

DESGEORGES, A., GABAY, C., SILACCI, P., NOVICK, D., ROUX-LOMBARD, P., GRAU, G., DAYER, J. M., VISCHER, T. & GUERNE, P. A. 1997. Concentrations and origins of soluble interleukin 6 receptor-alpha in serum and synovial fluid. *J Rheumatol,* 24**,** 1510-1516.

DESHMUKH, V., HU, H., BARROGA, C., BOSSARD, C., KC, S., DELLAMARY, L., STEWART, J., CHIU, K., IBANEZ, M., PEDRAZA, M., SEO, T., DO, L., CHO, S., CAHIWAT, J., TAM, B., TAMBIAH, J. R. S., HOOD, J., LANE, N. E. & YAZICI, Y. 2018. A small-molecule inhibitor of the Wnt pathway (SM04690) as a potential disease modifying agent for the treatment of osteoarthritis of the knee. *Osteoarthritis Cartilage,* 26**,** 18-27.

DESTACHE, C. J., BELGUM, T., CHRISTENSEN, K., SHIBATA, A., SHARMA, A. & DASH, A. 2009. Combination antiretroviral drugs in PLGA nanoparticle for HIV-1. *BMC Infectious Diseases,* 9**,** 198.

DEVEZA, L. A., NELSON, A. E. & LOESER, R. F. 2019. Phenotypes of osteoarthritis: current state and future implications. *Clin Exp Rheumatol,* 37 Suppl 120**,** 64-72.

DHAR, S., GU, F. X., LANGER, R., FAROKHZAD, O. C. & LIPPARD, S. J. 2008. Targeted delivery of cisplatin to prostate cancer cells by aptamer functionalized Pt(IV) prodrug-PLGA–PEG nanoparticles. *Proceedings of the National Academy of Sciences,* 105**,** 17356-17361.

DI DONATO, C., LACOVINO, R., ISERNIA, C., MALGIERI, G., VARELA-GARCIA, A., CONCHEIRO, A. & ALVAREZ-LORENZO, C. 2020. Polypseudorotaxanes of Pluronic® F127 with Combinations of α- and β-Cyclodextrins for Topical Formulation of Acyclovir. *Nanomaterials* 10.

DI MAGGIO, N., PICCININI, E., JAWORSKI, M., TRUMPP, A., WENDT, D. J. & MARTIN, I. 2011. Toward modeling the bone marrow niche using scaffold-based 3D culture systems. *Biomaterials,* 32**,** 321-329.

DIÉGUEZ, L., DARWISH, N., MIR, M., MARTÍNEZ, E., MORENO, M. & SAMITIER, J. 2009. Effect of the refractive index of buffer solutions in evanescent optical biosensors *Sensor Letters,* 7**,** 851-855.

DIEPPE, P. A. & LOHMANDER, L. S. 2005. Pathogenesis and management of pain in osteoarthritis. *The Lancet,* 365**,** 965-973.

DIETRICH, T., LEESON, R., GUGLIOTTA, B. & PETERSEN, B. 2014. Efficacy and Safety of Low Dose Subcutaneous Diclofenac in the Management of Acute Pain: A Randomized Double-Blind Trial. *Pain Practice,* 14**,** 315-323.

DINARELLO, C. A. 2013. Overview of the interleukin-1 family of ligands and receptors. *Semin Immunol,* 25**,** 389-93.

DINIZ, I. M. A., CHEN, C., XU, X., ANSARI, S., ZADEH, H. H., MARQUES, M. M., SHI, S. & MOSHAVERINIA, A. 2015. Pluronic F-127 hydrogel as a promising scaffold for encapsulation of dental-derived mesenchymal stem cells. *Journal of Materials Science: Materials in Medicine* 26**,** 153.

DOBSON, K. R. & SKERRY, T. M. 2001. The NMDA-type glutamate receptor antagonist MK801 regulates differentiation of rat bone marrow osteoprogenitors and influences adipogenesis [abstract]. *Bone,* 28**,** S75-S75.

DODD, J. S., RALEIGH, J. A. & GROSS, T. S. 1999. Osteocyte hypoxia: a novel mechanotransduction pathway. *American Journal of Physiology-Cell Physiology,* 277**,** C598-C602.

DRESNER-POLLAK, R., GELB, N., RACHMILEWITZ, D., KARMELI, F. & WEINREB, M. 2004. Interleukin 10-deficient mice develop osteopenia, decreased bone formation, and mechanical fragility of long bones. *Gastroenterology,* 127**,** 792-801.

DUQUE, G., HUANG, D. C., DION, N., MACORITTO, M., RIVAS, D., LI, W., YANG, X. F., LI, J., LIAN, J., MARINO, F. T., BARRALET, J., LASCAU, V., DESCHÊNES, C., STE-MARIE, L.-G. & KREMER, R. 2011. Interferon-γ plays a role in bone formation in vivo and rescues osteoporosis in ovariectomized mice. *Journal of Bone and Mineral Research,* 26**,** 1472-1483.

DURYMANOV, M., KAMALETDINOVA, T., LEHMANN, S. E. & REINEKE, J. 2017. Exploiting passive nanomedicine accumulation at sites of enhanced vascular permeability for non-cancerous applications. *Journal of Controlled Release,* 261**,** 10-22.

E.C.A. 2017. *What are the regulatory definitions for "Ambient", "Room Temperature" and "Cold Chain"? (European Compliance Academy)* [Online]. https://www.gmp-compliance.org/gmp-news/what-are-the-regulatory-definitions-for-ambient-room-temperature-and-cold-chain. Available: https://www.gmp-compliance.org/gmp-news/what-are-the-regulatory-definitions-for-ambient-room-temperature-and-cold-chain [Accessed 20 June 2020 2020].

EDMONDSON, R., BROGLIE, J. J., ADCOCK, A. F. & YANG, L. 2014. Three-dimensional cell culture systems and their applications in drug discovery and cell-based biosensors. *Assay and drug development technologies,* 12**,** 207-218.

EHRLICH, M. G., MANKIN, H. J., JONES, H., WRIGHT, R., CRISPEN, C. & VIGLIANI, G. 1977. Collagenase and collagenase inhibitors in osteoarthritic and normal cartilage. *The Journal of Clinical Investigation,* 59**,** 226-233.

ELSAID, K. A., UBHE, A., SHAMAN, Z. & D'SOUZA, G. 2016. Intra-articular interleukin-1 receptor antagonist (IL1-ra) microspheres for posttraumatic osteoarthritis: in vitro biological activity and in vivo disease modifying effect. *J Exp Orthop,* 3**,** 18.

EMERY, C. A., ROOS, E. M., VERHAGEN, E., FINCH, C. F., BENNELL, K. L., STORY, B., SPINDLER, K., KEMP, J. & LOHMANDER, L. S. 2015. OARSI Clinical Trials Recommendations: Design and conduct of clinical trials for primary prevention of osteoarthritis by joint injury prevention in sport and recreation. *Osteoarthritis Cartilage,* 23**,** 815-25.

ENGLUND, M., ROOS, E. M. & LOHMANDER, L. S. 2003. Impact of type of meniscal tear on radiographic and symptomatic knee osteoarthritis: A sixteen-year followup of meniscectomy with matched controls. *Arthritis & Rheumatism,* 48**,** 2178-2187.

ENGLUND, M., GUERMAZI, A., ROEMER, F. W., ALIABADI, P., YANG, M., LEWIS, C. E., TORNER, J., NEVITT, M. C., SACK, B. & FELSON, D. T. 2009. Meniscal tear in knees without surgery and the development of radiographic osteoarthritis among middle-aged and elderly persons: The multicenter osteoarthritis study. *Arthritis & Rheumatism,* 60**,** 831-839.

ENSIGN, L. M., CONE, R. & HANES, J. 2012. Oral drug delivery with polymeric nanoparticles: The gastrointestinal mucus barriers. *Advanced Drug Delivery Reviews,* 64**,** 557-570.

ESSA, E. A., BONNER, M. C. & BARRY, B. W. 2002. Human skin sandwich for assessing shunt route penetration during passive and iontophoretic drug and liposome delivery. *Journal of Pharmacy and Pharmacology,* 54**,** 1481-1490.

EVANS, K. E. & FOX, S. W. 2007. Interleukin-10 inhibits osteoclastogenesis by reducing NFATc1 expression and preventing its translocation to the nucleus. *BMC cell biology,* 8.

EVERETT, E. 2018. *Novel antimicrobial restorative materials for the control of dental disease.* PhD, Cardiff University

FAHLGREN, A., BRATENGEIER, C., SEMEINS, C. M., KLEIN-NULEND, J. & BAKKER, A. D. 2018. Supraphysiological loading induces osteocyte-mediated osteoclastogenesis in a novel in vitro model for bone implant loosening. *Journal of Orthopaedic Research,* 36**,** 1425-1434.

FALCONER, J., HAYES, K. W. & CHANG, R. W. 1992. Effect of ultrasound on mobility in osteoarthritis of the knee. A randomized clinical trial. *Arthritis & Rheumatism,* 5**,** 29-35.

FAN, W., LI, J., YUAN, L., CHEN, J., WANG, Z., WANG, Y., GUO, C., MO, X. & YAN, Z. 2018. Intra-articular injection of kartogenin-conjugated polyurethane nanoparticles attenuates the progression of osteoarthritis. *Drug Deliv,* 25**,** 1004-1012.

FATHALLA, D., ABDEL-MAGEED, A., ABDEL-HAMID, F. & AHMED, M. 2014. In-vitro and In-vivo Evaluation of Niosomal Gel Containing Aceclofenac for Sustained Drug Delivery. *Int J Pharm Sci Res,* 1**,** 11.

FAZZALARI, N. L. 2011. Bone fracture and bone fracture repair *Osteoporosis international* 22**,** 2003-2006.

FDA, U. S. 2018. Liposome Drug Products; Chemistry, Manufacturing, and Controls; Human Pharmacokinetics and Bioavailability; Labeling Documentation. Guidance for Industry; April 2018 Pharmaceutical Quality/CMC. *In:* U.S. DEPARTMENT OF HEALTH AND HUMAN SERVICES FOOD AND DRUG ADMINISTRATION CENTER FOR DRUG EVALUATION AND RESEARCH (CDER): SILVER SPRING, M., USA, 2018. (ed.).

FDA, U. S. 2019a. *Inactive Ingredient Search for Approved Drug Products* [Online]. Available: https://www.accessdata.fda.gov/scripts/cder/iig/index.cfm?event=browseByLetter.page&Letter=C [Accessed 19/10/19 2019].

FDA, U. S. 2019b. *FDA Approved Drug Database* [Online]. Available: https://www.accessdata.fda.gov/scripts/cder/daf/index.cfm [Accessed 03/01/2019 2019].

FERNANDES, J., TARDIF, G., MARTEL-PELLETIER, J., LASCAU-COMAN, V., DUPUIS, M., MOLDOVAN, F., SHEPPARD, M., KRISHNAN, B. R. & PELLETIER, J. P. 1999. In vivo transfer of interleukin-1 receptor antagonist gene in osteoarthritic rabbit knee joints: prevention of osteoarthritis progression. *Am J Pathol,* 154**,** 1159-69.

FICHTER, M., KORNER, U., SCHOMBURG, J., JENNINGS, L., COLE, A. A. & MOLLENHAUER, J. 2006. Collagen degradation products modulate matrix metalloproteinase expression in cultured articular chondrocytes. *J Orthop Res,* 24**,** 63-70.

FICK, A. 1855. V. On liquid diffusion. *The London, Edinburgh, and Dublin Philosophical Magazine and Journal of Science,* 10**,** 30-39.

FITZGERALD, J. B., JIN, M., DEAN, D., WOOD, D. J., ZHENG, M. H. & GRODZINSKY, A. J. 2004. Mechanical Compression of Cartilage Explants Induces Multiple Time-dependent Gene Expression Patterns and Involves Intracellular Calcium and Cyclic AMP. *Journal of Biological Chemistry,* 279**,** 19502-19511.

FLOOD, S., PARRI, R., WILLIAMS, A., DUANCE, V. & MASON, D. 2007. Modulation of interleukin-6 and matrix metalloproteinase 2 expression in human fibroblast-like synoviocytes by functional ionotropic glutamate receptors. *Arthritis Rheum,* 56**,** 2523-2534.

FLORENCE, C. S., ZHOU, C., LUO, F. & XU, L. 2016. The Economic Burden of Prescription Opioid Overdose, Abuse, and Dependence in the United States, 2013. *Medical care,* 54**,** 901-906.

FONTE, P., SOARES, S., COSTA, A., ANDRADE, J. C., SEABRA, V., REIS, S. & SARMENTO, B. 2012. Effect of cryoprotectants on the porosity and stability of insulin-loaded PLGA nanoparticles after freeze-drying. *Biomatter,* 2**,** 329-339.

FOREMAN, M. A., GU, Y., HOWL, J. D., JONES, S. & PUBLICOVER, S. J. 2005. Group III metabotropic glutamate receptor activation inhibits Ca2+ influx and nitric oxide synthase activity in bone marrow stromal cells. *Journal of Cellular Physiology,* 204**,** 704-713.

FOX, D. B. & WARNOCK, J. J. 2011. Cell-based Meniscal Tissue Engineering: A Case for Synoviocytes. *Clinical Orthopaedics and Related Research* 469**,** 2806-2816.

FRANCESCHI, C., BONAFÈ, M., VALENSIN, S., OLIVIERI, F., DE LUCA, M., OTTAVIANI, E. & DE BENEDICTIS, G. 2000. Inflamm-aging: An Evolutionary Perspective on Immunosenescence. *Annals of the New York Academy of Sciences,* 908**,** 244-254.

FRANZ-ODENDAAL, T. A., HALL, B. K. & WITTEN, P. E. 2006. Buried alive: How osteoblasts become osteocytes. *Developmental Dynamics,* 235**,** 176-190.

FREUNDLICH, B., KIVITZ, A. & JAFFE, J. S. 2014. Nearly pain-free self-administration of subcutaneous methotrexate with an autoinjector: results of a phase 2 clinical trial in patients with rheumatoid arthritis who have functional limitations. *Journal of clinical rheumatology : practical reports on rheumatic & musculoskeletal diseases,* 20**,** 256-260.

FRISBIE, D. D., GHIVIZZANI, S. C., ROBBINS, P. D., EVANS, C. H. & MCILWRAITH, C. W. 2002. Treatment of experimental equine osteoarthritis by in vivo delivery of the equine interleukin-1 receptor antagonist gene. *Gene Ther,* 9**,** 12-20.

FROST, G. I. 2007. Recombinant human hyaluronidase (rHuPH20): an enabling platform for subcutaneous drug and fluid administration. *Expert Opin Drug Deliv,* 4**,** 427-440.

FROST, H. M. 1996. Perspectives: A proposed general model of the “mechanostat” (suggestions from a new skeletal-biologic paradigm). *The Anatomical Record,* 244**,** 139-147.

FROST-CHRISTENSEN, L. N., MASTBERGEN, S. C., VIANEN, M. E., HARTOG, A., DEGROOT, J., VOORHOUT, G., VAN WEES, A. M., LAFEBER, F. P. & HAZEWINKEL, H. A. 2008. Degeneration, inflammation, regeneration, and pain/disability in dogs following destabilization or articular cartilage grooving of the stifle joint. *Osteoarthritis Cartilage,* 16**,** 1327-35.

FRYE, S. R., YEE, A., ESKIN, S. G., GUERRA, R., CONG, X. & MCINTIRE, L. V. 2005. cDNA microarray analysis of endothelial cells subjected to cyclic mechanical strain: importance of motion control. *Physiological Genomics,* 21**,** 124-130.

FUCHS, E. & RAGHAVAN, S. 2002. Getting under the skin of epidermal morphogenesis. *Nat Rev Genet,* 3**,** 199-209.

FUNG LING CHAU, J., FOOK LEONG, W. & LI, B. 2009. Signaling pathways governing osteoblast proliferation, differentiation and function. *Histology and Histopathology* 24**,** 1593-1606.

FURLAN, A. D., SANDOVAL, J. A., MAILIS-GAGNON, A. & TUNKS, E. 2006. Opioids for chronic noncancer pain: a meta-analysis of effectiveness and side effects. *Canadian Medical Association Journal,* 174**,** 1589-1594.

FURMAN, B. D., MANGIAPANI, D. S., ZEITLER, E., BAILEY, K. N., HORNE, P. H., HUEBNER, J. L., KRAUS, V. B., GUILAK, F. & OLSON, S. A. 2014. Targeting pro-inflammatory cytokines following joint injury: acute intra-articular inhibition of interleukin-1 following knee injury prevents post-traumatic arthritis. *Arthritis Research & Therapy,* 16**,** R134.

GAIKWAD, V. 2010. Formulation and evaluation of In-Situ gel of metoprolol tartrate for nasal delivery. *Journal of Pharmacy Research* 3**,** 788-793.

GALARZA TORRE, A., SHAW, J. E., WOOD, A., GILBERT, H. T. J., DOBRE, O., GENEVER, P., BRENNAN, K., RICHARDSON, S. M. & SWIFT, J. 2018. An immortalised mesenchymal stem cell line maintains mechano-responsive behaviour and can be used as a reporter of substrate stiffness. *Scientific reports,* 8**,** 8981.

GANDHI, A., PAUL, A., SEN, S. O. & SEN, K. K. 2015. Studies on thermoresponsive polymers: Phase behaviour, drug delivery and biomedical applications. *Asian Journal of Pharmaceutical Sciences,* 10**,** 99-107.

GAO, Y., MORITA, I., MARUO, N., KUBOTA, T., MUROTA, S. & ASO, T. 1998. Expression of IL-6 Receptor and GP130 in Mouse Bone Marrow Cells During Osteoclast Differentiation. *Bone,* 22**,** 487-493.

GARCÍA-LÓPEZ, S., MEIKLE, M. C., VILLANUEVA, R. E., MONTAÑO, L., MASSÓ, F., RAMÍREZ-AMADOR, V. & BOJALIL, R. 2005. Mechanical deformation inhibits IL-10 and stimulates IL-12 production by mouse calvarial osteoblasts in vitro. *Archives of Oral Biology,* 50**,** 449-452.

GAUDIO, A., PENNISI, P., BRATENGEIER, C., TORRISI, V., LINDNER, B., MANGIAFICO, R. A., PULVIRENTI, I., HAWA, G., TRINGALI, G. & FIORE, C. E. 2010. Increased sclerostin serum levels associated with bone formation and resorption markers in patients with immobilization-induced bone loss. *J Clin Endocrinol Metab,* 95**,** 2248-53.

GEE, K., GUZZO, C., CHE MAT, N. F., MA, W. & KUMAR, A. 2009. The IL-12 family of cytokines in infection, inflammation and autoimmune disorders. *Inflamm Allergy Drug Targets,* 8**,** 40-52.

GENDRON, C., KASHIWAGI, M., LIM, N. H., ENGHILD, J. J., THØGERSEN, I. B., HUGHES, C., CATERSON, B. & NAGASE, H. 2007. Proteolytic activities of human ADAMTS-5: comparative studies with ADAMTS-4. *Journal of Biological Chemistry,* 282**,** 18294-18306.

GENEVER, P. G. & SKERRY, T. M. 2001. Regulation of spontaneous glutamate release activity in osteoblastic cells and its role in differentiation and survival: evidence for intrinsic glutamatergic signaling in bone. *The FASEB Journal,* 15**,** 1586-1588.

GERSTENFELD, L. C., CULLINANE, D. M., BARNES, G. L., GRAVES, D. T. & EINHORN, T. A. 2003. Fracture healing as a post-natal developmental process: molecular, spatial, and temporal aspects of its regulation. *J Cell Biochem,* 88**,** 873-84.

GEURTS, J., VAN DEN BRAND, B. T., WOLF, A., ABDOLLAHI-ROODSAZ, S., ARNTZ, O. J., KRACHT, M., VAN DEN BERG, W. B. & VAN DE LOO, F. A. 2011. Toll-like receptor 4 signalling is specifically TGF-beta-activated kinase 1 independent in synovial fibroblasts. *Rheumatology (Oxford),* 50**,** 1216-25.

GEURTS, J., JURIC, D., MULLER, M., SCHAREN, S. & NETZER, C. 2018. Novel Ex Vivo Human Osteochondral Explant Model of Knee and Spine Osteoarthritis Enables Assessment of Inflammatory and Drug Treatment Responses. *Int J Mol Sci,* 19**,** 1314.

GHALME, S., MANKAR, A. & BHALERAO, Y. J. 2016. Biomaterials in Hip Joint Replacement. *International Journal of Materials Science and Engineering,* 4**,** 113-125.

GHOURI, A. & CONAGHAN, P. G. 2019. Update on novel pharmacological therapies for osteoarthritis. *Therapeutic Advances in Musculoskeletal Disease,* 11**,** 1759720X19864492.

GIBALDI, M. & FELDMAN, S. 1967. Establishment of sink conditions in dissolution rate determinations. Theoretical considerations and application to nondisintegrating dosage forms. *Journal of Pharmaceutical Sciences,* 56**,** 1238-1242.

GILBERT, J. C., HADGRAFT, J., BYE, A. & BROOKES, L. G. 1986. Drug release from Pluronic F-127 gels. *International Journal of Pharmaceutics,* 32**,** 223-228.

GILBERT, S. J., BONNET, C. S., STADNIK, P., DUANCE, V. C., MASON, D. J. & BLAIN, E. J. 2018. Inflammatory and degenerative phases resulting from anterior cruciate rupture in a non-invasive murine model of post-traumatic osteoarthritis. *Journal of Orthopaedic Research,* 36**,** 2118-2127.

GILBERT, S. J., BONNET, C. S. & MASON, D. J. 2020. The use of a 3-dimensional mechanical loading model of human stem cell derived osteocytes to study the 'mechanosome' [abstract]. *Osteoarthritis and Cartilage,* 28**,** S183.

GILLQUIST, J. & MESSNER, K. 1999. Anterior Cruciate Ligament Reconstruction and the Long Term Incidence of Gonarthrosis. *Sports Medicine,* 27**,** 143-156.

GIOFFREDI, E., BOFFITO, M., CALZONE, S., GIANNITELLI, S. M., RAINER, A., TROMBETTA, M., MOZETIC, P. & CHIONO, V. 2016. Pluronic F127 Hydrogel Characterization and Biofabrication in Cellularized Constructs for Tissue Engineering Applications. *Procedia CIRP,* 49**,** 125-132.

GLYN-JONES, S., PALMER, A. J. R., AGRICOLA, R., PRICE, A. J., VINCENT, T. L., WEINANS, H. & CARR, A. J. 2015. Osteoarthritis. *The Lancet,* 386**,** 376-387.

GOKAY, N. S., YILMAZ, I., KOMUR, B., DEMIROZ, A. S., GOKCE, A., DERVISOGLU, S. & GOKAY, B. V. 2016. A Comparison of the Effects of Neuronal Nitric Oxide Synthase and Inducible Nitric Oxide Synthase Inhibition on Cartilage Damage. *BioMed Research International* 2016**,** 8.

GOLDBERG, M. & GOMEZ-ORELLANA, I. 2003. Challenges for the oral delivery of macromolecules. *Nature Reviews Drug Discovery,* 2**,** 289-295.
GOLDBERG, R. L., HUFF, J. P., LENZ, M. E., GLICKMAN, P., KATZ, R. & THONAR, E. J.-M. A. 1991. Elevated plasma levels of hyaluronate in patients with osteoarthritis and rheumatoid arthritis. *Arthritis & Rheumatism,* 34**,** 799-807.
GOLDRING, M. B. & MARCU, K. B. 2009. Cartilage homeostasis in health and rheumatic diseases. *Arthritis Res Ther,* 11**,** 224.
GOLUB, E. E. & BOESZE-BATTAGLIA, K. 2007. The role of alkaline phosphatase in mineralization. *Current Opinion in Orthopaedics,* 18**,** 444-448.
GONG, C., QI, T., WEI, X., QU, Y., WU, Q., LUO, F. & QIAN, F. 2013. Thermosensitive polymeric hydrogels as drug delivery systems *Current Medicinal Chemistry* 20**,** 79-94.
GOSSAN, N., BOOT-HANDFORD, R. & MENG, Q.-J. 2015. Ageing and osteoarthritis: a circadian rhythm connection. *biogerontology* 16**,** 209-219.
GOUTTEBARGE, V., INKLAAR, H., BACKX, F. & KERKHOFFS, G. 2015. Prevalence of osteoarthritis in former elite athletes: a systematic overview of the recent literature. *Rheumatol. Int* 35**,** 405-418.
GRAVES, D. T., JIANG, Y. & VALENTE, A. J. 1999. The expression of monocyte chemoattractant protein-1 and other chemokines by osteoblasts. *Frontiers in Bioscience* 4**,** 571-580.
GREENBLATT, M. B., TSAI, J. N. & WEIN, M. N. 2017. Bone Turnover Markers in the Diagnosis and Monitoring of Metabolic Bone Disease. *Clinical Chemistry,* 63**,** 464-474.
GU, G., MULARI, M., PENG, Z., HENTUNEN, T. A. & VÄÄNÄNEN, H. K. 2005. Death of osteocytes turns off the inhibition of osteoclasts and triggers local bone resorption. *Biochemical and Biophysical Research Communications,* 335**,** 1095-1101.
GU, Y. & PUBLICOVER, S. J. 2000. Expression of functional metabotropic glutamate receptors in primary cultured rat osteoblasts. Cross-talk with N-methyl-D-aspartate receptors. *Journal of Biological Chemistry,* 275**,** 34252-34259.
GU, Y., GENEVER, P. G., SKERRY, T. M. & PUBLICOVER, S. J. 2002. The NMDA type glutamate receptors expressed by primary rat osteoblasts have the same electrophysiological characteristics as neuronal receptors. *Calcif Tissue Int,* 70**,** 194-203.
GUO, D. D., XU, C. X., QUAN, J. S., SONG, C. K., JIN, H., KIM, D. D., CHOI, Y. J., CHO, M. H. & CHO, C. S. 2009. Synergistic anti-tumor activity of paclitaxel-incorporated conjugated linoleic acid-coupled poloxamer thermosensitive hydrogel in vitro and in vivo. *Biomaterials,* 30**,** 4777-4785.
GÜRSOY, A., EROĞLU, L., ULUTIN, S., TAŞYÜREK, M., FESSI, H., PUISIEUX, F. & DEVISSAGUET, J. P. 1989. Evaluation of indomethacin nanocapsules for their physical stability and inhibitory activity on inflammation and platelet aggregation. *International Journal of Pharmaceutics,* 52**,** 101-108.
GUZMAN, R. E., EVANS, M. G., BOVE, S., MORENKO, B. & KILGORE, K. 2003. Mono-iodoacetate-induced histologic changes in subchondral bone and articular cartilage of rat femorotibial joints: an animal model of osteoarthritis. *Toxicol Pathol,* 31**,** 619-24.
HAAS, S. & STRAUB, R. H. 2012. Disruption of rhythms of molecular clocks in primary synovial fibroblasts of patients with osteoarthritis and rheumatoid arthritis, role of IL-1beta/TNF. *Arthritis Res Ther,* 14**,** R122.
HAJATI, A.-K., ALSTERGREN, P., NÄSSTRÖM, K., BRATT, J. & KOPP, S. 2009. Endogenous Glutamate in Association With Inflammatory and Hormonal Factors Modulates Bone

Tissue Resorption of the Temporomandibular Joint in Patients With Early Rheumatoid Arthritis. *Journal of Oral and Maxillofacial Surgery,* 67**,** 1895-1903.
HALYABAR, O., MEHTA, J., RINGOLD, S., RUMSEY, D. G. & HORTON, D. B. 2019. Treatment Withdrawal Following Remission in Juvenile Idiopathic Arthritis: A Systematic Review of the Literature. *Pediatric Drugs,* 21**,** 469-492.
HAMILTON, C. J., REID, L. S. & JAMAL, S. A. 2013. Organic nitrates for osteoporosis: an update. *BoneKey reports,* 2**,** 259.
HAMMACHER, A., WARD, L. D., WEINSTOCK, J., TREUTLEIN, H., YASUKAWA, K. & SIMPSON, R. J. 1994. Structure-function analysis of human IL-6: identification of two distinct regions that are important for receptor binding. *Protein Sci,* 3**,** 2280-93.
HAN, X., GELEIN, R., CORSON, N., WADE-MERCER, P., JIANG, J., BISWAS, P., FINKELSTEIN, J. N., ELDER, A. & OBERDÖRSTER, G. 2011. Validation of an LDH assay for assessing nanoparticle toxicity. *Toxicology,* 287**,** 99-104.
HANI, U. & SHIVAKUMAR, H. G. 2013. Development of Miconazole nitrate Thermosensitive Bioadhesive Vaignal Gel for Vaginal Candidiasis. *American Journal of Advanced Drug Delivery* 3**,** 358-368.
HAO, Z., MA, Y., WU, J., LI, X., CHEN, H., SHEN, J. & WANG, H. 2017. Osteocytes regulate osteoblast differentiation and osteoclast activity through Interleukin-6 under mechanical loading. *RSC Adv.,* 7**,** 50200-50209.
HART, P. H., AHERN, M. J., SMITH, M. D. & FINLAY-JONES, J. J. 1995. Regulatory effects of IL-13 on synovial fluid macrophages and blood monocytes from patients with inflammatory arthritis. *Clin Exp Immunol,* 99**,** 331-7.
HARTJEN, N., BRAUER, L., REISS, B., CLAASSEN, H., BEILEKE, S., GARREIS, F., HOOGEBOOM, S., TSOKOS, M., ETZOLD, S., MULLER-HILKE, B., GELSE, K., MULLER, T., GOLDRING, M. B., PAULSEN, F. & SCHICHT, M. 2018. Evaluation of surfactant proteins A, B, C, and D in articular cartilage, synovial membrane and synovial fluid of healthy as well as patients with osteoarthritis and rheumatoid arthritis. *PLoS One,* 13**,** e0203502.
HAUSMANN, L. R. M., YOUK, A., KWOH, C. K., IBRAHIM, S. A., HANNON, M. J., WEINER, D. K., GALLAGHER, R. M. & PARKS, A. 2017. Testing a Positive Psychological Intervention for Osteoarthritis. *Pain Medicine* 18**,** 1908-1920.
HAYAMI, T., PICKARSKI, M., ZHUO, Y., WESOLOWSKI, G. A., RODAN, G. A. & DUONG, L. T. 2006. Characterization of articular cartilage and subchondral bone changes in the rat anterior cruciate ligament transection and meniscectomized models of osteoarthritis. *Bone,* 38**,** 234-43.
HAYFLICK, L. & MOORHEAD, P. S. 1961. The serial cultivation of human diploid cell strains. *Exp Cell Res,* 25**,** 585-621.
HAYFLICK, L. 1965. The limited in vitro lifetime of human diploid cell strains. *Experimental Cell Research,* 37**,** 614-636.
HE, C., KIM, S. W. & LEE, D. S. 2008. In situ gelling stimuli-sensitive block copolymer hydrogels for drug delivery. *Journal of Controlled Release,* 127**,** 189-207.
HEARD, B. J., BARTON, K. I., CHUNG, M., ACHARI, Y., SHRIVE, N. G., FRANK, C. B. & HART, D. A. 2015. Single intra-articular dexamethasone injection immediately post-surgery in a rabbit model mitigates early inflammatory responses and post-traumatic osteoarthritis-like alterations. *Journal of Orthopaedic Research,* 33**,** 1826-1834.
HEILAND, G. R., ZWERINA, K., BAUM, W., KIREVA, T., DISTLER, J. H., GRISANTI, M., ASUNCION, F., LI, X., OMINSKY, M., RICHARDS, W., SCHETT, G. & ZWERINA, J. 2010.

Neutralisation of Dkk-1 protects from systemic bone loss during inflammation and reduces sclerostin expression. *Ann Rheum Dis,* 69**,** 2152-2159.
HEITEMEYER, U., CLAES, L., HIERHOLZER, G. & KÖRBER, M. 1990. Significance of postoperative stability for bony reparation of comminuted fractures. An experimental study. *Arch Orthop Trauma Surg,* 109**,** 144-149.
HENDERSON, B. & PETTIPHER, E. R. 1989. Arthritogenic actions of recombinant IL-1 and tumour necrosis factor alpha in the rabbit: evidence for synergistic interactions between cytokines in vivo. *Clinical and experimental immunology,* 75**,** 306-310.
HENDRIKS, J., RIESLE, J. & VAN BLITTERSWIJK, C. A. 2007. Co-culture in cartilage tissue engineering. *Journal of Tissue Engineering and Regenerative Medicine,* 1**,** 170-178.
HENRIKSEN, M., GRAVEN-NIELSEN, T., AABOE, J., ANDRIACCHI, T. P. & BLIDDAL, H. 2010. Gait changes in patients with knee osteoarthritis are replicated by experimental knee pain. *Arthritis Care & Research,* 62**,** 501-509.
HEPPER, C. T., HALVORSON, J. J., DUNCAN, S. T., GREGORY, A. J. M., DUNN, W. R. & SPINDLER, K. P. 2009. The Efficacy and Duration of Intra-articular Corticosteroid Injection for Knee Osteoarthritis: A Systematic Review of Level I Studies. *JAAOS - Journal of the American Academy of Orthopaedic Surgeons,* 17**,** 638-646.
HERRLING, P. L. 1997. *Excitatory amino acids: clinical results with antagonists* Academic Press
HIGAKI, M., ISHIHARA, T., IZUMO, N., TAKATSU, M. & MIZUSHIMA, Y. 2005. Treatment of experimental arthritis with poly(D, L-lactic/glycolic acid) nanoparticles encapsulating betamethasone sodium phosphate. *Annals of the Rheumatic Diseases,* 64**,** 1132-1136.
HIGUCHI, H., SHIRAKURA, K., KIMURA, M., TERAUCHI, M., SHINOZAKI, T., WATANABE, H. & TAKAGISHI, K. 2006. Changes in biochemical parameters after anterior cruciate ligament injury. *International orthopaedics,* 30**,** 43-47.
HIGUCHI, W. I. 1962. Analysis of Data on the Medicament Release from Ointments. *Journal of Pharmaceutical Sciences,* 51**,** 802-804.
HILAL, G., MARTEL-PELLETIER, J., PELLETIER, J.-P., RANGER, P. & LAJEUNESSE, D. 1998. Osteoblast-like cells from human subchondral osteoarthritic bone demonstrate an altered phenotype in vitro: Possible role in subchondral bone sclerosis. *Arthritis & Rheumatism,* 41**,** 891-899.
HILIGSMANN, M., COOPER, C., ARDEN, N., BOERS, M., BRANCO, J. C., BRANDI, M. L., BRUYÈRE, O., GUILLEMIN, F., HOCHBERG, M. C., HUNTER, D. J., KANIS, J. A., KVIEN, T. K., LASLOP, A., PELLETIER, J.-P., PINTO, D., REITER-NIESERT, S., RIZZOLI, R., ROVATI, L. C., SEVERENS, J. L. H., SILVERMAN, S., TSOUDEROS, Y., TUGWELL, P. & REGINSTER, J.-Y. 2013. Health economics in the field of osteoarthritis: an expert's consensus paper from the European Society for Clinical and Economic Aspects of Osteoporosis and Osteoarthritis (ESCEO). *Semin Arthritis Rheum,* 43**,** 303-13.
HILL, C. L., GALE, D. G., CHAISSON, C. E., SKINNER, K., KAZIS, L., GALE, M. E. & FELSON, D. T. 2001. Knee effusions, popliteal cysts, and synovial thickening: association with knee pain in osteoarthritis. *The Journal of Rheumatology,* 28**,** 1330-1337.
HILL, P. A. 1998. Bone Remodelling. *British Journal of Orthodontics,* 25**,** 101-107.
HINOI, E., FUJIMORI, S., NAKAMURA, Y. & YONEDA, Y. 2001. Group III metabotropic glutamate receptors in rat cultured calvarial osteoblasts. *Biochem Biophys Res Commun,* 281**,** 341-346.

HINOI, E., FUJIMORI, S., TAKARADA, T., TANIURA, H. & YONEDA, Y. 2002a. Facilitation of glutamate release by ionotropic glutamate receptors in osteoblasts. *Biochem Biophys Res Commun,* 297**,** 452-458.

HINOI, E., FUJIMORI, S., TAKEMORI, A., KURABAYASHI, H., NAKAMURA, Y. & YONEDA, Y. 2002b. Demonstration of expression of mRNA for particular AMPA and kainate receptor subunits in immature and mature cultured rat calvarial osteoblasts. *Brain Res,* 943**,** 112-116.

HINOI, E., FUJIMORI, S. & YONEDA, Y. 2003. Modulation of cellular differentiation by N-methyl-d-aspartate receptors in osteoblasts. *The FASEB Journal,* 17**,** 1-23.

HINOI, E., TAKARADA, T., UESHIMA, T., TSUCHIHASHI, Y. & YONEDA, Y. 2004. Glutamate signaling in peripheral tissues. *European Journal of Biochemistry,* 271**,** 1-13.

HINOI, E., OHASHI, R., MIYATA, S., KATO, Y., IEMATA, M., HOJO, H., TAKARADA, T. & YONEDA, Y. 2005. Excitatory amino acid transporters expressed by synovial fibroblasts in rats with collagen-induced arthritis. *Biochemical Pharmacology,* 70**,** 1744-1755.

HINOI, E., TAKARADA, T., UNO, K., INOUE, M., MURAFUJI, Y. & YONEDA, Y. 2007. Glutamate Suppresses Osteoclastogenesis through the Cystine/Glutamate Antiporter. *The American Journal of Pathology,* 170**,** 1277-1290.

HINTON, P. V., RACKARD, S. M. & KENNEDY, O. D. 2018. In Vivo Osteocyte Mechanotransduction: Recent Developments and Future Directions *Biomechanics,* 16**,** 746-753.

HIXSON, A. W. & CROWELL, J. H. 1931. Dependence of Reaction Velocity upon surface and Agitation. *Industrial & Engineering Chemistry,* 23**,** 923-931.

HOCHBERG, M., GUERMAZI, A., GUEHRING, H., AYDEMIR, A., WAX, S., FLEURANCEAU-MOREL, P., REINSTRUP BIHLET, A., BYRJALSEN, I., RAGNAR ANDERSEN, J. & ECKSTEIN, F. 2018. OP0059 Efficacy and safety of intra-articular sprifermin in symptomatic radiographic knee osteoarthritis: pre-specified analysis of 3-year data from a 5-year randomised, placebo-controlled, phase ii study [abstract]. *Annals of the Rheumatic Diseases,* 77**,** 80-81.

HOFBAUER, L. C. & HEUFELDER, A. E. 2001. Role of receptor activator of nuclear factor-kappaB ligand and osteoprotegerin in bone cell biology. *J Mol Med (Berl),* 79**,** 243-53.

HOFMANN, S., SEITLINGER, G., DJAHANI, O. & PIETSCH, M. 2011. The painful knee after TKA: a diagnostic algorithm for failure analysis. *Knee Surgery, Sports Traumatology, Arthroscopy,* 19**,** 1442.

HOLYOAK, D. T., TIAN, Y. F., VAN DER MEULEN, M. C. H. & SINGH, A. 2016. Osteoarthritis: Pathology, mouse models, and nanoparticle injectable systems for targeted treatment. *Annals of biomedical engineering,* 44**,** 2062-2075.

HOMANDBERG, G. A., WEN, C. & HUI, F. 1998. Cartilage damaging activities of fibronectin fragments derived from cartilage and synovial fluid. *Osteoarthritis and Cartilage,* 6**,** 231-244.

HONORÉ, T., DAVIES, S. N., DREJER, J., FLETCHER, E. J., JACOBSEN, P., LODGE, D. & NIELSEN, F. E. 1988. Quinoxalinediones: Potent Competitive Non-NMDA Glutamate Receptor Antagonists. *Science,* 241**,** 701-703.

HORWOOD, N. J., ELLIOTT, J., MARTIN, T. J. & GILLESPIE, M. T. 2001. IL-12 Alone and in Synergy with IL-18 Inhibits Osteoclast Formation In Vitro. *The Journal of Immunology,* 166**,** 4915-4921.

HRONIK-TUPAJ, M., RICE, W. L., CRONIN-GOLOMB, M., KAPLAN, D. L. & GEORGAKOUDI, I. 2011. Osteoblastic differentiation and stress response of human mesenchymal stem cells exposed to alternating current electric fields. *BioMedical Engineering OnLine,* 10.

HSU, J. D. & ROBINSON, R. A. 1969. Studies on the healing of long-bone fractures in hereditary pituitary insufficient mice. *J Surg Res,* 9**,** 535-6.

HUANG, H., QUAN, Y. Y., WANG, X. P. & CHEN, T. S. 2016. Gold Nanoparticles of Diameter 13 nm Induce Apoptosis in Rabbit Articular Chondrocytes. *Nanoscale Res Lett,* 11.

HUANG, S., SONG, X., LI, T., XIAO, J., CHEN, Y., GONG, X., ZENG, W., YANG, L. & CHEN, C. 2017. Pellet coculture of osteoarthritic chondrocytes and infrapatellar fat pad-derived mesenchymal stem cells with chitosan/hyaluronic acid nanoparticles promotes chondrogenic differentiation. *Stem Cell Res Ther,* 8**,** 264.

HUANG, W., TSUI, C. P., TANG, C. Y. & GU, L. 2018. Effects of Compositional Tailoring on Drug Delivery Behaviours of Silica Xerogel/Polymer Core-shell Composite Nanoparticles. *Scientific Reports,* 8**,** 13002.

HUGGETT, J., VAUGHAN-THOMAS, A. & MASON, D. 2000. The open reading frame of the Na+-dependent glutamate transporter GLAST-1 is expressed in bone and a splice variant of this molecule is expressed in bone and brain. *FEBS Letters,* 485**,** 13-18.

HUGGETT, J. F., MUSTAFA, A., O'NEAL, L. & MASON, D. J. 2002. The glutamate transporter GLAST-1 (EAAT-1) is expressed in the plasma membrane of osteocytes and is responsive to extracellular glutamate concentration. *Biochem Soc Trans,* 30**,** 890-893.

HUI, A. Y., MCCARTY, W. J., MASUDA, K., FIRESTEIN, G. S. & SAH, R. L. 2012. A systems biology approach to synovial joint lubrication in health, injury, and disease. *WIREs Systems Biology and Medicine,* 4**,** 15-37.

HUNTER, D. J., MARCH, L. & SAMBROOK, P. N. 2003. The association of cartilage volume with knee pain. *Osteoarthritis and Cartilage,* 11**,** 725-729.

HUNTER, L. J., WOOD, D. M. & DARGAN, P. I. 2011. The patterns of toxicity and management of acute nonsteroidal anti-inflammatory drug (NSAID) overdose. *Open Access Emergency Medicine : OAEM,* 3**,** 39-48.

ICHISEKI, T., MATSUMOTO, T., NISHINO, M., KANEUJI, A. & KATSUDA, S. 2004. Oxidative stress and vascular permeability in steroid-induced osteonecrosis model. *Journal of Orthopaedic Science,* 9**,** 509-515.

IGARASHI, K., SAEKI, S. & SHINODA, H. 2013. Diurnal rhythms in the incorporation and secretion of 3H-proline and 3H-galactose by cartilage cells and osteoblasts in various bone-forming sites in growing rats. *Orthodontic Waves,* 72**,** 11-15.

IGNATIUS, A., BLESSING, H., LIEDERT, A., SCHMIDT, C., NEIDLINGER-WILKE, C., KASPAR, D., FRIEMERT, B. & CLAES, L. 2005. Tissue engineering of bone: effects of mechanical strain on osteoblastic cells in type I collagen matrices. *Biomaterials,* 26**,** 311-318.

IIZUKA, M., YAO, R. & WAINAPEL, S. 2005. Saphenous nerve injury following medial knee joint injection: A case report. *Archives of Physical Medicine and Rehabilitation,* 86**,** 2062-2065.

ILESANMI-OYELERE, B. L., SCHOLLUM, L., KUHN-SHERLOCK, B., MCCONNELL, M., MROS, S., COAD, J., ROY, N. C. & KRUGER, M. C. 2019. Inflammatory markers and bone health in postmenopausal women: a cross-sectional overview. *Immunity & Ageing,* 16**,** 15.

INGHAM, B., BRENTNALL, D. W., DALE, E. A. & MCFADZEAN, J. A. 1977. Arthropathy induced by antibacterial fused N-alkyl-4-pyridone-3-carboxylic acids. *Toxicology Letters,* 1**,** 21-26.

INGWERSEN, S. H., OHRSTROM, J. K., PETERSEN, P., DRUSTRUP, J., BRUNO, L. & NORDHOLM, L. 1994. Human Pharmacokinetics of the Neuroprotective Agent NBQX. *Am J Ther,* 1**,** 296-303.

INSALL, J. 1974. The Pridie Debridement Operation for Osteoarthritis of the Knee. *Clinical Orthopaedics and Related Research (1976-2007),* 101**,** 61-67.

ISHIHARA, G., KOJIMA, T., SAITO, Y. & ISHIGURO, N. 2009a. Roles of metalloproteinase-3 and aggrecanase 1 and 2 in aggrecan cleavage during human meniscus degeneration. *Orthopedic reviews,* 1**,** e14.

ISHIHARA, T., KUBOTA, T., CHOI, T. & HIGAKI, M. 2009b. Treatment of Experimental Arthritis with Stealth-Type Polymeric Nanoparticles Encapsulating Betamethasone Phosphate. *Journal of Pharmacology and Experimental Therapeutics,* 329**,** 412-417.

ISHIMI, Y., MIYAURA, C., JIN, C. H., AKATSU, T., ABE, E., NAKAMURA, Y., YAMAGUCHI, A., YOSHIKI, S., MATSUDA, T. & HIRANO, T. 1990. IL-6 is produced by osteoblasts and induces bone resorption. *J Immunol,* 145**,** 3297-3303.

JACKSON, R. W., REED, C. A., ISRAEL, J. A., ABOU-KEER, F. K. & GARSIDE, H. 1970. Production of a standard experimental fracture. *Can J Surg,* 13**,** 415-20.

JAIN, A., MISHRA, S. K., VUDDANDA, P. R., SINGH, S. K., SINGH, R. & SINGH, S. 2014. Targeting of diacerein loaded lipid nanoparticles to intra-articular cartilage using chondroitin sulfate as homing carrier for treatment of osteoarthritis in rats. *Nanomedicine: Nanotechnology, Biology and Medicine,* 10**,** e1031-e1040.

JALAAL, M., COTTRELL, G., BALMFORTH, N. & STOEBER, B. 2017. On the rheology of Pluronic F127 aqueous solutions. *Journal of Rheology,* 61**,** 139-146.

JAMES, S., FOX, J., AFSARI, F., LEE, J., CLOUGH, S., KNIGHT, C., ASHMORE, J., ASHTON, P., PREHAM, O., HOOGDUIJN, M., PONZONI, RAQUEL DE ALMEIDA R., HANCOCK, Y., COLES, M. & GENEVER, P. 2015. Multiparameter Analysis of Human Bone Marrow Stromal Cells Identifies Distinct Immunomodulatory and Differentiation-Competent Subtypes. *Stem Cell Reports,* 4**,** 1004-1015.

JANSEN, N. W., ROOSENDAAL, G., HOOIVELD, M. J., BIJLSMA, J. W., VAN ROON, J. A., THEOBALD, M. & LAFEBER, F. P. 2008. Interleukin-10 protects against blood-induced joint damage. *Br J Haematol,* 142**,** 953-61.

JEAN, Y. H., WEN, Z. H., CHANG, Y. C., HUANG, G. S., LEE, H. S., HSIEH, S. P. & WONG, C. S. 2005. Increased concentrations of neuro-excitatory amino acids in rat anterior cruciate ligament-transected knee joint dialysates: a microdialysis study. *J Orthop Res,* 23**,** 569-75.

JEFFREY, J. E. & ASPDEN, R. M. 2006. The Biophysical Effects of a Single Impact Load on Human and Bovine Articular Cartilage. *Proceedings of the Institution of Mechanical Engineers, Part H: Journal of Engineering in Medicine,* 220**,** 677-686.

JEON, J., MALDA, J., SCHROBBACK, K., IRAWAN, D., MASUDA, K., SAH, R., HUTMACHER, D. & KLEIN, T. 2010. *3-D Tissue Engineering (Chapter 13): Engineering cartilage tissue with zonal properties. ,* Boston, Artech House.

JIN, P., WIRAJA, C., ZHAO, J., ZHANG, J., ZHENG, L. & XU, C. 2017. Nitric Oxide Nanosensors for Predicting the Development of Osteoarthritis in Rat Model. *ACS Applied Materials & Interfaces,* 9**,** 25128-25137.

JO, J., CHOI, S., OH, J., LEE, S.-G., CHOI, S. Y., KIM, K. K. & PARK, C. 2019. Conventionally used reference genes are not outstanding for normalization of gene expression in human cancer research. *BMC Bioinformatics,* 20**,** 245.

JOHNSON, A. R., PAVLOVSKY, A. G., ORTWINE, D. F., PRIOR, F., MAN, C.-F., BORNEMEIER, D. A., BANOTAI, C. A., MUELLER, W. T., MCCONNELL, P., YAN, C., BARAGI, V., LESCH, C., ROARK, W. H., WILSON, M., DATTA, K., GUZMAN, R., HAN, H.-K. & DYER, R. D. 2007. Discovery and Characterization of a Novel Inhibitor of Matrix Metalloprotease-13 That Reduces Cartilage Damage in Vivo without Joint Fibroplasia Side Effects. *Journal of Biological Chemistry,* 282**,** 27781-27791.

JOHNSON, C. I., ARGYLE, D. J. & CLEMENTS, D. N. 2016. In vitro models for the study of osteoarthritis. *The Veterinary Journal,* 209**,** 40-49.

JONES, D. H., KONG, Y.-Y. & PENNINGER, J. M. 2002. Role of RANKL and RANK in bone loss and arthritis. *Annals of the Rheumatic Diseases,* 61**,** ii32-ii39.

JONES, G. B., COLLINS, D. S., HARRISON, M. W., THYAGARAJAPURAM, N. R. & WRIGHT, J. M. 2017. Subcutaneous drug delivery: An evolving enterprise. *Sci Transl Med,* 9.

JONES, S. A. & ROSE-JOHN, S. 2002. The role of soluble receptors in cytokine biology: the agonistic properties of the sIL-6R/IL-6 complex. *Biochim Biophys Acta,* 1592**,** 251-63.

JUNG, Y.-S., PARK, W., PARK, H., LEE, D.-K. & NA, K. 2017. Thermo-sensitive injectable hydrogel based on the physical mixing of hyaluronic acid and Pluronic F-127 for sustained NSAID delivery. *Carbohydrate Polymers,* 156**,** 403-408.

JUSTICE, B. A., BADR, N. A. & FELDER, R. A. 2009. 3D cell culture opens new dimensions in cell-based assays. *Drug Discovery Today,* 14**,** 102-107.

KAASALAINEN, M., MÄKILÄ, E., RIIKONEN, J., KOVALAINEN, M., JÄRVINEN, K., HERZIG, K.-H., LEHTO, V.-P. & SALONEN, J. 2012. Effect of isotonic solutions and peptide adsorption on zeta potential of porous silicon nanoparticle drug delivery formulations. *International Journal of Pharmaceutics,* 431**,** 230-236.

KABANOV, A. V., BATRAKOVA, E. V. & ALAKHOV, V. Y. 2002. Pluronic® block copolymers as novel polymer therapeutics for drug and gene delivery. *Journal of Controlled Release,* 82**,** 189-212.

KAISER, H. F. 1974. An index of factorial simplicity. *Psychometrika,* 39**,** 31-36.

KAISER, K., PRYSTAZ, K., VIKMAN, A., HAFFNER-LUNTZER, M., BERGDOLT, S., STRAUSS, G., WAETZIG, G. H., ROSE-JOHN, S. & IGNATIUS, A. 2018. Pharmacological inhibition of IL-6 trans-signaling improves compromised fracture healing after severe trauma. *Naunyn-Schmiedeberg's archives of pharmacology,* 391**,** 523-536.

KALARITI, N., LEMBESSIS, P., PAPAGEORGIOU, E., PISSIMISSIS, N. & KOUTSILIERIS, M. 2007. Regulation of the mGluR5, EAAT1 and GS expression by glucocorticoids in MG-63 osteoblast-like osteosarcoma cells. *J Musculoskelet Neuronal Interact,* 7**,** 113-118.

KAMEKURA, S., KAWASAKI, Y., HOSHI, K., SHIMOAKA, T., CHIKUDA, H., MARUYAMA, Z., KOMORI, T., SATO, S., TAKEDA, S., KARSENTY, G., NAKAMURA, K., CHUNG, U. I. & KAWAGUCHI, H. 2006. Contribution of runt-related transcription factor 2 to the pathogenesis of osteoarthritis in mice after induction of knee joint instability. *Arthritis Rheum,* 54**,** 2462-2470.

KANBE, K., INOUE, K., XIANG, C. & CHEN, Q. 2006. Identification of clock as a mechanosensitive gene by large-scale DNA microarray analysis: downregulation in osteoarthritic cartilage. *Mod Rheumatol,* 16**,** 131-136.

KANG, M. L., KO, J.-Y., KIM, J. E. & IM, G.-I. 2014. Intra-articular delivery of kartogenin-conjugated chitosan nano/microparticles for cartilage regeneration. *Biomaterials,* 35**,** 9984-9994.

KAPADIA, B. H., BERG, R. A., DALEY, J. A., FRITZ, J., BHAVE, A. & MONT, M. A. 2016. Periprosthetic joint infection. *The Lancet,* 387**,** 386-394.

KAPOOR, M., MARTEL-PELLETIER, J., LAJEUNESSE, D., PELLETIER, J.-P. & FAHMI, H. 2011. Role of proinflammatory cytokines in the pathophysiology of osteoarthritis. *Nat Rev Rheumatol,* 7**,** 33-42.

KARSDAL, M. A., LEEMING, D. J., DAM, E. B., HENRIKSEN, K., ALEXANDERSEN, P., PASTOUREAU, P., ALTMAN, R. D. & CHRISTIANSEN, C. 2008. Should subchondral bone turnover be targeted when treating osteoarthritis? *Osteoarthritis and Cartilage,* 16**,** 638-646.

KARVONEN, R. L., MILLER, P. R., NELSON, D. A., GRANDA, J. L. & FERNÁNDEZ-MADRID, F. 1998. Periarticular osteoporosis in osteoarthritis of the knee. *The Journal of rheumatology,* 25**,** 2187-2194.

KASSEBAUM, N. J., ARORA, M., BARBER, R. M., BHUTTA, Z. A., BROWN, J., CARTER, A., CASEY, D. C., CHARLSON, F. J., COATES, M. M., COGGESHALL, M., CORNABY, L., DANDONA, L., DICKER, D. J., ERSKINE, H. E., FERRARI, A. J., FITZMAURICE, C., FOREMAN, K., FOROUZANFAR, M. H., FULLMAN, N. & AL., E. 2016. Global, regional, and national disability-adjusted life-years (DALYs) for 315 diseases and injuries and healthy life expectancy (HALE), 1990-2015: a systematic analysis for the Global Burden of Disease Study 2015. *Lancet,* 388**,** 1603-1658.

KAVANAUGH, A., VAN VOLLENHOVEN, R. F., FLEISCHMANN, R., EMERY, P., SAINSBURY, I., FLORENTINUS, S., CHEN, S., GUERETTE, B., KUPPER, H. & SMOLEN, J. S. 2018. Testing treat-to-target outcomes with initial methotrexate monotherapy compared with initial tumour necrosis factor inhibitor (adalimumab) plus methotrexate in early rheumatoid arthritis. *Ann Rheum Dis,* 77**,** 289-292.

KAWASHIMA, N. & STASHENKO, P. 1999. Expression of bone-resorptive and regulatory cytokines in murine periapical inflammation. *Archives of Oral Biology,* 44**,** 55-66.

KAY, A. G., STONE, A., FOX, J. M. & GENEVER, P. G. 2018. CD317 profiling distinguishes bone marrow stromal cell subtypes with distinct functional impact upon T cell proliferation and polarisation [abstract]. *Osteoarthritis and Cartilage,* 26**,** S296-S297.

KENKRE, J. S. & BASSETT, J. H. D. 2018. The bone remodelling cycle. *Annals of Clinical Biochemistry,* 55**,** 308-327.

KENNEDY, O. D., LAUDIER, D. M., MAJESKA, R. J., SUN, H. B. & SCHAFFLER, M. B. 2014. Osteocyte apoptosis is required for production of osteoclastogenic signals following bone fatigue in vivo. *Bone,* 64**,** 132-137.

KENNEDY, S., GHANDEHARI, H., SWEARINGEN, C., TAMBIAH, J. & HOCHBERG, M. 2018. OP0061 Treatment of knee osteoarthritis with sm04690 improved womac a1 'pain on walking' – results from a 52 week, randomised, double-blind, placebo-controlled, phase 2 study of a novel, intra-articular, wnt pathway inhibitor [abstract]. *Annals of the Rheumatic Diseases,* 77**,** 81-82.

KERNEK, C. B. & WRAY, J. B. 1973. Cellular proliferation in the formation of fracture callus in the rat tibia. *Clin Orthop Relat Res***,** 197-209.

KEVORKIAN, L., YOUNG, D. A., DARRAH, C., DONELL, S. T., SHEPSTONE, L., PORTER, S., BROCKBANK, S. M. V., EDWARDS, D. R., PARKER, A. E. & CLARK, I. M. 2004.

Expression profiling of metalloproteinases and their inhibitors in cartilage. *Arthritis & Rheumatism,* 50**,** 131-141.
KHATIB, N. 2018. *The Biomechanical and Biological Pathway of Tibiofemoral Focal Cartilage Defect Pathogenesis and Shortfalls of Microfracture Surgery* PhD, Cardiff University
KHATIB, N., BIGGS, P., WILSON, C., WILLIAMS, R., MASON, D. J. & HOLT, C. A. 2019. Dynamic medial knee overloading influences inflammation and bone remodeling in the degenerative knee [abstract]. *Osteoarthritis and Cartilage,* 27**,** S44.
KHOSLA, S. 2001. Minireview: The OPG/RANKL/RANK System *Endocrinology* 142**,** 5050-5055.
KIDD, B. L., INGLIS, J. J., VETSIKA, K., HOOD, V. C., DE FELIPE, C., BESTER, H., HUNT, S. P. & CRUWYS, S. C. 2003. Inhibition of inflammation and hyperalgesia in NK-1 receptor knock-out mice. *Neuroreport,* 14**,** 2189-92.
KIDD, B. L., PHOTIOU, A. & INGLIS, J. J. 2004. The role of inflammatory mediators on nociception and pain in arthritis. *Novartis Found Symp,* 260**,** 122-33; discussion 133-8, 277-9.
KIDD, L. J., STEPHENS, A. S., KULIWABA, J. S., FAZZALARI, N. L., WU, A. C. & FORWOOD, M. R. 2010. Temporal pattern of gene expression and histology of stress fracture healing. *Bone,* 46**,** 369-378.
KIM, H., PARK, H. & LEE, S. J. 2017. Effective method for drug injection into subcutaneous tissue. *Scientific reports,* 7.
KIM, J.-R., YOO, J. J. & KIM, H. A. 2018. Therapeutics in Osteoarthritis Based on an Understanding of Its Molecular Pathogenesis. *nt. J. Mol. Sci.,* 19**,** 674.
KIM, S. Y., HA, J. C. & LEE, Y. M. 2000. Poly(ethylene oxide)-poly(propylene oxide)-poly(ethylene oxide)/poly(ϵ-caprolactone) (PCL) amphiphilic block copolymeric nanospheres: II. Thermo-responsive drug release behaviors. *Journal of Controlled Release,* 65**,** 345-358.
KINDS, M. B., WELSING, P. M. J., VIGNON, E. P., BIJLSMA, J. W. J., VIERGEVER, M. A., MARIJNISSEN, A. C. A. & LAFEBER, F. P. J. G. 2011. A systematic review of the association between radiographic and clinical osteoarthritis of hip and knee. *Osteoarthritis and Cartilage,* 19**,** 768-778.
KINGSBURY, S. R., THARMANATHAN, P., KEDING, A., RONALDSON, S. J., GRAINGER, A., WAKEFIELD, R. J., ARUNDEL, C., BIRRELL, F., DOHERTY, M., VINCENT, T., WATT, F. E., DZIEDZIC, K., O'NEILL, T. W., ARDEN, N. K., SCOTT, D. L., DICKSON, J., GARROOD, T., GREEN, M., MENON, A., SHEERAN, T., TORGERSON, D. & CONAGHAN, P. G. 2018. Hydroxychloroquine Effectiveness in Reducing Symptoms of Hand Osteoarthritis: A Randomized Trial. *Ann Intern Med,* 168**,** 385-395.
KITAEVA, K. V., RUTLAND, C. S., RIZVANOV, A. A. & SOLOVYEVA, V. V. 2020. Cell Culture Based in vitro Test Systems for Anticancer Drug Screening. *Frontiers in Bioengineering and Biotechnology,* 8.
KITAURA, H., TATAMIYA, M., NAGATA, N., FUJIMURA, Y., EGUCHI, T., YOSHIDA, N. & NAKAYAMA, K. 2006. IL-18 induces apoptosis of adherent bone marrow cells in TNF-α mediated osteoclast formation in synergy with IL-12. *Immunology Letters,* 107**,** 22-31.
KLEIN-NULEND, J., HELFRICH, M. H., STERCK, J. G. H., MACPHERSON, H., JOLDERSMA, M., RALSTON, S. H., SEMEINS, C. M. & BURGER, E. H. 1998. Nitric Oxide Response to Shear Stress by Human Bone Cell Cultures Is Endothelial Nitric Oxide Synthase Dependent. *Biochemical and Biophysical Research Communications,* 250**,** 108-114.

KLOPPENBURG, M., RAMONDA, R., BOBACZ, K., KWOK, W. Y., ELEWAUT, D., HUIZINGA, T. W. J., KROON, F. P. B., PUNZI, L., SMOLEN, J. S., VANDER CRUYSSEN, B., WOLTERBEEK, R., VERBRUGGEN, G. & WITTOEK, R. 2018. Etanercept in patients with inflammatory hand osteoarthritis (EHOA): a multicentre, randomised, double-blind, placebo-controlled trial. *Ann Rheum Dis,* 77**,** 1757-1764.

KLOUDA, L. 2015. Thermoresponsive hydrogels in biomedical applications: A seven-year update. *European Journal of Pharmaceutics and Biopharmaceutics,* 97**,** 338-349.

KOENDERS, M. I., LUBBERTS, E., OPPERS-WALGREEN, B., VAN DEN BERSSELAAR, L., HELSEN, M. M., DI PADOVA, F. E., BOOTS, A. M., GRAM, H., JOOSTEN, L. A. & VAN DEN BERG, W. B. 2005. Blocking of interleukin-17 during reactivation of experimental arthritis prevents joint inflammation and bone erosion by decreasing RANKL and interleukin-1. *Am J Pathol,* 167**,** 141-149.

KOMIYA, S., KAWABATA, R., ZENMYO, M., HASHIMOTO, S. & INOUE, A. 2000. Increased concentrations of nitrate and nitrite in the cyst fluid suggesting increased nitric oxide synthesis in solitary bone cysts. *Journal of Orthopaedic Research,* 18**,** 281-288.

KOMPEL, A. J., ROEMER, F. W., MURAKAMI, A. M., DIAZ, L. E., CREMA, M. D. & GUERMAZI, A. 2019. Intra-articular Corticosteroid Injections in the Hip and Knee: Perhaps Not as Safe as We Thought? *Radiology,* 293**,** 656-663.

KOSUWON, W., SIRICHATIWAPEE, W., WISANUYOTIN, T., JEERAVIPOOLVARN, P. & LAUPATTARAKASEM, W. 2010. Efficacy of symptomatic control of knee osteoarthritis with 0.0125% of capsaicin versus placebo. *J Med Assoc Thai,* 93**,** 1188-1195.

KOTAKE, S., SATO, K., KIM, K. J., TAKAHASHI, N., UDAGAWA, N., NAKAMURA, I., YAMAGUCHI, A., KISHIMOTO, T., SUDA, T. & KASHIWAZAKI, S. 1996. Interleukin-6 and soluble interleukin-6 receptors in the synovial fluids from rheumatoid arthritis patients are responsible for osteoclast-like cell formation. *Journal of Bone and Mineral Research,* 11**,** 88-95.

KOU, L., XIAO, S., SUN, R., BAO, S., YAO, Q. & CHEN, R. 2019. Biomaterial-engineered intra-articular drug delivery systems for osteoarthritis therapy. *Drug delivery,* 26**,** 870-885.

KRAMER, I., HALLEUX, C., KELLER, H., PEGURRI, M., GOOI, J. H., WEBER, P. B., FENG, J. Q., BONEWALD, L. F. & KNEISSEL, M. 2010. Osteocyte Wnt/β-Catenin Signaling Is Required for Normal Bone Homeostasis. *Molecular and Cellular Biology,* 30**,** 3071-3085.

KRAUS, V. B., STABLER, T. V., KONG, S. Y., VARJU, G. & MCDANIEL, G. 2007. Measurement of synovial fluid volume using urea. *Osteoarthritis and Cartilage,* 15**,** 1217-1220.

KRAUS, V. B., BIRMINGHAM, J., STABLE, T. V., FENG, S., TAYLOR, D. C., MOORMAN, C. T., GARRETT, W. E. & TOTH, A. P. 2012. Effects of intraarticular IL1-Ra for acute anterior cruciate ligament knee injury: a randomized controlled pilot trial (NCT00332254). *Osteoarthritis and Cartilage,* 20**,** 271-278.

KRAUS, V. B., CONAGHAN, P. G., AAZAMI, H. A., MEHRA, P., KIVITZ, A. J., LUFKIN, J., HAUBEN, J., JOHNSON, J. R. & BODICK, N. 2018. Synovial and systemic pharmacokinetics (PK) of triamcinolone acetonide (TA) following intra-articular (IA) injection of an extended-release microsphere-based formulation (FX006) or standard crystalline suspension in patients with knee osteoarthritis (OA). *Osteoarthritis and Cartilage,* 26**,** 34-42.

KRINGELBACH, T. M., ASLAN, D., NOVAK, I., ELLEGAARD, M., SYBERG, S., ANDERSEN, C. K., KRISTIANSEN, K. A., VANG, O., SCHWARZ, P. & JORGENSEN, N. R. 2015. Fine-tuned

ATP signals are acute mediators in osteocyte mechanotransduction. *Cell Signal,* 27**,** 2401-2409.
KUIJT, M.-T. K., INKLAAR, H., GOUTTEBARGE, V. & FRINGS-DRESEN, M. H. W. 2012. Knee and ankle osteoarthritis in former elite soccer players: a systematic review. *J Sc Med Sport* 15**,** 480-487.
KULKARNI, R. N., BAKKER, A. D., EVERTS, V. & KLEIN-NULEND, J. 2012. Mechanical loading prevents the stimulating effect of IL-1β on osteocyte-modulated osteoclastogenesis. *Biochem Biophys Res Commun,* 420**,** 11-16.
KUMARI, A., YADAV, S. K. & YADAV, S. C. 2010. Biodegradable polymeric nanoparticles based drug delivery systems. *Colloids and Surfaces B: Biointerfaces,* 75**,** 1-18.
KUNDU, S. K., YOSHIDA, M. & SHIBAYAMA, M. 2010. Effect of salt content on the rheological properties of hydrogel based on oligomeric electrolyte. *J Phys Chem B,* 114**,** 1541-1547.
KUSHNER, I. & SOMERVILLE, J. A. 1971. Permeability of human synovial membrane to plasma proteins. Relationship to molecular size and inflammation. *Arthritis & Rheumatism,* 14**,** 560-570.
KUTUKCULER, N., CAGLAYAN, S. & AYDOGDU, F. 1998. Study of pro-inflammatory (TNF-alpha, IL-1alpha, IL-6) and T-cell-derived (IL-2, IL-4) cytokines in plasma and synovial fluid of patients with juvenile chronic arthritis: correlations with clinical and laboratory parameters. *Clin Rheumatol,* 17**,** 288-92.
KUYINU, E. L., NARAYANAN, G., NAIR, L. S. & LAURENCIN, C. T. 2016. Animal models of osteoarthritis: classification, update, and measurement of outcomes. *Journal of Orthopaedic Surgery and Research,* 11.
KWAN TAT, S., PADRINES, M., THEOLEYRE, S., HEYMANN, D. & FORTUN, Y. 2004. IL-6, RANKL, TNF-alpha/IL-1: interrelations in bone resorption pathophysiology. *Cytokine Growth Factor Rev,* 15**,** 49-60.
KWAN TAT, S., AMIABLE, N., PELLETIER, J.-P., BOILEAU, C., LAJEUNESSE, D., DUVAL, N. & MARTEL-PELLETIER, J. 2009. Modulation of OPG, RANK and RANKL by human chondrocytes and their implication during osteoarthritis. *Rheumatology,* 48**,** 1482-1490.
KWAN TAT, S., LAJEUNESSE, D., PELLETIER, J.-P. & MARTEL-PELLETIER, J. 2010. Targeting subchondral bone for treating osteoarthritis: what is the evidence? *Best practice & research. Clinical rheumatology,* 24**,** 51-70.
KWON, R. Y., TEMIYASATHIT, S., TUMMALA, P., QUAH, C. C. & JACOBS, C. R. 2010. Primary cilium-dependent mechanosensing is mediated by adenylyl cyclase 6 and cyclic AMP in bone cells. *Faseb j,* 24**,** 2859-68.
LADISLAS, R. 2000. Cellular and molecular mechanisms of aging and age related diseases. *Pathol Oncol Res,* 6**,** 3-9.
LAM, F. F. Y. & NG, E. S. K. 2010. Substance P and glutamate receptor antagonists improve the anti-arthritic actions of dexamethasone in rats. *British Journal of Pharmacology,* 159**,** 958-969.
LAMPROPOULOU-ADAMIDOU, K., LELOVAS, P., KARADIMAS, E. V., LIAKOU, C., TRIANTAFILLOPOULOS, I. K., DONTAS, I. & PAPAIOANNOU, N. A. 2014. Useful animal models for the research of osteoarthritis. *European Journal of Orthopaedic Surgery & Traumatology,* 24**,** 263-271.

LANAS, A., GARCIA-TELL, G., ARMADA, B. & OTEO-ALVARO, A. 2011. Prescription patterns and appropriateness of NSAID therapy according to gastrointestinal risk and cardiovascular history in patients with diagnoses of osteoarthritis. *BMC Medicine,* 9.

LANGER, R. & PEPPAS, N. 1983. Chemical and Physical Structure of Polymers as Carriers for Controlled Release of Bioactive Agents: A Review. *Journal of Macromolecular Science, Part C,* 23**,** 61-126.

LAROUI, H., GROSSIN, L., LÉONARD, M., STOLTZ, J.-F., GILLET, P., NETTER, P. & DELLACHERIE, E. 2007. Hyaluronate-Covered Nanoparticles for the Therapeutic Targeting of Cartilage. *Biomacromolecules,* 8**,** 3879-3885.

LARSEN, C., ØSTERGAARD, J., LARSEN, S. W., JENSEN, H., JACOBSEN, S., LINDEGAARD, C. & ANDERSEN, P. H. 2008. Intra-articular depot formulation principles: Role in the management of postoperative pain and arthritic disorders. *Journal of Pharmaceutical Sciences,* 97**,** 4622-4654.

LARSEN, S. W., ØSTERGAARD, J., YAGHMUR, A., JENSEN, H. & LARSEN, C. 2013. Use of in vitro release models in the design of sustained and localized drug delivery systems for subcutaneous and intra-articular administration. *Journal of Drug Delivery Science and Technology,* 23**,** 315-324.

LARSSON, P., ENGQVIST, H., BIERMANN, J., WERNER RÖNNERMAN, E., FORSSELL-ARONSSON, E., KOVÁCS, A., KARLSSON, P., HELOU, K. & PARRIS, T. Z. 2020. Optimization of cell viability assays to improve replicability and reproducibility of cancer drug sensitivity screens. *Scientific Reports,* 10.

LARSSON, S., ENGLUND, M., STRUGLICS, A. & LOHMANDER, L. S. 2015. Interleukin-6 and tumor necrosis factor alpha in synovial fluid are associated with progression of radiographic knee osteoarthritis in subjects with previous meniscectomy. *Osteoarthritis Cartilage,* 23**,** 1906-1914.

LASLETT, L. L., DORÉ, D. A., QUINN, S. J., BOON, P., RYAN, E., WINZENBERG, T. M. & JONES, G. 2012. Zoledronic acid reduces knee pain and bone marrow lesions over 1 year: a randomised controlled trial. *Annals of the Rheumatic Diseases,* 71**,** 1322-1328.

LASLETT, L. L. & JONES, G. 2014. Capsaicin for osteoarthritis pain. *Prog Drug Res,* 68**,** 277-291.

LAWAND, N. B., MCNEARNEY, T. & WESTLUND, K. N. 2000. Amino acid release into the knee joint: key role in nociception and inflammation. *Pain,* 86**,** 69-74.

LAZIC, S. E., CLARKE-WILLIAMS, C. J. & MUNAFÒ, M. R. 2018. What exactly is 'N' in cell culture and animal experiments? *PLOS Biology,* 16**,** e2005282.

LE GRAVERAND-GASTINEAU, M. P. H. 2009. OA clinical trials: current targets and trials for OA. Choosing molecular targets: what have we learned and where we are headed? *Osteoarthritis and Cartilage,* 17**,** 1393-1401.

LEARMONTH, I. D., YOUNG, C. & RORABECK, C. 2007. The operation of the century: total hip replacement. *Lancet,* 370**,** 1508-1519.

LEE, C., HUNSCHE, E., BALSHAW, R., KONG, S. X. & SCHNITZER, T. J. 2005. Need for common internal controls when assessing the relative efficacy of pharmacologic agents using a meta-analytic approach: case study of cyclooxygenase 2-selective inhibitors for the treatment of osteoarthritis. *Arthritis Rheum,* 53**,** 510-518.

LEE, M. K., KIM, M. Y., KIM, S. & LEE, J. 2009. Cryoprotectants for freeze drying of drug nano-suspensions: Effect of freezing rate. *Journal of Pharmaceutical Sciences,* 98**,** 4808-4817.

LEE, T. C., STAINES, A. & TAYLOR, D. 2002. Bone adaptation to load: microdamage as a stimulus for bone remodelling. *Journal of anatomy,* 201**,** 437-446.
LEE, W.-C. & CHU, I.-M. 2008. Preparation and degradation behavior of polyanhydrides nanoparticles. *Journal of Biomedical Materials Research Part B: Applied Biomaterials,* 84B**,** 138-146.
LEMENTOWSKI, P. W. & ZELICOF, S. B. 2008. Obesity and osteoarthritis *Am J Orthop (Belle Mead NJ),* 37**,** 148-151.
LEMOINE, D., FRANCOIS, C., KEDZIEREWICZ, F., PREAT, V., HOFFMAN, M. & MAINCENT, P. 1996. Stability study of nanoparticles of poly(ε-caprolactone), poly(d,l-lactide) and poly(d,l-lactide-co-glycolide). *Biomaterials,* 17**,** 2191-2197.
LEUNG, Y. Y., HAALAND, B., HUEBNER, J. L., WONG, S. B. S., TJAI, M., WANG, C., CHOWBAY, B., THUMBOO, J., CHAKRABORTY, B., TAN, M. H. & KRAUS, V. B. 2018. Colchicine lack of effectiveness in symptom and inflammation modification in knee osteoarthritis (COLKOA): a randomized controlled trial. *Osteoarthritis Cartilage,* 26**,** 631-640.
LEVICK, J. R. 1980. Contributions of the lymphatic and microvascular systems to fluid absorption from the synovial cavity of the rabbit knee. *J Physiol,* 306**,** 445-461.
LEVY, M. D., TORZILLI, P. A. & WARREN, R. F. 1982. The Effect of Medial Meniscectomy on Anterior-Posterior Motion of the Knee. *Journal of bone and joint surgery* 64-A**,** 884-888.
LI, B. & ASPDEN, R. M. 1997. Material Properties of Bone from the Femoral Neck and Calcar Femorale of Patients with Osteoporosis or Osteoarthritis. *Osteoporosis International,* 7**,** 450-456.
LI, J., WAN, Z., LIU, H., LI, H., LIU, L., LI, R., GUO, Y., CHEN, W., ZHANG, X. & ZHANG, X. 2013. Osteoblasts subjected to mechanical strain inhibit osteoclastic differentiation and bone resorption in a co-culture system. *Ann Biomed Eng,* 41**,** 2056-2066.
LI, W., LI, J., GAO, J., LI, B., XIA, Y., MENG, Y., YU, Y., CHEN, H., DAI, J., WANG, H. & GUO, Y. 2011. The fine-tuning of thermosensitive and degradable polymer micelles for enhancing intracellular uptake and drug release in tumors. *Biomaterials,* 32**,** 3832-3844.
LI, X., ZHOU, Z.-Y., ZHANG, Y.-Y. & YANG, H.-L. 2016. IL-6 Contributes to the Defective Osteogenesis of Bone Marrow Stromal Cells from the Vertebral Body of the Glucocorticoid-Induced Osteoporotic Mouse. *PLOS ONE,* 11**,** e0154677.
LIAO, C., CHENG, T., WANG, S., ZHANG, C., JIN, L. & YANG, Y. 2017. Shear stress inhibits IL-17A-mediated induction of osteoclastogenesis via osteocyte pathways. *Bone,* 101**,** 10-20.
LIBBEY, J. E., HANAK, T. J., DOTY, D. J., WILCOX, K. S. & FUJINAMI, R. S. 2016. NBQX, a highly selective competitive antagonist of AMPA and KA ionotropic glutamate receptors, increases seizures and mortality following picornavirus infection. *Experimental neurology,* 280**,** 89-96.
LIEBERTHAL, J., SAMBAMURTHY, N. & SCANZELLO, C. R. 2015. Inflammation in joint injury and post-traumatic osteoarthritis. *Osteoarthritis Cartilage,* 23**,** 1825-1834.
LIN, C.-C. & METTERS, A. T. 2006. Hydrogels in controlled release formulations: Network design and mathematical modeling. *Advanced Drug Delivery Reviews,* 58**,** 1379-1408.
LIN, T.-H., YANG, R.-S., TANG, C.-H., WU, M.-Y. & FU, W.-M. 2008. Regulation of the maturation of osteoblasts and osteoclastogenesis by glutamate. *European Journal of Pharmacology,* 589**,** 37-44.

LIN, Y., LIU, L., JIANG, H., ZHOU, J. & TANG, Y. 2017. Inhibition of interleukin-6 function attenuates the central sensitization and pain behavior induced by osteoarthritis. *European Journal of Pharmacology,* 811**,** 260-267.

LIN, Y.-Y., TANAKA, N., OHKUMA, S., IWABUCHI, Y., TANNE, Y., KAMIYA, T., KUNIMATSU, R., HUANG, Y.-C., YOSHIOKA, M., MITSUYOSHI, T., TANIMOTO, K., TANAKA, E. & TANNE, K. 2010. Applying an excessive mechanical stress alters the effect of subchondral osteoblasts on chondrocytes in a co-culture system. *European Journal of Oral Sciences,* 118**,** 151-158.

LINDBLAD, S. & HEDFORS, E. 1987. Arthroscopic and immunohistologic characterization of knee joint synovitis in osteoarthritis. *Arthritis & Rheumatism,* 30**,** 1081-1088.

LINDBLAD, S. S., MYDEL, P., HELLVARD, A., JONSSON, I. M. & BOKAREWA, M. I. 2012. The N-methyl-d-aspartic acid receptor antagonist memantine ameliorates and delays the development of arthritis by enhancing regulatory T cells. *Neurosignals,* 20**,** 61-71.

LIONIKAITE, V., HENNING, P., DREVINGE, C., SHAH, F. A., PALMQUIST, A., WIKSTRÖM, P., WINDAHL, S. H. & LERNER, U. H. 2019. Vitamin A decreases the anabolic bone response to mechanical loading by suppressing bone formation. *The FASEB Journal,* 33**,** 5237-5247.

LIPPENS, E., SWENNEN, I., GIRONÈS, J., DECLERCQ, H., VERTENTEN, G., VLAMINCK, L., GASTHUYS, F., SCHACHT, E. & CORNELISSEN, R. 2011. Cell survival and proliferation after encapsulation in a chemically modified Pluronic® F127 hydrogel. *Journal of Biomaterials Applications,* 27**,** 828-839.

LISIGNOLI, G., TONEGUZZI, S., GRASSI, F., PIACENTINI, A., TSCHON, M., CRISTINO, S., GUALTIERI, G. & FACCHINI, A. 2002. Different chemokines are expressed in human arthritic bone biopsies: IFN-gamma and IL-6 differently modulate IL-8, MCP-1 and rantes production by arthritic osteoblasts. *Cytokine,* 20**,** 231-238.

LITTLE, C. B., MEEKER, C. T., GOLUB, S. B., LAWLOR, K. E., FARMER, P. J., SMITH, S. M. & FOSANG, A. J. 2007. Blocking aggrecanase cleavage in the aggrecan interglobular domain abrogates cartilage erosion and promotes cartilage repair. *The Journal of Clinical Investigation,* 117**,** 1627-1636.

LITTLE, C. B. & SMITH, M. M. 2008. Animal Models of Osteoarthritis *Current Rheumatology Reviews* 4**,** 175-182.

LITTLE, C. B. & HUNTER, D. J. 2013. Post-traumatic osteoarthritis: from mouse models to clinical trials. *Nat Rev Rheumatol,* 9**,** 485-97.

LIU, D., YAO, S. & WISE, G. E. 2006. Effect of interleukin-10 on gene expression of osteoclastogenic regulatory molecules in the rat dental follicle. *Eur J Oral Sci,* 114**,** 42-49.

LIU, X.-H., KIRSCHENBAUM, A., YAO, S. & LEVINE, A. C. 2005. Cross-Talk between the Interleukin-6 and Prostaglandin E2 Signaling Systems Results in Enhancement of Osteoclastogenesis through Effects on the Osteoprotegerin/Receptor Activator of Nuclear Factor-κB (RANK) Ligand/RANK System. *Endocrinology,* 146**,** 1991-1998.

LIU, Y., LU, W.-L., WANG, J.-C., ZHANG, X., ZHANG, H., WANG, X.-Q., ZHOU, T.-Y. & ZHANG, Q. 2007. Controlled delivery of recombinant hirudin based on thermo-sensitive Pluronic® F127 hydrogel for subcutaneous administration: In vitro and in vivo characterization. *Journal of Controlled Release,* 117**,** 387-395.

LIU, Y., KRISHNAMURTHY, A., HENSVOLD, A. H., JOSHUA, V., SUN, M., ENGSTROM, M., WÄHÄMAA, H., MALMSTRÖM, V., JOPLING, L. A., RETHI, B. & CATRINA, A. 2016.

AB0078 Role of IL-8 and Its Receptor in Anti-Citrullinated Protein Antibody Mediated Osteoclastogenesis in RA [abstract]. *Annals of the Rheumatic Diseases,* 75**,** 923-923.
LIU, Y., FU, S., LIN, L., CAO, Y., XIE, X., YU, H., CHEN, M. & LI, H. 2017. Redox-sensitive Pluronic F127-tocopherol micelles: synthesis, characterization, and cytotoxicity evaluation. *International journal of nanomedicine,* 12**,** 2635-2644.
LIVAK, K. J. & SCHMITTGEN, T. D. 2001. Analysis of relative gene expression data using real-time quantitative PCR and the 2(-Delta Delta C(T)) Method. *Methods,* 25**,** 402-408.
LIVSHITS, G., ZHAI, G., HART, D. J., KATO, B. S., WANG, H., WILLIAMS, F. M. & SPECTOR, T. D. 2009. Interleukin-6 is a significant predictor of radiographic knee osteoarthritis: The Chingford Study. *Arthritis Rheum,* 60**,** 2037-2045.
LOESER, R. F., GOLDRING, S. R., SCANZELLO, C. R. & GOLDRING, M. B. 2012. Osteoarthritis: A disease of the joint as an organ. *Arthritis & Rheumatism,* 64**,** 1697-1707.
LOHMANDER, L. S., HOERRNER, L. A. & LARK, M. W. 1993. Metalloproteinases, tissue inhibitor, and proteoglycan fragments in knee synovial fluid in human osteoarthritis. *Arthritis & Rheumatism,* 36**,** 181-189.
LOHMANDER, L. S. & ROOS, H. 1994. Knee ligament injury, surgery and osteoarthrosis: Truth or consequences? *Acta Orthopaedica Scandinavica,* 65**,** 605-609.
LOHMANDER, L. S., ROOS, H., DAHLBERG, L., HOERRNER, L. A. & LARK, M. W. 1994. Temporal patterns of stromelysin-1, tissue inhibitor, and proteoglycan fragments in human knee joint fluid after injury to the cruciate ligament or meniscus. *Journal of Orthopaedic Research,* 12**,** 21-28.
LOHMANDER, L. S., ATLEY, L. M., PIETKA, T. A. & EYRE, D. R. 2003. The release of crosslinked peptides from type II collagen into human synovial fluid is increased soon after joint injury and in osteoarthritis. *Arthritis & Rheumatism,* 48**,** 3130-3139.
LOHMANDER, L. S., ÖSTENBERG, A., ENGLUND, M. & ROOS, H. 2004. High prevalence of knee osteoarthritis, pain, and functional limitations in female soccer players twelve years after anterior cruciate ligament injury. *Arthritis & Rheumatism,* 50**,** 3145-3152.
LOHMANDER, L. S., ENGLUND, P. M., DAHL, L. L. & ROOS, E. M. 2007. The Long-term Consequence of Anterior Cruciate Ligament and Meniscus Injuries:Osteoarthritis. *The American Journal of Sports Medicine,* 35**,** 1756-1769.
LOHMANDER, L. S., HELLOT, S., DREHER, D., KRANTZ, E. F., KRUGER, D. S., GUERMAZI, A. & ECKSTEIN, F. 2014. Intraarticular sprifermin (recombinant human fibroblast growth factor 18) in knee osteoarthritis: a randomized, double-blind, placebo-controlled trial. *Arthritis Rheumatol,* 66**,** 1820-1831.
LORDAN, S. & HIGGINBOTHAM, C. L. 2012. Effect of serum concentration on the cytotoxicity of clay particles. *Cell Biol Int,* 36**,** 57-61.
LORENZ, J. & GRÄSSEL, S. 2014. Experimental Osteoarthritis Models in Mice. *In:* SINGH, S. R. & COPPOLA, V. (eds.) *Mouse Genetics: Methods and Protocols.* New York, NY: Springer New York.
LOTZ, M., CARSON, D. A. & VAUGHAN, J. H. 1987. Substance P activation of rheumatoid synoviocytes: neural pathway in pathogenesis of arthritis. *Science,* 235**,** 893-895.
LOURENÇO, C. F., SANTOS, R., BARBOSA, R. M., GERHARDT, G., CADENAS, E. & LARANJINHA, J. 2011. In vivo modulation of nitric oxide concentration dynamics upon glutamatergic neuronal activation in the hippocampus. *Hippocampus,* 21**,** 622-630.
LOWNEY, J. J., NORTON, L. A., SHAFER, D. M. & ROSSOMANDO, E. F. 1995. Orthodontic forces increase tumor necrosis factor α in the human gingival sulcus. *American Journal of Orthodontics and Dentofacial Orthopedics,* 108**,** 519-524.

LOZO, E., RIECKE, K., SCHWABE, R., VORMANN, J. & STAHLMANN, R. 2002. Synergistic Effect of Ofloxacin and Magnesium Deficiency on Joint Cartilage in Immature Rats. *Antimicrobial Agents and Chemotherapy,* 46**,** 1755-1759.

LU, H.-D., ZHAO, H.-Q., WANG, K. & LV, L.-L. 2011. Novel hyaluronic acid–chitosan nanoparticles as non-viral gene delivery vectors targeting osteoarthritis. *International Journal of Pharmaceutics,* 420**,** 358-365.

LU, Y., ZHAO, Q., LIU, Y., ZHANG, L., LI, D., ZHU, Z., GAN, X. & YU, H. 2018. Vibration loading promotes osteogenic differentiation of bone marrow-derived mesenchymal stem cells via p38 MAPK signaling pathway. *Journal of Biomechanics,* 71**,** 67-75.

LUO, C. Y., WANG, L., SUN, C. & LI, D. J. 2011. Estrogen enhances the functions of CD4(+)CD25(+)Foxp3(+) regulatory T cells that suppress osteoclast differentiation and bone resorption in vitro. *Cell Mol Immunol,* 8**,** 50-58.

LUO, G., LI, F., LI, X., WANG, Z.-G. & ZHANG, B. 2018. TNF-α and RANKL promote osteoclastogenesis by upregulating RANK via the NF-κB pathway. *Molecular medicine reports,* 17**,** 6605-6611.

LYKE, K. E., BURGES, R., CISSOKO, Y., SANGARE, L., DAO, M., DIARRA, I., KONE, A., HARLEY, R., PLOWE, C. V., DOUMBO, O. K. & SZTEIN, M. B. 2004. Serum Levels of the Proinflammatory Cytokines Interleukin-1 Beta (IL-1β), IL-6, IL-8, IL-10, Tumor Necrosis Factor Alpha, and IL-12(p70) in Malian Children with Severe Plasmodium falciparum Malaria and Matched Uncomplicated Malaria or Healthy Controls. *Infection and immunity* 72**,** 5630-5637.

MACHADO, G. C., MAHER, C. G., FERREIRA, P. H., PINHEIRO, M. B., LIN, C.-W. C., DAY, R. O. & MCLACHLAN, A. J. 2015. Efficacy and safety of paracetamol for spinal pain and osteoarthritis: systematic review and meta-analysis of randomised placebo controlled trials. *BMJ,* 350.

MAIORANO, G., SABELLA, S., SORCE, B., BRUNETTI, V., MALVINDI, M. A., CINGOLANI, R. & POMPA, P. P. 2010. Effects of cell culture media on the dynamic formation of protein-nanoparticle complexes and influence on the cellular response. *ACS Nano,* 4**,** 7481-7491.

MAJITHIYA, R. J., GHOSH, P. K., UMRETHIA, M. L. & MURTHY, R. S. R. 2006. Thermoreversible-mucoadhesive Gel for nasal delivery of sumatriptan. *AAPS PharmSciTech,* 7**,** E80-E86.

MAJUMDAR, M. K., ASKEW, R., SCHELLING, S., STEDMAN, N., BLANCHET, T., HOPKINS, B., MORRIS, E. A. & GLASSON, S. S. 2007. Double-knockout of ADAMTS-4 and ADAMTS-5 in mice results in physiologically normal animals and prevents the progression of osteoarthritis. *Arthritis Rheum,* 56**,** 3670-3674.

MAKADIA, H. K. & SIEGEL, S. J. 2011. Poly Lactic-co-Glycolic Acid (PLGA) as Biodegradable Controlled Drug Delivery Carrier. *Polymers,* 3**,** 1377-1397.

MALEMUD, C. J. & SCHULT, M. E. 2008. Is there a final common pathway for arthritis? *Future Rheumatology,* 3**,** 253-268.

MALEMUD, C. J. 2015. Biologic basis of osteoarthritis: state of the evidence. *Curr Opin Rheumatol,* 27**,** 289-294.

MALEMUD, C. J. 2017. Chapter Seven - Matrix Metalloproteinases and Synovial Joint Pathology. *In:* KHALIL, R. A. (ed.) *Progress in Molecular Biology and Translational Science.* Academic Press.

MALICH, G., MARKOVIC, B. & WINDER, C. 1997. The sensitivity and specificity of the MTS tetrazolium assay for detecting the in vitro cytotoxicity of 20 chemicals using human cell lines. *Toxicology,* 124**,** 179-192.

MALININ, T. & OUELLETTE, E. A. 2000. Articular cartilage nutrition is mediated by subchondral bone: a long-term autograft study in baboons. *Osteoarthritis and Cartilage,* 8**,** 483-491.

MALVERN. 2007. *Sample dispersion and refractive index guide (Reference Manual)* [Online]. Available: https://www.malvernpanalytical.com/en/assets/Sample-dispersion-and-refractive-index-guide-English-MAN0396-1-0_tcm50-11599.pdf [Accessed 11/9/2019 2019].

MANN, G. N., JACOBS, T. W., BUCHINSKY, F. J., ARMSTRONG, E. C., LI, M., KE, H. Z., MA, Y. F., JEE, W. S. & EPSTEIN, S. 1994. Interferon-gamma causes loss of bone volume in vivo and fails to ameliorate cyclosporin A-induced osteopenia. *Endocrinology,* 135**,** 1077-1083.

MANSELL, J. P., TARLTON, J. F. & BAILEY, A. J. 1997. Biochemical evidence for altered subchondral bone collagen metabolism in osteoarthritis of the hip. *Br J Rheumatol,* 36**,** 16-19.

MANSELL, J. P. & BAILEY, A. J. 1998. Abnormal cancellous bone collagen metabolism in osteoarthritis. *The Journal of Clinical Investigation,* 101**,** 1596-1603.

MARINO, A. & GIOTTA, N. 2008. Letter: Cinacalcet, fetuin-A and interleukin-6. *Nephol Dial Transplant* 23**,** 1460-1461.

MARKER, C. L. & POMONIS, J. D. 2012. The monosodium iodoacetate model of osteoarthritis pain in the rat. *Methods Mol Biol,* 851**,** 239-248.

MARTIN, R. B. 2000. Toward a unifying theory of bone remodeling. *Bone,* 26**,** 1-6.

MARTIN, T. J. & SIMS, N. A. 2015. RANKL/OPG; Critical role in bone physiology *Reviews in Endocrine and Metabolic Disorders* 16**,** 131-139.

MASON, D. J., SUVA, L. J., GENEVER, P. G., PATTON, A. J., STEUCKLE, S., HILLAM, R. A. & SKERRY, T. M. 1997. Mechanically regulated expression of a neural glutamate transporter in bone: a role for excitatory amino acids as osteotropic agents? *Bone,* 20**,** 199-205.

MASON, D. J. & HUGGETT, J. F. 2002. Glutamate transporters in bone. *J Musculoskelet Neuronal Interact,* 2**,** 406-414.

MASON, D. J. 2004. Glutamate signalling and its potential application to tissue engineering of bone. *Eur Cell Mater,* 7**,** 12-25; discussion 25-6.

MASON, D. J., BONNET, C. S., GILBERT, S. J., GENEVER, P. & ELFORD, C. 2018. Unpublished: 3D Y201 co-culture system for NC3R grant

MASON, L., MOORE, R. A., DERRY, S., EDWARDS, J. E. & MCQUAY, H. J. 2004. Systematic review of topical capsaicin for the treatment of chronic pain. *BMJ,* 328**,** 991.

MASSELLA, D., CELASCO, E., SALAUN, F., FERRI, A. & BARRESI, A. A. 2018. Overcoming the Limits of Flash Nanoprecipitation: Effective Loading of Hydrophilic Drug into Polymeric Nanoparticles with Controlled Structure. *Polymers (Basel),* 10.

MASSICOTTE, F., LAJEUNESSE, D., BENDERDOUR, M., PELLETIER, J. P., HILAL, G., DUVAL, N. & MARTEL-PELLETIER, J. 2002. Can altered production of interleukin-1β, interleukin-6, transforming growth factor-β and prostaglandin E2 by isolated human subchondral osteoblasts identify two subgroups of osteoarthritic patients. *Osteoarthritis and Cartilage,* 10**,** 491-500.

MATEEN, S., MOIN, S., SHAHZAD, S. & KHAN, A. Q. 2017. Level of inflammatory cytokines in rheumatoid arthritis patients: Correlation with 25-hydroxy vitamin D and reactive oxygen species. *PloS one,* 12**,** e0178879-e0178879.

MATSUI, Y., IWASAKI, N., KON, S., TAKAHASHI, D., MORIMOTO, J., MATSUI, Y., DENHARDT, D. T., RITTLING, S., MINAMI, A. & UEDE, T. 2009. Accelerated development of aging-associated and instability-induced osteoarthritis in osteopontin-deficient mice. *Arthritis Rheum,* 60**,** 2362-2371.

MATTYASOVSZKY, S. G., HOFMANN, A., BROCHHAUSEN, C., RITZ, U., KUHN, S., WOLLSTÄDTER, J., SCHULZE-KOOPS, H., MÜLLER, L. P., WATZER, B. & ROMMENS, P. M. 2010. The effect of the pro-inflammatory cytokine tumor necrosis factor-alpha on human joint capsule myofibroblasts. *Arthritis Research & Therapy,* 12.

MAUDENS, P., MEYER, S., SEEMAYER, C. A., JORDAN, O. & ALLEMANN, E. 2018. Self-assembled thermoresponsive nanostructures of hyaluronic acid conjugates for osteoarthritis therapy. *Nanoscale,* 10**,** 1845-1854.

MAYOL, L., QUAGLIA, F., BORZACCHIELLO, A., AMBROSIO, L. & ROTONDA, M. I. L. 2008. A novel poloxamers/hyaluronic acid in situ forming hydrogel for drug delivery: Rheological, mucoadhesive and in vitro release properties. *European Journal of Pharmaceutics and Biopharmaceutics,* 70**,** 199-206.

MCALINDON, T. E., BANNURU, R. R., SULLIVAN, M. C., ARDEN, N. K., BERENBAS, F., BIERMA-ZEINSTRA, S. M., HAWKER, G. A., HENROTIN, Y., HUNTER, D. J., KAWAGUCHI, H., KWOH, K., LOHMANDER, S., RANNOU, F., ROOS, E. M. & UNDERWOOD, M. 2014. OARSI guidelines for the non-surgical management of knee osteoarthritis. *Osteoarthritis and Cartilage,* 22**,** 363-388.

MCALINDON, T. E., DRIBAN, J. B., HENROTIN, Y., HUNTER, D. J., JIANG, G. L., SKOU, S. T., WANG, S. & SCHNITZER, T. 2015. OARSI Clinical Trials Recommendations: Design, conduct, and reporting of clinical trials for knee osteoarthritis. *Osteoarthritis and Cartilage,* 23**,** 747-760.

MCALINDON, T. E., LAVALLEY, M. P., HARVEY, W. F., PRICE, L. L., DRIBAN, J. B., ZHANG, M. & WARD, R. J. 2017. Effect of intra-articular triamcinolone vs saline on knee cartilage volume and pain in patients with knee osteoarthritis: a randomized clinical trial. *JAMA,* 167.

MCALLISTER, T. N. & FRANGOS, J. A. 1999. Steady and transient fluid shear stress stimulate NO release in osteoblasts through distinct biochemical pathways. *J Bone Miner Res,* 14**,** 930-936.

MCBRIDE, S. H. & SILVA, M. J. 2012. Adaptive and Injury Response of Bone to Mechanical Loading. *BoneKEy osteovision,* 1.

MCCALL, R. L. & SIRIANNI, R. W. 2013. PLGA nanoparticles formed by single- or double-emulsion with vitamin E-TPGS. *Journal of visualized experiments : JoVE***,** 51015.

MCCOY, A. M. 2015. Animal Models of Osteoarthritis: Comparisons and Key Considerations. *Vet Pathol,* 52**,** 803-818.

MCCRAE, F., SHOULS, J., DIEPPE, P. & WATT, I. 1992. Scintigraphic assessment of osteoarthritis of the knee joint. *Annals of the Rheumatic Diseases,* 51**,** 938-942.

MCDEVITT, C. A. & MUIR, H. 1976. Biochemical changes in the cartilage of the knee in experimental and natural osteoarthritis in the dog. *J Bone Joint Surg Br,* 58**,** 94-101.

MCGREGOR, N. E., MURAT, M., ELANGO, J., POULTON, I. J., WALKER, E. C., CRIMEEN-IRWIN, B., HO, P. W. M., GOOI, J. H., MARTIN, T. J. & SIMS, N. A. 2019. IL-6 exhibits both cis-

and trans-signaling in osteocytes and osteoblasts, but only trans-signaling promotes bone formation and osteoclastogenesis. *J Biol Chem,* 294**,** 7850-7863.
MCMASTERS, J., POH, S., LIN, J. B. & PANITCH, A. 2017. Delivery of anti-inflammatory peptides from hollow PEGylated poly(NIPAM) nanoparticles reduces inflammation in an ex vivo osteoarthritis model. *J Control Release,* 258**,** 161-170.
MCNEARNEY, T., SPEEGLE, D., LAWAND, N., LISSE, J. & WESTLUND, K. N. 2000. Excitatory amino acid profiles of synovial fluid from patients with arthritis. *J Rheumatol,* 27**,** 739-745.
MCNEARNEY, T., BAETHGE, B. A., CAO, S., ALAM, R., LISSE, J. R. & WESTLUND, K. N. 2004. Excitatory amino acids, TNF-α , and chemokine levels in synovial fluids of patients with active arthropathies. *Clinical & Experimental Immunology,* 137**,** 621-627.
MCNEARNEY, T. A., MA, Y., CHEN, Y., TAGLIALATELA, G., YIN, H., ZHANG, W.-R. & WESTLUND, K. N. 2010. A peripheral neuroimmune link: glutamate agonists upregulate NMDA NR1 receptor mRNA and protein, vimentin, TNF-α, and RANTES in cultured human synoviocytes. *American journal of physiology. Regulatory, integrative and comparative physiology,* 298**,** R584-R598.
MELZACK, R., CODERRE, T. J., KATZ, J. & VACCARINO, A. L. 2001. Central Neuroplasticity and Pathological Pain. *Annals of the New York Academy of Sciences,* 933**,** 157-174.
METCALF, M. H. & BARRETT, G. R. 2004. Prospective Evaluation of 1485 Meniscal Tear Patterns in Patients with Stable Knees. *The American Journal of Sports Medicine,* 32**,** 675-680.
METSELAAR, J. M., WAUBEN, M. H. M., WAGENAAR-HILBERS, J. P. A., BOERMAN, O. C. & STORM, G. 2003. Complete remission of experimental arthritis by joint targeting of glucocorticoids with long-circulating liposomes. *Arthritis & Rheumatism,* 48**,** 2059-2066.
METZGER, C. E., BREZICHA, J. E., ELIZONDO, J. P., NARAYANAN, S. A., HOGAN, H. A. & BLOOMFIELD, S. A. 2017. Differential responses of mechanosensitive osteocyte proteins in fore- and hindlimbs of hindlimb-unloaded rats. *Bone,* 105**,** 26-34.
METZGER, C. E., GONG, S., ACEVES, M., BLOOMFIELD, S. A. & HOOK, M. A. 2019. Osteocytes reflect a pro-inflammatory state following spinal cord injury in a rodent model. *Bone,* 120**,** 465-475.
MILLER, K. E., HOFFMAN, E. M., SUTHARSHAN, M. & SCHECHTER, R. 2011. Glutamate pharmacology and metabolism in peripheral primary afferents: physiological and pathophysiological mechanisms.
. *Pharmacol Ther.,* 130**,** 283-209.
MILLER, R. R., CAPPOLA, A. R., SHARDELL, M. D., HAWKES, W. G., YU-YAHIRO, J. A., HEBEL, J. R. & MAGAZINER, J. 2006. Persistent changes in interleukin-6 and lower extremity function following hip fracture. *J Gerontol A Biol Sci Med Sci,* 61**,** 1053-1058.
MIN, K. H., KIM, J. H., BAE, S. M., SHIN, H., KIM, M. S., PARK, S., LEE, H., PARK, R. W., KIM, I. S., KIM, K., KWON, I. C., JEONG, S. Y. & LEE, D. S. 2010. Tumoral acidic pH-responsive MPEG-poly(beta-amino ester) polymeric micelles for cancer targeting therapy. *J Control Release,* 144**,** 259-266.
MINA-OSORIO, P. 2015. Basics of Drug Development in Rheumatology. *Arthritis & Rheumatology,* 67**,** 2581-2590.
MIOSSEC, P., BRIOLAY, J., DECHANET, J., WIJDENES, J., MARTINEZ-VALDEZ, H. & BANCHEREAU, J. 1992. Inhibition of the production of proinflammatory cytokines

and immunoglobulins by interleukin-4 in an ex vivo model of rheumatoid synovitis. *Arthritis & Rheumatism,* 35**,** 874-883.

MIOSSEC, P., CHOMARAT, P., DECHANET, J., MOREAU, J. F., ROUX, J. P., DELMAS, P. & BANCHEREAU, J. 1994. Interleukin-4 inhibits bone resorption through an effect on osteoclasts and proinflammatory cytokines in an ex vivo model of bone resorption in rheumatoid arthritis. *Arthritis Rheum,* 37**,** 1715-1722.

MIZUNO, S. & OGAWA, R. 2011. Using changes in hydrostatic and osmotic pressure to manipulate metabolic function in chondrocytes. *American Journal of Physiology-Cell Physiology,* 300**,** C1234-C1245.

MOEN, G.-H., MOEN, A., SCHISTAD, E. I. & GJERSTAD, J. 2017. Local up-regulation of interferon-γ (IFN-γ) following disc herniation is involved in the inflammatory response underlying acute lumbar radicular pain. *Cytokine,* 97**,** 181-186.

MOHAMED, S. G., SUGIYAMA, E., SHINODA, K., TAKI, H., HOUNOKI, H., ABDEL-AZIZ, H. O., MARUYAMA, M., KOBAYASHI, M., OGAWA, H. & MIYAHARA, T. 2007. Interleukin-10 inhibits RANKL-mediated expression of NFATc1 in part via suppression of c-Fos and c-Jun in RAW264.7 cells and mouse bone marrow cells. *Bone,* 41**,** 592-602.

MOHR, K., SOMMER, M., BAIER, G., SCHÖTTLER, S., OKWIEKA, P., TENZER, S., LANDFESTER, K., MAILÄNDER, V., SCHMIDT, M. & MEYER, R. G. 2014. Aggregation Behavior of Polystyrene-Nanoparticles in Human Blood Serum and its Impact on the in vivo Distribution in Mice. *Journal of nanomedicine and nanotechnology* 5**,** 1-10.

MOMEN-HERAVI, F., BALAJ, L., ALIAN, S., TRACHTENBERG, A., HOCHBERG, F., SKOG, J. & KUO, W. 2012. Impact of Biofluid Viscosity on Size and Sedimentation Efficiency of the Isolated Microvesicles. *Frontiers in Physiology,* 3.

MONTERO-JULIAN, F. A., LIAUTARD, J., FLAVETTA, S., ROMAGNE, F., GAILLARD, J. P., BROCHIER, J., KLEIN, B. & BRAILLY, H. 1994. Immunoassay for functional human soluble interleukin-6 receptor in plasma based on ligand/receptor interactions. *J Immunol Methods,* 169**,** 111-121.

MOORE, E. E., BENDELE, A. M., THOMPSON, D. L., LITTAU, A., WAGGIE, K. S., REARDON, B. & ELLSWORTH, J. L. 2005. Fibroblast growth factor-18 stimulates chondrogenesis and cartilage repair in a rat model of injury-induced osteoarthritis. *Osteoarthritis Cartilage,* 13**,** 623-631.

MOREAU, M., LUSSIER, B., PELLETIER, J. P., MARTEL-PELLETIER, J., BEDARD, C., GAUVIN, D. & TRONCY, E. 2014. A medicinal herb-based natural health product improves the condition of a canine natural osteoarthritis model: a randomized placebo-controlled trial. *Res Vet Sci,* 97**,** 574-581.

MOREIRA, F. A., MOLCHANOV, M. L. & GUIMARAES, F. S. 2004. Ionotropic glutamate-receptor antagonists inhibit the aversive effects of nitric oxide donor injected into the dorsolateral periaqueductal gray of rats. *Psychopharmacology (Berl),* 171**,** 199-203.

MORGEN, M., TUNG, D., BORAS, B., MILLER, W., MALFAIT, A. M. & TORTORELLA, M. 2013. Nanoparticles for improved local retention after intra-articular injection into the knee joint. *Pharm Res,* 30**,** 257-268.

MORIISHI, T., FUKUYAMA, R., ITO, M., MIYAZAKI, T., MAENO, T., KAWAI, Y., KOMORI, H. & KOMORI, T. 2012. Osteocyte network; a negative regulatory system for bone mass augmented by the induction of Rankl in osteoblasts and Sost in osteocytes at unloading. *PLoS One,* 7**,** e40143.

MORIMOTO, R., UEHARA, S., YATSUSHIRO, S., JUGE, N., HUA, Z., SENOH, S., ECHIGO, N., HAYASHI, M., MIZOGUCHI, T., NINOMIYA, T., UDAGAWA, N., OMOTE, H., YAMAMOTO, A., EDWARDS, R. H. & MORIYAMA, Y. 2006. Secretion of L-glutamate from osteoclasts through transcytosis. *The EMBO Journal,* 25**,** 4175-4186.

MORITA, Y., KITAURA, H., YOSHIMATSU, M., FUJIMURA, Y., KOHARA, H., EGUCHI, T. & YOSHIDA, N. 2010. IL-18 Inhibits TNF-α-Induced Osteoclastogenesis Possibly via a T Cell-Independent Mechanism in Synergy with IL-12 In Vivo. *Calcified tissue international,* 86**,** 242-248.

MORRISETTE-THOMAS, V., COHEN, A. A., FÜLÖP, T., RIESCO, É., LEGAULT, V., LI, Q., MILOT, E., DUSSEAULT-BÉLANGER, F. & FERRUCCI, L. 2014. Inflamm-aging does not simply reflect increases in pro-inflammatory markers. *Mechanisms of Ageing and Development,* 139**,** 49-57.

MROSEK, E. H., LAHM, A., ERGGELET, C., UHL, M., KURZ, H., EISSNER, B. & SCHAGEMANN, J. C. 2006. Subchondral bone trauma causes cartilage matrix degeneration: an immunohistochemical analysis in a canine model. *Osteoarthritis Cartilage,* 14**,** 171-178.

MUELLER, T. D., ZHANG, J. L., SEBALD, W. & DUSCHL, A. 2002. Structure, binding, and antagonists in the IL-4/IL-13 receptor system. *Biochim Biophys Acta,* 1592**,** 237-250.

MÜHL, H. & PFEILSCHIFTER, J. 2003. Anti-inflammatory properties of pro-inflammatory interferon-γ. *International Immunopharmacology,* 3**,** 1247-1255.

MULCAHY, L. E., TAYLOR, D., LEE, T. C. & DUFFY, G. P. 2011. RANKL and OPG activity is regulated by injury size in networks of osteocyte-like cells. *Bone,* 48**,** 182-188.

MÜLLER, R. H., RADTKE, M. & WISSING, S. A. 2002. Solid lipid nanoparticles (SLN) and nanostructured lipid carriers (NLC) in cosmetic and dermatological preparations. *Advanced Drug Delivery Reviews,* 54**,** S131-S155.

MUSUMECI, T., VENTURA, C. A., GIANNONE, I., RUOZI, B., MONTENEGRO, L., PIGNATELLO, R. & PUGLISI, G. 2006. PLA/PLGA nanoparticles for sustained release of docetaxel. *International Journal of Pharmaceutics,* 325**,** 172-179.

MYKLEBUST, G. & BAHR, R. 2005. Return to play guidelines after anterior cruciate ligament surgery. *British Journal of Sports Medicine,* 39**,** 127-131.

NAAHIDI, S., JAFARI, M., LOGAN, M., WANG, Y., YUAN, Y., BAE, H., DIXON, B. & CHEN, P. 2017. Biocompatibility of hydrogel-based scaffolds for tissue engineering applications. *Biotechnol Adv,* 35**,** 530-544.

NAGAR, G., MANN, M. & GUPTA, R. A. 2019. Mucoadhesive Sustained Release Formulation of Lamivudine. *Journal of Drug Delivery and Therapeutics,* 9**,** 47-52.

NAGATA, N., KITAURA, H., YOSHIDA, N. & NAKAYAMA, K. 2003. Inhibition of RANKL-induced osteoclast formation in mouse bone marrow cells by IL-12: involvement of IFN-γ possibly induced from non-T cell population. *Bone,* 33**,** 721-732.

NAKASHIMA, T., HAYASHI, M., FUKUNAGA, T., KURATA, K., OH-HORA, M., FENG, J. Q., BONEWALD, L. F., KODAMA, T., WUTZ, A., WAGNER, E. F., PENNINGER, J. M. & TAKAYANAGI, H. 2011. Evidence for osteocyte regulation of bone homeostasis through RANKL expression. *Nature Medicine,* 17**,** 1231-1234.

NAKAZAWA, F., MATSUNO, H., YUDOH, K., WATANABE, Y., KATAYAMA, R. & KIMURA, T. 2002. Corticosteroid treatment induces chondrocyte apoptosis in an experimental arthritis model and in chondrocyte cultures. *Clinical and Experimental Rheumatology* 20**,** 773-781.

NAMBA, S., NAKANO, R., KITANAKA, T., KITANAKA, N., NAKAYAMA, T. & SUGIYA, H. 2017. ERK2 and JNK1 contribute to TNF-alpha-induced IL-8 expression in synovial fibroblasts. *PLoS One,* 12**,** e0182923.

NASI, S., EA, H.-K., SO, A. & BUSSO, N. 2017. Revisiting the Role of Interleukin-1 Pathway in Osteoarthritis: Interleukin-1α and -1β, and NLRP3 Inflammasome Are Not Involved in the Pathological Features of the Murine Menisectomy Model of Osteoarthritis. *Frontiers in pharmacology,* 8.

NCBI. 2019. *Ethyl acetate* [Online]. PubChem database. Available: https://pubchem.ncbi.nlm.nih.gov/compound/Ethyl-acetate [Accessed 30 sept 2019].

NELSON, F., BILLINGHURST, R. C., PIDOUX, I., REINER, A., LANGWORTHY, M., MCDERMOTT, M., MALOGNE, T., SITLER, D. F., KILAMBI, N. R., LENCZNER, E. & POOLE, A. R. 2006. Early post-traumatic osteoarthritis-like changes in human articular cartilage following rupture of the anterior cruciate ligament. *Osteoarthritis and Cartilage,* 14**,** 114-119.

NENCINI, S., RINGUET, M., KIM, D.-H., CHEN, Y.-J., GREENHILL, C. & IVANUSIC, J. J. 2017. Mechanisms of nerve growth factor signaling in bone nociceptors and in an animal model of inflammatory bone pain. *Molecular pain,* 13.

NETRAVALI, N. A., GIORI, N. J. & ANDRIACCHI, T. P. 2010. Partial medial meniscectomy and rotational differences at the knee during walking. *Journal of Biomechanics,* 43**,** 2948-2953.

NEUHOLD, L. A., KILLAR, L., ZHAO, W., SUNG, M.-L. A., WARNER, L., KULIK, J., TURNER, J., WU, W., BILLINGHURST, C., MEIJERS, T., POOLE, A. R., BABIJ, P. & DEGENNARO, L. J. 2001. Postnatal expression in hyaline cartilage of constitutively active human collagenase-3 (MMP-13) induces osteoarthritis in mice. *The Journal of Clinical Investigation,* 107**,** 35-44.

NGUYEN, C. & RANNOU, F. 2017. The safety of intra-articular injections for the treatment of knee osteoarthritis: a critical narrative review. *Expert Opinion on Drug Safety,* 16**,** 897-902.

NIAZVAND, F., KHORSANDI, L., ABBASPOUR, M., ORAZIZADEH, M., VARAA, N., MAGHZI, M. & AHMADI, K. 2017. Curcumin-loaded poly lactic-co-glycolic acid nanoparticles effects on mono-iodoacetate -induced osteoarthritis in rats. *Vet Res Forum,* 8**,** 155-161.

NICE. 2015. *Non-steroidal anti -inflammatory drugs* [Online]. Available: https://www.nice.org.uk/advice/ktt13/chapter/evidence-context [Accessed 08/06/18 2018].

NIE, S., HSIAO, W. L. W., PAN, W. & YANG, Z. 2011. Thermoreversible Pluronic F127-based hydrogel containing liposomes for the controlled delivery of paclitaxel: in vitro drug release, cell cytotoxicity, and uptake studies. *International journal of nanomedicine,* 6**,** 151-166.

NIISSALO, S., HUKKANEN, M., IMAI, S., TÖRNWALL, J. & KONTTINEN, Y. T. 2002. Neuropeptides in Experimental and Degenerative Arthritis. *Annals of the New York Academy of Sciences,* 966**,** 384-399.

NOBLE, B. S., PEET, N., STEVENS, H. Y., BRABBS, A., MOSLEY, J. R., REILLY, G. C., REEVE, J., SKERRY, T. M. & LANYON, L. E. 2003. Mechanical loading: biphasic osteocyte survival and targeting of osteoclasts for bone destruction in rat cortical bone. *American Journal of Physiology-Cell Physiology,* 284**,** C934-C943.

NOGUEIRA, E., GOMES, A. C., PRETO, A. & CAVACO-PAULO, A. 2016. Folate-targeted nanoparticles for rheumatoid arthritis therapy. *Nanomedicine: Nanotechnology, Biology and Medicine,* 12**,** 1113-1126.

NORDHOLM, L., SHEARDOWN, M. & HONORÉ, T. 1997. 8 - The NBQX Story. *In:* HERRLING, P. L. (ed.) *Excitatory Amino Acids.* San Diego: Academic Press.

NORVELL, S. M., ALVAREZ, M., BIDWELL, J. P. & PAVALKO, F. M. 2004. Fluid shear stress induces beta-catenin signaling in osteoblasts. *Calcif Tissue Int,* 75**,** 396-404.

NOVAKOFSKI, K. D., TORRE, C. J. & FORTIER, L. A. 2012. Interleukin-1α, -6, and -8 decrease Cdc42 activity resulting in loss of articular chondrocyte phenotype. *Journal of Orthopaedic Research,* 30**,** 246-251.

NOWELL, M. A., RICHARDS, P. J., HORIUCHI, S., YAMAMOTO, N., ROSE-JOHN, S., TOPLEY, N., WILLIAMS, A. S. & JONES, S. A. 2003. Soluble IL-6 receptor governs IL-6 activity in experimental arthritis: blockade of arthritis severity by soluble glycoprotein 130. *J Immunol,* 171**,** 3202-3209.

NÜESCH, E., DIEPPE, P., REICHENBACH, S., WILLIAMS, S., IFF, S. & JÜNI, P. 2011. All cause and disease specific mortality in patients with knee or hip osteoarthritis: population based cohort study. *BMJ,* 342**,** d1165.

NUKI, G. & FERGUSON, J. 1971. Studies on the nature and significance of macromolecular complexes in the rheology of synovial fluid from normal and diseased human joints. *J. Rheologica Acta,* 10**,** 8-14.

OEHLER, S., NEUREITER, D., MEYER-SCHOLTEN, C. & AIGNER, T. 2002. Subtyping of osteoarthritic synoviopathy. *Clinical and Experimental Rheumatology,* 20**,** 633-640.

OHURA, T., TAKAHASHI, M. & OHURA, N. J. 2008. Influence of external forces (pressure and shear force) on superficial layer and subcutis of porcine skin and effects of dressing materials: are dressing materials beneficial for reducing pressure and shear force in tissues? *Wound Repair Regen,* 16**,** 102-7.

ØIESTAD, B. E., ENGEBRETSEN, L., STORHEIM, K. & RISBERG, M. A. 2009. Winner of the 2008 Systematic Review Competition: Knee Osteoarthritis after Anterior Cruciate Ligament Injury. *The American journal of sports medicine.,* 37**,** 1434-1443.

OLIVE, J., D'ANJOU, M. A., GIRARD, C., LAVERTY, S. & THEORET, C. L. 2009. Imaging and histological features of central subchondral osteophytes in racehorses with metacarpophalangeal joint osteoarthritis. *Equine Vet J,* 41**,** 859-864.

OLIVIER, J.-C. 2005. Drug Transport to Brain with Targeted Nanoparticles. *NeuroRX,* 2**,** 108-119.

OLKKU, A. & MAHONEN, A. 2008. Wnt and steroid pathways control glutamate signalling by regulating glutamine synthetase activity in osteoblastic cells. *Bone,* 43**,** 483-493.

OLYMPUS. 2020. *Olympus Filter Cube Overview* [Online]. Available: http://webtools.olympus.eu/micro/fluorophore/en-GB/Cube/Fluorophore/29?fluoroId=2 [Accessed 28th May 2020].

ONOE, Y., MIYAURA, C., KAMINAKAYASHIKI, T., NAGAI, Y., NOGUCHI, K., CHEN, Q. R., SEO, H., OHTA, H., NOZAWA, S., KUDO, I. & SUDA, T. 1996. IL-13 and IL-4 inhibit bone resorption by suppressing cyclooxygenase-2-dependent prostaglandin synthesis in osteoblasts. *The Journal of Immunology,* 156**,** 758-764.

OPREE, A. & KRESS, M. 2000. Involvement of the proinflammatory cytokines tumor necrosis factor-alpha, IL-1 beta, and IL-6 but not IL-8 in the development of heat hyperalgesia: effects on heat-evoked calcitonin gene-related peptide release from rat skin. *J Neurosci,* 20**,** 6289-6293.

ORCHARD, J. W. 2020. Is there a place for intra-articular corticosteroid injections in the treatment of knee osteoarthritis? *BMJ,* 368**,** l6923.
ORTH, P., CUCCHIARINI, M., KOHN, D. & MADRY, H. 2013. Alterations of the subchondral bone in osteochondral repair--translational data and clinical evidence. *Eur Cell Mater,* 25**,** 299-316; discussion 314-6.
OSTEOARTHRITIS RESEARCH SOCIETY INTERNATIONAL, O. A. R. S. I. 2016. Osteoarthritis: A Serious Disease. *Submitted to the U.S. FDA* https://www.oarsi.org/education/oarsi-resources/oarsi-white-paper-oa-serious-disease.
PAAVOLA, A., KILPELAINEN, I., YLIRUUSI, J. & ROSENBERG, P. 2000. Controlled release injectable liposomal gel of ibuprofen for epidural analgesia. *Int J Pharm,* 199**,** 85-93.
PALMQVIST, P., PERSSON, E., CONAWAY, H. H. & LERNER, U. H. 2002. IL-6, leukemia inhibitory factor, and oncostatin M stimulate bone resorption and regulate the expression of receptor activator of NF-kappa B ligand, osteoprotegerin, and receptor activator of NF-kappa B in mouse calvariae. *J Immunol,* 169**,** 3353-3362.
PANDIT, N. K. & WANG, D. 1998. Salt effects on the diffusion and release rate of propranolol from poloxamer 407 gels. *International Journal of Pharmaceutics,* 167**,** 183-189.
PANTSULAIA, I., KALICHMAN, L. & KOBYLIANSKY, E. 2010. Association between radiographic hand osteoarthritis and RANKL, OPG and inflammatory markers. *Osteoarthritis and Cartilage,* 18**,** 1448-1453.
PANYAM, J. & LABHASETWAR, V. 2012. Biodegradable nanoparticles for drug and gene delivery to cells and tissue. *Advanced Drug Delivery Reviews,* 64**,** 61-71.
PAP, T., DANKBAR, B., WEHMEYER, C., KORB-PAP, A. & SHERWOOD, J. 2020. Synovial fibroblasts and articular tissue remodelling: Role and mechanisms. *Semin Cell Dev Biol,* 101**,** 140-145.
PARADA-TURSKA, J., RZESKI, W., MAJDAN, M., KANDEFER-SZERSZEN, M. & TURSKI, W. A. 2006. Effect of glutamate receptor antagonists and antirheumatic drugs on proliferation of synoviocytes in vitro. *Eur J Pharmacol,* 535**,** 95-97.
PARK, J. S., YANG, H. N., JEON, S. Y., WOO, D. G., KIM, M. S. & PARK, K.-H. 2012. The use of anti-COX2 siRNA coated onto PLGA nanoparticles loading dexamethasone in the treatment of rheumatoid arthritis. *Biomaterials,* 33**,** 8600-8612.
PARK, K. M., LEE, S. Y., JOUNG, Y. K., NA, J. S., LEE, M. C. & PARK, K. D. 2009. Thermosensitive chitosan–Pluronic hydrogel as an injectable cell delivery carrier for cartilage regeneration. *Acta Biomaterialia,* 5**,** 1956-1965.
PARPURA, V., LIU, F., JEFTINIJA, K. V., HAYDON, P. G. & JEFTINIJA, S. D. 1995. Neuroligand-evoked calcium-dependent release of excitatory amino acids from Schwann cells. *The Journal of Neuroscience,* 15**,** 5831-5839.
PARVIZI, J., NUNLEY, R. M., BEREND, K. R., LOMBARDI, A. V., RUH, E. L., CLOHISY, J. C., HAMILTON, W. G., DELLA VALLE, C. J. & BARRACK, R. L. 2014. High level of residual symptoms in young patients after total knee arthroplasty. *Clin Orthop Relat Res* 472**,** 133-137.
PASCARELLI, N. A., MORETTI, E., TERZUOLI, G., LAMBOGLIA, A., RENIERI, T., FIORAVANTI, A. & COLLODEL, G. 2013. Effects of gold and silver nanoparticles in cultured human osteoarthritic chondrocytes. *J Appl Toxicol,* 33**,** 1506-1513.
PATEL, T. D., JACKMAN, A., RICE, F. L., KUCERA, J. & SNIDER, W. D. 2000. Development of sensory neurons in the absence of NGF/TrkA signaling in vivo. *Neuron,* 25**,** 345-357.

PATHAK, J. L., BAKKER, A. D., LUYTEN, F. P., VERSCHUEREN, P., LEMS, W. F., KLEIN-NULEND, J. & BRAVENBOER, N. 2016. Systemic Inflammation Affects Human Osteocyte-Specific Protein and Cytokine Expression. *Calcif Tissue Int,* 98**,** 596-608.

PATTON, A. J., GENEVER, P. G., BIRCH, M. A., SUVA, L. J. & SKERRY, T. M. 1998. Expression of an N-Methyl-D-Aspartate-Type Receptor by Human and Rat Osteoblasts and Osteoclasts Suggests a Novel Glutamate Signaling Pathway in Bone. *Bone,* 22**,** 645-649.

PAVELKA, K. 2012. A comparison of the therapeutic efficacy of diclofenac in osteoarthritis: a systematic review of randomised controlled trials. *Curr Med Res Opin,* 28**,** 163-178.

PAVLIN, M. & BREGAR, V. B. 2012. Stability of nanoparticle suspensions in different biologically relevant media. *Digest Journal of Nanomaterials and Biostructures,* 7**,** 1389-1400.

PEARLE, A. D., SCANZELLO, C. R., GEORGE, S., MANDL, L. A., DICARLO, E. F., PETERSON, M., SCULCO, T. P. & CROW, M. K. 2007. Elevated high-sensitivity C-reactive protein levels are associated with local inflammatory findings in patients with osteoarthritis. *Osteoarthritis Cartilage,* 15**,** 516-523.

PEJOVIC, M., STANKOVIC, A. & MITROVIC, D. R. 1995. Determination of the apparent synovial permeability in the knee joint of patients suffering from osteoarthritis and rheumatoid arthritis. *Rheumatology,* 34**,** 520-524.

PELEGRINO, M. T., DE ARAÚJO, D. R. & SEABRA, A. B. 2018. S-nitrosoglutathione-containing chitosan nanoparticles dispersed in Pluronic F-127 hydrogel: Potential uses in topical applications. *Journal of Drug Delivery Science and Technology,* 43**,** 211-220.

PELLETIER, J.-P., CARON, J. P., EVANS, C., ROBBINS, P. D., GEORGESCU, H. I., JOVANOVIC, D., FERNANDES, J. C. & MARTEL-PELLETIER, J. 1997. In vivo suppression of early experimental osteoarthritis by interleukin-1 receptor antagonist using gene therapy. *Arthritis & Rheumatism,* 40**,** 1012-1019.

PEZET, S., ONTENIENTE, B., JULLIEN, J., JUNIER, M. P., GRANNEC, G., RUDKIN, B. B. & CALVINO, B. 2001. Differential regulation of NGF receptors in primary sensory neurons by adjuvant-induced arthritis in the rat. *Pain,* 90**,** 113-125.

PFAFFL, M. W., TICHOPAD, A., PRGOMET, C. & NEUVIANS, T. P. 2004. Determination of stable housekeeping genes, differentially regulated target genes and sample integrity: BestKeeper--Excel-based tool using pair-wise correlations. *Biotechnology letters* 26**,** 509-515.

PHILP, A. M., DAVIS, E. T. & JONES, S. W. 2017. Developing anti-inflammatory therapeutics for patients with osteoarthritis. *Rheumatology* 56**,** 869-881.

PICKARSKI, M., HAYAMI, T., ZHUO, Y. & DUONG, L. T. 2011. Molecular changes in articular cartilage and subchondral bone in the rat anterior cruciate ligament transection and meniscectomized models of osteoarthritis. *BMC Musculoskeletal Disorders,* 12**,** 197.

PIECHA, D., WEIK, J., KHEIL, H., BECHER, G., TIMMERMANN, A., JAWORSKI, A., BURGER, M. & HOFMANN, M. W. 2010. Novel selective MMP-13 inhibitors reduce collagen degradation in bovine articular and human osteoarthritis cartilage explants. *Inflammation Research* 59**,** 379-389.

PIEMONTESE, M., XIONG, J., FUJIWARA, Y., THOSTENSON, J. D. & O'BRIEN, C. A. 2016. Cortical bone loss caused by glucocorticoid excess requires RANKL production by osteocytes and is associated with reduced OPG expression in mice. *American Journal of Physiology-Endocrinology and Metabolism,* 311**,** E587-E593.

PIEPOLI, T., MENNUNI, L., ZERBI, S., LANZA, M., ROVATI, L. C. & CASELLI, G. 2009. Glutamate signaling in chondrocytes and the potential involvement of NMDA receptors in cell proliferation and inflammatory gene expression. *Osteoarthritis and Cartilage,* 17**,** 1076-1083.

PILICHOU, A., PAPASSOTIRIOU, I., MICHALAKAKOU, K., FESSATOU, S., FANDRIDIS, E., PAPACHRISTOU, G. & TERPOS, E. 2008. High levels of synovial fluid osteoprotegerin (OPG) and increased serum ratio of receptor activator of nuclear factor-κB ligand (RANKL) to OPG correlate with disease severity in patients with primary knee osteoarthritis. *Clinical Biochemistry,* 41**,** 746-749.

PINGGUAN-MURPHY, B. & NAWI, I. 2012. Upregulation of matrix synthesis in chondrocyte-seeded agarose following sustained bi-axial cyclic loading. *Clinics,* 67**,** 939-944.

PISKIN, A., GULBAHAR, M. Y., TOMAK, Y., GULMAN, B., HOKELEK, M., KERIMOGLU, S., KOKSAL, B., ALIC, T. & KABAK, Y. B. 2007. Osteoarthritis models after anterior cruciate ligament resection and medial meniscectomy in rats. A histological and immunohistochemical study. *Saudi Med J,* 28**,** 1796-1802.

PITSILLIDES, A. A., RAWLINSON, S. C., SUSWILLO, R. F., BOURRIN, S., ZAMAN, G. & LANYON, L. E. 1995. Mechanical strain-induced NO production by bone cells: a possible role in adaptive bone (re)modeling? *The FASEB Journal,* 9**,** 1614-1622.

POND, S. M. & TOZER, T. N. 1984. First-Pass Elimination Basic Concepts and Clinical Consequences. *Clinical Pharmacokinetics,* 9**,** 1-25.

POULET, B., HAMILTON, R. W., SHEFELBINE, S. & PITSILLIDES, A. A. 2011. Characterizing a novel and adjustable noninvasive murine joint loading model. *Arthritis & Rheumatism,* 63**,** 137-147.

POWELL, T. R., POWELL-SMITH, G., HADDLEY, K., MCGUFFIN, P., QUINN, J., SCHALKWYK, L. C., FARMER, A. E. & D'SOUZA, U. M. 2014. Mood-stabilizers differentially affect housekeeping gene expression in human cells. *International Journal of Methods in Psychiatric Research,* 23**,** 279-288.

POZGAN, U., CAGLIC, D., ROZMAN, B., NAGASE, H., TURK, V. & TURK, B. 2010. Expression and activity profiling of selected cysteine cathepsins and matrix metalloproteinases in synovial fluids from patients with rheumatoid arthritis and osteoarthritis. *Biol Chem,* 391**,** 571-579.

PRAUSNITZ, M. R. & LANGER, R. 2008. Transdermal drug delivery. *Nature Biotechnology,* 26**,** 1261-1268.

PRIDEAUX, M., LOVERIDGE, N., PITSILLIDES, A. A. & FARQUHARSON, C. 2012. Extracellular Matrix Mineralization Promotes E11/gp38 Glycoprotein Expression and Drives Osteocytic Differentiation. *PLOS ONE,* 7**,** e36786.

PRIDEAUX, M., WIJENAYAKA, A. R., KUMARASINGHE, D. D., ORMSBY, R. T., EVDOKIOU, A., FINDLAY, D. M. & ATKINS, G. J. 2014. SaOS2 Osteosarcoma Cells as an In Vitro Model for Studying the Transition of Human Osteoblasts to Osteocytes. *Calcified Tissue International,* 95**,** 183-193.

PRIDEAUX, M., SCHUTZ, C., WIJENAYAKA, A. R., FINDLAY, D. M., CAMPBELL, D. G., SOLOMON, L. B. & ATKINS, G. J. 2016. Isolation of osteocytes from human trabecular bone. *Bone,* 88**,** 64-72.

PRITZKER, K. 2003. *Pathology of osteoarthritis* Oxford, Oxford University Press

PRITZKER, K. P. H., GAY, S., JIMENEZ, S. A., OSTERGAARD, K., PELLETIER, J. P., REVELL, P. A., SALTER, D. & VAN DEN BERG, W. B. 2006. Osteoarthritis cartilage histopathology: grading and staging. *Osteoarthritis and Cartilage,* 14**,** 13-29.

PROKOP, A. & DAVIDSON, J. M. 2008. Nanovehicular Intracellular Delivery Systems. *Journal of Pharmaceutical Sciences,* 97**,** 3518-3590.

PROMEGA. 2020. *Quantitative Real-Time PCR* [Online]. Available: https://www.promega.co.uk/resources/guides/nucleic-acid-analysis/pcr-amplification/ [Accessed 28th May 2020].

PUENPATOM, R. A. & VICTOR, T. W. 2009. Increased prevalence of metabolic syndrome in individuals with osteoarthritis: an analysis of NHANES III data. *Postgrad Med,* 121**,** 9-20.

PULAI, J. I., CHEN, H., IM, H.-J., KUMAR, S., HANNING, C., HEGDE, P. S. & LOESER, R. F. 2005. NF-κB Mediates the Stimulation of Cytokine and Chemokine Expression by Human Articular Chondrocytes in Response to Fibronectin Fragments. *The Journal of Immunology,* 174**,** 5781-5788.

PUNO, R. M., VAUGHAN, J. J., STETTEN, M. L. & JOHNSON, J. R. 1991. Long-term effects of tibial angular malunion on the knee and ankle joints. *Journal of orthopaedic trauma,* 5**,** 247-254.

PUNZI, L., GALOZZI, P., LUISETTO, R., FAVERO, M., RAMONDA, R., OLIVIERO, F. & SCANU, A. 2016. Post-traumatic arthritis: overview on pathogenic mechanisms and role of inflammation. *RMD Open,* 2.

QI, R., SHEN, M., CAO, X., GUO, R., TIAN, X., YU, J. & SHI, X. 2011. Exploring the dark side of MTT viability assay of cells cultured onto electrospun PLGA-based composite nanofibrous scaffolding materials. *Analyst,* 136**,** 2897-2903.

RAAB-CULLEN, D. M., THIEDE, M. A., PETERSEN, D. N., KIMMEL, D. B. & RECKER, R. R. 1994. Mechanical loading stimulates rapid changes in periosteal gene expression. *Calcified Tissue International,* 55**,** 473-478.

RAE, P. J. & NOBLE, J. 1989. Arthroscopic drilling of osteochondral lesions of the knee. *The Journal of Bone and Joint Surgery. British volume,* 71-B**,** 534-534.

RAGGATT, L. J. & PARTRIDGE, N. C. 2010. Cellular and molecular mechanisms of bone remodeling. *The Journal of biological chemistry,* 285**,** 25103-25108.

RAJESHWARI, H. R., DHAMECHA, D., JAGWANI, S., PATIL, D., HEGDE, S., POTDAR, R., METGUD, R., JALALPURE, S., ROY, S., JADHAV, K., TIWARI, N. K., KODURU, S., HUGAR, S. & DODAMANI, S. 2017. Formulation of thermoreversible gel of cranberry juice concentrate: Evaluation, biocompatibility studies and its antimicrobial activity against periodontal pathogens. *Materials Science and Engineering: C,* 75**,** 1506-1514.

RALSTON, S. H., HO, L.-P., HELFRICH, M. H., GRABOWSKI, P. S., JOHNSTON, P. W. & BENJAMIN, N. 1995. Nitric oxide: A cytokine-induced regulator of bone resorption. *Journal of Bone and Mineral Research,* 10**,** 1040-1049.

RAMME, A. J., LENDHEY, M., RAYA, J. G., KIRSCH, T. & KENNEDY, O. D. 2016. A novel rat model for subchondral microdamage in acute knee injury: a potential mechanism in post-traumatic osteoarthritis. *Osteoarthritis Cartilage,* 24**,** 1776-1785.

RAYCHAUDHURI, S. P. & RAYCHAUDHURI, S. K. 2009. The regulatory role of nerve growth factor and its receptor system in fibroblast-like synovial cells. *Scand J Rheumatol,* 38**,** 207-215.

REBOUL, P., PELLETIER, J. P., TARDIF, G., CLOUTIER, J. M. & MARTEL-PELLETIER, J. 1996. The new collagenase, collagenase-3, is expressed and synthesized by human chondrocytes but not by synoviocytes. A role in osteoarthritis. *The Journal of Clinical Investigation,* 97**,** 2011-2019.

REDLICH, K., GORTZ, B., HAYER, S., ZWERINA, J., DOERR, N., KOSTENUIK, P., BERGMEISTER, H., KOLLIAS, G., STEINER, G., SMOLEN, J. S. & SCHETT, G. 2004. Repair of local bone erosions and reversal of systemic bone loss upon therapy with anti-tumor necrosis factor in combination with osteoprotegerin or parathyroid hormone in tumor necrosis factor-mediated arthritis. *Am J Pathol,* 164**,** 543-555.

REDLICH, K. & SMOLEN, J. S. 2012. Inflammatory bone loss: pathogenesis and therapeutic intervention. *Nature Reviews Drug Discovery,* 11**,** 234-250.

REEUWIJK, K. G., DE ROOIJ, M., VAN DIJK, G. M., VEENHOF, C., STEULTJENS, M. P. & DEKKER, J. 2010. Osteoarthritis of the hip or knee: which coexisting disorders are disabling? *Clin Rheumatol,* 29**,** 739-747.

REINER, A. & LEVITZ, J. 2018. Glutamatergic Signaling in the Central Nervous System: Ionotropic and Metabotropic Receptors in Concert. *Neuron,* 98**,** 1080-1098.

REVELL, P. A., MAYSTON, V., LALOR, P. & MAPP, P. 1988. The synovial membrane in osteoarthritis: a histological study including the characterisation of the cellular infiltrate present in inflammatory osteoarthritis using monoclonal antibodies. *Annals of the Rheumatic Diseases,* 47**,** 300-307.

RHEE, D. K., MARCELINO, J., BAKER, M., GONG, Y., SMITS, P., LEFEBVRE, V., JAY, G. D., STEWART, M., WANG, H., WARMAN, M. L. & CARPTEN, J. D. 2005. The secreted glycoprotein lubricin protects cartilage surfaces and inhibits synovial cell overgrowth. *The Journal of Clinical Investigation,* 115**,** 622-631.

RIANCHO, J. A., ZARRABEITIA, M. T., OLMOS, J. M., AMADO, J. A. & GONZALEZ-MACIAS, J. 1993. Effects of interleukin-4 on human osteoblast-like cells. *Bone and Mineral,* 21**,** 53-61.

RICCI, E. J., LUNARDI, L. O., NANCLARES, D. M. A. & MARCHETTI, J. M. 2005. Sustained release of lidocaine from Poloxamer 407 gels. *International Journal of Pharmaceutics,* 288**,** 235-244.

RIDKER, P. M., EVERETT, B. M., THUREN, T., MACFADYEN, J. G., CHANG, W. H., BALLANTYNE, C., FONSECA, F., NICOLAU, J., KOENIG, W., ANKER, S. D., KASTELEIN, J. J. P., CORNEL, J. H., PAIS, P., PELLA, D., GENEST, J., CIFKOVA, R., LORENZATTI, A., FORSTER, T., KOBALAVA, Z., VIDA-SIMITI, L., FLATHER, M., SHIMOKAWA, H., OGAWA, H., DELLBORG, M., ROSSI, P. R. F., TROQUAY, R. P. T., LIBBY, P. & GLYNN, R. J. 2017. Antiinflammatory Therapy with Canakinumab for Atherosclerotic Disease. *N Engl J Med,* 377**,** 1119-1131.

RIFFAULT, M., SIX, J. L., NETTER, P., GILLET, P. & GROSSIN, L. 2015. PLGA-Based Nanoparticles: a Safe and Suitable Delivery Platform for Osteoarticular Pathologies. *Pharm Res,* 32**,** 3886-3898.

RIGOGLOU, S. & PAPAVASSILIOU, A. G. 2013. The NF-κB signalling pathway in osteoarthritis. *The International Journal of Biochemistry & Cell Biology,* 45**,** 2580-2584.

RINAUDO, M., ROZAND, Y., MATHIEU, P. & CONROZIER, T. 2009. Role of Different Pre-Treatments on Composition and Rheology of Synovial Fluids. *Polymers* 1**,** 16-34.

RITCHLIN, C. & HAAS-SMITH, S. A. 2001. Expression of interleukin 10 mRNA and protein by synovial fibroblastoid cells. *J Rheumatol,* 28**,** 698-705.

RIZVI, S. A. A. & SALEH, A. M. 2018. Applications of nanoparticle systems in drug delivery technology. *Saudi Pharmaceutical Journal,* 26**,** 64-70.

ROBLING, A. G., NIZIOLEK, P. J., BALDRIDGE, L. A., CONDON, K. W., ALLEN, M. R., ALAM, I., MANTILA, S. M., GLUHAK-HEINRICH, J., BELLIDO, T. M., HARRIS, S. E. & TURNER, C. H.

2008. Mechanical stimulation of bone in vivo reduces osteocyte expression of Sost/sclerostin. *J Biol Chem,* 283**,** 5866-5875.
RODRIGUEZ-MERCHAN, E. C. 2018. Topical therapies for knee osteoarthritis. *Postgraduate Medicine,* 130**,** 607-612.
ROOS, H., LAURÉN, M., ADALBERTH, T., ROOS, E. M., JONSSON, K. & LOHMANDER, L. S. 1998. Knee osteoarthritis after meniscectomy: Prevalence of radiographic changes after twenty-one years, compared with matched controls. *Arthritis & Rheumatism,* 41**,** 687-693.
ROSE-JOHN, S. 2012. IL-6 trans-signaling via the soluble IL-6 receptor: importance for the pro-inflammatory activities of IL-6. *International journal of biological sciences,* 8**,** 1237-1247.
ROSNER, B., NEICUN, J., YANG, J. C. & ROMAN-URRESTARAZU, A. 2019. Opioid prescription patterns in Germany and the global opioid epidemic: Systematic review of available evidence. *PloS one,* 14**,** e0221153-e0221153.
ROTHENFLUH, D. A., BERMUDEZ, H., O'NEIL, C. P. & HUBBELL, J. A. 2008. *Biofunctional polymer nanoparticles for intra-articular targeting and retention in cartilage*.
RUBBERT-ROTH, A. & FINCKH, A. 2009. Treatment options in patients with rheumatoid arthritis failing initial TNF inhibitor therapy: a critical review. *Arthritis Research & Therapy,* 11.
RUBIN, J., MURPHY, T. C., ZHU, L., ROY, E., NANES, M. S. & FAN, X. 2003. Mechanical Strain Differentially Regulates Endothelial Nitric-oxide Synthase and Receptor Activator of Nuclear κB Ligand Expression via ERK1/2 MAPK. *Journal of Biological Chemistry* 278**,** 34018-34025.
RUEL-GARIÉPY, E. & LEROUX, J.-C. 2004. In situ-forming hydrogels—review of temperature-sensitive systems. *European Journal of Pharmaceutics and Biopharmaceutics,* 58**,** 409-426.
RUMNEY, R. M. H., SUNTERS, A., REILLY, G. C. & GARTLAND, A. 2012. Application of multiple forms of mechanical loading to human osteoblasts reveals increased ATP release in response to fluid flow in 3D cultures and differential regulation of immediate early genes. *Journal of Biomechanics,* 45**,** 549-554.
RUSSO, E. & VILLA, C. 2019. Poloxamer Hydrogels for Biomedical Applications. *Pharmaceutics,* 11**,** 671.
RUTJES, A. W. S., JUNI, P., DA COSTA, B. R., TRELLE, S., NUESCH, E. & REICHENBACH, S. 2012. Viscosupplementation for osteoarthritis of the knee: a systematic review and meta-analysis. *Ann Intern Med,* 157**,** 180-191.
RYAN, S. M., MCMORROW, J., UMERSKA, A., PATEL, H. B., KORNERUP, K. N., TAJBER, L., MURPHY, E. P., PERRETTI, M., CORRIGAN, O. I. & BRAYDEN, D. J. 2013. An intra-articular salmon calcitonin-based nanocomplex reduces experimental inflammatory arthritis. *Journal of Controlled Release,* 167**,** 120-129.
SADOUK, M. B., PELLETIER, J. P., TARDIF, G., KIANSA, K., CLOUTIER, J. M. & MARTEL-PELLETIER, J. 1995. Human synovial fibroblasts coexpress IL-1 receptor type I and type II mRNA. The increased level of the IL-1 receptor in osteoarthritic cells is related to an increased level of the type I receptor. *Laboratory investigation; a journal of technical methods and pathology,* 73**,** 347-355.
SAFIEH-GARABEDIAN, B., POOLE, S., ALLCHORNE, A., WINTER, J. & WOOLF, C. J. 1995. Contribution of interleukin-1 beta to the inflammation-induced increase in nerve growth factor levels and inflammatory hyperalgesia. *Br J Pharmacol,* 115**,** 1265-1275.

SAHOO, S., CHAKRABORTI, C. K. & MISHRA, S. C. 2011. Qualitative analysis of controlled release ciprofloxacin/carbopol 934 mucoadhesive suspension. *Journal of advanced pharmaceutical technology & research,* 2**,** 195-204.

SALATA, O. V. 2004. Applications of nanoparticles in biology and medicine. *Journal of Nanobiotechnology,* 2**,** 3.

SALTER, D. M., WALLACE, W. H. B., ROBB, J. E., CALDWELL, H. & WRIGHT, M. O. 2000. Human Bone Cell Hyperpolarization Response to Cyclical Mechanical Strain Is Mediated by an Interleukin-1β Autocrine/Paracrine Loop. *Journal of Bone and Mineral Research,* 15**,** 1746-1755.

SALTER, D. M., WRIGHT, M. O. & MILLWARD-SADLER, S. J. 2004. NMDA receptor expression and roles in human articular chondrocyte mechanotransduction. *Biorheology,* 41**,** 273-281.

SANCHEZ, C., DEBERG, M. A., BELLAHCENE, A., CASTRONOVO, V., MSIKA, P., DELCOUR, J. P., CRIELAARD, J. M. & HENROTIN, Y. E. 2008. Phenotypic characterization of osteoblasts from the sclerotic zones of osteoarthritic subchondral bone. *Arthritis Rheum,* 58**,** 442-455.

SANCHEZ, C., GABAY, O., SALVAT, C., HENROTIN, Y. E. & BERENBAUM, F. 2009. Mechanical loading highly increases IL-6 production and decreases OPG expression by osteoblasts. *Osteoarthritis Cartilage,* 17**,** 473-481.

SANCHEZ, C., PESESSE, L., GABAY, O., DELCOUR, J.-P., MSIKA, P., BAUDOUIN, C. & HENROTIN, Y. E. 2012. Regulation of subchondral bone osteoblast metabolism by cyclic compression. *Arthritis & Rheumatism,* 64**,** 1193-1203.

SANDY, J. D., FLANNERY, C. R., NEAME, P. J. & LOHMANDER, L. S. 1992. The structure of aggrecan fragments in human synovial fluid. Evidence for the involvement in osteoarthritis of a novel proteinase which cleaves the Glu 373-Ala 374 bond of the interglobular domain. *The Journal of Clinical Investigation,* 89**,** 1512-1516.

SANDY, J. D. & VERSCHAREN, C. 2001. Analysis of aggrecan in human knee cartilage and synovial fluid indicates that aggrecanase (ADAMTS) activity is responsible for the catabolic turnover and loss of whole aggrecan whereas other protease activity is required for C-terminal processing in vivo. *Biochemical Journal,* 358**,** 615-626.

SATO, K., SUEMATSU, A., OKAMOTO, K., YAMAGUCHI, A., MORISHITA, Y., KADONO, Y., TANAKA, S., KODAMA, T., AKIRA, S., IWAKURA, Y., CUA, D. J. & TAKAYANAGI, H. 2006. Th17 functions as an osteoclastogenic helper T cell subset that links T cell activation and bone destruction. *J Exp Med,* 203**,** 2673-2682.

SAWA, N., FUJIMOTO, H., SAWA, Y. & YAMASHITA, J. 2019. Alternating Differentiation and Dedifferentiation between Mature Osteoblasts and Osteocytes. *Scientific Reports,* 9.

SAWA, S., KAMIMURA, D., JIN, G. H., MORIKAWA, H., KAMON, H., NISHIHARA, M., ISHIHARA, K., MURAKAMI, M. & HIRANO, T. 2006. Autoimmune arthritis associated with mutated interleukin (IL)-6 receptor gp130 is driven by STAT3/IL-7-dependent homeostatic proliferation of CD4+ T cells. *J Exp Med,* 203**,** 1459-1470.

SCANZELLO, C. R., MCKEON, B., SWAIM, B. H., DICARLO, E., ASOMUGHA, E. U., KANDA, V., NAIR, A., LEE, D. M., RICHMOND, J. C., KATZ, J. N., CROW, M. K. & GOLDRING, S. R. 2011. Synovial inflammation in patients undergoing arthroscopic meniscectomy: Molecular characterization and relationship to symptoms. *Arthritis & Rheumatism,* 63**,** 391-400.

SCHEMITSCH, E. H., KOWALSKI, M. J. & SWIONTKOWSKI, M. F. 1996. Soft-tissue blood flow following reamed versus unreamed locked intramedullary nailing: a fractured sheep tibia model. *Ann Plast Surg,* 36**,** 70-75.

SCHENK, M. & MUELLER, C. 2008. The mucosal immune system at the gastrointestinal barrier. *Best Practice & Research Clinical Gastroenterology,* 22**,** 391-409.

SCHIEKER, M., MINDEHOLM, L. & PRAESTGAARD, J. 2018. Interleukin-1β inhibition with canakinumab associates with reduced rates of total hip and knee replacement (THR/TKR) and osteoarthritis (OA) symptoms: exploratory results from the canakinumab anti-inflammatory thrombosis outcomes study (CANTOS) [abstract]. *Arthritis Rheumatol,* 70.

SCHLAAK, J. F., PFERS, I., MEYER ZUM BÜSCHENFELDE, K. H. & MÄRKER-HERMANN, E. 1996. Different cytokine profiles in the synovial fluid of patients with osteoarthritis, rheumatoid arthritis and seronegative spondylarthropathies. *Clin Exp Rheumatol,* 14**,** 155-162.

SCHUERWEGH, A. J., DOMBRECHT, E. J., STEVENS, W. J., VAN OFFEL, J. F., BRIDTS, C. H. & DE CLERCK, L. S. 2003. Influence of pro-inflammatory (IL-1 alpha, IL-6, TNF-alpha, IFN-gamma) and anti-inflammatory (IL-4) cytokines on chondrocyte function. *Osteoarthritis Cartilage,* 11**,** 681-687.

SCOTT, A., KHAN, K. M., DURONIO, V. & HART, D. A. 2008. Mechanotransduction in Human Bone. *Sports Medicine* 38**,** 139-160.

SCOTT, L. J. 2017. Tocilizumab: A Review in Rheumatoid Arthritis. *Drugs,* 77**,** 1865-1879.

SCULLY, N., EVANS, S. L., MASON, D. J. & EVANS, B. A. J. 2013. Mimicking osteocytes in vivo using 3D collagen gels: development of a novel tool to study osteocyte biology [abstract]. *Endocrine Abstracts* 31.

SCULLY, N. 2015. *Differentiation of osteoblasts to osteocytes in 3D type I collagen gels - a novel tool to study osteocyte responses to mechanical loading.* PhD, Cardiff University

SEFTON, M. V., MAY, M. H., LAHOOTI, S. & BABENSEE, J. E. 2000. Making microencapsulation work: conformal coating, immobilization gels and in vivo performance. *Journal of Controlled Release,* 65**,** 173-186.

SEIDEL, M. F., HERGUIJUELA, M., FORKERT, R. & OTTEN, U. 2010. Nerve Growth Factor in Rheumatic Diseases. *Seminars in Arthritis and Rheumatism,* 40**,** 109-126.

SEIDLITZ, E. P., SHARMA, M. K. & SINGH, G. 2010. Extracellular glutamate alters mature osteoclast and osteoblast functions. *Can J Physiol Pharmacol,* 88**,** 929-936.

SENDZIK, J., LODE, H. & STAHLMANN, R. 2009. Quinolone-induced arthropathy: an update focusing on new mechanistic and clinical data. *International Journal of Antimicrobial Agents,* 33**,** 194-200.

SEO, S. J., MAHAPATRA, C., SINGH, R. K., KNOWLES, J. C. & KIM, H. W. 2014. Strategies for osteochondral repair: Focus on scaffolds. *J Tissue Eng,* 5.

SHAKYA, A. K., AL-NAJJAR, B. O., DEB, P. K., NAIK, R. R. & TEKADE, R. K. 2018. Chapter 8 - First-Pass Metabolism Considerations in Pharmaceutical Product Development. *In:* TEKADE, R. K. (ed.) *Dosage Form Design Considerations.* Academic Press.

SHANMUGARAJAN, S., KAWANABE, N., KOIDE, M., TSURUGA, E., ARROYO, J. E., KEY, L. L., JR. & REDDY, S. V. 2009. IL-12 stimulates the osteoclast inhibitory peptide-1 (OIP-1/hSca) gene expression in CD4+ T cells. *Journal of cellular biochemistry,* 107**,** 104-111.

SHAPIRO, F., KOIDE, S. & GLIMCHER, M. J. 1993. Cell origin and differentiation in the repair of full-thickness defects of articular cartilage. *J Bone Joint Surg Am,* 75**,** 532-553.
SHARMA, L., LOU, C., CAHUE, S. & DUNLOP, D. D. 2000. The mechanism of the effect of obesity in knee osteoarthritis: The mediating role of malalignment. *Arthritis & Rheumatism,* 43**,** 568-575.
SHIN, S., CHO, C. & OH, I. 2000a. Enhanced efficacy by percutaneous absorption of piroxicam from the poloxamer gel in rats. *Int J Pharm,* 193**,** 213-218.
SHIN, S.-C., KIM, J.-Y. & OH, I.-J. 2000b. Mucoadhesive and Physicochemical Characterization of Carbopol-Poloxamer Gels Containing Triamcinolone Acetonide. *Drug Development and Industrial Pharmacy,* 26**,** 307-312.
SHRIVASTAVA, A. K., SINGH, H. V., RAIZADA, A., SINGH, S. K., PANDEY, A., SINGH, N., YADAV, D. S. & SHARMA, H. 2015. Inflammatory markers in patients with rheumatoid arthritis. *Allergologia et Immunopathologia,* 43**,** 81-87.
SILBERBERG, M., SILBERBERG, R. & HASLER, M. 1966. Fine structure of articular cartilage in mice receiving cortisone acetate. *Arch Pathol,* 82**,** 569-582.
SILFVERSWÄRD, C. J., SISASK, G., LARSSON, S., OHLSSON, C., FROST, A., LJUNGGREN, O. S. & NILSSON, O. 2008. Bone formation in interleukin-4 and interleukin-13 depleted mice, Acta Orthopaedica. *Acta Orthopaedica,* 79**,** 410-420.
SILVER, N., BEST, S., JIANG, J. & THEIN, S. L. 2006. Selection of housekeeping genes for gene expression studies in human reticulocytes using real-time PCR. *BMC molecular biology* 7.
SIMS, N. A. & WALSH, N. C. 2010. GP130 cytokines and bone remodelling in health and disease. *BMB Reports. Korean Society for Biochemistry and Molecular Biology - BMB Reports,* 43**,** 513-523.
SINGH, A., AGARWAL, R., DIAZ-RUIZ, C. A., WILLETT, N. J., WANG, P., LEE, L. A., WANG, Q., GULDBERG, R. E. & GARCÍA, A. J. 2014. Nano-engineered particles for enhanced intra-articular retention and delivery of proteins. *Advanced healthcare materials,* 3**,** 1562-1567.
SINGH, R. & LILLARD, J. W. 2009. Nanoparticle-based targeted drug delivery. *Experimental and Molecular Pathology,* 86**,** 215-223.
SINGH, T. & NEWMAN, A. B. 2011. Inflammatory markers in population studies of aging. *Ageing Research Reviews,* 10**,** 319-329.
SITTICHOKECHAIWUT, A., EDWARDS, J. H., SCUTT, A. M. & REILLY, G. C. 2010. Short Bouts of Mechanical Loading are as Effective as Dexamethasone at Inducing Matrix Production by Human Bone Marrow Mesenchymal Stem Cells *European Cells and Materials,* 20**,** 45-57.
SKIRVING, A. P., DAY, R., MACDONALD, W. & MCLAREN, R. 1987. Carbon fiber reinforced plastic (CFRP) plates versus stainless steel dynamic compression plates in the treatment of fractures of the tibiae in dogs. *Clin Orthop Relat Res,* 224**,** 117-124.
SKOU, S. T., ROOS, E. M., LAURSEN, M. B., RATHLEFF, M. S., ARENDT-NIELSEN, L., SIMONSEN, O. & RASMUSSEN, S. 2015. A randomized, controlled trial of total knee replacement. *N Engl J Med* 373**,** 1596-1606.
SMITH, L. E., RIMMER, S. & MACNEIL, S. 2006. Examination of the effects of poly(N-vinylpyrrolidinone) hydrogels in direct and indirect contact with cells. *Biomaterials,* 27**,** 2806-2812.
SOARES, S., FONTE, P., COSTA, A., ANDRADE, J., SEABRA, V., FERREIRA, D., REIS, S. & SARMENTO, B. 2013. Effect of freeze-drying, cryoprotectants and storage conditions

on the stability of secondary structure of insulin-loaded solid lipid nanoparticles. *International Journal of Pharmaceutics,* 456**,** 370-381.

SOKOLOVE, J. & LEPUS, C. M. 2013. Role of inflammation in the pathogenesis of osteoarthritis: latest findings and interpretations. *Therapeutic advances in musculoskeletal disease,* 5**,** 77-94.

SOMJEN, D., BINDERMAN, I., BERGER, E. & HARELL, A. 1980. Bone remodelling induced by physical stress is prostaglandin E2 mediated. *Biochim Biophys Acta,* 627**,** 91-100.

SON, G.-H., LEE, B.-J. & CHO, C.-W. 2017. Mechanisms of drug release from advanced drug formulations such as polymeric-based drug-delivery systems and lipid nanoparticles. *Journal of Pharmaceutical Investigation,* 47**,** 287-296.

SONG, J. Q., DONG, F., LI, X., XU, C. P., CUI, Z., JIANG, N., JIA, J. J. & YU, B. 2014. Effect of treadmill exercise timing on repair of full-thickness defects of articular cartilage by bone-derived mesenchymal stem cells: an experimental investigation in rats. *PLoS One,* 9**,** e90858.

SONG, R.-H., D. TORTORELLA, M., MALFAIT, A.-M., ALSTON, J. T., YANG, Z., ARNER, E. C. & GRIGGS, D. W. 2007. Aggrecan degradation in human articular cartilage explants is mediated by both ADAMTS-4 and ADAMTS-5. *Arthritis & Rheumatism,* 56**,** 575-585.

SOPPIMATH, K. S., AMINABHAVI, T. M., KULKARNI, A. R. & RUDZINSKI, W. E. 2001. Biodegradable polymeric nanoparticles as drug delivery devices. *Journal of Controlled Release,* 70**,** 1-20.

SPECTOR, T. D., HART, D. J., NANDRA, D., DOYLE, D. V., MACKILLOP, N., GALLIMORE, J. R. & PEPYS, M. B. 1997. Low-level increases in serum C-reactive protein are present in early osteoarthritis of the knee and predict progressive disease. *Arthritis Rheum,* 40**,** 723-727.

STADELMANN, V. A., TERRIER, A. & PIOLETTI, D. P. 2008. Microstimulation at the bone–implant interface upregulates osteoclast activation pathways. *Bone,* 42**,** 358-364.

STANNUS, O. P., JONES, G., BLIZZARD, L., CICUTTINI, F. M. & DING, C. 2013. Associations between serum levels of inflammatory markers and change in knee pain over 5 years in older adults: a prospective cohort study. *Ann Rheum Dis,* 72**,** 535-540.

STEFANOVIC-RACIC, M., STADLER, J., GEORGESCU, H. I. & EVANS, C. H. 1994. Nitric oxide synthesis and its regulation by rabbit synoviocytes. *J Rheumatol,* 21**,** 1892-1898.

STERNER, B., HARMS, M., WÖLL, S., WEIGANDT, M., WINDBERGS, M. & LEHR, C. M. 2016. The effect of polymer size and charge of molecules on permeation through synovial membrane and accumulation in hyaline articular cartilage. *European Journal of Pharmaceutics and Biopharmaceutics,* 101**,** 126-136.

STEVENS, R., PETERSEN, D., ERVIN, J., NEZZER, J., NIEVES, Y., CAMPBELL, J., GUEDES, K., BURGES, R. & HANSON, P. 2017. OP0167 Efficacy and safety of CNTX-4975 in subjects with moderate to severe osteoarthritis knee pain: 24-week, randomized, double-blind, placebo-controlled, dose-ranging study [abstract]. *Annals of the Rheumatic Diseases,* 76**,** 121-121.

STEVENSON, S., HUNZIKER, E. B., HERRMANN, W. & SCHENK, R. K. 1990. Is longitudinal bone growth influenced by diurnal variation in the mitotic activity of chondrocytes of the growth plate? *J Orthop Res,* 8**,** 132-135.

STRANDBERG, T. & TILVIS, R. 2000. C-Reactive Protein, Cardiovascular Risk Factors and Mortality in a Prospective Study in the Elderly *Atherioscler Thromb Vasc Biol. ,* 20**,** 1057-1060.

STROBER, W. 1997. Trypan Blue Exclusion Test of Cell Viability. *Current Protocols in Immunology,* 21**,** A.3B.1-A.3B.2.

STROJAN, K., LEONARDI, A., BREGAR, V. B., KRIŽAJ, I., SVETE, J. & PAVLIN, M. 2017. Dispersion of Nanoparticles in Different Media Importantly Determines the Composition of Their Protein Corona. *PloS one,* 12**,** e0169552.

STRUGLICS, A., LARSSON, S., PRATTA, M. A., KUMAR, S., LARK, M. W. & LOHMANDER, L. S. 2006. Human osteoarthritis synovial fluid and joint cartilage contain both aggrecanase- and matrix metalloproteinase-generated aggrecan fragments. *Osteoarthritis Cartilage,* 14**,** 101-113.

STUPINA, T. A., STEPANOV, M. A. & TEPLEN'KII, M. P. 2015. Role of subchondral bone in the restoration of articular cartilage. *Bull Exp Biol Med,* 158**,** 820-823.

STURMER, T., BRENNER, H., KOENIG, W. & GUNTHER, K. P. 2004. Severity and extent of osteoarthritis and low grade systemic inflammation as assessed by high sensitivity C reactive protein. *Ann Rheum Dis,* 63**,** 200-205.

SUDA, T., TAKAHASHI, N., UDAGAWA, N., JIMI, E., GILLESPIE, M. T. & MARTIN, T. J. 1999. Modulation of osteoclast differentiation and function by the new members of the tumor necrosis factor receptor and ligand families. *Endocr Rev,* 20**,** 345-357.

SUN, Y., MAUERHAN, D. R., HONEYCUTT, P. R., KNEISL, J. S., NORTON, J. H., HANLEY, E. N. & GRUBER, H. E. 2010. Analysis of meniscal degeneration and meniscal gene expression. *BMC Musculoskeletal Disorders,* 11.

SURI, S., GILL, S. E., MASSENA DE CAMIN, S., WILSON, D., MCWILLIAMS, D. F. & WALSH, D. A. 2007. Neurovascular invasion at the osteochondral junction and in osteophytes in osteoarthritis. *Ann Rheum Dis,* 66**,** 1423-1428.

SUTTON, S., CLUTTERBUCK, A., HARRIS, P., GENT, T., FREEMAN, S., FOSTER, N., BARRETT-JOLLEY, R. & MOBASHERI, A. 2009. The contribution of the synovium, synovial derived inflammatory cytokines and neuropeptides to the pathogenesis of osteoarthritis. *Vet J,* 179**,** 10-24.

SWAIN, S., SARMANOVA, A., COUPLAND, C., DOHERTY, M. & ZHANG, W. 2019. Comorbidities in Osteoarthritis: A systematic review and meta-analysis of observational studies. *Arthritis Care & Research,* 72**,** 991-1000.

SWÄRD, P., FROBELL, R., ENGLUND, M., ROOS, H. & STRUGLICS, A. 2012. Cartilage and bone markers and inflammatory cytokines are increased in synovial fluid in the acute phase of knee injury (hemarthrosis) – a cross-sectional analysis. *Osteoarthritis and Cartilage,* 20**,** 1302-1308.

SYLVESTER, J., EL MABROUK, M., AHMAD, R., CHAUDRY, A. & ZAFARULLAH, M. 2012. Interleukin-1 Induction of Aggrecanase Gene Expression in Human Articular Chondrocytes is Mediated by Mitogen-Activated Protein Kinases. *Cellular Physiology and Biochemistry,* 30**,** 563-574.

SZCZESNIAK, A. M., GILBERT, R. W., MUKHIDA, M. & ANDERSON, G. I. 2005. Mechanical loading modulates glutamate receptor subunit expression in bone. *Bone,* 37**,** 63-73.

TAKAHASHI, J. S., HONG, H.-K., KO, C. H. & MCDEARMON, E. L. 2008. The genetics of mammalian circadian order and disorder: implications for physiology and disease. *Nat Rev Genet,* 9**,** 764-775.

TAKARADA, T., HINOI, E., FUJIMORI, S., TSUCHIHASHI, Y., UESHIMA, T., TANIURA, H. & YONEDA, Y. 2004. Accumulation of [3H]glutamate in cultured rat calvarial osteoblasts. *Biochemical Pharmacology,* 68**,** 177-184.

TAMI, A. E., NASSER, P., SCHAFFLER, M. B. & KNOTHE TATE, M. L. 2003. Noninvasive fatigue fracture model of the rat ulna. *J Orthop Res,* 21**,** 1018-1024.
TAN, S. D., KUIJPERS-JAGTMAN, A. M., SEMEINS, C. M., BRONCKERS, A. L., MALTHA, J. C., VON DEN HOFF, J. W., EVERTS, V. & KLEIN-NULEND, J. 2006. Fluid shear stress inhibits TNFalpha-induced osteocyte apoptosis. *J Dent Res,* 85**,** 905-909.
TANAKA, S. M., LI, J., DUNCAN, R. L., YOKOTA, H., BURR, D. B. & TURNER, C. H. 2003. Effects of broad frequency vibration on cultured osteoblasts. *Journal of Biomechanics,* 36**,** 73-80.
TANAMAS, S., HANNA, F. S., CICUTTINI, F. M., WLUKA, A. E., BERRY, P. & URQUHART, D. M. 2009. Does knee malalignment increase the risk of development and progression of knee osteoarthritis? A systematic review. *Arthritis Care & Research,* 61**,** 459-467.
TAT, S. K., PELLETIER, J.-P., LAJEUNESSE, D., FAHMI, H., DUVAL, N. & MARTEL-PELLETIER, J. 2008. Differential modulation of RANKL isoforms by human osteoarthritic subchondral bone osteoblasts: Influence of osteotropic factors. *Bone,* 43**,** 284-291.
TATSUMI, S., ISHII, K., AMIZUKA, N., LI, M., KOBAYASHI, T., KOHNO, K., ITO, M., TAKESHITA, S. & IKEDA, K. 2007. Targeted Ablation of Osteocytes Induces Osteoporosis with Defective Mechanotransduction. *Cell Metabolism,* 5**,** 464-475.
TEMENOFF, J. S. & MIKOS, A. G. 2000. Review: tissue engineering for regeneration of articular cartilage. *Biomaterials,* 21**,** 431-440.
TEN DIJKE, P., KRAUSE, C., DE GORTER, D. J. J., LÖWIK, C. W. G. M. & VAN BEZOOIJEN, R. L. 2008. Osteocyte-Derived Sclerostin Inhibits Bone Formation: Its Role in Bone Morphogenetic Protein and Wnt Signaling. *JBJS,* 90**,** 31-35.
TETTEH, E. K. & MORRIS, S. 2014. Evaluating the administration costs of biologic drugs: development of a cost algorithm. *Health economics review,* 4**,** 26.
THIBAULT, M., POOLE, R. A. & BUSCHMANN, M. D. 2002. Cyclic compression of cartilage/bone explants in vitro leads to physical weakening, mechanical breakdown of collagen and release of matrix fragments. *Journal of Orthopaedic Research,* 20**,** 1265-1273.
THING, M., MERTZ, N., ÅGÅRDH, L., LARSEN, S. W., ØSTERGAARD, J. & LARSEN, C. 2019. Simulated synovial fluids for in vitro drug and prodrug release testing of depot injectables intended for joint injection. *Journal of Drug Delivery Science and Technology,* 49**,** 169-176.
THOMAS, A. C., HUBBARD-TURNER, T., WIKSTROM, E. A. & PALMIERI-SMITH, R. M. 2017. Epidemiology of Posttraumatic Osteoarthritis. *Journal of Athletic Training,* 52**,** 491-496.
THOMPSON, M., HUNT, B., SMITH, A. & JOYCE, T. 2015. Wear tests of a potential biolubricant for orthopaedic biopolymers. *Lubricants* 3**,** 80-90.
THOMPSON, P. W., KIRWAN, J. R., JONES, D. D. & CURREY, H. L. 1988. Serum cytidine deaminase levels after withdrawal of non-steroidal anti-inflammatory treatment in rheumatoid arthritis. *Annals of the Rheumatic Diseases,* 47**,** 308-312.
TIWARI, A., KARKHUR, Y., KEENEY, J. A. & AGGARWAL, A. 2018. Rapid destructive osteoarthritis of the hip after intra-articular steroid injection. *Arthroplasty Today,* 4**,** 184-186.
TJALMA, W., HUIZING, M. T. & PAPADIMITRIOU, K. 2017. The smooth and bumpy road of trastuzumab administration: from intravenous (IV) in a hospital to subcutaneous (SC) at home. *Facts, views & vision in ObGyn,* 9**,** 51-55.

TOMLINSON, E. 1987. Theory and practice of site-specific drug delivery. *Advanced Drug Delivery Reviews,* 1**,** 87-198.

TROEBERG, L. & NAGASE, H. 2012. Proteases involved in cartilage matrix degradation in osteoarthritis. *Biochimica et Biophysica Acta (BBA) - Proteins and Proteomics,* 1824**,** 133-145.

TSUCHIDA, A. I., BEEKHUIZEN, M., BOT, A. G. J., GEURTS, B., BEKKERS, J. E. J., DHERT, W. J. A., CREEMERS, L. B. & SARIS, D. B. F. 2012. The Role of IL-6 in Osteoarthritis and Cartilage Regeneration [abstract]. *ORS 2012 annual meeting poster presentation* Poster N. 1709.

TU, X., RHEE, Y., CONDON, K. W., BIVI, N., ALLEN, M. R., DWYER, D., STOLINA, M., TURNER, C. H., ROBLING, A. G., PLOTKIN, L. I. & BELLIDO, T. 2012. Sost downregulation and local Wnt signaling are required for the osteogenic response to mechanical loading. *Bone,* 50**,** 209-217.

TURNER, C. H., AKHTER, M. P., RAAB, D. M., KIMMEL, D. B. & RECKER, R. R. 1991. A noninvasive, in vivo model for studying strain adaptive bone modeling. *Bone,* 12**,** 73-79.

TURNER, C. H., TAKANO, Y., OWAN, I. & MURRELL, G. A. 1996. Nitric oxide inhibitor L-NAME suppresses mechanically induced bone formation in rats. *American Journal of Physiology-Endocrinology and Metabolism,* 270**,** E634-E639.

TURNER, C. H., WARDEN, S. J., BELLIDO, T., PLOTKIN, L. I., KUMAR, N., JASIUK, I., DANZIG, J. & ROBLING, A. G. 2009. Mechanobiology of the skeleton. *Sci Signal,* 2**,** pt3.

UDAGAWA, N., TAKAHASHI, N., YASUDA, H., MIZUNO, A., ITOH, K., UENO, Y., SHINKI, T., GILLESPIE, M. T., MARTIN, T. J., HIGASHIO, K. & SUDA, T. 2000. Osteoprotegerin produced by osteoblasts is an important regulator in osteoclast development and function. *Endocrinology,* 141**,** 3478-3484.

URIST, M. R. & MCLEAN, F. C. 1941. Calcification and ossification. I. Calcification in the callus in healing fractures in normal rats *J. Bone Joint Surg. ,* 23**,** 1-16.

VAN DALEN, S. C. M., BLOM, A. B., SLÖETJES, A. W., HELSEN, M. M. A., ROTH, J., VOGL, T., VAN DE LOO, F. A. J., KOENDERS, M. I., VAN DER KRAAN, P. M., VAN DEN BERG, W. B., VAN DEN BOSCH, M. H. J. & VAN LENT, P. L. E. M. 2017. Interleukin-1 is not involved in synovial inflammation and cartilage destruction in collagenase-induced osteoarthritis. *Osteoarthritis and Cartilage,* 25**,** 385-396.

VAN DEN BERG, W. B., JOOSTEN, L. A. & VAN LENT, P. L. 2007. Murine antigen-induced arthritis. *Methods Mol Med,* 136**,** 243-253.

VAN DIJK, G. M., VEENHOF, C., SPREEUWENBERG, P., COENE, N., BURGER, B. J., VAN SCHAARDENBURG, D., VAN DEN ENDE, C. H., LANKHORST, G. J. & DEKKER, J. 2010. Prognosis of limitations in activities in osteoarthritis of the hip or knee: a 3-year cohort study. *Arch Phys Med Rehabil,* 91**,** 58-66.

VAN MEEGEREN, M. E. R., ROOSENDAAL, G., JANSEN, N. W. D., WENTING, M. J. G., VAN WESEL, A. C. W., VAN ROON, J. A. G. & LAFEBER, F. P. J. G. 2012. IL-4 alone and in combination with IL-10 protects against blood-induced cartilage damage. *Osteoarthritis and Cartilage,* 20**,** 764-772.

VAN OSCH, G. J., VAN DER KRAAN, P. M., BLANKEVOORT, L., HUISKES, R. & VAN DEN BERG, W. B. 1996. Relation of ligament damage with site specific cartilage loss and osteophyte formation in collagenase induced osteoarthritis in mice. *J Rheumatol,* 23**,** 1227-1232.

VAN WALSEM, A., PANDHI, S., NIXON, R. M., GUYOT, P., KARABIS, A. & MOORE, R. A. 2015. Relative benefit-risk comparing diclofenac to other traditional non-steroidal anti-inflammatory drugs and cyclooxygenase-2 inhibitors in patients with osteoarthritis or rheumatoid arthritis: a network meta-analysis. *Arthritis research & therapy,* 17**,** 66.

VAN WEEREN, R. 2014. 11 - Joint physiology: Responses to exercise and training. *In:* HINCHCLIFF, K. W., KANEPS, A. J. & GEOR, R. J. (eds.) *Equine Sports Medicine and Surgery (Second Edition).* W.B. Saunders.

VAN'T HOF, R. J., HOCKING, L., WRIGHT, P. K. & RALSTON, S. H. 2000. Nitric oxide is a mediator of apoptosis in the rheumatoid joint. *Rheumatology,* 39**,** 1004-1008.

VANDESOMPELE, J., DE PRETER, K., PATTYN, F., POPPE, B., VAN ROY, N., DE PAEPE, A. & SPELEMAN, F. 2002. Accurate normalization of real-time quantitative RT-PCR data by geometric averaging of multiple internal control genes. *Genome Biology,* 3.

VANGSNESS, C. T., BURKE, W. S., NARVY, S. J., MACPHEE, R. D. & FEDENKO, A. N. 2011. Human knee synovial fluid cytokines correlated with grade of knee osteoarthritis--a pilot study. *Bull NYU Hosp Jt Dis,* 69**,** 122-127.

VASTA, V., MEACCI, E., FARNARARO, M. & BRUNI, P. 1993. Glutamine Utilization in Resting and Stimulated Platelets. *The Journal of Biochemistry,* 114**,** 163-166.

VAZQUEZ, M. 2013. *Development of a novel in vitro 3D osteocyte-osteoblast co-culture model to investigate mechanically induced signalling* PhD, Cardiff University

VAZQUEZ, M., EVANS, B. A. J., RICCARDI, D., EVANS, S. L., RALPHS, J. R., DILLINGHAM, C. M. & MASON, D. J. 2014. A New Method to Investigate How Mechanical Loading of Osteocytes Controls Osteoblasts. *Frontiers in Endocrinology,* 5.

VENKATESH, M. P., ANIS, S. & PRAMOD KUMAR, T. M. 2013. Design and development of an injectable in situ forming drug delivery system of methotrexate for the treatment of rheumatoid arthritis. *Journal of Drug Delivery Science and Technology,* 23**,** 445-453.

VIJAYAN GANGADHARAN, V., WANG, R., ULZHÖFER, B., LUO, C., BARDONI, R., KUMAR BALI, K., AGARWAL, N., TEGEDER, I., HILDEBRANDT, U., NAGY, G. G., TODD, A. J., GHIRRI, A., HÄUSSLER, A., SPRENGEL, R., SEEBURG, P. H., MACDERMOTT, A. B., LEWIN, G. R. & KUNER, R. 2011. Peripheral calcium-permeable AMPA receptors regulate chronic inflammatory pain in mice. *J Clin Invest,* 121**,** 1608-1623.

VINCENT, H. K., PERCIVAL, S. S., CONRAD, B. P., SEAY, A. N., MONTERO, C. & VINCENT, K. R. 2013. Hyaluronic Acid (HA) Viscosupplementation on Synovial Fluid Inflammation in Knee Osteoarthritis: A Pilot Study. *Open Orthop J,* 7**,** 378-384.

VINOGRADOV, S. V., BRONICH, T. K. & KABANOV, A. V. 2002. Nanosized cationic hydrogels for drug delivery: preparation, properties and interactions with cells. *Advanced Drug Delivery Reviews,* 54**,** 135-147.

VON PORAT, A., ROOS, E. M. & ROOS, H. 2004. High prevalence of osteoarthritis 14 years after an anterior cruciate ligament tear in male soccer players: a study of radiographic and patient relevant outcomes. *Annals of the Rheumatic Diseases,* 63**,** 269-273.

VUOLTEENAHO, K., MOILANEN, T., KNOWLES, R. G. & MOILANEN, E. 2007. The role of nitric oxide in osteoarthritis. *Scandinavian Journal of Rheumatology,* 36**,** 247-258.

WALSH, C. A., BIRCH, M. A., FRASER, W. D., GINTY, A. F. & GALLAGHER, J. A. 2000. Cytokine expression by cultured osteoblasts from patients with osteoporotic fractures. *International Journal of Experimental Pathology,* 81**,** 159-163.

WALSH, D. A., BONNET, C. S., TURNER, E. L., WILSON, D., SITU, M. & MCWILLIAMS, D. F. 2007. Angiogenesis in the synovium and at the osteochondral junction in osteoarthritis. *Osteoarthritis Cartilage,* 15**,** 743-751.

WALTON, M. 1977. Degenerative joint disease in the mouse knee; histological observations. *J Pathol,* 123**,** 109-122.

WANG, B., DU, T., WANG, Y., YANG, C., ZHANG, S. & CAO, X. 2011. Focal adhesion kinase signaling pathway is involved in mechanotransduction in MG-63 cells. *Biochem Biophys Res Commun,* 410**,** 671-676.

WANG, H., LIU, J., TAO, S., CHAI, G., WANG, J., HU, F.-Q. & YUAN, H. 2015. Tetracycline-grafted PLGA nanoparticles as bone-targeting drug delivery system. *International journal of nanomedicine,* 10**,** 5671-5685.

WANG, J., WANG, X., CAO, Y., HUANG, T., SONG, D. X. & TAO, H. R. 2018. Therapeutic potential of hyaluronic acid/chitosan nanoparticles for the delivery of curcuminoid in knee osteoarthritis and an in vitro evaluation in chondrocytes. *Int J Mol Med,* 42**,** 2604-2614.

WANG, L., HINOI, E., TAKEMORI, A. & YONEDA, Y. 2005. Release of Endogenous Glutamate by AMPA Receptors Expressed in Cultured Rat Costal Chondrocytes. *Biological and Pharmaceutical Bulletin,* 28**,** 990-993.

WANG, R., HUGHES, T., BECK, S., VAKIL, S., LI, S., PANTANO, P. & DRAPER, R. K. 2012. Generation of toxic degradation products by sonication of Pluronic® dispersants: implications for nanotoxicity testing. *Nanotoxicology,* 7**,** 1272-1281.

WANG, Y., CHEN, X., CAO, W. & SHI, Y. 2014. Plasticity of mesenchymal stem cells in immunomodulation: pathological and therapeutic implications. *Nat Immunol,* 15**,** 1009-1016.

WARD, M. A. & GEORGIOU, T. K. 2010. Thermoresponsive terpolymers based on methacrylate monomers: Effect of architecture and composition. *Journal of Polymer Science Part A: Polymer Chemistry,* 48**,** 775-783.

WATT, F. E., PATERSON, E., FREIDIN, A., KENNY, M., JUDGE, A., SAKLATVALA, J., WILLIAMS, A. & VINCENT, T. L. 2016. Acute Molecular Changes in Synovial Fluid Following Human Knee Injury: Association With Early Clinical Outcomes. *Arthritis & rheumatology (Hoboken, N.J.),* 68**,** 2129-2140.

WATT, F. E., CORP, N., KINGSBURY, S. R., FROBELL, R., ENGLUND, M., FELSON, D. T., LEVESQUE, M., MAJUMDAR, S., WILSON, C., BEARD, D. J., LOHMANDER, L. S., KRAUS, V. B., ROEMER, F., CONAGHAN, P. G., MASON, D. J., ARTHRITIS RESEARCH, U. K. & OSTEOARTHRITIS CRYSTAL DISEASE CLINICAL STUDY GROUP EXPERT WORKING, G. 2019. Towards prevention of post-traumatic osteoarthritis: report from an international expert working group on considerations for the design and conduct of interventional studies following acute knee injury. *Osteoarthritis and cartilage,* 27**,** 23-33.

WEBB, P. 1992. Temperatures of skin, subcutaneous tissue, muscle and core in resting men in cold, comfortable and hot conditions. *Eur J Appl Physiol Occup Physiol,* 64**,** 471-476.

WEHLING, P., EVANS, C., WEHLING, J. & MAIXNER, W. 2017. Effectiveness of intra-articular therapies in osteoarthritis: a literature review. *Therapeutic Advances in Musculoskeletal Disease,* 9**,** 183-196.

WEIN, M. N., SPATZ, J., NISHIMORI, S., DOENCH, J., ROOT, D., BABIJ, P., NAGANO, K., BARON, R., BROOKS, D., BOUXSEIN, M., PAJEVIC, P. D. & KRONENBERG, H. M. 2015.

HDAC5 controls MEF2C-driven sclerostin expression in osteocytes. *Journal of bone and mineral research : the official journal of the American Society for Bone and Mineral Research,* 30**,** 400-411.

WEINSTEIN, A. M., ROME, B. N., REICHMANN, W. M., COLLINS, J. E., BURBINE, S. A., THORNHILL, T. S., WRIGHT, J., KATZ, J. N. & LOSINA, E. 2013. Estimating the Burden of Total Knee Replacement in the United States. *The Journal of Bone and Joint Surgery. American volume,* 95**,** 385-392.

WERNER, B. C., CANCIENNE, J. M., BURRUS, M. T., PARK, J. S., PERUMAL, V. & COOPER, M. T. 2016. Risk of Infection After Intra-articular Steroid Injection at the Time of Ankle Arthroscopy in a Medicare Population. *Arthroscopy,* 32**,** 350-354.

WHITE, A. A., PANJABI, M. M. & SOUTHWICK, W. O. 1977. The four biomechanical stages of fracture repair. *J Bone Joint Surg Am,* 59**,** 188-192.

WHITMIRE, R. E., WILSON, S. D., SINGH, A., LEVENSTON, M. E., MURTHY, N. & GARCÍA, A. J. 2012. Self-assembling nanoparticles for intra-articular delivery of anti-inflammatory proteins. *Biomaterials,* 33**,** 7665-7675.

WIKRAMANAYAKE, T. C., STOJADINOVIC, O. & TOMIC-CANIC, M. 2014. Epidermal Differentiation in Barrier Maintenance and Wound Healing. *Advances in wound care,* 3**,** 272-280.

WILLIAMS, A. C. 2015. *Topical and transdermal drug delivery* Elsevier.

WILLIAMS, A. S., TOPLEY, N., DOJCINOV, S., RICHARDS, P. J. & WILLIAMS, B. D. 2001. Amelioration of rat antigen-induced arthritis by liposomally conjugated methotrexate is accompanied by down-regulation of cytokine mRNA expression. *Rheumatology (Oxford),* 40**,** 375-383.

WINKLER, D. G., SUTHERLAND, M. K., GEOGHEGAN, J. C., YU, C., HAYES, T., SKONIER, J. E., SHPEKTOR, D., JONAS, M., KOVACEVICH, B. R., STAEHLING-HAMPTON, K., APPLEBY, M., BRUNKOW, M. E. & LATHAM, J. A. 2003. Osteocyte control of bone formation via sclerostin, a novel BMP antagonist. *The EMBO Journal,* 22**,** 6267.

WOJDASIEWICZ, P., PONIATOWSKI, Ł. A. & SZUKIEWICZ, D. 2014. The Role of Inflammatory and Anti-Inflammatory Cytokines in the Pathogenesis of Osteoarthritis. *Mediators Inflamm,* 2014**,** 19.

WOLFE, F. 1997. The C-reactive protein but not erythrocyte sedimentation rate is associated with clinical severity in patients with osteoarthritis of the knee or hip. *J Rheumatol,* 24**,** 1486-1488.

WOLFF, J. 1892. *Das Gesetz der Transformation der Knochen. Berlin: A Hirschwald,* Berlin, Germany, G. Grotesche Verlagsbuchhandlung.

WONG, M., WUETHRICH, P., EGGLI, P. & HUNZIKER, E. 1996. Zone-specific cell biosynthetic activity in mature bovine articular cartilage: A new method using confocal microscopic stereology and quantitative autoradiography. *Journal of Orthopaedic Research,* 14**,** 424-432.

WONG, M., ZIRING, D., KORIN, Y., DESAI, S., KIM, S., LIN, J., GJERTSON, D., BRAUN, J., REED, E. & SINGH, R. R. 2008. TNFα blockade in human diseases: Mechanisms and future directions. *Clinical Immunology,* 126**,** 121-136.

WONG, P. K., QUINN, J. M., SIMS, N. A., VAN NIEUWENHUIJZE, A., CAMPBELL, I. K. & WICKS, I. P. 2006. Interleukin-6 modulates production of T lymphocyte-derived cytokines in antigen-induced arthritis and drives inflammation-induced osteoclastogenesis. *Arthritis Rheum,* 54**,** 158-168.

WOO, S. M., ROSSER, J., DUSEVICH, V., KALAJZIC, I. & BONEWALD, L. F. 2011. Cell line IDG-SW3 replicates osteoblast-to-late-osteocyte differentiation in vitro and accelerates bone formation in vivo. *J Bone Miner Res,* 26**,** 2634-2646.

WOOLF, A. D. & PFLEGER, B. 2003. Burden of major musculoskeletal conditions. *Bull World Health Organ,* 81**,** 646-656.

WORLD HEALTH ORGANISATION, W. H. O. 2013. *Priority Medicines for Europe and the World 2013 Update: 6.12 Osteoarthritis* [Online]. https://www.who.int/medicines/areas/priority_medicines/Ch6_12Osteo.pdf. [Accessed 13/01/2020 2020].

WU, G., CHEN, L., LI, H., DENG, C.-L. & CHEN, X.-F. 2014. Comparing Microspheres with Different Internal Phase of Polyelectrolyte as Local Drug Delivery System for Bone Tuberculosis Therapy. *BioMed Research International,* 2014**,** 8.

WU, Q., ZHOU, X., HUANG, D., JI, Y. & KANG, F. 2017. IL-6 Enhances Osteocyte-Mediated Osteoclastogenesis by Promoting JAK2 and RANKL Activity *In Vitro*. *Cellular Physiology and Biochemistry,* 41**,** 1360-1369.

WU, X., FENG, X., HE, Y., GAO, Y., YANG, S., SHAO, Z., YANG, C., WANG, H. & YE, Z. 2016. IL-4 administration exerts preventive effects via suppression of underlying inflammation and TNF-α-induced apoptosis in steroid-induced osteonecrosis. *Osteoporos Int,* 27**,** 1827-1837.

XIA, B., DI, C., ZHANG, J., HU, S., JIN, H. & TONG, P. 2014. Osteoarthritis pathogenesis: a review of molecular mechanisms. *Calcified tissue international,* 95**,** 495-505.

XIE, F., XIAO, P., CHEN, D., XU, L. & ZHANG, B. 2012. miRDeepFinder: a miRNA analysis tool for deep sequencing of plant small RNAs. *Plant molecular biology* 80**,** 75-84.

XIE, W., DOLDER, S., SIEGRIST, M., WETTERWALD, A. & HOFSTETTER, W. 2016. Glutamate Receptor Agonists and Glutamate Transporter Antagonists Regulate Differentiation of Osteoblast Lineage Cells. *Calcif Tissue Int,* 99**,** 142-154.

XIONG, J., ONAL, M., JILKA, R. L., WEINSTEIN, R. S., MANOLAGAS, S. C. & O'BRIEN, C. A. 2011. Matrix-embedded cells control osteoclast formation. *Nature Medicine,* 17**,** 1235-1241.

XU, L. X., KUKITA, T., KUKITA, A., OTSUKA, T., NIHO, Y. & IIJIMA, T. 1995. Interleukin-10 selectively inhibits osteoclastogenesis by inhibiting differentiation of osteoclast progenitors into preosteoclast-like cells in rat bone marrow culture system. *J Cell Physiol,* 165**,** 624-629.

XU, P., GULLOTTI, E., TONG, L., HIGHLEY, C. B., ERRABELLI, D. R., HASAN, T., CHENG, J.-X., KOHANE, D. S. & YEO, Y. 2009. Intracellular drug delivery by poly(lactic-co-glycolic acid) nanoparticles, revisited. *Molecular pharmaceutics,* 6**,** 190-201.

YAMADA, A., TAKAMI, M., KAWAWA, T., YASUHARA, R., ZHAO, B., MOCHIZUKI, A., MIYAMOTO, Y., ETO, T., YASUDA, H., NAKAMICHI, Y., KIM, N., KATAGIRI, T., SUDA, T. & KAMIJO, R. 2007. Interleukin-4 inhibition of osteoclast differentiation is stronger than that of interleukin-13 and they are equivalent for induction of osteoprotegerin production from osteoblasts. *Immunology,* 120**,** 573-579.

YAMMANI, R. R., CARLSON, C. S., BRESNICK, A. R. & LOESER, R. F. 2006. Increase in production of matrix metalloproteinase 13 by human articular chondrocytes due to stimulation with S100A4: Role of the receptor for advanced glycation end products. *Arthritis & Rheumatism,* 54**,** 2901-2911.

YAN, Y., WANG, L., GE, L. & PATHAK, J. L. 2020. Osteocyte-Mediated Translation of Mechanical Stimuli to Cellular Signaling and Its Role in Bone and Non-bone-Related Clinical Complications. *Current Osteoporosis Reports,* 18**,** 67-80.

YANG, A., LU, Y., XING, J., LI, Z., YIN, X., DOU, C., DONG, S., LUO, F., XIE, Z., HOU, T. & XU, J. 2018. IL-8 Enhances Therapeutic Effects of BMSCs on Bone Regeneration via CXCR2-Mediated PI3k/Akt Signaling Pathway. *Cell Physiol Biochem,* 48**,** 361-370.

YANG, J.-Y., CHO, S. W., AN, J. H., JUNG, J. Y., KIM, S. W., KIM, S. Y., KIM, J. E. & SHIN, C. S. 2013. Osteoblast-Targeted Overexpression of TAZ Increases Bone Mass In Vivo. *PLOS ONE,* 8**,** e56585.

YANG, N. H., NAYEB-HASHEMI, H., CANAVAN, P. K. & VAZIRI, A. 2010. Effect of frontal plane tibiofemoral angle on the stress and strain at the knee cartilage during the stance phase of gait. *Journal of Orthopaedic Research,* 28**,** 1539-1547.

YANG, X., RICCIARDI, B. F., HERNANDEZ-SORIA, A., SHI, Y., PLESHKO CAMACHO, N. & BOSTROM, M. P. 2007. Callus mineralization and maturation are delayed during fracture healing in interleukin-6 knockout mice. *Bone,* 41**,** 928-936.

YANG, Z., SCHMITT, J. F. & LEE, E. H. 2011. Immunohistochemical Analysis of Human Mesenchymal Stem Cells Differentiating into Chondrogenic, Osteogenic, and Adipogenic Lineages. *Mesenchymal Stem Cell Assays and Applications. Methods in Molecular Biology (Methods and Protocols),* 698**,** 353-366.

YAVROPOULOU, M. P. & YOVOS, J. G. 2016. The molecular basis of bone mechanotransduction. *Journal of musculoskeletal & neuronal interactions,* 16**,** 221-236.

YI, L., LI, Z., JIANG, H., CAO, Z., LIU, J. & ZHANG, X. 2018. Gene Modification of Transforming Growth Factor beta (TGF-beta) and Interleukin 10 (IL-10) in Suppressing Mt Sonicate Induced Osteoclast Formation and Bone Absorption. *Med Sci Monit,* 24**,** 5200-5207.

YIN, Q.-Q., WU, L., GOU, M.-L., QIAN, Z.-Y., ZHANG, W.-S. & LIU, J. 2009. Long-lasting infiltration anaesthesia by lidocaine-loaded biodegradable nanoparticles in hydrogel in rats. *Acta Anaesthesiologica Scandinavica,* 53**,** 1207-1213.

YORIMITSU, M., NISHIDA, K., SHIMIZU, A., DOI, H., MIYAZAWA, S., KOMIYAMA, T., NASU, Y., YOSHIDA, A., WATANABE, S. & OZAKI, T. 2008. Intra-articular injection of interleukin-4 decreases nitric oxide production by chondrocytes and ameliorates subsequent destruction of cartilage in instability-induced osteoarthritis in rat knee joints. *Osteoarthritis and Cartilage,* 16**,** 764-771.

YOSHIMATSU, M., KITAURA, H., FUJIMURA, Y., EGUCHI, T., KOHARA, H., MORITA, Y. & YOSHIDA, N. 2009. IL-12 inhibits TNF-α induced osteoclastogenesis via a T cell-independent mechanism in vivo. *Bone,* 45**,** 1010-1016.

YOU, L., TEMIYASATHIT, S., LEE, P., KIM, C. H., TUMMALA, P., YAO, W., KINGERY, W., MALONE, A. M., KWON, R. Y. & JACOBS, C. R. 2008. Osteocytes as mechanosensors in the inhibition of bone resorption due to mechanical loading. *Bone,* 42**,** 172-179.

YUAN, X. L., MENG, H. Y., WANG, Y. C., PENG, J., GUO, Q. Y., WANG, A. Y. & LU, S. B. 2014. Bone–cartilage interface crosstalk in osteoarthritis: potential pathways and future therapeutic strategies. *Osteoarthritis and Cartilage,* 22**,** 1077-1089.

ZAUNER, W., FARROW, N. A. & HAINES, A. M. R. 2001. In vitro uptake of polystyrene microspheres: effect of particle size, cell line and cell density. *Journal of Controlled Release,* 71**,** 39-51.

ZHANG, B., HOU, R., ZOU, Z., LUO, T., ZHANG, Y., WANG, L. & WANG, B. 2018. Mechanically induced autophagy is associated with ATP metabolism and cellular viability in osteocytes in vitro. *Redox Biology,* 14**,** 492-498.

ZHANG, C., BAKKER, A. D., KLEIN-NULEND, J. & BRAVENBOER, N. 2019. Studies on Osteocytes in Their 3D Native Matrix Versus 2D In Vitro Models. *Current Osteoporosis Reports,* 17**,** 207-216.

ZHANG, G. H., YOON, Y. W., LEE, K. S., MIN, S. S., HONG, S. K., PARK, J. Y. & HAN, H. C. 2003. The glutamatergic N-methyl-D-aspartate and non-N-methyl-D-aspartate receptors in the joint contribute to the induction, but not maintenance, of arthritic pain in rats. *Neurosci Lett,* 351**,** 177-180.

ZHANG, J.-M. & AN, J. 2007. Cytokines, inflammation, and pain. *International anesthesiology clinics,* 45**,** 27-37.

ZHANG, L., GU, F. X., CHAN, J. M., WANG, A. Z., LANGER, R. S. & FAROKHZAD, O. C. 2008. Nanoparticles in Medicine: Therapeutic Applications and Developments. *Clinical Pharmacology & Therapeutics,* 83**,** 761-769.

ZHANG, S.-S., XIA, W.-T., XU, J., XU, H.-L., LU, C.-T., ZHAO, Y.-Z. & WU, X.-Q. 2017. Three-dimensional structure micelles of heparin-poloxamer improve the therapeutic effect of 17β-estradiol on endometrial regeneration for intrauterine adhesions in a rat model. *International journal of nanomedicine,* 12**,** 5643-5657.

ZHANG, W., JONES, A. & DOHERTY, M. 2004. Does paracetamol (acetaminophen) reduce the pain of osteoarthritis? A meta-analysis of randomised controlled trials. *Ann Rheum Dis,* 63**,** 901-907.

ZHANG, Y.-H., HEULSMANN, A., TONDRAVI, M. M., MUKHERJEE, A. & ABU-AMER, Y. 2001. Tumor Necrosis Factor-α (TNF) Stimulates RANKL-induced Osteoclastogenesis via Coupling of TNF Type 1 Receptor and RANK Signaling Pathways. *Journal of Biological Chemistry,* 276**,** 563-568.

ZHAO, B. & IVASHKIV, L. B. 2011. Negative regulation of osteoclastogenesis and bone resorption by cytokines and transcriptional repressors. *Arthritis Research & Therapy,* 13**,** 234.

ZHAO, F., ZHAO, Y., LIU, Y., CHANG, X., CHEN, C. & ZHAO, Y. 2011. Cellular uptake, intracellular trafficking, and cytotoxicity of nanomaterials. *Small,* 7**,** 1322-1337.

ZHONG, H., CHAN, G., HU, Y., HU, H. & OUYANG, D. 2018. A Comprehensive Map of FDA-Approved Pharmaceutical Products. *Pharmaceutics* 10**,** 263.

ZHOU, Y., LIU, S.-Q., PENG, H., YU, L., HE, B. & ZHAO, Q. 2015. In vivo anti-apoptosis activity of novel berberine-loaded chitosan nanoparticles effectively ameliorates osteoarthritis. *International Immunopharmacology,* 28**,** 34-43.

ZHUO, Q., YANG, W., CHEN, J. & WANG, Y. 2012. Metabolic syndrome meets osteoarthritis. *Nat Rev Rheumatol,* 8**,** 729-737.

ZIEN, A., AIGNER, T., ZIMMER, R. & LENGAUER, T. 2001. Centralization: a new method for the normalization of gene expression data. *Bioinformatics,* 17**,** S323-S331.

ZILLE, H., PAQUET, J., HENRIONNET, C., SCALA-BERTOLA, J., LEONARD, M., SIX, J. L., DESCHAMP, F., NETTER, P., VERGES, J., GILLET, P. & GROSSIN, L. 2010. Evaluation of intra-articular delivery of hyaluronic acid functionalized biopolymeric nanoparticles in healthy rat knees. *Biomed Mater Eng,* 20**,** 235-242.

ZREIQAT, H., BELLUOCCIO, D., SMITH, M. M., WILSON, R., ROWLEY, L. A., JONES, K., RAMASWAMY, Y., VOGL, T., ROTH, J., BATEMAN, J. F. & LITTLE, C. B. 2010. S100A8 and S100A9 in experimental osteoarthritis. *Arthritis Res Ther,* 12**,** R16.

ZUPAN, J., KOMADINA, R. & MARC, J. 2012. The relationship between osteoclastogenic and anti-osteoclastogenic pro-inflammatory cytokines differs in human osteoporotic and osteoarthritic bone tissues. *Journal of Biomedical Science,* 19**,** 28.

Research Contributions and Awards

Conferences (Abstracts Accepted)

2020 British Orthopaedic Research Society (Oral Presentation)

2019 Orthopaedic Research Society (Podium Presentation and Poster Presentation)

2018 European Orthopaedic Research Society (Oral Presentation)

2018 Bone Research Society (Poster Presentation)

2018 Cardiff Institute of Tissue Engineering and Repair (CITER) Annual Scientific Meeting (ASM) (Oral Presentation)

2017 11th world meeting of pharmaceutics, biopharmaceutics and pharmaceutical technology (Poster Presentation)

2017 CITER ASM (Oral Presentation)

2016 British Orthopaedic Research Society (Oral Presentation)

Awards

Best oral presentation 2018 CITER ASM

CITER international conference travel bursary 2018

Appendix

9.1 Calibration Curves

The DNQX peak area calibration curve (Figure 9.1) was obtained by identifying the peak areas from serial dilutions in H_2O of 10, 5, 2.5, 1.25, 0.625, 0.3125, 0.15625, 0.078125 and 0.0390625mM DNQX dissolved in dH_2O (n=3). The equation used to calculate DNQX concentration from sample peak area is: $y = 5082.4x$, with y=peak area and x=DNQX concentration. The Calibration coefficient calculated from Figure 9.1 (5082.4) was then utilized to calculate DNQX concentrations from drug release studies and diffusion studies.

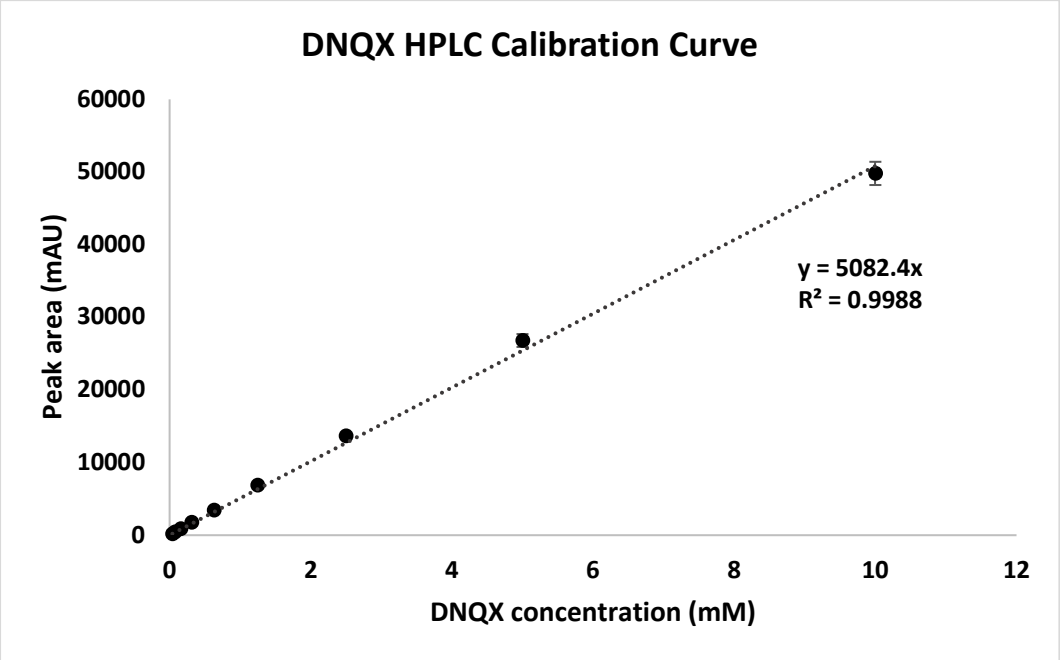

Figure 9.1: HPLC calibration curve for the quantification of DNQX isolated from PLGA nanoparticles (section 2.2) and Pluronic F-127 hydrogels (section 2.3) (n=3).

The NBQX peak area calibration curve (Figure 9.2) was obtained by identifying the peak areas from serial dilutions in H_2O of 2.5, 1.25, 0.625, 0.3125, 0.15625, 0.078125 and 0.0390625, 0.01953125, 0.009765625 and 0.004882813mM DNQX dissolved in dH_2O (n=3). The equation used to calculate DNQX concentration from sample peak area is: $y = 6611.3x$, with y=peak area and x=NBQX concentration. The Calibration coefficient calculated from Figure 9.2 (6611.3) was then utilized to calculate NBQX concentrations from drug release studies.

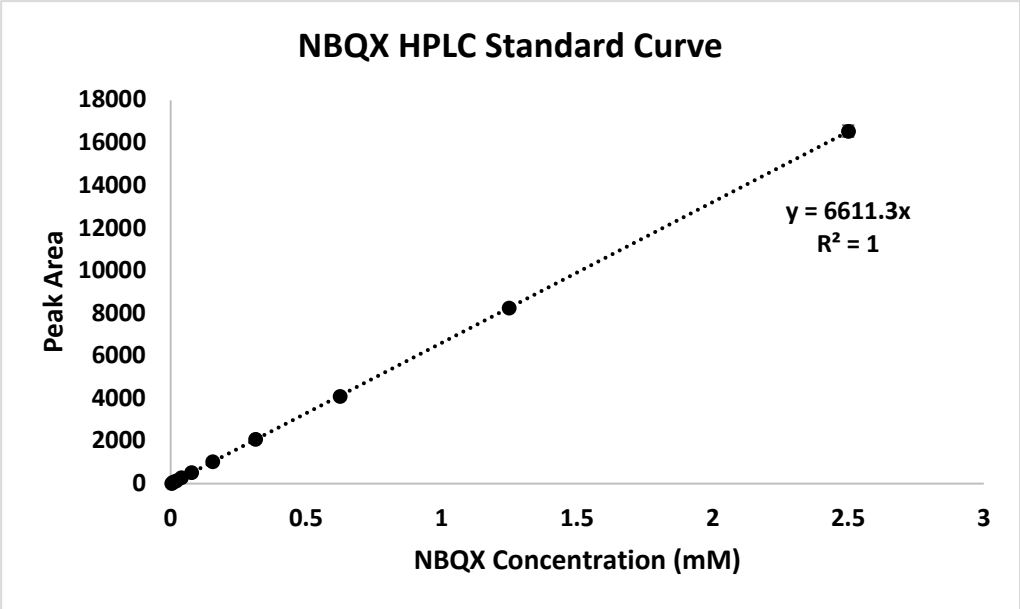

Figure 9.2: HPLC calibration curve for the quantification of NBQX isolated from PLGA nanoparticle release studies (section 2.2) (n=3).

When quantifying nitrite concentration within media samples (methods section 2.11). A standard curve was run alongside every experiment in triplicate to ensure reliability of nitrite quantification (Figure 9.3).

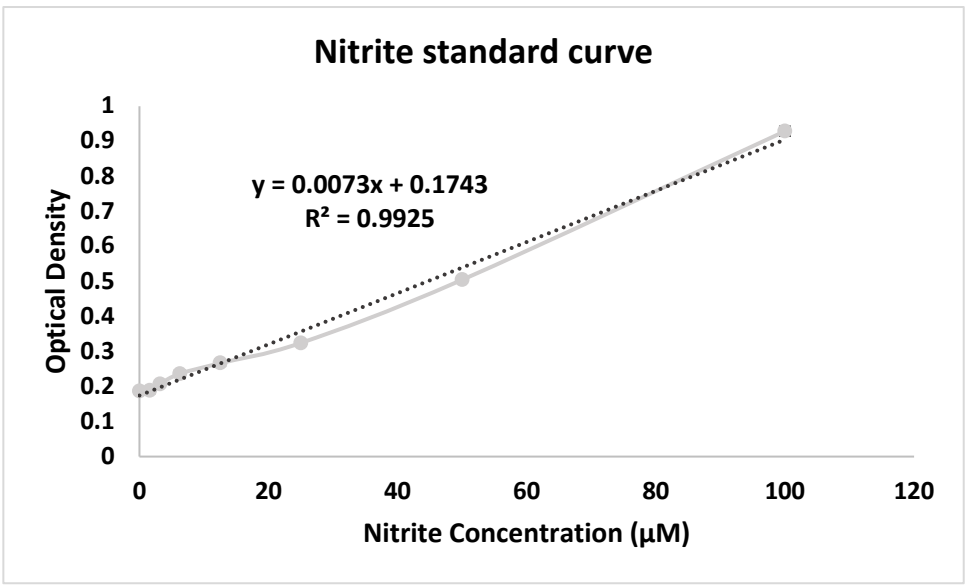

Figure 9.3: Griess Reagent System assay standard curve (n=3).

9.2 HPLC GluR Antagonist Peaks

DNQX and NBQX were detected using HPLC. DNQX was detected at a retention time of 8.5 minutes at a wavelength of 276nm (Figure 9.4A). NBQX was detected at a retention time of 2.6 minutes at a wavelength of 254nm (Figure 9.4B).

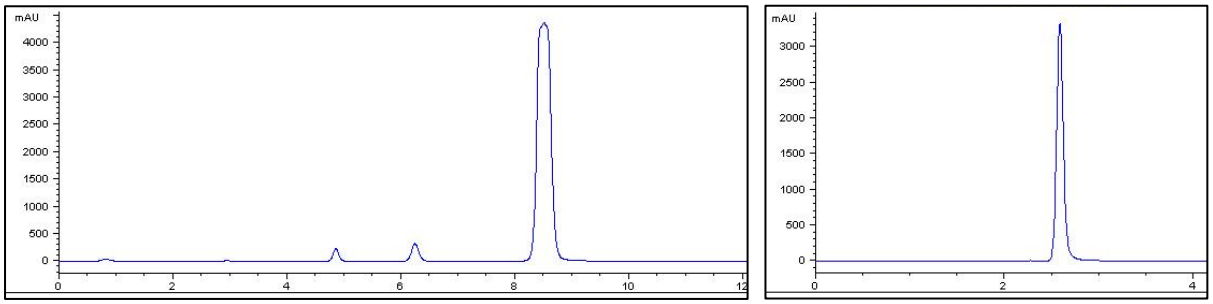

Figure 9.4: HPLC detection peaks for A) DNQX and B) NBQX. Both peaks were quantified using calibration coefficients established from serial dilutions of each drug (Figure 9.1 and Figure 9.2).

9.3 qRT-PCR

9.3.1 Reference Gene Stability Values

Reference genes act as internal controls for performing qRT-PCR. The geNorm algorithm within RefFinder software was used to identify the most stable combination of reference genes (section 2.9.5.2). The outputs of this analysis are shown in Figure 9.5.

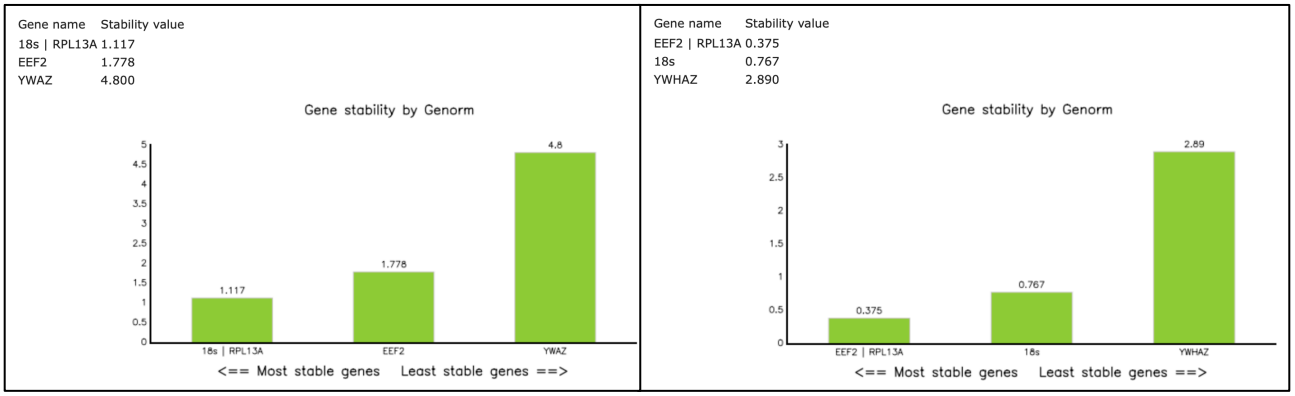

Figure 9.5: qRT-PCR reference gene stability ratings as calculated by geNorm algorithm within RefFinder software (described in section 2.9.5.2). A) 3D Y201 loading study. B) 3D Y201 IL-6/sIL-6r study.

9.3.2 Melting Curves

Each gene in results chapters 5 and 6 for gene expression analysis of both the 3D Y201 loading studies and 3D Y201 IL-6/sIL-6r inflammatory study produced a qRT-PCR melting curve as shown in Table 9.1.

Table 9.1: qRT-PCR melting curves for all genes described in results chapters 5 and 6 (analysis described in methods section 2.9).

Analyte	Study	
	IL-6 inflammatory study	**Cell loading study**
opg	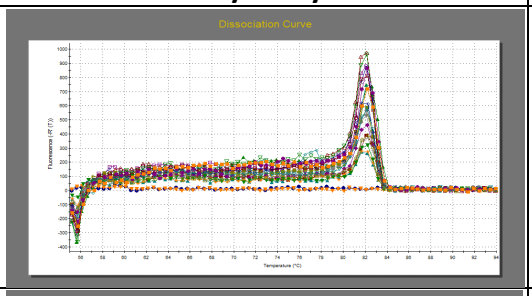	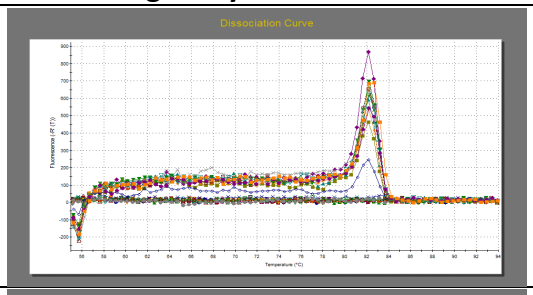
ocn	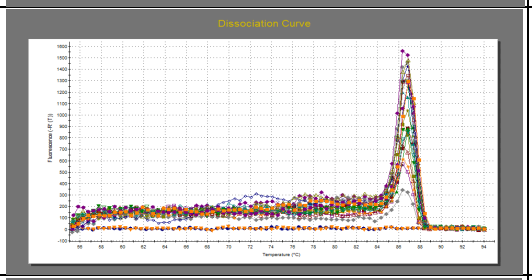	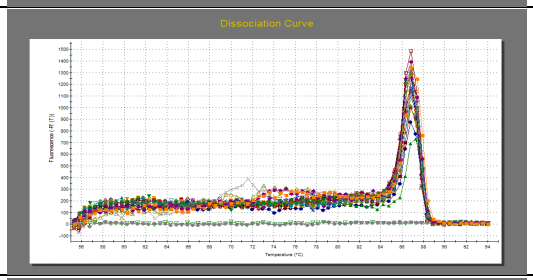
Col-I	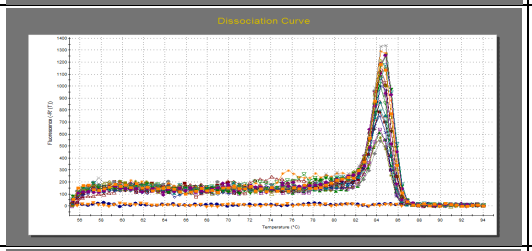	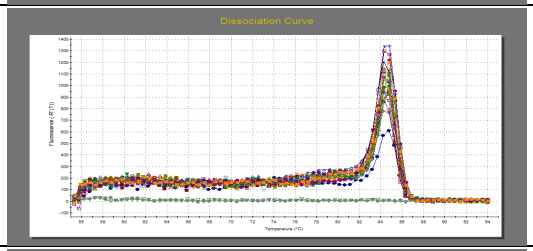
alp	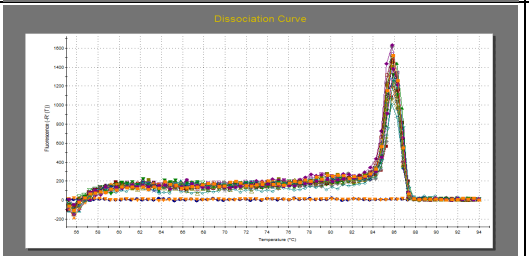	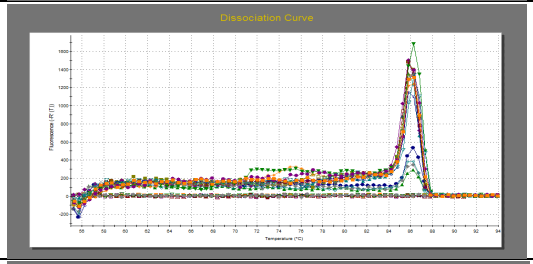
il-6	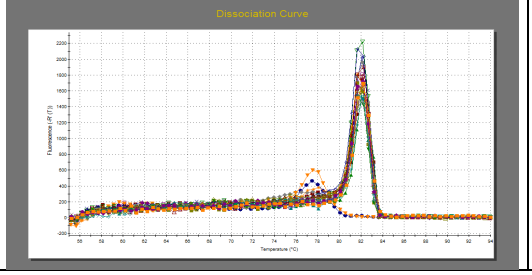	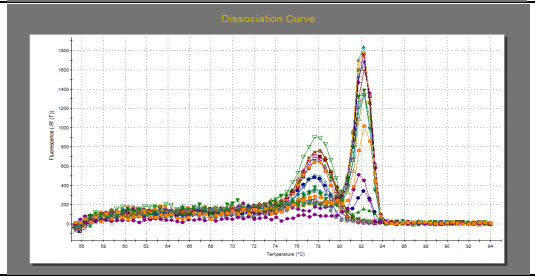

grik-1	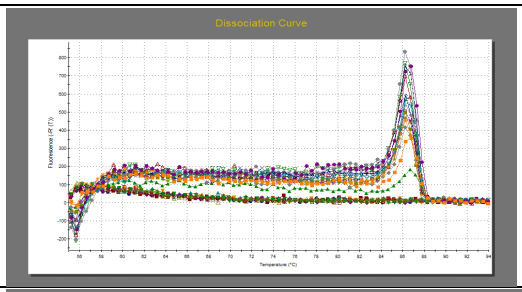	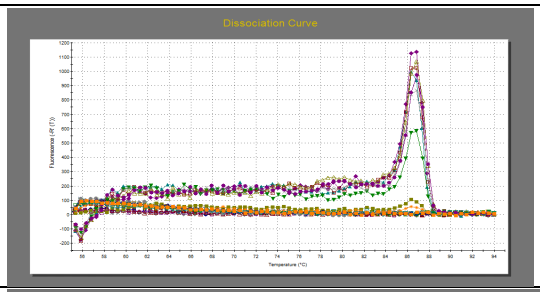
gria-1	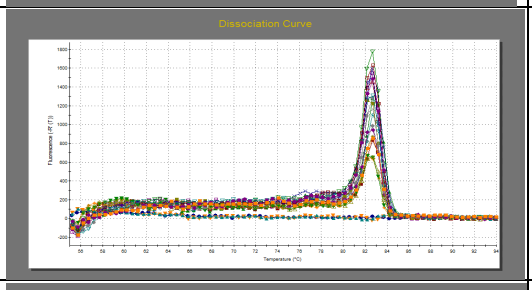	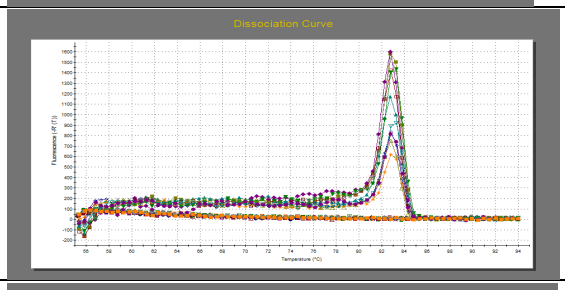
eaat-1	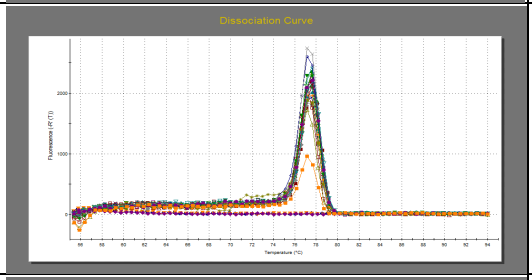	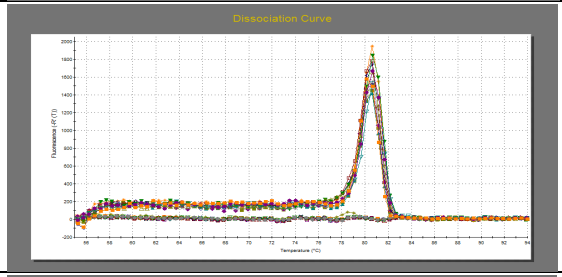
eaat-3	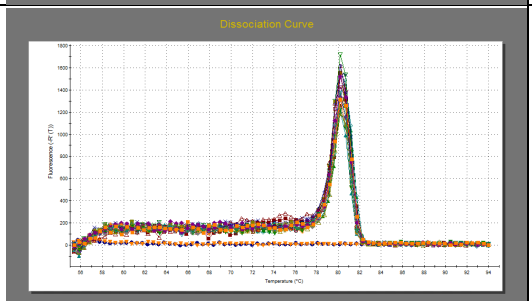	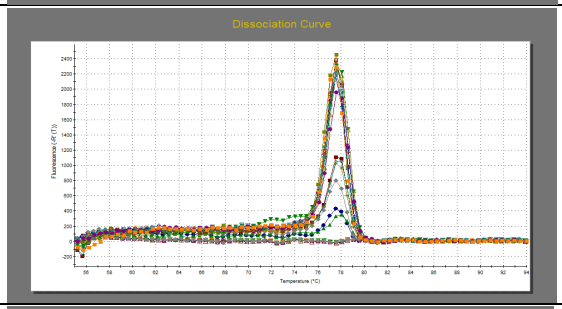
18s	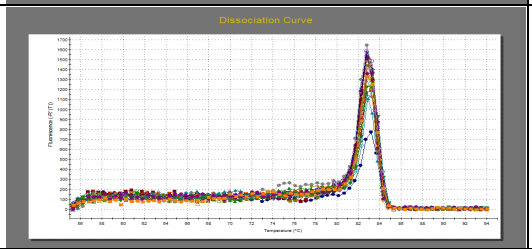	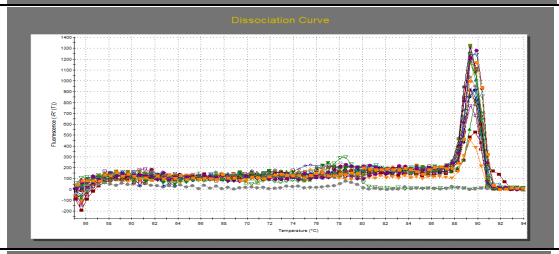
ywhaz	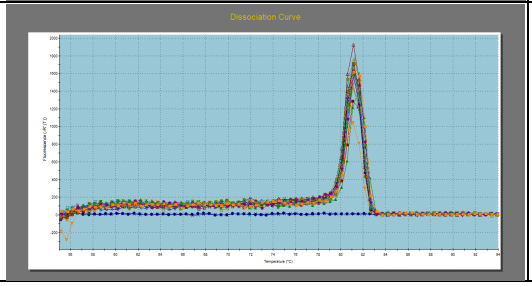	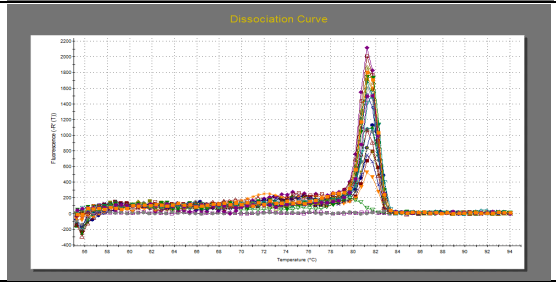

eef2	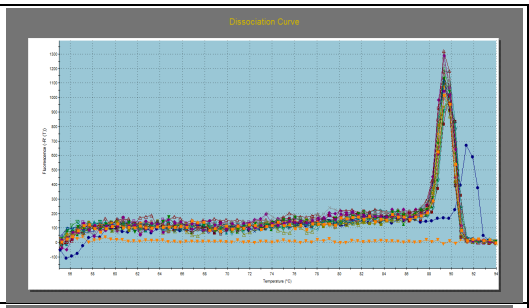	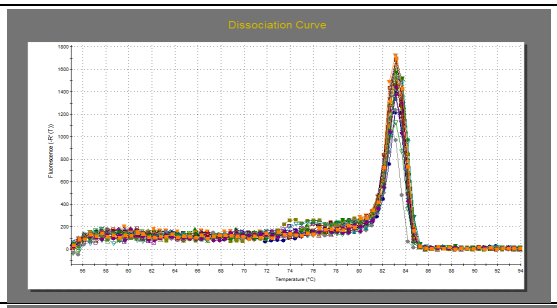
rpl13a	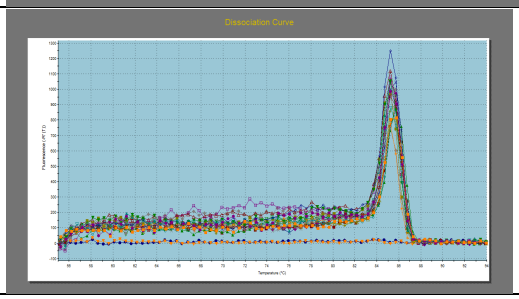	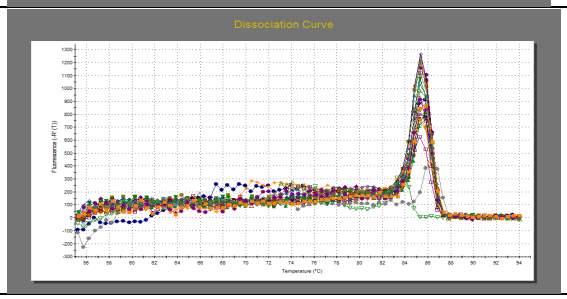

9.3.3 Example Standard Curves

Table 9.2: Example qRT-PCR standard curves for genes described in results chapters 5 and 6 (analysis described in methods section 2.9).

Analyte	Standard Curve	Source
ocn	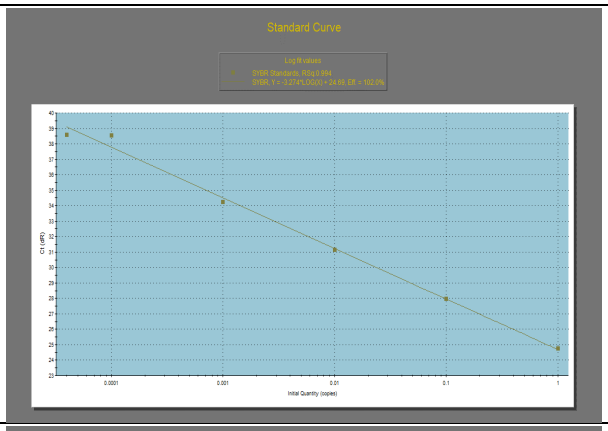	**Carole Elford**
col-1a1	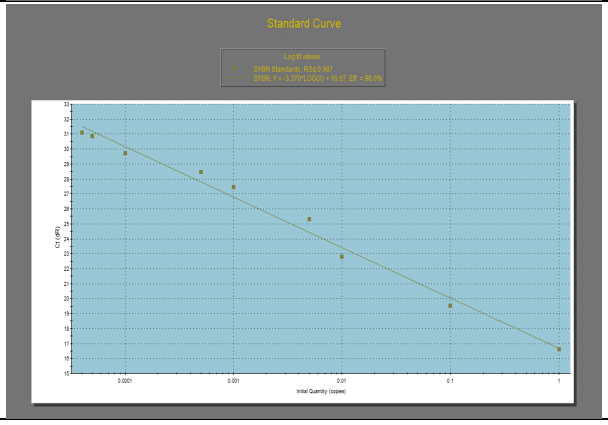	**Carole Elford**

Il-6	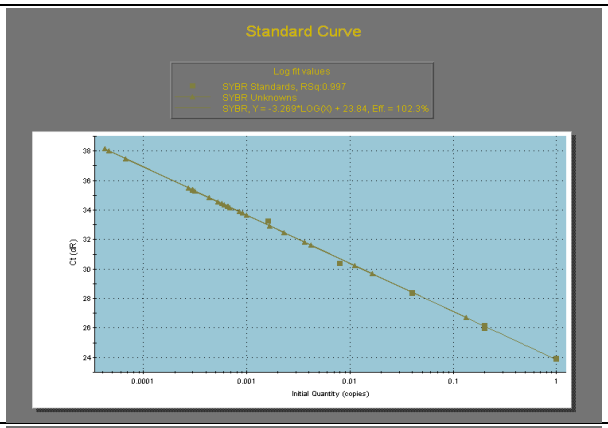	**Sophie Gilbert**
grik-1	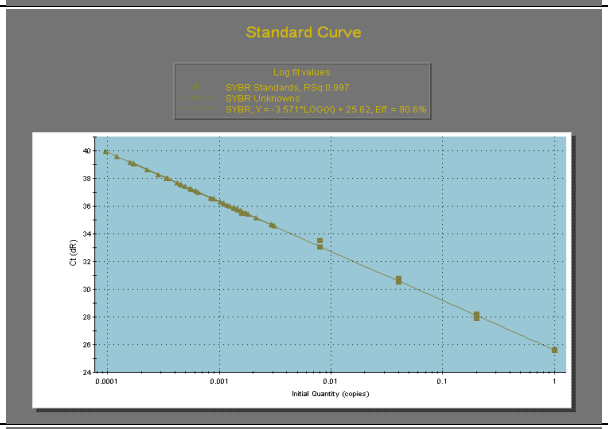	**Cleo Bonnet**
gria-1	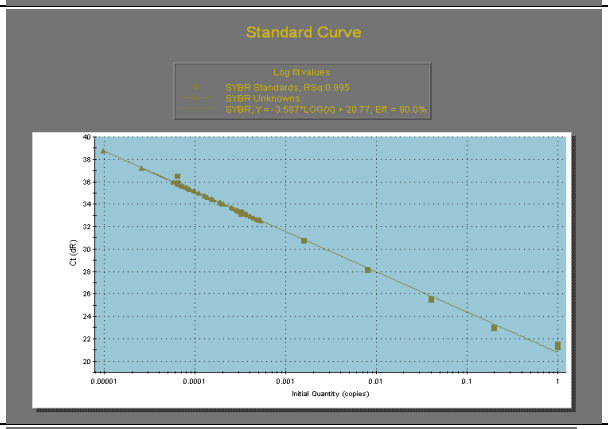	**Cleo Bonnet**
eaat-3	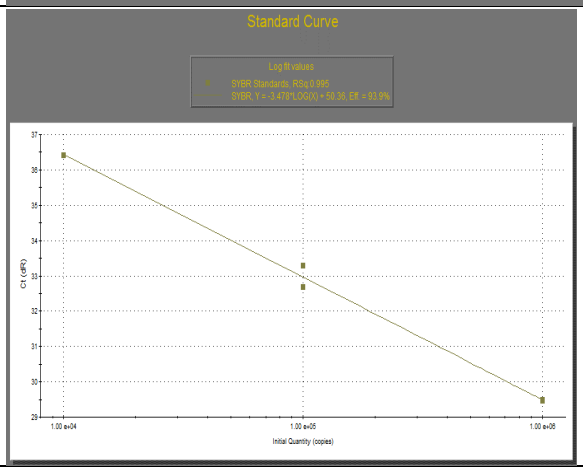	**This thesis and Karen Brakspear**

18s	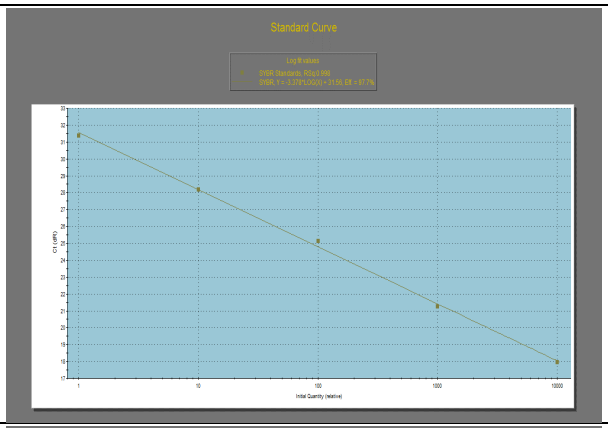	**Sophie Gilbert**
ywhaz	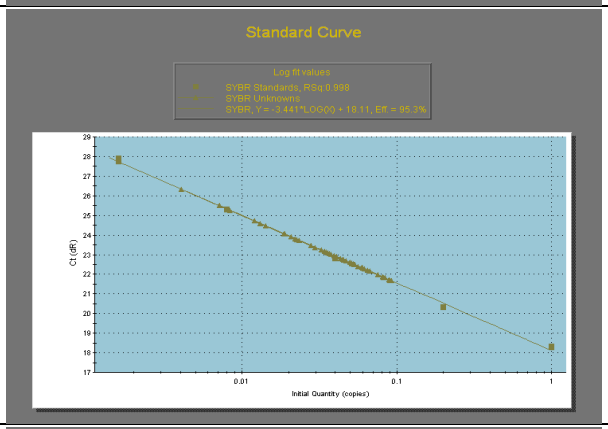	**Sophie Gilbert**
rpl13a	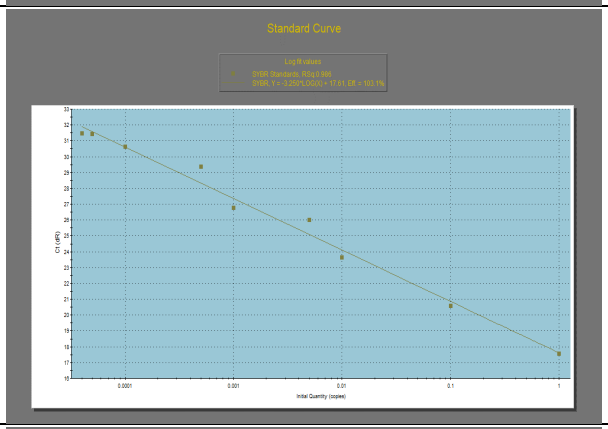	**Carole Elford**
eef2	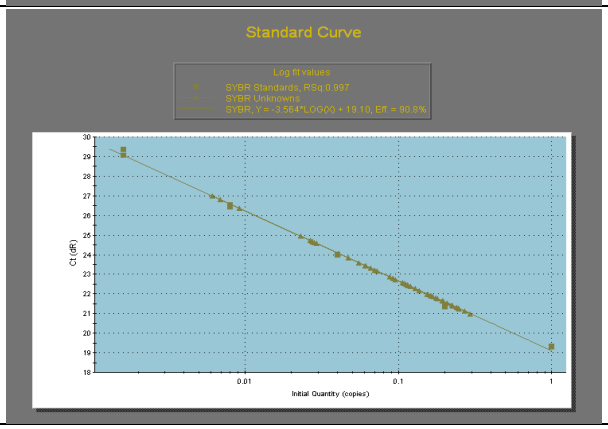	**Sophie Gilbert**

9.4 3D Cell Culture Layouts

9.4.1 3D Osteogenically Differentiated Y201 MSC Loading Study

Control 1 (1hr)	Control 2 (1hr)	Control 1 (24hrs)	Control 2 (24hrs)
Control 3 (1hr)	Control 4 (1hr)	Control 3 (24hrs)	Control 4 (24hrs)
+NBQX 1 (1hr)	+NBQX 2 (1hr)	+NBQX 1 (24hrs)	+NBQX 2 (24hrs)
+NBQX 3 (1hr)	+NBQX 4 (1hr)	+NBQX 3 (24hrs)	+NBQX 4 (24hrs)

Figure 9.6: Silicon plate layout for Y201 MSC loading study (methods section 2.6).

Cell culture plate layout for the cell loading study (methods section 2.6.). 3 plates were used to compare unloaded, physiological load (0.07mm displacement; 500μstrain) and pathophysiological loads (0.7mm displacement; 5000μstrain). Time point shown on table corresponds to the time samples were extracted after loading.

9.4.2 3D osteogenically differentiated Y201 IL-6/sIL-6r inflammatory study

Cntrl 1	IL-6/sIL-6r 1	IL-6/sIL-6r +NBQX 1	IL-6/sIL-6r +NBQX +NP 1
Cntrl 2	IL-6/sIL-6r 2	IL-6/sIL-6r +NBQX 2	IL-6/sIL-6r +NBQX +NP 2
Cntrl 3	IL-6/sIL-6r 3	IL-6/sIL-6r +NBQX 3	IL-6/sIL-6r +NBQX +NP 3
Cntrl 4	IL-6/sIL-6r 4	IL-6/sIL-6r +NBQX 4	IL-6/sIL-6r +NBQX +NP 4

Figure 9.7: Plastic plate layout for Y201 MSC IL-6/sIL-6r inflammatory study (methods section 2.7).

Cell culture plate layout for IL-6/sIL-6r experiment (Methods section 2.7). 2 plates were used corresponding to two timepoints (24 and 72hrs) after inflammatory stimulus. Cntrl wells: no inflammatory stimulus applied; IL-6/sIL-6r wells: application of IL-6 (5ng/ml) and sIL-6r (40ng/ml) inflammatory stimulus; IL-6/sIL-6r + NBQX wells: 1 hour application of NBQX (200μM), 1 hour after application of inflammatory stimulus (IL-6/sIL-6r); IL-6/sIL-6r + NBQX + NP wells: The same as NBQX wells but with the addition of 10mg/ml NBQX loaded freeze dried PLGA nanoparticles following removal of NBQX treated media after 1 hour

9.5 Assay Plate Layouts

Plate assays were carried out using Y201 MSC culture media from either the 3D Y201 loading study (section 2.6) or the 3D Y201 IL-6/sIL-6r inflammatory study (section 2.7).

9.5.1 Griess Assay (Nitrite Release)

Griess Assays (section 2.11) plate layouts for experimental samples are depicted in Figure 9.8 and Figure 9.9

9.5.1.1 Y201 loading study

Std 1 100 µM	Std 1 100 µM	Std 1 100 µM		Phys 1 1hr (-NBQX)	Phys 1 1hr (-NBQX)	Phys 1 24hrs (-NBQX)	Phys 1 24hrs (-NBQX)	Path 1 1hr (-NBQX)	Path 1 1hr (-NBQX)	Path 1 24hr (-NBQX)	Path 1 24hr (-NBQX)
Std 2 50 µM	Std 2 50 µM	Std 2 50 µM		Phys 2 1hr (-NBQX)	Phys 2 1hr (-NBQX)	Phys 2 24hrs (-NBQX)	Phys 2 24hrs (-NBQX)	Path 2 1hr (-NBQX)	Path 2 1hr (-NBQX)	Path 2 24hr (-NBQX)	Path 2 24hr (-NBQX)
Std 3 25 µM	Std 3 25 µM	Std 3 25 µM		Phys 3 1hr (-NBQX)	Phys 3 1hr (-NBQX)	Phys 3 24hrs (-NBQX)	Phys 3 24hrs (-NBQX)	Path 3 1hr (-NBQX)	Path 3 1hr (-NBQX)	Path 3 24hr (-NBQX)	Path 3 24hr (-NBQX)
Std 4 12.5 µM	Std 4 12.5 µM	Std 4 12.5 µM		Phys 4 1hr (-NBQX)	Phys 4 1hr (-NBQX)	Phys 4 24hrs (-NBQX)	Phys 4 24hrs (-NBQX)	Path 4 1hr (-NBQX)	Path 4 1hr (-NBQX)	Path 4 24hr (-NBQX)	Path 4 24hr (-NBQX)
Std 5 6.25 µM	Std 5 6.25 µM	Std 5 6.25 µM		Phys 1 1hr (+NBQX)	Phys 1 1hr (+NBQX)	Phys 1 24hrs (+NBQX)	Phys 1 24hrs (+NBQX)	Path 1 1hr (+NBQX)	Path 1 1hr (+NBQX)	Path 1 24hr (+NBQX)	Path 1 24hr (+NBQX)
Std 6 3.13 µM	Std 6 3.13 µM	Std 6 3.13 µM		Phys 2 1hr (+NBQX)	Phys 2 1hr (+NBQX)	Phys 2 24hrs (+NBQX)	Phys 2 24hrs (+NBQX)	Path 2 1hr (+NBQX)	Path 2 1hr (+NBQX)	Path 2 24hr (+NBQX)	Path 2 24hr (+NBQX)
Std 7 1.56 µM	Std 7 1.56 µM	Std 7 1.56 µM		Phys 3 1hr (+NBQX)	Phys 3 1hr (+NBQX)	Phys 3 24hrs (+NBQX)	Phys 3 24hrs (+NBQX)	Path 3 1hr (+NBQX)	Path 3 1hr (+NBQX)	Path 3 24hr (+NBQX)	Path 3 24hr (+NBQX)
Blnk 0 µM	Blnk 0 µM	Blnk 0 µM		Phys 4 1hr (+NBQX)	Phys 4 1hr (+NBQX)	Phys 4 24hrs (+NBQX)	Phys 4 24hrs (+NBQX)	Path 4 1hr (+NBQX)	Path 4 1hr (+NBQX)	Path 4 24hr (+NBQX)	Path 4 24hr (+NBQX)

Figure 9.8: Plate layout for Griess assay of media from 3D Y201 loading study (section 2.6).

9.5.1.2 Y201 IL-6/sIL-6 study

Std 1 100µM	Std 1 100µM	Std 1 100µM		Cntrl 1 24hr	Cntrl 1 24hr	IL-6 1 24hr	IL-6 1 24hr	NBQX 1 24hr	NBQX 1 24hr	NP 1 24hr	NP 1 24hr
Std 2 50µM	Std 2 50µM	Std 2 50µM		Cntrl 2 24hr	Cntrl 2 24hr	IL-6 2 24hr	IL-6 2 24hr	NBQX 2 24hr	NBQX 2 24hr	NP 2 24hr	NP 2 24hr
Std 3 25µM	Std 3 25µM	Std 3 25µM		Cntrl 3 24hr	Cntrl 3 24hr	IL-6 3 24hr	IL-6 3 24hr	NBQX 3 24hr	NBQX 3 24hr	NP 3 24hr	NP 3 24hr
Std 4 12.5µM	Std 4 12.5µM	Std 4 12.5µM		Cntrl 4 24hr	Cntrl 4 24hr	IL-6 4 24hr	IL-6 4 24hr	NBQX 4 24hr	NBQX 4 24hr	NP 4 24hr	NP 4 24hr
Std 5 6.25µM	Std 5 6.25µM	Std 5 6.25µM		Cntrl 1 72hr	Cntrl 1 72hr	IL-6 1 72hr	IL-6 1 72hr	NBQX 1 72hr	NBQX 1 72hr	NP 1 72hr	NP 1 72hr
Std 6 3.13µM	Std 6 3.13µM	Std 6 3.13µM		Cntrl 2 72hr	Cntrl 2 72hr	IL-6 2 72hr	IL-6 2 72hr	NBQX 2 72hr	NBQX 2 72hr	NP 2 72hr	NP 2 72hr
Std 7 1.56µM	Std 7 1.56µM	Std 7 1.56µM		Cntrl 3 72hr	Cntrl 3 72hr	IL-6 3 72hr	IL-6 3 72hr	NBQX 3 72hr	NBQX 3 72hr	NP 3 72hr	NP 3 72hr
Blank 0µM	Blank 0µM	Blank 0µM		Cntrl 4 72hr	Cntrl 4 72hr	IL-6 4 72hr	IL-6 4 72hr	NBQX 4 72hr	NBQX 4 72hr	NP 4 72hr	NP 4 72hr

Figure 9.9: Plate layout for Griess assay for media from 3D Y201 IL-6/sIL-6r inflammatory study (section 2.7).

9.5.2 Multiplex Electrochemiluminescence

Std 1	Std 1	Cntrl 1 24hr	Cntrl 1 24hr	IL-6 1 24hr	IL-6 1 24hr	NBQX 1 24hr	NBQX 1 24hr	NP 1 24hr	NP 1 24hr	Path 1 1hr (-NBQX)	Path 1 24hr (-NBQX)
Std 2	Std 2	Cntrl 2 24hr	Cntrl 2 24hr	IL-6 2 24hr	IL-6 2 24hr	NBQX 2 24hr	NBQX 2 24hr	NP 2 24hr	NP 2 24hr	Path 2 1hr (-NBQX)	Path 2 24hr (-NBQX)
Std 3	Std 3	Cntrl 3 24hr	Cntrl 3 24hr	IL-6 3 24hr	IL-6 3 24hr	NBQX 3 24hr	NBQX 3 24hr	NP 3 24hr	NP 3 24hr	Path 3 1hr (-NBQX)	Path 3 24hr (-NBQX)
Std 4	Std 4	Cntrl 4 24hr	Cntrl 4 24hr	IL-6 4 24hr	IL-6 4 24hr	NBQX 4 24hr	NBQX 4 24hr	NP 4 24hr	NP 4 24hr	Path 4 1hr (-NBQX)	Path 4 24hr (-NBQX)
Std 5	Std 5	Cntrl 1 72hr	Cntrl 1 72hr	IL-6 1 72hr	IL-6 1 72hr	NBQX 1 72hr	NBQX 1 72hr	NP 1 72hr	NP 1 72hr	Path 1 1hr (+NBQX)	Path 1 24hr (+NBQX)
Std 6	Std 6	Cntrl 2 72hr	Cntrl 2 72hr	IL-6 2 72hr	IL-6 2 72hr	NBQX 2 72hr	NBQX 2 72hr	NP 2 72hr	NP 2 72hr	Path 2 1hr (+NBQX)	Path 2 24hr (+NBQX)
Std 7	Std 7	Cntrl 3 72hr	Cntrl 3 72hr	IL-6 3 72hr	IL-6 3 72hr	NBQX 3 72hr	NBQX 3 72hr	NP 3 72hr	NP 3 72hr	Path 3 1hr (+NBQX)	Path 3 24hr (+NBQX)
BLANK 1	BLANK 1	Cntrl 4 72hr	Cntrl 4 72hr	IL-6 4 72hr	IL-6 4 72hr	NBQX 4 72hr	NBQX 4 72hr	NP 4 72hr	NP 4 72hr	Path 4 1hr (+NBQX)	Path 4 24hr (+NBQX)

Figure 9.10: Plate layout for ECL assay (section 2.10) using media from the 3D y201 loading and IL-6/sIL-6r inflammatory studies (sections 2.6 and 2.7).

9.5.3 Enzyme linked immunosorbent assays

Std 1	Std 1	Std 1	Cntrl 1 24hrs	IL-6 1 24hrs	IL-6 1 24hrs	NBQX 1 24hrs	NBQX 1 24hrs	NP 1 24hrs	NP 1 24hrs	Path 1 1hr (-NBQX)	Path 1 24hr (-NBQX)
Std 4	Std 2	Std 2	Cntrl 2 24hrs	IL-6 2 24hrs	IL-6 2 24hrs	NBQX 2 24hrs	NBQX 2 24hrs	NP 2 24hrs	NP 2 24hrs	Path 2 1hr (-NBQX)	Path 2 24hr (-NBQX)
Std 7	Std 3	Std 3	Cntrl 3 24hrs	IL-6 3 24hrs	IL-6 3 24hrs	NBQX 3 24hrs	NBQX 3 24hrs	NP 3 24hrs	NP 3 24hrs	Path 3 1hr (-NBQX)	Path 3 24hr (-NBQX)
BLANK	Std 4	Std 4	Cntrl 4 24hrs	IL-6 4 24hrs	IL-6 4 24hrs	NBQX 4 24hrs	NBQX 4 24hrs	NP 4 24hrs	NP 4 24hrs	Path 4 1hr (-NBQX)	Path 4 24hr (-NBQX)
Dilution 0	Std 5	Std 5	Cntrl 1 72hrs	IL-6 1 72hrs	IL-6 1 72hrs	NBQX 1 72hrs	NBQX 1 72hrs	NP 1 72hrs	NP 1 72hrs	Path 1 1hr (+NBQX)	Path 1 24hr (+NBQX)
Dilution 1:2	Std 6	Std 6	Cntrl 2 72hrs	IL-6 2 72hrs	IL-6 2 72hrs	NBQX 2 72hrs	NBQX 2 72hrs	NP 2 72hrs	NP 2 72hrs	Path 2 1hr (+NBQX)	Path 2 24hr (+NBQX)
Dilution 1:4	Std 7	Std 7	Cntrl 3 72hrs	IL-6 3 72hrs	IL-6 3 72hrs	NBQX 3 72hrs	NBQX 3 72hrs	NP 3 72hrs	NP 3 72hrs	Path 3 1hr (+NBQX)	Path 3 24hr (+NBQX)
Dilution 1:8	BLANK	BLANK	Cntrl 4 72hrs	IL-6 4 72hrs	IL-6 4 72hrs	NBQX 4 72hrs	NBQX 4 72hrs	NP 4 72hrs	NP 4 72hrs	Path 4 1hr (+NBQX)	Path 4 24hr (+NBQX)

Figure 9.11: ELISA plate layout for media samples aliquoted from the 3D Y201 loading and IL-6/sIL-6r inflammatory studies (section 2.6 and 2.7) for experimental methods described in methods section 2.10.

9.6 Microfluidic Synthesized PLGA Nanoparticle Agglomeration Findings

A microfluidic synthesis methodology, as described in methods section 2.2.1.1, was used to develop GluR antagonist loaded PLGA nanoparticles. These nanoparticles presented with consistent agglomeration, rendering them as visible 'clumps' as opposed to a dispersion of nanoscale particles (Figure 9.12). The results of these findings are presented in this section. The microfluidic nanoparticle synthesis method was replaced with a double emulsion method for the encapsulation of water-soluble drugs (methods section 2.2.1.2) the findings from which are described in results chapter 3.

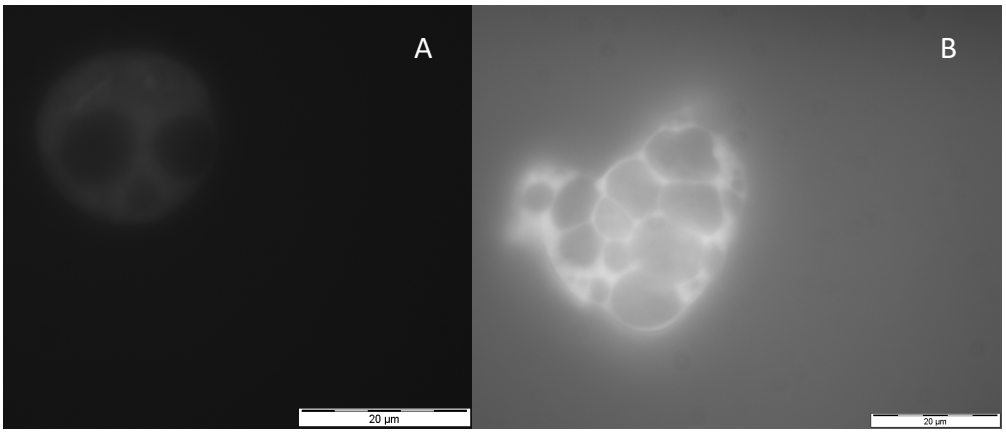

Figure 9.12: Microscopy images of PLGA particle agglomerates identified in the micrometre range. Scale bar=20μm. A) 10mM DNQX load. B) 50mM DNQX load.

9.7 Further details relating to introduction

The tables in Section 9.7 provide additional detail to support the literature reviewed in the introduction of this thesis.

9.7.1 Bone Mechanical and Inflammatory Biomarker Table

Table 9.3: A summary of some of the inflammatory molecules and signalling proteins involved in the maintenance of healthy bone and their involvement in the mechanical and inflammatory response of bone (supporting introduction section 1.4.2).

Biomarker	Abbrev.	Activity	Bone cell release	Mechanical regulated	Bone remodelling / inflammatory activity	Reference
Glutamate	Glu	Excitatory Amino Acid (EAA), glutamatergic signalling agonist, inflammatory mediator and associated with the mechanical regulation of bone physiology and arthritic joint degeneration.	Osteocytes, osteoblasts and osteoclasts all express glutamate signalling machinery.	Osteocyte expressed glutamate transporters have been identified as significantly down regulated following osteogenic loading. Inhibition of glutamate receptors (GluRs) shown to significantly reduce lameness, inflammation and joint degeneration in an anterior cruciate ligament (ACL) rupture post traumatic OA (PTOA) mouse *in vivo* model.	Plasma glutamate levels significantly correlate with extent of temporomandibular joint (TMJ) bone resorption in rheumatoid arthritis (RA) patients. Addition of pro-inflammatory cytokines (TNFα and IFNγ) inhibits glutamate release from human osteoblasts. Inhibition of GluR with NBQX shown to significantly reduce lameness, inflammation, *il-6* expression and joint degeneration in inflammatory, antigen induced arthritis (AIA) *in vivo* mouse models.	(Genever and Skerry, 2001, Chenu, 2002, Mason, 2004, McNearney et al., 2004, Hajati et al., 2009, McNearney et al., 2010, Seidlitz et al., 2010, Brakspear and Mason, 2012, Bonnet et al., 2015, Xie et al., 2016, Bonnet et al., 2019, Bonnet et al., 2020)

Sclerostin	SOST	Osteocyte derived mechanical regulator of bone physiology, Wnt signalling inhibitor.	Primarily Osteocyte expressed.	Expression repressed by mechanical loading and increased during immobilization.	Pro-inflammatory cytokines (TNFα and IL-6) upregulate osteoblast SOST expression	(Turner et al., 2009, Gaudio et al., 2010, Redlich and Smolen, 2012, Baron and Kneissel, 2013)
Osteoprotegerin	OPG	RANKL decoy receptor. Osteoblast and osteocyte derived inhibitor of osteoclast differentiation and activity.	Osteoblast and osteocyte expressed.	Mechanical loading activates osteocyte OPG release resulting in decreased osteoclast activity.	Down regulated by proinflammatory cytokines (IL-6 and TNFα) in osteoblasts. In combination with anti-TNF antibodies OPG treatment prevented bone loss in an inflammatory arthritis mouse model.	(Suda et al., 1999, Hofbauer and Heufelder, 2001, Redlich et al., 2004, Kramer et al., 2010, Redlich and Smolen, 2012)
Interferon-γ	IFN-γ	Neuropathic pain stimulant, pro- and anti-inflammatory cytokine	Primarily an immune cell derived cytokine but shown to be expressed in OA and osteoporotic human subchondral bone samples.	In an *ex vivo* human trabecular bone core loading model IFN-γ expression was down regulated along with OPG in loaded cores vs unloaded suggesting a bone resorptive response to load.	IFN-γ and TNFα treatment shown to have proapoptotic affects and inhibit glutamate release from human osteoblasts *in vitro.* IFN-γ knockout induces bone loss. However, IFN-γ treatment has shown contradictory effects both promoting bone formation through low dose sustained treatment while promoting bone loss in short term acute treatment. IFN-γ down regulated IL-8 production in osteoblasts isolated from PTOA and RA patients *in vitro*.	(Mann et al., 1994, Genever and Skerry, 2001, Lisignoli et al., 2002, Mühl and Pfeilschifter, 2003, Sato et al., 2006, Stadelmann et al., 2008, Duque et al., 2011, Buchwald et al., 2012, Zupan et al., 2012, Malemud, 2017, Moen et al., 2017)

Interleukin-10	IL-10	Anti-inflammatory cytokine, plays a role in bone formation.	Immune and inflammatory cell derived cytokine. Released by mouse calvarial osteoblasts.	Mechanically induced strain on mouse calvarial osteoblasts in monolayer *in vitro* down regulated IL-10 release vs unloaded cells.	IL-10 exposure Inhibits osteoclast formation. Antibody blockade of IL-10 from Tc_{REG} immune cells reduced osteoclast suppression *in vitro.* IL-10 inhibits osteoclastogenesis via reduction of NFATc1 expression *in vitro.* IL-10 knockout mice have reduced expression of osteoblast and osteocyte markers in association with spontaneous alveolar bone loss.	(García-López et al., 2005, Liu et al., 2006, Evans and Fox, 2007, Mohamed et al., 2007, Jansen et al., 2008, Claudino et al., 2010, Luo et al., 2011, Buchwald et al., 2012, Yi et al., 2018)
Interleukin-12p70	IL-12p70	Stimulatory factor for T cells. Potential to inhibit osteoclastogenesis.	Immune and inflammatory cell derived cytokine. Released by mouse calvarial osteoblasts.	Mechanically induced strain on mouse calvarial osteoblasts in monolayer *in vitro* temporarily up regulated IL-12 release vs unloaded cells.	IL-12 shown to inhibit osteoclast formation *in vitro* on Maurine osteoblasts co-cultured with spleen cells. IL-12 shown to inhibit osteoclast production via stimulation of osteoclast inhibitory peptide-1 expression in CD4+ T cells.	(Horwood et al., 2001, Nagata et al., 2003, García-López et al., 2005, Kitaura et al., 2006, Gee et al., 2009, Shanmugarajan et al., 2009, Morita et al., 2010)
Interleukin-13	IL-13	Anti-inflammatory cytokine.	Primarily produced by T-lymphocytes along with IL-4. Also produced by stromal cells.	In a mechanical fracture mouse model, IL-4/IL-13 knockout mice were not found to have any difference on fracture healing and bone formation compared to wild type mice.	Represses osteoclastogenesis and osteoclast function with IL-4 via inhibition of RANKL and induces OPG production in osteoblasts.	(Hart et al., 1995, Yamada et al., 2007, Silfverswärd et al., 2008, Bhattacharjee et al., 2013, Wojdasiewicz et al., 2014)

Interleukin-1β	IL-1β	Pro-inflammatory cytokine.	Primarily produced by immune cells (monocytes and macrophages). Although has been shown to be expressed in human osteoblasts taken from human osteoporotic fractures.	IL-1β released in response to mechanical stimulation of human primary osteoblasts *in vitro.*	Overproduction associated with bone loss primarily due to increased activation of osteoclasts and inhibition of osteoblast activity.	(Salter et al., 2000, Walsh et al., 2000, Massicotte et al., 2002, Redlich and Smolen, 2012, Dinarello, 2013)
Interleukin-2	IL-2	Pro-inflammatory cytokine.	Primarily derived from T-helper 1 cells.	IL-2 levels significantly increased in human tooth loading model *in vivo.*	In a rat periapical bone lesion model, a delayed increased in IL-2 expression was identified in periapical lesions following pulp exposure.	(Kutukculer et al., 1998, Kawashima and Stashenko, 1999, Başaran et al., 2006, Boshtam et al., 2017)
Interleukin-4	IL-4	Anti-inflammatory cytokine linked to the function of IL-13.	Primarily produced by T-lymphocytes along with IL-13.	In a mechanical fracture mouse model, IL-4/IL-13 knockout mice were not found to have any difference on fracture healing and bone formation compared to wild type mice.	Represses osteoclastogenesis and osteoclast function with IL-13 via inhibition of RANKL and induces OPG production in osteoblasts. IL-4 also supresses nuclear factor kappa beta (NF-κB), MAPK and calcium signalling during osteoclastogenesis.	(Mueller et al., 2002, Schuerwegh et al., 2003, Yamada et al., 2007, Silfverswärd et al., 2008, Zhao and Ivashkiv, 2011, Bhattacharjee et al., 2013)

Interleukin-6	IL-6	Pro-inflammatory cytokine involved in osteoclast signalling and playing a role in bone resorption.	produced by monocytes and macrophages. Reported expressed in osteoblasts primarily but also reported in osteoclasts and osteocytes.	Mechanical loading increased IL-6 production and reduced OPG production in primary mice osteoblasts *in vitro.* osteocyte expressed IL-6 upregulated in loaded limbs vs unloaded in rat model. An *in vitro*, MLO-Y4 study indicated IL-6 is produced by shear stress and may modulate bone mass via reduction of osteoblast activity.	IL-6 stimulation has been well established to inhibit osteoblast activity and upregulate osteoclast activity. IL-6 has been shown to increase osteocyte controlled osteoclastogenesis via increasing RANKL and Janus Kinase-2 (JAK2) activity in mouse osteocyte cell line MLO-Y4 cells *in vitro*. *In vivo* inhibition of IL-6 trans-signalling (via soluble receptor) in a mouse osteotomy model significantly improved fracture healing.	(Ishimi et al., 1990, Hammacher et al., 1994, Gao et al., 1998, Chenoufi et al., 2001, Kwan Tat et al., 2004, Sanchez et al., 2009, Sims and Walsh, 2010, Redlich and Smolen, 2012, Bakker et al., 2014, Metzger et al., 2017, Kaiser et al., 2018)
Interleukin-8	IL-8	Pro-inflammatory chemokine, plays a role in neutrophil chemotaxis.	Expressed by macrophages and monocytes. Also expressed by both osteoblasts and osteocytes.	IL-8 levels significantly increased in human tooth loading model *in vivo*. Increased IL-8 levels were shown to be concomitant with knee loading in a catabolic joint environment in human OA patients.	Increased IL-8 levels in RA patient synovial fluid have been linked to RANKL mediated osteoclast induced bone loss. IL-8 treatment of human osteoblasts cells in vitro increased RANKL expression and protein production.	(Graves et al., 1999, Bendre et al., 2003, Başaran et al., 2006, Davidson and Patel, 2014, Liu et al., 2016, Namba et al., 2017, Yang et al., 2018, Khatib et al., 2019)

Tumour necrosis factor-α	TNFα	Pro-inflammatory cytokine, involved in both osteoblast signalling and osteoclastogenic signalling. Often synergistic with activity of IL-1β.	Reported to have been expressed by osteoblasts isolated from human osteoporotic fractures.	Increased TNF-α along with IL-8 and IL-6 levels were shown to be concomitant with knee loading in a catabolic joint environment in human OA patients. TNF-α and IL-1β treatment of MLO-Y4 mouse osteocytes inhibited mechanically induced NO production *in vitro.* increased TNF-α levels have been identified in human gingival sulcus following orthodontic tooth movement.	Release of TNFα inhibits osteoblast activity and upregulates osteoclast activity. TNFα induced osteoclast recruitment thought to be central to pathogenesis in inflammatory disorders including RA. Induces RANKL and RANK expression and stimulates osteoclastogenesis.	(Henderson and Pettipher, 1989, Lowney et al., 1995, Azuma et al., 2000, Walsh et al., 2000, Zhang et al., 2001, Bodmer et al., 2002, Massicotte et al., 2002, Wong et al., 2008, Redlich and Smolen, 2012, Luo et al., 2018, Khatib et al., 2019)

9.7.2 Commonly Used Pharmaceutical Therapies for OA Table

Table 9.4: A summary of commonly used pharmaceutical therapies for OA management. List of pharmaceuticals taken from Arthritis UK website accessed 10/06/19.

Pharmaceutical Type	**Evidence**	**Side Effects**	**Approved Drugs**
Non-Steroidal Anti-inflammatory Drugs (NSAID)	Oral non-selective NSAIDs estimated effect size for pain vs placebo: 0.37; 95% Confidence interval (CI) 0.26, 0.49 (Lee et al., 2005).	Renal and gastrointestinal safety concerns. Increased risk of cardiovascular event with COX-2 inhibitors and traditional NSAIDs ibuprofen and diclofenac. Associated with oral usage (McAlindon et al., 2014, NICE, 2015).	Asparin, Ibuprofen, Naproxen, Diclofenac, Celecoxib, Mefenamic acid, Etoricoxib, Indomethacin, Piroxicam, Meloxicam, Ketoprofen, Culindac, Diflunisal, Nabumetone, Oxaprozin, Tolmetin, Salsalate, Fenoprofen, Etodolac, Flurbiprofen, Ketorolac, Meclofenamate,
	Oral COX-2 inhibitors estimated effect size for pain vs placebo: 0.44; 95% CI 0.33, 0.55 (Lee et al., 2005).		
	Topical NSAIDs no estimated effect size for pain available but a Cochrane comparative effectiveness review found topical NSAIDs to be of comparable efficacy to oral NSAIDs for knee OA (Chou et al., 2011).	Topical NSAIDs associated with decreased risk of GI tract complications but increased risk of dermatological adverse effects (Chou et al., 2011).	

Analgesics	In a 2010 systematic review (SR) and meta-analysis found low level effect for paracetamol (oral) on OA pain. 10 eligible trials, estimated effect size for pain vs placebo: 0.18; 95% CI 0.11, 0.25 (Bannuru et al., 2010). Using data from a SR and Randomised control trial (RCT) In a 2011 comparative efficacy review capsaicin (0.075%, topical) was superior to placebo for 50% pain reduction in neuropathic and musculo-skeletal pain (Mason et al., 2004).	Increased risk of adverse events associated with paracetamol usage including gastro-intestinal (GI) and organ failure (McAlindon et al., 2014). Increased risk of local adverse events (burning sensation and withdrawal associated with adverse events (McAlindon et al., 2014)).	Capsaicin, Lidocaine, Methyl Salicylate, Trolamine, Paracetamol (Acetaminophen).
Opioid Analgesics	Opioid therapy estimated effect size for Western Ontario and McMaster Universities Osteoarthritis index (WOMAC) scored joint function vs placebo: -0.26; 95% CI -0.35, -0.17.(da Costa et al., 2014).	Significant withdrawal from treatment due to adverse events. Four times as likely to withdraw compared to placebo for adverse events and three times as likely due to severe adverse events.	Codeine, Morphine, Tramadol, Acetaminophen with Codeine, Fentanyl, Hydrocodone,

	Overall Opioids estimated size effect for knee and hip pain vs placebo: -0.28; 95% CI -0.35, -0.20 (da Costa et al., 2014).	Adverse events include nausea, vomiting, dizziness and constipation. There is also a risk of dependence (da Costa et al., 2014).	Acetaminophen with Hydrocodone (Vicodin), Hydromorphone, Meperidine, Oxycodone.
Steroids	Intra-articular (IA) corticosteroid injections have been clinically demonstrated to deliver a significant short-term decrease in pain vs hyaluronic acid injections by two SRs. 7 eligible trials with an effect size of -0.39 (95% CI; -0.65, -0.12) favouring corticosteroids vs hyaluronic acid after 2 weeks. However, by 8 weeks hyaluronic acid injections proved to be more effective vs steroid injection (effect size 0.22; 95% CI -0.05, 0.49) (Bannuru et al., 2009).	Post-injection pain flaire, skin atrophy and facial flushing are potential side effects of localised steroid injections (Cole and Schumacher, 2005). There is evidence in animal models to suggest IA steroid injections may cause joint destruction with Depo-Medrone (10mg/kg) injection having been shown to increase joint degradation by 50% saline controls in a PTOA mouse model (Bonnet et al., 2020). In a review of patient notes and radiographic data from knee (152 patients) and hip (307 patients) who had received steroid injections, 8% of patients reported adverse events. These events, included osteonecrosis (0.7%), rapid progressive OA (6.7%) and subchondral insufficiency fracture (0.9%) (Kompel et al., 2019). This review indicates steroid injection may result in adverse events in some OA	Prednisolone, Betamethasone, Cortisone, Dexamethasone, Hydrocortisone, Methylprednisolone.

		sufferers and highlights a need for improved understanding of the risk factors linked to these events.	
Other	One review found that compared to IA corticosteroid injection, IA hyaluronic acid (HA) injection had a significantly improved effect on knee joint pain by 8 weeks (effect size 0.22; 95% CI -0.05, 0.49), 12 weeks (effect size 0.35; 95% CI -0.05, 0.49) and at 26 weeks (effect size 0.39; 95% CI -0.05, 0.49). This is from an SR containing 7 eligible trials (Bannuru et al., 2009). IA HA Estimated effect size for: Pain vs placebo: -0.37 (95% CI; -0.46, -0.28) Physical function vs placebo: -0.33 (95% CI; -0.43, -0.22) (Bannuru et al., 2011, Rutjes et al., 2012).	Increased risk of adverse events, reported transient pain at injection site compared to placebo (relative risk 1.08) (Arrich et al., 2005).	Hyaluronic acid.

9.7.3 Pre-clinical Glutamate Receptor Signaling Studies to Treat Arthritis Table

Table 9.5: A summary of studies carried out to assess the impact of glutamate receptor activation and cytokine modulation on various models of arthritis.

Model	**Treatment Regime**	**Control**	**Outcome**				**Reference**
			Pain	**Swelling**	**Tissue specific effects**	**Other**	
Collagen Induced Arthritis (CIA, Mouse)	Administered intraperitoneally every 12 hours in a volume of 100μl starting from time 0 of CIA induction. Initial loading dose of 20mg/kg and 24 hours following, a maintenance dose of 1mg/kg every 12 hours. Experiment was discontinued at day 43.	Phosphate buffered saline (PBS) treated vehicle control.			Significant reduction in **synovitis** (p=0.007) and reduction in **cartilage erosion** frequency (p=0.007).	Up-regulation of Foxp3 in spleen CD4+T cells followed by increase in CD4+CD25+ regulatory T cells.	(Lindblad et al., 2012)

AIA (rat)	Treatment administered 15 minutes before arthritis induction. A single IA injection of NMDA receptor antagonist AP7 (10nmol) plus KA/AMPA receptor antagonist CNQX (10nmol) at a volume of 100μl. joint allodenia and swelling were measured on days 1, 2, 3, 4 and 7 and histological sections taken on day 7.	Control with no drug treatment	A combination of AP7 and CNQX (10nmol) reduced allodenia as measured by knee extension angle by 28% after 2 days. A combination of high dose oral dexamethasone (0.5mg/kg/day) and glutamate receptor antagonists AP7, RP67580 and CNQX resulted in a significant reduction in allodynia vs controls over 7 days ($p<0.001$) and dexamethasone alone over 2 days ($p<0.001$).	Swelling was reduced by 40 percent on day 2 and reduced to 33% by day 7 following treatment with AP7 and CNQX ($p=0.01$ vs controls). When combined with high dose oral dexamethasone (0.5mg/kg/day) significant reductions in swelling were maintained over 7 days vs controls ($p<0.001$).		Both AP7 + CNQX treated and dexamethasone (0.5mg/kg/day) + AP7, RP67580 and CNQX) treated groups had significantly reduced knee blood flow compared to controls ($p<0.05$).	(Lam and Ng, 2010)

Mice with GluA1 and GluA2 AMPA receptor genetic deletions in peripheral neurones, in kaolin induced unilateral knee arthritis.	Nociception in control vs genetically modified mice assessed. Chronic pain sensitivity analysed up to 18 days. Systemic administration of GYKI 52466 AMPA receptor antagonist was delivered to wildtype mice once per day following arthritis induction.	Wild type mice.	Genetically modified mice (SNS-GluA1$^{-/-}$) had a significantly increased hyperalgesia threshold compared to GRIA1 positive mice over 18 days ($p<0.05$). Intra-peritoneal administration of glutamate receptor antagonist GYKI52466 negated the difference overserved between GluA1 negative and positive mice over 18 days. These results indicate a key role for AMPA receptors in peripheral				(Vijayan Gangadharan et al., 2011)

			and arthritic nociception.				
Human fibroblast like synoviocyte (FLS) *in vitro* testing.	Glutamate stimulated human FLSs were treated with MK801 (100μM) a non-competitive NMDA receptor antagonist; D-AP5 (10μM), a competitive NMDA receptor antagonist; CFM-2 (10μM) a non-competitive AMPA receptor antagonist and NBQX (150μM) a competitive AMPA/KA receptor antagonist. IL-6 release was quantified by enzyme	Antagonist free human FLSs.	Inhibition of NMDA receptors on human RA FLS with non-competitive antagonist MK801 increased proMMP-2 release ($p<0.05$). 6 ($p<0.001$).			Non-NMDA (AMPA/KA) GluR antagonist (NBQX) reduced cellular RA FLS production of IL-6 ($p<0.001$).	(Flood et al., 2007)

	linked immunosorbent assay (ELISA) and MMP expression and activity was measured by gelatin zymography.						
AIA rat	A single intra-articular injection of GluR antagonist NBQX (2.5mM) at the point of arthritic induction.	AIA and Naive controls.	NBQX administration reduced gait abnormalities (stance width and stride length) (days 1-2) to a non-significant difference ($p>0.05$).	NBQX administration reduced knee swelling ($p<0.0001$ days 1-21).	NBQX administration reduced joint severity scores ($p<0.001$) vs AIA groups. NBQX significantly reduced **bone cell (primary human osteoblast (hOB))** mineralisation (2 and 5 days; $p<0.001$). NBQX		(Bonnet et al., 2015)

					significantly reduced **meniscus** IL-6 mRNA levels ($p<0.05$).		
MNX rat	A single intra-articular injection of GluR antagonist NBQX (25mM) immediately following surgical arthritic induction.	Sham operated vehicle controls and naïve controls.	NBQX administration reduced weight bearing differences to naive levels that were significantly lower than vehicle controls ($p<0.05$).	NBQX significantly reduced swelling (days 7 and 8) compared to vehicle controls ($p<0.05$ and $p<0.01$) with NBQX reducing swelling similar to that of the naive treatment group.	NBQX administration (12.5 and 25mM) reduced joint severity scores to that of naive animals indicating reduced degradative effects compared with vehicle groups.	At day 21 histologically determined inflammation was significantly reduced compared to vehicle controls ($p<0.05$) with no significant difference compared to naive controls.	(Bonnet et al., 2017)
ACLr mice	A single intra-articular injection of GluR antagonist NBQX	placebo control injections.		NBQX significantly reduced swelling (days 1 and 2)	NBQX administration reduced ACLr	No histological increase in inflammation	(Bonnet et al., 2017,

	(20mM) immediately following ACL rupture.			compared to vehicle controls ($p<0.05$ and $p<0.01$) with NBQX showing no significant increase in swelling compared to day 0 over 21 days.	induced **cartilage** loss and **bone** remodelling changes($p<0.001$) and reduced ACLr joint severity score significantly (29%; $p<0.001$). two injections of NBQX (0 and 24hrs) resulted in a significantly reduced joint severity score compared to 1 injection ($p<0.05$) and reduced levels to that of naive groups.	was observed in NBQX treatment groups.	Bonnet et al., 2020)

9.7.4 Nanoparticle Studies in the Treatment of OA Table

Table 9.6: Summary of papers investigating the use of nanoparticles in the treatment of OA, highlighting particle characteristics and in vitro and in vivo effects. Sections with bold borders indicate a study in which in vivo application of nanoparticles has delivered an antiarthritic effect.

NP type / Size	**Drug load (EE/DL)**	**Testing** ***In vitro***		**Testing** ***In vivo***		**Reference**
		Model	**Study outcome**	**Model**	**Study outcome**	
PEG-immunoliposomes 150-250nm	Collagen II antibodies.	Porcine articular chondrocytes from healthy compared to arthritic tissue.	Nanoparticles bind preferentially to arthritic primary articular porcine chondrocytes.	Dunkin-Hartley-guinea pig spontaneous OA development model.	Visualisation of IV injected nanoparticle localisation preferentially to areas of degraded cartilage.	(Cho et al., 2014)

Condroitin sulphate (ChS)– solid lipid nanoparticles (SLN). 396+/-2.7nm	Diacerein (DL: 15.59%).	PBS release study through dialysis membrane.	Release studies: burst up to 1hr followed by release up to 16hrs and increased bioavailability of diacerein 2.8-fold.	Charles foster rat sodium iodoacetate chemically induced OA model treated for 12 weeks orally with nanoparticles compared to free drug.	Nanoparticle loaded drug was identified in significantly higher concentrations than free drug in cartilage ($p<0.01$) and synovial fluid ($p<0.001$) (12wks). ChS nanoparticle drug treatment groups had improved joint scores (grade 1, stages 1.5-1) compared to free drug (grade 2, stage 2).	(Jain et al., 2014)

ChS conjugated SLNs SLN: 143.4+/-0.9nm CS-SLN: 154+/-1.1nm	Aceclofenac SLN: 76.53+/-2.5% EE CS-SLN: 65.38+/-1.7% EE	Drug release via dialysis tube (molecular weight cut off, 15KDa). Release media Ethanol:PBS (50:50).	Sustained drug release over 24hrs. 65.25% from SLN nanoparticles and 57.82% release from ChS-SLN nanoparticles at 24hrs.	After three days SLN, ChS-SLN and free drug administered intra-venously and readings taken over 48hrs.	Percentage drug uptake in the knee joint at 24hrs 0.34% for free drug, 5.16% for SLN nanoparticles and 10.63% for ChS-SLN. ChS-SLN delivered percentage reduction in oedema for up to 12hrs (52.35%) vs 8 (36.57%) and 4 (40.53%) for SLN and free drug respectively.	(Bishnoi et al., 2014)
HA/chitosan – pEGFP 150-350nm	Non-viral plasmid DNA.	Rabbit knee chondrocytes incubated for 4hrs with NPs and monitored for DNA transfection efficiency.	HA/chitosan nanoparticles delivered significantly higher transfection than chitosan particles alone for up to 4 days ($p<0.05$).	N/A	N/A	(Lu et al., 2011)

Poly(propylene sulphide) nanoparticles functionalised with collagen II binding peptide. 38nm or 96nm	WYRGRL ligand peptide for selective nanoparticle binding to collagen Iiα1.	N/A	N/A	IA injection of nanoparticles into mice knees. Localisation and retention quantified using confocal laser scanning microscopy.	Peptide functionalised nanoparticles targeted articular cartilage up to 72-fold more than nanoparticles with a non-specific peptide sequence at 24hrs ($p<0.01$).	(Rothenfluh et al., 2008)
Chitosan based nanoparticles 50-400nm	Berberine (BBR) EE: 22.3% at chitosan/BBR ratio 1:1 to 45.8% CS/BBR ratio 4:1.	Drug release of free BBR compared to BBR loaded Chitosan nanoparticles in PBS.	Free BBR release was 90.5% after 24hrs. The BBR loaded chitosan nanoparticles cumulative release over three days was 55.7% with slowing release over the next 4 days.	ACLT medial meniscal resection rat OA model. IA injection with free drug compared to BBR loaded nanoparticles and joint histology analysed after 10 weeks post-surgery.	Significantly higher BBR concentration in synovial fluid from nanoparticles compared to free BBR up to 96hrs ($p<0.001$). cartilage histopathology scores were significantly improved for BBR loaded nanoparticle group (4.52) compared to OA group (9.62; $p<0.001$) and free BBR groups (5.58; $p<0.05$).	(Zhou et al., 2015)

Bovine serum albumin (BSA) nanoparticles and HA coated BSA-nanoparticles. 108+/-5.9nm	At 1:5 brucine to BSA ratio 48.9+/-1.1% EE and 4.2+/-0.1% DL	Cellular uptake study into chondrocytes isolated from articular cartilage from New Zealand white rabbits.	HA coated BSA nanoparticles demonstrated increased cellular uptake (7ug/mg) vs non-coated nanoparticles (<4ug/mg) over 60 minutes ($p<0.01$).	Male Sprague Dawley (SD) rats biodistribution studies over 14 days following IA injection.	Only HA coated nanoparticles remained in the joint after 14 days compared to all other groups.	(Chen et al., 2013)
Range of cationic polymeric nanoparticle formulations for different testing: 37.5:37.5:25 D10P:D20P-VivoTag:Eudragit RL100 nanoparticles used for *in vivo* testing. 100-150nm	Fluorescent tagged nanoparticles.	Viscosity measurements of human OA synovial fluid with and without nanoparticle application. PBS release studies from 1mg/ml nanoparticles.	Viscosity measurements indicated that hydrogels, formed after the addition of nanoparticles to synovial fluid, did not alter the viscosity. Approximately 20% peptide release over 6 days at a linear release rate.	Retention of fluorescent nanoparticles within knee joint of female SD rats following IA injection.	74% retention of fluorescent NPs within knee joint at 1 week compared to 23% after 2 days for free peptide.	(Morgen et al., 2013)

Kartogenin (KGN) conjugated with low/medium molecular weight chitosan nanoparticles and microparticles. 150+/-39nm	KGN-chitosan concentration 0.05% (w/v) on nanoparticles.	Investigation into chondrogenic differentiation of human MSCs following free drug and nanoparticle exposure. Release study into PBS from 100mg of particles.	Release studies demonstrated 30-50% release over 7 weeks. Increased stimulation of chondrogenic markers than unconjugated KGN (GAG, $p<0.05$; COL2A1; $p<0.01$; aggrecan, $p<0.05$).	Surgically induced (ACLT) rat OA.	Nanoparticle treatment groups showed significantly lower OA Research Society International (OARSI) cartilage histopathology assessment score changes than unconjugated KGN ($P<0.05$) and vehicle controls ($p<0.01$) after 14 weeks.	(Kang et al., 2014)
HA - salmon calcitonin-chitosan nanocomplexes HA:chitosan ratio- 5:2=193+/-21nm 5:1=193+/-33nm 10:1=163+/-5nm	Anti-inflammatory effects of HA and salmon calcitonin-chitosan. salmon calcitonin-chitosan association	salmon calcitonin-chitosan release studies into PBS. salmon calcitonin-chitosan and HA treated SW1353 chondrocyte cell line cells.	Up to 40% salmon calcitonin-chitosan release within the first hour followed by sustained release over 24hrs. Salmon calcitonin-chitosan and HA down regulated NR4A2 expression in PGE2 and IL-1β treated SW1353 cells ($p<0.01$) compared to treatment free controls.	K/BxN inflammatory mouse model treated with IA injection of nanoparticles compare to PBS controls.	A significant reduction in knee diameter ($p<0.001$) compared to PBS controls; a significant reduction ankle in NR4A2 expression ($p<0.01$) and a significant reduction in joint histology score ($p<0.01$) compared to PBS controls.	(Ryan et al., 2013)

	efficiency of up to 99.52%.		Salmon calcitonin-chitosan and HA down regulated the expression of MMP-13 expression in IL-1β treated cells ($p<0.001$).			
μ-RAFT-TEGM copolymer self-assembling nanoparticles 270+/-5nm	IL-1Ra tethered to particle surface. 250ng IL-1Ra/100μg particles.	The HIG-82 synoviocyte cell line was incubated for 2hrs with IL-1Ra or BSA loaded nanoparticles and analysed for binding via confocal microscopy and flow cytometry.	IL-1Ra loaded particles bioactivity on HIG-82 synoviocytes showed higher particle co-localisation to cells than BSA loaded controls representing 44% of cells whereas BSA particles represented 2.7%.	Male Lewis rats were treated with 50μl of either nanoparticles or soluble IL-1Ra protein (5μg IL-1Ra) via intra-articular injection.	IL-1Ra tethered nanoparticles increased IL-1Ra retention time to 20% signal over 10 days with untethered IL-1Ra dropping to less than 20% by 3 days. Half-life enhanced from 0.96 days to 3.01.	(Whitmire et al., 2012)
PLGA (50:50) nanoparticles encapsulated into PLGA microspheres. Nanoparticles in	Brucine loaded nanoparticles and NIMs. EE nanoparticles: 80.29+/-0.22%	Release studies into PBS.	Burst release of brucine from microparticles into PBS quantified as 41%, this was reduced to 9% from NIMs encapsulated with nanoparticles.	Male SD-rats with airpouch, subcutaneous injection model used for pharmacokinetic studies.	Rats IA injected with fluorescent labelled nanoparticles, microparticles and NIMs. NIMS shown to be retained within the joint after 11	(Chen et al., 2014)

microspheres (NIMs) nanoparticle size: 260+/-12nm Microparticle size: 8.99µm NIM size: 12.38 µm	EE NIMs: 83.37+/-0.24%				days and nanoparticles after 7 day.	
Protein complexed pHEMA-pyridine nanoparticles. Nanoparticle size corresponds to BSA:polymer ratio 2:1 ratio: 303+/-13nm 1.875:1 ratio: 500+/-22nm 1.5:1 ratio: 910+/-46nm.	BSA and FN tethered to nanoparticles.	Assessment of FN nanoparticle bioactivity using FN cell binding domain specific monoclonal antibody HFN7.1.	FN nanoparticle binding ability was significantly greater than BSA loaded nanoparticles and unloaded nanoparticles ($p<0.001$).	Evaluated the relationship between nanoparticle size and joint retention time following IA injection of BSA loaded NPs into male Lewis rat stifle joints.	Joint retention of 900nm and 500nm nanoparticles significantly higher than soluble protein at 14 days ($p<0.05$). 900nm showed the most retention (half-life 2.5 days) vs 500nm particles (1.9days half-life).	(Singh et al., 2014)

Fibronectin (FN):polymer ratio. 2:1 ratio: 200nm						
PLGA nanoparticles covered with HA or Poly-vinyl alcohol (PVA). 600-700nm	Dextran-Fluorescein isothiocyante (FITC) loaded nanoparticles.	Primary rat chondrocyte cell viability and cellular uptake studies.	HA coated nanoparticles were shown to elicit no decrease in cell viability on primary rat chondrocytes and synoviocytes up to 72 hours. HA coated nanoparticles shown to have increased uptake into primary rat chondrocytes compared to PVA coated nanoparticles at 6, 12 and 24hrs.	IA nanoparticle injections into rat knees at 0 and 1 week. Rats were then culled 1 week after injection.	No change in expression of early inflammatory markers (IL-1β and TNFα) was observed as a consequence of nanoparticle injection ($p>0.05$).	(Laroui et al., 2007) (Zille et al., 2010)
Iron-Ethylcellulose magnetic nanoparticles 430+/-40nm	Diclofenac sodium loaded through adsorption to particle surface or absorption into particle core.	Drug release studies into PBS via dialysis bag (2KDa cut-off).	Drug release studies demonstrated a biphasic release profile. Initial burst release of diclofenac up to 1 hour followed by sustained release up to the next 48 hours.	N/A	N/A	(Arias et al., 2009)

	Adsoption:8-12% EE Absorption: up to 54% EE.					
Avidin-FITC and NeutrAvidin-FITC quantum dots (QDs) 7nm	QD particle identification for drug delivery into the cartilage.	Cartilage explant disks harvested from femoropatellar grooves of 1-2-week-old bovine calf knee joints.	Comparison of solutes demonstrated that having a diameter of less than 10nm can allow for full thickness cartilage penetration. Avidin had 400-fold increased uptake compared to NeutrAvidin and >90% of Avidin was retained within explants for 15 days.	N/A	N/A	(Bajpayee et al., 2014)
Chitosan and HA nanoparticles Size dependant on chitosan:HA ratio ranging from	pDNA encoding IL-1 receptor antagonist gene.	Release studies into PBS (pH6.8) over 15 days.	Sustained release achieved over 15 days with a 22% burst release of encapsulated pDNA.	N/A	N/A	(Deng et al., 2018)

144.9+/-2.8nm at 4:1 ratio to approximately 500nm at 1:1 ratio.		Anti-inflammatory effect of nanoparticles treatment on IL-1β treated primary Sprague-Dawley rat synoviocytes.	nanoparticle treatment decreased the expression of MMP-3, MMP-13, COX-2 and iNOS mRNA ($p<0.05$) and protein ($p<0.05$) compared to untreated controls.			
Chitosan and HA nanoparticles 164.68+/-14.21nm	Curcuminoid. Optimum loading capacity 38.44%.	PBS release study through dialysis bag (2kDa cut off). Primary chondrocytes from SD rats.	Curcumin release from nanoparticles went from 40% (1hr) to 74% (72hrs) over time. Primary chondrocytes from SD rats showed enhanced proliferation (36.4% compared to 13.62% in controls), suppressed apoptosis ($p<0.01$ vs negative control) and decreased MMP-13 and MMP-1 expression ($p<0.01$ compared to controls)	OA model in SD rats (MCL, ACL and meniscal severance)	nanoparticles alleviated joint lesions, increased levels of collagen II mRNA and decreased levels of MMP-1 and MMP-13 mRNA ($p<0.01$ compared to control).	(Wang et al., 2018)

			upon treatment with nanoparticles			
Melanin nanoparticles (MNPs) encapsulated within poly(L-lysine) (PLL). MNPS: 5.8+/-2.1nm PLL-MNPs: 42.5+/-1.6nm	MNPs for photoacoustic glycosaminoglycan (GAG) targeting in cartilage.	Cartilage samples extracted from 10-week-old Sprague-Dawley rats treated with PLL-MNPs or MNPs alone.	Cartilage treated with PLL-MNPs showed higher uptake (2580 PA intensity) than MNPs alone (1425 photoacoustic intensity) and increased retention within the cartilage, demonstrating a stronger GAG affinity than MNPs alone.	Surgical meniscal destabilisation (DMM) mouse model.	MNPs could not effectively aggregate to detect cartilage degeneration within OA joints. PLL-MNPs accurately provided information as to the extent of OA related cartilage degeneration allowing for visualisation of degeneration *in vivo* as opposed to *ex vivo.*	(Chen et al., 2018)
KGN coated polyurethane nanoparticles. 25nm diameter	Small molecule KGN bonded to nanoparticles.	Saline release study Primary chondrocytes	Release of approximately 20% of drug load occurred over 30 days with burst release of the initial 10% within the first 5 days. Polyurethane nanoparticles-KGN did not	10-week-old male SD rat ACLT OA model.	Cartilage in polyurethane nanoparticle-KGN treatment group 12 weeks after IA injection showed less extensive cartilage destruction, with OARSI scores significantly less in nanoparticle treatment	(Fan et al., 2018)

		isolated from SD rats treated with polyurethane nanoparticles-KGN.	increase secretion of IL-6 compared to untreated controls at 24 and 48 hours ($p>0.05$). Additionally, no cytotoxicity from PN-KGNs were observed on chondrocytes.		groups compared to all other groups ($p<0.05$).	
HA conjugated to thermosensitive dibenzocyclooctyne (DBCO)-amine and pNiPAM-azide, thermoresponsive nanoparticles Three nanoparticle preparations: HA nano 1: 239+/-95nm. HA nano 2: 133+/-64nm.	HA conjugated to nanoparticles.	Human fibroblast-like synoviocytes exposed to HA conjugates MTT cell viability assay.	Cell viability did not decrease with HA nano 1 or 2 at concentrations used *in vivo*.	Week-old male C57BL/6 mice surgical meniscal destabilisation (DMM) model. HA nano 1 IA injected 7 and 35 days after surgery and treatment groups evaluated at day 63.	HA nano 1 reduced Vascular endothelial growth factor (VEGF) ($p<0.05$), IL-1β ($p<0.001$) and TNFα ($p<0.01$) plasma levels vs untreated OA groups and OARSI scores were significantly reduced in the media tibia and medial femur compared to OA groups ($p<0.001$).	(Maudens et al., 2018)

HA nano 3: 223+/-55nm.						
Condroitin sulphate-HA nanoaprticles. Size effected by CS:HA ratio: Largest 1:1=650nm Smallest 4:1=100nm	Condroitin sulphate-HA nanoparticles with no drug load used to treat cells.	Articular chondrocytes and infrapatellar fat pad derived MSCs from human OA patients were co-cultured in monolayer and in pellets with monocultures used as controls.	There was increased expression of collagen type II and aggrecan from pellet coculture after 3 weeks exposure to chondroitin sulphate-HA nanoparticles ($p<0.05$).	N/A	N/A	(Huang et al., 2017)
PLGA Nanoparticles. 136nm	Curcumin loaded nanoparticles. EE:97+/-0.45%.	N/A	N/A	Male Wistar rat mono-iodoacetate (MIA) OA model. Gavaged with either Curcumin or Nanoparticle encapsulated curcumin for 14 consecutive days and	Encapsulating curcumin in PLGA nanoparticles reduced Mankin knee joint scores compared to MIA controls ($p<0.001$) and free curcumin treated ($p<0.01$) groups.	(Niazvand et al., 2017)

				knee joints analysed histologically.		
Hollow thermoresponsive poly(N-isopropylacrylamide) (pNIPAM) nanoparticles with Sulfated 2-acrylamido-2-methyl-1-propanesulfonic acid was copolymerized in the shell. Hollow PEGylated nanoparticles: 293+/-1.4nm	Anti-inflammatory mitogen-activated protein kinase-activated protein kinase 2-inhibiting cell-penetrating peptide (KAFAK). Hollow PEGylated nanoparticles drug loading: 0.498+/-0.087mg/mg.	PBS release study Nanoparticle uptake into RAW 264.7 macrophages, monitored. *Ex vivo* bovine cartilage explant model. Cartilage explants exposed to an 'OA inducing' environment via the removal of native aggrecan.	KAFAK released over 4 days with initial burst release of 79% within 24 hours. Macrophage uptake of PEGylated nanoparticles occurred within 24 hours. Sustained KAFAK release from hollow nanoparticles resulted in significant IL-6 reductions from day 4 compared to controls ($p<0.05$) continuing to decrease to day 8 ($p<0.001$).	N/A	N/A	(McMasters et al., 2017)

Gold nanoparticles (AuNPs) Three size batches: 2.94nm 13.19nm 44.74nm	No drug load just comparison of the effects of gold nanoparticle diameter.	Primary articular chondrocytes from 4-week-old New Zealand white rabbits, cell viability studies (CCK-8 assay) measurement of reactive oxygen species and measurement of mitochondrial membrane potential.	13nm AuNPs induced a reduction in chondrocyte cell viability at 0.2 ($p<0.05$) and 2nM ($p<0.01$), increased chondrocyte apoptosis ($p<0.01$ vs all other groups) and increased levels of reactive oxygen species ($p<0.01$ vs controls). 3 and 45nm AuNPs had no significant effect on articular chondrocytes indicating a size dependant cytotoxicity of AuNPs.	N/A	N/A	(Huang et al., 2016)
Gold (Au) and silver (Ag) nanoparticles AuNP: 50nm AgNP: 65nm	Effects of different concentrations of Au and AgNPs tested.	Exposure of Ag and Au nanoparticles to primary human OA chondrocytes.	There was a dose dependant cytotoxic effect of both NP types. 160µM and 250µM NP reduced cell viability ($p<0.01$). Au but not AgNPs were identified	N/A	N/A	(Pascarelli et al., 2013)

			in cell cytoplasm and endocytotic vesicles. Increased gene expression of MMP-3 ($p<0.001$) and MMP-1, MMP-13, ADAMTS-4 and ADAMTS-5 ($p<0.01$) was observed for both NPs at 160µM.			
Nanostructure lipid carrier	Ginger extract at 5% w/w ratio with nanostructure lipid carrier. With a 6-gingerol content of 11.18%.	Modified Franz Cell Diffusion release study.	92% of 6-gingerol released from nanoparticle lipid carrier after 24 hours.	Clinical trial: Patients apply ginger-nanoparticle lipid carrier topically around knee index three times a day, 59 patients were completed and reported for baseline testing.	Results following 12 weeks of treatment indicated ginger extract-nanoparticle lipid carriers significantly improved knee joint pain, symptoms of OA, daily activities and quality of life (KOOS), index of severity for OA and patient global assessment ($p<0.05$ vs baseline). There were no safety issues of adverse events.	(Müller et al., 2002, Amorndoljai et al., 2015)

Cationic Avidin (7nm) conjugated to dexamethasone (DEX). 4 different formulations: -Av+DEX -PEG Av+DEX -PEG Av-ester-DEX -PEG Av-hydrazone-DEX.	DEX conjugated in different formulations to Avidin. Drug loading content: Av+DEX: 33.2+/-4.8% PEG Av+DEX-32.8+/-3.6% PEG Av: ester-DEX: 2.2+/-0.3% PEG Av-hydrazone-DEX: 1.9+/-0.1%.	PBS release studies via dialysis membrane (3.5KDa cut off). Cartilage explants were extracted from 1 to 2-week-old bovine calf knees and treated with IL-1a with or without DEX conjugated avidin formulations and free DEX.	Av-DEX and PEG Av-DEX demonstrated the quickest drug release (70% release in 3 hours), conjugation of DEX increased release rate (14.4- and 57.3-hour half-lives for PEG Av-ester-DEX and PEG Av-hydrazone-DEX respectively). Single dose of Avidin-DEX reduced IL-1a induced sGAG loss over 3 weeks ($p<0.05$), rescued IL-1a induced cell death ($p<0.0001$) and didn't cause cytotoxicity while restoring GAG synthesis levels ($p<0.0001$) vs untreated controls.	N/A	N/A	(Bajpayee et al., 2016)

PLGA nanoparticles coated with HA. 335nm mean particle diameter.	Fluorescently labelled nanoparticles to identify in cells.	Human primary chondrocytes and synoviocytes were assayed for nanoparticle internalisation, Lactate dehydrogenase (LDH) activity, mitochondrial activity (MTT assay), inflammatory response (qRT-PCR), NO, PGE_2.	Nanoparticles were detected in cell cytoplasm after 8 hours.	The effect of Intra-articular nanoparticle injection into young male Wistar Han rats was histologically analysed on sections extracted from joints 3- or 7-days post injection.	No adverse side effects were demonstrated compared to saline controls (cartilage abnormalities, synovial inflammation, subchondral bone remodelling).	(Riffault et al., 2015)